Shakil Mahmud • Research Monograph

SHAKIL MAHMUD EDITORIAL & RESEARCH MONOGRAPHS

The Universal Chronicle

The epic 13.8-billion-year chronicle of reality: from cosmic inflation and stellar nucleosynthesis to planetary intelligence and cosmic horizons.

SHAKIL MAHMUD

Independent Scholar & Systems Researcher

SHAKIL MAHMUD EDITORIAL & RESEARCH SERIES

First Collected Edition • Dhaka & Singapore • 2026

The Universal Chronicle

The epic 13.8-billion-year chronicle of reality: from cosmic inflation and stellar nucleosynthesis to planetary intelligence and cosmic horizons.

LIBRARY & CATALOGING-IN-PUBLICATION DATA

Title: The Universal Chronicle
Author: Shakil Mahmud
Series: Shakil Mahmud Editorial & Research Series (Monograph Collection)
Subjects: Science -- History -- Philosophy -- Mathematics -- Civilization
Published: Dhaka & Singapore, 2026
Format: Digital Monograph Offprint (PDF) • Complete 20-Part Collected Edition
Permanent URI: https://shakilmahmud.com/series/universe/

Suggested Academic Citation:
Mahmud, Shakil. (2026). *The Universal Chronicle: The Complete 20-Part Collected Monograph*. Shakil Mahmud Research Series. https://shakilmahmud.com/series/universe/

Open Scholarly Access: This collected monograph is published under Open Scholarly Access for personal study, academic citation, university pedagogy, and non-commercial research.

© 2026 Shakil Mahmud. All rights reserved. Typeset and published at Dhaka and Singapore.

Shakil Mahmud • Research Monograph

EDITORIAL PREFACE

Preface: The Scaffolding of Reality

Across 13.8 billion years, the cosmos evolved from a singularity of unimaginable temperature and density into an expanding web of billions of galaxies, trillions of stars, and conscious observers. This monograph delivers an authoritative chronicle of cosmic evolution: inflation, nucleosynthesis, cosmic microwave background, stellar lifecycles, supermassive black holes, and the ultimate thermodynamic destiny of reality.

The purpose of this collected monograph is not merely didactic exposition, but the systematic synthesis of conceptual revolutions. Each chapter examines an intellectual threshold where old paradigms faltered and new mathematical or physical insight illuminated deeper structures of reality.

— Shakil Mahmud
Dhaka & Singapore, 2026

INDEX OF PARTS

Table of Contents

PHASE I: ANCIENT & CLASSICAL FOUNDATIONS

PART I	**The Beginning Before Time — Cosmic Inflation, the Quantum Vacuum, and the Planck Epoch** *The Beginning Before Time — Cosmic Inflation, the Quantum Vacuum, and the Planck Epoch*	2,752 words
PART II	**The Crucible of Matter — Quark-Gluon Plasma, Baryogenesis, and Primordial Nucleosynthesis** *The Crucible of Matter — Quark-Gluon Plasma, Baryogenesis, and Primordial Nucleosynthesis*	3,039 words
PART III	**The Clearing of the Heavens — Recombination, the Cosmic Microwave Background, and the Dark Ages** *The Clearing of the Heavens — Recombination, the Cosmic Microwave Background, and the Dark Ages*	2,476 words
PART IV	**Cosmic Dawn — Population III Hyperstars, the First Galaxies, and Reionization** *Cosmic Dawn — Population III Hyperstars, the First Galaxies, and Reionization*	2,101 words
PART V	**The Alchemists of the Universe — Stellar Nucleosynthesis, Supernovae, and the Forging of Heavy Elements** *The Alchemists of the Universe — Stellar Nucleosynthesis, Supernovae, and the Forging of Heavy Elements*	2,322 words

PHASE II: MEDIEVAL TRANSFORMATIONS

PART VI	**The Architecture of Galaxies — Spiral Arms, Supermassive Black Holes, and the Milky Way** *The Architecture of Galaxies — Spiral Arms, Supermassive Black Holes, and the Milky Way*	2,481 words
PART VII	**The Solar Cradle — The Protoplanetary Disk, Planetesimal Accretion, and the Young Sun** *The Solar Cradle — The Protoplanetary Disk, Planetesimal Accretion, and the Young Sun*	2,420 words
PART VIII	**The Violent Genesis — The Hadean Earth, Theia Giant Impact, and the Birth of the Moon** *The Violent Genesis — The Hadean Earth, Theia Giant Impact, and the Birth of the Moon*	1,922 words
PART IX	**The Primordial Cradle — Volcanic Degassing, Cometary Bombardment, and the First Oceans** *The Primordial Cradle — Volcanic Degassing, Cometary Bombardment, and the First Oceans*	2,078 words
PART X	**The Spark of Abiogenesis — Alkaline Hydrothermal Vents, Prebiotic Chemistry, and the RNA World** *The Spark of Abiogenesis — Alkaline Hydrothermal Vents, Prebiotic Chemistry, and the RNA World*	2,446 words

PHASE III: THE MODERN SCIENTIFIC REVOLUTION

PART XI	**The Oxygen Catastrophe & The Miracle — Cyanobacteria and the Great Oxidation Event** *The Oxygen Catastrophe & The Miracle — Cyanobacteria and the Great Oxidation Event*	2,285 words
PART XII	**The Leap to Complexity — Endosymbiosis, Eukaryotes, and the Genesis of Cellular Specialization** *The Leap to Complexity — Endosymbiosis, Eukaryotes, and the Genesis of Cellular Specialization*	2,212 words
PART XIII	**The Cambrian Crucible — Snowball Earth Thaw, Multicellular Body Plans, and the Apex Predators** *The Cambrian Crucible — Snowball Earth Thaw, Multicellular Body Plans, and the Apex Predators*	2,004 words
PART XIV	**The Conquest of Land — Primitive Forests, Arthropod Pioneers, and the Tetrapod Revolution** *The Conquest of Land — Primitive Forests, Arthropod Pioneers, and the Tetrapod Revolution*	2,541 words
PART XV	**The Dinosaur Empire & The Impact — The Mesozoic World and the Mammalian Dawn** *The Dinosaur Empire & The Impact — The Mesozoic World and the Mammalian Dawn*	2,454 words

PHASE IV: CONTEMPORARY HORIZONS & SYNTHESIS

PART XVI	**The Upright Ape — The Rift Valley, Bipedalism, and the Mastery of Fire** *The Upright Ape — The Rift Valley, Bipedalism, and the Mastery of Fire*	2,067 words
PART XVII	**The Cognitive Revolution — Homo sapiens, Symbolic Language, and Abstract Thought** *The Cognitive Revolution — Homo sapiens, Symbolic Language, and Abstract Thought*	2,093 words
PART XVIII	**The Domestication of Nature — The Neolithic Spark, Cuneiform, and the Rise of Cities** *The Domestication of Nature — The Neolithic Spark, Cuneiform, and the Rise of Cities*	2,149 words
PART XIX	**The Harnessing of Logic — Electromagnetism, Turing Machines, and the Solid-State Transistor** *The Harnessing of Logic — Electromagnetism, Turing Machines, and the Solid-State Transistor*	2,193 words

Shakil Mahmud • Research Monograph

PART XX **The Synthetic Mind — Neural Networks, Transformers, and the Dawn of Planetary Intelligence** 2,136 words

The Synthetic Mind — Neural Networks, Transformers, and the Dawn of Planetary Intelligence

SHAKIL MAHMUD RESEARCH MONOGRAPHS • PART I

The Beginning Before Time — Cosmic Inflation, the Quantum Vacuum, and the Planck Epoch

The Beginning Before Time — Cosmic Inflation, the Quantum Vacuum, and the Planck Epoch

2,752 words • October 30, 2026 • Permanent URI



Plate I: *Figure: Cosmic inflation and quantum spacetime fluctuations during the Planck epoch ($t \leq 10^{-43}$ s), driving the exponential metric expansion of spacetime from subatomic scales to cosmological horizons.*

Before there were stars, atoms, or even the passage of time itself, the universe existed as an unimaginable physical state: an unbroken symmetry where space, matter, and the fundamental forces of reality were compressed into a single quantum continuum. Within the first septillionth of a second, a violent exponential expansion of spacetime—cosmic inflation—stretched microscopic quantum ripples into the vast cosmic web that now cradles two trillion galaxies.

The Boundary of Knowledge: What Actually Happened at t = 0?

Popular representations of the Big Bang invariably imagine a firecracker exploding inside an empty black room. A blinding point of light flashes, debris hurtles outwards, and planets coalesce within the void. This mental model is profoundly incorrect in two fundamental ways: first, the Big Bang was not an explosion of matter *through* space, but the rapid, metric expansion *of space itself*; second, there was no pre-existing "outside" room into which the universe could expand.

In classical General Relativity, working backward through the Friedmann-Lemaître-Robertson-Walker (FLRW) metric leads to a mathematical singularity at t = 0. At this boundary, the scale factor of the universe $a(t) \to 0$, causing energy density, spacetime curvature, and temperature to diverge toward infinity:

The Singularity Theorems of Hawking and Penrose
In 1970, Roger Penrose and Stephen Hawking demonstrated mathematically that if General Relativity holds true and energy satisfies reasonable positivity conditions (the strong energy condition), an initial gravitational singularity was physically inevitable. However, physicists do not interpret this infinite density as an actual physical event, but rather as the precise point where Albert Einstein's classical theory breaks down and must surrender to quantum mechanics.

Shakil Mahmud • Research Monograph

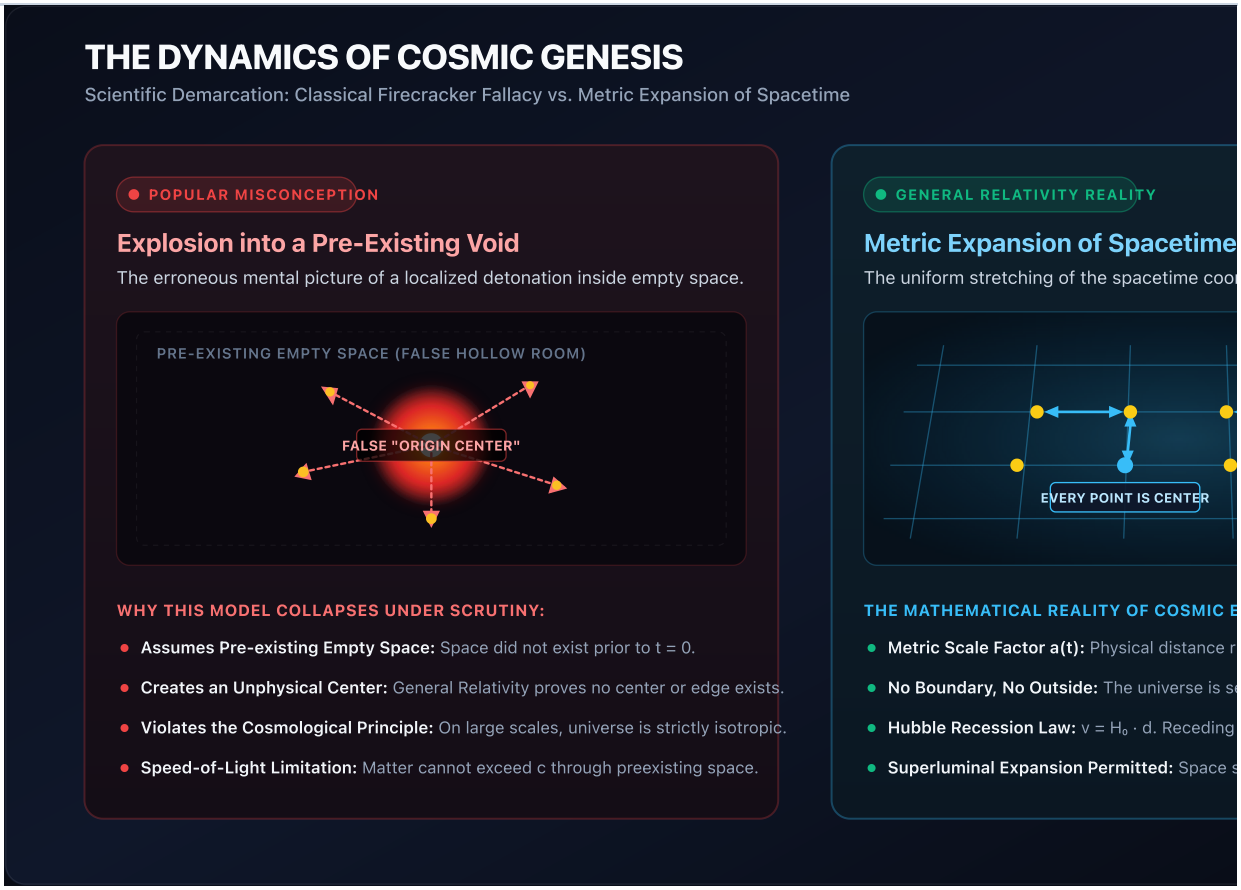


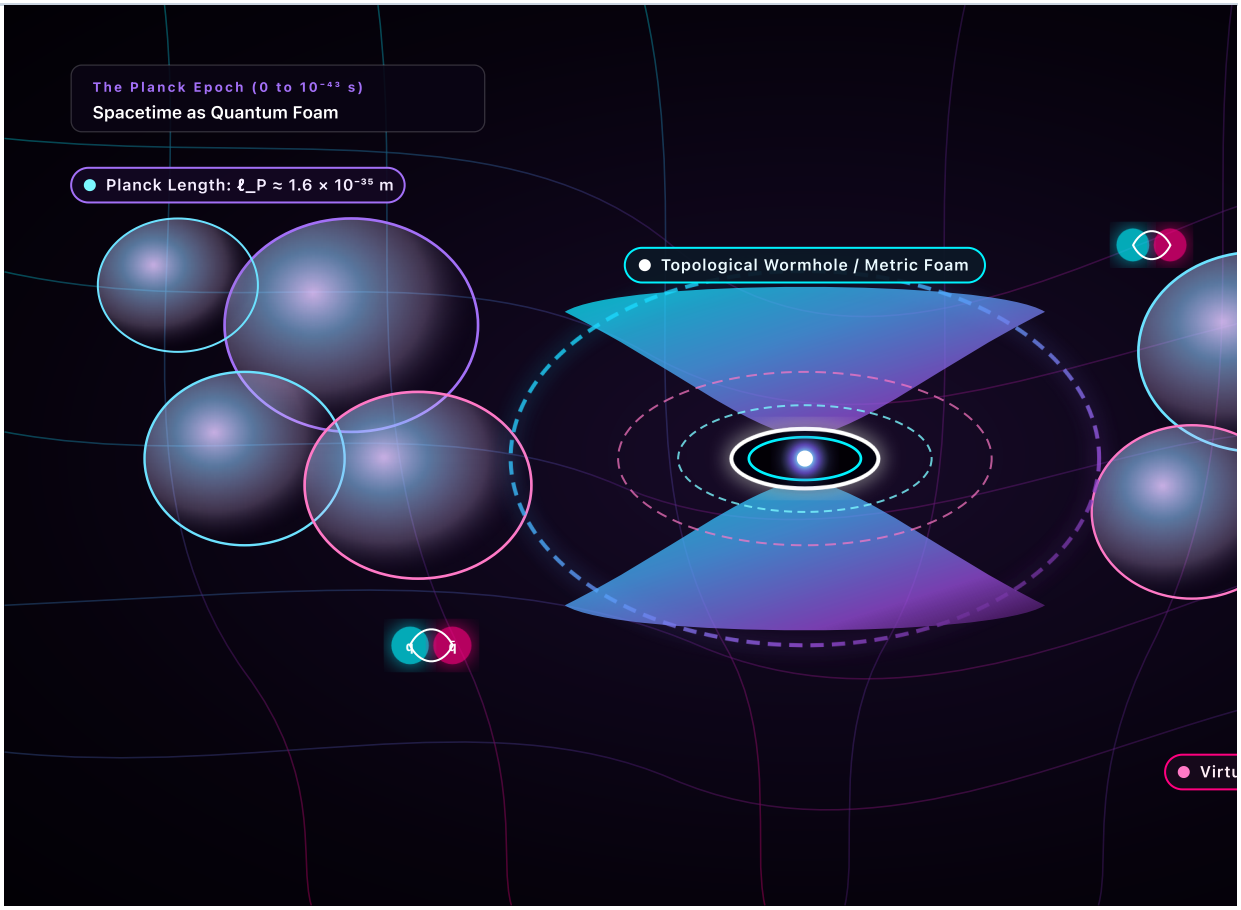
Figure 1.1: The Dynamics of Cosmic Genesis. Contrasting the popular firecracker misconception (an explosion of matter inside a preexisting empty room) with General Relativity reality: the uniform metric expansion of spacetime itself, with no central origin and no external boundary.

The Planck Epoch (0 to 10^{-43} seconds): Spacetime as Quantum Foam

To understand the earliest reachable frontier of physics, we must encounter the fundamental constants of nature: Planck's reduced constant $\hbar$ (the currency of quantum mechanics), Newton's gravitational constant G (the curvature of gravity), and the speed of light c (the maximum velocity of information). Combining these three constants yields the natural scales of the universe at which classical descriptions of geometry cease to function:

- **Planck Time (t_P):** $\sqrt{(\hbar G/c^5)} \approx 5.391 \times 10^{-44}$ seconds
- **Planck Length (l_P):** $\sqrt{(\hbar G/c^3)} \approx 1.616 \times 10^{-35}$ meters
- **Planck Energy (E_P):** $\sqrt{(\hbar c^5/G)} \approx 1.22 \times 10^{19}$ GeV $\approx 1.956 \times 10^9$ Joules
- **Planck Density (ρ_P):** $c^5/(\hbar G^2) \approx 5.155 \times 10^{96}$ kg/m^3

During the Planck Epoch, the energy of individual particles and gravitational curvature were so extreme that the de Broglie wavelength of any particle was smaller than its own event horizon. At this scale, spacetime was not the smooth, continuous fabric described by Einstein. Instead, as John Archibald Wheeler famously formulated, spacetime was a violent, boiling **quantum foam**—a chaotic topological froth where wormholes, microscopic black holes, and temporal geometries flickered into and out of existence faster than light could traverse a proton.



Wheeler's Quantum Spacetime Foam in the Planck Epoch ($t \leq 10^{-43}$ s). At the Planck scale ($\ell_P \approx 1.6 \times 10^{-35}$ m), quantum zero-point metric fluctuations overwhelm smooth Riemannian geometry. Spacetime dissolves into a chaotic, bubbling topological foam of Planck-mass virtual black holes and transient microscopic wormholes fluctuating at $T \sim 10^{32}$ K.

At these blistering temperatures (T ≈ 10^{32} Kelvin), all four fundamental forces of nature—Gravity, the Strong Nuclear Force, the Weak Nuclear Force, and Electromagnetism—were unified into a single, perfectly symmetric superforce. There was no distinction between matter and radiation, between a quark and an electron, or even between "here" and "there."

Spontaneous Symmetry Breaking: The Fracturing of the Superforce

As the nascent spacetime expanded, its energy density fell below the Planck threshold at t ≈ 10^{-43} s. This cooling triggered the first great phase transition in cosmic history: **gravitational decoupling**. Gravity froze out from the unified superforce, becoming a distinct geometric interaction described by curved spacetime.

The remaining three forces remained bound together under what particle physicists term the **Grand Unified Theory (GUT) epoch**. For a fleeting interval between 10^{-43} s and 10^{-36} s, the universe was governed by a GUT gauge group (such as SU(5) or SO(10)). Gauge bosons known as X and Y bosons mediated transitions directly between leptons and quarks, allowing baryonic matter to fluctuate without conservation of baryon number.

When the temperature plunged past T ≈ 10^{28} K (~ 10^{15} GeV), the strong nuclear force broke away from the electroweak force. Much like water abruptly crystallizing into rigid ice when cooling past zero degrees Celsius, the Higgs-like scalar fields governing grand unification experienced **spontaneous symmetry breaking**. This phase transition did not occur smoothly across the entire universe—it left the universe supercooled in a high-energy false vacuum state, setting the stage for the most astonishing event in cosmic history.

Shakil Mahmud • Research Monograph

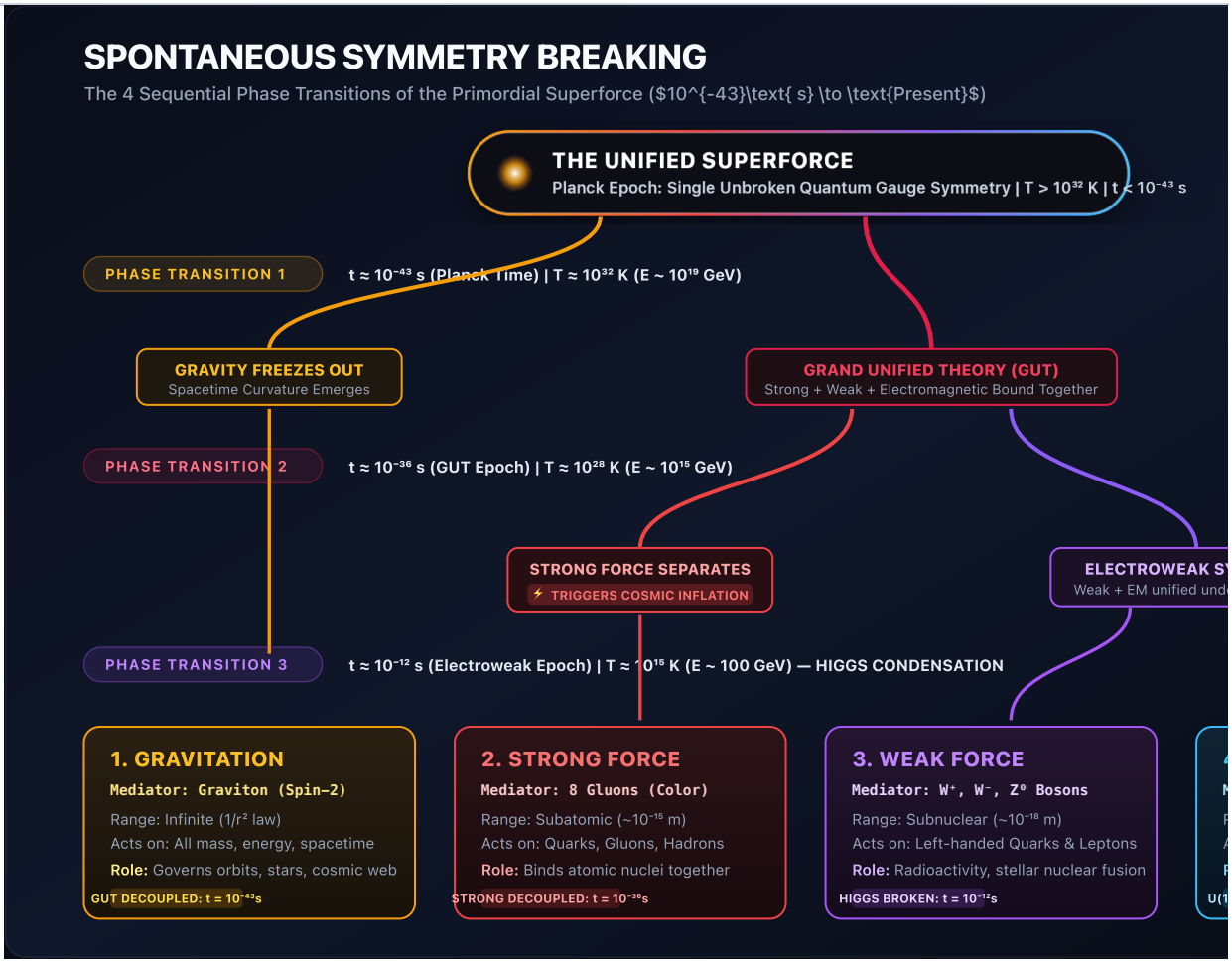


Figure 1.2: Spontaneous Symmetry Breaking & Force Decoupling. Step-by-step chronology of the primordial Superforce fracturing into the four modern fundamental forces (Gravity, Strong Force, Weak Force, and Electromagnetism) as the cosmic temperature plummeted from > 10^{32} K down to 10^{15} K.

The Three Fatal Flaws of the Standard Big Bang Model

By the late 1970s, the classic Big Bang theory was universally accepted following the 1965 discovery of the Cosmic Microwave Background (CMB) by Arno Penzias and Robert Wilson. Yet, as theoretical cosmologists interrogated the equations, three catastrophic paradoxes emerged that threatened to dismantle the entire paradigm:

1. The Horizon Problem (Thermal Equilibrium Without Communication)

When we point radio telescopes at opposite sides of the observable night sky, we are measuring CMB photons that were emitted 13.8 billion years ago from regions separated by roughly 28 billion light-years today. Under standard decelerating FLRW expansion, these two regions were separated by tens of millions of light-years at recombination (t = 380,000 years), while their maximum causal horizon (the distance light could have traveled since t = 0) was only 380,000 light-years. They could never have exchanged a single photon, shared energy, or equalized temperatures. Yet, satellite measurements (COBE, WMAP, Planck) show their temperatures match to within **1 part in 100,000** (2.7255 ± K). How could two regions that never touched be in such immaculate thermal equilibrium?

2. The Flatness Problem (Fine-Tuning of Ω)

The curvature of our universe is dictated by the cosmic density parameter Ω = ρ / ρ_c, where ρ_c is the critical density required for a spatially flat universe (k = 0). In standard general relativity, any deviation from Ω = 1 is unstable and grows exponentially with time: if Ω had been 1.000000000000001 at the Planck epoch, the universe would have recollapsed in a Big Crunch within microseconds; if it had been 0.999999999999999, the universe would have expanded so aggressively that atoms would never have coalesced into stars. Modern observational data demonstrates that today, 13.8 billion years later, Ω = 1.00 ± 0.002. For Ω to remain this close to flat today, it had to be tuned to Ω = 1 ± 10^{-60} at the Planck time—an unscientific miracle of fine-tuning.

3. The Relic Magnetic Monopole Problem

Grand Unified Theories predict that during the spontaneous symmetry breaking of the GUT force, topological defects in the Higgs field should have condensed in immense quantities. The most prominent of these are stable, supermassive magnetic monopoles (m ~ 10^{16} GeV). Had standard cosmology occurred, these monopoles would have saturated the universe, dominating its mass density and collapsing the geometry trillions of years ago. Yet, decades of ultrasensitive detectors have detected zero confirmed magnetic monopoles.

The Miracle of Cosmic Inflation: Alan Guth's Exponential Expansion

In December 1979, a 32-year-old postdoctoral researcher at SLAC named **Alan Guth** realized that these three existential paradoxes could be resolved simultaneously by a single mechanism: what if, for an imperceptible fraction of a second, the universe underwent an exponential super-expansion driven by negative vacuum pressure?

Guth postulated that during the GUT phase transition, the universe became trapped in a "false vacuum"—a local minimum of an unknown scalar potential field, designated the **Inflaton Field** (ϕ). According to the stress-energy tensor of general relativity, a scalar field dominated by its potential energy V(ϕ) exhibits a peculiar property: its pressure is equal to the negative of its energy density:

The Equation of State for Repulsive Gravity

$$P = -\rho c^2$$

In Einstein's second Friedmann acceleration equation:

$$\ddot{a} = -\frac{4\pi G}{3}\left(\rho + \frac{3P}{c^2}\right)a$$

Substituting P = -ρ c^2 flips the sign inside the parentheses from positive to negative:

$$\ddot{a} = +\frac{8\pi G}{3}\rho a$$

Rather than slowing down due to gravitational attraction, spacetime experiences **unbridled gravitational repulsion**!

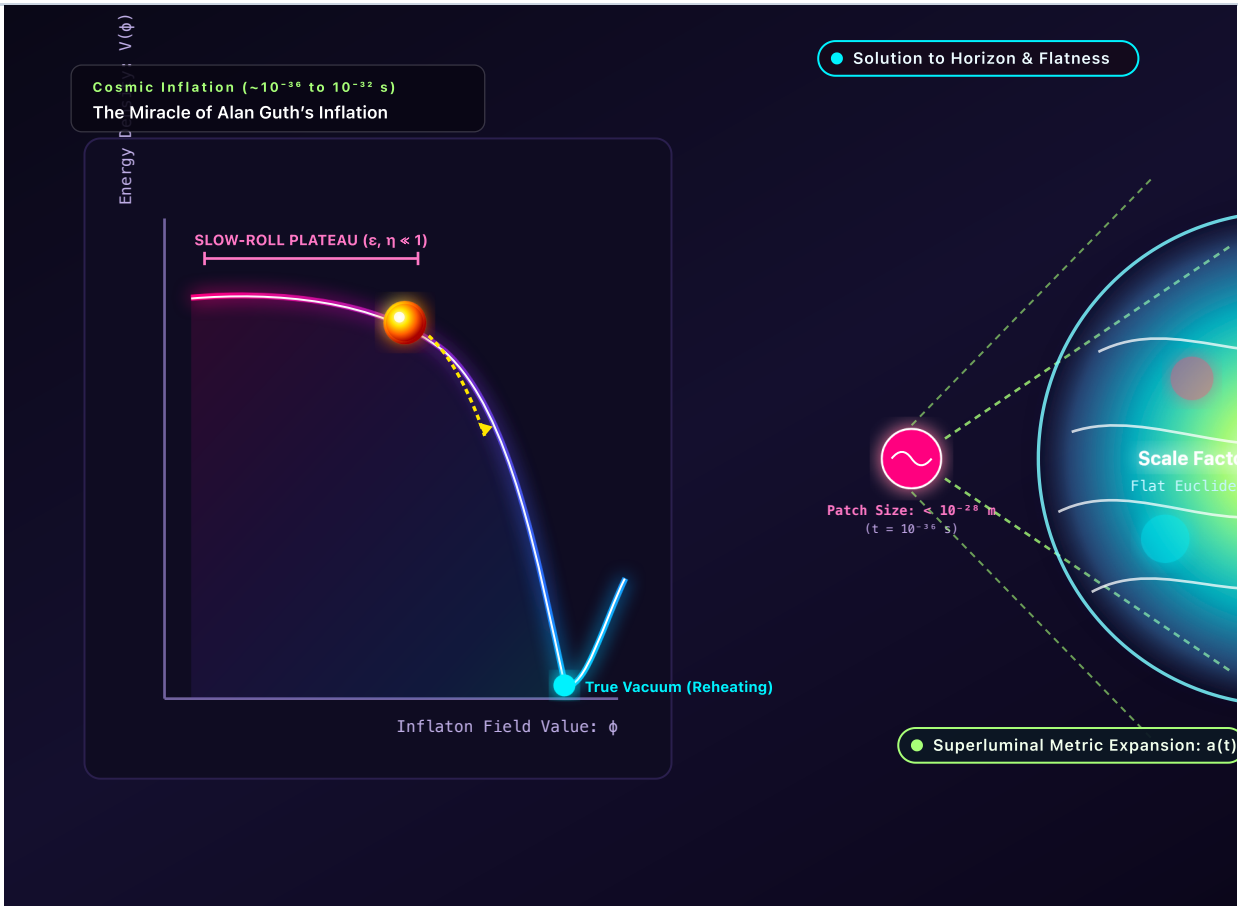
Between t ≈ 10^{-36} seconds and t ≈ 10^{-32} seconds, the scale factor a(t) did not expand linearly or polynomially. It grew exponentially according to de Sitter spacetime geometry:

$$a(t) = a_0 \exp\left(H_{\text{inf}} \cdot t\right)$$

During this unimaginably brief interval of 10^{-32} seconds, spacetime expanded by a factor of at least **10^{26} to 10^{30}** (equivalent to roughly 60 e-folds of expansion, N = ln(a_f / a_i) ≥ 60). A volume smaller than a single subatomic proton was stretched to the size of a marble in less time than it takes light to cross an atomic nucleus. The consequences of this runaway expansion completely resolved the cosmological crises:

- **Horizon Problem Solved:** The entire observable universe today originated from a microscopic patch that had ample time to achieve complete thermal equilibrium before inflation began. Inflation then tore this tiny, equilibrated region apart, propelling points far beyond the speed of light away from one another.
- **Flatness Problem Solved:** Just as blowing up a wrinkled balloon to planetary proportions makes its surface appear completely flat to an ant walking upon it, exponential expansion stretched the curvature of spacetime so thoroughly that Ω was driven irresistibly toward 1.000000.
- **Monopole Problem Solved:** Any topological defects or heavy monopoles created prior to inflation were diluted across an unfathomable expanse of empty volume, leaving at most one monopole in many observable universes.

Shakil Mahmud • Research Monograph



Cosmic Inflaton Potential $V(\phi)$ & False Vacuum Expansion (10^{-36} s $\leq t \leq 10^{-32}$ s). The scalar inflaton field ϕ rolls slowly down a flat potential plateau ($\epsilon, \eta \ll 1$), trapped in a false vacuum state. The constant potential energy density acts as negative pressure ($P = -\rho c^2$), driving exponential de Sitter spacetime expansion ($a(t) \propto e^{Ht}$) by over 60 e-folds.

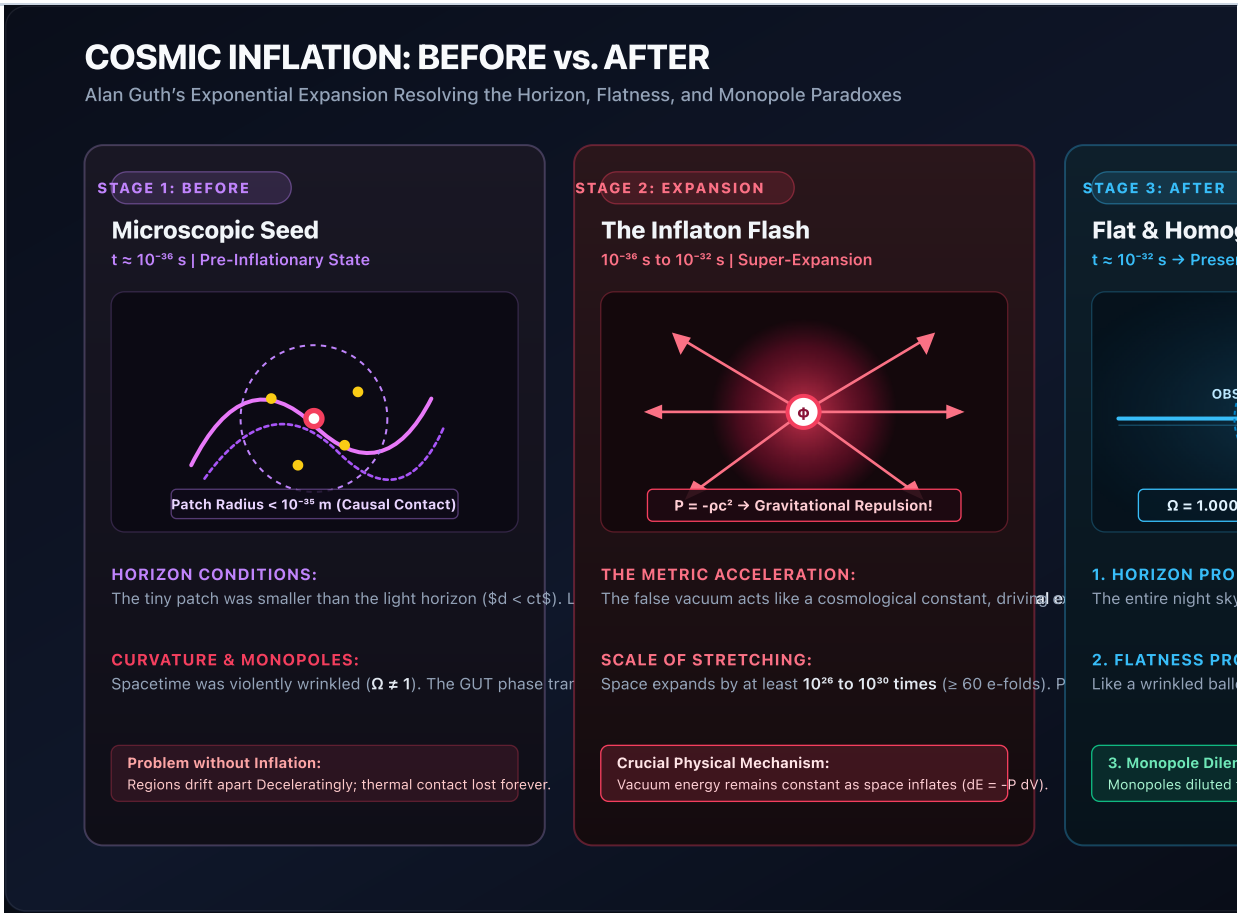


Figure 1.3: Cosmic Inflation Before vs. After. A three-stage comparative sequence showing how exponential de Sitter super-expansion (a(t) ∝ e^{Ht}) stretched a microscopic patch in causal equilibrium to cosmological proportions, ironing out spatial curvature ($\Omega \to 1.000$) and resolving the horizon paradox.

The Cosmic Rosetta Stone: How Quantum Fluctuations Became Galaxies

The most breathtaking triumph of inflationary theory—clarified by Andrei Linde, Andreas Albrecht, Paul Steinhardt, and Viatcheslav Mukhanov—is that it explains where galaxies, stars, and human beings came from.

Heisenberg's Uncertainty Principle (

$$\Delta E \cdot \Delta t \geq \frac{\hbar}{2}$$

) dictates that on subatomic scales, the vacuum can never be completely inert. Particles and fields must constantly fluctuate. Under normal circumstances, these microscopic quantum fluctuations appear and annihilate in fractions of a zeptosecond, averaging out to zero.

During cosmic inflation, however, the expansion rate of spacetime was far faster than the speed of light. Before a quantum ripple in the inflaton field could fluctuate back into nonexistence, spacetime stretched the crests and troughs of the wave **beyond the cosmic event horizon**. The quantum fluctuation was "frozen" into classical reality as a permanent overdensity or underdensity in the metric of space.

These frozen quantum ripples produced a nearly scale-invariant spectrum of primordial density perturbations ($n_s \approx 0.965$, precisely measured by the Planck space observatory). Hundreds of millions of years later, regions that were merely 0.001\% denser than their surroundings exerted greater gravitational pull, drawing in surrounding hydrogen gas to build the first stars, galaxies, and galaxy clusters. **Every structure in the cosmos today is the macroscopic fossil of a primordial quantum fluctuation.**

Shakil Mahmud • Research Monograph

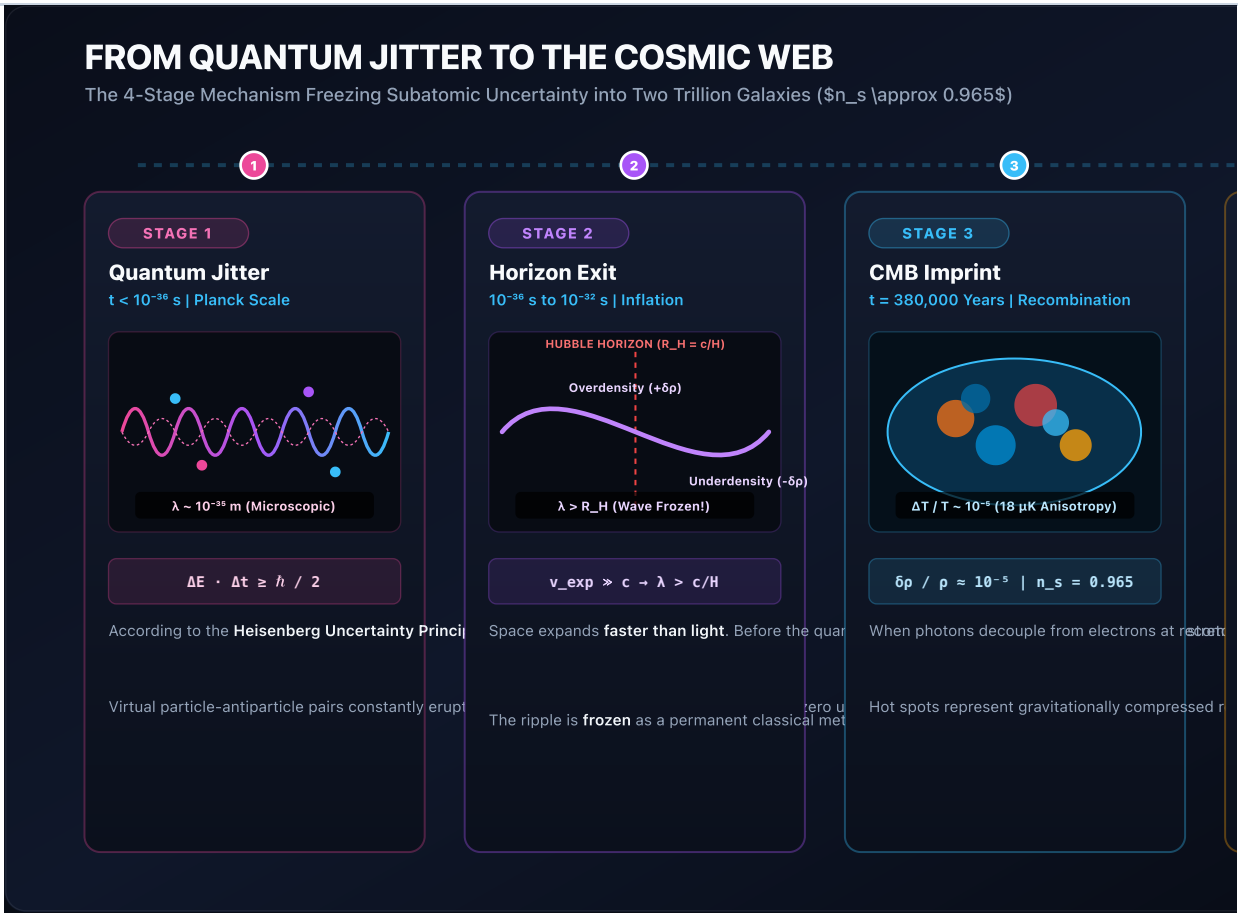


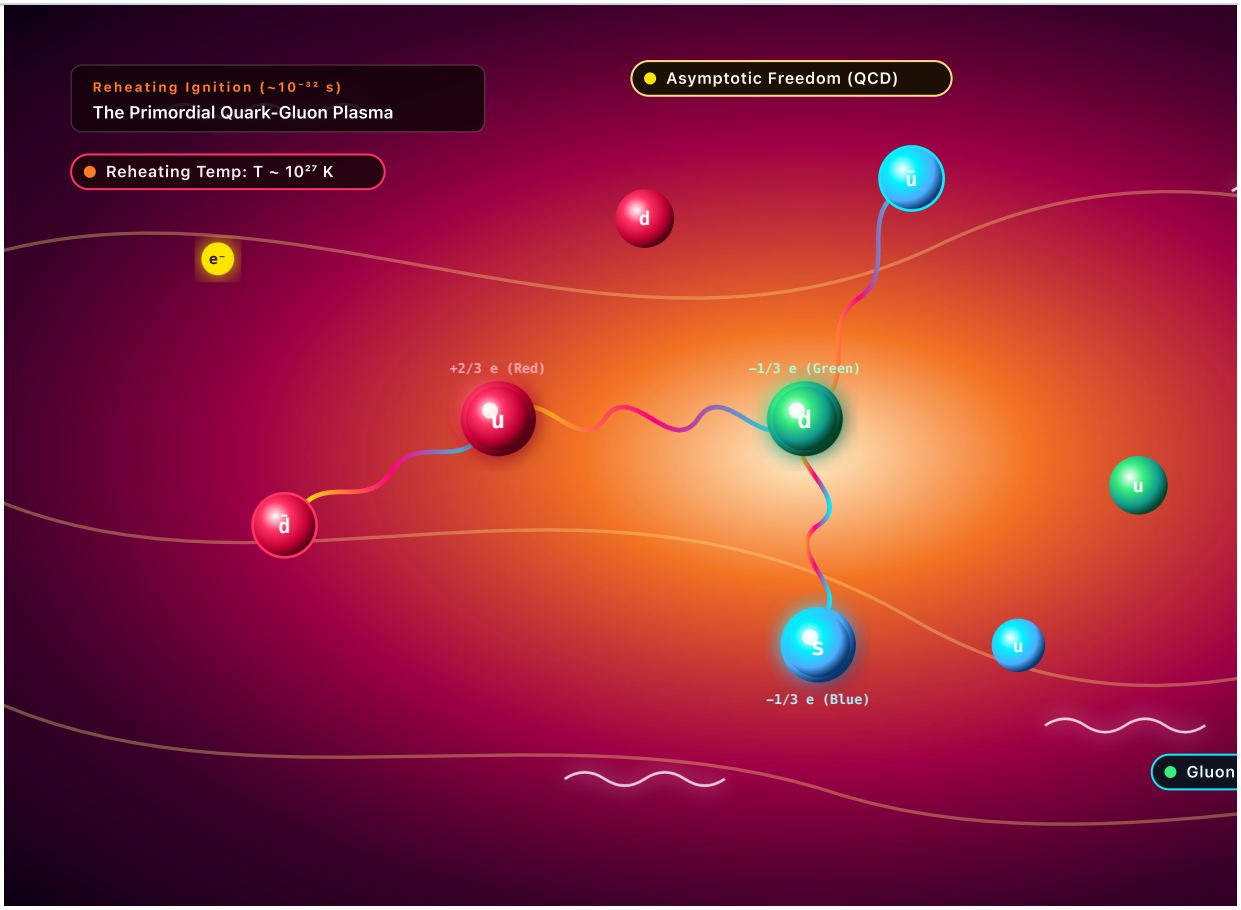
Figure 1.4: From Subatomic Uncertainty to the Cosmic Web. The four-stage conversion process: zero-point vacuum fluctuations are stretched across the cosmic event horizon during inflation, frozen as classical curvature ripples, imprinted on the Cosmic Microwave Background ($\Delta T/T \sim 10^{-5}$), and collapsed into galaxies.

Reheating: The Ignition of the Hot Big Bang

While inflation solved the paradoxes of cosmology, it presented a formidable new problem: exponential expansion stretched the universe into a state of absolute, frigid emptiness. Any pre-existing matter or radiation was diluted to zero density; the temperature dropped to absolute zero ($T \to$ K). How did the universe become the blistering, high-energy cauldron of the Hot Big Bang?

The answer is **Reheating**. As the inflaton field reached the bottom of its potential well ($V(\phi) \to 0$), it began oscillating violently around the minimum. Through parametric resonance and quantum field decay, the enormous potential energy stored in the false vacuum coupled to the Standard Model fields (gluons, quarks, leptons, gauge bosons). In a fraction of a second, the universe was inundated with a searing, relativistic thermal bath at temperatures exceeding T_{rh} ~ 10^{27} Kelvin.

Inflation ended. The scalar field vanished into a memory of cosmic expansion. And the true Hot Big Bang—the fiery, plasma-dominated era of particle physics—was officially ignited.



Primordial Reheating & The Relativistic Quark-Gluon Plasma ($t \sim 10^{-32}$ s). At the end of inflation, coherent inflaton oscillations decay via parametric resonance into the fundamental particles of the Standard Model. The universe is superheated to $T_{\rm rh} \sim 10^{27}$ K, birthing a dense, asymptotically free soup of quarks, gluons, and leptons—the physical start of the Hot Big Bang.

Shakil Mahmud • Research Monograph

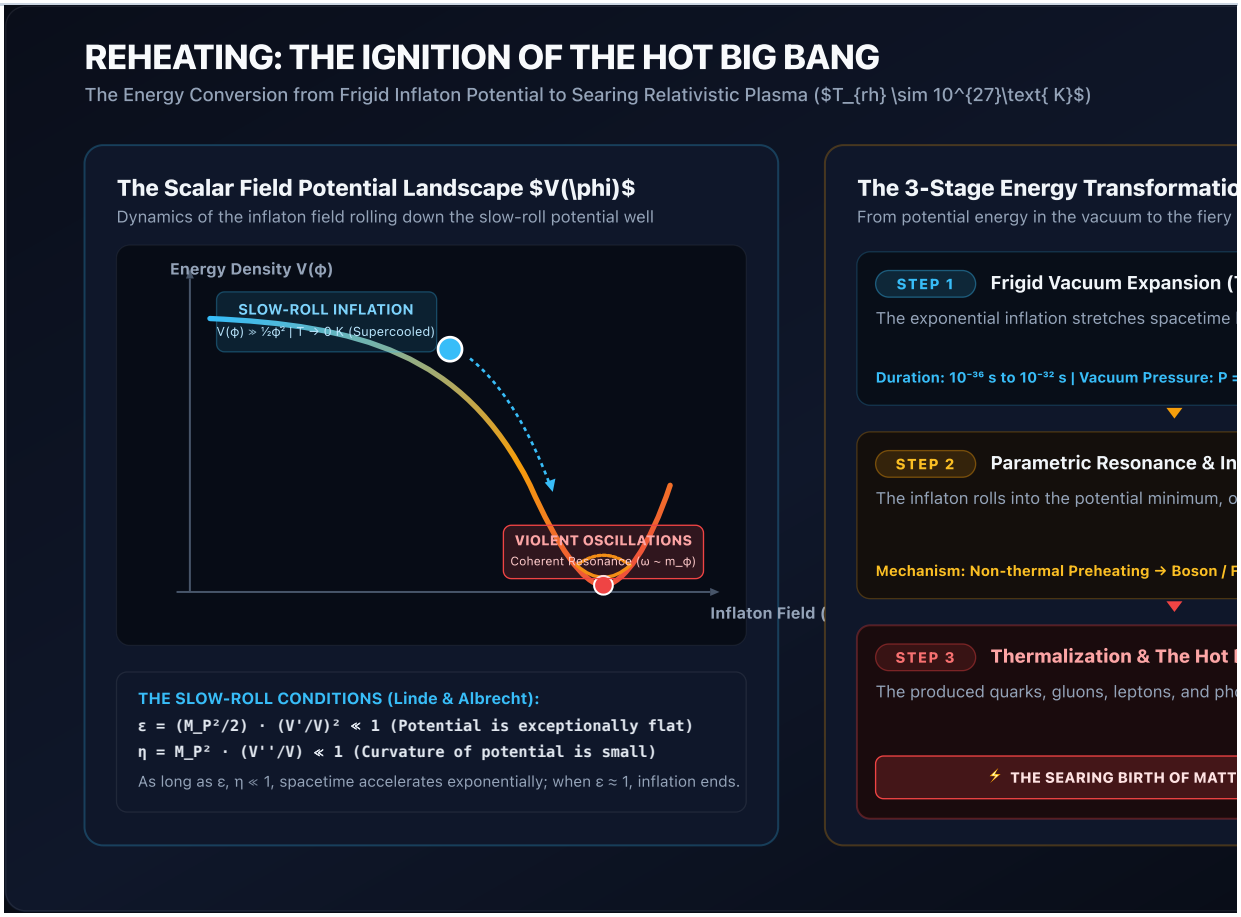


Figure 1.5: Reheating & The Thermal Ignition of the Cosmos. Energy transformation dynamics: the inflaton field rolls down the slow-roll potential V(ϕ) and undergoes violent coherent oscillations at the minimum, decaying into Standard Model quarks, gluons, and leptons at T_rh ~ 10^{27} K.

Chronology of Cosmic Genesis: The First Split-Second

Epoch	Time Elapsed (t)	Temperature (K)	Energy Scale (GeV)	Dominant Physical Phenomena
Planck Epoch	0 to 10^{-43} s	> 10^{32} K	10^{19} GeV	Unified superforce; spacetime behaves as chaotic quantum foam; classical GR breaks down.
GUT Epoch	10^{-43} to 10^{-36} s	10^{32} to 10^{28} K	10^{15} GeV	Gravity decouples; Strong and Electroweak forces unified; *X* and *Y* gauge bosons dominate.
Electroweak Symmetry Breaking & Inflation	10^{-36} to 10^{-32} s	Supercooled to < 10^{22} K	10^{14} to 10^{12} GeV	Inflaton field rolls down potential; exponential de Sitter expansion ($a \propto e^{Ht}$); space stretches ≥ 10^{26}×; quantum ripples frozen as cosmic seeds.
Reheating Epoch	10^{-32} to 10^{-12} s	Reheated to 10^{27} K	10^{12} to 10^{3} GeV	Inflaton decays into Standard Model quarks, leptons, and gauge bosons; Hot Big Bang thermal bath ignited.

Philosophical Epilogue: A Universe from Absolute Nothing?

In 1973, physicist Edward P. Tryon published a seminal paper in *Nature* titled simply: *"Is the Universe a Vacuum Fluctuation?"* Tryon proposed that our universe is a zero-energy system: the positive energy locked within all mass ($E = mc^2$) and thermal radiation is precisely balanced and canceled out by the negative gravitational potential energy of cosmic curvature ($U = -GMm/r$).

As Alan Guth famously summarized, *"The universe is the ultimate free lunch."* In the light of modern inflationary cosmology, the cosmos did not require a vast stockpile of matter and energy to be deposited at the beginning. It required only a tiny volume of empty space containing a quantum scalar field in a false vacuum state. The laws of quantum mechanics and general relativity did the rest.

In **Part 2** of *The Universal Chronicle*, we will step out of the inflationary vacuum and plunge into the blinding furnace of the first minutes: **The Crucible of Matter — Quark-Gluon Plasma, Baryogenesis, and the Creation of the First Atoms**.

Academic Citations & Foundational Literature

- **Guth, A. H. (1981).** "Inflationary universe: A possible solution to the horizon and flatness problems." *Physical Review D*, 23(2), 347–356. doi:10.1103/PhysRevD.23.347.
- **Linde, A. D. (1982).** "A new inflationary universe scenario: A possible solution of the horizon, flatness, homogeneity, isotropy and primordial monopole problems." *Physics Letters B*, 108(6), 389–393. doi:10.1016/0370-2693(82)91219-9.
- **Hawking, S. W., & Penrose, R. (1970).** "The singularities of gravitational collapse and cosmology." *Proceedings of the Royal Society of London. A. Mathematical and Physical Sciences*, 314(1519), 529–548. doi:10.1098/rspa.1970.0021.
- **Planck Collaboration (Akrami, Y., et al.) (2020).** "Planck 2018 results. X. Constraints on inflation." *Astronomy & Astrophysics*, 641, A10. doi:10.1051/0004-6361/201833887.
- **Mukhanov, V. F., & Chibisov, G. V. (1981).** "Quantum fluctuations and a nonsingular universe." *JETP Letters*, 33(10), 532–535.
- **Tryon, E. P. (1973).** "Is the Universe a Vacuum Fluctuation?" *Nature*, 246, 396–397. doi:10.1038/246396a0.
- **Weinberg, S. (2008).** *Cosmology*. Oxford University Press. ISBN: 978-0198526827.
- **Kolb, E. W., & Turner, M. S. (1990).** *The Early Universe*. Frontiers in Physics, Addison-Wesley. ISBN: 978-0201626742.

Citation: Mahmud, S. (2026). "The Beginning Before Time — Cosmic Inflation, the Quantum Vacuum, and the Planck Epoch." In The Universal Chronicle, Part 1. https://shakilmahmud.com/universal-chronicle-part-1-the-beginning-before-time/

Shakil Mahmud • Research Monograph

SHAKIL MAHMUD RESEARCH MONOGRAPHS • PART II

The Crucible of Matter — Quark-Gluon Plasma, Baryogenesis, and Primordial Nucleosynthesis

The Crucible of Matter — Quark-Gluon Plasma, Baryogenesis, and Primordial Nucleosynthesis

3,039 words • October 30, 2026 • Permanent URI

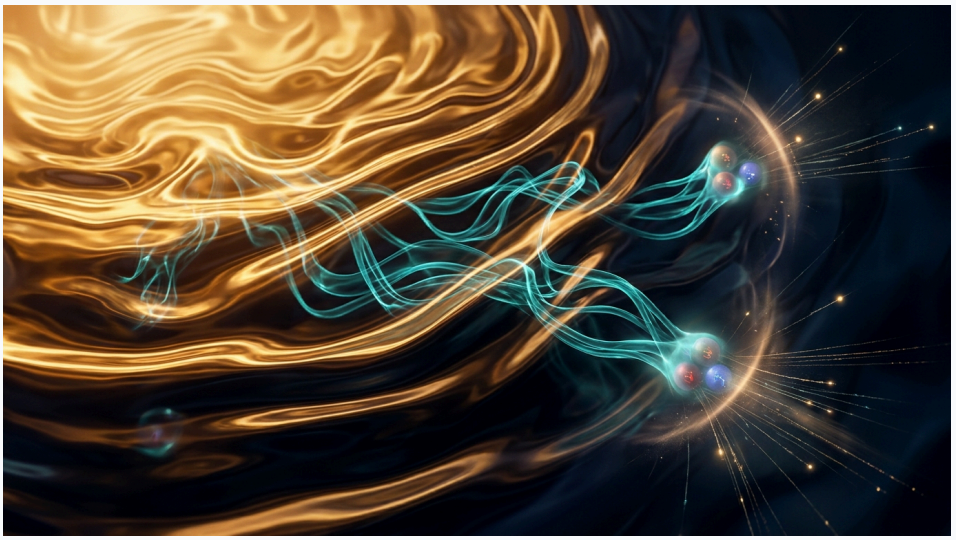


Plate II: *Figure: Relativistic hydrodynamic flow of the primordial quark-gluon plasma at trillion-degree temperatures, preceding color confinement into hadrons and the nucleosynthesis of hydrogen, helium-4, and trace lithium.*

During the opening twenty minutes of existence, the universe functioned as a single, cosmos-spanning thermonuclear reactor. In this blindingly dense furnace, the fundamental building blocks of matter emerged from a nearly frictionless fluid of unbound quarks, survived an existential annihilation against antimatter, and fused into the exact primordial chemical recipe—75% hydrogen and 25% helium—that powers every star shining in the night sky today.

The Electroweak Epoch (10^{-12} Seconds): How Particles Acquired Mass

Following the end of cosmic inflation and the turbulent fires of reheating, the universe expanded into the **Electroweak Epoch**. The cosmos was filled with a searing relativistic soup of leptons, quarks, and gauge bosons at temperatures exceeding 10^{15} K (E ~ 100 GeV). At these energies, the electromagnetic force and the weak nuclear force were indistinguishable, operating under a unified SU(2)_L × U(1)_Y electroweak gauge symmetry.

All fundamental particles were massless, hurtling through the cosmos at the speed of light. However, at t ≈ 10^{-12} seconds, the temperature dropped below the critical electroweak threshold (T_c ≈ 160 GeV). The scalar Higgs field underwent **electroweak symmetry breaking**, settling into a non-zero vacuum expectation value (v ≈ 246 GeV):

- **The Weak Gauge Bosons (W^+, W^-, and Z^0):** Strongly coupled to the Higgs field, acquiring immense inertial rest masses (≈ 80.4 GeV and 91.2 GeV). Because their carriers were now heavy, the weak nuclear force collapsed into a short-range interaction operating only within subatomic distances (10^{-18} meters).
- **The Photon (γ):** Remained completely uncoupled to the Higgs vacuum expectation value, preserving its zero rest mass. Electromagnetism became an infinite-range force governed by unbroken U(1)_{em} symmetry.
- **Fermions (Quarks & Charged Leptons):** Acquired distinct rest masses via Yukawa coupling to the Higgs condensate. The top quark coupled fiercely, becoming the heaviest elementary particle (173 GeV), while the electron coupled weakly (0.511 MeV).

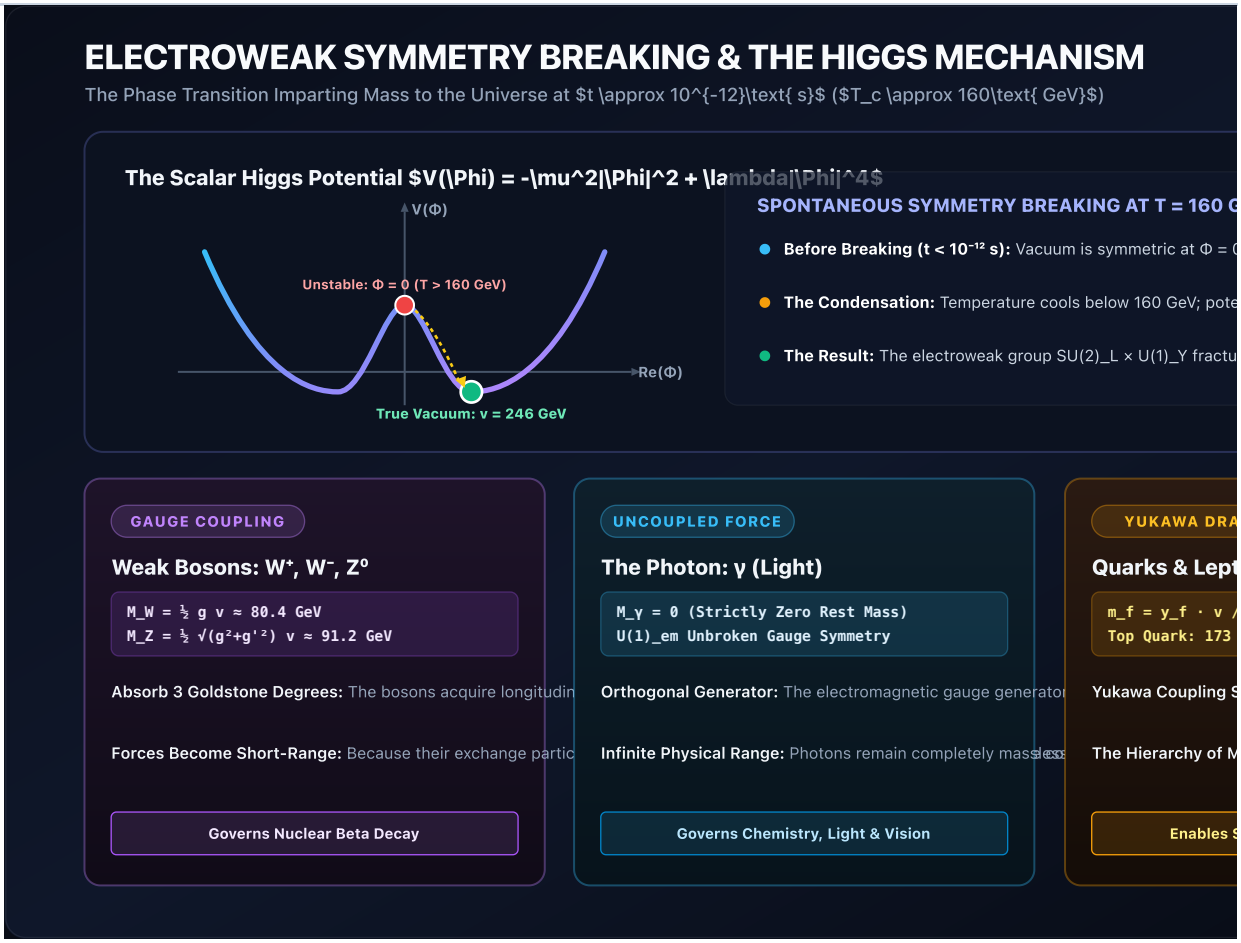


Figure 2.1: Electroweak Symmetry Breaking & Mass Acquisition. The scalar Higgs field rolls from the unstable origin into its non-zero vacuum expectation value (v = 246 GeV), giving heavy inertial rest masses to the W and Z gauge bosons while leaving the photon completely massless.

The Quark-Gluon Plasma: The Universe's "Perfect Liquid"

Between 10^{-12} and 10^{-5} seconds, the universe was dominated by a state of matter so extreme that it has only been recreated on Earth inside the core collision chambers of the Relativistic Heavy Ion Collider (RHIC) at Brookhaven and the Large Hadron Collider (LHC) at CERN: the **Quark-Gluon Plasma (QGP)**.

Under ordinary terrestrial conditions, the strong nuclear force is governed by *quantum chromodynamic (QCD) color confinement*: quarks can never exist in isolation. If you attempt to pull two quarks apart, the energy stored in the gluon flux tube between them increases linearly until it becomes energetically favorable to create a new quark-antiquark pair from the vacuum ($E = mc^2$).

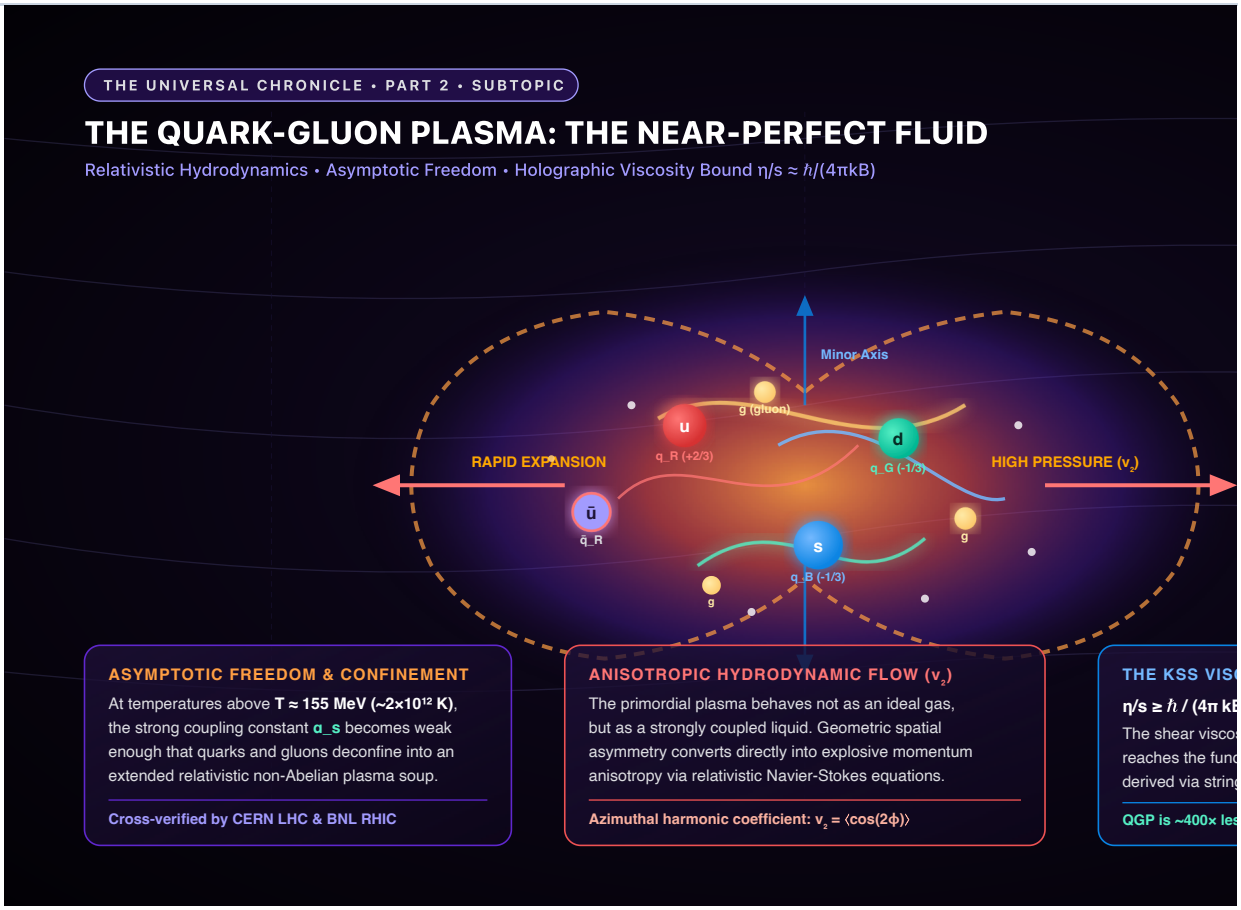
Asymptotic Freedom (Gross, Politzer, & Wilczek)
In 1973, David Gross, Frank Wilczek, and David Politzer demonstrated that the strong coupling constant α_s decreases logarithmically at ultra-high energies and microscopic distances. In the primordial universe, when densities exceeded nuclear saturation density (ρ > 10^{18} kg/m^3) and temperatures rose above 2×10^{12} K (T > 170 MeV), individual hadrons melted. Quarks, antiquarks, and gluons moved freely as an unconfined, deconfined plasma.

Crucially, experiments at RHIC and the LHC's ALICE detector revealed that the Quark-Gluon Plasma does not behave like an ideal gas of billiard-ball particles. Instead, it is a strongly coupled quantum fluid with the **lowest shear viscosity-to-entropy density ratio (η/s) ever measured in nature**—approaching the fundamental holographic Kovtun-Son-Starinets (KSS) quantum bound:

$$\frac{\eta}{s} \approx \frac{\hbar}{4\pi k_B}$$

The primordial universe was not an erratic gas; it was an ultra-dense, near-frictionless *perfect liquid* swirling with turbulent quantum vortices.

Shakil Mahmud • Research Monograph



Relativistic Hydrodynamic Flow & Asymptotic Freedom in the Quark-Gluon Plasma (10^{-12} s $\leq t \leq 10^{-5}$ s). In the ultra-relativistic deconfined plasma ($T \sim 2 \times 10^{12}$ K), the shear viscosity-to-entropy ratio reaches the quantum minimum holographic bound $\eta/s \approx \hbar/(4\pi k_B)$. Initial geometric asymmetry converts into explosive momentum anisotropy through anisotropic elliptic flow (v_2).

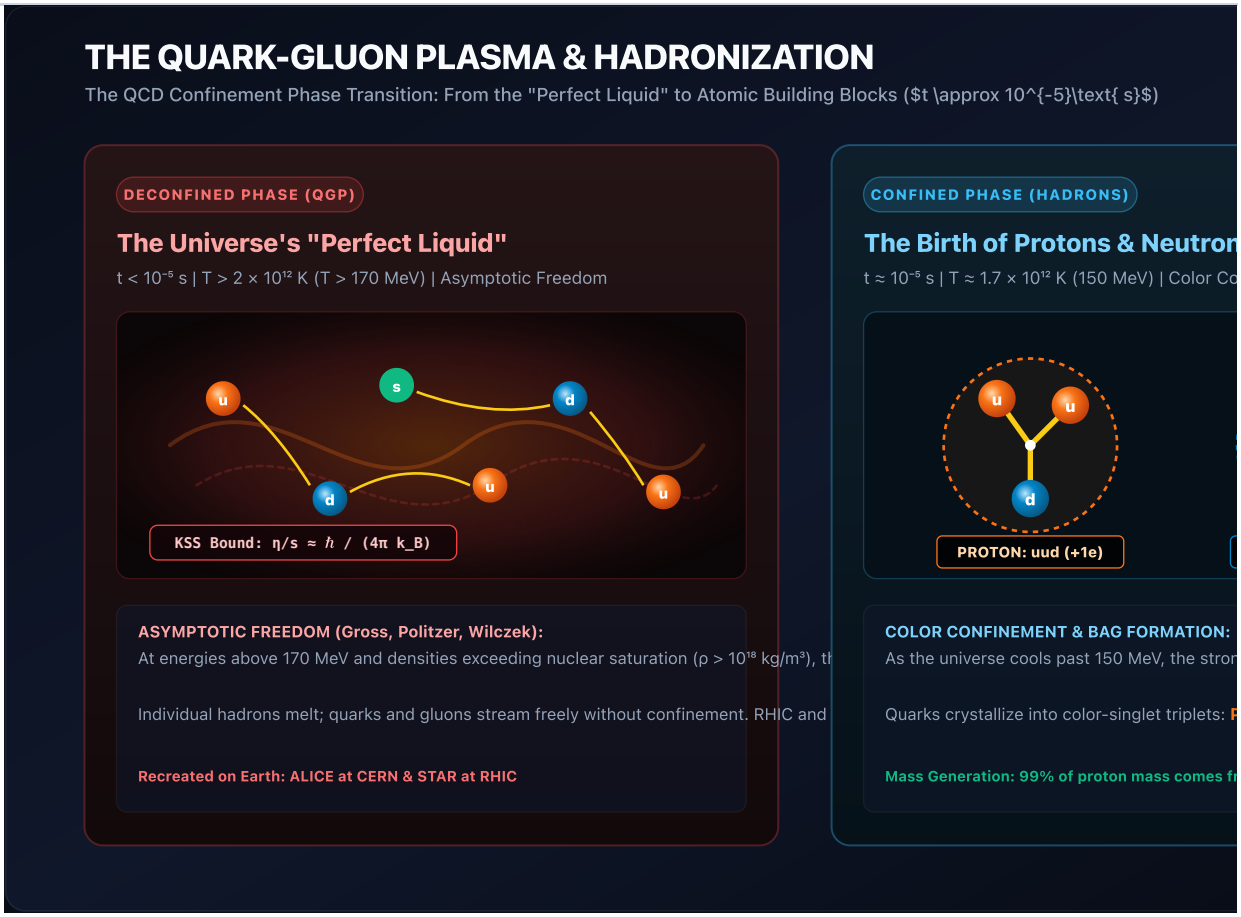


Figure 2.2: From Deconfined "Perfect Liquid" to Atomic Hadronization. Before 10^{-5} seconds, quarks and gluons moved freely as an ultra-dense, low-viscosity quantum liquid; cooling past 150 MeV triggered color confinement, binding quarks permanently into protons (uud) and neutrons (udd).

The Mystery of Baryogenesis: Why Anything Exists at All

One of the deepest enigmas in modern physics is why our universe is composed almost exclusively of matter rather than an equal mixture of matter and antimatter. The equations of Quantum Electrodynamics (QED) and the Standard Model are nearly symmetric: whenever pure energy transforms into matter via pair production ($\gamma + \gamma \rightarrow q + \bar{q}$), it generates particles and antiparticles in equal numbers.

Had this symmetry remained absolute during the early universe, then as the temperature cooled below particle creation thresholds, every quark would have encountered an antiquark, annihilating into pure gamma-ray photons:

$$q + \bar{q} \rightarrow \gamma + \gamma$$

The cosmos would have ended as an empty, sterile sea of cold radiation, completely devoid of protons, neutrons, atoms, stars, or observers. Yet, we observe a universe containing roughly 10^{80} protons and neutrons, with no macroscopic pockets of primordial antimatter detected anywhere in the observable cosmos.

The Three Sakharov Conditions (1967)

In 1967, Soviet nuclear physicist and dissident **Andrei Sakharov** identified the three mandatory mathematical conditions required to generate a net baryon asymmetry from an initially symmetric state:

- **1. Baryon Number (B) Violation:** There must exist physical processes that do not conserve the total number of baryons. In the Standard Model, non-perturbative electroweak *sphaleron* transitions can violate B while conserving B – L. In Grand Unified Theories, superheavy gauge bosons directly decay into unequal numbers of quarks and leptons.
- **2. C and CP Symmetry Violation:** Charge conjugation (C) and the combination of Charge conjugation and Parity (CP) must be violated. If CP were exact, the rate of a reaction producing matter ($\Gamma(X \rightarrow q + q)$) would precisely equal the rate of the conjugate reaction producing antimatter ($\Gamma(\bar{X} \rightarrow \bar{q} + \bar{q})$), resulting in zero net surplus. While CP violation is observed in the Cabibbo-Kobayashi-Maskawa (CKM) matrix of the quark sector, its magnitude is insufficient to explain the observed universe, pointing to undiscovered physics (such as leptogenesis via heavy Majorana neutrinos).
- **3. Departure from Thermal Equilibrium:** In strict thermodynamic equilibrium, the CPT theorem guarantees that the phase space density of matter and antimatter remains identical. Therefore, the baryon-generating reactions had to occur during a rapid out-of-equilibrium phase transition—such as bubble nucleation during a first-order phase transition or the decay of heavy particles during the expansion of the universe.

Shakil Mahmud • Research Monograph

Because these conditions were met, a microscopic asymmetry emerged: for every **1,000,000,000 antiquarks**, there were **1,000,000,001 quarks**. When the universe cooled and the great annihilation took place, one billion quark-antiquark pairs canceled out into a bath of light. **The entire tangible universe—every galaxy, every carbon atom, every drop of water, and every human brain—is made from the solitary, triumphant survivor of that one-in-a-billion excess.**



Figure 2.3: The Mystery of Baryogenesis & The Sakharov Mechanism. How the three Sakharov conditions generated a microscopic 1-in-a-billion matter excess: one billion quark-antiquark pairs annihilated into the cosmic radiation bath, leaving the solitary survivor surplus that constitutes all stars, galaxies, and living matter today.

Hadronization (T ≈ 10^{-5} Seconds): The Birth of Protons and Neutrons

By t ≈ 10 microseconds (10^{-5} s), the universe expanded and cooled to T ≈ 1.7 × 10^{12} K (150 MeV). At this temperature, the strong coupling constant α_s grew so powerful that the Quark-Gluon Plasma could no longer maintain asymptotic freedom. The universe underwent the **QCD confinement phase transition**, or *Hadronization*.

Quarks were bound permanently by gluon exchange into color-neutral composite particles (hadrons):

- **Protons (p = uud):** Two up quarks (+2/3 e each) and one down quark (-1/3 e), yielding an electric charge of +1. Stable against decay.
- **Neutrons (n = udd):** One up quark (+2/3 e) and two down quarks (-1/3 e each), yielding an electric charge of 0. A free neutron is slightly heavier than a proton (Δ m ≈ 1.293 MeV) and decays via beta decay (n ⟶ p + e^- + ν̄_e) with a half-life of roughly 879 seconds (14.6 minutes).
- **Mesons (π^+, π^-, π^0):** Quark-antiquark pairs that rapidly decayed into photons and leptons.



QCD Color Confinement & Hadronization ($t \approx 10^{-5}$ s). As the universe cools past $T_c \approx 155$ MeV, the gluon flux tube between separating quarks stretches with constant tension ($\sigma \approx 1$ GeV/fm). When the stored field energy exceeds $2m_q c^2$, the vacuum ruptures into new $q\bar{q}$ pairs, confining all quarks into color-singlet protons (uud), neutrons (udd), and pions ($u\bar{d}$).

At this moment, the universe entered the **Lepton Epoch** (t ≈ 10^-5 s to 1 second). The temperature was still high enough to generate copious electron-positron pairs (e^- + e^+ ↔ γ + γ), while neutrinos roamed freely. At (t ≈ 1 s)econd (T ≈ 10^{10} K ≈ 1 MeV), the weak interaction rate dropped below the Hubble expansion rate. **Neutrinos decoupled from the plasma**, streaming freely through space to form the *Cosmic Neutrino Background (CνB)*, an invisible relic that permeates the cosmos today at a temperature of K.

Big Bang Nucleosynthesis (T = 10 Seconds to 20 Minutes): The First Atoms

Between 10 seconds and 20 minutes after the Big Bang, the universe underwent its most critical chemical transformation: **Big Bang Nucleosynthesis (BBN)**. For the first and only time in cosmic history, the entire universe was dense and hot enough to function as an all-encompassing fusion reactor.

1. The Neutron-to-Proton Freeze-Out Ratio

Early in the lepton epoch, protons and neutrons converted back and forth effortlessly through weak interactions mediated by electron neutrinos:

$$n + \nu_e \leftrightarrow p + e^- \quad \text{and} \quad n + e^+ \leftrightarrow p + \bar{\nu}_e$$

Because the neutron is 1.293 MeV heavier than the proton, the Boltzmann distribution favored the lower-energy proton state (n/p ∝ e^{-Δ m / k_B T}). When the temperature dropped below 0.8 MeV (t ≈ 1 s), the weak reactions became too slow to keep pace with the expansion. The ratio **froze out at roughly n/p ≈ 1/6**.

Over the next several minutes, free neutrons underwent beta decay (n → p + e^- + ν̄_e). By the time nuclear fusion could begin in earnest, the ratio had shifted to approximately **n/p ≈ 1/7** (one neutron for every seven protons).

2. The Deuterium Bottleneck

To build heavier nuclei, the universe had to start by fusing a proton and a neutron into a deuterium nucleus (heavy hydrogen):

$$p + n \rightarrow {}^2\mathrm{H} + \gamma$$

Shakil Mahmud • Research Monograph

The binding energy of deuterium is relatively fragile: E_b = 2.22 MeV. Although the average thermal energy of the universe was well below 2.22 MeV, the ratio of photons to baryons was immense—approximately **two billion photons for every single baryon** ($\eta \approx 6 \times 10^{-10}$). In this high-energy Planckian tail of the blackbody radiation spectrum, there were millions of gamma-ray photons capable of instantly shattering any newly formed deuterium back into a lone proton and neutron.

This delay is known as the **Deuterium Bottleneck**. Fusion could not proceed until the universe cooled to $T \approx 8 \times 10^{8}$ K (0.08 MeV), at roughly t ≈ 3 minutes.

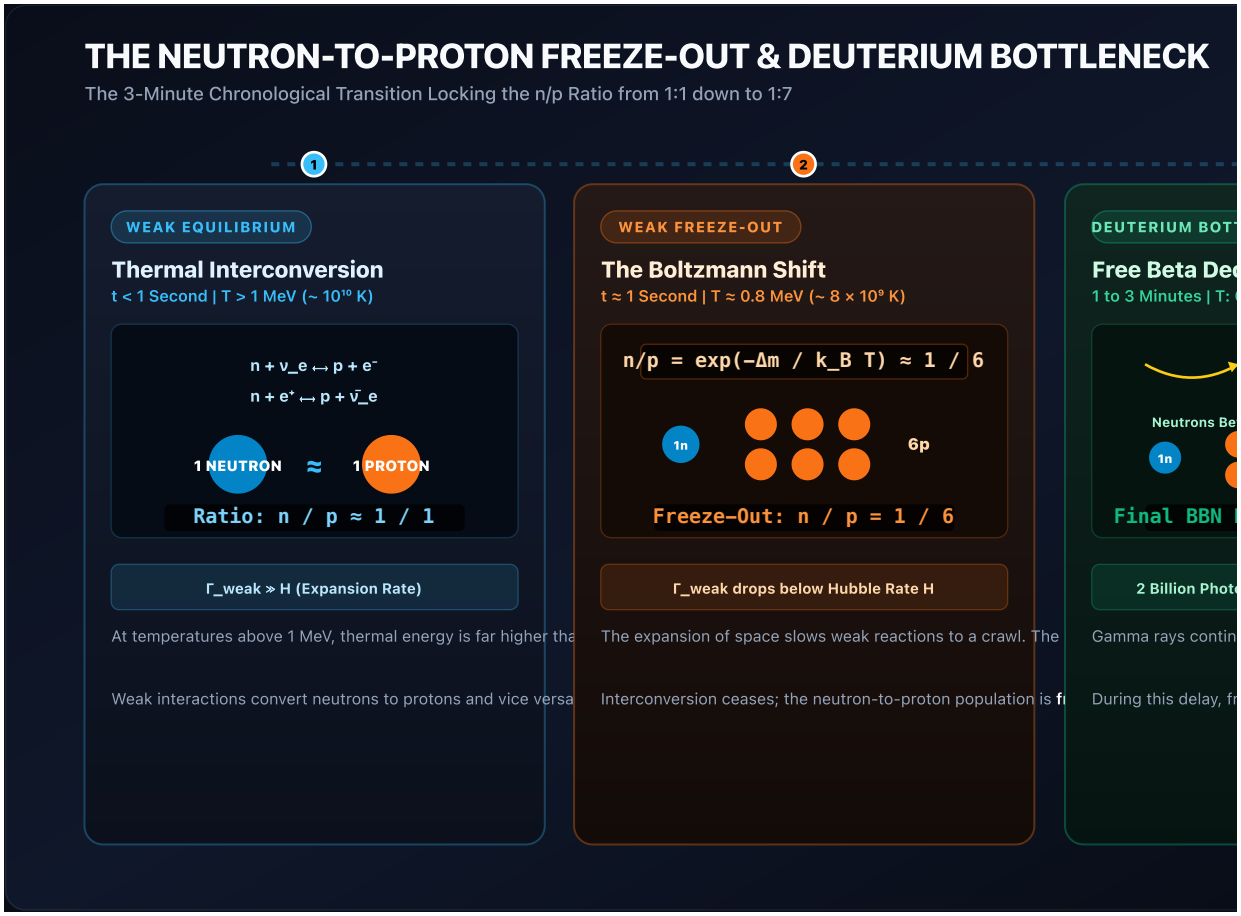


Figure 2.4: The Neutron Freeze-Out & The Deuterium Bottleneck. At t ≈ 1 s, the neutron-to-proton ratio froze out at 1:6; intense blackbody gamma radiation delayed deuterium formation for 3 minutes, during which free neutrons underwent beta decay until the population locked at exactly 1 neutron for every 7 protons.

3. The Fusion Cascade to Helium-4

Once the temperature fell low enough for deuterium to survive, an explosive cascade of nuclear reactions consumed nearly all available neutrons in seconds:

- $^{2}H + p \rightarrow {}^{3}He + \gamma$ (Helium-3)
- $^{2}H + n \rightarrow {}^{3}H + \gamma$ (Tritium)
- $^{2}H + {}^{2}H \rightarrow {}^{3}He + n$
- $^{3}H + {}^{2}H \rightarrow {}^{4}He + n$ (Helium-4)
- $^{3}He + {}^{2}H \rightarrow {}^{4}He + p$ (Helium-4)

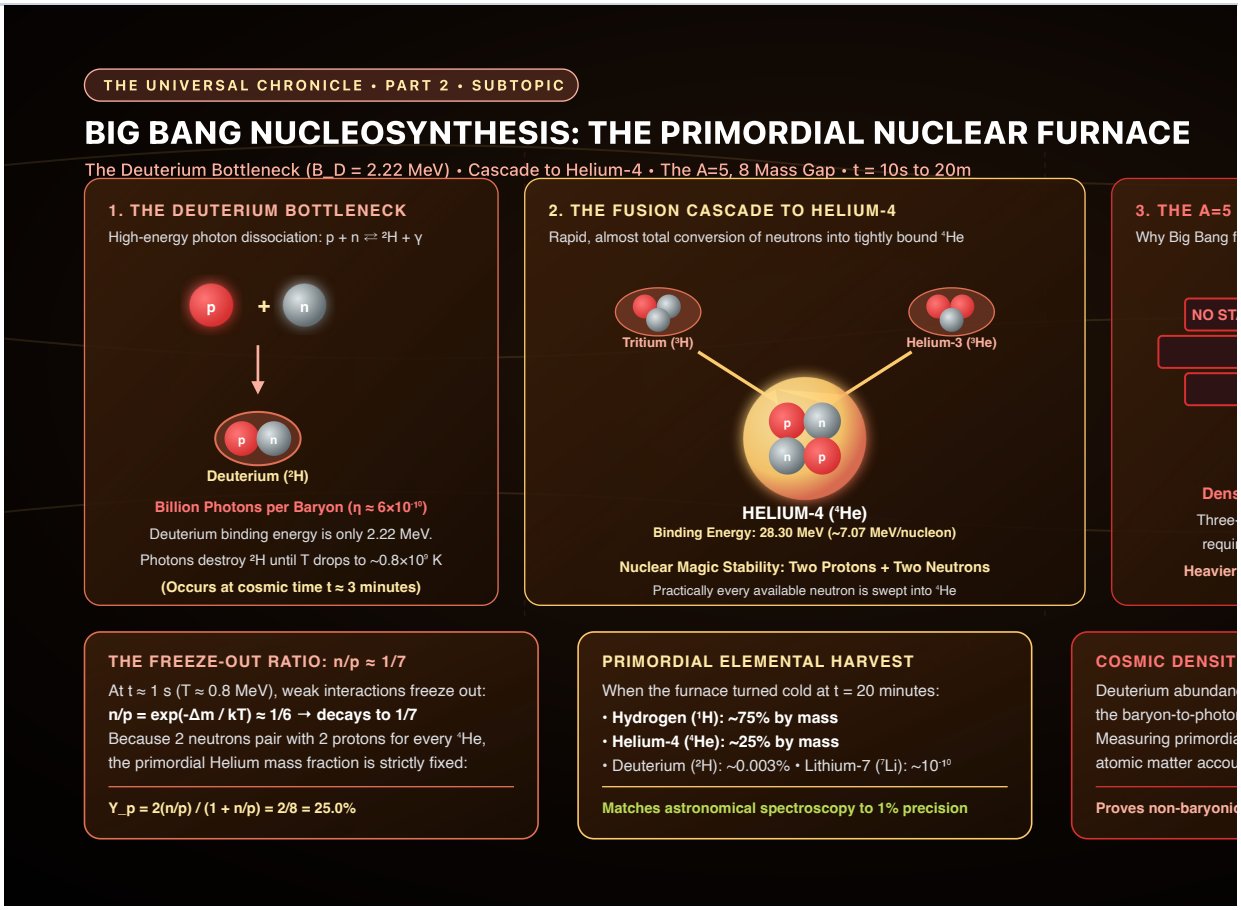
Because Helium-4 (^{4}He) has an exceptionally tight binding energy (28.3 MeV, or 7.07 MeV per nucleon), it acts as a nuclear "black hole"—virtually all available neutrons were bound into Helium-4 nuclei. With an initial ratio of 1 neutron to 7 protons, a simple calculation reveals the ultimate mass fraction of the universe:

Calculating the Primordial Helium Abundance (Y_p)
Consider 16 nucleons: 2 neutrons and 14 protons (a 1:7 ratio). The 2 neutrons combine with 2 protons to form a single ^{4}He nucleus (mass = 4). This leaves 14 – 2 = 12 free protons (Hydrogen nuclei, mass = 12).

The mass fraction of Helium-4 is therefore:

$$Y_p = \frac{\text{Mass of Helium}}{\text{Total Mass}} = \frac{4}{4+12} = \frac{4}{16} = 25\%$$

The remaining 75% of the baryonic mass stayed as free protons—the nuclei of ordinary **Hydrogen**.



The Primordial Fusion Furnace & The $A = 5, 8$ Mass Gaps ($t = 10$ s to 20 min). Overcoming the Deuterium Bottleneck at $T \sim 0.8 \times 10^9$ K, nuclear reactions sweep nearly all cosmic neutrons ($n/p \approx 1/7$) into exceptionally stable Helium-4 (^{4}He, $B \approx 28.3$ MeV). Absence of stable nuclei at mass numbers $A = 5$ and $A = 8$ halts nucleosynthesis, locking primordial matter at ~75% Hydrogen and ~25% Helium.

4. Why the Big Bang Could Not Forge Carbon or Iron

Why did nucleosynthesis halt at helium? Why didn't the universe continue fusing carbon, nitrogen, oxygen, and iron, as massive stars do?

There are two insurmountable nuclear bottlenecks in nature: **there are no stable nuclei with mass numbers A = 5 or A = 8**. If Helium-4 captures a proton or neutron, it forms ^{5}Li or ^{5}He, both of which disintegrate instantaneously (10^{-21} s). If two Helium-4 nuclei fuse, they form Beryllium-8 (^{8}Be), which decays back into two alpha particles with a half-life of just 10^{-16} seconds.

In the dense, gravitational cores of red giant stars, this bottleneck is overcome via the *triple-alpha process* (^{4}He + ^{4}He + ^{4}He → ^{12}C), which requires sustained, immense densities and millions of years. In the early universe, the cosmic expansion was so rapid that by t ≈ 20 minutes, the temperature and density had plummeted far below the threshold for nuclear fusion. The cosmic forge closed forever.

Only trace quantities of heavier isotopes managed to form: a tiny remnant of unburned Deuterium (^{2}H/H ≈ 2.5 × 10^-5), Helium-3 (^{3}He/H ≈ 10^-5), and a whisper of Lithium-7 (^{7}Li/H ≈ 1.6 × 10^{-10}).

Shakil Mahmud • Research Monograph

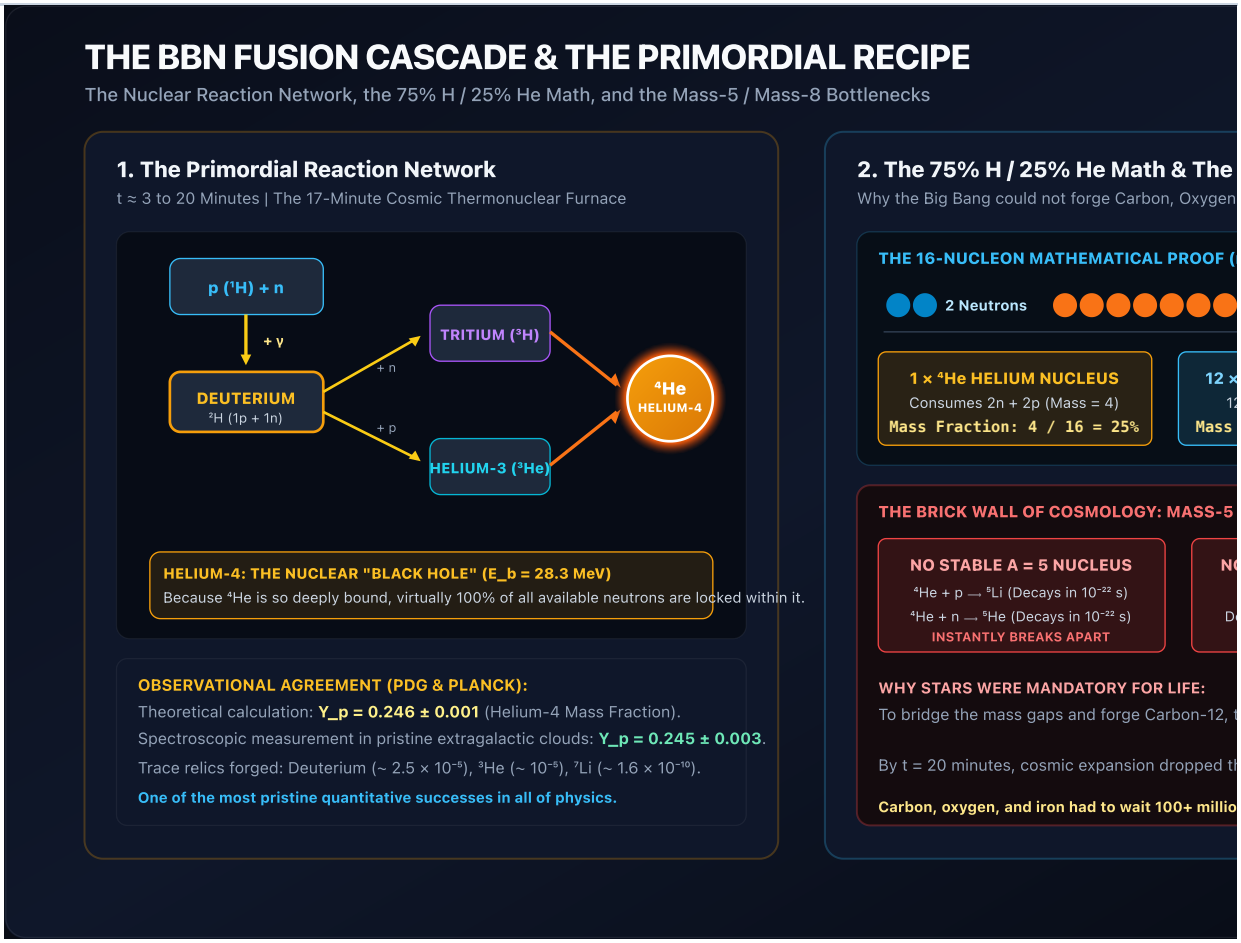


Figure 2.5: The Primordial Thermonuclear Recipe & The Mass-5/8 Wall. The nuclear fusion reaction network consumed virtually all neutrons into Helium-4 nuclei, yielding the universal mass fraction of 75% Hydrogen and 25% Helium; unstable mass numbers A = 5 and A = 8 halted Big Bang fusion, reserving heavier elements for stellar interiors.

Chronology Table: From Quark Soup to the First Atomic Nuclei

Stage / Epoch	Time Elapsed	Temperature (K)	Energy Scale	Key Physical Transitions
Electroweak Symmetry Breaking	10^{-12} s	10^{15} K	100 GeV	Higgs field acquires vacuum expectation value; W^±, Z^0 acquire mass; electromagnetism separates from weak force.
Quark-Gluon Plasma (QGP)	10^{-12} to 10^{-5} s	> 2 × 10^{12} K	> 170 MeV	Asymptotic freedom; quarks and gluons roam unbound as a near-zero-viscosity quantum perfect liquid.
Baryogenesis Era	10^{-11} to 10^{-6} s	~ 10^{13} K	~ 1 GeV	Sakharov conditions generate a 1-in-a-billion matter surplus; mutual annihilation leaves pure matter residue and cosmic photon bath.
Hadronization	10^{-5} s (10 μ s)	1.7 × 10^{12} K	150 MeV	Color confinement locks quarks into protons (uud) and neutrons (udd). Mesons decay.
Neutrino Decoupling	1.0 s	10^{10} K	1 MeV	Weak force freezes out; n/p ratio freezes at ~ 1/6; neutrinos decouple to form the Cosmic Neutrino Background (CνB).
Deuterium Bottleneck	10 to 180 s	10^{9} to 8 × 10^ K	0.1 MeV	High photon-to-baryon ratio delays fusion; free neutrons decay until n/p ≈ 1/7.
Primordial Nucleosynthesis (BBN)	3 to 20 min	8 × 10^{8} to 3 × 10^ K	< 0.05 MeV	Nuclear fusion cascade; forms 75% ^{1}H, 25% ^{4}He, trace Deuterium, ^{3}He, and ^{7}Li. Cosmic expansion halts fusion.

The Legacy: The Golden Fingerprint of the Big Bang

Big Bang Nucleosynthesis stands alongside the Cosmic Microwave Background and cosmological redshift as one of the three foundational observational pillars of the Big Bang model. In 1948, Ralph Alpher, Hans Bethe, and George Gamow published their landmark *αβγ paper* predicting that the universe must be predominantly hydrogen and helium formed in the opening minutes.

Modern spectroscopic observations of pristine, metal-poor intergalactic gas clouds and ancient dwarf galaxies confirm these calculations with breathtaking accuracy: the primordial helium fraction is measured to be $Y_p = 0.245 \pm 0.003$, matching the mathematical predictions of BBN to within fractions of a percent. The ratio of primordial deuterium directly constrains the total density of baryonic matter in the cosmos ($\Omega_b h^2 \approx 0.022$), proving that ordinary atomic matter accounts for barely **5% of the total energy density of the universe**.

The stage was set. The atomic nuclei were forged. Yet, the universe remained an opaque, blinding fog of free electrons and protons where light could not travel. In **Part 3** of *The Universal Chronicle*, we will explore the great clearing of the heavens: **The Clearing of the Heavens — Recombination, the Cosmic Microwave Background, and the 100-Million-Year Dark Ages**.

Academic Citations & Foundational Literature

- **Alpher, R. A., Bethe, H., & Gamow, G. (1948).** "The origin of chemical elements." *Physical Review*, 73(7), 803–804. doi:10.1103/PhysRev.73.803.
- **Sakharov, A. D. (1967).** "Violation of CP invariance, C asymmetry, and baryon asymmetry of the universe." *Soviet Physics Uspekhi*, 161(5), 61–64. doi:10.1070/PU1991v034n05ABEH002497.
- **Wagoner, R. V., Fowler, W. A., & Hoyle, F. (1967).** "On the synthesis of elements at very high temperatures." *The Astrophysical Journal*, 148, 3–49. doi:10.1086/149126.
- **Gross, D. J., & Wilczek, F. (1973).** "Ultraviolet behavior of non-Abelian gauge theories." *Physical Review Letters*, 30(26), 1343–1346. doi:10.1103/PhysRevLett.30.1343.
- **Politzer, H. D. (1973).** "Reliable perturbative results for strong interactions?" *Physical Review Letters*, 30(26), 1346–1349. doi:10.1103/PhysRevLett.30.1346.
- **ALICE Collaboration (Abelev, B., et al.) (2013).** "Centrality dependence of charged particle production at large transverse momentum in Pb-Pb collisions at $\sqrt{s_{NN}}$ = 2.76 TeV." *Physics Letters B*, 720(1–3), 52–62. doi:10.1016/j.physletb.2013.01.051.
- **Fields, B. D., Molaro, P., & Sarkar, S. (2020).** "Big-Bang Nucleosynthesis." In *Review of Particle Physics (Particle Data Group)*, *Progress of Theoretical and Experimental Physics*, 2020(8), 083C01. doi:10.1093/ptep/ptaa104.
- **Kovtun, P., Son, D. T., & Starinets, A. O. (2005).** "Viscosity in strongly interacting quantum field theories from black hole physics." *Physical Review Letters*, 94(11), 111601. doi:10.1103/PhysRevLett.94.111601.

Citation: Mahmud, S. (2026). "The Crucible of Matter — Quark-Gluon Plasma, Baryogenesis, and Primordial Nucleosynthesis." In The Universal Chronicle, Part 2. https://shakilmahmud.com/universal-chronicle-part-2-the-crucible-of-matter/

Shakil Mahmud • Research Monograph

SHAKIL MAHMUD RESEARCH MONOGRAPHS • PART III

The Clearing of the Heavens — Recombination, the Cosmic Microwave Background, and the Dark Ages

The Clearing of the Heavens — Recombination, the Cosmic Microwave Background, and the Dark Ages

2,476 words • October 30, 2026 • Permanent URI



Plate III: *Figure: The surface of last scattering at approx 1100$ (380,000 years post-Big Bang): electrons bind to nuclei during recombination, releasing the cosmic microwave background (CMB) radiation and plunging the universe into the Cosmic Dark Ages.*

For the first 380,000 years of cosmic history, the universe was completely blind. Space was filled with an impenetrable, glowing white-hot plasma where photons could not travel a fraction of a millimeter without crashing into free electrons. Then, in an epoch-defining phase transition known as Recombination, atomic nuclei captured those electrons, the universe abruptly turned transparent, and the first light broke free across the cosmos—initiating the mysterious, silent hundred-million-year epoch of the Cosmic Dark Ages.

The Foggy Furnace: Why the Early Universe Was Opaque

In the aftermath of Big Bang Nucleosynthesis, the universe had cooled from billions of degrees to tens of thousands of degrees. Although atomic nuclei (protons, alpha particles, and trace lithium) were already fully assembled, they could not retain orbital electrons. The thermal energy of the radiation bath was far higher than the ionization energy of hydrogen (13.6 eV), keeping all matter in a fully ionized plasma state.

Whenever a photon attempted to travel through this plasma, it instantly collided with an unattached, free electron via **Thomson scattering** ($\sigma_T = (8\pi/3)\, r_e^2 \approx 6.65 \times 10^{-29}$ m^2). Because the density of free electrons was immense, the mean free path of a photon—the average distance light could travel before being deflected—was infinitesimally short:

$$\lambda_{\text{mfp}} = \frac{1}{n_e \sigma_T}$$

Photons were trapped in an endless, diffusive random walk, scattering billions of times per second. The universe was an optically thick, completely opaque glowing fog—much like the blinding, luminous interior of the Sun today. If an observer had existed inside this epoch, they would have been immersed in an omnidirectional, uniform glare with zero visibility.

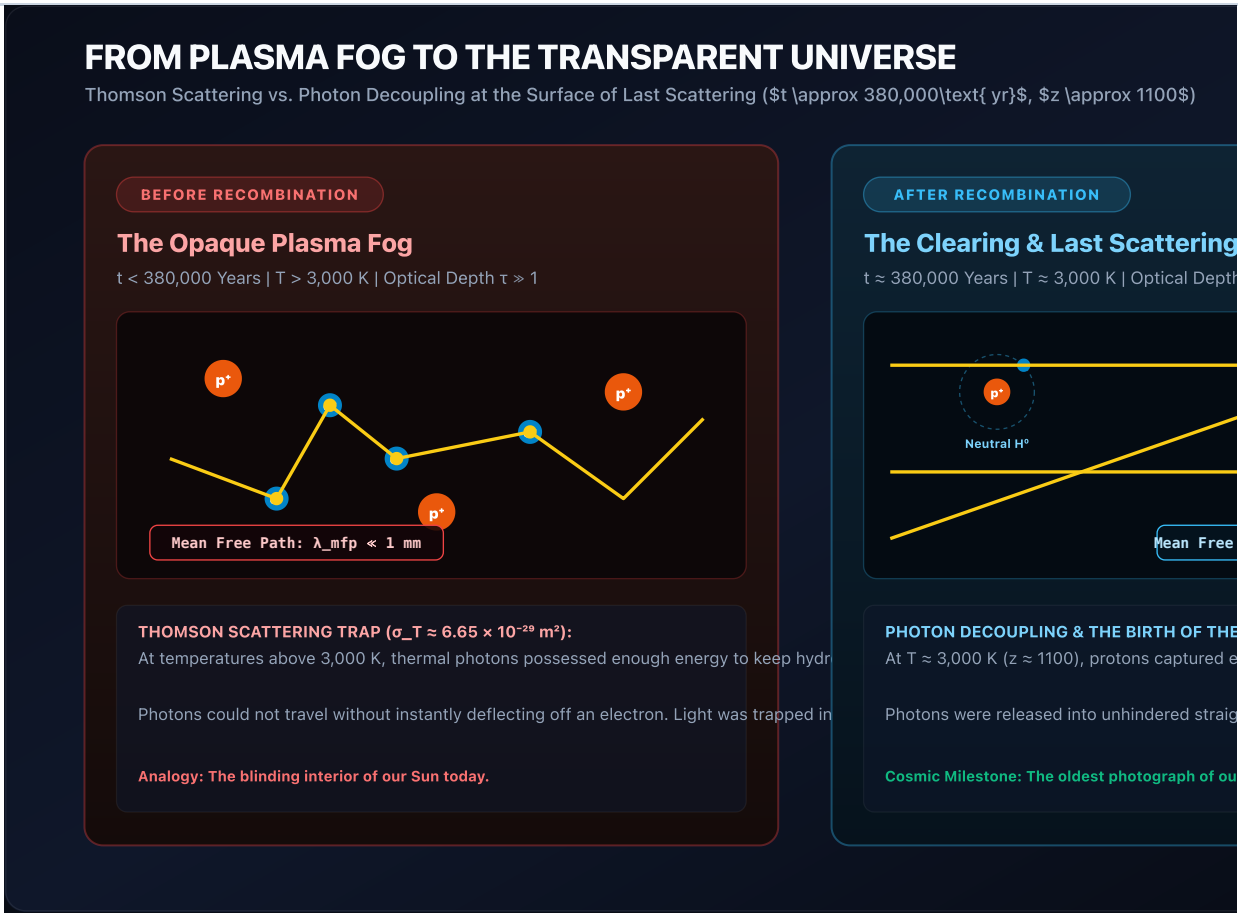


Figure 3.1: The Clearing of the Heavens. Before 380,000 years, photons were trapped in an endless Thomson scattering random walk off free electrons; once atomic nuclei captured electrons at Recombination, optical depth collapsed below unity and the first light broke free across the cosmos.

Matter-Radiation Equality (t ≈ 50,000 Years): The Shift of Power

As the universe expanded, the energy densities of matter and radiation diluted at fundamentally different rates:

- **Matter Density (ρ_m):** Dilutes strictly with the expansion of spatial volume: ρ_m(a) ∝ a^{-3}.
- **Radiation Energy Density (ρ_r):** Dilutes with spatial volume (a^{-3}) *plus* an additional factor of a^{-1} because cosmological expansion stretches the wavelength of individual photons (λ ∝ a, hence E = hc/λ ∝ a^{-1}). Therefore: ρ_r(a) ∝ a^{-4}.

Because radiation diluted faster than matter, their densities eventually crossed at a critical junction known as **Matter-Radiation Equality** (z_{eq} ≈ 3400, corresponding to t ≈ 51,000 years):

The Cosmic Transition to Gravitational Clustering
Prior to equality, the relativistic pressure of radiation dominated the universe, suppressing the gravitational collapse of matter. Once matter took the gravitational helm (ρ_m > ρ_r), cold dark matter could begin collapsing into gravitational potential wells without being blown apart by radiation pressure, laying the silent groundwork for the future cosmic web.

Shakil Mahmud • Research Monograph

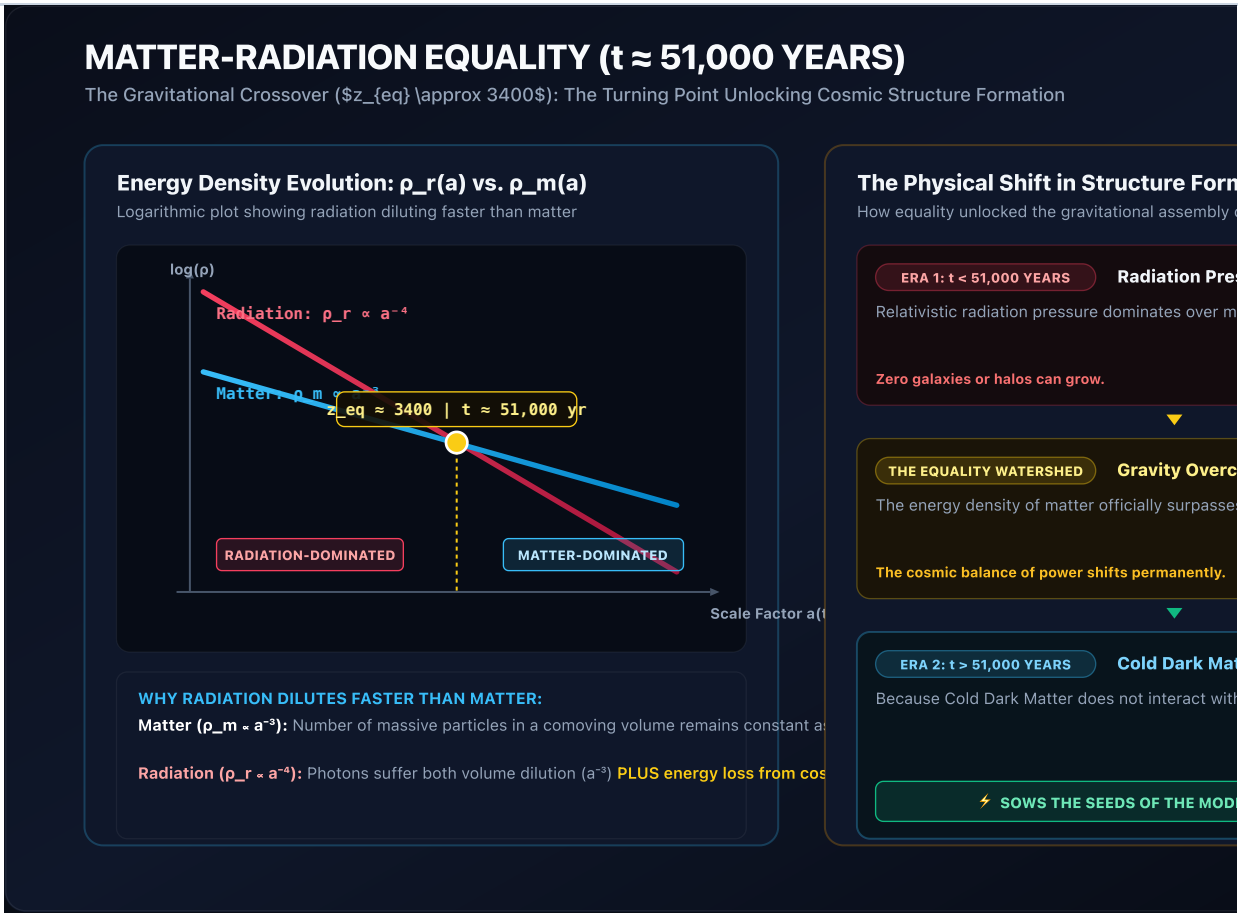


Figure 3.2: Matter-Radiation Equality & The Gravitational Turning Point. Radiation energy density diluted faster ($\propto a^{-4}$) than matter density ($\propto a^{-3}$); their crossing at t ≈ 51,000 years ($z_{eq} \approx 3400$) allowed Cold Dark Matter to begin unhindered gravitational collapse, forming the scaffolding of galaxies.

The Physics of Recombination (z ≈ 1100, t ≈ 380,000 Years): The Great Neutralization

A student of atomic physics might expect recombination to occur when the average thermal kinetic energy of the universe ($k_B T$) dropped below the binding energy of the hydrogen ground state ($E_I = 13.6$ eV), which corresponds to a temperature of approximately 157,000 K. Yet, the universe did not recombine until it cooled to a mere **3,000 K** ($k_B T \approx 0.26$ eV)—a delay of hundreds of thousands of years!

The reason for this immense delay lies in the **baryon-to-photon ratio** ($\eta = n_b / n_\gamma \approx 6 \times 10^{-10}$). Because there were nearly two billion high-energy photons for every proton and electron, the high-energy exponential Wien tail of the Planck blackbody radiation curve contained an overwhelming surplus of ionizing photons ($h\nu > 13.6$ eV), even when the average temperature was far below 13.6 eV.

The equilibrium ionization fraction $X_e = n_e / (n_p + n_H)$ is governed by the **Saha Ionization Equation**:

$$\frac{X_e^2}{1 - X_e} = \frac{1}{n_b} \left(\frac{m_e k_B T}{2\pi \hbar^2} \right)^{3/2} \exp\left(-\frac{E_I}{k_B T}\right)$$

Furthermore, when an electron falls directly into the ground state of a hydrogen atom ($e^- + p \rightarrow H(1s) + \gamma$), it emits a Lyman-continuum ultraviolet photon (13.6 eV). In the dense plasma, this newly emitted photon was instantly reabsorbed by an adjacent neutral atom, re-ionizing it. Net recombination could only proceed through a slow, bottlenecked detour formulated by Jim Peebles: electrons captured into excited 2s or 2p states, followed by **two-photon decay from the 2s state** ($H(2s) \rightarrow H(1s) + \gamma_1 + \gamma_2$), which has an agonizingly slow transition rate of just $8.22\ s^{-1}$.

By t ≈ 380,000 years (z ≈ 1090), the ionization fraction plummeted below 10^{-4}. Free electrons were locked into neutral, bound hydrogen and helium atoms. In a geological blink of an eye, the free electron density vanished.

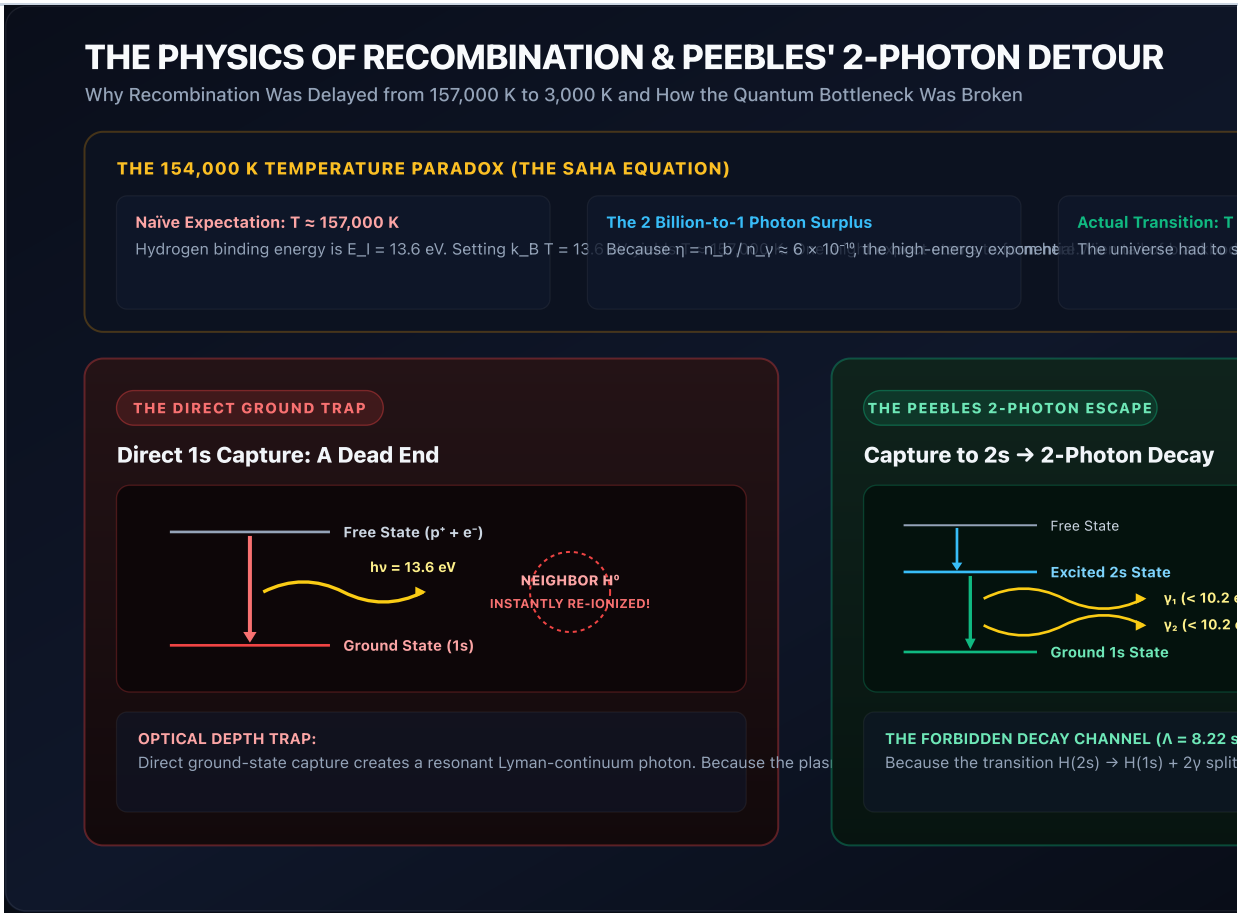


Figure 3.3: Recombination & Peebles' 2-Photon Escape Channel. Direct ground-state electron capture was an optical trap because emitted 13.6 eV photons instantly re-ionized neighbor atoms; recombination could only succeed via excited 2s capture and forbidden two-photon decay (2s ⟶ 1s + 2γ), permanently locking neutral atoms.

Photon Decoupling: The Birth of the Cosmic Microwave Background

With the disappearance of free electrons, the Thomson scattering optical depth (τ) dropped below unity:

$$\tau = \int \sigma_T n_e c \, dt < 1$$

Suddenly, the mean free path of light expanded to the edge of the universe. Photons were no longer scattered, trapped, or refracted. **The heavens cleared.**

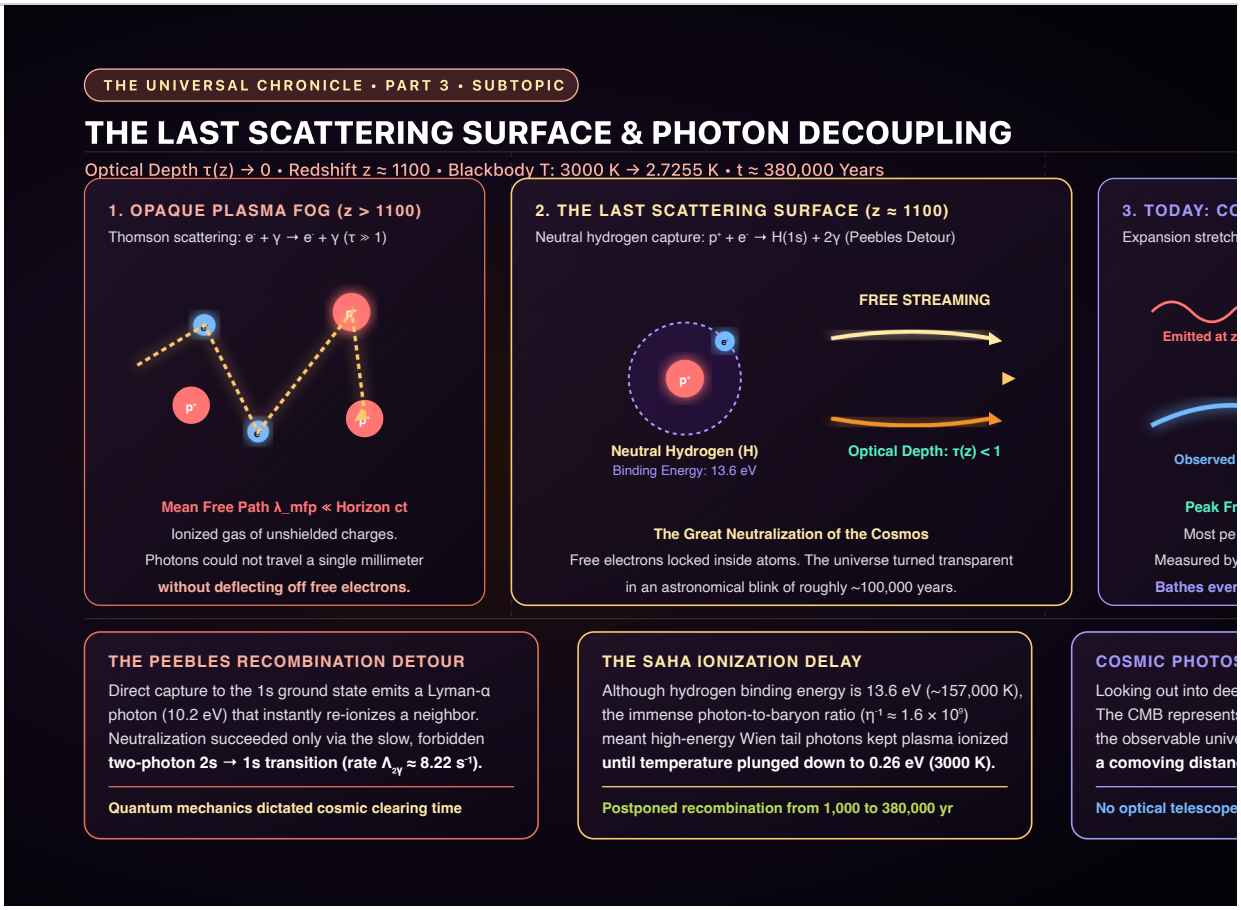
The last layer of plasma that scattered these photons is called the **Surface of Last Scattering**. The light released at that moment was an intense, warm, incandescent glow—radiating at 3,000 K, equivalent to the golden-orange light of a low-wattage incandescent lightbulb. Over the subsequent 13.8 billion years of cosmic expansion, spacetime stretched the wavelength of these photons by a factor of 1,100 ($z \approx 1090$):

$$\lambda_{\text{today}} = \lambda_{\text{emission}} \times (1 + z) \approx 1100 \times \lambda_{\text{emission}}$$

That ancient visible orange glow was redshifted out of the visible spectrum, through the infrared, and into the microwave band. Today, it bathes every cubic centimeter of the cosmos in a faint, uniform sea of approximately **411 photons per cubic centimeter**, cooled to an icy **2.72548 ± 0.00057 K**: the **Cosmic Microwave Background (CMB)**.

The Most Perfect Blackbody in the Universe
In 1990, the Far-Infrared Absolute Spectrophotometer (FIRAS) aboard NASA's COBE satellite measured the spectral energy distribution of the CMB. The data points matched Max Planck's theoretical blackbody radiation formula so flawlessly that the error bars were narrower than the thickness of the printed curve line—confirming with unprecedented precision that the early universe was in complete thermal equilibrium.

Shakil Mahmud • Research Monograph

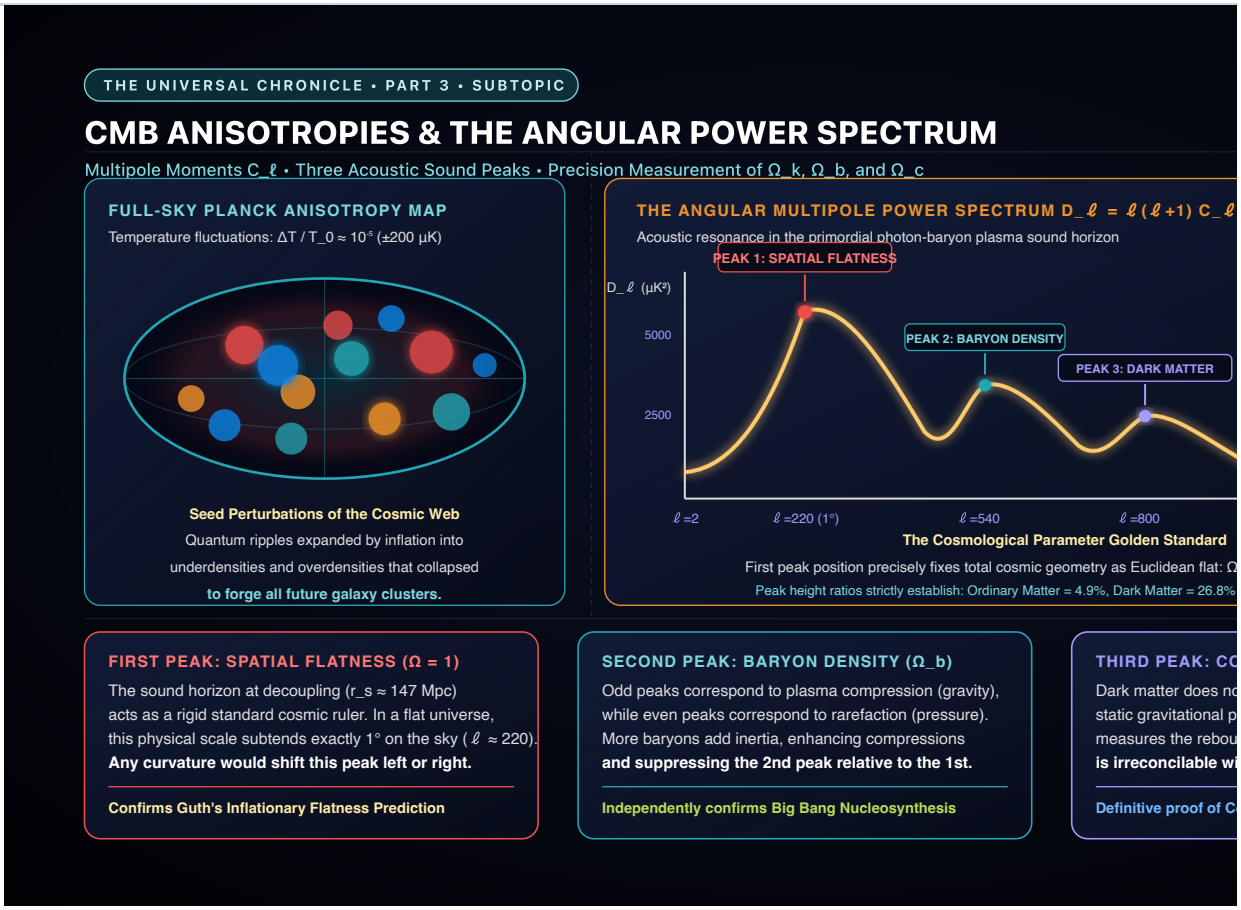


The Surface of Last Scattering & Cosmological Redshift ($z \approx 1100, t \approx 380,000$ yr). Recombination neutralizes the primordial plasma, causing optical depth $\tau(z)$ to drop through unity. Free electrons decouple from photons, releasing an incandescent 3,000 K blackbody photosphere. Over 13.8 billion years, metric expansion stretches these photons by a factor of $(1 + z) \approx 1100$, shifting peak wavelengths from near-infrared (1μm) into the 2.7255 K microwave background.

The Cosmic Rosetta Stone: Reading the Ripples of the CMB

When Arno Penzias and Robert Wilson discovered the CMB in 1965 at Bell Labs, it appeared completely smooth and isotropic. However, theoretical cosmologists recognized that if the universe were 100% smooth, gravity would have had no starting points to gather matter into galaxies.

In 1992, COBE detected the first **temperature anisotropies**—microscopic fluctuations on the order of **$\Delta T / T \approx 10^{-5}$ (one part in 100,000)**, representing temperature differences of barely 30 microkelvins. Subsequent orbital observatories—NASA's WMAP (2001–2010) and ESA's Planck satellite (2009–2018)—mapped these ripples across the entire celestial sphere with ultra-high angular resolution.



The CMB Angular Multipole Power Spectrum C_ℓ & Acoustic Sound Horizon. Temperature fluctuations ($\Delta T/T_0 \sim 10^{-5}$) across the Planck all-sky map decomposed into spherical harmonics. Peak 1 ($\ell \approx 220, \theta \approx 1^\circ$) confirms Euclidean spatial flatness ($\Omega_k \approx 0$). Peak 2 measures cosmic baryon density ($\Omega_b h^2$), and Peak 3 demonstrates the gravitational dominance of Cold Dark Matter ($\Omega_c h^2$).

Baryon Acoustic Oscillations (BAO): Sound Waves of Creation

These temperature ripples are not random noise; they are the frozen acoustic harmonics of the primordial universe. Prior to recombination, regions of overdensity pulled matter inward via gravity, while radiation pressure pushed outward. This tug-of-war set up compression and rarefaction sound waves traveling through the plasma at more than half the speed of light ($c_s = c / \sqrt{(3(1 + 3\rho_b/4\rho_\gamma))} \approx 0.57c$).

When recombination occurred, the sound waves were suddenly frozen in time. Decomposing these temperature ripples into spherical harmonics produces the legendary **CMB Angular Power Spectrum**:

- **The 1st Acoustic Peak ($l \approx 220$):** Represents the fundamental sound wave that had just reached maximum compression at recombination. Its angular size on the sky (0.8°) acts as a cosmic surveyor's rod, proving that **spatial curvature is flat ($\Omega_k = 0.0007 \pm 0.0019$)**.
- **The 2nd Acoustic Peak ($l \approx 540$):** Measures the maximum rarefaction (rebound) of the sound wave. The ratio of the second to first peak reveals the exact density of ordinary baryonic matter: **$\Omega_b \approx 4.9\%$**.
- **The 3rd Acoustic Peak ($l \approx 800$):** Measures the second compression cycle, directly constraining the density of **Cold Dark Matter ($\Omega_c \approx 26.8\%$)**, while the remainder is Dark Energy ($\Omega_\Lambda \approx 68.3\%$).

Shakil Mahmud • Research Monograph

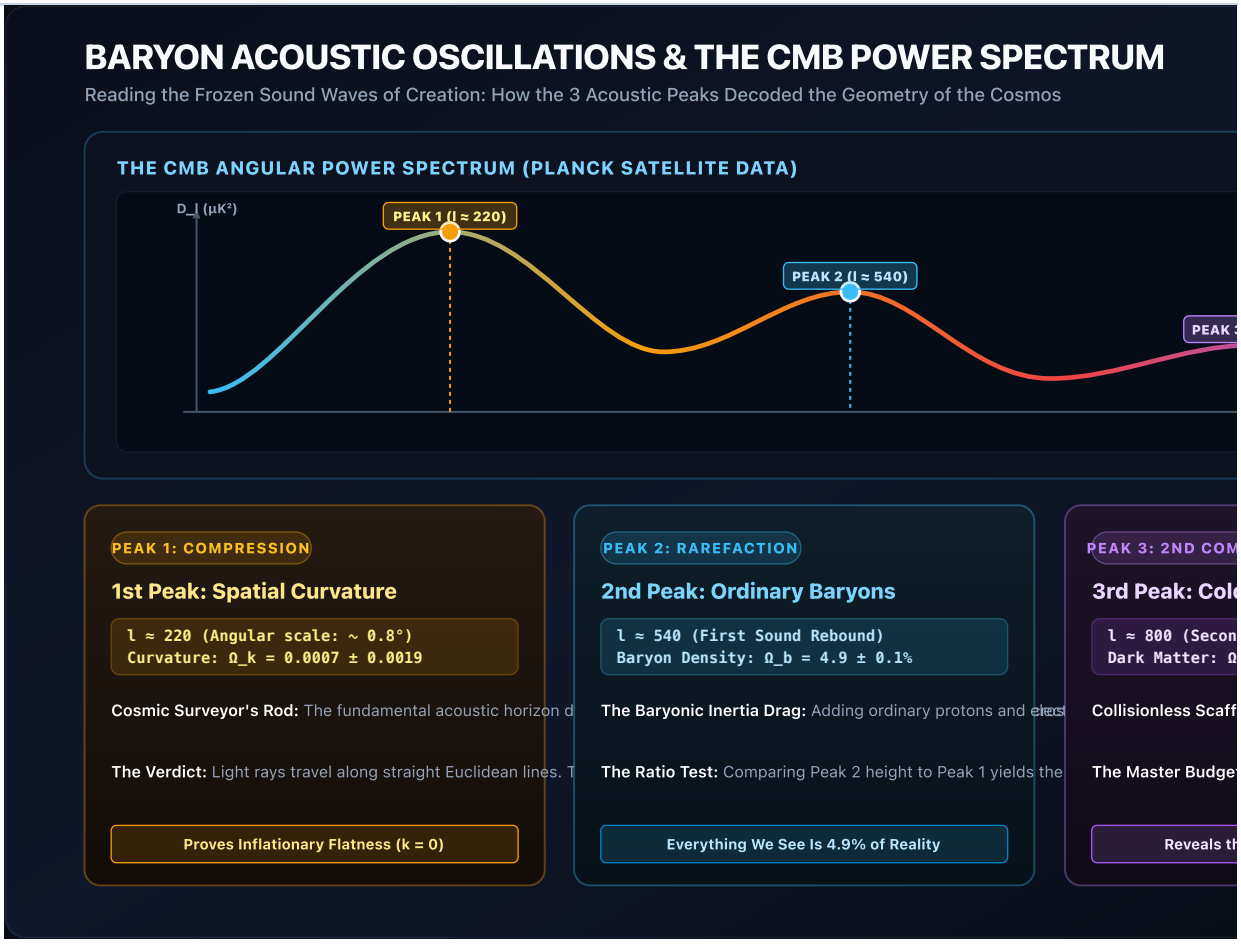


Figure 3.4: The Frozen Sound Waves of Creation (BAO & The CMB Spectrum). The tug-of-war between gravity and radiation pressure generated relativistic sound waves ($c_s \approx 0.57c$) frozen at Recombination; the three acoustic peaks decode the universe's spatial flatness (Peak 1), ordinary baryon density (Peak 2), and Cold Dark Matter density (Peak 3).

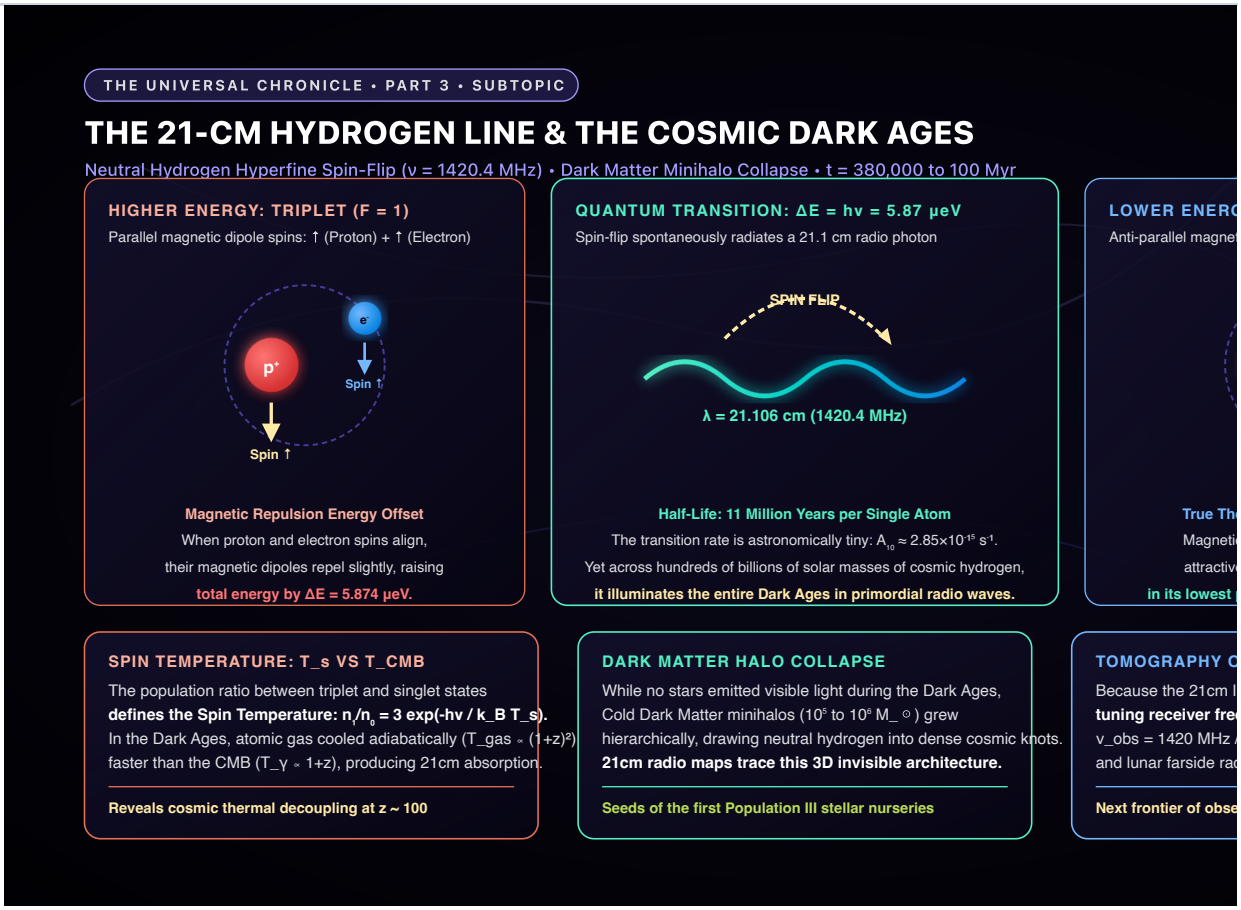
The Cosmic Dark Ages (t = 380,000 to 100 Million Years): The Silent Abyss

Once the last scattering photons decoupled and redshifted into invisible infrared wavelengths, the universe was plunged into an epoch of utter, pitch-black darkness: the **Cosmic Dark Ages**.

There was not a single star, galaxy, quasar, or accretion disk in existence. The cosmos was a vast, cold, expanding ocean of neutral gas: 75% neutral atomic hydrogen and 25% helium, with no heavy elements. No chemical combustion was possible, and no stellar fusion had ignited. For over 100 million years, an observer traveling through the universe would have experienced total sensory void.

Yet, this darkness was not passive. Beneath the veil of invisibility, the invisible hand of **Cold Dark Matter** was orchestrating the future of the universe. Because dark matter interacts only through gravity and does not scatter photons, it had already begun collapsing into vast, invisible filaments and spherical halos during the radiation era. During the Dark Ages, ordinary hydrogen and helium gas fell gravitationally into these deep dark matter gravitational wells.

The only electromagnetic radiation emitted throughout the entire Dark Ages was the subtle **21-centimeter line**—a hyperfine radio transition produced when the spin of a hydrogen atom's solitary electron flips from parallel to antiparallel relative to the proton's nuclear spin ($\Delta E = 5.87 \times 10^{-6}$ eV). This faint, ancient radio signal, redshifted into low-frequency meters-long radio waves today, represents the ultimate frontier of modern radio astronomy (such as the Square Kilometre Array).



The 21-cm Hydrogen Hyperfine Transition & The Cosmic Dark Ages ($t = 380,000$ to 100 Myr). Neutral atomic hydrogen in the unlit universe experiences a ground-state hyperfine spin-flip: when the electron spin transitions from parallel ($F = 1$ triplet) to anti-parallel ($F = 0$ singlet) relative to the proton, it radiates a 21.1 cm radio photon ($\Delta E = 5.87 \mu\text{eV}, \nu = 1420.4$ MHz). This whisper of radiation maps the invisible collapse of Cold Dark Matter minihalos before the first stars ignited.

Shakil Mahmud • Research Monograph

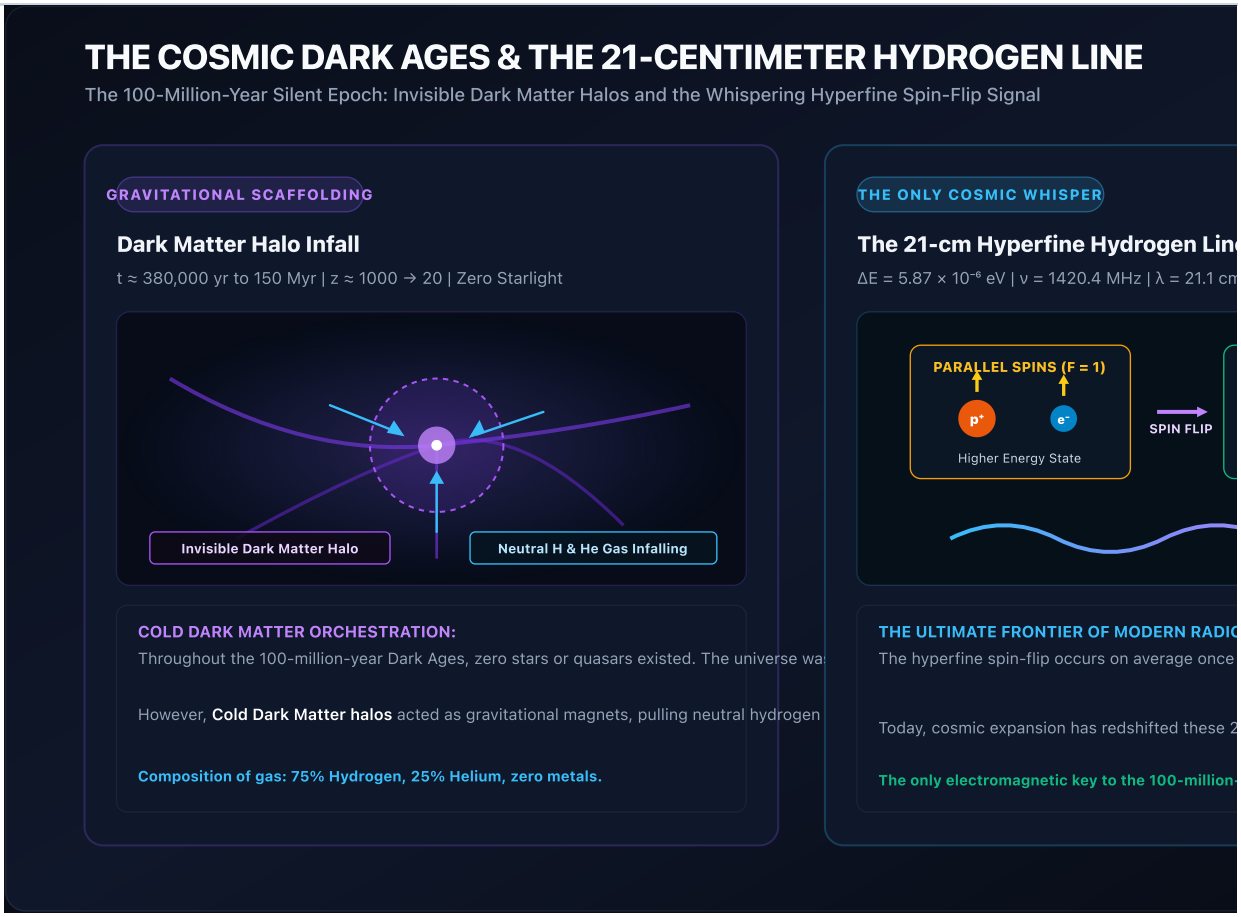


Figure 3.5: The 100-Million-Year Silent Abyss & The 21cm Hydrogen Line. During the starless Dark Ages, invisible Dark Matter halos gathered neutral hydrogen into deep gravitational wells; the solitary whisper of radiation throughout this epoch was the 21cm hyperfine spin-flip (parallel to antiparallel electron-proton spin), now targeted by modern radio astronomy arrays.

Chronology Table: From Plasma Fog to the Edge of Starlight

Epoch / Event	Redshift (z)	Cosmic Time (t)	Temperature (K)	Physical Characteristics
Matter-Radiation Equality	z ≈ 3400	51,000 years	~ 9, K	Matter energy density surpasses radiation; dark matter begins unhindered gravitational collapse.
Recombination Era	z ≈ 1300 → 1000	260,000 → 380,000 yr	4,000 → 3, K	Electrons combine with protons via 2-photon decay (2s → 1s); ionization drops from 100% to <0.01%.
Photon Decoupling (Last Scattering)	z ≈ 1090	380,000 years	2, K	Optical depth drops below 1; photons stream freely across space; the Cosmic Microwave Background is released.
The Cosmic Dark Ages	z ≈ 1000 → 20	380,000 yr to 150 Myr	3,000 → K	Zero stellar light; space is cold and black; neutral hydrogen gas accumulates inside dark matter halos; 21-cm hyperfine radio emission.
Cosmic Dawn (First Stars)	z ≈ 20 → 15	~ 150 → 250 Myr	~ K	Gravitational gas collapse reaches critical density; Population III hypermassive stars ignite; Reionization begins.

The Verdict: How the CMB Anchors Modern Cosmology

The discovery and precision mapping of the Cosmic Microwave Background transformed cosmology from philosophical speculation into an exact physical science. Every fundamental parameter of our universe—its age (13.787 ± 0.020 billion years), its spatial flatness, its expansion rate ($H_0 \approx 67.4$ km/s/Mpc), and its cosmic recipe (68.3% Dark Energy, 26.8% Cold Dark Matter, 4.9% Baryonic Matter)—is encoded directly into the subtle thermal ripples of the last scattering surface.

As the Dark Ages progressed, gravitational potential wells grew deeper. Massive primordial hydrogen gas clouds began to cool via molecular hydrogen rotational transitions, slowly falling inward under their own immense gravity. In **Part 4** of *The Universal Chronicle*, the silence will finally shatter: **Cosmic Dawn — Population III Monster Stars, the First Galaxies, and the Epoch of Reionization**.

Academic Citations & Foundational Literature

- **Penzias, A. A., & Wilson, R. W. (1965).** "A Measurement of Excess Antenna Temperature at 4080 Mc/s." *The Astrophysical Journal*, 142, 419–421. doi:10.1086/148307.
- **Dicke, R. H., Peebles, P. J. E., Roll, P. G., & Wilkinson, D. T. (1965).** "Cosmic Black-Body Radiation." *The Astrophysical Journal*, 142, 414–419. doi:10.1086/148306.
- **Peebles, P. J. E. (1968).** "Recombination of the Primeval Plasma." *The Astrophysical Journal*, 153, 1–11. doi:10.1086/149628.
- **Sunyaev, R. A., & Zel'dovich, Y. B. (1970).** "Small-scale fluctuations of relic radiation." *Astrophysics and Space Science*, 7(1), 3–19. doi:10.1007/BF00653471.
- **Mather, J. C., et al. (1990).** "A measurement of the cosmic microwave background spectrum by the COBE FIRAS instrument." *The Astrophysical Journal*, 354, L37–L40. doi:10.1086/185717.
- **Smoot, G. F., et al. (1992).** "Structure in the COBE differential microwave radiometer first-year maps." *The Astrophysical Journal*, 396, L1–L5. doi:10.1086/186504.
- **Planck Collaboration (Aghanim, N., et al.) (2020).** "Planck 2018 results. VI. Cosmological parameters." *Astronomy & Astrophysics*, 641, A6. doi:10.1051/0004-6361/201833910.
- **Hu, W., & Dodelson, S. (2002).** "Cosmic Microwave Background Anisotropies." *Annual Review of Astronomy and Astrophysics*, 40(1), 171–216. doi:10.1146/annurev.astro.40.060401.093926.

Citation: Mahmud, S. (2026). "The Clearing of the Heavens — Recombination, the Cosmic Microwave Background, and the Dark Ages." In The Universal Chronicle, Part 3. https://shakilmahmud.com/universal-chronicle-part-3-the-clearing-of-the-heavens/

Shakil Mahmud • Research Monograph

SHAKIL MAHMUD RESEARCH MONOGRAPHS • PART IV

Cosmic Dawn — Population III Hyperstars, the First Galaxies, and Reionization

Cosmic Dawn — Population III Hyperstars, the First Galaxies, and Reionization

2,101 words • October 30, 2026 • Permanent URI

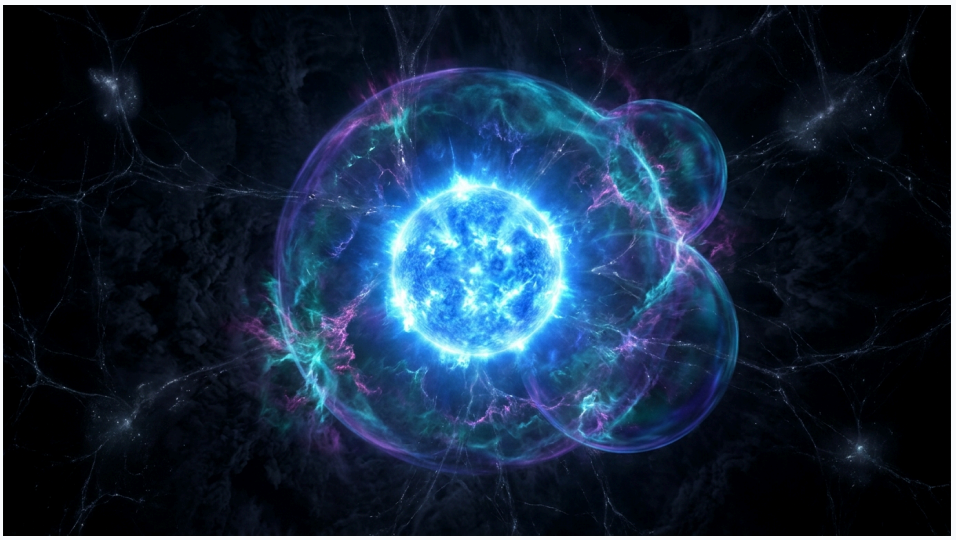


Plate IV: *Figure: Cosmic Dawn (~100–250 Ma): the birth of pristine, metal-free Population III hyperstars (100–300 M ⊙) collapsing from molecular hydrogen clouds, blazing with ultraviolet radiation to trigger the Epoch of Reionization.*

For over one hundred million years after the Big Dawn, the universe was an unbroken, lightless desert of neutral hydrogen and cold dark matter. Then, deep within the gravitational wells of primordial mini-halos, pristine gas collapsed under immense pressure to ignite the first stars in cosmic history: Population III hyperstars. Colossal, scorching, and short-lived, these stellar titans illuminated the Cosmic Dawn, flooded the cosmos with ionizing ultraviolet radiation, and sowed the very first seeds of the periodic table.

The Physics of Primordial Collapse: The Molecular Hydrogen Bottleneck

In modern stellar nurseries (such as the Orion Nebula), interstellar gas clouds collapse and fragment efficiently into low-mass stars like our Sun. This occurs because the modern interstellar medium is enriched with "metals"—astronomical shorthand for any element heavier than helium, such as carbon, oxygen, silicon, and iron. These heavy elements and dust grains possess thousands of closely spaced electronic and fine-structure transitions (such as [C II] at 158\,μm and [O I] at 63\,μm) that radiate infrared photons with exquisite efficiency, cooling clouds down to a frigid 10 K.

In the primordial universe, however, there were zero dust grains and zero heavy elements. The gas consisted purely of 75% hydrogen and 25% helium. Atomic hydrogen cannot radiate energy efficiently below 10,000 K because its first electronic excitation level (n=1 → n=2, Lyman-α) requires an enormous 10.2 eV of thermal energy.

The only coolant available in the entire early cosmos was trace amounts of **molecular hydrogen (H_2)**, formed through fragile gas-phase catalytic pathways mediated by free electrons:

- $H + e^- \rightarrow H^- + \gamma$
- $H^- + H \rightarrow H_2 + e^-$

Because molecular hydrogen is a homonuclear diatomic molecule, it has no permanent electric dipole moment. Its cooling is restricted to quadrupole rotational transitions ($J = 2 \rightarrow 0$), which have an energy spacing corresponding to $T \approx 512$ K. As a result, primordial gas clouds could not cool below roughly **200 to 300 K**.

The Jeans Mass: Why the First Stars Were Giants

The minimum mass required for a gas cloud to overcome thermal gas pressure and collapse under self-gravity is defined by the **Jeans Mass (M_J)**:

$$M_J \propto \left(\frac{k_B T}{G \mu m_H}\right)^{3/2} \rho^{-1/2}$$

Because the temperature floor of the primordial gas (T ~ 200– K) was twenty to thirty times higher than in modern molecular clouds (T ~ K), the Jeans mass in primordial mini-halos was enormous: typically **100 to 1,000 Solar Masses ($M_\odot$)**. Rather than fragmenting into thousands of tiny stars, primordial gas clouds collapsed into solitary, massive proto-stellar cores that accreted matter at ferocious rates ($\dot{M}$ ~ 10^{-3} to 10^{-2} $M_\odot$ /year).

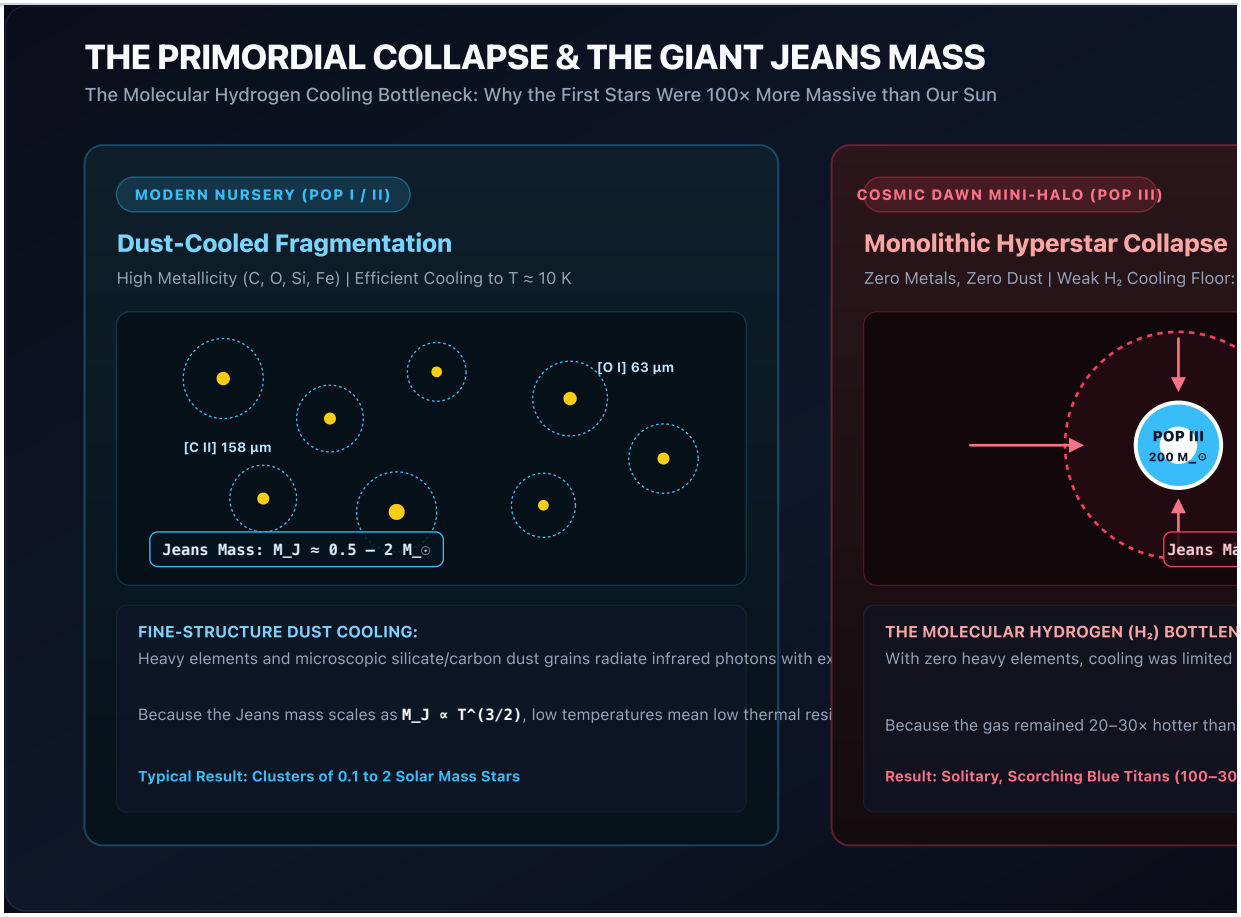


Figure 4.1: The Molecular Hydrogen Bottleneck & Jeans Mass Scaling. Without heavy elements (C, O, Fe) to radiate heat at low temperatures, pristine gas could only cool via inefficient H2 rotational transitions down to ~200 K. Because Jeans mass scales as M_J ∝ T^(3/2) / ρ^(1/2), primordial collapse fragments were 100 to 1,000 times more massive than modern stellar nurseries.

Population III Hyperstars: The Blue Titans of the Dawn

The stars that ignited at Cosmic Dawn ($z \sim 20–30$, or $t \approx 100–200$ million years) were unlike anything existing in our galaxy today. Designated **Population III stars**, these titans possessed masses ranging from **30 $M_\odot$ to upwards of 300 $M_\odot$**.

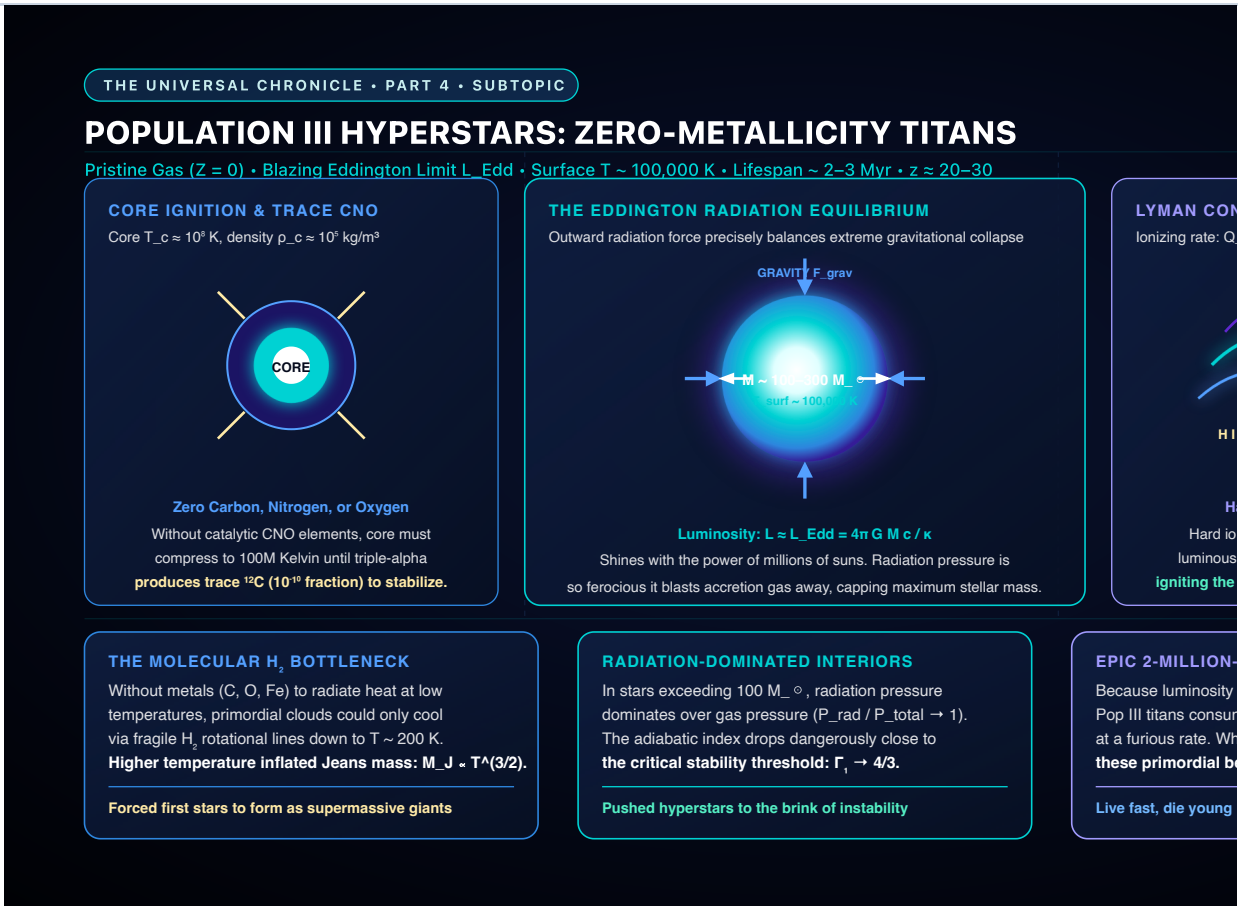
Anatomy of a Population III Hyperstar

Surface Temperature: Because they possessed zero carbon to catalyze the CNO cycle, Population III stars had to contract until their central core temperatures reached a staggering 10^8 K to initiate the triple-alpha process and produce trace carbon. This intense core compression caused their surfaces to burn at blistering effective temperatures exceeding **100,000 K** (compared to 5, K for our Sun).

Luminosity: They shone close to the theoretical *Eddington limit*, radiating millions of times more energy than the Sun ($L \sim 10^6–10^7 L_\odot$). Their emission peaked not in visible light, but in hard, ionizing extreme ultraviolet (EUV) radiation.

Because they burned through their nuclear fuel with reckless ferocity, Population III hyperstars lived spectacularly brief lives. While our Sun has a lifespan of 10 billion years, a 200 $M_\odot$ primordial star consumed its core hydrogen in barely **2 to 3 million years**.

Shakil Mahmud • Research Monograph



Population III Hyperstar Structure & The Eddington Radiation Limit (z \approx 20\text{–}30). Formed from pristine $Z = 0$ primordial hydrogen and helium, hypermassive stars (100\text{–}300 M_\odot) compressed core temperatures to $T_c \sim 10^8$ K to initiate trace carbon production via the triple-alpha process. Operating near the Eddington limit (L \sim 10^6\text{–}10^7 L_\odot) with surface temperatures $T_{\text{eff}} \sim 100,000$ K, these giants flooded the universe with extreme ultraviolet Lyman continuum radiation before dying within 2–3 million years.

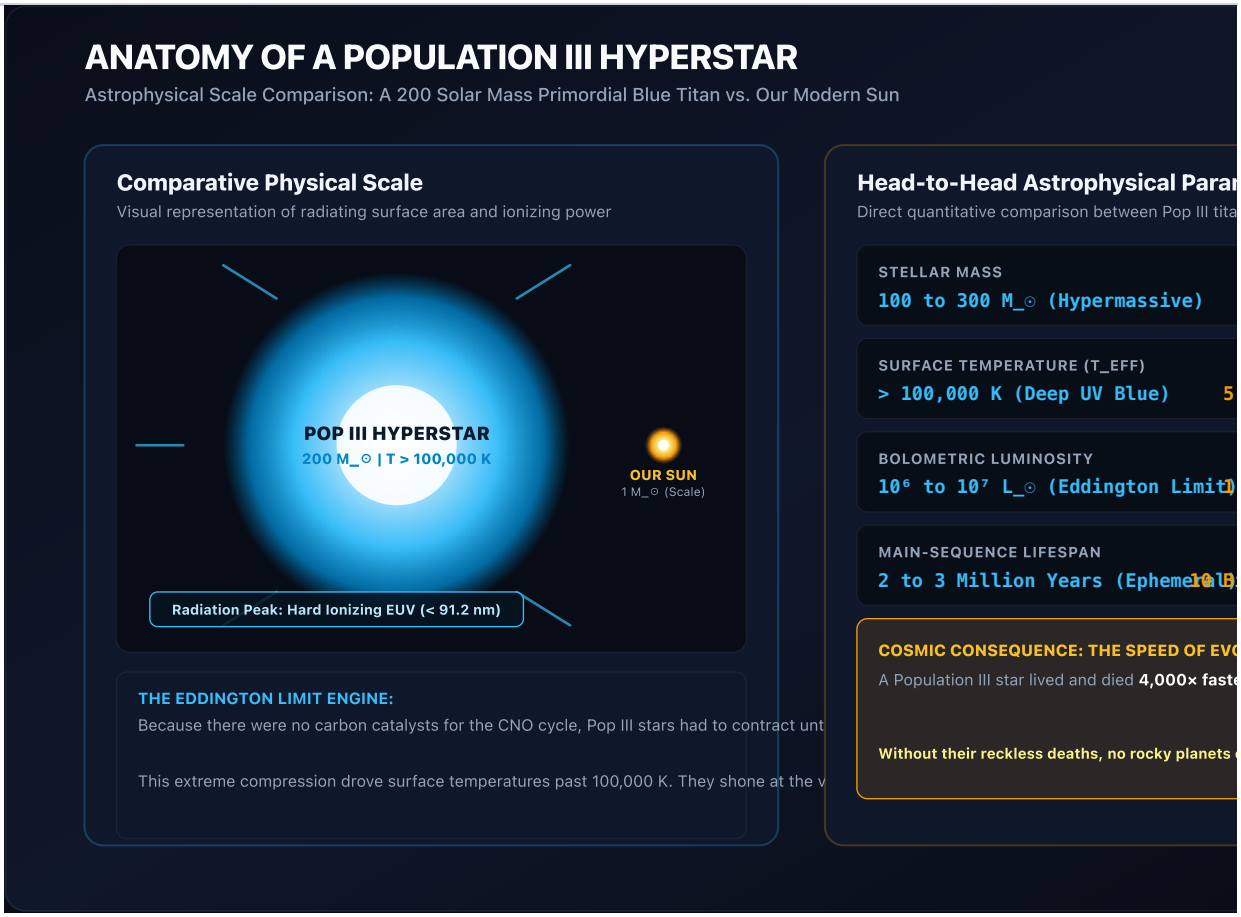


Figure 4.2: Anatomy of a Population III Hyperstar. Spanning 100 to 300+ solar masses, these zero-metallicity behemoths operated at 99% of the Eddington luminosity limit. Lacking dust grains to drive radiation winds, they experienced zero mass loss during their short 2–3 million year lifespans, burning at surface temperatures exceeding 100,000 K.

Catastrophic Deaths: Pair-Instability Supernovae and Black Hole Seeds

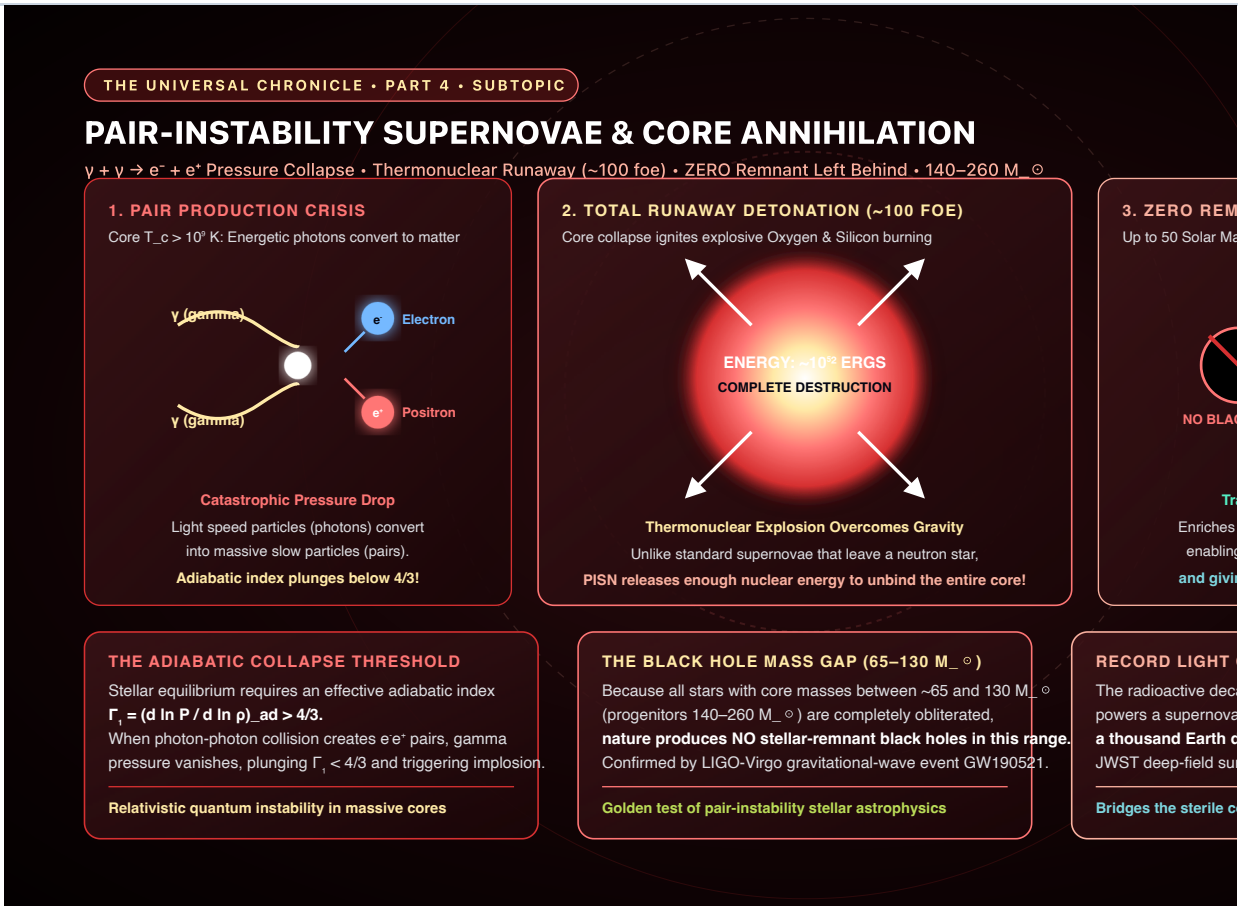
When a Population III hyperstar exhausted its core fuel, its fate depended strictly on its initial mass, leading to some of the most violent astrophysical phenomena in cosmic history:

1. Pair-Instability Supernovae (PISN: 140–260 $M_\odot$)

In stars with helium core masses between 64 $M_\odot$ and 133 $M_\odot$, core temperatures reached 10^9 K. At this threshold, the average thermal photons became so energetic that they spontaneously converted into electron-positron pairs via quantum pair production ($\gamma + \gamma \rightarrow e^+ + e^-$).

This conversion abruptly replaced radiation pressure (which supports the star against gravity) with matter pressure, causing the adiabatic index Γ_1 to drop below the critical stability limit of 4/3. The core suffered an instantaneous, runaway gravitational collapse. The sudden compression ignited catastrophic, explosive oxygen and silicon burning, releasing more thermonuclear energy than the gravitational binding energy of the entire star. **The entire star was completely obliterated in a single blast with zero remnant left behind—no neutron star, no black hole.** Up to 50 $M_\odot$ of pure synthesized iron, nickel, carbon, and oxygen was hurled into the surrounding pristine cosmos.

Shakil Mahmud • Research Monograph



Pair-Instability Supernova Core Annihilation (M = 140\text{–}260 M_\odot). In helium cores exceeding $64 M_\odot$ (T_c > 10^9\text{ K}), high-energy gamma rays spontaneously convert into electron-positron pairs ($\gamma + \gamma \rightarrow e^- + e^+$). The sudden collapse of photon radiation pressure plunges the adiabatic index below 4/3, triggering runaway core collapse and explosive thermonuclear detonation ($\sim 10^{52}$ ergs) that obliterates the entire star with ZERO remnant left behind.

2. Direct Collapse to Intermediate-Mass Black Holes (> 260 M_⊙)

For primordial stars exceeding 260 M_⊙, the thermonuclear explosion was unable to overcome the immense gravitational potential. The star collapsed directly and completely into an **Intermediate-Mass Black Hole (IMBH)** of 100 to 1,000 M_⊙. These primordial stellar corpses provided the elusive gravitational "seeds" that grew via hyper-Eddington accretion into the billion-solar-mass supermassive black holes observed at high redshifts by the James Webb Space Telescope.

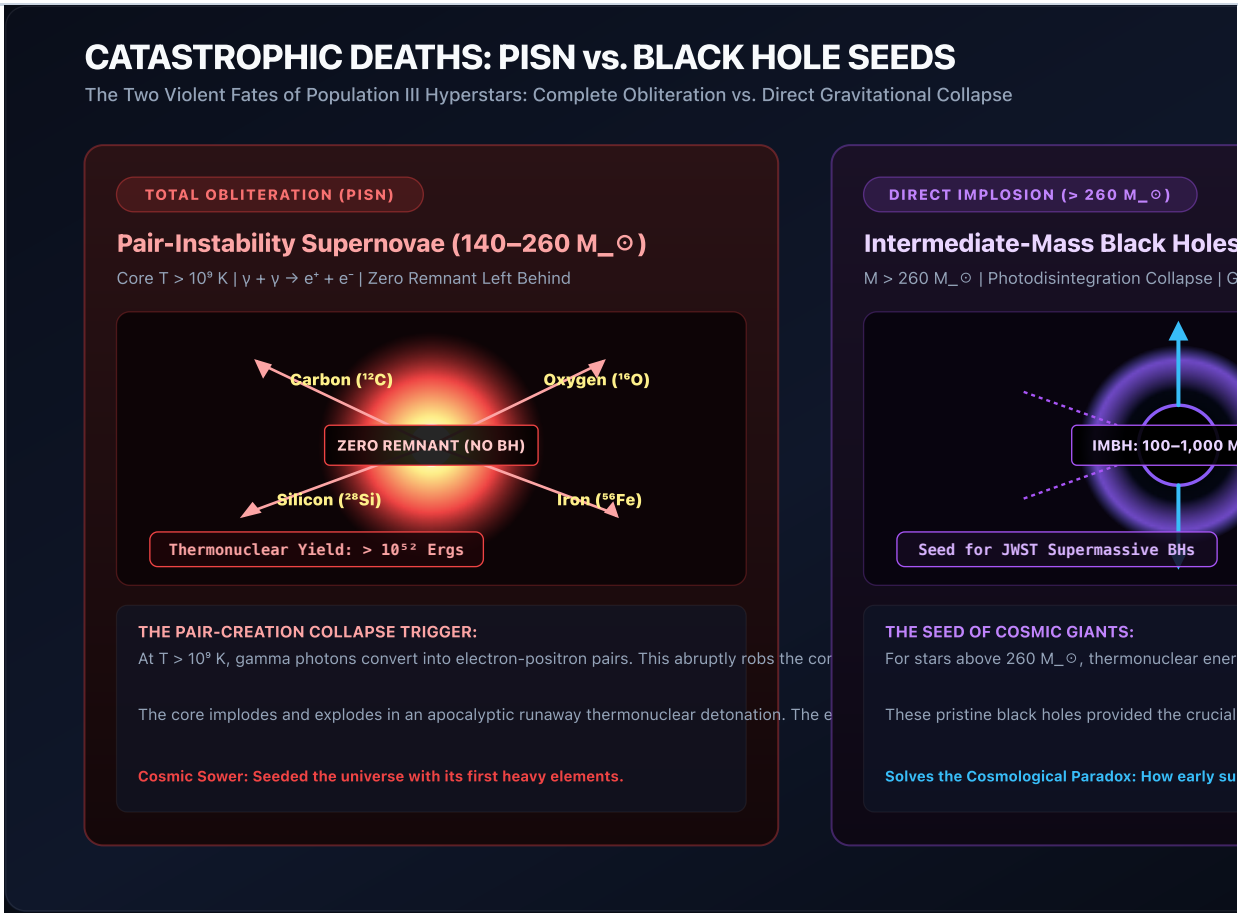


Figure 4.3: Fate Bifurcation of Population III Hyperstars. Between 140 and 260 $M_{\odot}$, energetic gamma rays convert into electron-positron pairs, dropping core radiation pressure and triggering catastrophic runaway fusion that obliterates the star with zero remnant. Above 260 $M_{\odot}$, photodisintegration robs energy, driving total gravitational collapse into an Intermediate-Mass Black Hole (IMBH).

The Epoch of Reionization (EoR): Ionizing the Cosmos

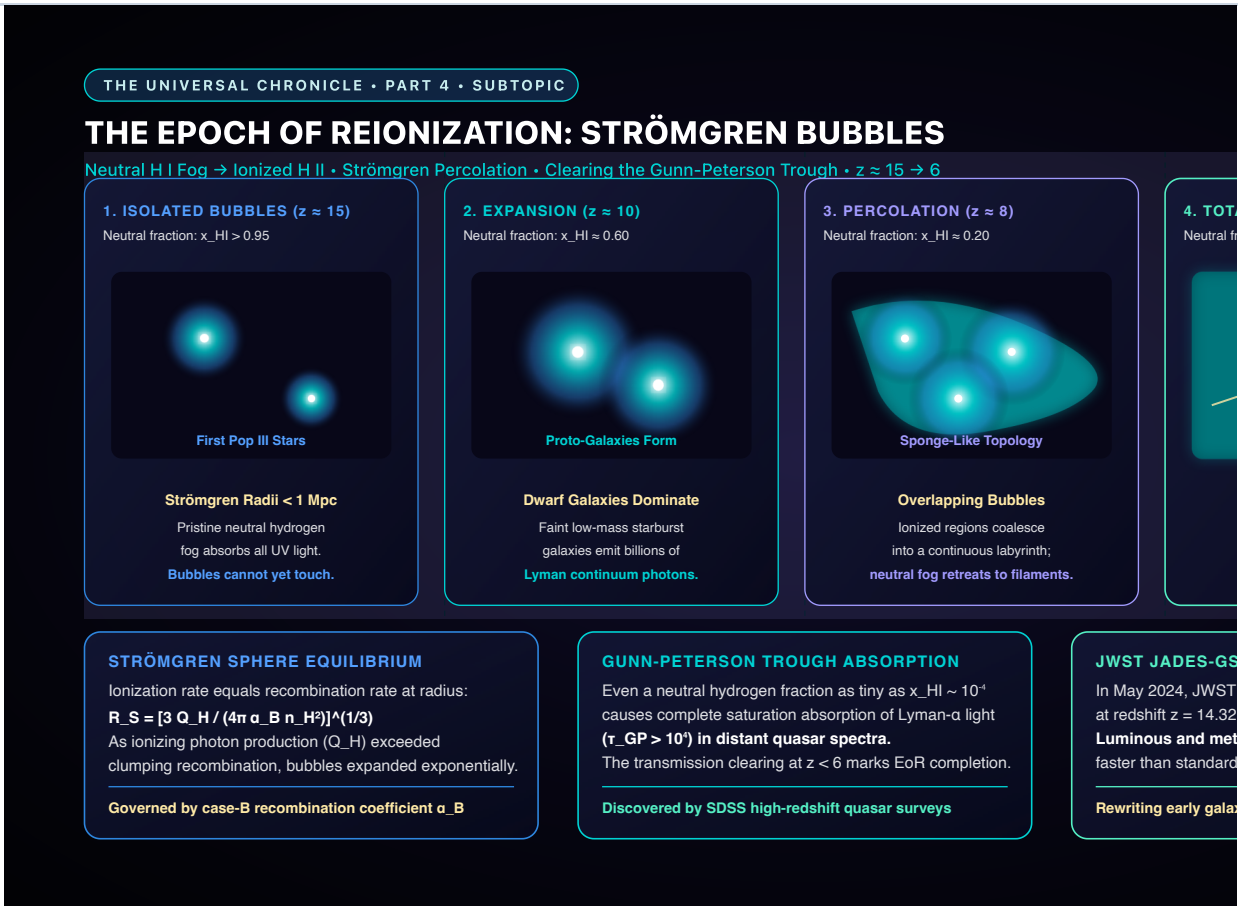
As the first stars ignited and aggregated into proto-galaxies, their ferocious extreme ultraviolet radiation began ionizing the surrounding neutral hydrogen gas. Each star created a localized **Strömgren sphere**—an expanding bubble of transparent, ionized plasma (H II):

$$\mathrm{H}^0 + h\nu(\geq 13.6\ \mathrm{eV}) \rightarrow p + e^-$$

Throughout the **Epoch of Reionization** ($z \approx 12 \rightarrow 6$, corresponding to $t \approx 300$ million to 1 billion years), these isolated bubbles grew, overlapped, and merged across cosmological distances. By redshift $z \approx 6$, over 99.9% of all intergalactic hydrogen had been re-ionized back into a hot, diffuse plasma (T ~ 10^ K).

Astronomers confirmed the timeline of this transformation through observations of high-redshift quasars using the **Gunn-Peterson Trough**: at $z > 6.2$, the spectrum of distant quasars is completely blotted out blueward of the Lyman-α line by residual neutral hydrogen fog, while at $z < 6$, the spectrum clears as the universe becomes fully transparent to ultraviolet light once more.

Shakil Mahmud • Research Monograph



Percolation of Strömgren Bubbles During the Epoch of Reionization ($z \approx 15 \to 6$). Chronological progression of cosmic ionization: isolated ionized hydrogen spheres (H_{II}) carved by Pop III stars expand and merge under ionizing radiation from primeval dwarf galaxies. Overlapping bubbles form a connected topological sponge, culminating in the complete clearing of the Gunn-Peterson optical trough at $z \approx 6$ ($t \sim 1$ Gyr).

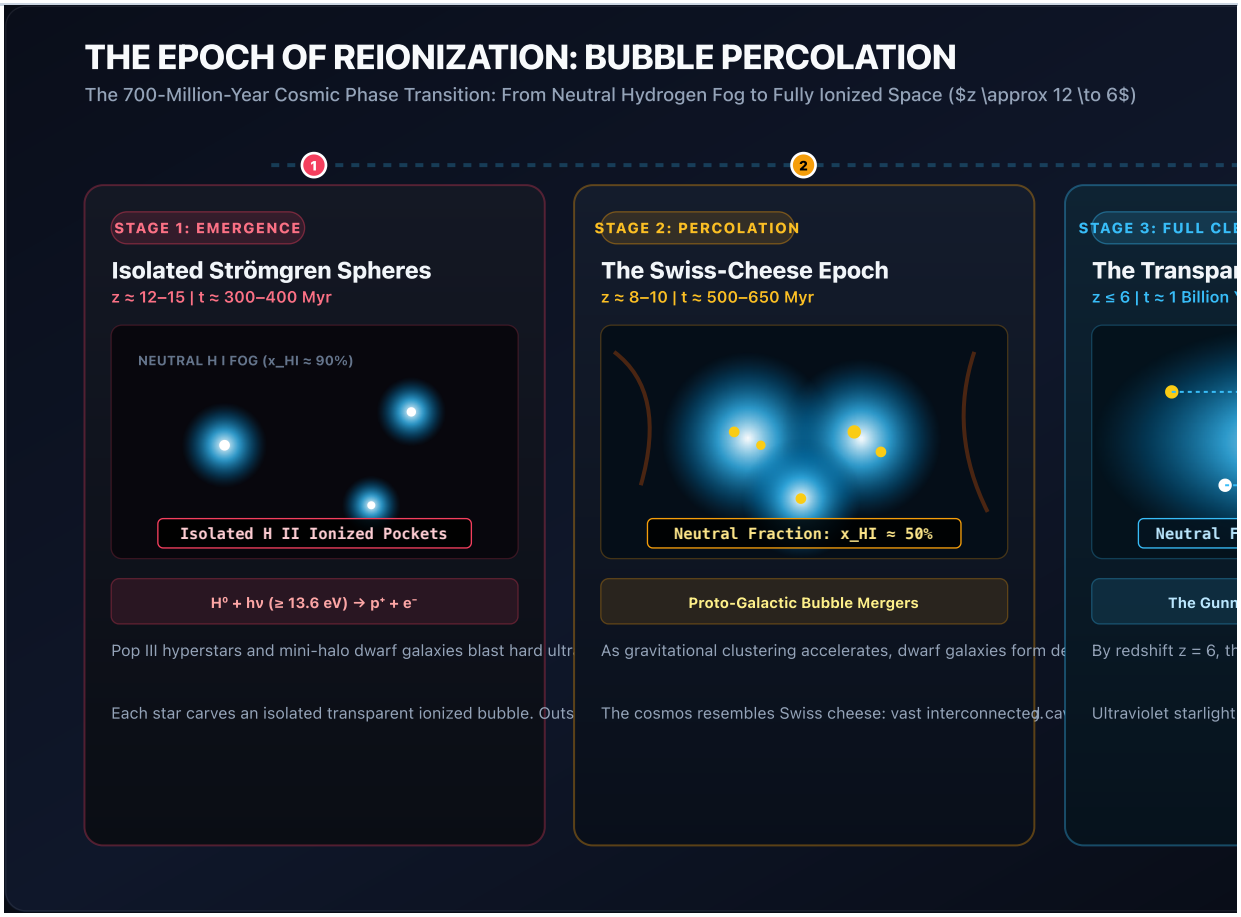


Figure 4.4: The Epoch of Reionization (EoR) Percolation. From z ≈ 20 to z ≈ 6, ionizing UV photons from Pop III hyperstars carved expanding ionized hydrogen (H II) Strömgren bubbles. As galactic density peaked, bubbles coalesced and percolated across cosmic space, permanently clearing the neutral hydrogen fog and completing the second great optical transition.

The Revolution of the James Webb Space Telescope (JWST)

Launched on Christmas Day 2021, NASA's James Webb Space Telescope (JWST) was engineered specifically to peer through cosmic redshift and capture the infrared signatures of the first galaxies. In its first two years of operations, JWST shattered previous theoretical models by discovering luminous, mature galaxies far earlier than standard cosmological simulations had predicted:

- **JADES-GS-z14-0 (z = 14.32):** Observed just 290 million years after the Big Bang, this galaxy spans over 1,600 light-years across and contains hundreds of millions of solar masses in stars, proving that star formation ignited with unexpected vigor deep inside the Dark Ages.
- **GN-z11 (z = 10.6):** Confirmed to host an active, luminous supermassive black hole accreting matter at over five times its theoretical Eddington limit just 400 million years after t=0.

Shakil Mahmud • Research Monograph

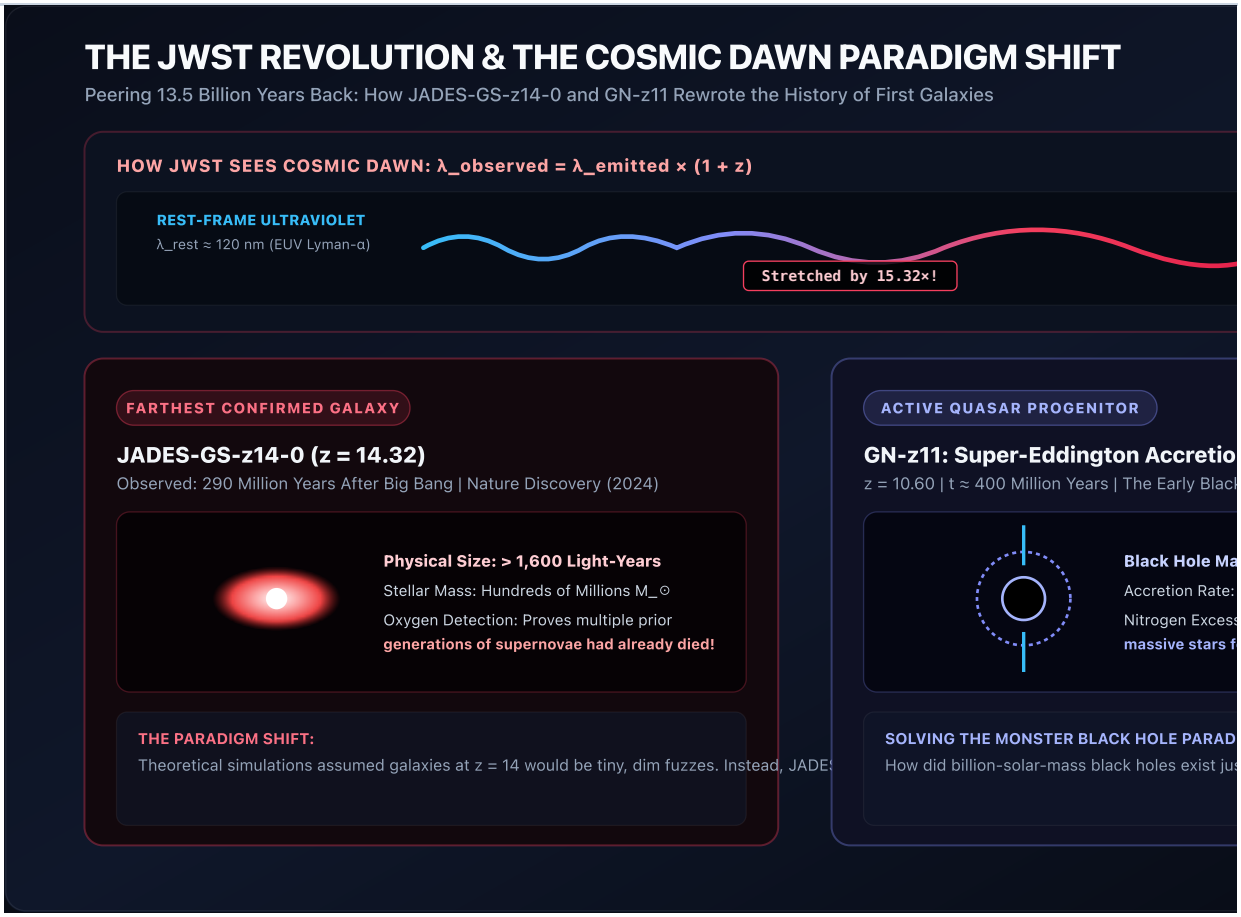


Figure 4.5: The High-Redshift Cosmic Dawn Revolution. Observations with the James Webb Space Telescope (such as JADES-GS-z14-0 at z = 14.32, just 290 million years post-Big Bang) revealed unexpectedly luminous, massive early galaxies. This requires hyper-efficient early gas accretion, top-heavy initial mass functions, or direct-collapse supermassive black hole seeds.

Chronology Table: From Dark Ages to Cosmic Dawn

Cosmic Epoch	Redshift (z)	Time Elapsed (t)	Characteristic Phenomena
Dark Ages Minimum	z ≈ 30–50	50–100 Myr	Cold dark matter mini-halos (10^5–10^6 $M_\odot$) form; pristine gas accumulates; H_2 cooling initiates.
Ignition of Population III Stars	z ≈ 20–30	100–180 Myr	First stars ignite; masses 50–300 $M_\odot$; $T_{eff} > 100$, K; EUV radiation carves first Strömgren spheres.
First Supernovae & Chemical Enrichment	z ≈ 15–20	180–270 Myr	Pair-instability supernovae obliterate first stars; first carbon, oxygen, and iron enrich the intergalactic medium; Population II star formation begins.
Proto-Galaxy Assembly	z ≈ 10–15	270–480 Myr	Mergers of mini-halos create first dwarf galaxies (JADES-GS-z14-0, GN-z11); early black hole seeds grow via rapid accretion.
Overlap & Completion of Reionization	z ≈ 6–8	650 Myr to 1 Gyr	Ionized bubbles merge; intergalactic medium reaches >99.9\% ionization; Gunn-Peterson trough clears.

The Legacy: A Chemically Transformed Universe

The reign of Population III stars was brief, violent, and utterly transformative. Before them, the universe was sterile, composed solely of hydrogen and helium. Through their fierce thermonuclear cores and cataclysmic pair-instability deaths, these ancient titans synthesized and dispersed the universe's first heavy nuclei—the initial carbon, oxygen, nitrogen, and magnesium.

Once the metallicity of gas clouds crossed a critical threshold ($Z_{crit} \approx 10^{-5.5} Z_\odot$), dust grains formed, efficient fine-structure cooling took over, and the cosmos transitioned forever to **Population II stellar generations**—smaller, stable stars capable of forming solar systems. In **Part 5** of *The Universal Chronicle*, we will explore the great stellar alchemists that followed: **The Alchemists of the Universe — Stellar Nucleosynthesis, Supernovae, and the Forging of Heavy Elements**.

Academic Citations & Foundational Literature

- **Barkana, R., & Loeb, A. (2001).** "In the beginning: the first sources of light and the reionization of the universe." *Physics Reports*, 349(2), 125–238. doi:10.1016/S0370-1573(01)00019-9.
- **Bromm, V., & Larson, R. B. (2004).** "The First Stars." *Annual Review of Astronomy and Astrophysics*, 42(1), 79–118. doi:10.1146/annurev.astro.42.053102.134034.
- **Heger, A., & Woosley, S. E. (2002).** "The Nucleosynthetic Signature of Population III." *The Astrophysical Journal*, 567(1), 532–543. doi:10.1086/338487.
- **Fan, X., Carilli, C. L., & Keating, B. (2006).** "Observational Constraints on Cosmic Reionization." *Annual Review of Astronomy and Astrophysics*, 44(1), 415–462. doi:10.1146/annurev.astro.44.051905.092521.
- **Robertson, B. E., et al. (2015).** "Cosmic reionization and early star-forming galaxies: a joint analysis of new constraints from Planck and the Hubble Space Telescope." *The Astrophysical Journal Letters*, 802(2), L19. doi:10.1088/2041-8205/802/2/L19.
- **Carniani, S., et al. (JADES Collaboration) (2024).** "A shining cosmic dawn: spectroscopic confirmation of two luminous galaxies at z ~ 14." *Nature*, 633, 318–322. doi:10.1038/s41586-024-07680-y.
- **Gunn, J. E., & Peterson, B. A. (1965).** "On the Density of Neutral Hydrogen in Intergalactic Space." *The Astrophysical Journal*, 142, 1633–1636. doi:10.1086/148444.

Citation: Mahmud, S. (2026). "Cosmic Dawn — Population III Hyperstars, the First Galaxies, and Reionization." In The Universal Chronicle, Part 4. https://shakilmahmud.com/universal-chronicle-part-4-cosmic-dawn/

Shakil Mahmud • Research Monograph

SHAKIL MAHMUD RESEARCH MONOGRAPHS • PART V

The Alchemists of the Universe — Stellar Nucleosynthesis, Supernovae, and the Forging of Heavy Elements

The Alchemists of the Universe — Stellar Nucleosynthesis, Supernovae, and the Forging of Heavy Elements

2,322 words • October 30, 2026 • Permanent URI



Plate V: *Figure: Concentric onion-shell burning within a massive supergiant star and the terminal core-collapse supernova explosion, forging carbon, oxygen, silicon, and iron before rapid neutron-capture (r-process) disseminates gold and uranium across the cosmos.*

The Big Bang was a profoundly conservative chemist: in its opening minutes, it synthesized only the simplest elements—hydrogen, helium, and a trace of lithium. Left to itself, the universe would have remained an inert cosmic desert incapable of producing rocks, water, or life. To build a living universe, the cosmos required alchemists: massive stars that crushed light nuclei into the rich periodic table within their searing cores, died in cataclysmic supernova detonations, and collided as neutron stars to scatter the building blocks of planets across interstellar space.

The Stellar Engine: How Stars Defy Coulomb Repulsion

Every atomic nucleus carries a positive electric charge proportional to its atomic number (Z). Because like charges repel according to Coulomb's law, two approaching nuclei experience an electrostatic repulsion barrier that grows exponentially as they draw nearer:

$$U_C(r) = \frac{Z_1 Z_2 e^2}{4\pi\varepsilon_0 r}$$

In classical Newtonian mechanics, for two protons to collide and fuse, the core temperature of a star would have to exceed 10^9 K—a temperature that ordinary main-sequence stars like our Sun (T_{core} ≈ 1.5 × 10^ K) never reach. How, then, do stars shine?

Quantum Tunneling and the Gamow Window
In 1928, George Gamow discovered that quantum mechanics allows particles to behave as wavefunctions. Even when a proton lacks the classical kinetic energy to climb the Coulomb barrier, there is a finite probability (P ≈ exp(-2π η_G)) that it will **tunnel directly through the barrier** into the attractive domain of the strong nuclear force (r ≈ 10^{-15} m). The convolution of the Maxwell-Boltzmann energy distribution and the quantum tunneling probability creates a narrow energy sweet spot—the **Gamow Window**—where stellar fusion takes place.

In stars with masses similar to our Sun (M ≤ 1.3 M_ ⊙), hydrogen fuses into helium primarily via the **Proton-Proton (p-p) Chain**, releasing 26.73 MeV per Helium-4 nucleus. In stars heavier than 1.3 M_ ⊙ , where core temperatures exceed 1.8 × 10^ K, the **CNO (Carbon-Nitrogen-Oxygen) Cycle** dominates, using carbon, nitrogen, and oxygen nuclei as nuclear catalysts to fuse protons at a rate proportional to T^{16}–T^{20}.

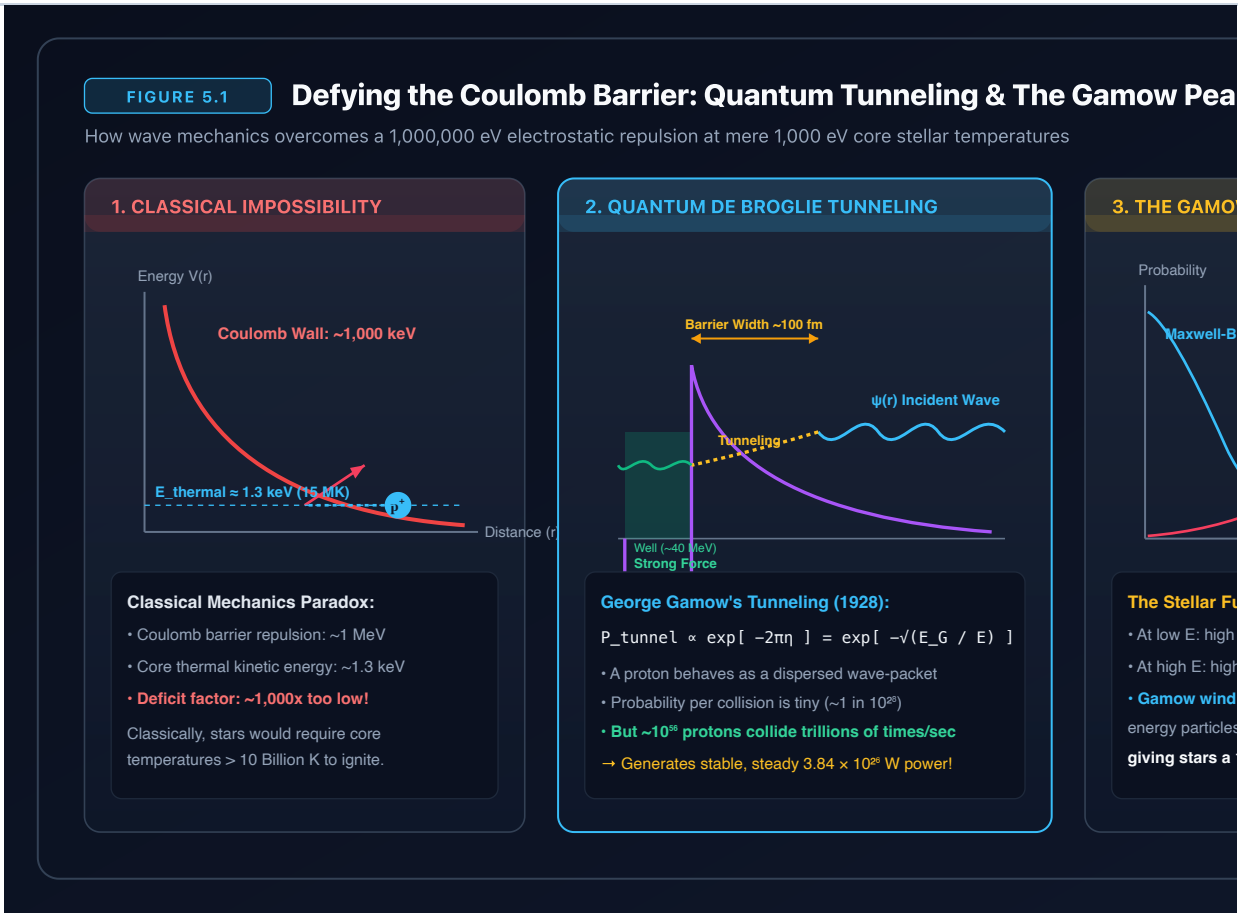


Figure 5.1: Defying the Coulomb Barrier (Quantum Tunneling & The Gamow Peak). Positively charged protons face a 1,000,000 eV electrostatic repulsion wall that thermal kinetic energy (1.3 keV at 15 MK) could never overcome classically. By treating protons as de Broglie matter waves, quantum mechanical barrier penetration multiplied by the Maxwell-Boltzmann thermal tail isolates a narrow energy sweet spot—the Gamow Peak (15–25 keV)—enabling stable stellar burning across billions of years.

The Onion-Skin Crucible: Burning Stages of a 25 $M_\odot$ Supergiant

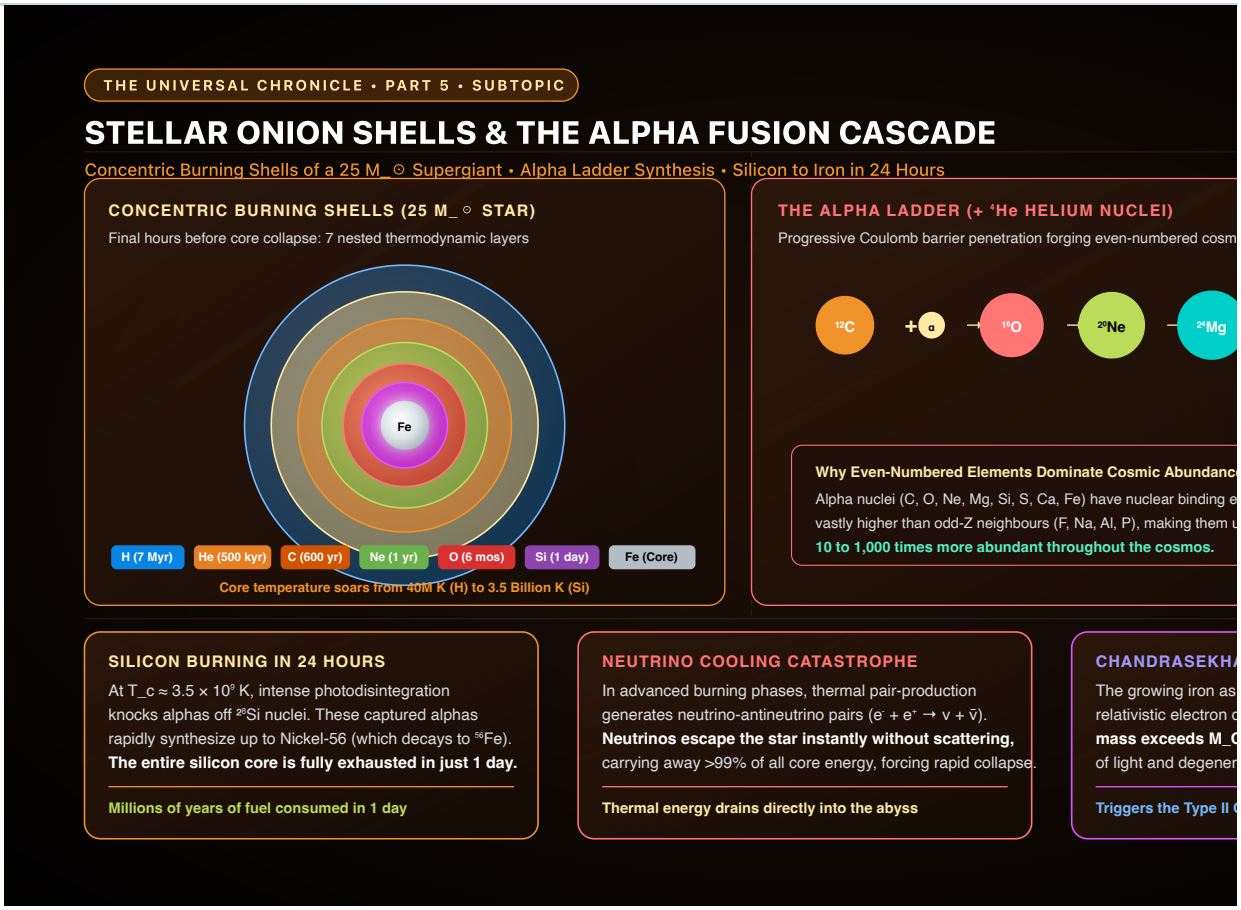
When a star with mass $M \geq 8\ M_\odot$ exhausts its central core hydrogen, hydrostatic equilibrium is disrupted. With radiation pressure diminished, gravity compresses the inert helium core, driving core temperatures up to 2×10^8 K and densities to 10^4 g/cm^3. At this threshold, the **Triple-Alpha Process** ignites:

$$3\,{}^4\mathrm{He} \rightarrow {}^{12}\mathrm{C} + \gamma \quad \text{followed by} \quad {}^{12}\mathrm{C} + {}^4\mathrm{He} \rightarrow {}^{16}\mathrm{O} + \gamma$$

This cycle of exhaustion, gravitational contraction, heating, and ignition repeats with increasing speed and violence, transforming the interior of a massive evolved star into a concentric **onion-skin structure** of burning nuclear shells:

- **1. Hydrogen Burning Shell (T ~ 4 × 10^ K):** Fuses hydrogen into helium. Duration: ≈ 7 million years.
- **2. Helium Burning Shell (T ~ 2 × 10^ K):** Fuses helium into carbon and oxygen. Duration: ≈ 500,000 years.
- **3. Carbon Burning Shell (T ~ 8 × 10^ K):** Fuses ${}^{12}\mathrm{C} + {}^{12}\mathrm{C} \rightarrow {}^{20}\mathrm{Ne}, {}^{24}\mathrm{Mg}, {}^{23}\mathrm{Na}$. Duration: ≈ 600 years.
- **4. Neon Burning Shell (T ~ 1.5 × 10^ K):** Photodisintegrates neon, triggering alpha capture: ${}^{20}\mathrm{Ne}(\alpha,\gamma){}^{24}\mathrm{Mg}$. Duration: ≈ 1 year.
- **5. Oxygen Burning Shell (T ~ 2.0 × 10^ K):** Fuses ${}^{16}\mathrm{O} + {}^{16}\mathrm{O} \rightarrow {}^{28}\mathrm{Si}, {}^{32}\mathrm{S}, {}^{31}\mathrm{P}$. Duration: ≈ 6 months.
- **6. Silicon Burning Core (T ~ 3.5 × 10^ K):** Photodisintegration rearrangement creates a rapid alpha-capture cascade up to ${}^{56}\mathrm{Ni}$, which decays into ${}^{56}\mathrm{Fe}$. Duration: **Barely 24 hours!**

Shakil Mahmud • Research Monograph



Concentric Onion-Skin Fusion Shells & The Alpha Ladder in a $25M_{\odot}$ Supergiant. Hydrostatic equilibrium drives progressive core compression, reaching $T_c \approx 3.5 \times 10^9$ K in the central silicon engine. Successive alpha-particle captures ($+^4$He) forge the dominant cosmic elements (^{12}C $\rightarrow^{16}$ O $\rightarrow^{20}$ Ne $\rightarrow^{24}$ Mg $\rightarrow^{28}$ Si $\rightarrow^{56}$ Ni $\rightarrow^{56}$ Fe), burning from 7 million years for hydrogen down to a terminal 24-hour sprint for silicon.

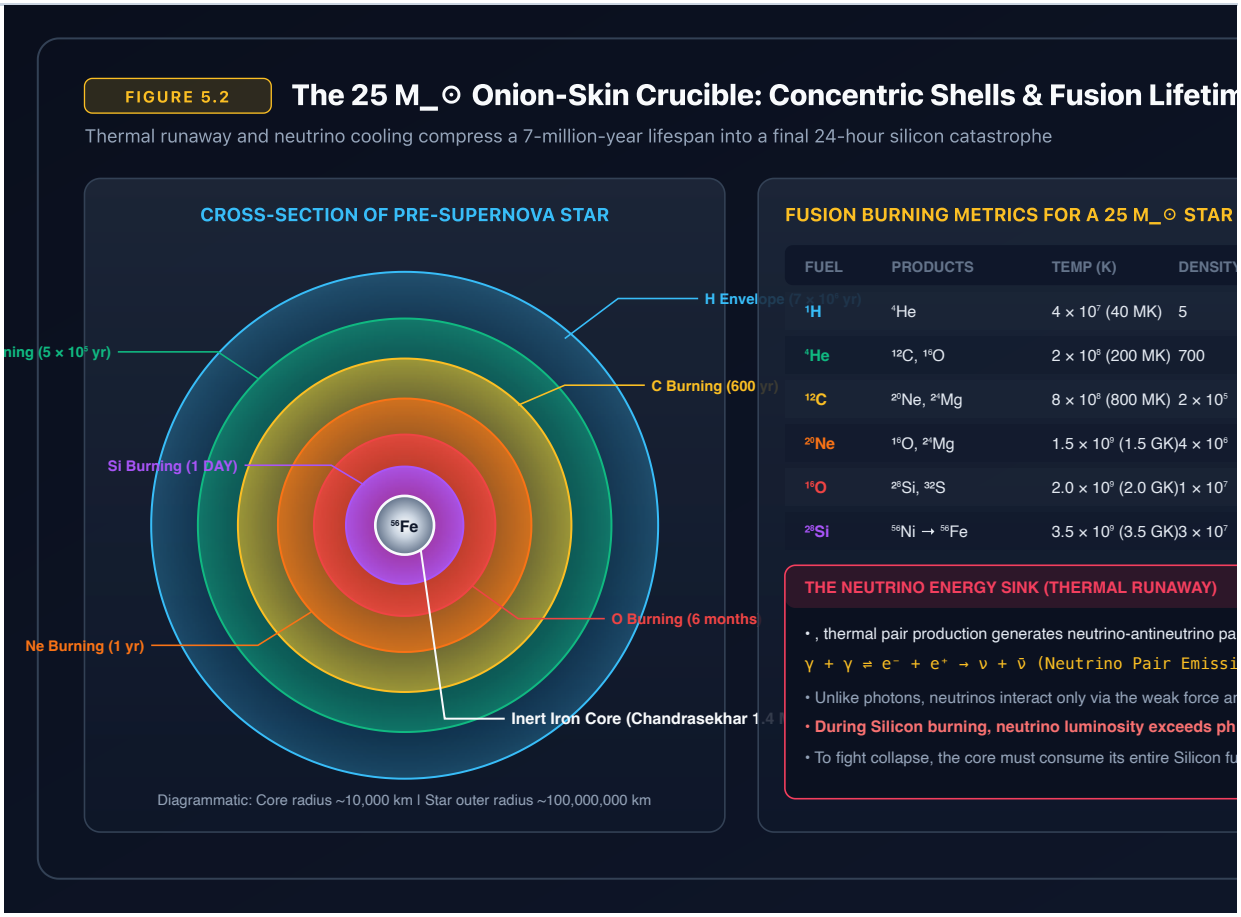


Figure 5.2: The Concentric Onion-Skin Crucible & Fusion Lifetimes. As massive stars exhaust successive core fuels, higher temperatures ignite outer concentric burning shells around an ever-denser core. Above 1 billion Kelvin, runaway pair-production neutrino emission drains energy straight into the vacuum, compressing a 7-million-year hydrogen lifespan into 600 years for carbon, 6 months for oxygen, and a frantic 24-hour terminal sprint for silicon.

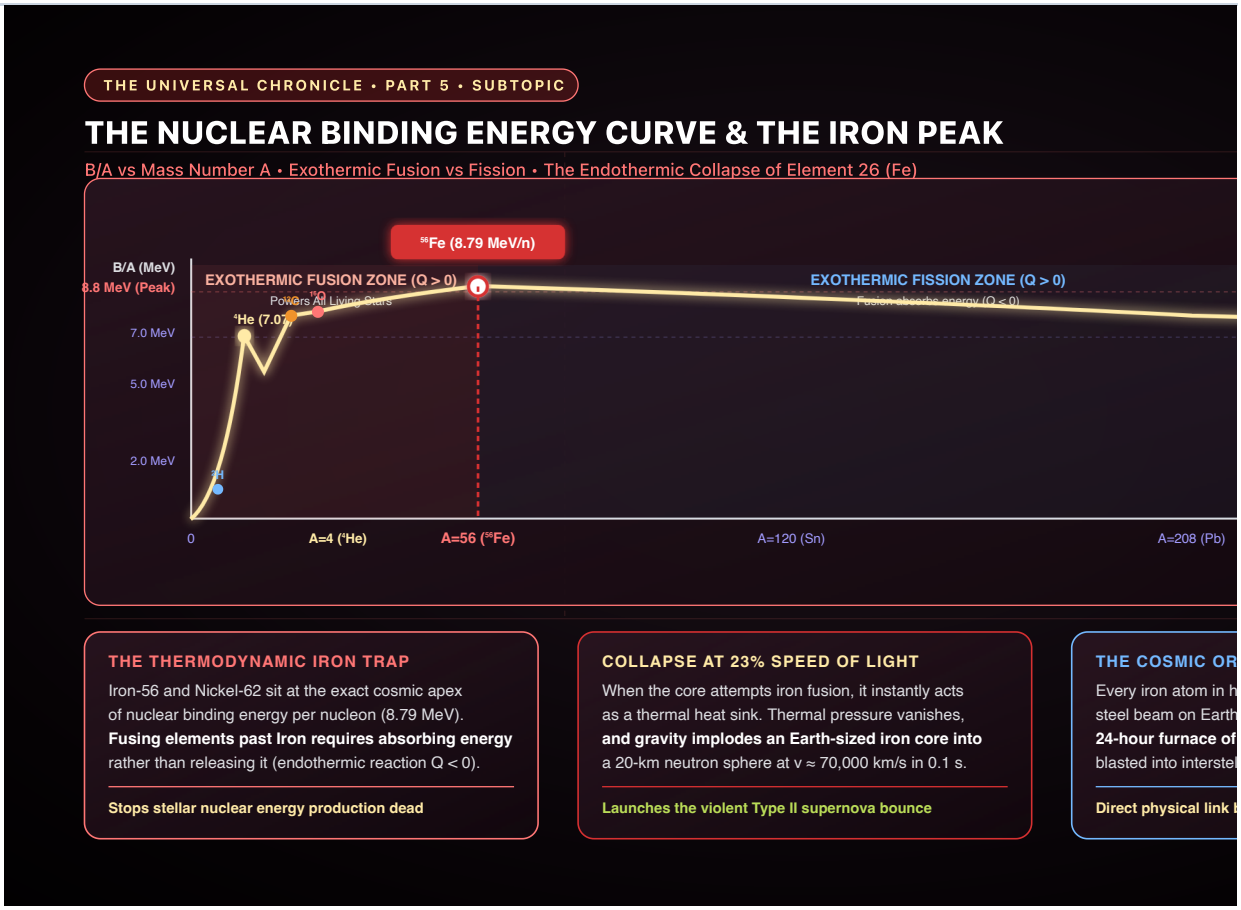
The Iron Catastrophe: Why Fusion Halts at Element 26

For millions of years, the star fought off gravitational collapse through exothermic nuclear fusion: whenever light nuclei fuse, the resulting nucleus has a lower mass than its constituents ($E = \Delta m c^2$), and the mass defect is converted into thermal radiation pressure that supports the weight of the star.

However, the binding energy per nucleon curve peaks precisely at the iron-group nuclei—specifically **Nickel-62, Iron-58, and Iron-56** (B/A ≈ 8.8 MeV per nucleon):

The Thermodynamic Valley of Stability
Iron-56 has zero extractable nuclear fusion energy. Attempting to fuse iron with another nucleus is strictly **endothermic**—it absorbs thermal energy from the core rather than releasing it. The moment an iron core accumulates inside a massive star, the nuclear engine dies. The thermal pressure supporting the core drops to zero in a fraction of a second.

Shakil Mahmud • Research Monograph



The Nuclear Binding Energy Curve & The Iron Peak Catastrophe. Binding energy per nucleon (B/A) peaks at Iron-56 and Nickel-62 ($8.79\ \text{MeV/nucleon}$). To the left, exothermic fusion (Q > 0) powers living stars; to the right, exothermic fission (Q > 0) operates. Fusing iron is strictly endothermic (Q < 0), stealing core thermal heat and triggering gravitational collapse at 23% the speed of light within 100 milliseconds.

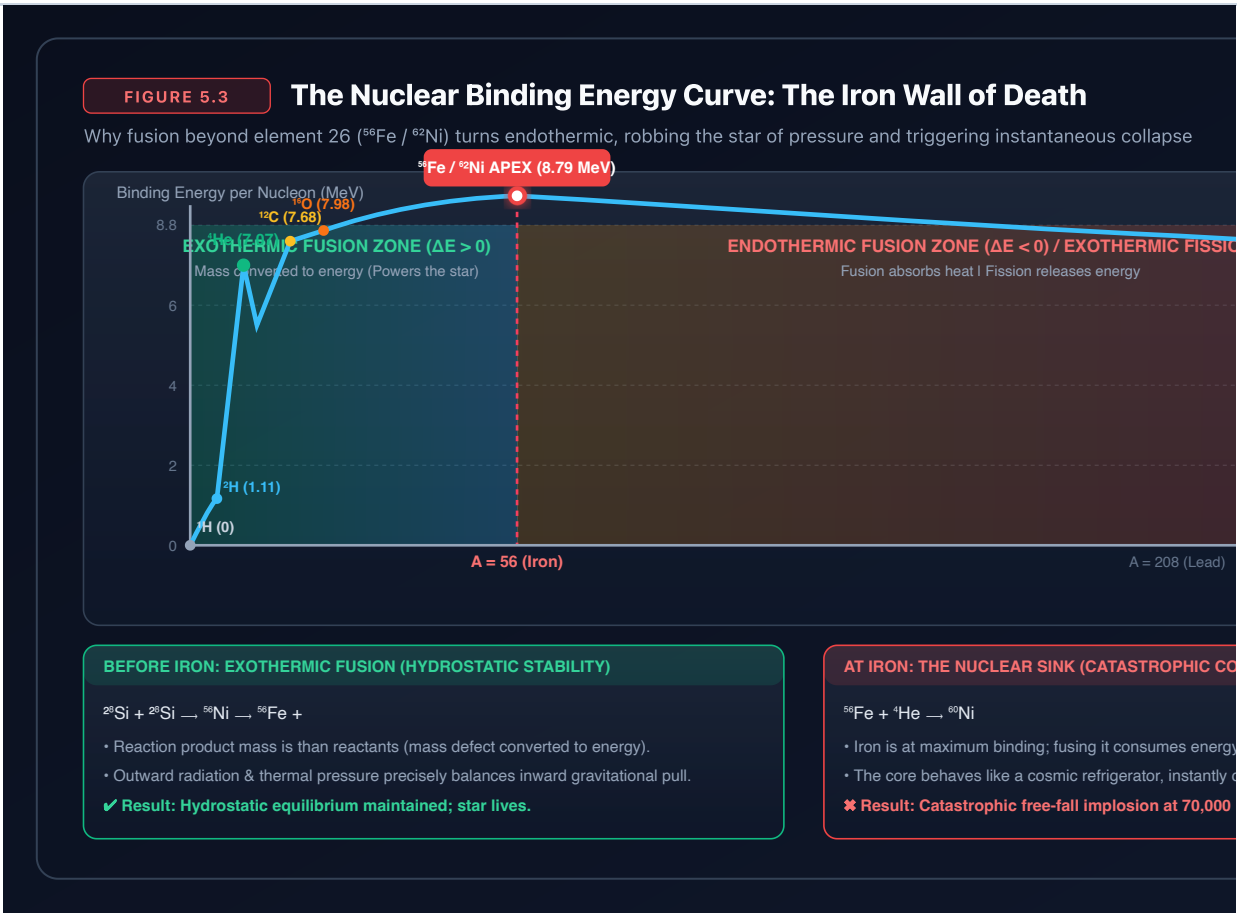


Figure 5.3: The Nuclear Binding Energy Curve & The Iron Wall of Death. Nuclear binding energy per nucleon peaks at Iron-56 (8.79 MeV) and Nickel-62 (8.795 MeV). Nucleosynthesis prior to iron is exothermic (yielding net energy to resist gravity); fusing past iron is endothermic, actively absorbing heat from the core and causing immediate loss of thermal pressure support.

Core-Collapse Supernovae: When a Star Rebounds off Nuclear Density

Once the mass of the iron core exceeds the **Chandrasekhar Mass Limit** (M_{Ch} ≈ 1.44 M_ ⊙), electron degeneracy pressure—the quantum resistance of electrons against occupying identical quantum states—can no longer withstand gravity. The core collapses catastrophically:

1. Electron Capture & Photodisintegration (Milliseconds 0 to 100)

As density surges past 10^{11} g/cm^3, energetic gamma rays smash into iron nuclei, shattering them back into alpha particles and free neutrons (photodisintegration). Simultaneously, electrons are crushed directly into protons via electron capture (inverse beta decay):

$$p + e^- \rightarrow n + \nu_e$$

This process completely neutralizes the core into a ball of pure neutrons, draining the core of electron degeneracy pressure. The iron core—an object roughly the diameter of the Earth—collapses down to a sphere just **20 kilometers in diameter** in less than **100 milliseconds**, plunging inward at nearly 25% of the speed of light (70,000 km/s).

2. The Nuclear Rebound and the Neutrino Shockwave

When the core reaches nuclear saturation density (ρ_nuc ≈ 3 × 10^{14} g/cm^3), the strong nuclear force suddenly transitions from attractive to fiercely repulsive. **Neutron degeneracy pressure** halts the collapse like an unyielding concrete wall. The infalling outer core slams into this rigid ball of nuclear matter and **rebounds**, creating an outwards-propagating supersonic shockwave.

Although the shock initially stalls as it tears through the outer iron mantle, it is revitalized by an unfathomable flood of neutrinos escaping the proto-neutron star. A core-collapse supernova unleashes **10^{46} Joules of energy (10^{53} ergs)**—more energy than our Sun will radiate in its entire 10-billion-year lifetime. Astonishingly, **99% of this energy is carried away by neutrinos**, 1% becomes kinetic energy blasting the star apart, and barely 0.01% is emitted as visible light.

For several weeks, the exploding star outshines its entire host galaxy of hundreds of billions of stars, hurtling tens of solar masses of synthesized carbon, oxygen, neon, and silicon across interstellar space at 10,000 km/s.

Shakil Mahmud • Research Monograph

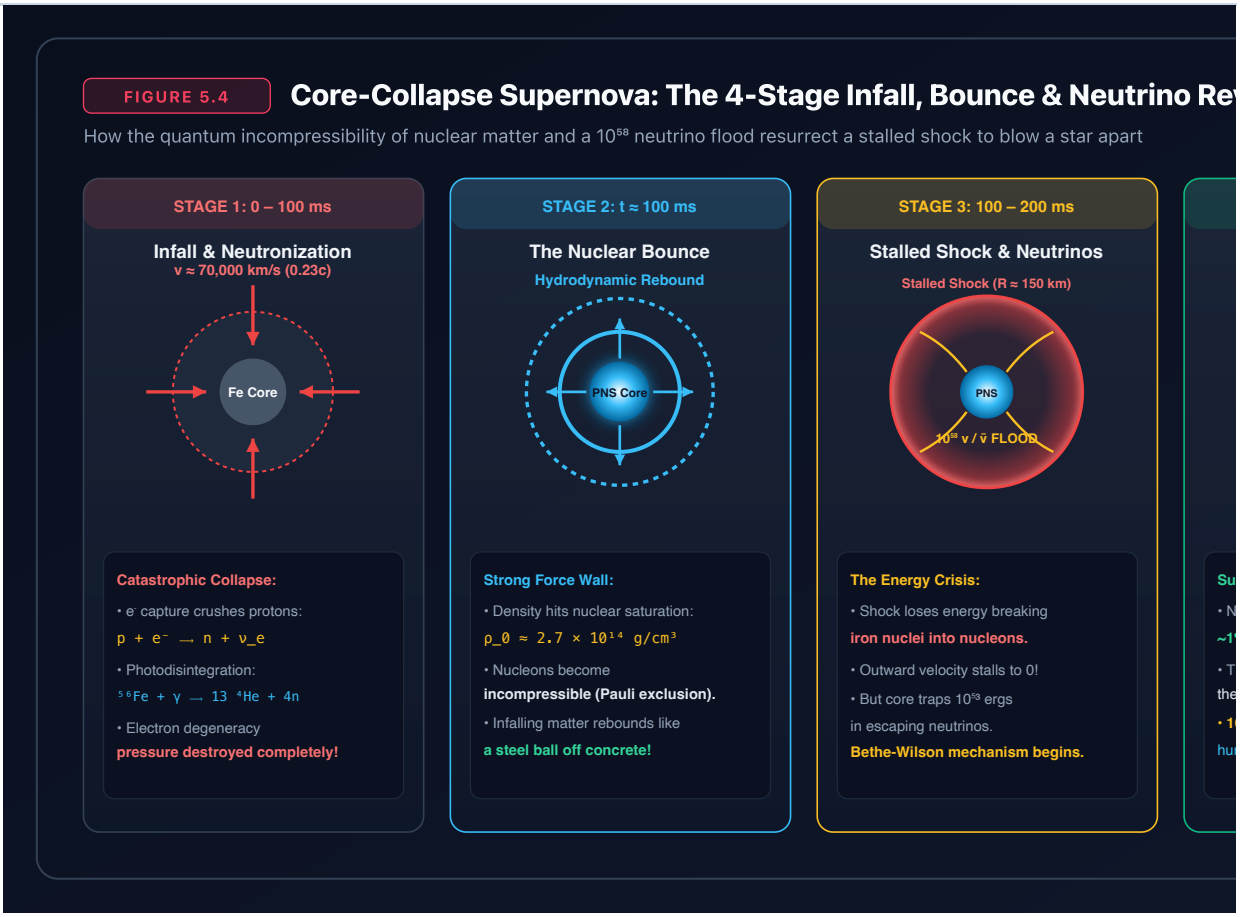


Figure 5.4: Core-Collapse Supernova Anatomy (Infall, Bounce & Neutrino Revival). Within 100 milliseconds, electron capture and photodisintegration trigger a free-fall collapse at 23% the speed of light. Rebounding off incompressible nuclear saturation density, the outgoing shock stalls in the dense infalling mantle until the Bethe-Wilson mechanism—1% neutrino energy reabsorption—revives the blastwave into a catastrophic 10^{44}-Joule supernova detonation.

Beyond Iron: The Slow (s) and Rapid (r) Neutron Capture Processes

Because fusion cannot produce elements heavier than iron, elements such as copper, zinc, silver, iodine, barium, gold, platinum, and uranium must be forged through **neutron capture**. Because neutrons carry zero electric charge, they experience no Coulomb repulsion barrier, slipping effortlessly into atomic nuclei:

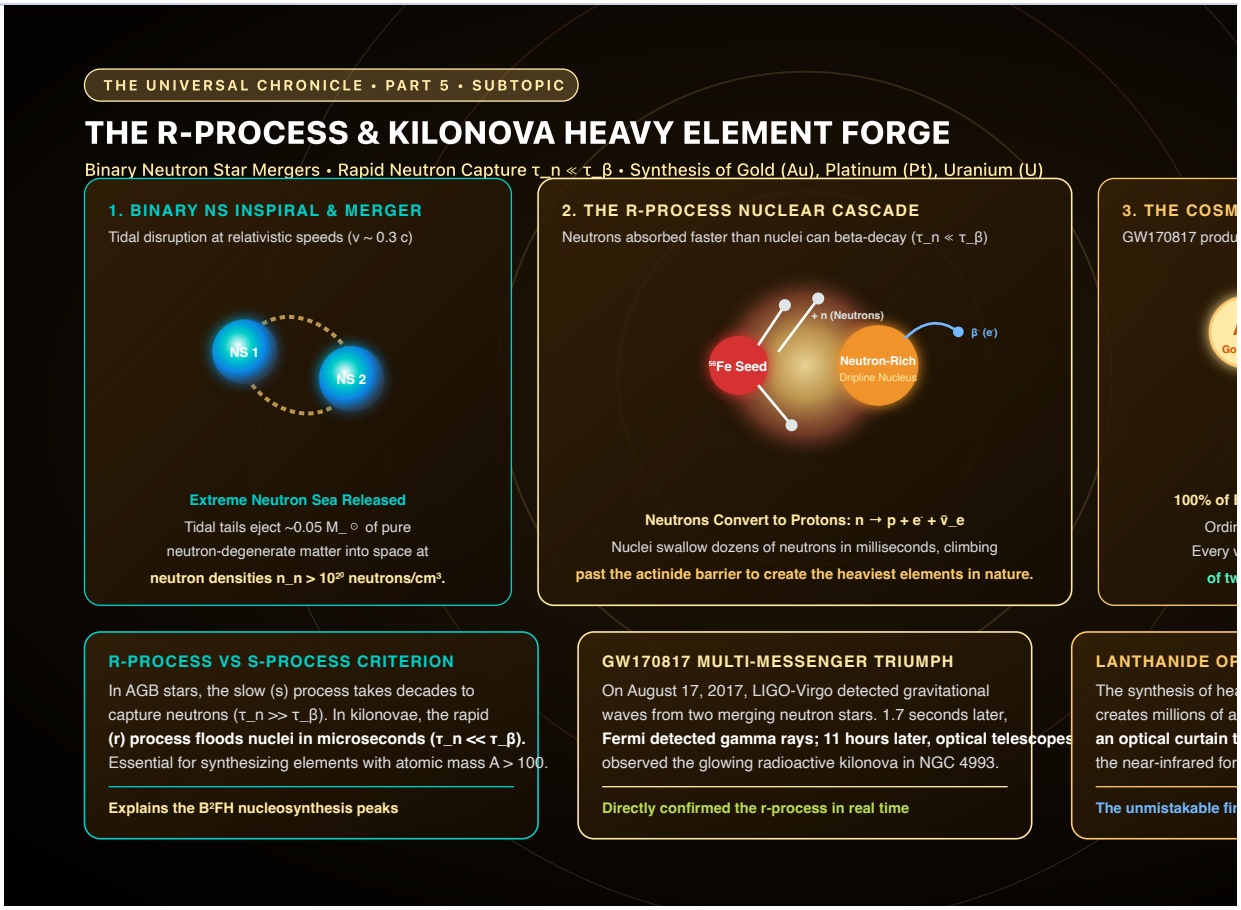
1. The s-Process (Slow Neutron Capture)

Occurs over thousands of years inside low- to intermediate-mass Asymptotic Giant Branch (AGB) stars. The neutron flux is low: an atomic nucleus captures a neutron, and if it becomes unstable, it has ample time to undergo beta decay ($n \rightarrow p + e^- + \bar{\nu}_e$) into a new element with a higher atomic number before the next neutron arrives. The s-process builds half of the elements heavier than iron, including **strontium, barium, yttrium, and lead**.

2. The r-Process (Rapid Neutron Capture in Kilonovae & Mergers)

Requires an extreme, violent environment where the neutron flux exceeds 10^{20} neutrons/cm^3/s. Nuclei are bombarded by hundreds of neutrons in a fraction of a second, bloated far out toward the "neutron drip line" before cascading down via successive beta decays into stable, heavy, neutron-rich elements.

In 2017, the LIGO-Virgo gravitational wave observatory detected **GW170817**: the inspiral and collision of two neutron stars in the galaxy NGC 4993. Follow-up observations across electromagnetic bands (from gamma rays to optical and infrared) confirmed the radioactive glow of a **Kilonova**. The merger synthesized and ejected over **ten times the mass of the Earth in pure gold and platinum**, proving conclusively that neutron star mergers are the primary cosmic forge of gold, platinum, europium, and uranium.



The Rapid Neutron-Capture (*r*-Process) Forge in Binary Neutron Star Mergers. Extreme relativistic collision (GW170817) floods ejecta with ultra-dense neutron flux (n_n > 10^{20}\text{ neutrons/cm}^{3}). Because neutron capture is thousands of times faster than beta decay ($\tau_n \ll \tau_\beta$), iron seed nuclei swell to the neutron dripline before beta-decaying into precious metals, synthesizing over 10 Earth masses of pure Gold (^{197}Au), Platinum (^{195}Pt), and Uranium (^{238}U).

Shakil Mahmud • Research Monograph

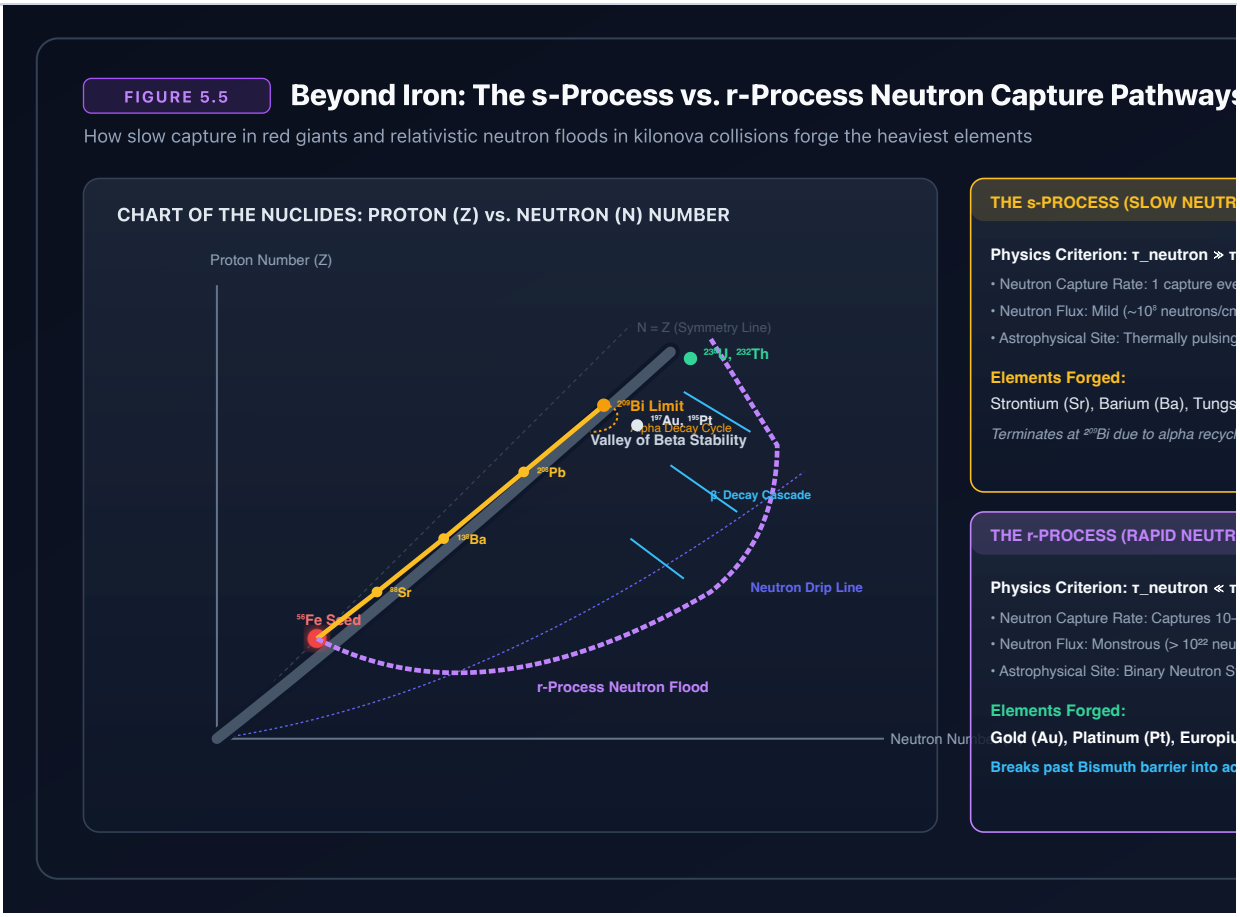


Figure 5.5: Forging Heavy Elements Beyond Iron (s-Process vs. r-Process). Elements heavier than iron require neutron capture free of Coulomb repulsion. The slow (s) process in pulsating AGB stars captures neutrons over decades, strictly following the Valley of Beta Stability up to Bismuth-209. The rapid (r) process in binary neutron star mergers (kilonovae) floods nuclei with over 10^{22} neutrons/cm^3, plunging into neutron-rich radioactive territory to forge gold, platinum, and uranium.

The Cosmic Genealogy of the Periodic Table

Origin Mechanism	Key Elements Synthesized	Cosmic Environment	Human / Terrestrial Importance
Big Bang Nucleosynthesis	Hydrogen (^{1}H), Helium (^{4}He), trace Lithium (^{7}Li)	Cosmic furnace (t = 3–20 min)	Water molecules (H_2O), stellar fuel for the Sun.
Low & Medium Mass Stars (AGB)	Carbon (^{12}C), Nitrogen (^{14}N), s-process (Sr, Ba, Pb)	Planetary nebulae & stellar winds	Organic chemistry, DNA/RNA backbones, amino acids.
Core-Collapse Supernovae (Type II)	Oxygen (^{16}O), Silicon (^{28}Si), Magnesium (^{24}Mg), Sulfur (^{32}S)	Massive exploding stars ($M > 8\ M_\odot$)	Atmospheric oxygen, rocky planetary crusts (SiO_2).
Type Ia Supernovae (White Dwarfs)	Iron (^{56}Fe), Nickel, Chromium, Cobalt	Thermonuclear explosion of degenerate white dwarf	Hemoglobin in blood, Earth's molten iron core & magnetic field.
Neutron Star Mergers (Kilonovae)	Gold (^{197}Au), Platinum (^{195}Pt), Uranium (^{238}U), Europium	Relativistic collision of two neutron stars	Heavy jewelry, nuclear fuel, geothermal heating of Earth's mantle.
Cosmic Ray Spallation	Boron (^{11}B), Beryllium (^{9}Be), Lithium (^{6}Li)	High-energy cosmic rays shattering nuclei	Trace minerals, high-tech industrial alloys.

Carl Sagan's Truism: We Are Star-Stuff

In 1957, Margaret Burbidge, Geoffrey Burbidge, William Fowler, and Fred Hoyle published their monumental paper *"Synthesis of the Elements in Stars"* (known universally as B^{2}FH), establishing the mathematical and nuclear architecture of stellar nucleosynthesis.

Their discovery revealed an extraordinary truth that astronomer Carl Sagan would later poeticize: **"The cosmos is within us. We are made of star-stuff. We are a way for the cosmos to know itself."**

The nitrogen in our DNA, the calcium in our bones, the iron in our red blood cells, and the silicon in our microchips were not created at the beginning of time. They were forged inside the crushing pressure of ancient stellar cores that lived and died billions of years before the Earth existed. When those stars perished in fire, they hurled their ashes across the galaxy, enriching the interstellar gas clouds that would one day coalesce into our solar system.

In **Part 6** of *The Universal Chronicle*, we will examine how these enriched clouds gathered into majestic rotating disk galaxies: **The Architecture of Galaxies — Spiral Arms, Supermassive Black Holes, and the Milky Way**.

Academic Citations & Foundational Literature

- **Burbidge, E. M., Burbidge, G. R., Fowler, W. A., & Hoyle, F. (1957).** "Synthesis of the Elements in Stars." *Reviews of Modern Physics*, 29(4), 547–650. doi:10.1103/RevModPhys.29.547.
- **Bethe, H. A. (1939).** "Energy Production in Stars." *Physical Review*, 55(5), 434–456. doi:10.1103/PhysRev.55.434.
- **Woosley, S. E., Heger, A., & Weaver, T. A. (2002).** "The evolution and explosion of massive stars." *Reviews of Modern Physics*, 74(4), 1015–1071. doi:10.1103/RevModPhys.74.1015.
- **Abbott, B. P., et al. (LIGO Scientific Collaboration and Virgo Collaboration) (2017).** "GW170817: Observation of Gravitational Waves from a Binary Neutron Star Inspirall." *Physical Review Letters*, 119(16), 161101. doi:10.1103/PhysRevLett.119.161101.
- **Thielemann, F.-K., et al. (2011).** "What are the sources of the r-process?" *Progress in Particle and Nuclear Physics*, 66(2), 346–353. doi:10.1016/j.ppnp.2011.01.032.
- **Nomoto, K., Kobayashi, C., & Tominaga, N. (2013).** "Nucleosynthesis in Stars and the Chemical Enrichment of Galaxies." *Annual Review of Astronomy and Astrophysics*, 51(1), 457–509. doi:10.1146/annurev-astro-082812-140956.

Citation: Mahmud, S. (2026). "The Alchemists of the Universe — Stellar Nucleosynthesis, Supernovae, and the Forging of Heavy Elements." In The Universal Chronicle, Part 5. https://shakilmahmud.com/universal-chronicle-part-5-the-alchemists-of-the-universe/

Shakil Mahmud • Research Monograph

SHAKIL MAHMUD RESEARCH MONOGRAPHS • PART VI

The Architecture of Galaxies — Spiral Arms, Supermassive Black Holes, and the Milky Way

The Architecture of Galaxies — Spiral Arms, Supermassive Black Holes, and the Milky Way

2,481 words • October 30, 2026 • Permanent URI



Plate VI: *Figure: Grand-design spiral structure of the Milky Way, stabilized by an invisible spherical dark matter halo and powered by accretion flows surrounding the supermassive black hole Sagittarius A* at the galactic nucleus.*

Galaxies are the great island empires of the cosmos—sprawling gravitational architectures containing hundreds of billions of stars, interstellar dust nurseries, and supermassive black holes. Far from being random clusters of stars, spiral galaxies like our Milky Way are dynamic, self-regulating machines shaped by the invisible scaffolding of dark matter halos, sculpted into graceful rotating disks by the conservation of angular momentum, and pinned in equilibrium around central gravitational singularities.

From Primordial Halos to Rotating Disks: Conservation of Angular Momentum

In the standard ΛCDM (Lambda Cold Dark Matter) cosmological framework, galaxies do not assemble in isolation. They form at the intersections of the **Cosmic Web**—a vast, sponge-like network of dark matter filaments woven during the first fractions of a second following the Big Bang.

As primordial gas fell into these dark matter potential wells, it was subjected to tidal gravitational torques from neighboring overdensities. This tidal shearing imparted a net orbital angular momentum (J) to the collapsing gas cloud. While dark matter particles are collisionless and remain suspended in a vast, spherical or triaxial halo, baryonic gas is collisional and dissipative: when gas clouds collide, they shock, heat up, and radiate away their thermal energy via electromagnetic radiation.

The Disk Formation Theorem
Because gas can radiate away kinetic energy parallel to the rotation axis through collisions, but cannot eliminate its net angular momentum perpendicular to the axis ($J = I\omega$ = constant), the collapsing gas cloud inevitably collapses along its rotational poles while resisting collapse along its equatorial plane. In a few hundred million years, a turbulent, three-dimensional spherical gas cloud is flattened into a thin, centrifugally supported, rotating **galactic disk**.

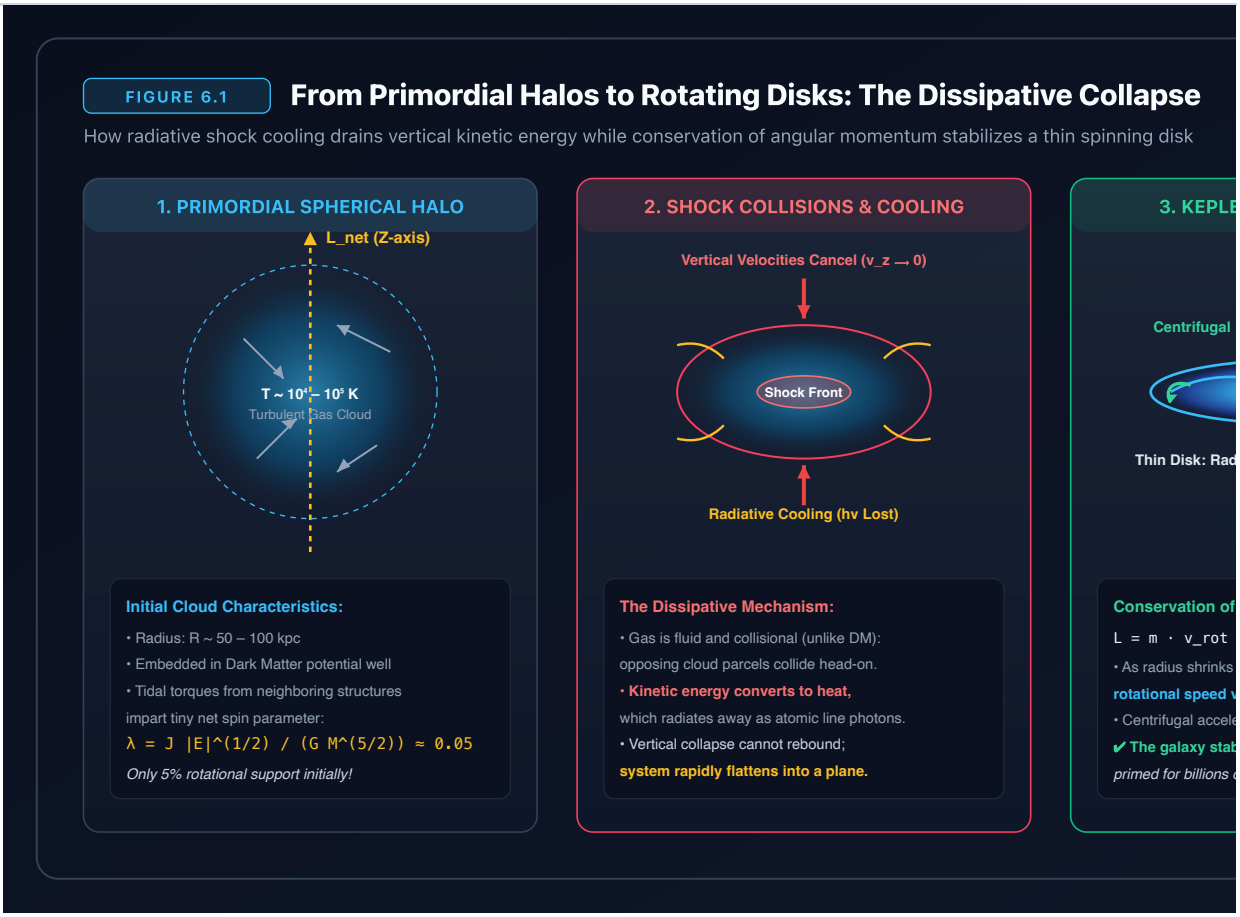


Figure 6.1: From Spherical Halo to Rotating Disk (The Dissipative Collapse). Gas embedded in a dark matter halo possesses a small initial spin ($\lambda \approx 0.05$). Unlike dark matter, colliding gas parcels undergo radiative shock cooling that cancels vertical kinetic energy ($v_z \to 0$), while conservation of angular momentum ($L = m \cdot v \cdot r$) halts radial collapse once centrifugal force balances gravity, settling into a stable, razor-thin rotating disk.

The Winding Dilemma: Why Spiral Arms Are Not Physical Structures

When astronomers in the early 20th century first photographed grand-design spiral galaxies like Messier 51 (the Whirlpool Galaxy), they encountered a fundamental mathematical paradox known as the **Winding Dilemma**.

Galaxies exhibit *differential rotation*: stars near the galactic center complete an orbit far faster than stars on the outer periphery. In the Milky Way, a star at 2 kpc orbits in ~ 50 million years, while our Sun at 8 kpc requires ~ 230 million years. If spiral arms were rigid, physical strings of stars tied together, the inner sections would wind tightly around the core like spaghetti on a fork, wiping out all visible spiral structure within two or three rotations (~ 500 million years). Yet, spiral galaxies have persisted with open, majestic arms for over ten billion years!

The Lin-Shu Density Wave Theory (1964)

In 1964, mathematicians **Chia-Chiao Lin and Frank Shu** formulated the definitive resolution: **spiral arms are not physical objects made of the same stars; they are propagating gravitational density waves**—cosmic traffic jams traveling through the galactic disk.

Shakil Mahmud • Research Monograph

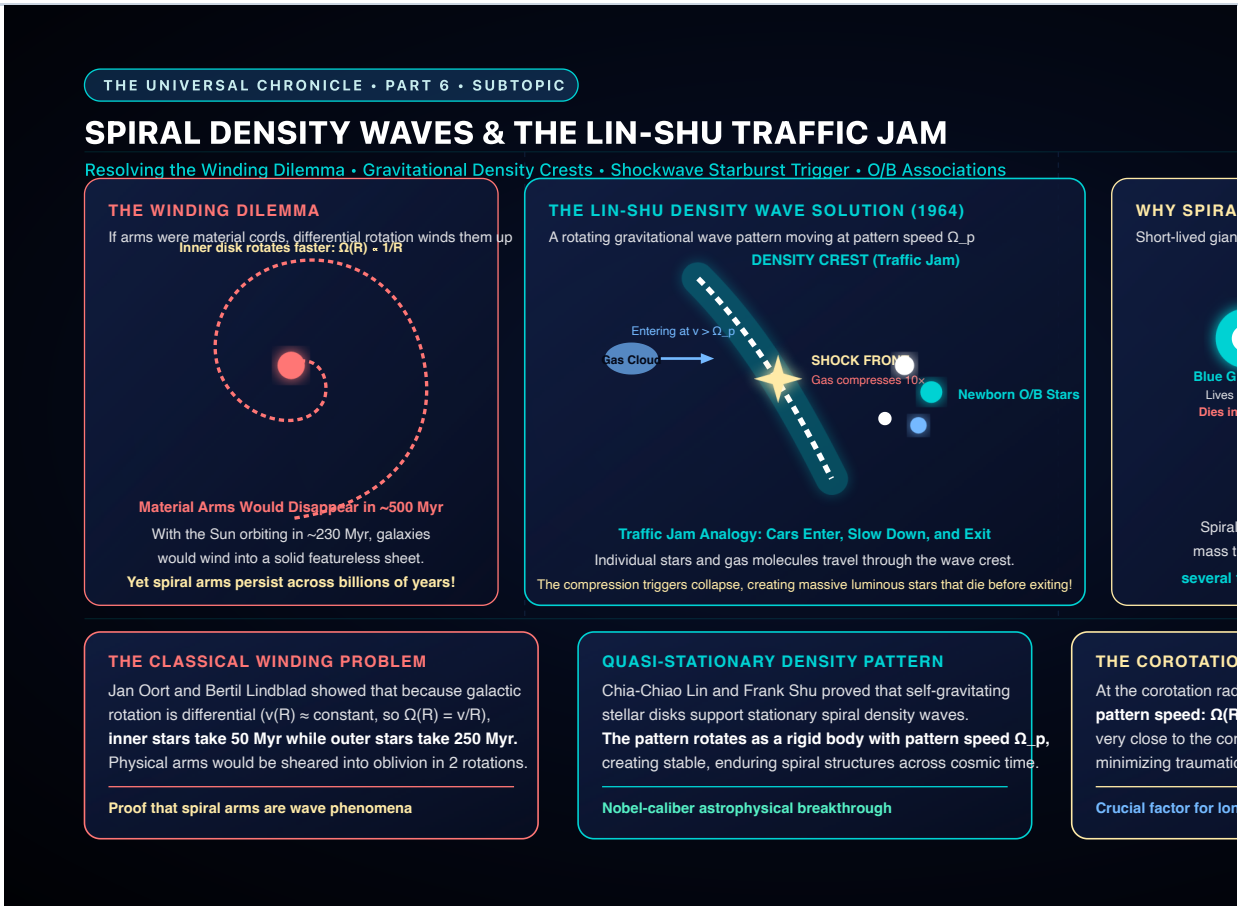


Figure 6.2a: Kinematic density wave mechanics and stellar traffic jam. As interstellar gas clouds orbit differentially into the rotating spiral potential well, shock compression triggers runaway gravitational collapse into luminous O- and B-type starburst clusters, illuminating the grand-design spiral arms before massive stars die in supernovae.

Consider a slow-moving highway truck: cars bunch together behind the truck, move slowly through the high-density cluster, and accelerate away once past it. The high-density traffic jam remains stationary or moves slowly, even though individual cars constantly enter and exit it. Similarly, stars and interstellar gas clouds orbit freely through the disk, moving in and out of the spiral arms:

- **Shock Compression:** As diffuse interstellar gas plows into the crest of a gravitational density wave, it is compressed violently, triggering gravitational collapse.
- **Starburst Nurseries:** The compressed gas fragments into dense molecular clouds, birthing thousands of bright, massive, hot O- and B-type stars.
- **Why Arms Look Blue:** Massive O/B stars are millions of times more luminous than ordinary stars, radiating intense blue-white light. Because these titans live only 5 to 20 million years, they die in supernovae before they can exit the other side of the spiral arm! Consequently, the spiral arms shine with brilliant electric blue starlight and pink hydrogen-emission (H II) nebulae, while older, yellow-red dwarf stars like our Sun disperse smoothly across the inter-arm disk.

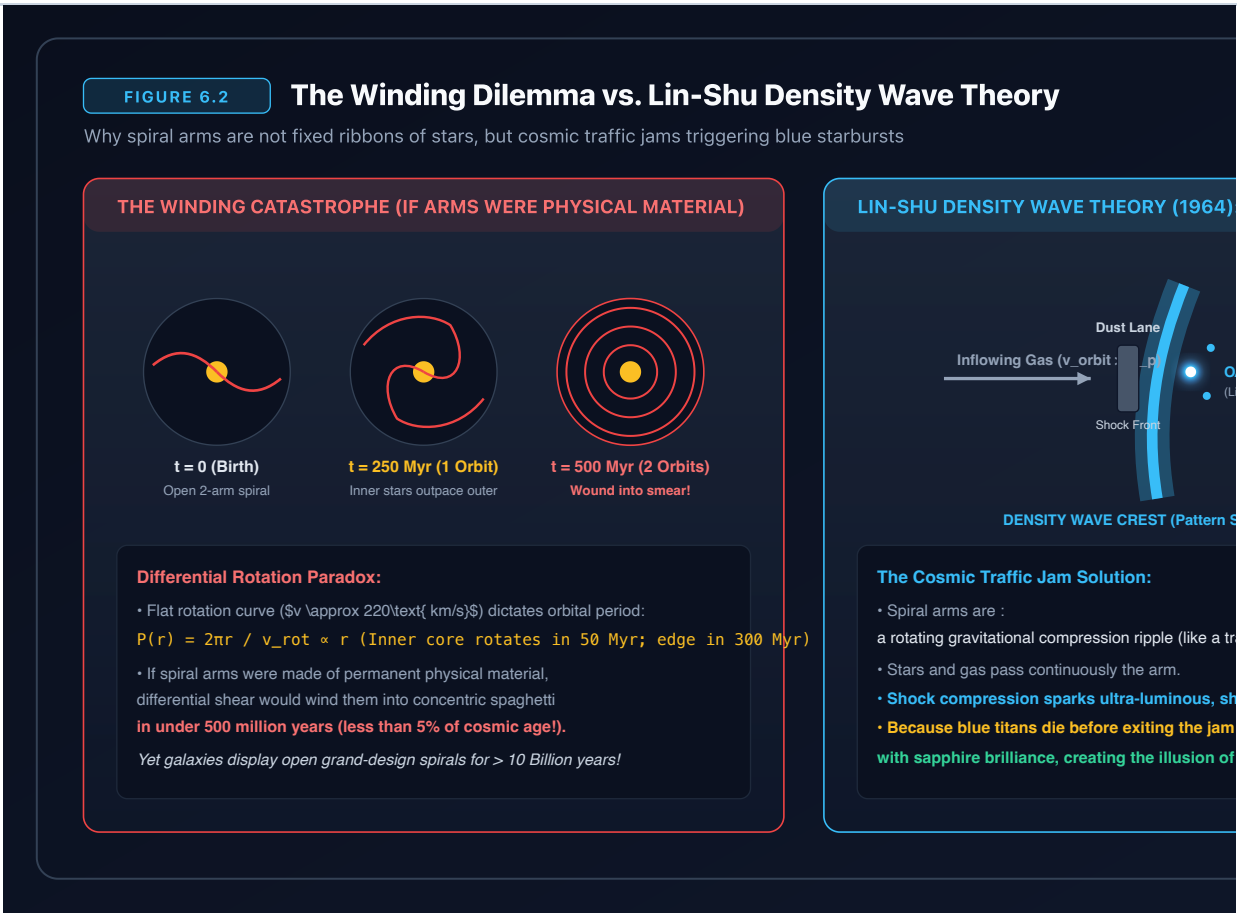


Figure 6.2: The Winding Dilemma vs. Lin-Shu Density Waves. If spiral arms were physical material, differential rotation would tightly wind and destroy them in under 500 million years. The Lin-Shu theory resolves this: spiral arms are rotating gravitational density compression waves (pattern speed Ω_p) through which interstellar gas flows, compresses into dark dust shock lanes, and sparks brilliant blue O/B starbursts before exiting.

The Heart of the Whirlpool: Supermassive Black Holes and Co-Evolution

At the exact gravitational center of virtually every massive galaxy lies a gravitational monster: a **Supermassive Black Hole (SMBH)** containing millions to billions of times the mass of the Sun. In the heart of our own Milky Way, concealed behind 26,000 light-years of obscuring interstellar dust in the constellation Sagittarius, lies **Sagittarius A* (Sgr A*)**—a singularity possessing a mass of $\mathbf{4.297 \pm 0.012 \times 10^6\ M_\odot}$, confined within a volume smaller than the orbit of Mercury.

For decades, astronomers debated whether central black holes were passive byproducts of galaxy formation or active directors. In the early 2000s, astrophysicists discovered the **M–σ Relation** (Ferrarese & Merritt, Gebhardt et al.):

$$M_{\rm BH} \propto \sigma_*^{4\ \text{to}\ 5}$$

There exists an astonishingly tight power-law correlation between the mass of a galaxy's central black hole (M_{BH}) and the velocity dispersion (σ_*) of stars in the galaxy's central bulge—even though the black hole's direct gravitational pull extends only a few light-years, while the stellar bulge spans tens of thousands of light-years! How could a tiny central speck dictate the kinematics of an entire galaxy?

Active Galactic Nucleus (AGN) Feedback

The answer is **AGN Feedback**. In the early universe, when immense inflows of cold gas plunged into the galactic center, the black hole accreted matter at ferocious rates, becoming an ultra-luminous *Quasar*. The accretion disk radiated colossal energies, launching relativistic plasma jets and radiation-driven winds at thousands of kilometers per second. These winds blasted through the host galaxy, heating and expelling the cold gas required for star formation—effectively "quenching" the galaxy and shutting down both star birth and black hole growth simultaneously. Galaxies and their central black holes grew in intimate lockstep.

Shakil Mahmud • Research Monograph

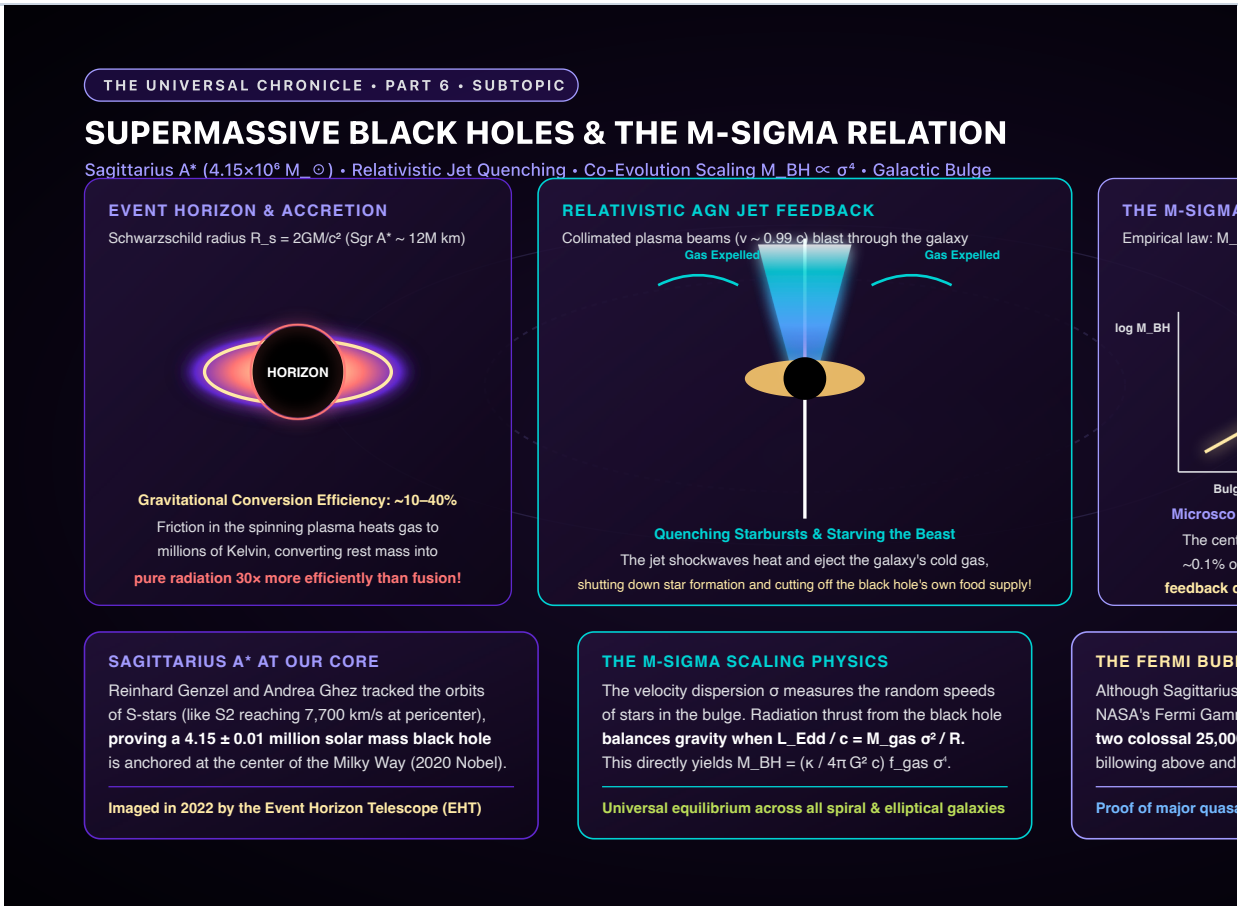


Figure 6.3a: Quasar wind feedback and the SMBH M\text{–}\sigma co-evolution law. Relativistic plasma jets and radiation pressure driven by the accretion disk of Sagittarius A* sweep cool star-forming molecular gas out of the central bulge, terminating star formation and locking black hole mass in strict power-law proportion to stellar velocity dispersion ($M_{\rm BH} \propto \sigma_*^{4\ \text{to}\ 5}$).

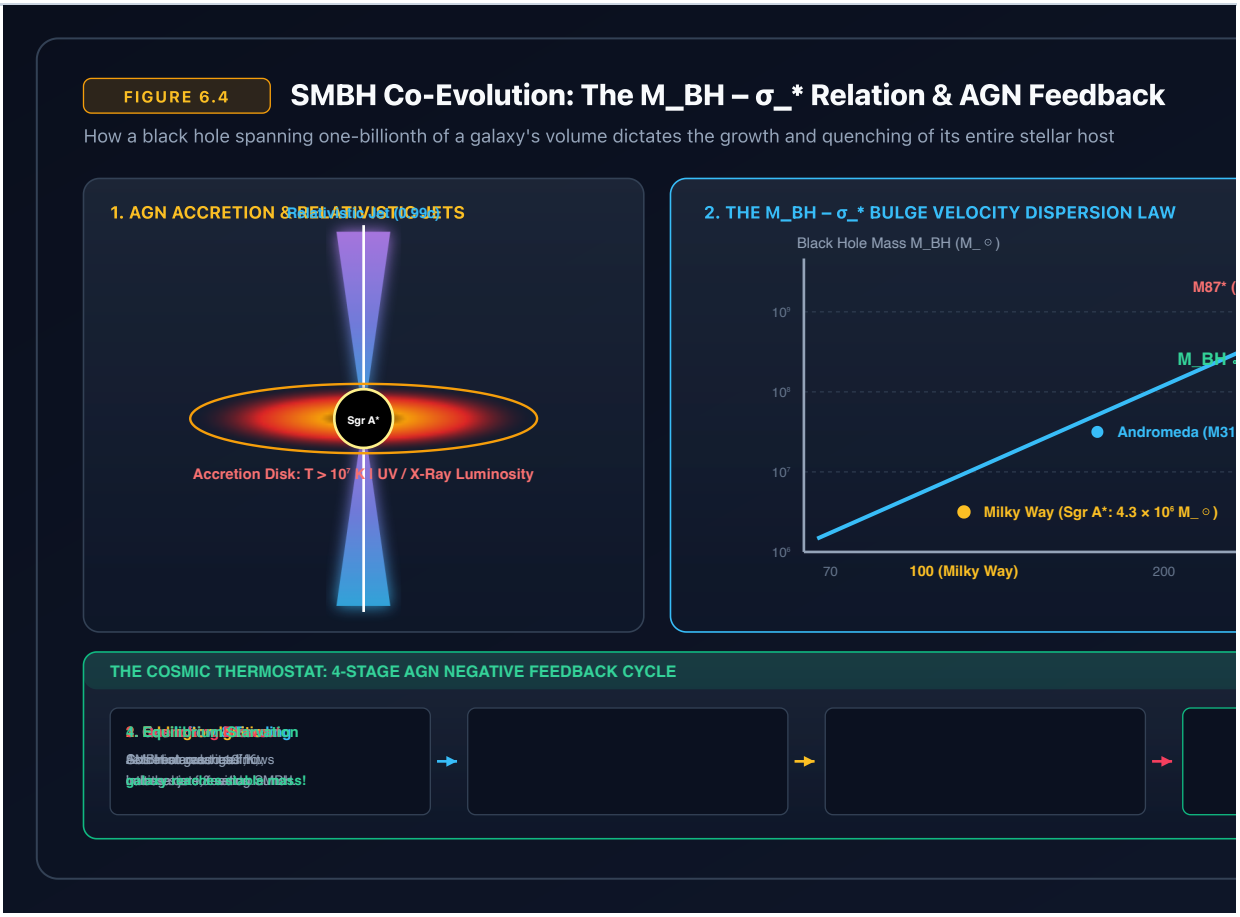


Figure 6.3: Supermassive Black Hole Co-Evolution & AGN Feedback. The empirical $M_{BH} \propto \sigma_*^{4.4}$ relation links central black hole mass to host bulge stellar velocities across five orders of magnitude. Active galactic nucleus (AGN) feedback acts as a cosmic thermostat: when infalling gas pushes accretion toward the Eddington limit, relativistic jets and magnetic winds heat the interstellar reservoir to 10^7 K, blowing away fuel and quenching runaway starbursts.

Vera Rubin's Triumph: The Invisible Giant of Dark Matter

According to classical Keplerian mechanics, orbital velocities in a gravitationally bound system should decrease with distance from the central mass ($v \propto r^{-1/2}$)—exactly as Neptune moves far slower than Mercury in our solar system. In the 1970s, astronomer **Vera Rubin** and instrument maker **Kent Ford** measured the optical emission lines of ionized gas across the disks of dozens of spiral galaxies.

Instead of falling off at large radii, the orbital velocities **remained flat ($v(r) \approx$ constant)** all the way to the visible edge of the disks. In the Milky Way, stars 60,000 light-years from the center are orbiting at over 220 km/s—velocities so high that the gravitational pull of all visible stars, gas, and dust combined is insufficient to hold them. By all laws of physics, the galaxy should have flown apart like a loose spinning wheel.

Rubin's flat rotation curves provided the undeniable empirical proof that spiral galaxies are embedded inside enormous, quasi-spherical **Dark Matter Halos**. In our Milky Way, while visible baryonic stars and gas account for roughly $6 \times 10^{10}\ M_\odot$, the invisible dark matter halo extends over 600,000 light-years into intergalactic space with a total mass exceeding $\mathbf{1.1 \times 10^{12}\ M_\odot}$. Over **85% of the Milky Way's mass is completely invisible**.

Shakil Mahmud • Research Monograph

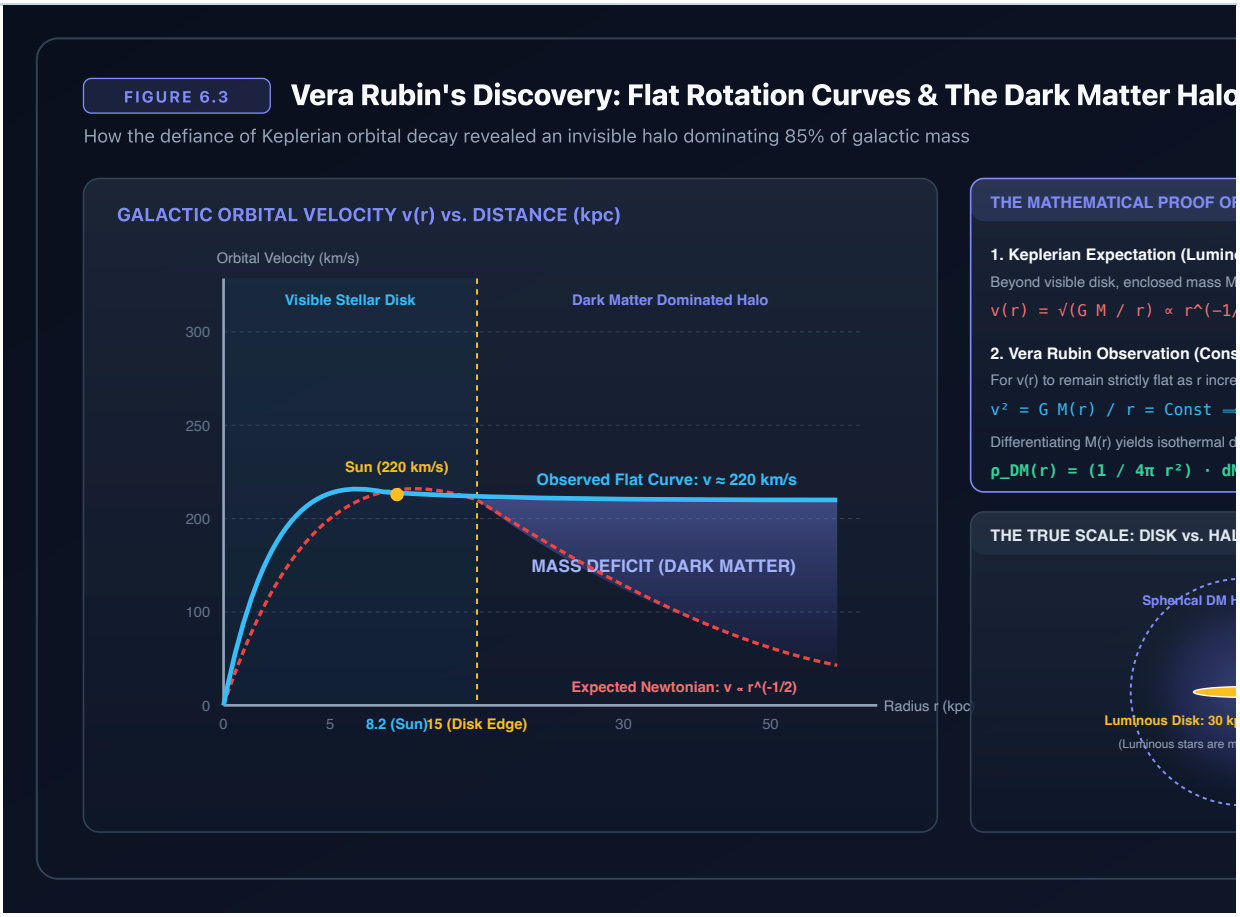


Figure 6.4: Vera Rubin's Discovery (Flat Rotation Curves & The Dark Matter Halo). Classical Keplerian mechanics dictates orbital velocity should decay as $v \propto r^{-1/2}$ beyond the optical disk edge (15 kpc). Vera Rubin and Kent Ford's spectroscopic measurements proved velocities remain flat (~220 km/s) out to tens of kiloparsecs, mathematically requiring an invisible isothermal dark matter halo with density profile $\rho_{DM}(r) \propto r^{-2}$ comprising 85% of total galactic mass.

Anatomy of our Island Home: The Structure of the Milky Way

Our galaxy is classified as an **SBbc barred spiral galaxy**, spanning roughly 100,000 light-years in diameter and hosting between 100 and 400 billion stars. It consists of four distinct structural components:

- **1. The Central Bar and Bulge:** A rotating peanut-shaped central bar of older stars spanning 27,000 light-years, housing Sagittarius A* and dense stellar populations.
- **2. The Thin Disk:** A razor-thin sheet with a vertical scale height of only ~ 300 parsecs (~ 1,000 light-years). Contains the vast majority of interstellar gas, active star-forming regions, and metal-rich *Population I* stars like our Sun.
- **3. The Thick Disk:** Extends to a scale height of ~ 1 kpc (~ 3,300 light-years), populated by older, intermediate-metallicity stars born during the turbulent early merger history of the galaxy.
- **4. The Stellar & Dark Matter Halo:** A diffuse, spherical swarm of ancient, metal-poor *Population II* stars and over 150 dense **Globular Clusters**—relic stellar fossils dating back to the first billion years after the Big Bang—all shrouded within the colossal dark matter halo.

The Galactic Habitable Zone: Finding Safe Harbor in the Cosmos

Just as a planetary system possesses a circumstellar habitable zone where liquid water can exist on a planet's surface, a galaxy possesses a **Galactic Habitable Zone (GHZ)** (formulated by Guillermo Gonzalez, Donald Brownlee, and Peter Ward)—a ring-like region where complex biological life can emerge and survive over geological timescales:

If a planetary system forms too close to the galactic center ($r < 4$ kpc), stellar densities are so extreme that gravitational encounters strip planets from their orbits. Furthermore, frequent nearby supernovae, relativistic gamma-ray bursts (GRBs), and active flares from the central supermassive black hole repeatedly strip planetary atmospheres with lethal ionizing radiation.

Conversely, if a star forms too far on the galactic periphery ($r > 10$ kpc), the chemical evolution of the galaxy has been too sluggish: the metallicity ([Fe/H]) is too low to provide the heavy elements (iron, silicon, magnesium) required to condense rocky terrestrial planets or form metallic planetary cores capable of generating protective magnetic dynamos.

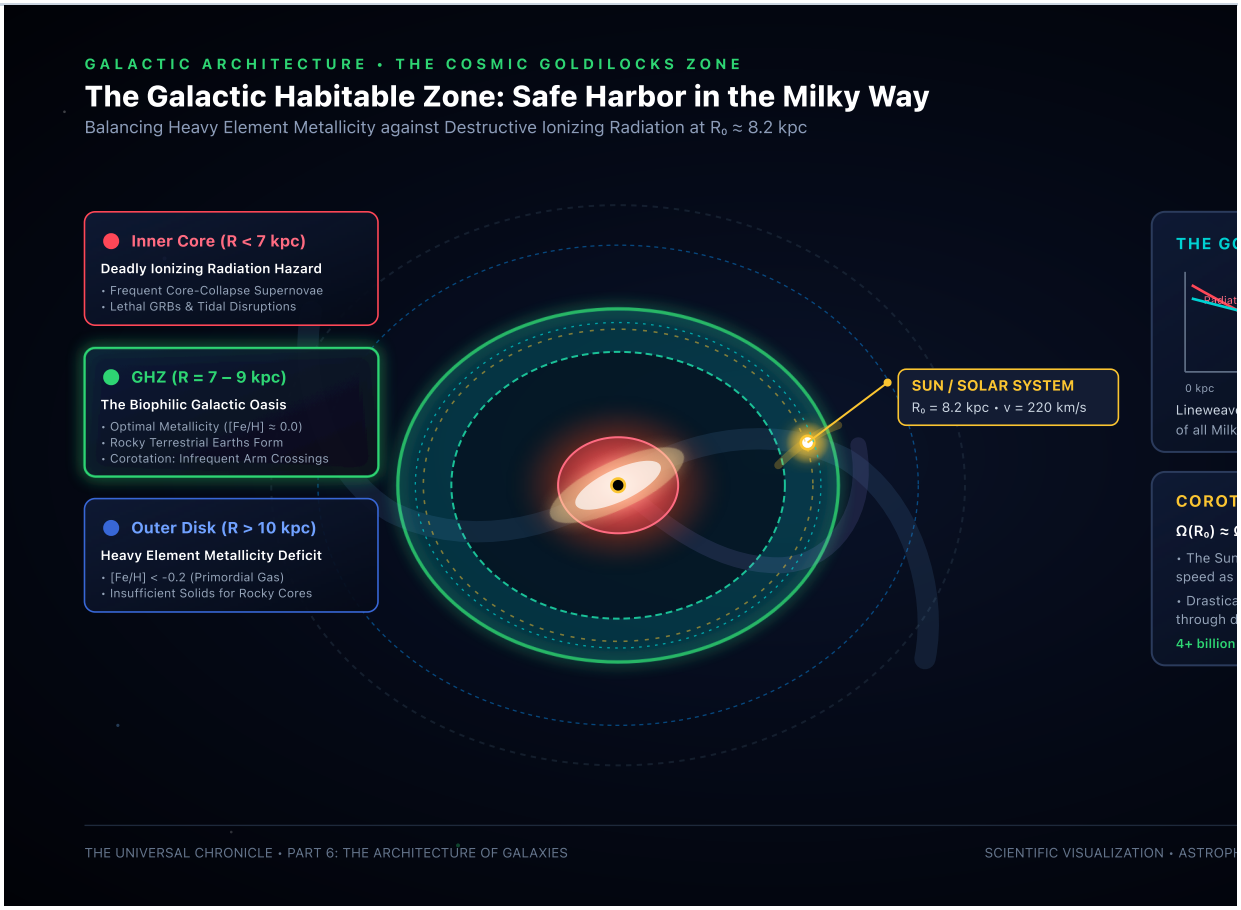


Figure 6.5a: The Galactic Habitable Zone (GHZ) in the Milky Way disk. An annular cosmic Goldilocks ring (r \approx 7\text{–}9\text{ kpc}) balancing heavy element abundance ($[\mathrm{Fe/H}] \approx 0.0$) against lethal core-collapse supernovae and gamma-ray burst radiation, where our Solar System orbits safely at $R_0 = 8.2$ kpc near the corotation radius.

Our Solar System orbits at a radius of **8.2 kpc (~ 26,700 light-years)** from the galactic core, nestled inside the local Orion-Cygnus Spur between the major Sagittarius and Perseus spiral arms. Here, in this tranquil cosmic oasis, stellar metallicity is optimal (Z ≈ Z_ ⊙), dangerous supernova sterilizations occur only once every few hundred million years, and the orbital velocity of the Sun matches the speed of the spiral density wave itself—preventing our star from crossing violent starburst shock fronts too frequently.

Shakil Mahmud • Research Monograph

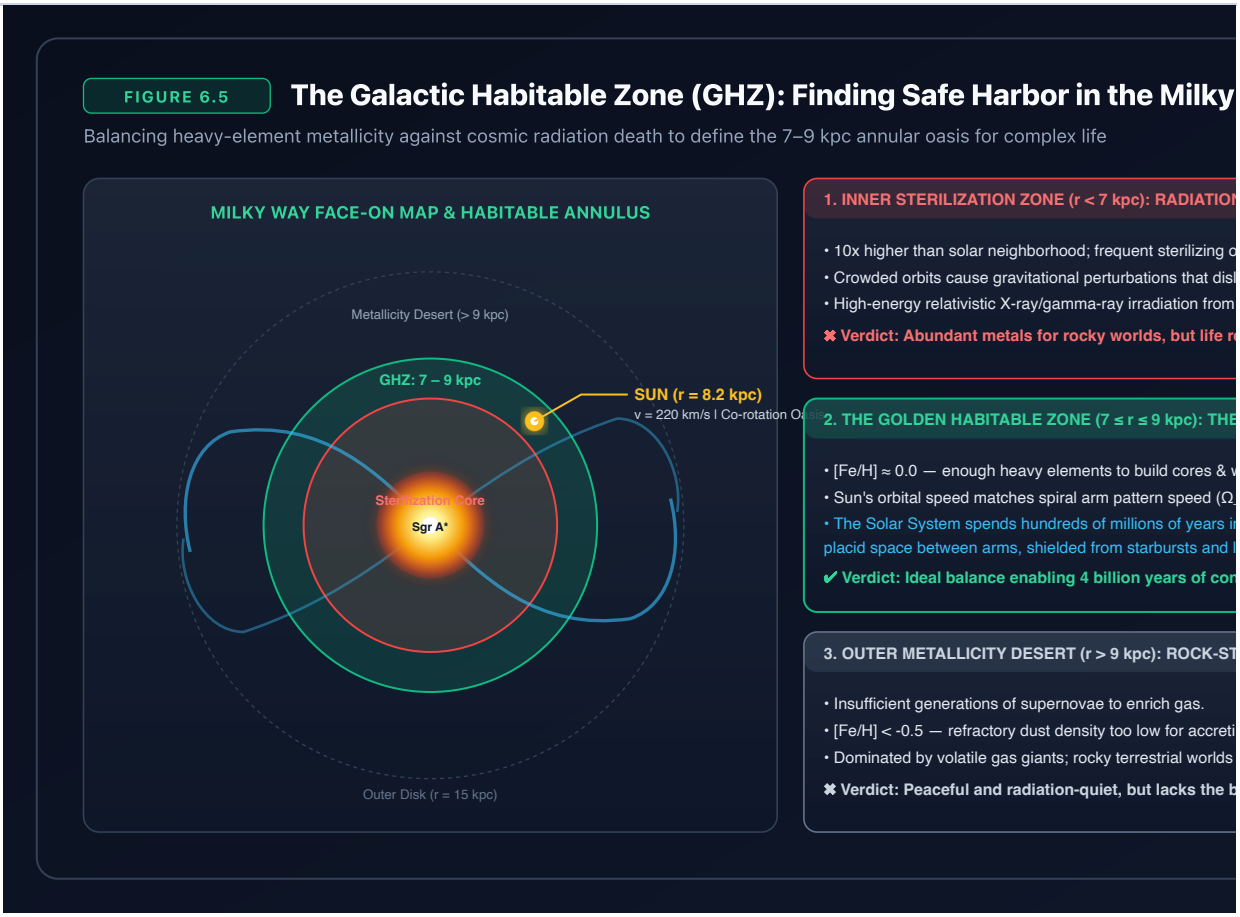


Figure 6.5: The Galactic Habitable Zone (GHZ). Complex biological evolution requires an annular balance between heavy-element availability and cosmic radiation hazards. The inner galaxy is sterilized by frequent supernovae, gamma-ray bursts, and stellar tidal disruptions; the outer rim lacks sufficient iron/silicon to condense terrestrial rocky planets. The Solar System resides at 8.2 kpc—a quiet, metal-rich co-rotation oasis where spiral arm crossing occurs only once every ~100–200 million years.

Structural Metrics of the Milky Way

Component / Parameter	Dimension / Value	Mass ($M_\odot$)	Key Physical Characteristics
Total Virial Mass	Radius ~ 200 kpc	~ 1.1×10^{12} $M_\odot$	Dominated (>85\%) by Cold Dark Matter halo.
Total Stellar Mass	Diameter ~ 30 kpc (~ 100,000 ly)	≈ 5.5 × 10^{10} $M_\odot$	100 to 400 billion stars.
Thin Disk	Scale height ~ 300 pc	≈ 4.5 × 10^{10} $M_\odot$	Houses spiral arms, gas reservoirs, Population I stars (e.g., Sun).
Thick Disk	Scale height ~ 1,000 pc	≈ 6×10^9 $M_\odot$	Older, metal-poor stars; relic of early galactic mergers.
Galactic Bulge & Bar	Length ~ 8 kpc	≈ 1.5 × 10^{10} $M_\odot$	Old Population II stars, triaxial rotating bar.
Sagittarius A* (SMBH)	R_{Schw} ≈ 12.7 million km	4.297 × 10^6 $M_\odot$	Central singularity, quiescent accretion disk.
Solar Position	R_0 = 8.2 kpc (26,700 ly)	—	Galactic Habitable Zone; orbital period 230 Myr at 220 km/s.

The Stage is Set: The Collapse of a Solar Cradle

Roughly 4.6 billion years ago—nearly nine billion years after the Big Bang—the Milky Way was a mature, chemically enriched spiral galaxy. In a quiet, suburban backwater of the galactic disk, inside the Orion spiral arm, a giant molecular cloud of cold hydrogen, helium, and synthesized stardust was drifting in space.

The universe had forged the space, the matter, the forces, the heavy elements, and the galactic harbor. Now, a localized trigger—the shockwave of a dying neighbor star—would disturb this peaceful cloud, initiating gravitational collapse. In **Part 7** of *The Universal Chronicle*, we will witness the birth of our home star system: **The Solar Cradle — The Protoplanetary Disk, Planetesimal Accretion, and the Young Sun**.

Academic Citations & Foundational Literature

- **Lin, C. C., & Shu, F. H. (1964).** "On the Spiral Structure of Disk Galaxies." *The Astrophysical Journal*, 140, 646–655. doi:10.1086/147955.

- **Rubin, V. C., & Ford, W. K. (1970).** "Rotation of the Andromeda Nebula from a Spectroscopic Survey of Emission Regions." *The Astrophysical Journal*, 159, 379–403. doi:10.1086/150317.
- **Ferrarese, L., & Merritt, D. (2000).** "A Fundamental Relation between Supermassive Black Holes and Their Host Galaxies." *The Astrophysical Journal Letters*, 539(1), L9–L12. doi:10.1086/312838.
- **Gonzalez, G., Brownlee, D., & Ward, P. (2001).** "The Galactic Habitable Zone: Galactic Chemical Evolution." *Icarus*, 152(1), 185–200. doi:10.1006/icar.2001.6617.
- **Bland-Hawthorn, J., & Gerhard, O. (2016).** "The Galaxy in Context: Structural, Kinematic, and Integrated Properties." *Annual Review of Astronomy and Astrophysics*, 54(1), 529–596. doi:10.1146/annurev-astro-081915-023441.
- **Event Horizon Telescope Collaboration (Akiyama, K., et al.) (2022).** "First Sagittarius A* Event Horizon Telescope Results. I. The Shadow of the Supermassive Black Hole in the Center of the Milky Way." *The Astrophysical Journal Letters*, 930(2), L12. doi:10.3847/2041-8213/ac6674.

Citation: Mahmud, S. (2026). "The Architecture of Galaxies — Spiral Arms, Supermassive Black Holes, and the Milky Way." In The Universal Chronicle, Part 6. https://shakilmahmud.com/universal-chronicle-part-6-the-architecture-of-galaxies/

Shakil Mahmud • Research Monograph

SHAKIL MAHMUD RESEARCH MONOGRAPHS • PART VII

The Solar Cradle — The Protoplanetary Disk, Planetesimal Accretion, and the Young Sun

The Solar Cradle — The Protoplanetary Disk, Planetesimal Accretion, and the Young Sun

2,420 words • October 30, 2026 • Permanent URI



Plate VII: *Figure: The primordial solar nebula (~4.57 Ga): a spinning circumstellar protoplanetary disk of gas, silicate dust, and ices coalescing into planetesimals and protoplanets around the young, luminous T-Tauri Proto-Sun.*

Roughly 4.567 billion years ago, deep within an unremarkable molecular gas cloud in the Milky Way's Orion Arm, a localized shockwave triggered the collapse of the Solar Nebula. In the furious gravitational vortex that followed, 99.86% of the matter pooled into a thermonuclear furnace—our young Sun—while the remaining fraction of a percent flattened into a rotating circumstellar disk of gas, mineral dust, and ice. Through aerodynamic drag, electrostatic adhesion, and chaotic orbital collisions, microscopic grains assembled into the architectural framework of our Solar System.

The Supernova Trigger: The Birth Certificate of the Solar System

How do we know precisely when the Solar System began? The answer is preserved inside the oldest macroscopic solid objects in our planetary system: **Calcium-Aluminum-rich Inclusions (CAIs)** found within primitive carbonaceous chondrite meteorites, such as the Allende meteorite that fell in Mexico in 1969.

Using ultra-high-precision uranium-lead (^{207}Pb–^{206}Pb) radiometric dating, cosmochemists have measured the condensation age of CAIs to be exactly **4.56730 ± 0.00016 billion years**. This date defines Year Zero of the Solar System.

The Fingerprint of Extinct Radionuclides
CAIs contain an excess of Magnesium-26 (^{26}Mg), the daughter isotope produced by the radioactive beta decay of **Aluminium-26 (^{26}Al)**. Because ^{26}Al has an astronomically brief half-life of just 717,000 years, it could not have lingered from primordial galactic history. It had to be synthesized in a nearby core-collapse supernova or asymptotic giant star and injected into the Solar Nebula **less than one million years before the gas collapsed**. The shockwave of that dying star compressed our cold parental molecular cloud, triggering its gravitational collapse.

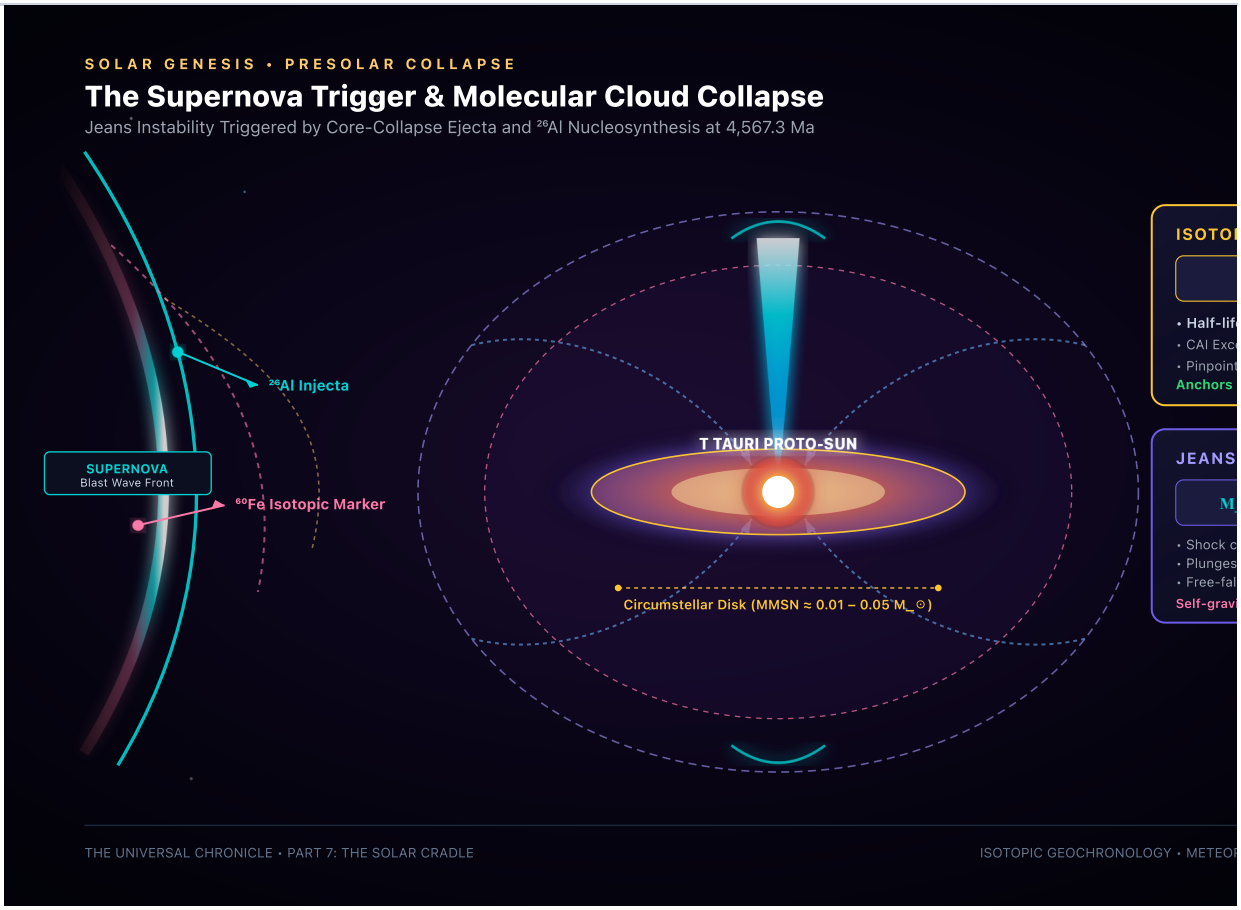


Figure 7.1a: Supernova shock front triggering presolar molecular cloud collapse. Core-collapse nucleosynthetic ejecta enriched with short-lived radionuclides (^{26}Al and ^{60}Fe) compressed the cold molecular cloud beyond its Jeans mass threshold, initiating rapid gravitational collapse into the spinning protostellar disk at $4,567.3$ Ma.

Shakil Mahmud • Research Monograph

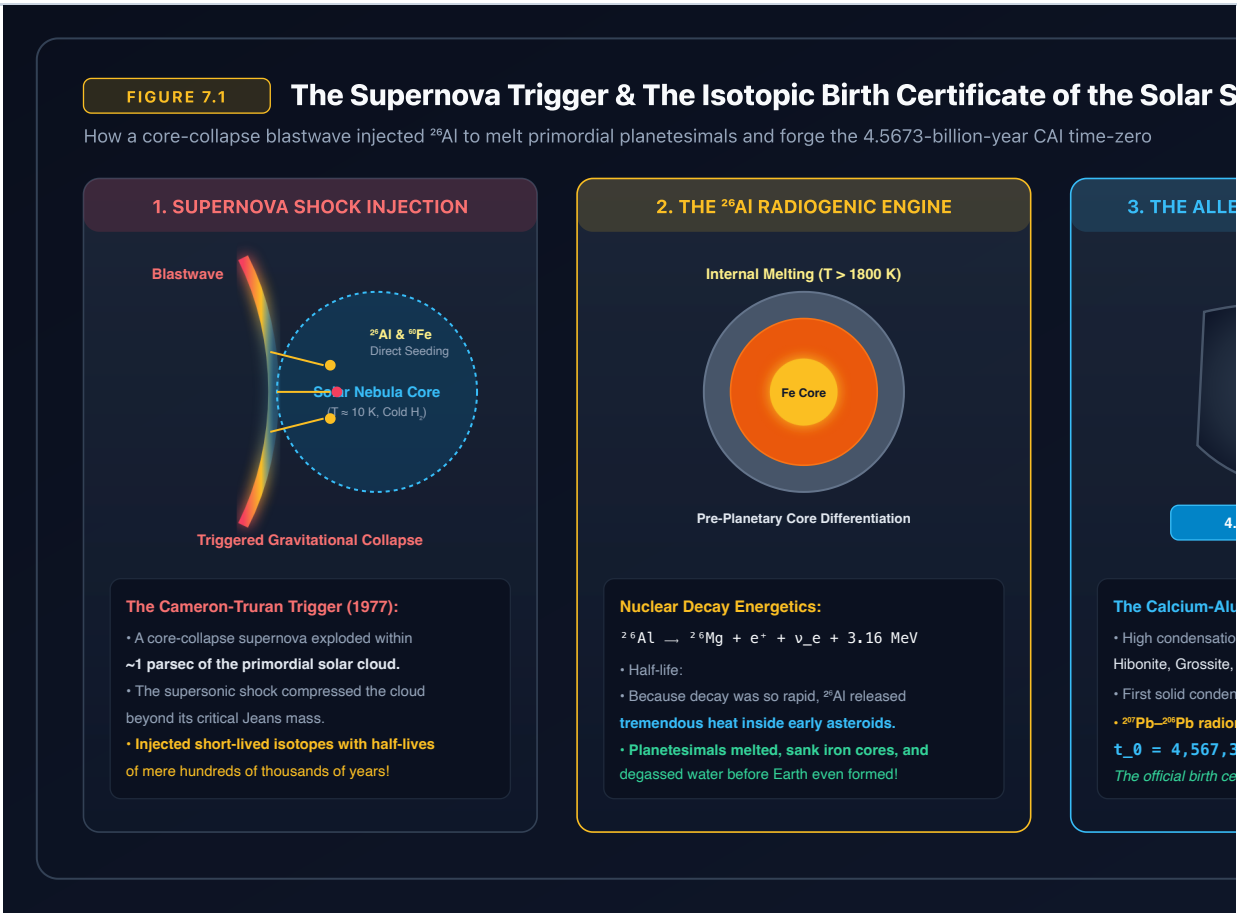


Figure 7.1: The Supernova Trigger & The CAI Chronometer (4.5673 Ga). A nearby core-collapse supernova compressed the cold molecular cloud core and injected short-lived radionuclides (^{26}Al and ^{60}Fe). The rapid radioactive decay of ^{26}Al (half-life: 717,000 years) melted primordial planetesimals from within, while refractory Calcium-Aluminum-rich Inclusions (CAIs) preserved in carbonaceous chondrites pin the birth of the Solar System to exactly 4,567.30 ± 0.16 million years ago.

The T Tauri Proto-Sun and the Minimum Mass Solar Nebula

As the rotating nebula collapsed, conservation of angular momentum flattened the outer gas and dust into a circumstellar accretion disk—the **Protoplanetary Disk**—spanning over 100 Astronomical Units (AU) across. At the center, gravitational potential energy converted into heat via Kelvin-Helmholtz contraction, forming the **Proto-Sun**.

During its first 10 million years, the young Sun was in the violent **T Tauri phase**: it was not yet powered by core nuclear fusion, but shone brightly via gravitational contraction. It was an unruly star, rotating rapidly with magnetic field strengths thousands of times stronger than today. It unleashed ferocious bipolar plasma jets and powerful stellar winds that bombarded the inner disk with extreme ultraviolet and X-ray radiation.

The mass distribution of this disk is traditionally modeled as the **Minimum Mass Solar Nebula (MMSN)** (Hayashi 1981): adding back the light hydrogen and helium gas that was lost from the planets yields an initial disk mass of roughly **0.01 to 0.05 M_⊙** (equivalent to 10 to 50 Jupiter masses of gas and dust).

The Condensation Sequence: Why Inner Planets Are Rocky and Outer Worlds Are Giants

The temperature across the protoplanetary disk dropped steeply with distance from the central proto-Sun: from over 1,800 K near the center to less than 30 K in the outer reaches. This thermodynamic gradient dictated the **chemical condensation sequence**:

1. The Refractory Inner Zone (r < 2.7 AU)

Close to the Sun, temperatures were far too high for volatile compounds (water, ammonia, methane) to condense. Only refractory materials with high sublimation temperatures could crystallize into solid mineral grains:

- Aluminum, titanium, and calcium oxides (T_{cond} ~ 1,500–1, K)
- Iron-nickel alloys (T_{cond} ~ 1, K)
- Magnesium-rich silicate minerals: Forsterite (Mg_2SiO_4) and Enstatite (MgSiO_3) (T_{cond} ~ 1,300–1, K)

Because refractory elements constituted barely **0.5% of the total nebula mass**, the inner solar system had very little solid raw material with which to build planets. The inner worlds—Mercury, Venus, Earth, and Mars—were starved of mass, remaining small, dense, rocky spheres.

2. The Snow Line (Frost Line) at ~ 2.7 AU

At an orbital distance of roughly 2.7 AU (the present-day location of the asteroid belt), the disk temperature dropped below **170 K**. At this boundary—the **Snow Line (Ice Line)**—water vapor could spontaneously desublimate into microscopic ice crystals.

Because oxygen and hydrogen are among the most abundant elements in the cosmos, the condensation of water ice multiplied the density of solid surface material by a factor of **four to five**! Beyond the snow line, planetary embryos had access to mountains of solid ice, enabling them to grow rapidly into massive icy-rocky cores.

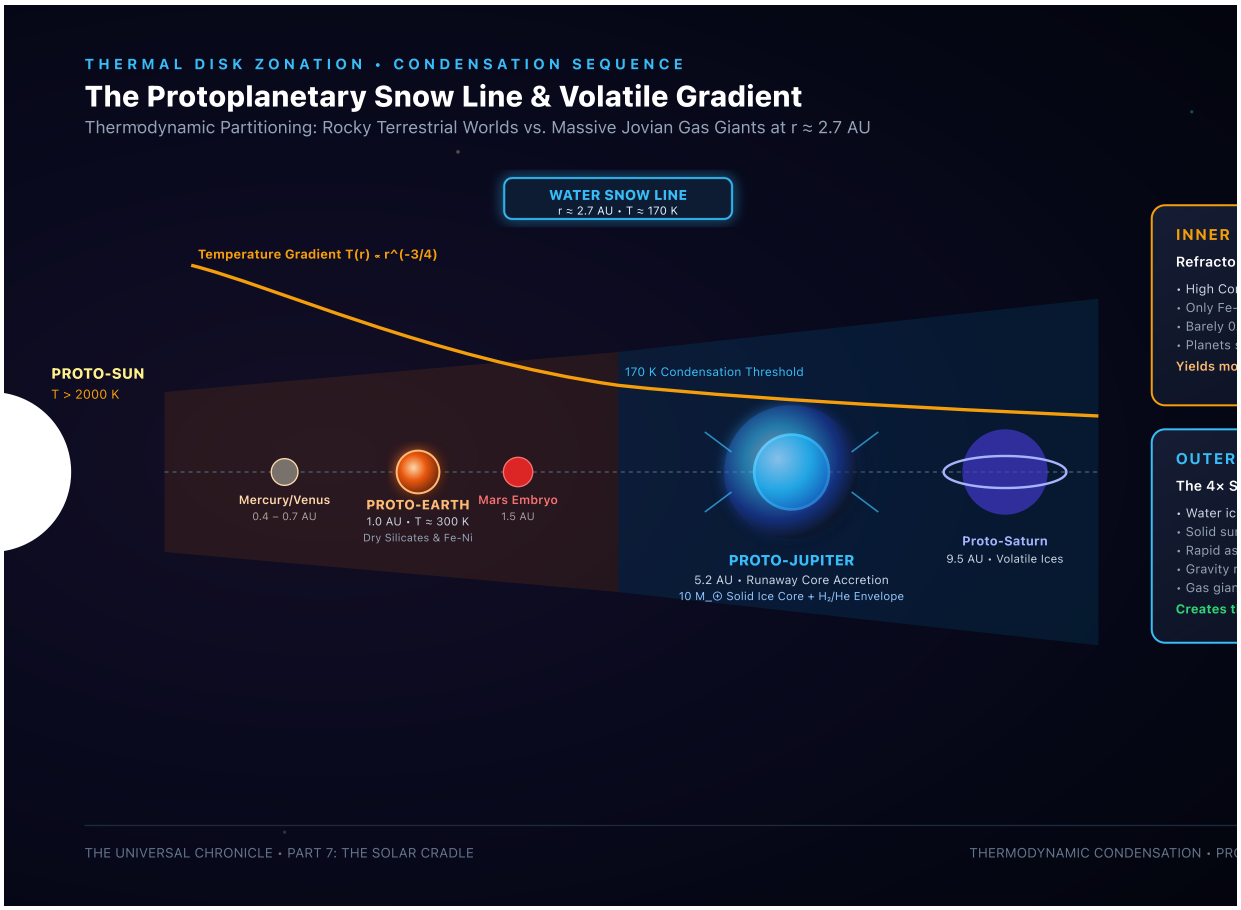


Figure 7.2a: Thermodynamic condensation sequence and the circumstellar snow line. At $r \approx 2.7$ AU ($T \approx 170$ K), water vapor freezes into solid ice crystals, quadrupling the solid surface density and fueling rapid accretion of massive $10 M_{\oplus}$ cores for Jupiter and Saturn, while inner terrestrial embryos remain small and rocky.

Shakil Mahmud • Research Monograph

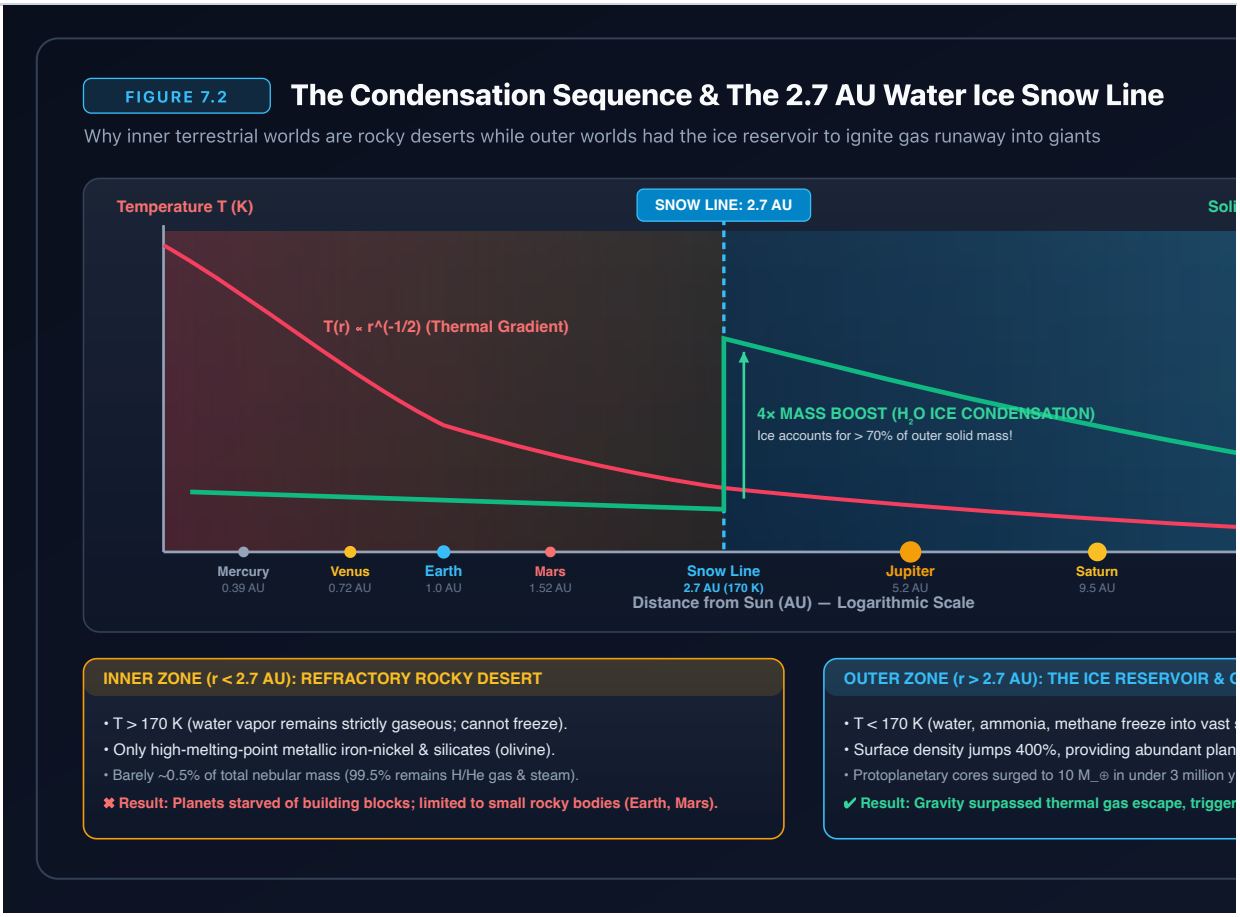


Figure 7.2: The Thermal Condensation Sequence & The 2.7 AU Snow Line. As temperature dropped with solar distance ($T \propto r^{-1/2}$), only high-temperature metallic iron and silicates could condense inside 2.7 AU, starving terrestrial planets of building material. Beyond the 170 K Snow Line, water vapor froze into solid ice grains, producing an instant 400% surge in solid surface density that provided the fuel for Jupiter's rapid core assembly.

From Dust to Planetesimals: The Physics of the Meter Barrier

How do sub-micron mineral dust grains grow into thousand-kilometer planetary embryos? This process is fraught with formidable aerodynamic bottlenecks:

1. The Electrostatic Growth Phase (Microns to Centimeters)

In the earliest phase, microscopic dust grains suspended in the laminar gas disk collide gently via Brownian motion. At relative velocities of a few centimeters per second, van der Waals and electrostatic forces cause the grains to stick together, forming porous, fluffy, fractal aggregates up to pebble sizes.

2. The Radial Drift & Bouncing Barrier (The Meter Trap)

When particles reach millimeter to meter sizes, electrostatic adhesion fails: at collision velocities above 1 m/s, pebbles bounce off one another or shatter into dust. Worse still is **gas drag**.

Because the gas disk is partially supported by outward radial gas pressure, it rotates around the Sun at slightly sub-Keplerian velocity ($\Delta v \approx 50$ m/s). Solid boulders, which do not feel gas pressure, attempt to orbit at full Keplerian velocity. As a result, boulders feel a relentless, supersonic "headwind" from the slower gas. This aerodynamic headwind drains the boulders of orbital angular momentum, causing a meter-sized rock at 1 AU to **spiral inward and vaporize into the young Sun in barely 100 years!**

The Streaming Instability Resolution (Youdin & Goodman 2005)
In 2005, astrophysicists Andrew Youdin and Jeremy Goodman discovered the mathematical mechanism that rescues planet formation: **The Streaming Instability**. As swarms of pebbles drift inward, their collective drag pushes back against the gas, slowing down the headwind. Pebbles behind them pile up into dense, turbulent clumping filaments.

When the local density of pebbles inside a filament exceeds the gas density by a factor of 100, the swarm becomes **gravitationally unstable**: the entire filament collapses directly under its own self-gravity in a matter of months, bypassing the meter-size barrier completely to forge **10 to 100-kilometer Planetesimals** in a single leap!

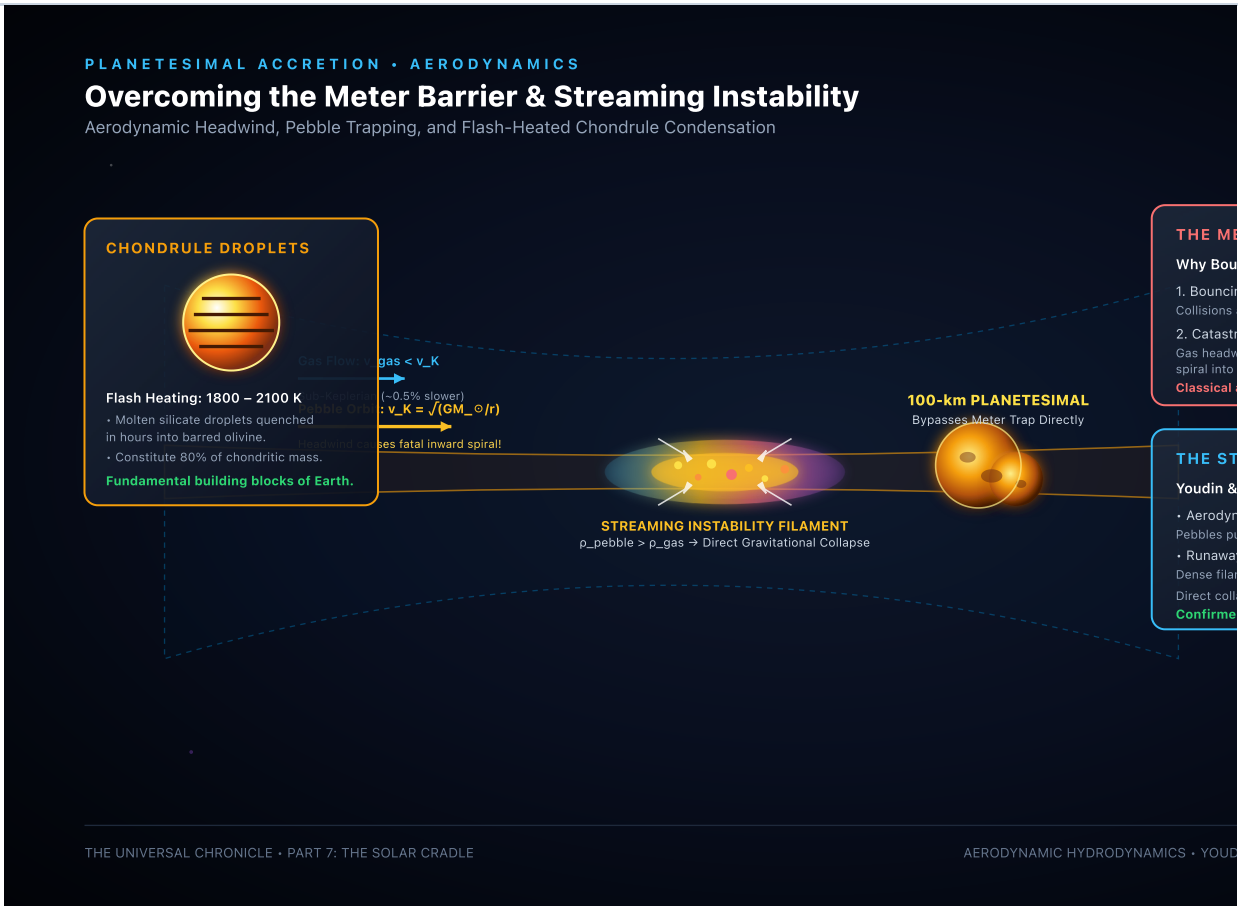


Figure 7.3a: Aerodynamic streaming instability and flash-heated chondrule clumping. Solid pebbles overcome the lethal meter-size radial drift barrier by aerodynamically clustering into dense turbulent filaments, where collective self-gravity triggers sudden gravitational collapse into 100 km-scale planetesimals and primitive chondritic asteroids.

This theoretical mechanism was dramatically confirmed in 2019 when NASA's New Horizons spacecraft flew past Kuiper Belt object **Arrokoth**, revealing a pristine, contact-binary planetesimal formed by the gentle gravitational coalescence of two swirling pebble clouds.

Shakil Mahmud • Research Monograph

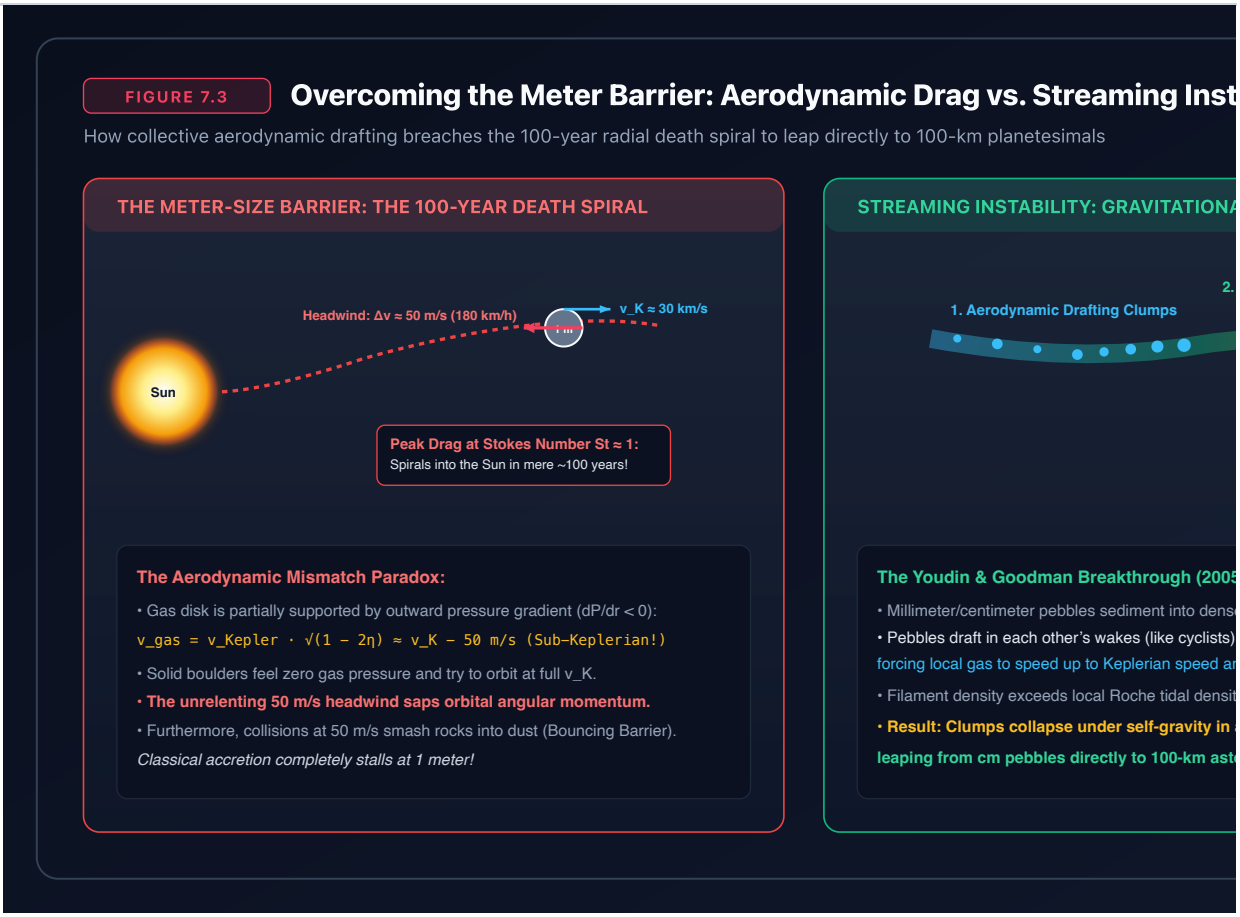


Figure 7.3: Overcoming the Meter Barrier (Streaming Instability). Outward radial gas pressure causes nebular gas to orbit at sub-Keplerian velocity, subjecting 1-meter boulders to a persistent 50 m/s headwind that spirals them into the Sun in under 100 years. The streaming instability resolves this: centimeter-sized pebbles draft collectively in dense midplane filaments, accelerating local gas to cancel drag until self-gravity directly collapses the swarm into 100-km planetesimals.

The Giant Planet Race: Core Accretion and the Grand Tack

Beyond the snow line, planetesimals grew via *runaway and oligarchic accretion* into a massive planetary embryo of roughly **10 to 15 Earth masses ($M_\oplus$)** in less than 3 million years. Once an embryo reached this critical mass, its escape velocity exceeded the thermal velocity of surrounding hydrogen and helium gas.

The embryo entered **runaway gas accretion**, vacuuming up enormous volumes of gas directly from the disk. This was the birth of **Jupiter**, followed closely by **Saturn**. This gas-capture window was brutally brief: within 3 to 10 million years, powerful T Tauri stellar winds from the young Sun and photoevaporation from nearby stars blew the gaseous disk away, freezing Jupiter at 318 $M_\oplus$ and Saturn at 95 $M_\oplus$. Further out, **Uranus and Neptune** formed too slowly to capture deep gas envelopes, remaining "ice giants" with thick water-methane-ammonia mantles.

The Grand Tack Hypothesis: How Jupiter Reshaped the Inner Solar System

In classical models, Mars should have accreted roughly the same mass as Earth or Venus. Why is Mars a diminutive world with barely 10% of Earth's mass? Furthermore, why is the Asteroid Belt mostly empty, containing barely 0.05\% of Earth's mass?

The leading explanation is the **Grand Tack Hypothesis** (Walsh et al. 2011). As Jupiter grew inside the gaseous disk, exchange of angular momentum with the gas caused it to **migrate inward toward the Sun**, plowing all the way to 1.5 AU (where Mars orbits today). Like a cosmic snowplow, Jupiter's gravity scattered the inner planetesimal disk, truncating the reservoir of planet-forming material outside 1 AU.

Before Jupiter could plunge into the Sun and become a "hot Jupiter," Saturn grew, caught up to Jupiter, and locked into a mutual **3:2 mean-motion orbital resonance**. The gravitational resonance opened a clear gap in the gas disk between them, reversing their torque and pulling both giant planets **"tacking" outward** to their present orbits. This dramatic migration left Mars starved of accretion material, carved out the asteroid belt, and delivered volatile-rich carbonaceous asteroids into the inner solar system.

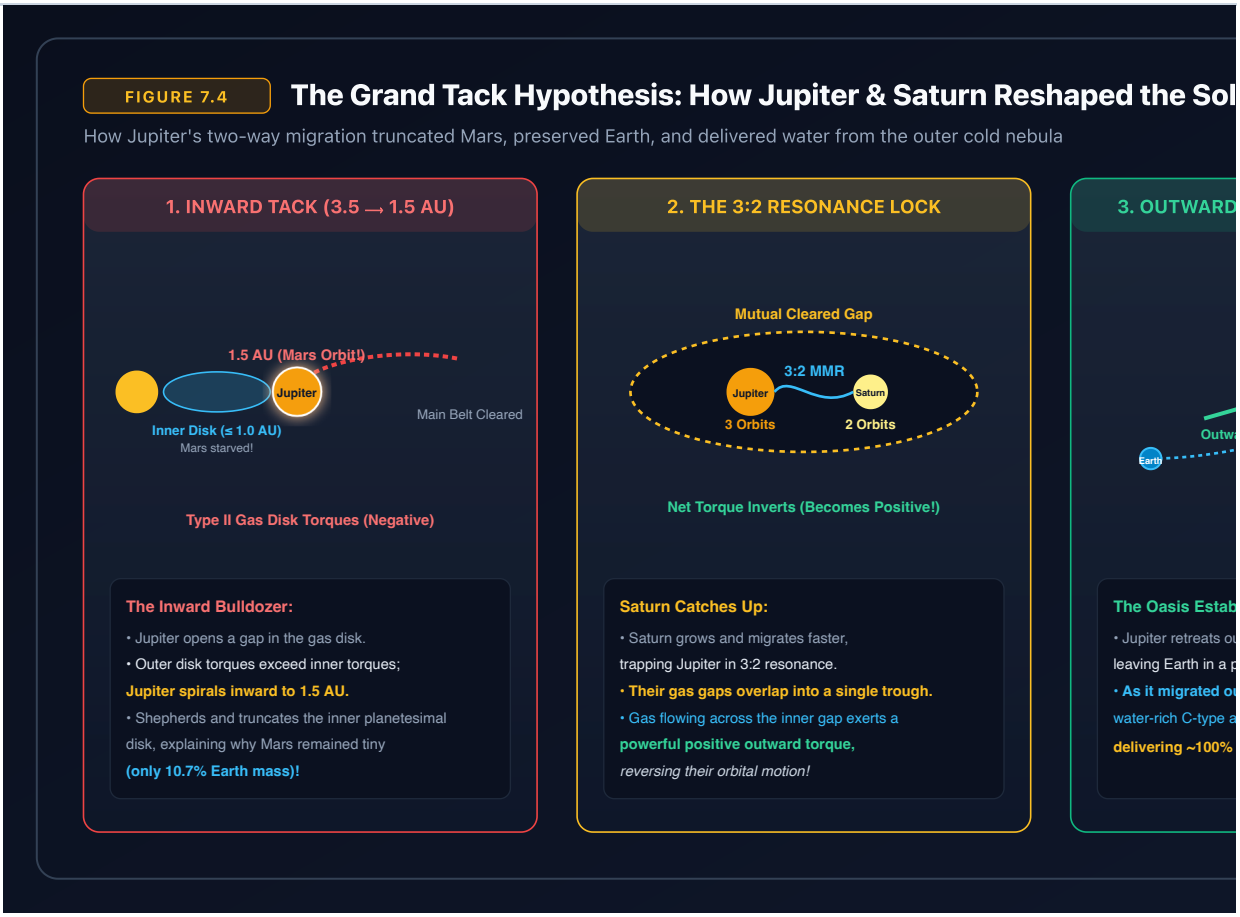


Figure 7.4: The Grand Tack Hypothesis (Walsh & Morbidelli 2011). Type II gas disk torques initially drove Jupiter inward to 1.5 AU, truncating the inner planetesimal disk and starving Mars. Once Saturn reached the 3:2 mean-motion resonance, their overlapping gas gap reversed net disk torques, "tacking" both gas giants outward to their current orbits while scattering water-rich C-type asteroids into the terrestrial zone to seed Earth's oceans.

The Inner Crucible: Oligarchic Growth and Proto-Earth

Inside the truncated inner disk (0.5 to 1.0 AU), the gas cleared, leaving behind a swarm of roughly **50 to 100 Moon- to Mars-sized protoplanetary embryos**. For the next 30 to 100 million years, these embryos orbited in chaotic, intersecting ellipses.

This was the era of giant impacts: planetary embryos smashed into one another at orbital velocities of 30 km/s, merging and shattering in violent, incandescent collisions. From this cosmic demolition derby emerged four survivors: Mercury, Venus, Earth, and Mars.

Shakil Mahmud • Research Monograph



Figure 7.5: The 3-Phase Assembly of Proto-Earth & Terrestrial Planets. Runaway growth via gravitational focusing ($t < 10^5$ yr) transitioned into oligarchic growth ($t \sim 10^6$ yr), producing dozens of Moon-to-Mars-sized planetary embryos spaced by mutual Hill radii. Once nebular gas dissipated, orbital crossings triggered a violent 100-million-year era of giant impacts that merged embryos into the four stable inner planets.

Chronology Table: Assembly of the Solar System

Stage / Milestone	Time from T_0	Key Physical Processes	Observable Relic / Evidence
Supernova Shock & Nebula Collapse	-1 Myr to 0	Gravitational collapse of molecular cloud; ^{26}Al and ^{60}Fe injection.	Isotopic anomalies in carbonaceous chondrites.
CAI Condensation (t_0)	0.00 Myr (4.5673 Ga)	First high-temperature minerals condense at >1, K.	Calcium-Aluminum-rich Inclusions in Allende meteorite.
Planetesimal Formation	0.1 to 1 Myr	Streaming instability concentrates pebbles; gravitational collapse into 10–100-km bodies.	Kuiper Belt object Arrokoth (contact binary).
Giant Planet Runaway Accretion	1 to 5 Myr	Jupiter and Saturn core accretion exceeds 10 $M_\oplus$; runaway gas capture.	Mass and atmospheric compositions of Jupiter/Saturn.
The Grand Tack & Disk Dispersal	3 to 10 Myr	Jupiter migrates to 1.5 AU, tacks outward with Saturn; solar winds blow gas away.	Truncated mass of Mars; structure of Asteroid Belt.
Terrestrial Giant Impacts	10 to 100 Myr	50–100 embryos collide chaotically to assemble Mercury, Venus, Earth, and Mars.	Earth-Moon system; planetary core-mantle differentiation.

Proto-Earth on the Brink of Cataclysm

By approximately 4.51 billion years ago—roughly 50 million years after the first CAIs condensed—our home planet had grown to roughly 90% of its current mass. Known as **Proto-Earth**, it was a searing, radioactive world heated by the decay of ^{26}Al and short-lived radionuclides, enveloped in a dense steam atmosphere.

Yet, the architecture of our world was not yet complete. Lurking nearby, sharing an unstable orbital resonance, was another planetary embryo roughly the size of Mars: a protoplanet that geochemists have named **Theia**. The inevitable collision between these two worlds would completely remake our planet, vaporize the oceans of magma, and forge the gravitational companion that stabilizes Earth's climate to this day.

In **Part 8** of *The Universal Chronicle*, we will witness the most violent day in our planet's history: **The Violent Genesis — The Hadean Earth, Theia Giant Impact, and the Birth of the Moon**.

Academic Citations & Foundational Literature

- **Connelly, J. N., et al. (2012).** "The Absolute Chronology and Thermal Processing of Solids in the Solar Protoplanetary Disk." *Science*, 338(6107), 651–655. doi:10.1126/science.1226919.
- **Hayashi, C. (1981).** "Structure of the Solar Nebula, Growth and Decay of Magnetic Fields and Effects of Magnetic and Turbulent Viscosities on the Nebula." *Progress of Theoretical Physics Supplement*, 70, 35–53. doi:10.1143/PTPS.70.35.
- **Youdin, A. N., & Goodman, J. (2005).** "Streaming Instabilities in Protoplanetary Disks." *The Astrophysical Journal*, 620(1), 459–469. doi:10.1086/426895.
- **Walsh, K. J., Morbidelli, A., Raymond, S. N., O'Brien, D. P., & Mandell, A. M. (2011).** "A low mass for Mars from Jupiter's early gas-driven migration." *Nature*, 475, 206–209. doi:10.1038/nature10201.
- **ALMA Partnership (Brogan, C. L., et al.) (2015).** "The 2014 ALMA Long Baseline Campaign: First Results from High Angular Resolution Observations toward the HL Tau Protoplanetary Disk." *The Astrophysical Journal Letters*, 808(1), L3. doi:10.1088/2041-8205/808/1/L3.
- **Stern, S. A., et al. (2019).** "Initial results from the flyby of New Horizons at the Kuiper Belt object (486958) Arrokoth." *Science*, 364(6441), eaaw9771. doi:10.1126/science.aaw9771.

Citation: Mahmud, S. (2026). "The Solar Cradle — The Protoplanetary Disk, Planetesimal Accretion, and the Young Sun." In The Universal Chronicle, Part 7. https://shakilmahmud.com/universal-chronicle-part-7-the-solar-cradle/

Shakil Mahmud • Research Monograph

SHAKIL MAHMUD RESEARCH MONOGRAPHS • PART VIII

The Violent Genesis — The Hadean Earth, Theia Giant Impact, and the Birth of the Moon

The Violent Genesis — The Hadean Earth, Theia Giant Impact, and the Birth of the Moon

1,922 words • October 30, 2026 • Permanent URI



Plate VIII: *Figure: The cataclysmic Giant Impact hypothesis (~4.51 Ga): Mars-sized protoplanet Theia collides with the proto-Earth, vaporizing silicates and ejecting a blazing debris disk that rapidly accreted to form the Moon.*

Four and a half billion years ago, the inner Solar System was an astronomical war zone of colliding protoplanets. In the most catastrophic event in our planet's history, an infant world named Theia struck the young Proto-Earth at ten kilometers per second. The cataclysmic energy vaporized both worlds into a swirling donut of incandescent silicate gas, plunged Theia's metallic core into Earth's center, and launched a glowing orbital ring from which our Moon coalesced in less than a millennium—bestowing upon Earth the gravitational gyroscope that made complex life possible.

The Hadean Infancy: Melting a Planet and the Iron Catastrophe

The earliest geological eon of Earth history is named the **Hadean** (after Hades, the Greek god of the underworld). In popular imagination, the Hadean is pictured as a static landscape of volcanic lava. In planetary physics, however, the Hadean was a dynamic crucible driven by extreme internal heat sources:

- **Short-Lived Radionuclides:** The decay of extinct isotopes injected by the ancestral supernova, primarily ^{26}Al ($t_{1/2} \approx 717{,}000$ yr) and ^{60}Fe ($t_{1/2} \approx 2.6$ Myr), pumped billions of joules of radioactive heat into the interior.
- **Gravitational Accretion Energy:** Every kinetic impact of an incoming planetesimal converted kinetic energy ($\frac{1}{2}mv^2$) directly into thermal energy upon impact.
- **Gravitational Core Differentiation:** The sinking of dense iron released additional potential energy, heating the planet by an additional 2,000 K.

Within its first 30 million years, Proto-Earth melted completely, transforming into a global **Magma Ocean** extending over 1,000 kilometers deep. In this molten bath occurred the defining geochemical event of our planet's interior: **The Iron Catastrophe**.

Goldschmidt Geochemical Classification

In 1923, Victor Goldschmidt demonstrated that elements partition according to their chemical affinities. Dense, metallic **siderophile ("iron-loving") elements**—primarily iron, nickel, cobalt, gold, and platinum—became immiscible in liquid silicates and sank under gravity toward the planet's center in massive metallic diapirs. Floating above them, the lighter **lithophile ("rock-loving") elements**—silicon, oxygen, aluminum, magnesium, and calcium—formed a thick silicate mantle. Earth had acquired its metallic core ($r \sim 3{,}480$ km), setting up the geodynamo that generates our protective magnetic shield.

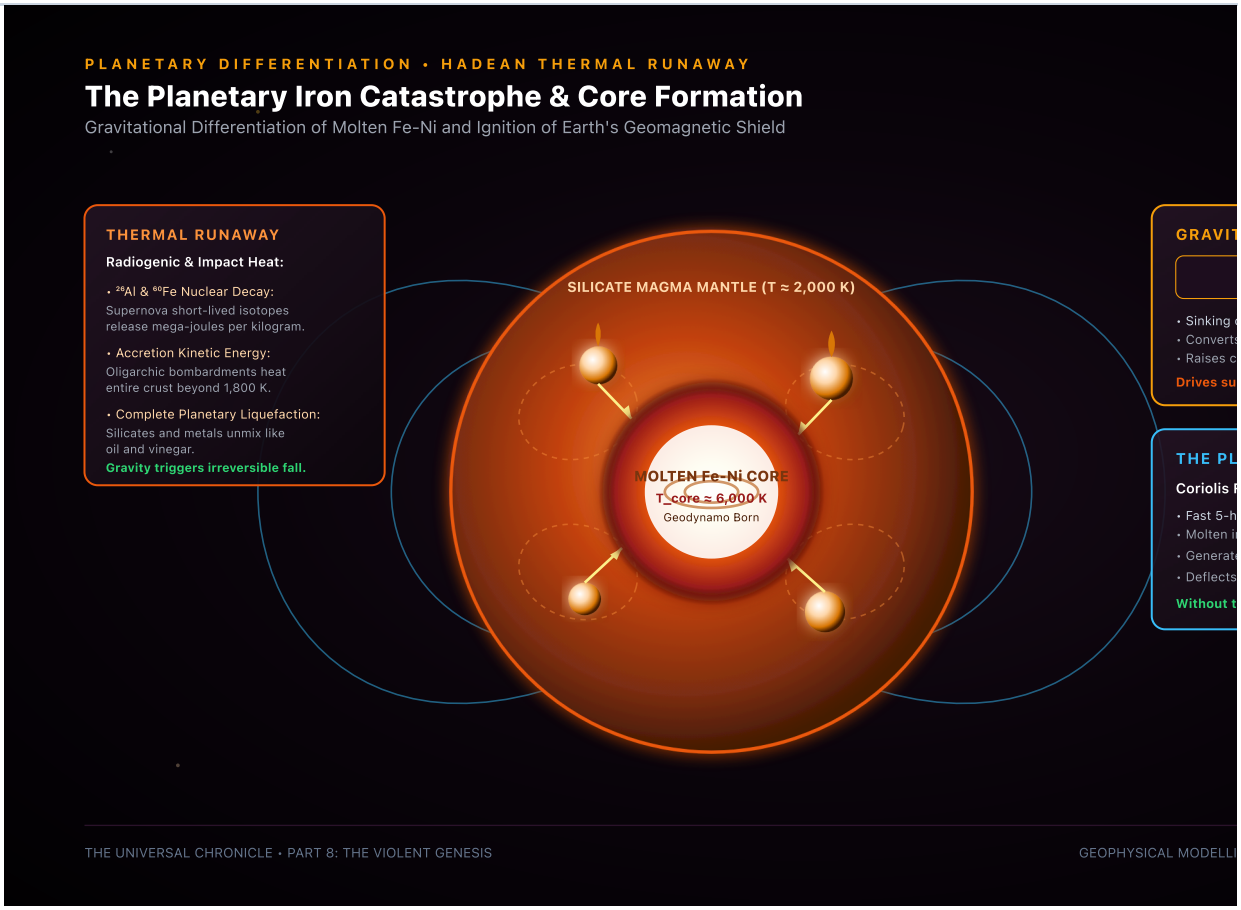


Figure 8.1a: The Planetary Iron Catastrophe and geodynamo ignition. Accretion impacts and short-lived radiogenic heating ($^{26}\mathrm{Al}$ and $^{60}\mathrm{Fe}$) induced wholesale planetary melting, allowing dense molten iron-nickel diapirs to sink catastrophically to Earth's center, releasing 2×10^{30} J of gravitational heat and establishing the protective dipolar geomagnetic shield.

Shakil Mahmud • Research Monograph

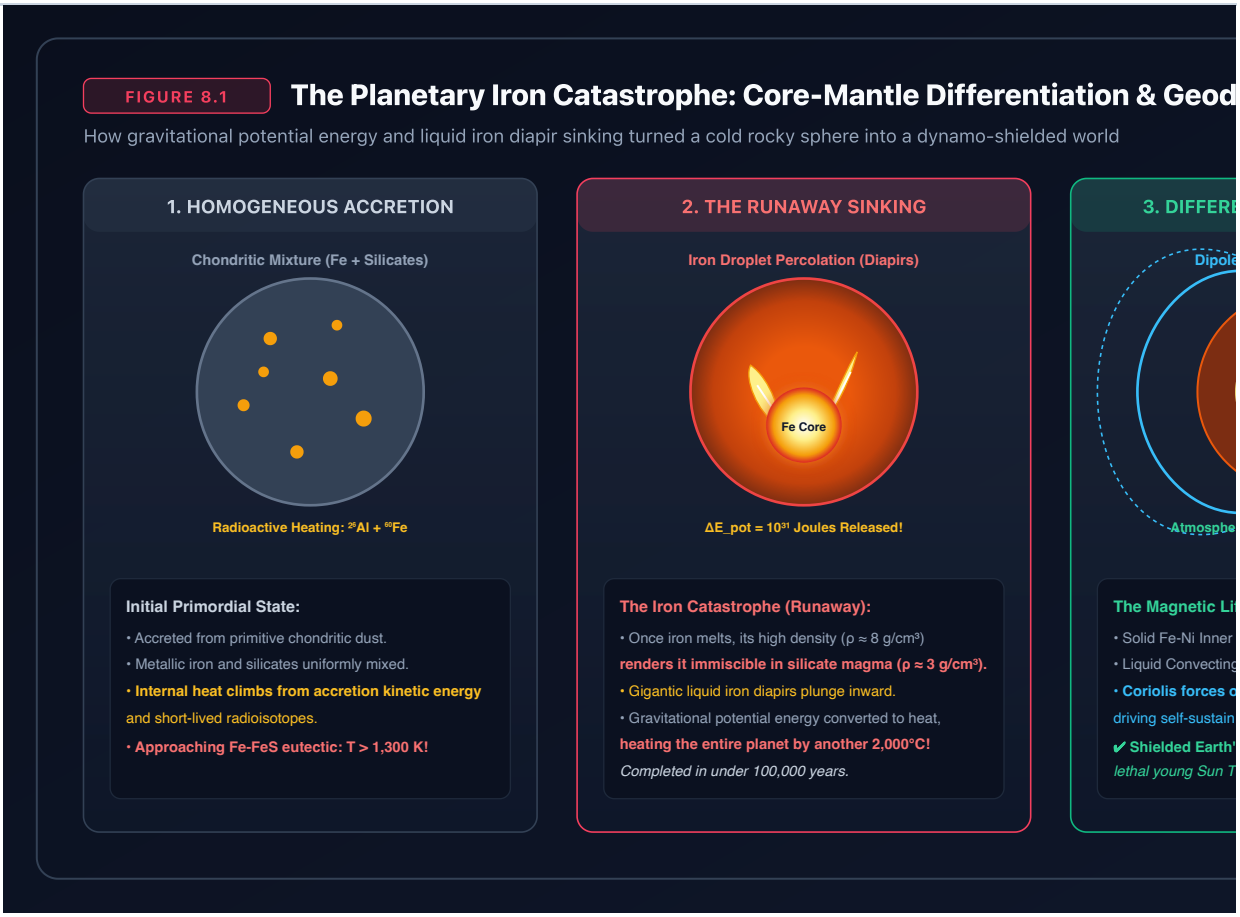


Figure 8.1: The Planetary Iron Catastrophe & Geodynamo. Radioactive decay of ^{26}Al and violent accretion impacts heated the infant Earth past 1,800 K, melting iron-nickel. Dense liquid iron droplets coalesced into massive diapirs that sank to Earth's center in under 100,000 years, liberating 10^{31} Joules of gravitational energy and establishing the convecting liquid outer core that powers our protective magnetic shield.

The Giant Impact: The Day Earth and Theia Collided

By approximately 4.51 billion years ago (t_0 + 50–70 million years), Proto-Earth had grown to roughly 90% of its current mass. But orbiting in the same chaotic neighborhood—likely originating at the Sun-Earth L_4 or L_5 Lagrange point before being nudged into an eccentric orbit—was another protoplanetary embryo roughly the size of Mars (10% of Earth's mass), named by astronomers **Theia** (after the Titaness who was the mother of Selene, the Moon).

At an oblique angle of approximately 45°, Theia slammed into Proto-Earth at a relative velocity exceeding **10 kilometers per second (36,000 km/h)**.

1. The Energetics of Annihilation

The kinetic energy unleashed in the collision was staggering: roughly **10^{31} Joules (10^{38} ergs)**—the equivalent of trillions of Tsar Bomba nuclear detonations. In less than 30 minutes, Theia was completely shattered. Its metallic core plowed straight through Proto-Earth's mantle and merged permanently with Earth's molten core, creating an oversized, ultra-dense metallic heart for our planet.

2. The Synestia Hypothesis: A Donut of Vaporized Rock

For decades, simple numerical models assumed Theia struck a glancing blow that kicked a solid/liquid debris disk into orbit. However, in 2017, planetary scientists Simon Lock and Sarah Stewart proved that a giant impact between rapidly rotating planets generates temperatures exceeding 4,000 to 6,000 K, far beyond the vaporization point of silicate rock (T_{vap} ≈ 2, K).

The collision transformed Earth into a **Synestia**—a colossal, rapidly rotating, donut-shaped mass of vaporized rock and supercritical fluid spanning over 100,000 kilometers across, rotating faster than its orbital velocity. Inside this vaporized rock cloud, the material of Earth and Theia was vigorously mixed, homogenizing their isotopic compositions.

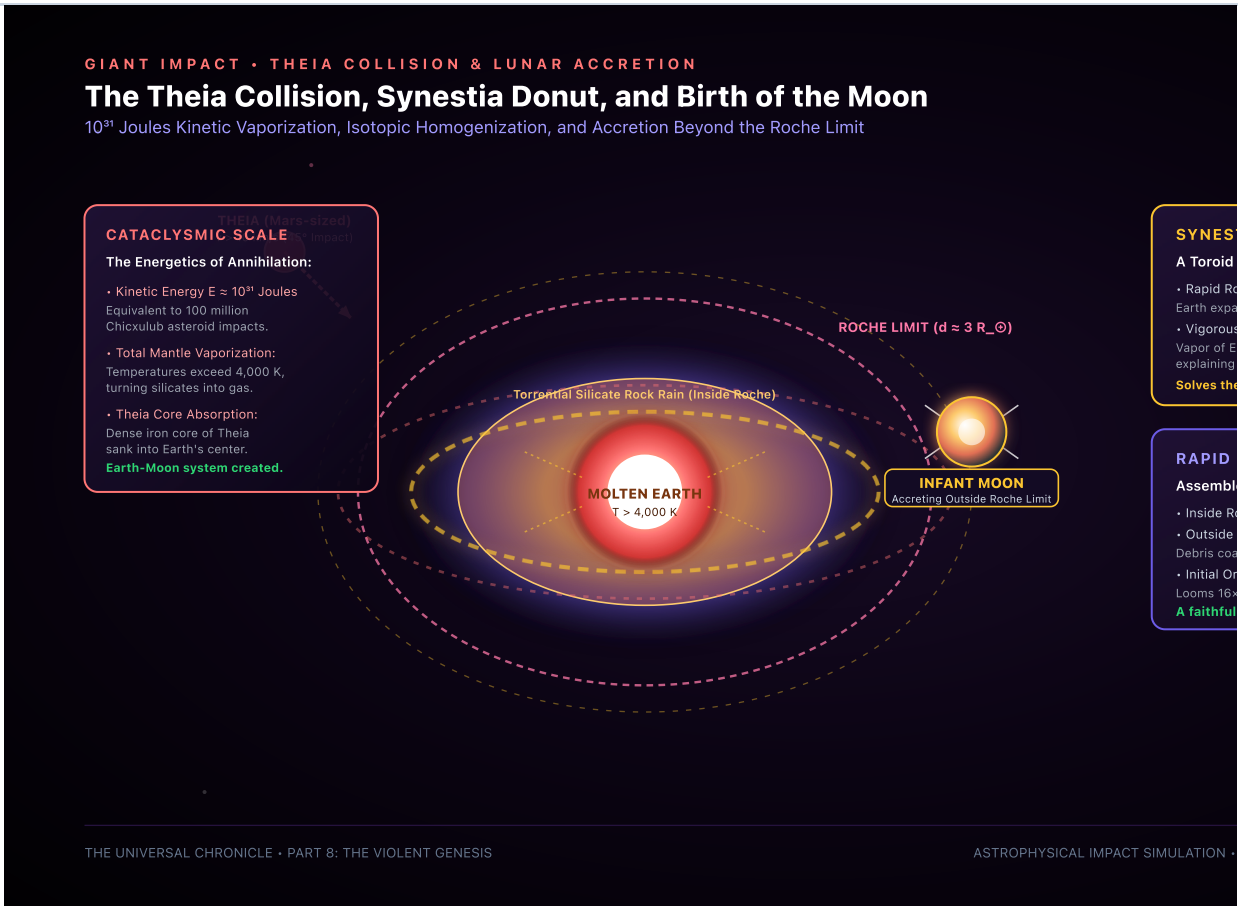


Figure 8.2a: The Theia giant impact and toroidal Synestia accretion. A Mars-sized protoplanet colliding at $10\ \mathrm{km/s}$ unleashed $10^{31}\ \mathrm{J}$, vaporizing the silicate mantle into a vast rapidly rotating Synestia donut, where isotopic signatures homogenized and debris beyond the Roche limit ($d \approx 3R_{\oplus}$) rapidly coalesced into the infant Moon.

Shakil Mahmud • Research Monograph

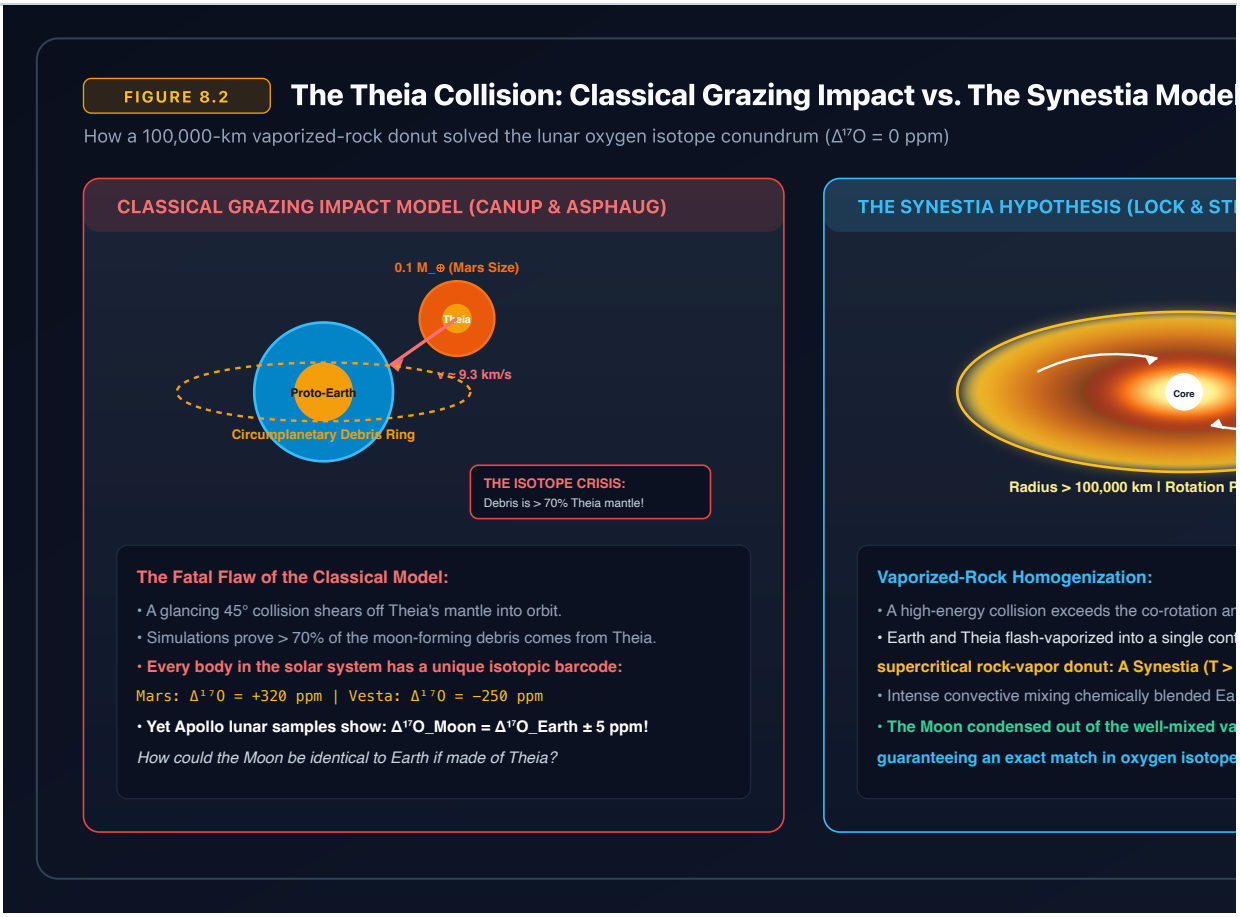


Figure 8.2: The Theia Collision & The Synestia Breakthrough (Lock & Stewart 2017). Classical grazing models failed because they predicted the Moon should be composed predominantly (> 70%) of Theia's mantle, contradicting identical Apollo oxygen isotope measurements ($\Delta^{17}O = 0$ ppm). The Synestia model resolves this: a high-energy collision vaporized both bodies into a giant, rapidly rotating rock-vapor donut spanning > 100,000 km, driving turbulent phase-mixing that completely homogenized Earth and lunar isotopic barcodes.

The Rapid Accretion of the Moon: Assembled in Centuries

As the outer perimeter of the vaporized synestia cooled, silicate rock droplets condensed like rain outside Earth's **Roche Limit** (~ 3–5 $R_\oplus \approx 18{,}000$ km)—the distance within which planetary tidal forces tear celestial bodies apart.

High-resolution supercomputer simulations reveal that once outside the Roche limit, gravitational instability caused this molten ring of debris to coalesce into the Moon with astonishing speed: not over millions of years, but in **barely 100 to 1,000 years!**

The Oxygen Isotope Fingerprint

Every celestial body in the Solar System possesses a distinct isotopic fingerprint: meteorites from Mars, Vesta, and chondrite parent bodies have unique ratios of Oxygen-17 to Oxygen-18 (Δ^{17}O). Yet, when Apollo astronauts brought back lunar basalt samples, mass spectrometers revealed that **Earth rocks and Moon rocks share an identical Δ^{17}O ratio to within a few parts per million**. The total vaporization and turbulent isotopic mixing inside the post-impact synestia explains this identical geochemical parentage perfectly.

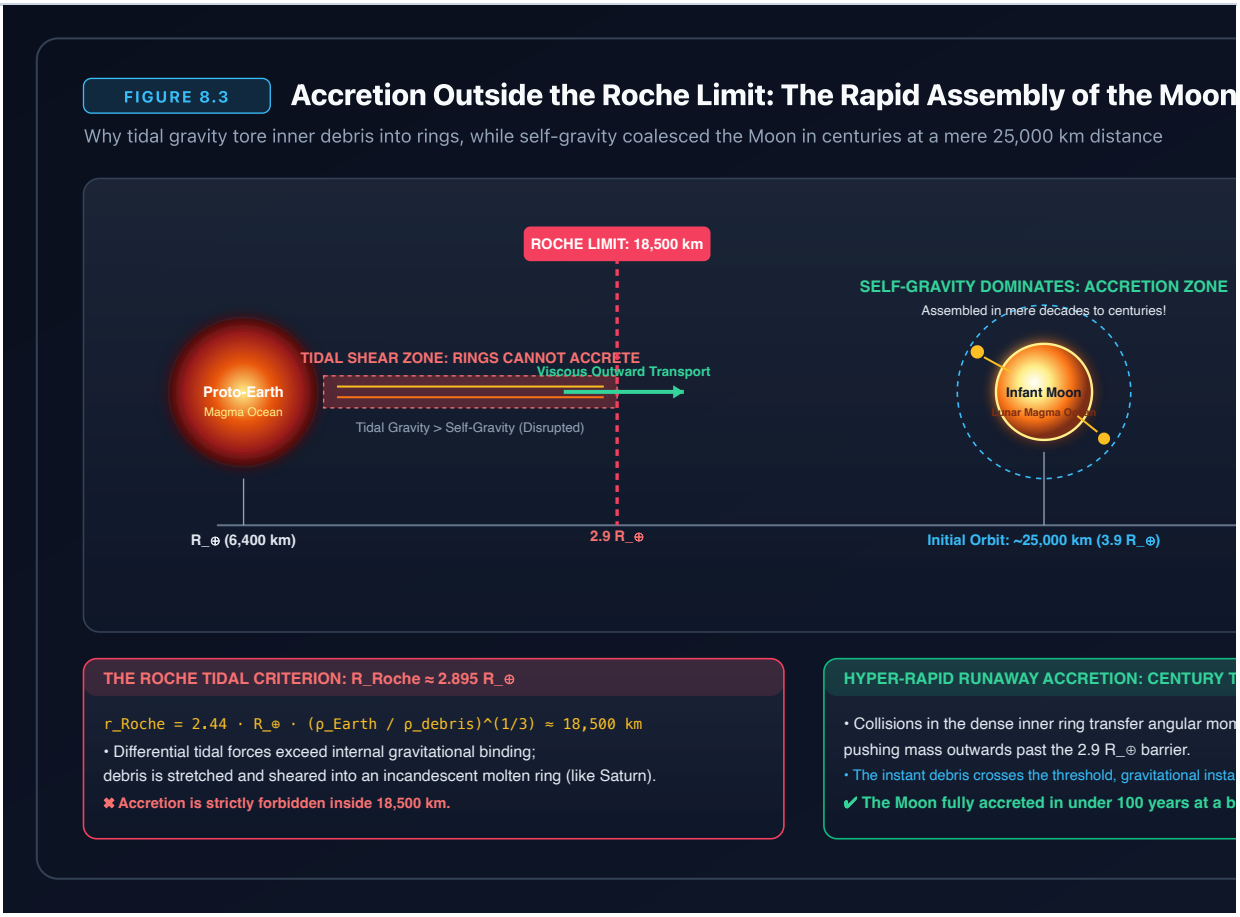


Figure 8.3: Accretion Outside the Roche Limit (18,500 km). Inside the fluid Roche limit (2.9 R_⊕), Earth's differential tidal gravity sheared debris into an incandescent, un-accretable molten ring. Viscous collisions pushed matter outward past 18,500 km, where self-gravity abruptly overpowered tidal forces, accreting the entire Moon in under 100 years at a blistering distance of only ~25,000 km.

The Moon's Indispensable Gifts: Why Earth Needs its Lunar Companion

Earth has the largest satellite relative to its own size of any terrestrial planet in the Solar System (M_{Moon} ≈ 1.2\% M_⊕). Without this oversized companion, Earth would be a vastly different, hostile world:

- **1. Gyroscopic Obliquity Stabilization (Touma & Wisdom 1993):** The gravitational torque of the Moon locks Earth's axial tilt into a remarkably stable variation between 22.1° and 24.5° over a 41,000-year Milankovitch cycle (currently 23.44°). Without the Moon, gravitational perturbations from Jupiter and Saturn would cause Earth's obliquity to swing wildly from 0° to over 85°—plunging the equator into permanent ice and scorching the poles, rendering sustained evolutionary ecosystems nearly impossible. (Mars, lacking a massive moon, experiences chaotic axial tilt swings up to 60°).
- **2. Braking the 5-Hour Day:** Immediately after the impact, Earth was spinning at a dizzying velocity, with a day lasting barely **5 hours**. Through gravitational tidal friction, the Moon has been transferring Earth's rotational angular momentum to its own orbital distance, slowing Earth's rotation down over billions of years to a comfortable 24-hour cycle.
- **3. Colossal Ancient Tides:** When the Moon first formed, it orbited at a distance of barely **25,000 kilometers** (compared to 384,400 km today), appearing sixteen times larger in the sky. Lunar tides were kilometers high, sweeping vast distances across ancient continental margins twice a day. These immense tidal cycles created dynamic intertidal flats with alternating wetting, drying, and salinity cycles that served as prime geological crucibles for prebiotic chemistry.

Shakil Mahmud • Research Monograph

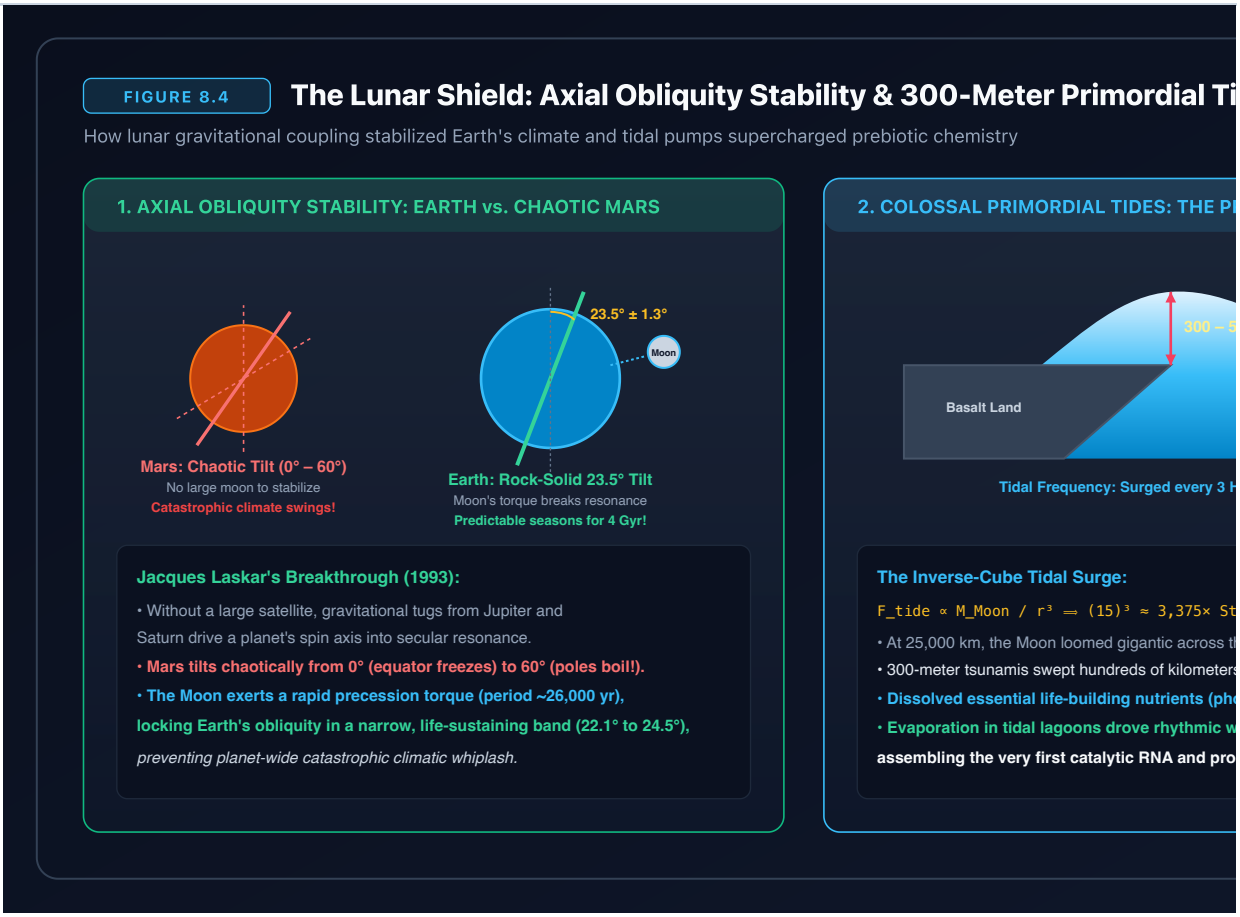


Figure 8.4: The Lunar Stabilizer & Megatides. Without the Moon, solar and Jovian perturbations would drive Earth's axial tilt into chaotic oscillations (0° to 60°, as seen on Mars), destroying climatic stability. The Moon's gravitational torque locks our tilt at 23.5° ± 1.3°. Simultaneously, its close 25,000-km orbit generated 300-meter megatides every 3 hours across a 5-hour Earth day, dissolving mineral nutrients and driving cyclic wet-dry prebiotic polymerization in volcanic tidal pools.

Comparative Metrics: Earth, Theia, and the Infant Moon

Property / Metric	Proto-Earth (Pre-Impact)	Theia (Impactor)	Modern Earth	The Moon
Mass	~ 0.90 M_⊕	~ 0.10 M_⊕ (Mars size)	5.972 × 10^{24} kg (1.0 M_⊕)	7.342 × 10^{22} kg (0.0123 M_⊕)
Radius	~ 6,100 km	~ 3,390 km	6,371 km	1,737 km
Core Mass Fraction	~ 30\%	~ 20–30\%	**32.5\%** (Oversized)	< **2\%** (Depleted)
Initial Day Length	~ 8–10 hours	Unknown	~ 5 hours (Post-impact)	Tidally locked (27.3 days)
Initial Orbital Distance	1.0 AU	~ 1.0 AU (Lagrange orbit)	1.0 AU	~ 25,000 km (384,400 km today)
Volatile Content (H2O, K)	Moderate	Moderate	Preserved / Replenished	Extremely depleted in volatiles

The Aftermath: The Freezing of the Magma Ocean

Following the departure of Theia and the coalescence of the Moon, Earth was enveloped in a glowing supercritical atmosphere of vaporized rock and high-pressure steam (> 100 bars). Surface temperatures hovered near 2,000 K, glowing dull orange in the dark of space.

Yet, the radiative physics of space is unforgiving. Radiating energy outward at hundreds of watts per square meter, the surface began to cool. Within two to three million years, the outer magma ocean froze into a brittle basaltic crust. Beneath this fragile shell, intense mantle convection churned, while volcanic degassing belched gigatons of steam, carbon dioxide, sulfur, and nitrogen into the cooling sky.

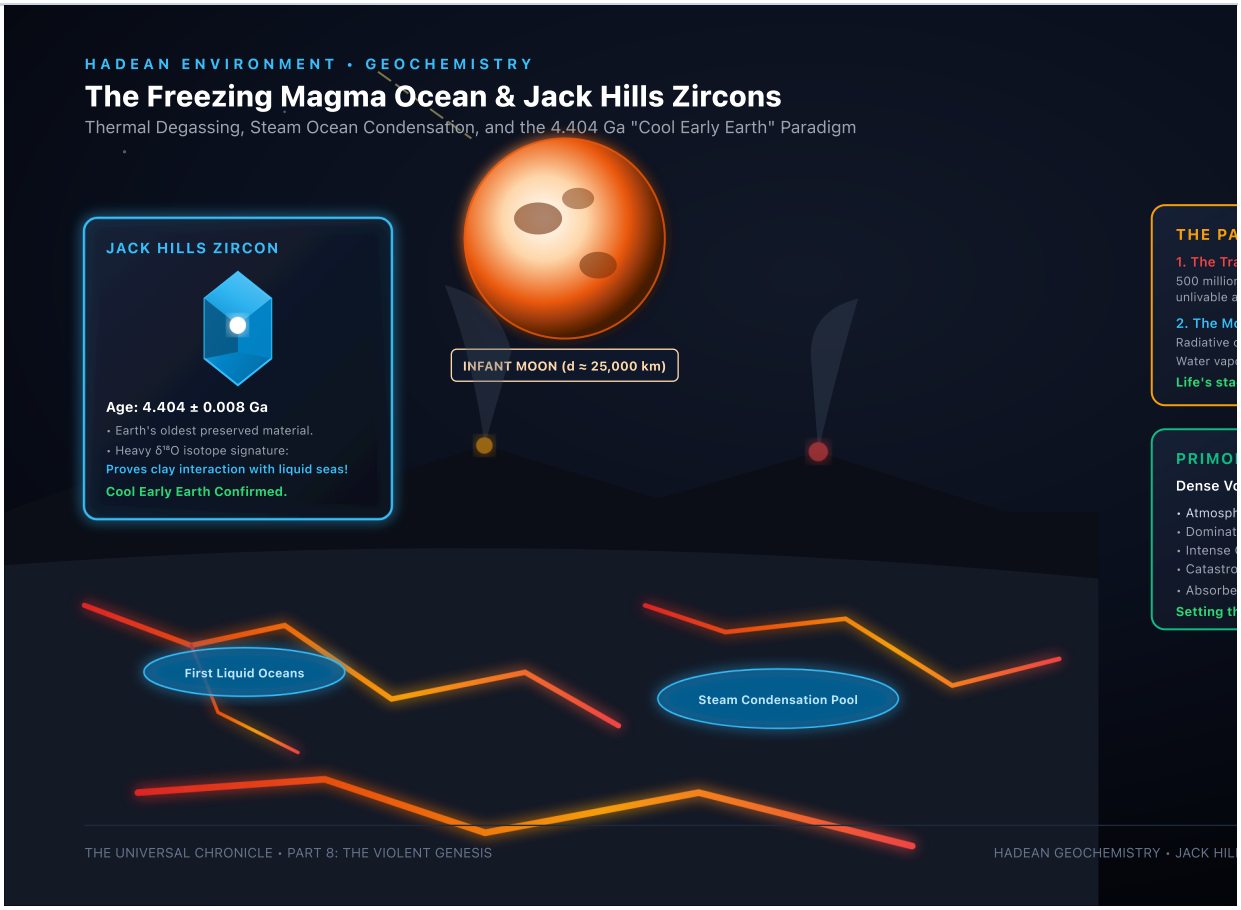


Figure 8.5a: Magma ocean solidification and the 4.404 Ga Jack Hills zircon evidence. Radiative cooling through space solidified a basaltic crust within millions of years, collapsing dense volcanic steam into torrential rains and warm acidic proto-oceans, directly verified by elevated $\delta^{18}O$ isotope ratios in ancient zircon crystals.

The stage was set for the greatest deluge in terrestrial history. When the atmospheric temperature finally dropped below the critical point of water, the steam clouds condensed into torrential, planetary rain. In **Part 9** of *The Universal Chronicle*, we will witness the birth of the hydrosphere: **The Primordial Cradle — Volcanic Degassing, Cometary Bombardment, and the First Oceans**.

Shakil Mahmud • Research Monograph

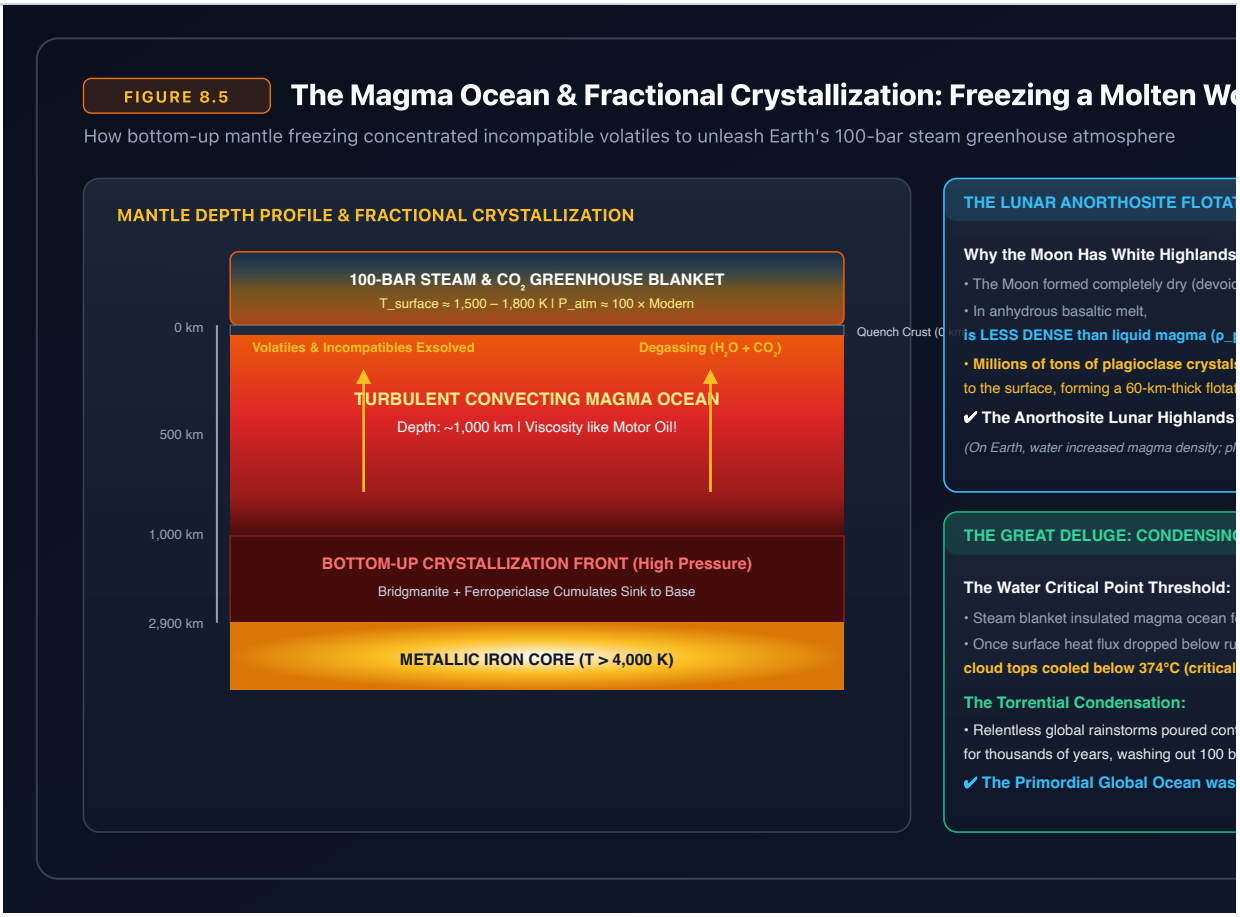


Figure 8.5: Freezing of the Magma Ocean & The Great Deluge. High pressure drove bottom-up crystallization of the 1,000-km-deep terrestrial magma ocean, concentrating incompatible volatile gases (H2O, CO2) into a dense 100-bar greenhouse steam blanket. While buoyant plagioclase floated on the dry Moon to form the white anorthosite highlands, Earth's steam atmosphere eventually cooled below 374°C, releasing torrential global rains that condensed into our first world ocean.

Academic Citations & Foundational Literature

- **Hartmann, W. K., & Davis, D. R. (1975).** "Satellite-sized planetesimals and lunar origin." *Icarus*, 24(4), 504–515. doi:10.1016/0019-1035(75)90070-6.
- **Cameron, A. G. W., & Ward, W. R. (1976).** "The Origin of the Moon." *Lunar and Planetary Science Conference Proceedings*, 7, 120–122.
- **Canup, R. M., & Asphaug, E. (2001).** "Origin of the Moon in a giant impact during the end of the Earth's formation." *Nature*, 412, 708–712. doi:10.1038/35089010.
- **Touma, J., & Wisdom, J. (1993).** "The Chaotic Obliquity of Mars." *Science*, 259(5099), 1294–1297. doi:10.1126/science.259.5099.1294.
- **Lock, S. J., & Stewart, S. T. (2017).** "The structure and evolution of synestias: A new type of planetary object formed by high-energy, high-angular-momentum giant impacts." *Journal of Geophysical Research: Planets*, 122(5), 950–982. doi:10.1002/2016JE005239.
- **Barboni, M., et al. (2017).** "Early formation of the Moon 4.51 billion years ago." *Science Advances*, 3(1), e1602365. doi:10.1126/sciadv.1602365.

Citation: Mahmud, S. (2026). "The Violent Genesis — The Hadean Earth, Theia Giant Impact, and the Birth of the Moon." In The Universal Chronicle, Part 8. https://shakilmahmud.com/universal-chronicle-part-8-the-violent-genesis/

SHAKIL MAHMUD RESEARCH MONOGRAPHS • PART IX

The Primordial Cradle — Volcanic Degassing, Cometary Bombardment, and the First Oceans

The Primordial Cradle — Volcanic Degassing, Cometary Bombardment, and the First Oceans

2,078 words • October 31, 2026 • Permanent URI



Plate IX: *Figure: The late Hadean Earth (~4.4–4.1 Ga): mantle convection and volcanic outgassing saturate the carbon-dioxide-rich atmosphere, unleashing torrential planetary rainfalls that cool the basaltic crust and condense the first global oceans.*

For over two centuries, geology envisioned the infant Earth as a dry, radioactive wasteland of boiling magma that persisted for half a billion years. In recent decades, however, microscopic crystal zircons from Western Australia revealed a radical truth: within barely 160 million years of the Solar System's birth, the surface cooled, supercritical steam clouds condensed into a torrential planetary deluge, and a vast, dark, global ocean swept across the world—illuminated by an immense Moon orbiting dangerously close in the sky.

The Collapse of the Steam Atmosphere: The Great Planetary Deluge

In the direct aftermath of the Theia giant impact, Earth was enveloped in a scorching, supercritical atmosphere composed primarily of water vapor (H_2O), carbon dioxide (CO_2), carbon monoxide (CO), molecular nitrogen (N_2), and sulfur gases. The atmospheric pressure at the molten surface was crushing—exceeding **100 to 200 bars** (equivalent to the hydrostatic pressure one to two kilometers beneath modern oceans).

Because water vapor is a potent greenhouse gas, it trapped planetary thermal radiation, creating a thermal blanket. However, as the outer magma ocean froze into an insulating basaltic crust, the heat flux from the planetary interior dropped by orders of magnitude. The top of the steam atmosphere radiated heat directly into the cold vacuum of space at the *Simpson-Nakajima runaway greenhouse limit* (~ 280–310 W/m^2).

The Condensation Point of a Supercritical Atmosphere
Under a crushing surface pressure of 100 atmospheres, water does not boil at 100°C (K); its condensation temperature is elevated to over **300°C (K)**. When the surface crust finally cooled past this critical threshold, the atmospheric moisture reached saturation. The steam atmosphere collapsed into a continuous, torrential rainfall that pounded the planet uninterrupted for **thousands of years**, filling the low-lying impact basins and tectonic depressions with liquid water.

Shakil Mahmud • Research Monograph

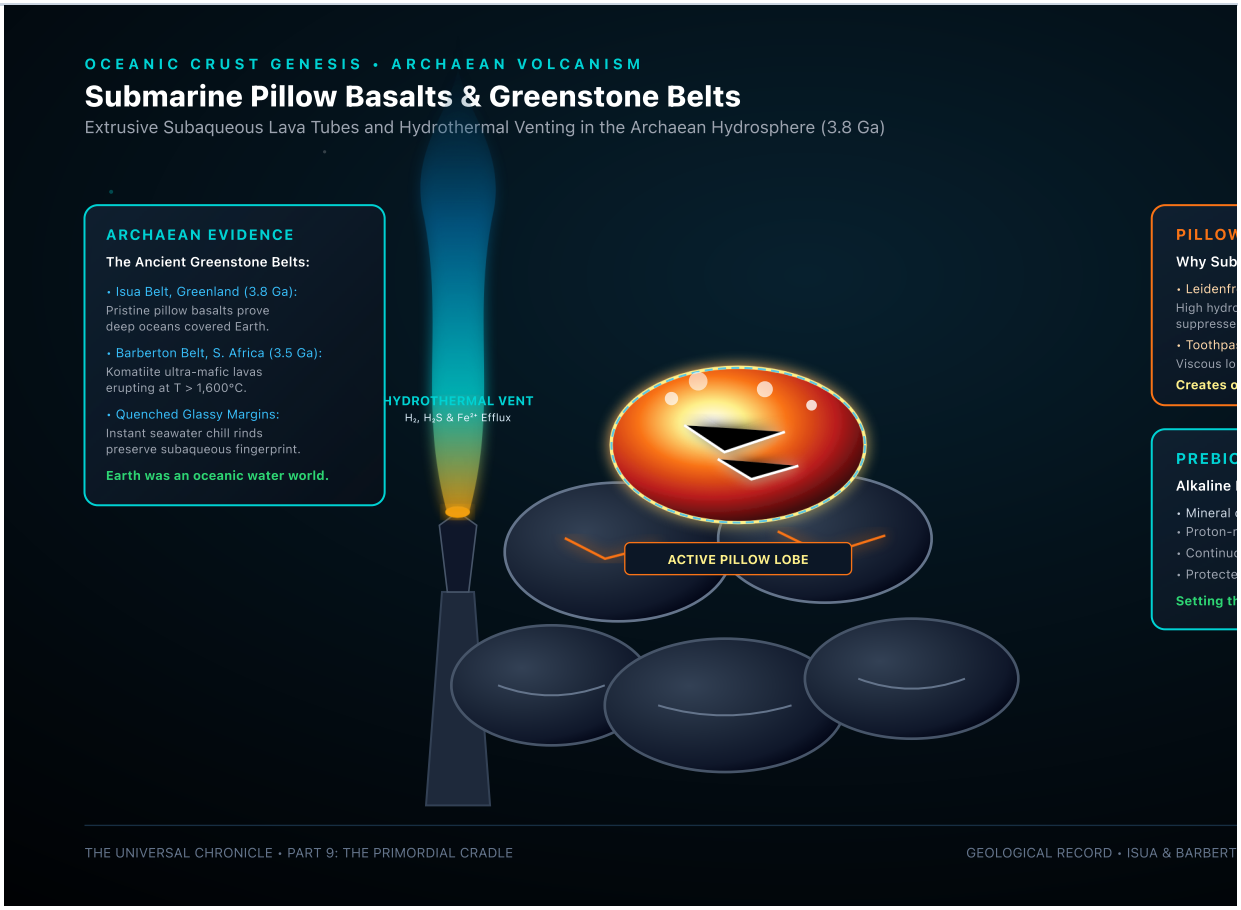


Figure 9.1a: Submarine pillow basalts and Archaean hydrothermal venting. High hydrostatic pressure in the newly condensed primordial ocean suppressed explosive boiling, allowing subaqueous komatiitic and basaltic lava lobes to quench into characteristic pillow structures preserved today in the 3.8 Ga Isua and Barberton greenstone belts.

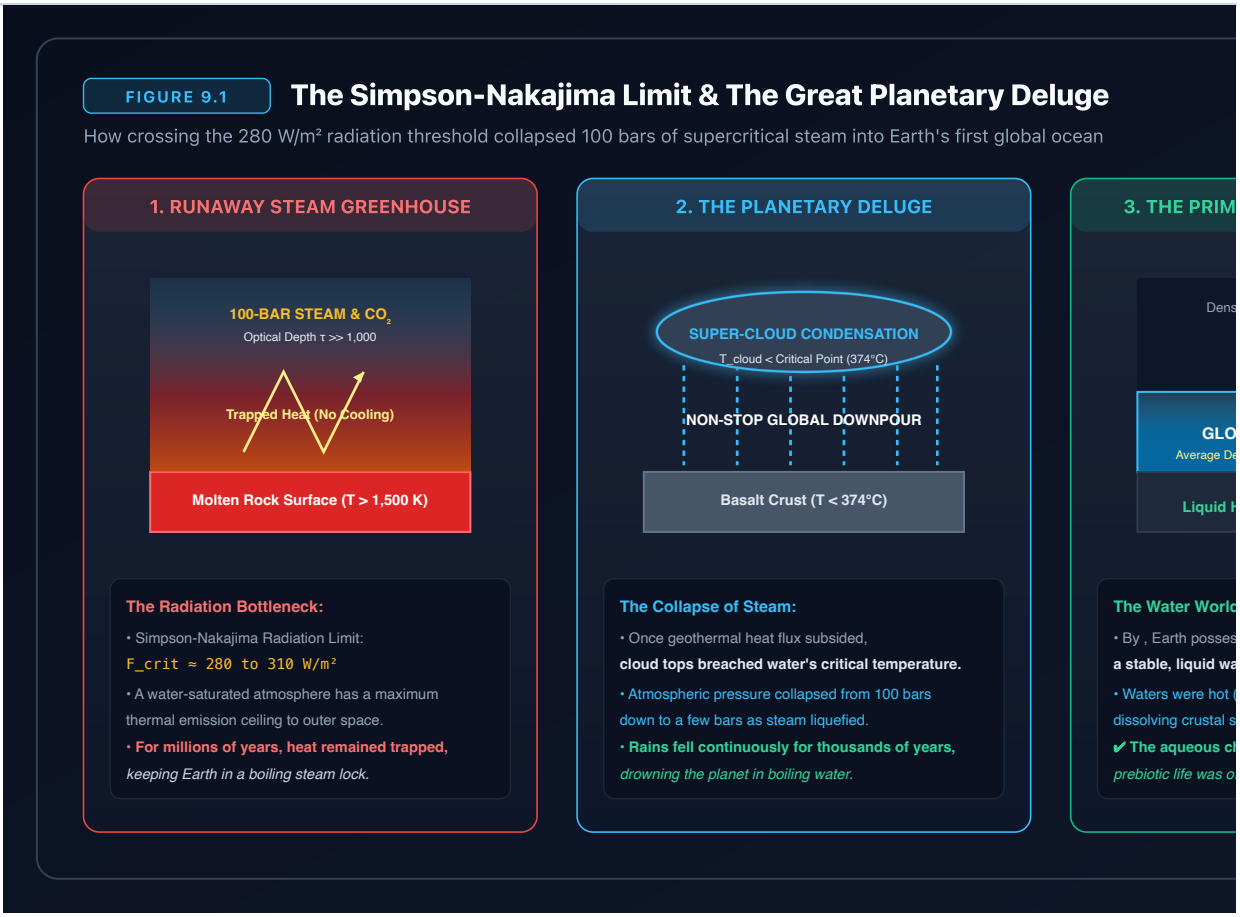


Figure 9.1: The Simpson-Nakajima Limit & The Great Planetary Deluge. A water-saturated atmosphere has an absolute thermal emission ceiling to space (~280–310 W/m^2). Once geothermal heat flux from magma cooling dropped below this threshold, cloud tops cooled below water's critical point (374°C), causing the 100-bar steam atmosphere to violently collapse in a thousands-of-years-long continuous global downpour that pooled into Earth's first world ocean.

Where Did Earth's Water Come From? Comets vs. Asteroids

One of the classic mysteries of planetary science is how Earth acquired its oceans. Because Earth formed inside the Solar System's snow line ($r < 2.7$ AU), where high temperatures prevented water ice from condensing, early planetary models assumed Earth must have formed completely bone-dry. The standard hypothesis for decades was that Earth's water was delivered late by a swarm of icy comets from the frozen outer Solar System.

The definitive test of this hypothesis lies in the **Deuterium-to-Hydrogen (D/H) Ratio**. Deuterium (^{2}H) is heavy hydrogen with an extra neutron. The ratio of D/H in Earth's oceans is defined as **SMOW (Vienna Standard Mean Ocean Water)**:

$$(D/H)_{\text{SMOW}} = (1.5576 \pm 0.001) \times 10^{-4}$$

Between 1986 and 2015, space missions analyzed the water vapor evaporating from comets:

- **Oort Cloud Comets (Halley, Hyakutake, Hale-Bopp):** Exhibited D/H ratios of (3.0 ± 0.5) × 10^{-4}—roughly **twice as high as Earth's oceans**.
- **Kuiper Belt Comet 67P/Churyumov-Gerasimenko:** In 2014, the ROSINA mass spectrometer aboard the European Space Agency's *Rosetta* orbiter measured a D/H ratio of (5.3 ± 0.7) × 10^{-4}—over **three times higher than Earth's oceans**!

If comets had delivered Earth's oceans, our water would be far richer in deuterium. Instead, isotopic measurements of **Carbonaceous Chondrite Asteroids** (specifically CI and CM chondrites from the outer asteroid belt) revealed a D/H ratio and nitrogen isotopic composition that matches Earth's ocean water with astonishing precision. Earth's water was delivered not by icy comets, but by **hydrated phyllosilicate minerals (clay minerals containing bound hydroxyl groups, OH$^-$)** inside carbonaceous asteroids scattered into the inner Solar System by the migration of Jupiter and Saturn!

Shakil Mahmud • Research Monograph

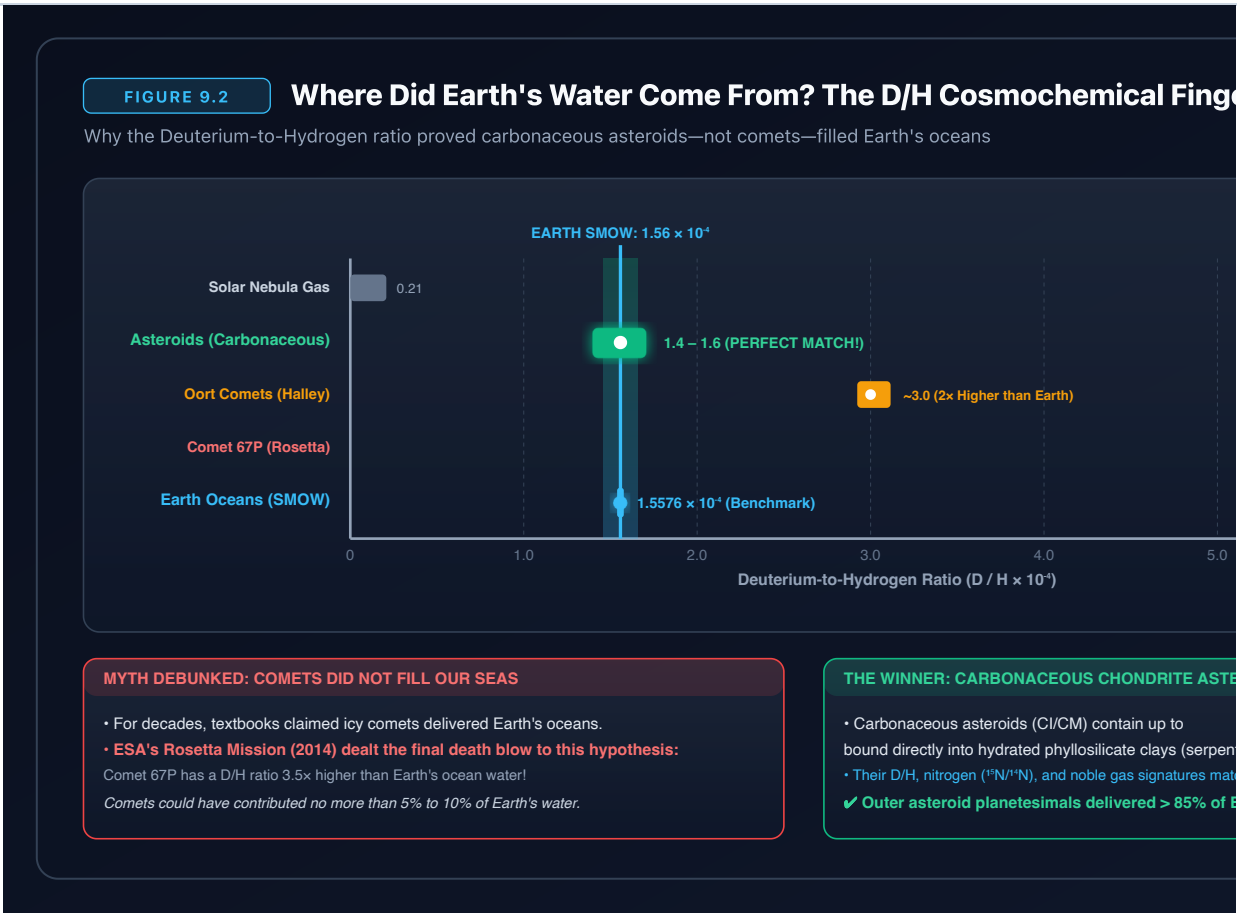


Figure 9.2: The D/H Ratio Fingerprint (Asteroids vs. Comets). Measuring deuterium-to-hydrogen ratios settled the debate over the origin of Earth's oceans. Oort cloud and Jupiter-family comets (like 67P) exhibit D/H values 2× to 3.5× higher than Earth's ocean benchmark (VSMOW = 1.5576×10^{-4}). In contrast, water-rich carbonaceous chondrite asteroids match Earth's exact isotopic barcode, proving asteroids from beyond 2.7 AU delivered > 85% of our oceans.

The Jack Hills Zircons: Physical Proof of a Cool, Wet Early Earth

Because plate tectonics and mantle convection constantly recycle the Earth's crust, no intact rock formations survive from the first 500 million years of Earth history. The oldest known intact rocks on Earth—the Acasta Gneiss in northern Canada—date to roughly 4.03 billion years ago. For generations, scientists believed the first 500 million years were lost forever.

Then, geochemists turned their attention to the **Jack Hills** in the desert of Western Australia. Embedded within younger Archean quartzites were microscopic, indestructible crystals of **Zircon ($ZrSiO_4$)** barely a tenth of a millimeter across.

The 4.404-Billion-Year-Old Time Capsule
In 2001, a team led by Simon Wilde and John Valley dated an individual zircon crystal (W74/2-36) using ion microprobe ($^{207}Pb/^{206}Pb$) uranium-lead dating to **4.404 ± 0.008 billion years old**—just 160 million years after the formation of the Solar System.

Crucially, analysis of the **Oxygen-18 isotopes ($\delta^{18}O$)** inside these ancient zircons revealed enriched values ($\delta^{18}O$ = 6.5 to 7.5‰), significantly higher than the mantle baseline (5.3‰). In petrology, such high $\delta^{18}O$ signatures can only be produced when rocks are altered at low temperatures by **liquid surface water** before being remelted into granitic magmas. The Jack Hills zircons provided indisputable chemical proof: **Earth had liquid oceans, continental granite crust, and a temperate surface climate by 4.4 billion years ago!**



Figure 9.3: The Jack Hills Zircons & The "Cool Early Earth" (4.404 Ga). Discovery of 4.4-billion-year-old zircon crystals ($ZrSiO_4$) in Western Australia shattered the myth of an unbroken 500-million-year molten Hadean hell. Their elevated oxygen isotope values ($\delta^{18}O$ = 6.5‰ to 7.5‰) require low-temperature weathering by liquid surface water and water-fluxed melting of granites, proving cool temperate oceans and continental crust existed just 160 million years after Earth formed.

The Faint Young Sun Paradox: Why Earth Did Not Freeze

The discovery of 4.4-billion-year-old oceans created a profound astrophysical paradox first articulated by **Carl Sagan and George Mullen in 1972**: the **Faint Young Sun Paradox**.

According to standard stellar evolution models, young main-sequence stars have a lower core density and temperature. 4.4 billion years ago, the Sun's core was fusing hydrogen at a slower rate, making our Sun **25% to 30% fainter** than it is today ($L \sim 0.70–0.75\ L_{\odot}$).

If modern Earth were suddenly exposed to a Sun 25% fainter, global surface temperatures would plunge to -30°C, freezing the entire planet into an irreversible, reflective "Snowball Earth." How did Earth maintain liquid oceans under a dim, faint young Sun?

Shakil Mahmud • Research Monograph

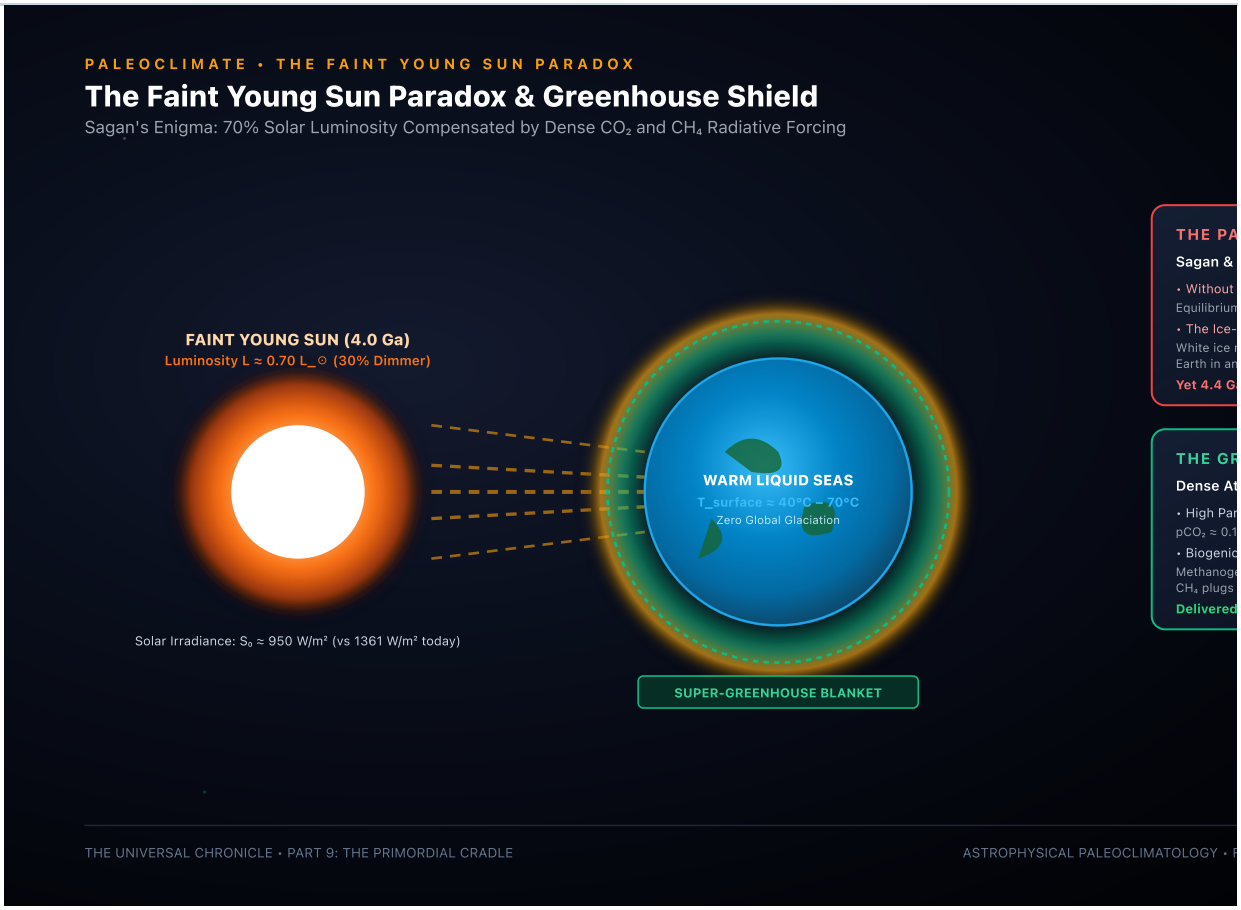


Figure 9.4a: The Faint Young Sun paradox and atmospheric greenhouse radiative forcing. Emitting only 70% of modern solar luminosity ($L \approx 0.70 L_{\odot}$), the young Sun would have locked Earth into an ice-albedo snowball without a dense greenhouse blanket of carbon dioxide (p\text{CO}_2 \approx 0.1\text{–}1.0\text{ bar}) and biogenic methane ($1,000$ ppm), delivering $+50^{\circ}\text{C}$ of warming.

The solution was a powerful, dense greenhouse atmosphere:

- **Carbon Dioxide Blanket:** The Hadean atmosphere contained between **0.5 and 5 bars of CO2** (hundreds of times higher than modern levels), released by continuous mantle outgassing and un-sequestered by modern continental carbonate weathering.
- **Methane Greenhouse (CH4):** Hydrothermal serpentinization reactions between seawater and ultramafic olivine rocks (Olivine + Water → Serpentine + Magnetite + Hydrogen) produced copious hydrogen, which combined with dissolved carbon to generate methane—a greenhouse gas 28 times more potent than CO2.
- **Reduced Surface Albedo:** With few exposed continents and no polar ice caps, the dark, iron-rich ocean absorbed over 90% of incident solar radiation.

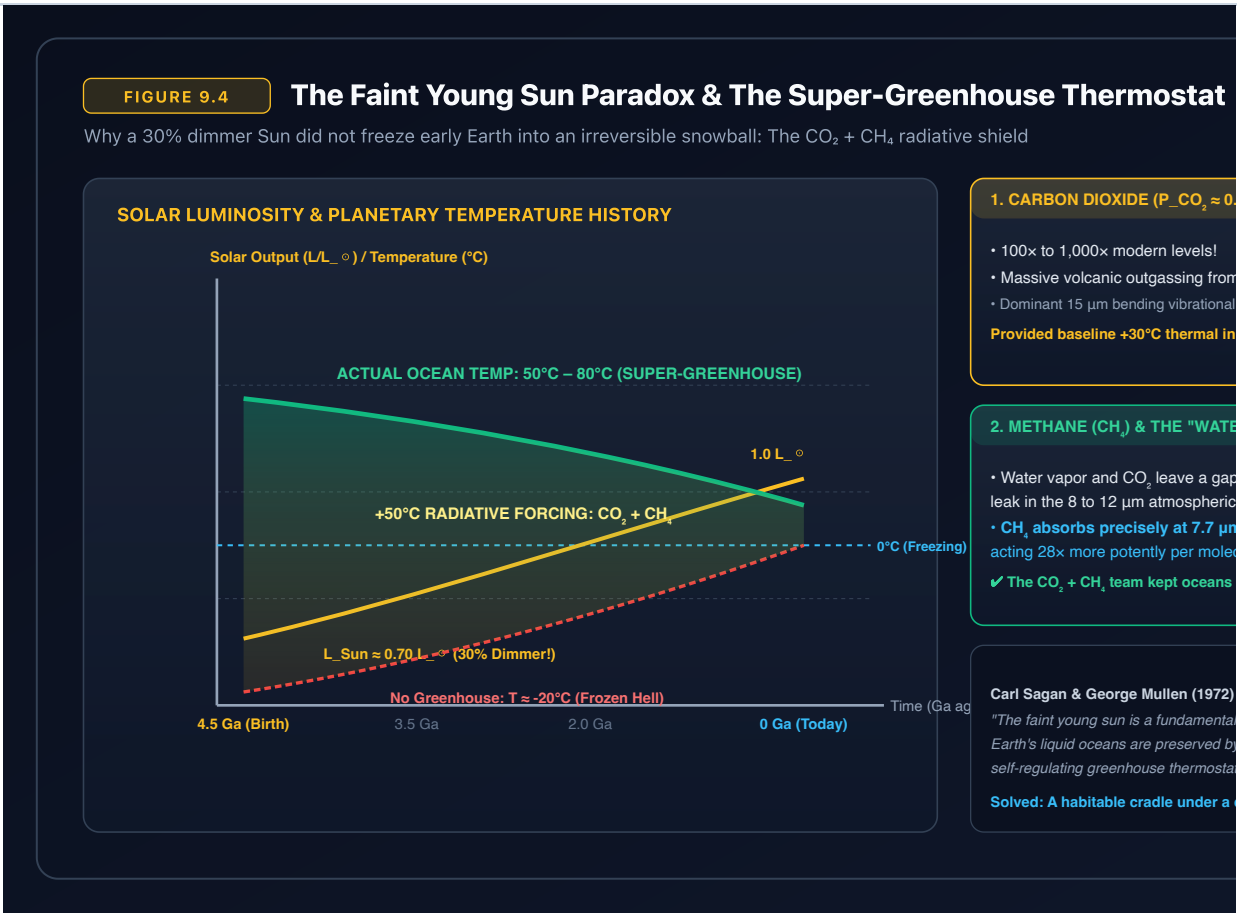


Figure 9.4: The Faint Young Sun Paradox & Radiative Forcing. At 4.5 Ga, the young Sun was 30% dimmer than today ($L \approx 0.70\ L_{\odot}$); under modern atmospheric greenhouse levels, Earth would have frozen into an irreversible -20°C snowball. A super-greenhouse atmosphere combining high carbon dioxide (0.1–1.0 bar) and potent methane (absorbing in the 8–12 μm water vapor window) provided +50°C of radiative forcing to sustain balmy, liquid oceans.

The Archean Ocean: A Ferrous, Green-Black Cauldron

If a time-traveler could stand on the shores of Earth 4.2 billion years ago, the landscape would be alien beyond imagination:

- **The Sky:** An orange-tinted or salmon-colored sky dominated by dense N2 and CO2, with zero free oxygen ($O_2 < 10^{-5}$ PAL). Heavy cloud cover generated frequent, violent lightning storms fueled by volcanic ash.
- **The Moon:** Hanging immense and luminous in the sky, orbiting at a fraction of its modern distance. Colossal, kilometers-high tides rushed in and out of coastal basins every few hours.
- **The Ocean:** An acidic, warm (40°C to 70°C), slightly effervescent sea saturated with dissolved ferrous iron (Fe^{2+}) and silica (SiO2). In the absence of oxygen, iron remained completely dissolved, tinting the ocean deep olive-green to black.

Shakil Mahmud • Research Monograph

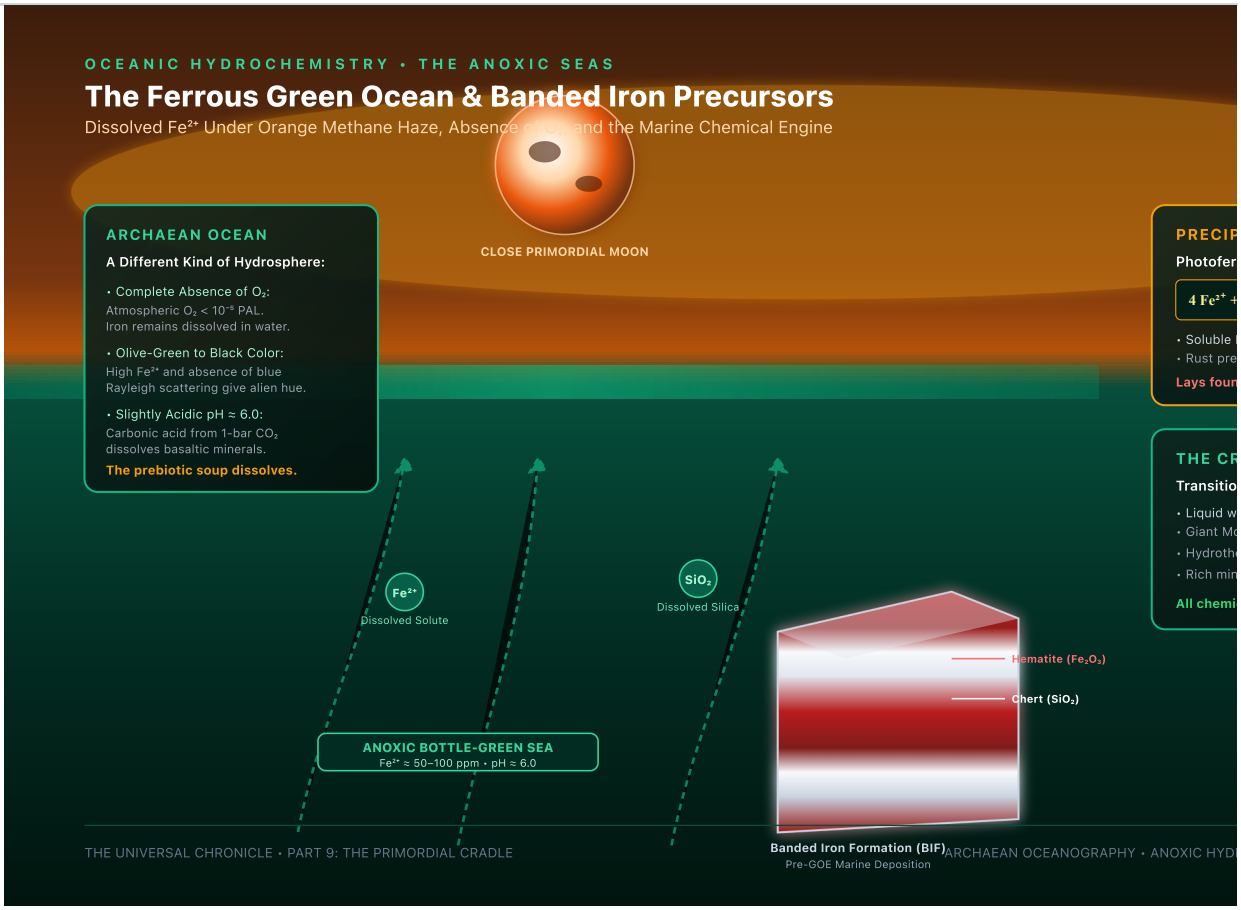


Figure 9.5a: The anoxic ferrous green ocean and pre-BIF sedimentation. In an atmosphere devoid of free oxygen (O_2 < 10^{-5}\text{ PAL}), iron dissolved completely as soluble ferrous ions (\text{Fe}^{2+} \approx 50\text{–}100\text{ ppm}), giving the global ocean an alien bottle-green to black tint beneath an orange methane haze before photoferrotrophy triggered the deposition of Banded Iron Formations.

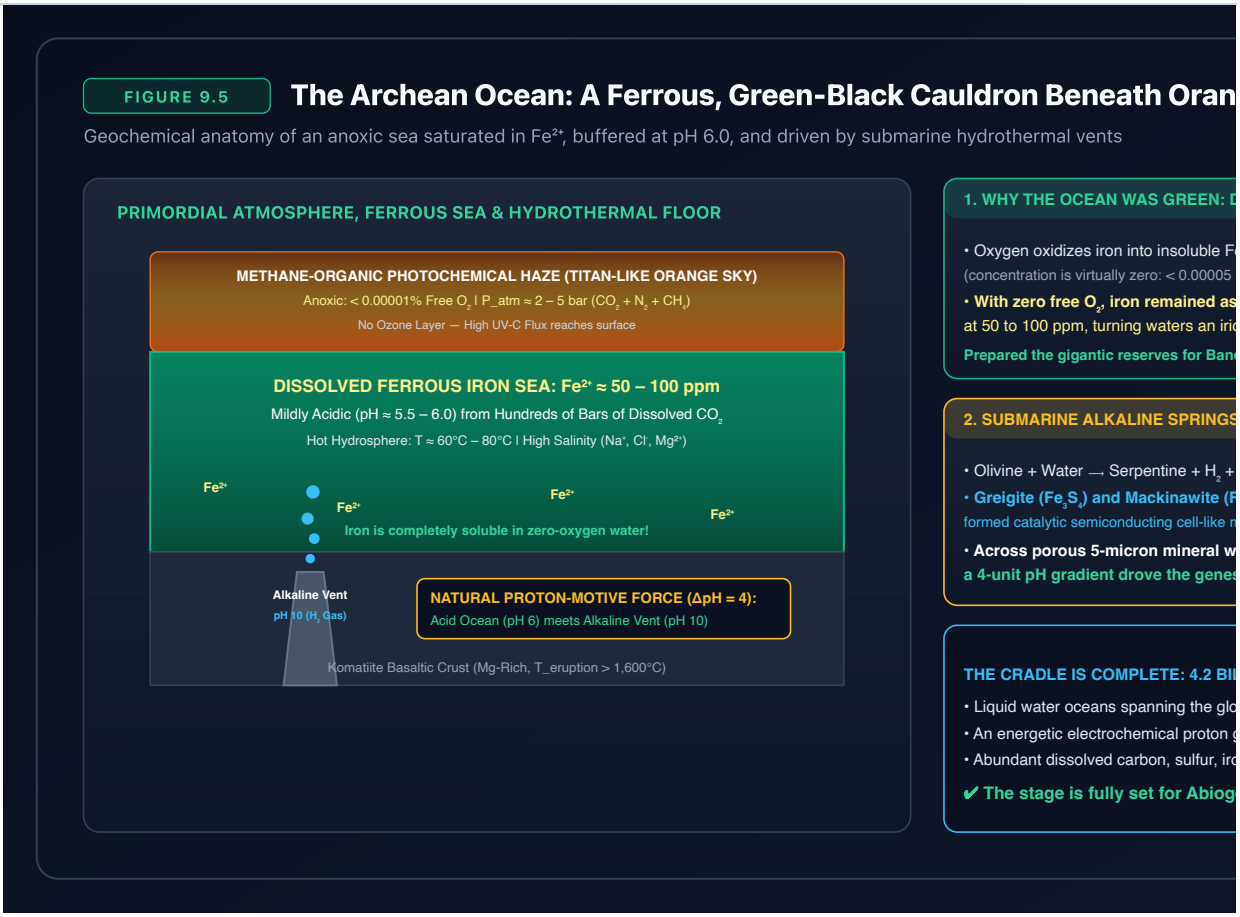


Figure 9.5: The Archean Hydrosphere & The Submarine Life Engine. The primordial ocean was an anoxic, hot (60°–80°C) bottle-green cauldron holding dissolved ferrous iron (Fe^{2+} ≈ 50–100 ppm) beneath an orange Titan-like organic haze. At submarine komatiite vents, alkaline hydrothermal fluids (pH 10) met acidic seawater (pH 6), creating a natural electrochemical proton-motive force (ΔpH = 4) across porous iron-sulfur chimneys that catalyzed the very first metabolic reactions.

Geochemical Profile of the Hadean / Early Archean Earth

System / Reservoir	Primary Composition	Estimated Temperature	Key Physical / Chemical Dynamics
Atmosphere	CO2 (80–90\%), N2 (10–15\%), CH4, CO, H2O	40° to 85°C	Pressure 1 to 10 bars; anoxic (no O2); resolving Faint Young Sun.
Hydrosphere (Oceans)	H2O saturated with Fe^{2+}, Mg^{2+}, Cl^-, SiO2	50° to 70°C	Volume 1.5 to 2.0× modern oceans; slightly acidic (pH 5.5–6.5); green/black hue.
Crust & Landmasses	Basaltic oceanic crust, tonalite-trondhjemite-granodiorite (TTG) proto-continents	300–500°C (Deep)	Thin, fast-moving proto-plates; high volcanic heat flux (3× modern).
Tidal Dynamics	Lunar distance 30,000–60,000 km	—	Day length 6 to 10 hours; tidal amplitudes 10 to 100 meters; massive intertidal flushing.
Ocean Floor	Ultramafic peridotite, komatiite, serpentine	Hydrothermal vents >300°C	Alkaline hydrothermal vents; serpentinization generating hydrogen (H2) and proton gradients.

The Cradle is Prepared: The Threshold of Life

By four billion years ago, the universe had achieved an extraordinary physical milestone. Out of quantum foam, inflationary expansion, nuclear nucleosynthesis, stellar explosions, galactic rotation, and planetary collision, a stable terrestrial world had emerged: an iron-core planet cloaked in protective magnetic fields, warmed by a dense greenhouse sky, and blanketed by deep, warm, mineral-rich oceans.

On the abyssal ocean floor, along the submarine volcanic fissures where the hot crust met the dark sea, alkaline hydrothermal vents were pumping chemical energy, catalytic transition metals (iron, nickel, sulfur), and proton concentration gradients into the water. The physical and chemical stage was set for the greatest qualitative leap in the history of matter: the transition from geochemical physics to self-replicating biological code.

In **Part 10** of *The Universal Chronicle*, we cross the threshold into Phase III: **The Spark of Abiogenesis — Alkaline Hydrothermal Vents, Prebiotic Chemistry, and the RNA World**.

Shakil Mahmud • Research Monograph

Academic Citations & Foundational Literature

- **Wilde, S. A., Valley, J. W., Peck, W. H., & Graham, C. M. (2001).** "Evidence from detrital zircons for the existence of continental crust and oceans on the Earth 4.4 Gyr ago." *Nature*, 409, 175–178. doi:10.1038/35051550.
- **Valley, J. W., et al. (2014).** "Hadean age for a post-magma-ocean zircon confirmed by atom-probe tomography." *Nature Geoscience*, 7, 219–223. doi:10.1038/ngeo2075.
- **Sagan, C., & Mullen, G. (1972).** "Earth and Mars: Evolution of Atmospheres and Surface Temperatures." *Science*, 177(4043), 52–56. doi:10.1126/science.177.4043.52.
- **Alexander, C. M. O'D., et al. (2012).** "The Provenance of Carbonaceous Chondrites and the Origin of Earth's Water." *Science*, 337(6095), 721–723. doi:10.1126/science.1223474.
- **Altwegg, K., et al. (2015).** "67P/Churyumov-Gerasimenko, a Jupiter family comet with a high D/H ratio." *Science*, 347(6220), 1261952. doi:10.1126/science.1261952.
- **Kasting, J. F. (1993).** "Earth's early atmosphere." *Science*, 259(5097), 920–926. doi:10.1126/science.11536547.
- **Sleep, N. H., Zahnle, K., & Neuhoff, P. S. (2001).** "Initiation of clement surface conditions on the earliest Earth." *Proceedings of the National Academy of Sciences*, 98(7), 3666–3672. doi:10.1073/pnas.071045698.

Citation: Mahmud, S. (2026). "The Primordial Cradle — Volcanic Degassing, Cometary Bombardment, and the First Oceans." In The Universal Chronicle, Part 9. https://shakilmahmud.com/universal-chronicle-part-9-the-primordial-cradle/

SHAKIL MAHMUD RESEARCH MONOGRAPHS • PART X

The Spark of Abiogenesis — Alkaline Hydrothermal Vents, Prebiotic Chemistry, and the RNA World

The Spark of Abiogenesis — Alkaline Hydrothermal Vents, Prebiotic Chemistry, and the RNA World

2,446 words • October 31, 2026 • Permanent URI

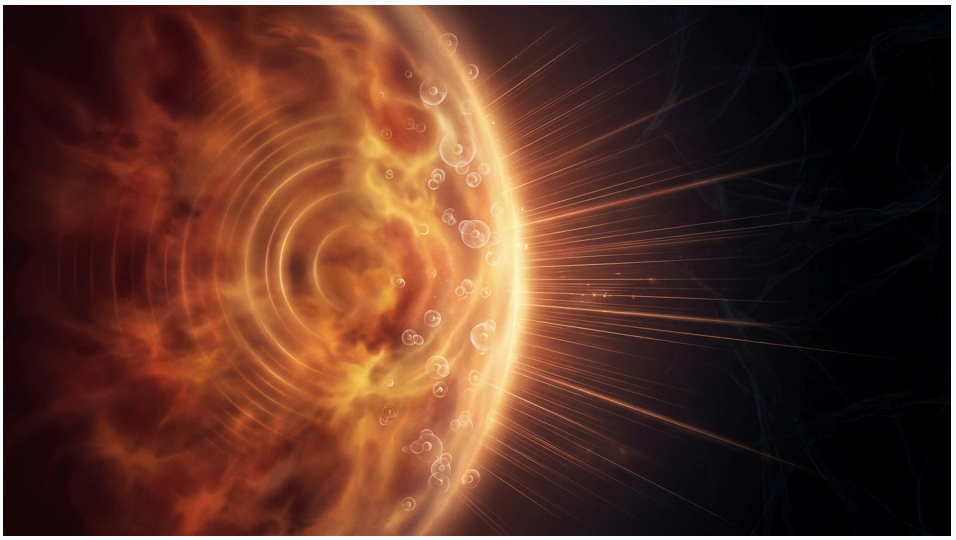


Plate X: *Figure: Deep-sea alkaline hydrothermal vents (~4.0 Ga): serpentine mineral chimneys catalyzing proton gradients, iron-sulfur clusters, and prebiotic nucleotide polymerization that sparked the RNA World and cellular metabolism.*

Four billion years ago, on the abyssal floor of Earth's dark, anoxic primordial ocean, a miraculous qualitative phase transition took place. Inorganic rocks began to behave like living cells. Within the porous mineral micro-chambers of alkaline hydrothermal vents, sustained natural electrochemical proton gradients drove the reduction of carbon dioxide into organic molecules. In this chemical incubator, catalytic strands of ribonucleic acid (RNA) learned to store digital information and duplicate themselves—crossing the cosmic threshold from physics and geochemistry into self-sustaining biological evolution.

What is Life? The Thermodynamic Challenge

To understand how life began, we must first define what life actually does in physical terms. In 1944, quantum pioneer Erwin Schrödinger published *"What is Life?"*, proposing that living organisms survive by drawing **negative entropy** ($\Delta S < 0$) from their environment. A living organism is not a static object like a diamond or a rock; it is a **non-equilibrium dissipative structure**—a continuous vortex of matter and energy that maintains internal structural order by degrading high-grade chemical energy and dissipating low-grade waste heat into its surroundings.

Modern biochemists define a minimal living system by three interconnected pillars:

- **1. Compartmentalization:** A semi-permeable physical boundary (lipid membrane) that separates the internal biochemical system from the chaotic external environment, preventing vital biomolecules from diffusing into oblivion.
- **2. Continuous Metabolism:** A self-sustaining network of chemical reactions that harvests external energy and carbon to synthesize cellular components and maintain an electrochemical charge across the membrane.
- **3. Digital Genetic Information:** Linear polymeric molecules (RNA or DNA) capable of storing sequence data that directs catalytic machinery, replicates with high fidelity, and exhibits Darwinian heritable variation.

Beyond the Primordial Soup: Why the Miller-Urey Flask was Incomplete

In 1953, Stanley Miller and Harold Urey conducted their famous spark-discharge experiment at the University of Chicago. By firing high-voltage electric sparks through a glass flask containing water, methane (CH_4), ammonia (NH_3), and hydrogen (H_2), Miller synthesized over twenty different amino acids, the chemical building blocks of proteins. For half a century, school textbooks taught that lightning striking a "primordial organic soup" in a warm pond gave birth to life.

However, modern cosmochemistry and planetary geology revealed two fatal problems with the open-soup hypothesis:

Shakil Mahmud • Research Monograph

1. The Neutral Atmosphere

Analysis of mantle oxidation states in Hadean zircons proves that early volcanic outgassing produced a *weakly reducing* or neutral atmosphere dominated by carbon dioxide (CO_2) and nitrogen (N_2), with only trace amounts of methane and hydrogen. When Miller-style spark experiments are repeated with CO_2 and N_2, amino acid yields drop to nearly zero.

2. The Dilution and Concentration Problem

Even if organic molecules rained into the open ocean, the volume of Earth's hydrosphere (1.4 × 10^{21} liters) would dilute them to vanishingly low nanomolar concentrations. Furthermore, polymerizing amino acids into proteins or nucleotides into RNA is a **condensation reaction** that eliminates a water molecule (A + B → AB + H_2O). In an open ocean filled with water, Le Chatelier's principle thermodynamically favors *hydrolysis* (breaking polymers apart) rather than polymer synthesis!

The Deep-Sea Alkaline Vent: Earth's Natural Electrochemical Reactor

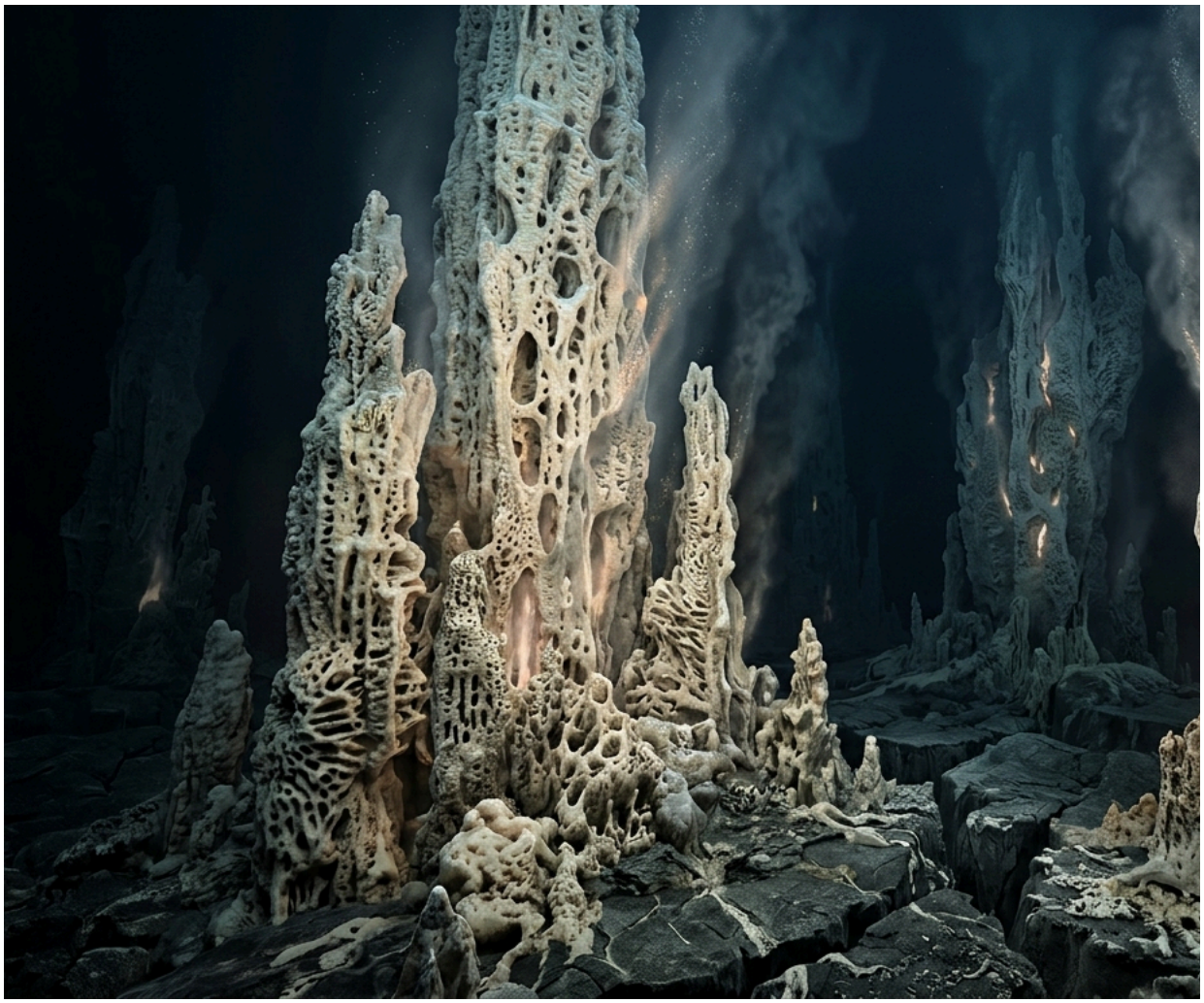
In 1989, geochemist **Michael Russell** proposed a revolutionary paradigm that has become the preeminent scientific model for abiogenesis: life originated not in sunlit surface ponds, but in **deep-sea alkaline hydrothermal vents** (such as the modern "Lost City" hydrothermal field discovered in 2000 along the Mid-Atlantic Ridge).

Crucially, Russell's model does not point to violent, volcanic "Black Smokers" (which spew acidic water at 350°C that destroys fragile biomolecules). Instead, it identifies mild, off-axis **Alkaline Vents** driven by a low-temperature geochemical reaction between seawater and mantle peridotite: **Serpentinization**.

$$\text{Olivine} + \text{Water} \rightarrow \text{Serpentine} + \text{Brucite} + \text{Magnetite} + \text{Hydrogen } (H_2)$$

The Natural Proton-Motive Force
Serpentinization generates warm (40°C to 90°C), strongly alkaline fluids (pH 9 to 11) saturated with dissolved hydrogen gas (H_2), methane, and hydrosulfide (HS^-). When these alkaline fluids seep upward into the Hadean ocean floor, they encounter the primordial ocean—which was mildly acidic (pH 5.5 to 6.0) due to hundreds of bars of dissolved atmospheric CO_2.

At the interface, calcium carbonate and iron-sulfur minerals (greigite, mackinawite) precipitated to build towering chimneys riddled with **microscopic, interconnected inorganic chambers** (micropores 10 to 100 micrometers across). Across the thin, catalytic, semi-conducting iron-sulfur walls of these pores, there existed an innate, natural pH gradient: **a differential of 4 to 5 pH units, creating a voltage of roughly 200 to 300 millivolts!**



Deep-Sea Geochemistry: Alkaline Hydrothermal Vent Spires (~4.0 Ga). Rising from the dark, fractured basaltic crust of the Hadean seafloor, porous white chimneys of calcium carbonate and serpentinite acted as Earth's earliest electrochemical reactors. Warm (70°C), hydrogen-rich alkaline fluids percolated into the cold, acidic ocean, establishing continuous proton and electron gradients that fueled prebiotic synthesis.

This natural electrical gradient across mineral walls is identical in magnitude, polarity, and orientation to the **proton-motive force (~ 200 mV)** that every living cell on Earth uses today to generate ATP via Peter Mitchell's chemiosmotic coupling! Before cells evolved lipid membranes and protein proton pumps, they utilized the **geological battery of the Earth itself**.

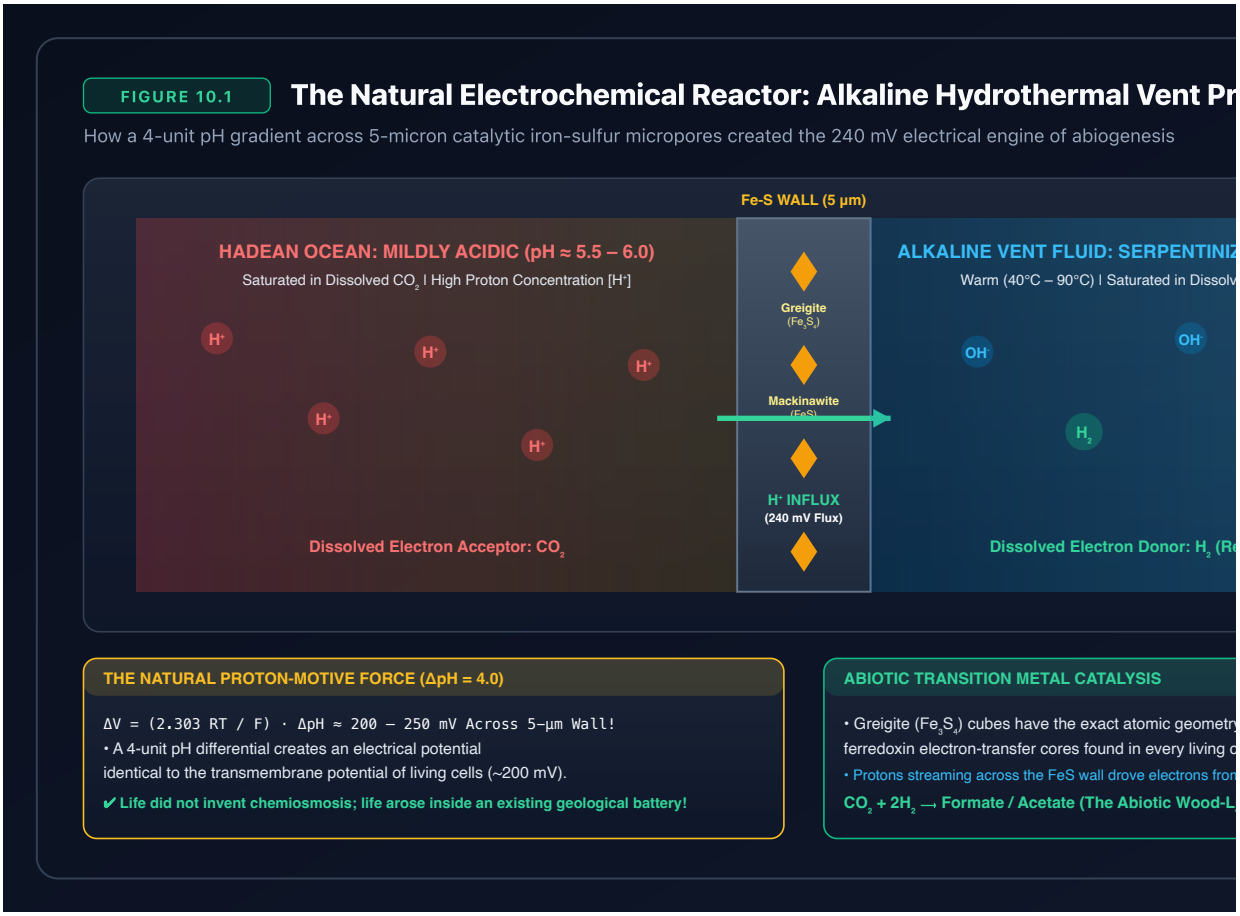


Figure 10.1: The Natural Electrochemical Reactor & Geological Proton-Motive Force. Alkaline hydrothermal chimneys formed porous, interconnected microcavities bounded by semi-permeable iron-sulfur mineral walls. Warm alkaline fluids (pH ~9–11) enriched in H_2 and HS^- seeped through one side, while cold, mildly acidic Hadean ocean water (pH ~5.5–6.0) laden with CO_2 washed the exterior. This sustained a 4-unit ΔpH gradient (~240 mV electrical potential) across 5-micron mineral membranes—powering life's first thermodynamic reactions long before biological ATP synthase evolved.

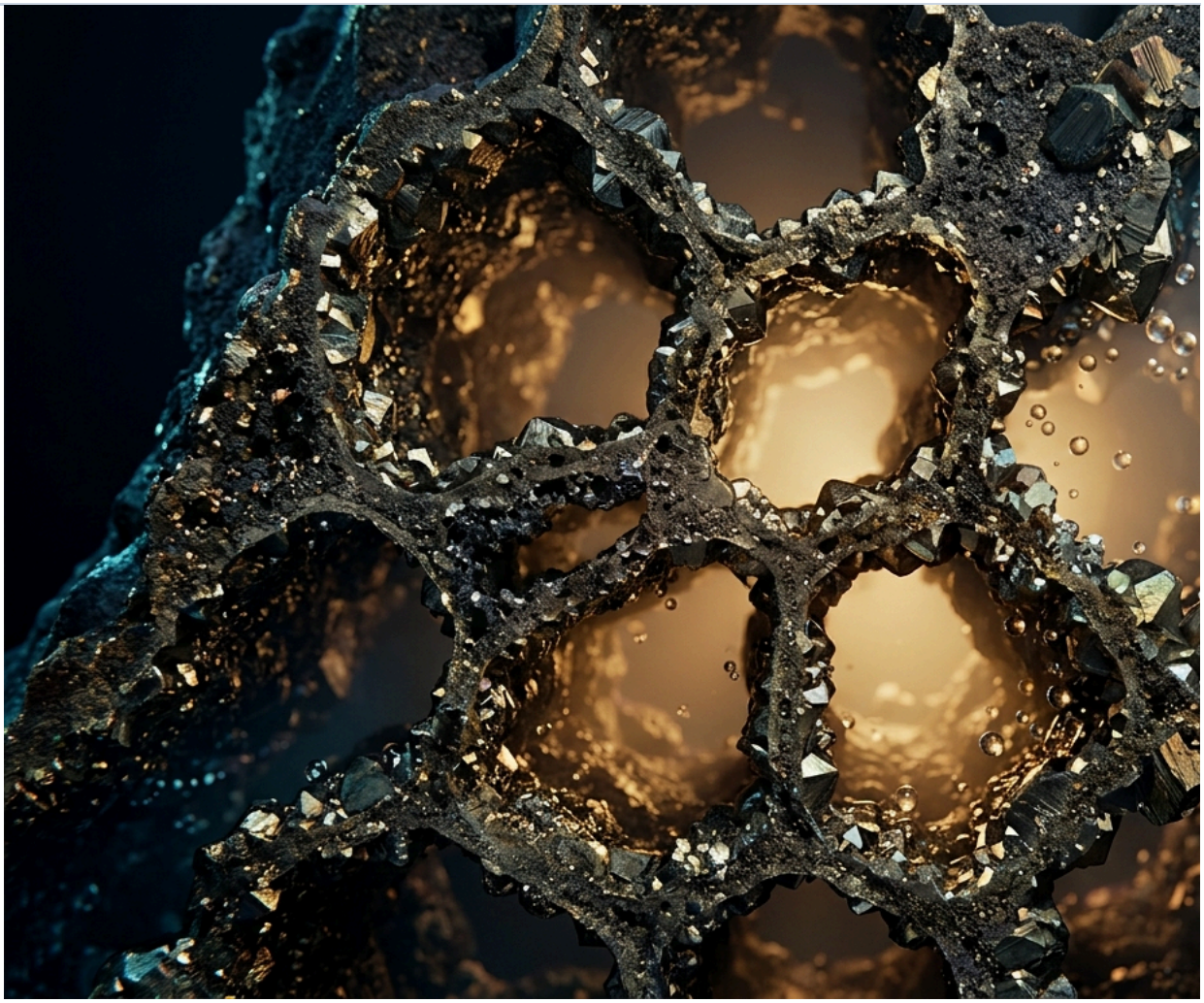
The Ancient Engine: The Wood-Ljungdahl Pathway

How did inorganic carbon dioxide become organic molecules? The most ancient metabolic pathway known to biology is the **Wood-Ljungdahl (acetyl-CoA) Pathway**. It is the only carbon-fixation pathway found in both ancient Archaea (methanogens) and Bacteria (acetogens), and the only one that releases energy rather than consuming it:

$$\text{CO}_2 + 2\text{H}_2 \to \text{Formate} / \text{Acetate} + \text{H}_2\text{O} \quad (\Delta G^\circ < 0)$$

Inside the vent micropores, the catalytic iron-sulfur minerals (FeS and NiS) acted as primitive, inorganic precursors to modern biological enzymes (such as carbon monoxide dehydrogenase and ferredoxin). Driven by the natural proton gradient across the mineral barrier, hydrogen transferred electrons directly to dissolved CO_2, synthesizing **formate, acetate, pyruvate, and acetyl-thioesters**—the foundational building blocks of biochemistry.

Shakil Mahmud • Research Monograph



Micro-Geochemistry: Catalytic Iron-Sulfur Micropores (~4.0 Ga). A microscopic cross-section inside an alkaline chimney reveals an interconnected labyrinth of semi-permeable inorganic micro-compartments lined with greigite (Fe_3S_4) and mackinawite (FeS). Acting as nature's primordial flow-cells, these metallic mineral walls catalyzed the Wood-Ljungdahl pathway, reducing CO_2 into foundational organic building blocks.

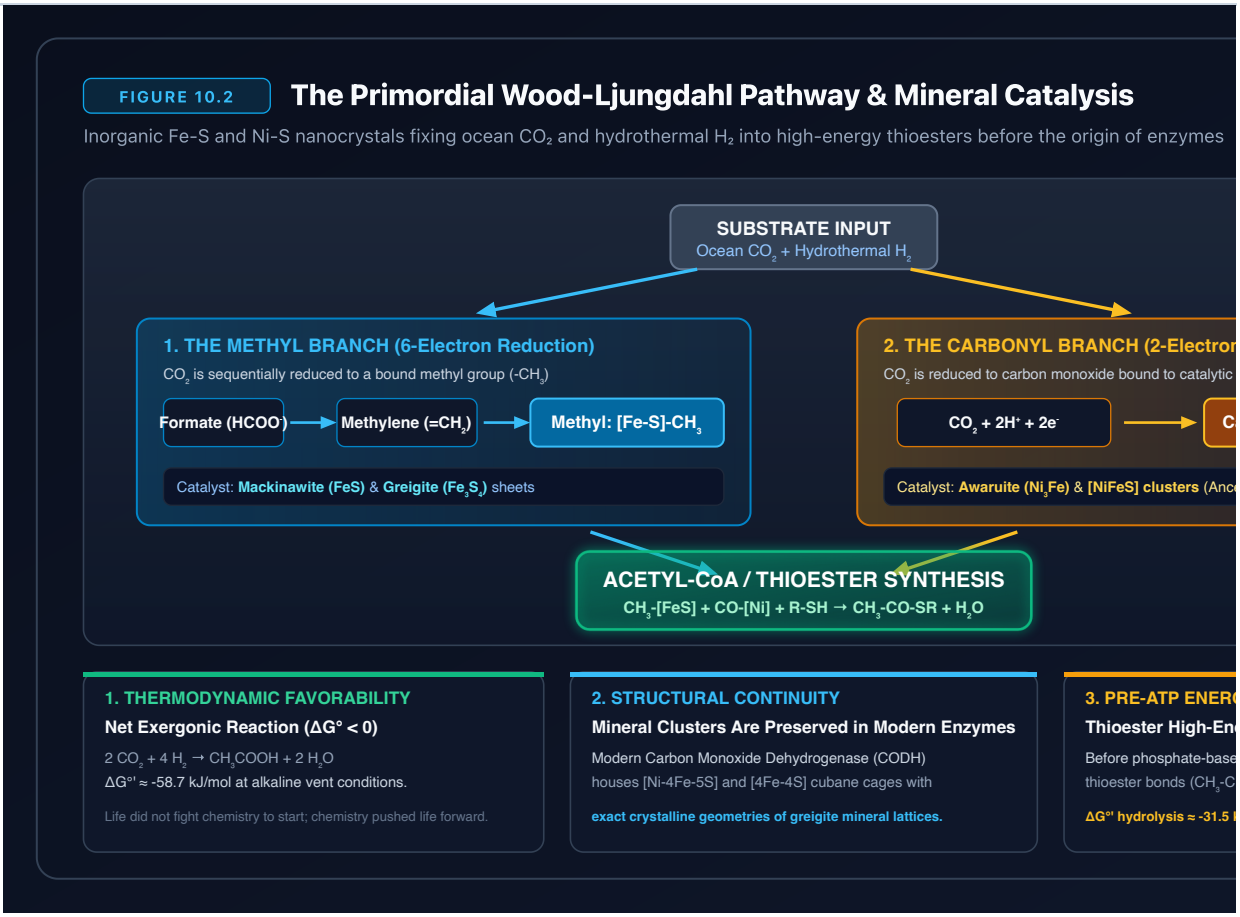


Figure 10.2: The Primordial Wood-Ljungdahl Pathway & Mineral Catalysis. The most ancient pathway of carbon fixation does not require energy input; it is net exergonic (ΔG°′ ≈ -58.7 kJ/mol). Greigite (Fe3S4) and mackinawite (FeS) sheets catalyzed the 6-electron methyl branch reducing CO2 to methyl-FeS, while awaruite (Ni3Fe) catalyzed the 2-electron carbonyl branch reducing CO2 to CO-Ni. Condensation of the two groups produced high-energy acetyl thioesters (CH3-CO-SR), the primordial precursor to ATP.

The RNA World: Solving the Molecular Chicken-and-Egg Paradox

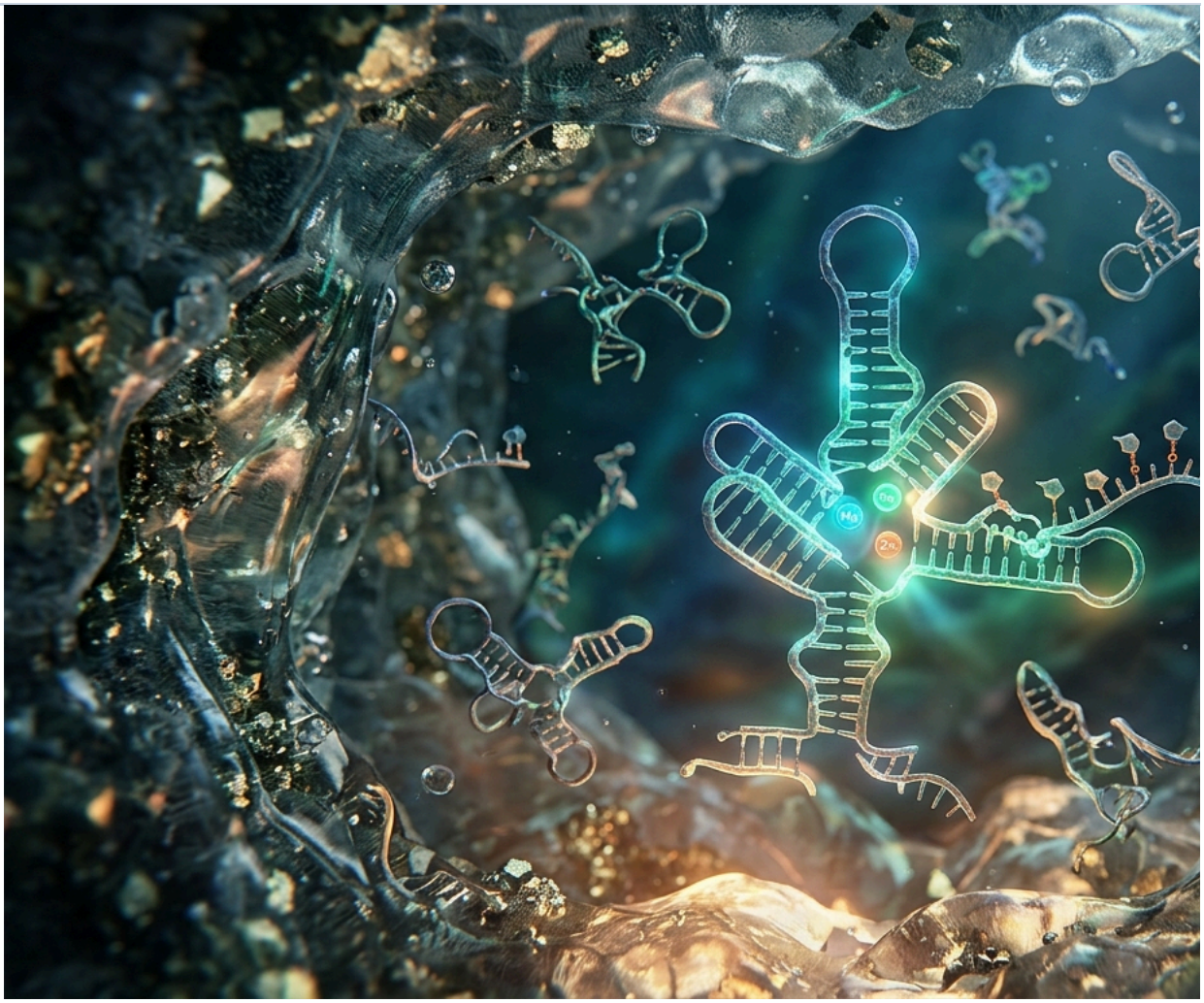
In modern biology, life operates through a strict division of labor between two classes of macromolecules:

- **DNA (The Blueprint):** Possesses high chemical stability to store genetic code, but is completely inert and cannot catalyze chemical reactions or replicate itself.
- **Proteins (The Workers):** Fold into intricate three-dimensional enzymes that carry out all catalytic and metabolic tasks, but cannot store or transmit heritable digital code.

DNA requires proteins to replicate; proteins require DNA to specify their amino acid sequences. How could either have originated in the absence of the other?

The Discovery of Ribozymes (Cech & Altman 1982)
In the 1980s, Thomas Cech and Sidney Altman discovered that **Ribonucleic Acid (RNA)** can perform both functions simultaneously! In addition to storing digital genetic information via its four nucleotide bases (Adenine, Cytosine, Guanine, Uracil), single-stranded RNA can fold back on itself into complex tertiary structures that act as true catalytic enzymes, termed **Ribozymes**.

Shakil Mahmud • Research Monograph



Molecular Prebiotic Biology: The RNA World Inside Hydrothermal Pores (~3.9 Ga). Solving the molecular chicken-and-egg paradox, folded ribonucleic acid (RNA) macromolecules acted simultaneously as genetic templates and enzymatic catalysts (ribozymes). Coordinated by divalent magnesium ions inside mineral cavities, these catalytic strands self-cleaved and polymerized complementary nucleotides, sparking Darwinian evolution.

The smoking gun of this evolutionary transition was revealed when structural biologists mapped the atomic structure of the **Ribosome**—the universal molecular factory in all living cells that builds proteins: the active catalytic site where amino acids are forged together (the peptidyl transferase center) is composed **100% of ribosomal RNA, with zero protein enzymes involved**! Proteins are literally the evolutionary creation of ancient, catalytic RNA.

During the **RNA World** epoch (t ≈ 4.0 to 3.8 billion years ago), self-assembling nucleotides (synthesized via formamide and cyanide pathways catalyzed by ultraviolet light and mineral surfaces) concentrated inside hydrothermal micropores via *thermophoresis* (thermal convection currents). Over millions of cycles of temperature and hydration fluctuations, RNA polymers grew, folded into catalytic ribozymes, and evolved the ability to catalyze their own template-directed replication.

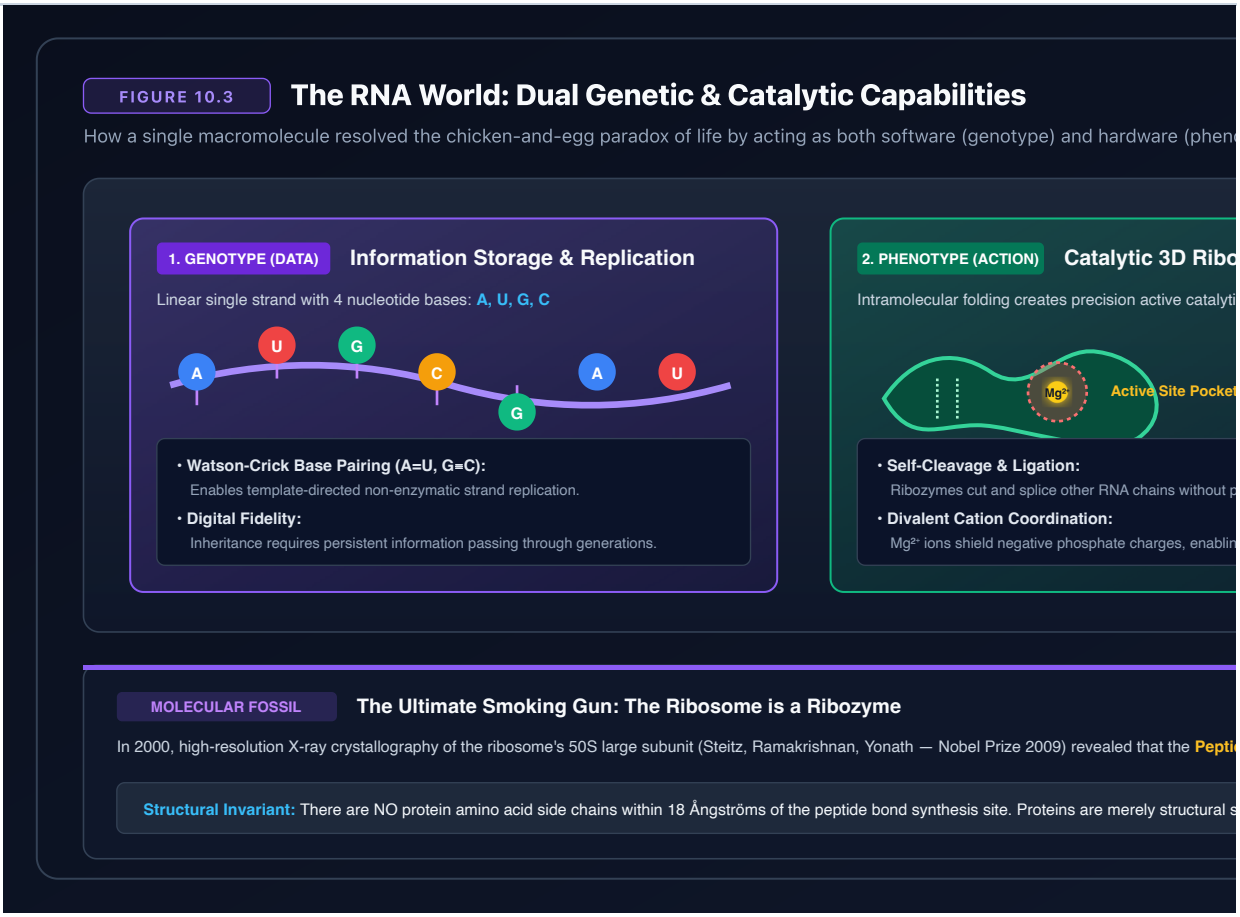


Figure 10.3: The RNA World: Dual Genetic & Catalytic Capabilities. RNA bridged the genotype-phenotype paradox by functioning simultaneously as informational storage (linear Watson-Crick sequence A, U, G, C) and catalytic machinery (complex 3D tertiary ribozyme folds stabilized by Mg^{2+} counter-ions). The ultimate molecular proof endures in every living cell: the Peptidyl Transferase Center (PTC) of the ribosome large subunit is 100% catalytic 23S rRNA, with zero protein amino acids within 18 Ångströms of the reaction core.

The Cellular Exodus: Escaping the Mineral Matrix

As catalytic RNA and metabolic reactions flourished inside the inorganic mineral cavities, another spontaneous physical process was underway: **lipid self-assembly**. Simple single-chain amphiphilic fatty acids (such as decanoic acid and glycerol phosphate) spontaneously aggregate into stable, microscopic **bilayer vesicles (liposomes)** when suspended in water.

Eventually, self-replicating RNA and peptide networks became encapsulated inside these lipid vesicles. To escape dependence on the geological proton gradients of the vent chimney, these proto-cells evolved their own membrane-bound proton pumps (precursors to the F_1F_0-ATP synthase complex). Once a proto-cell could maintain its own proton gradient across its own lipid membrane, **it was free**. It detached from the mineral vent chimney and drifted freely into the open ocean.

Shakil Mahmud • Research Monograph

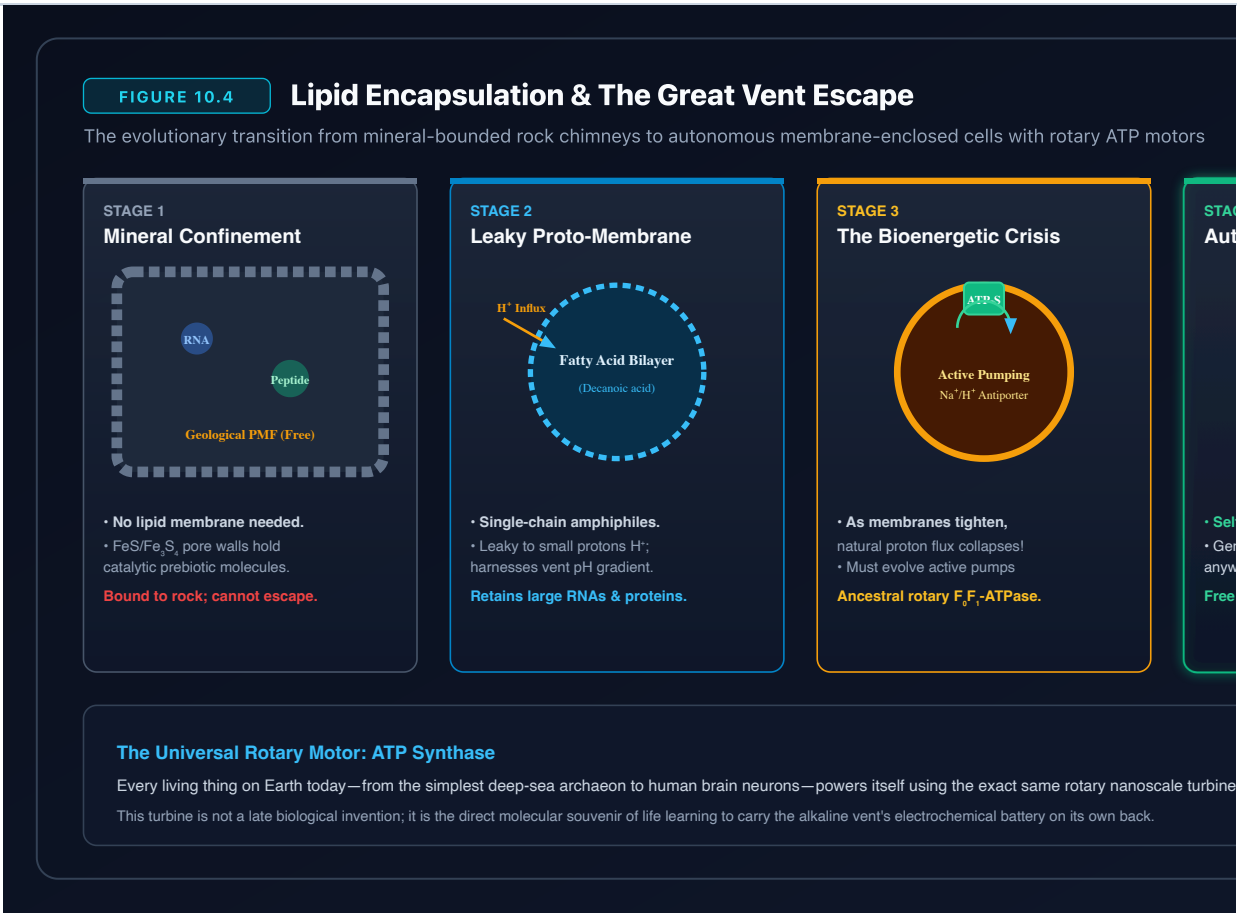


Figure 10.4: Lipid Encapsulation & The Cellular Exodus. The transition from rock-bound mineral incubators to free-living cells required overcoming a bioenergetic crisis. Primitive single-chain fatty acid vesicles were leaky, allowing geological protons to pass through. As phospholipid membranes became less permeable to retain genetic macromolecules, cells were forced to evolve active proton pumping (ancestral F0F1 rotary ATP synthase). Equipped with their own portable ion-gradient engine, cells broke free to colonize the global ocean.

LUCA: The Common Root of All Earthly Life

Every living organism that breathes, crawls, swims, or computes on Earth today—from the gut bacterium *E. coli* to an oak tree, a blue whale, or a human engineer—traces its uninterrupted biological lineage back to a solitary population of ancient single-celled organisms: **LUCA (The Last Universal Common Ancestor)**, living roughly **3.8 to 4.0 billion years ago**.

In 2016, genomicist William Martin and his team sequenced over 6.1 million prokaryotic genes and identified **355 universal gene families** shared across ancient Bacteria and Archaea. From these conserved genes, LUCA's exact biological portrait emerged:

- **Environment:** An obligate anaerobe living in a hot, dark, geochemically active hydrothermal environment rich in H2, CO2, and iron.
- **Metabolism:** Autotrophic, utilizing the Wood-Ljungdahl pathway to fix inorganic carbon directly using transition-metal clusters ([Fe_4S_4] and [NiFeS]).
- **Genetic Machinery:** Possessed a universal genetic code, a DNA genome, transcribed messenger RNA, and synthesized proteins using a modern 20-amino-acid ribosome.

Prebiotic Geochemistry vs. Universal Living Cell Architecture

Biochemical Feature	Hydrothermal Vent Prebiotic Origin	Modern Cellular Execution (LUCA & Descendants)
Compartmentalization	Microporous iron-sulfur/carbonate chimneys	Lipid bilayer cell membrane with embedded transport proteins
Energy Driving Force	Natural geological ΔpH gradient (9 → 6)	Chemiosmotic proton-motive force powering F_1F_0-ATP synthase
Carbon Fixation	Inorganic serpentinization & FeS catalysis	Wood-Ljungdahl (acetyl-CoA) metabolic pathway
Catalytic Machinery	Greigite ([Fe_4S_4]) & Mackinawite minerals	Ferredoxin, hydrogenase, and metalloenzyme cofactors
Information Storage	Catalytic, self-replicating Ribozymes (RNA World)	Double-stranded DNA genome with RNA intermediaries
Protein Synthesis	Peptide bonds catalyzed on RNA templates	Universal 70S/80S Ribosome (100% RNA catalytic core)

The Great Divergence: Bacteria and Archaea

Shortly after emerging from the vents, LUCA branched into the two primary domains of cellular life: **Bacteria** and **Archaea**. Interestingly, while both domains share an identical genetic code and core ribosome, their cell membrane lipids are fundamentally different:

- **Bacterial Lipids:** Unbranched fatty acids bound to D-glycerol via *ester* linkages.
- **Archaeal Lipids:** Branched isoprenoid hydrocarbon chains bound to L-glycerol via chemical *ether* linkages—providing immense structural stability that allowed Archaea to conquer extreme environments (hyper-saline pools, boiling acidic hot springs, and deep subsurface crust).

For the next billion years, Bacteria and Archaea held undisputed dominion over the planet. They colonized every drop of the global ocean, metabolizing hydrogen, sulfur, iron, and methane in complete darkness. But in the sunlit surface waters of the ocean, a group of photosynthetic bacteria was quietly developing a biochemical invention that would reshape the geology of the entire planet: **oxygenic photosynthesis**.

In **Part 11** of *The Universal Chronicle*, we will explore the most catastrophic and miraculous transformation in Earth's history: **The Oxygen Catastrophe & The Miracle — Cyanobacteria, the Great Oxidation Event, and the Huronian Snowball Earth**.

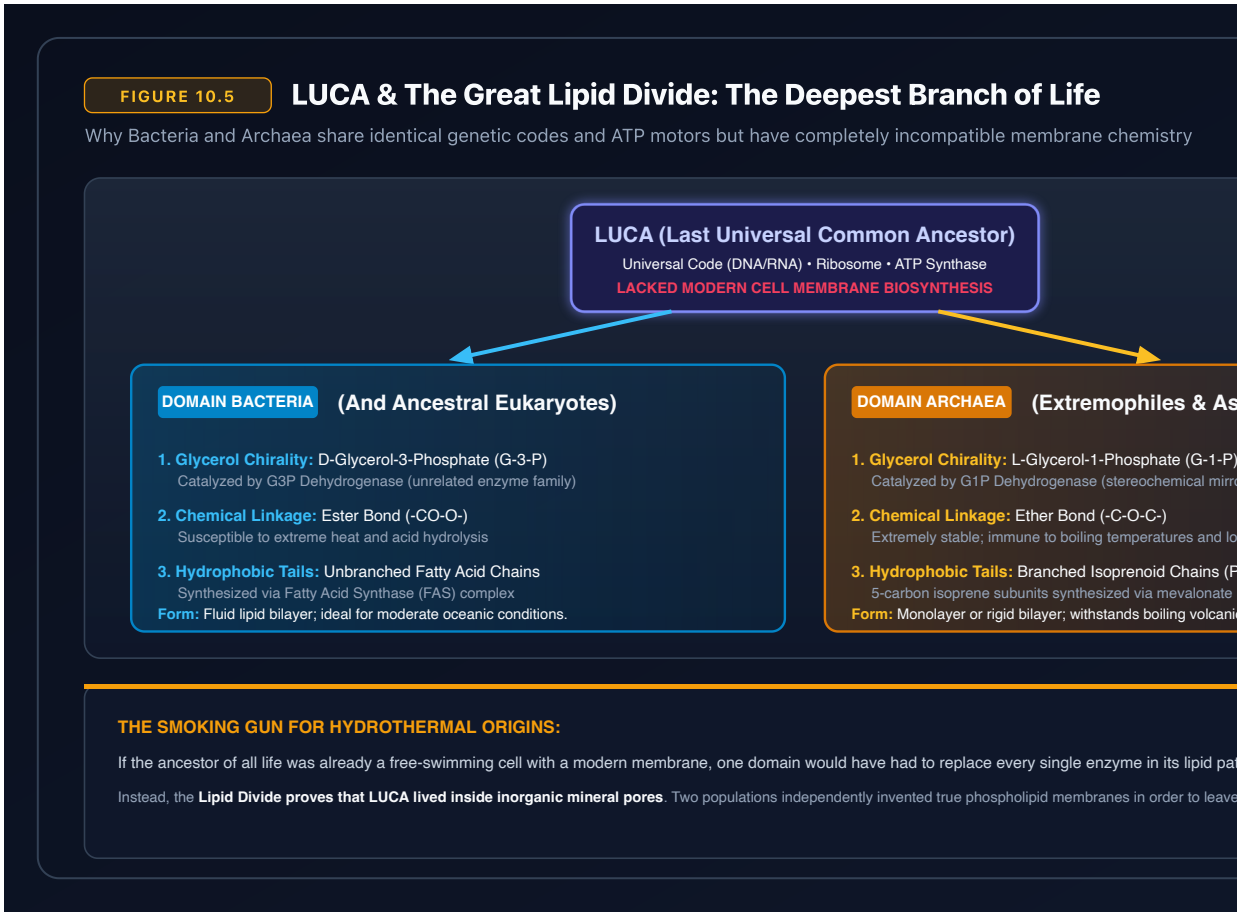


Figure 10.5: LUCA & The Great Lipid Divide. While Bacteria and Archaea share an identical genetic code and homologous rotary ATP synthase, their cell membranes are stereochemically and chemically incompatible. Bacteria synthesize D-glycerol-3-phosphate linked to straight fatty acids via ester bonds; Archaea synthesize L-glycerol-1-phosphate linked to branched isoprenoids via ether bonds. This fundamental divergence proves that LUCA lived inside inorganic mineral pores before modern lipid membranes were invented, giving rise to two independent lineages of cellular escape.

Academic Citations & Foundational Literature

- **Miller, S. L. (1953).** "A Production of Amino Acids Under Possible Primitive Earth Conditions." *Science*, 117(3046), 528–529. doi:10.1126/science.117.3046.528.
- **Russell, M. J., & Hall, A. J. (1997).** "The emergence of life from iron monosulphide bubbles at a submarine hydrothermal redox and pH front." *Journal of the Geological Society*, 154(3), 377–402. doi:10.1144/gsjgs.154.3.0377.
- **Martin, W., & Russell, M. J. (2003).** "On the origins of cells: a hypothesis for the evolutionary transitions from abiotic geochemistry to chemoautotrophic prokaryotes, and from replicating physical compartmentalization to biochemical organizations." *Philosophical Transactions of the Royal Society of London. Series B: Biological Sciences*, 358(1429), 59–85. doi:10.1098/rstb.2002.1183.
- **Lane, N., Allen, J. F., & Martin, W. (2010).** "How energy flow shaped the evolution of life." *Nature*, 467, 929–936. doi:10.1038/nature09486.
- **Gilbert, W. (1986).** "Origin of life: The RNA world." *Nature*, 319, 618. doi:10.1038/319618a0.

Shakil Mahmud • Research Monograph

- **Cech, T. R. (1986).** "A model for the RNA-catalyzed replication of RNA." *Proceedings of the National Academy of Sciences*, 83(12), 4360–4363. doi:10.1073/pnas.83.12.4360.
- **Weiss, M. C., et al. (2016).** "The physiology and habitat of the last universal common ancestor." *Nature Microbiology*, 1, 16116. doi:10.1038/nmicrobiol.2016.116.

Citation: Mahmud, S. (2026). "The Spark of Abiogenesis — Alkaline Hydrothermal Vents, Prebiotic Chemistry, and the RNA World." In The Universal Chronicle, Part 10. https://shakilmahmud.com/universal-chronicle-part-10-the-spark-of-abiogenesis/

SHAKIL MAHMUD RESEARCH MONOGRAPHS • PART XI

The Oxygen Catastrophe & The Miracle — Cyanobacteria and the Great Oxidation Event

The Oxygen Catastrophe & The Miracle — Cyanobacteria and the Great Oxidation Event

2,285 words • October 31, 2026 • Permanent URI



Plate XI: *Figure: Cyanobacterial stromatolite reefs flourishing in Paleoproterozoic shallow seas (~2.4–2.1 Ga), releasing photosynthetic oxygen that precipitated banded iron formations (BIFs) and triggered the Huronian Snowball Earth.*

Roughly 2.4 billion years ago, a humble photosynthetic microbe committed the greatest ecological crime and the greatest evolutionary miracle in planetary history. By evolving a biochemical nanomachinery capable of splitting water molecules, Cyanobacteria began releasing free diatomic oxygen into a world that had known only anaerobic tranquility. The corrosive gas precipitated billions of tons of dissolved iron into the ocean floor, extinguished the dominant anaerobic biosphere, obliterated Earth's greenhouse blanket to trigger a 300-million-year planetary ice age, and forged the thermodynamic foundation for complex multicellular life.

The Anoxic Earth: A World of Iron, Methane, and Sulfur

For the first half of Earth's existence—the entire Archean Eon (4.0 to 2.5 billion years ago)—the atmosphere was devoid of free diatomic oxygen ($O_2 < 10^{-5}$ of modern Present Atmospheric Level, PAL). In this anoxic world, anaerobic prokaryotes thrived across the global ocean:

- **Methanogens (Archaea):** Reduced volcanic carbon dioxide with hydrogen to generate methane ($CO_2 + 4H_2 \rightarrow CH_4 + 2H_2O$), filling the sky with a warm, smoggy greenhouse blanket that kept the Archean Earth warm under the Faint Young Sun.
- **Sulfate Reducers & Fermenters (Bacteria):** Recycled organic debris into hydrogen sulfide (H_2S) and organic acids in total darkness.
- **Anoxygenic Phototrophs:** Early photosynthetic bacteria (such as purple and green sulfur bacteria) harvested sunlight, but they did not use water as an electron donor. They relied on dissolved hydrogen sulfide ($H_2S \rightarrow 2H^+ + S + 2e^-$) or dissolved ferrous iron (Fe^{2+}). Because sulfur and iron springs were localized, early photosynthesis was chained to hydrothermal hotspots.

The Master Key: Cracking the Water Molecule

Water (H_2O) was infinite, blanketing the planet in oceans miles deep. But water holds onto its electrons with ferocious thermodynamic tenacity: the redox potential of the O_2 / H_2O half-reaction is +0.815 Volts. No biological enzyme on Earth could generate an electrochemical potential strong enough to rip an electron away from an oxygen atom.

Then, inside the ancestors of modern **Cyanobacteria** (blue-green algae), an extraordinary structural mutation occurred: the coupling of two distinct photosystems—Photosystem I and Photosystem II—into the **Z-Scheme of Photosynthesis**.

Shakil Mahmud • Research Monograph

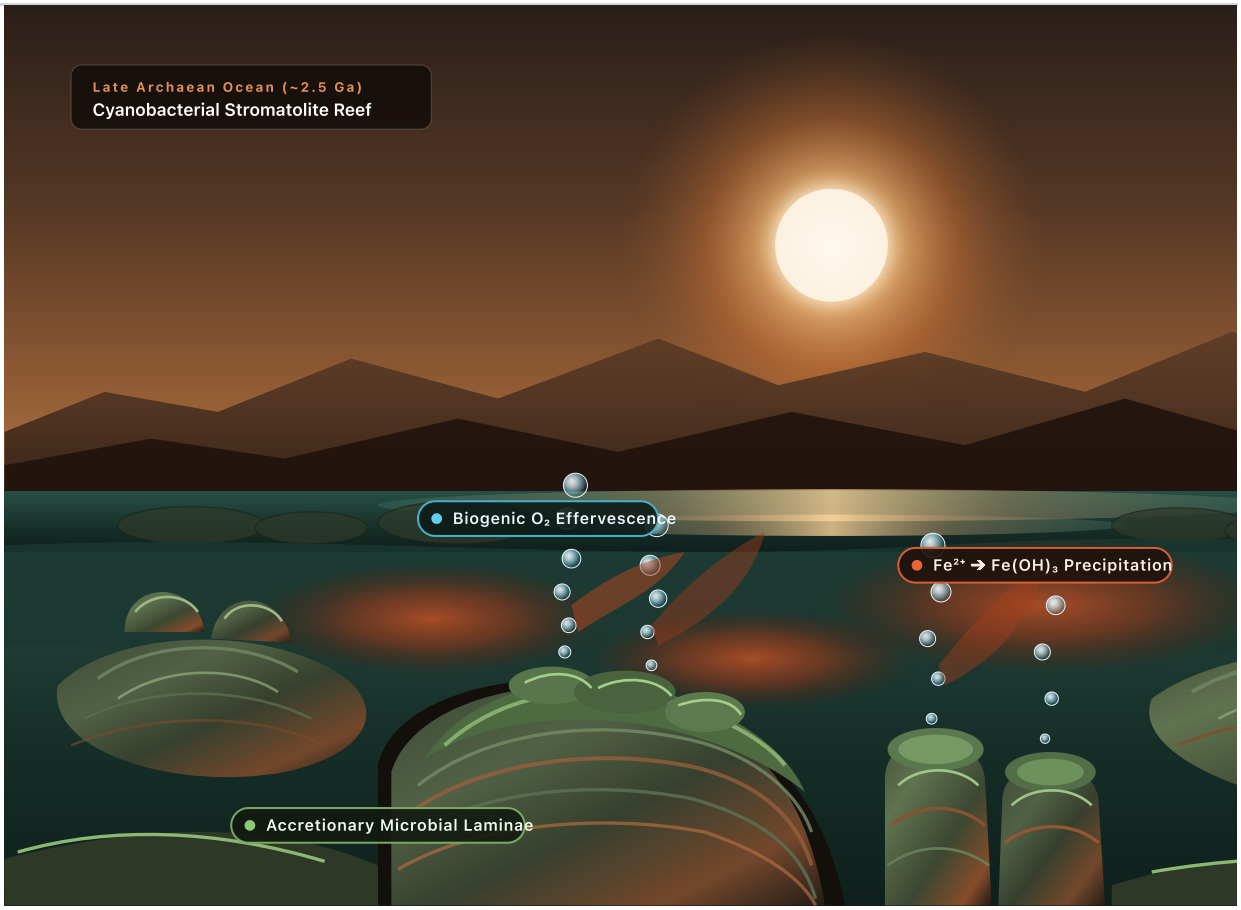


Figure 11.Sub1: Cyanobacterial Stromatolite Reefs in the Late Archaean Sea (~2.5 Ga). Coloured under a methane-hazed sky and a green ferrous ocean, layered bioherms of filamentous cyanobacteria release streams of oxygen bubbles (O_2). Where the biogenic gas contacts dissolved ferrous iron (Fe^{2+}), vibrant plumes of insoluble ferric oxyhydroxides precipitate and settle upon the tidal mudflats, capturing the earliest chemical battles of oxygenic photosynthesis.

The Manganese-Calcium Catalytic Core

Inside Photosystem II lies the **Oxygen-Evolving Complex (OEC)**, centered around an asymmetric inorganic cluster of four manganese atoms, one calcium atom, and five oxygen atoms (Mn_4CaO_5). Driven by absorbed photons of red sunlight (λ = 680 nm), chlorophyll reaction center P680 becomes the most powerful oxidizing agent in biological nature ($E^\circ \approx +1.25$ V).

Through four successive flashes of light (the Kok cycle), the cluster rips four electrons from two bound water molecules:

$$2\mathrm{H_2O} + 4h\nu \rightarrow \mathrm{O_2} + 4\mathrm{H^+} + 4e^-$$

The protons (H^+) drive ATP synthesis; the electrons reduce CO2 into sugars; and the molecular oxygen (O2) was discarded into the surrounding seawater as **toxic biological waste**.

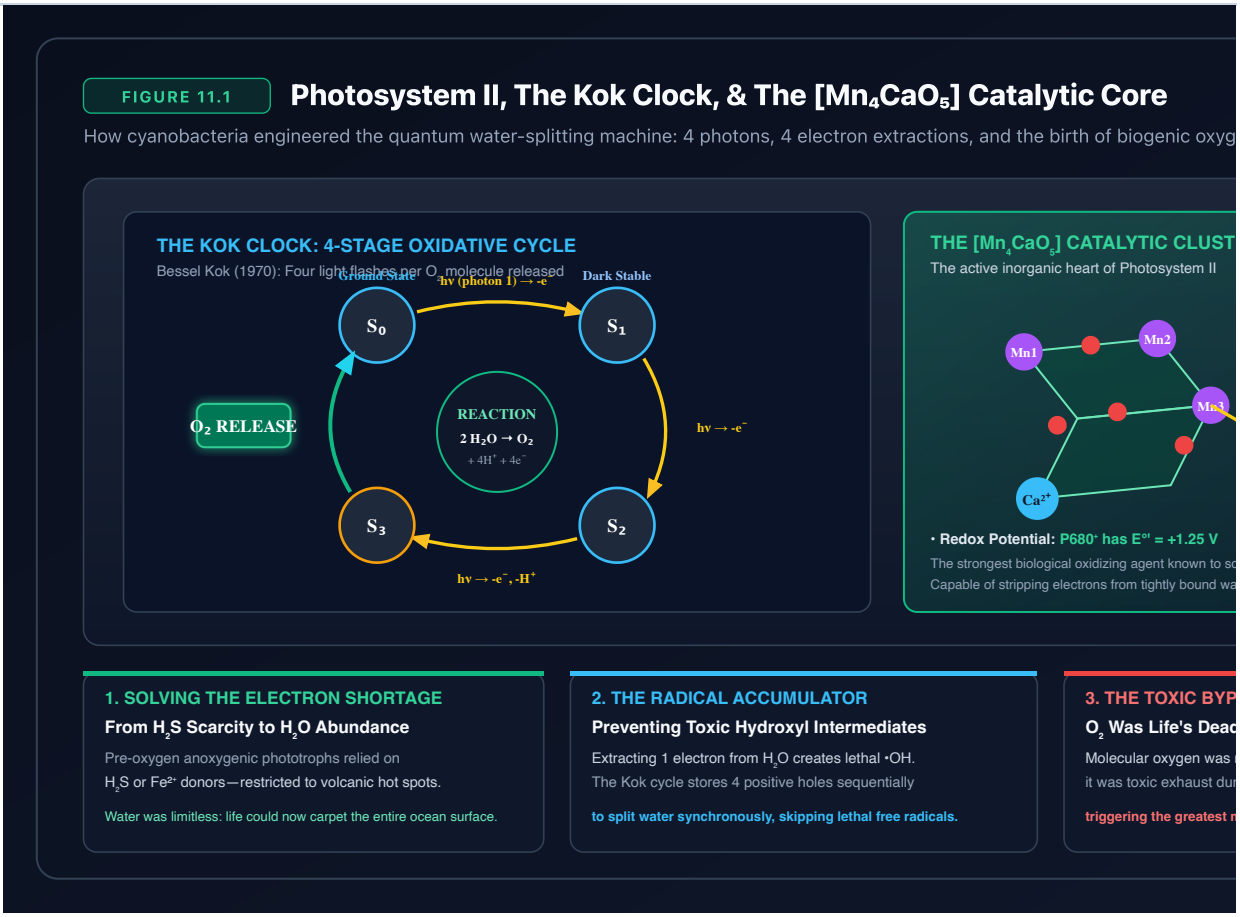


Figure 11.1: Photosystem II, The Kok Clock, & The [Mn4CaO5] Catalytic Core. Cyanobacteria achieved the ultimate quantum bioengineering breakthrough by coupling a manganese-calcium cubane cluster ([Mn4CaO5]) to the P680 reaction center (E°' = +1.25 V). Through Bessel Kok's 5-state cyclical clock (S0 to S4), the enzyme sequentially accumulates 4 solar photon excitations (4hν), abstracting 4 electrons and 4 protons from two bound water molecules while avoiding lethal hydroxyl free radical intermediates, before ejecting molecular oxygen (O2) into the world.

The Great Chemical Sinks: Banded Iron Formations

Cyanobacteria did not oxygenate the atmosphere overnight. For hundreds of millions of years (from roughly 2.8 to 2.4 billion years ago), the oxygen produced by microbial mats (stromatolites) was eagerly devoured by planetary chemical sinks.

The Archean oceans were vast chemical reservoirs of soluble **ferrous iron (Fe^{2+})**, leached from hydrothermal vents and basaltic crusts. As cyanobacterial blooms released free oxygen, the oxygen immediately oxidized the dissolved iron into insoluble **ferric iron (Fe^{3+})**:

$$4Fe^{2+} + O_2 + 10H_2O \rightarrow 4Fe(OH)_3 \downarrow + 8H^+$$

The precipitated ferric hydroxides settled to the abyssal ocean floor like red rust snow, consolidating into alternating seasonal layers of silver-black iron oxides (magnetite Fe_3O_4 and hematite Fe_2O3) and red chert silica (SiO2): **Banded Iron Formations (BIFs)**.

These majestic geological formations—stretching across thousands of square kilometers in the Hamersley Range of Western Australia, the Carajás of Brazil, and the Lake Superior region—contain over **90% of all minable iron ore on Earth**. The skyscrapers, bridges, cargo ships, and railways of modern human civilization are constructed from the fossilized rusted byproduct of cyanobacterial metabolism!

Shakil Mahmud • Research Monograph

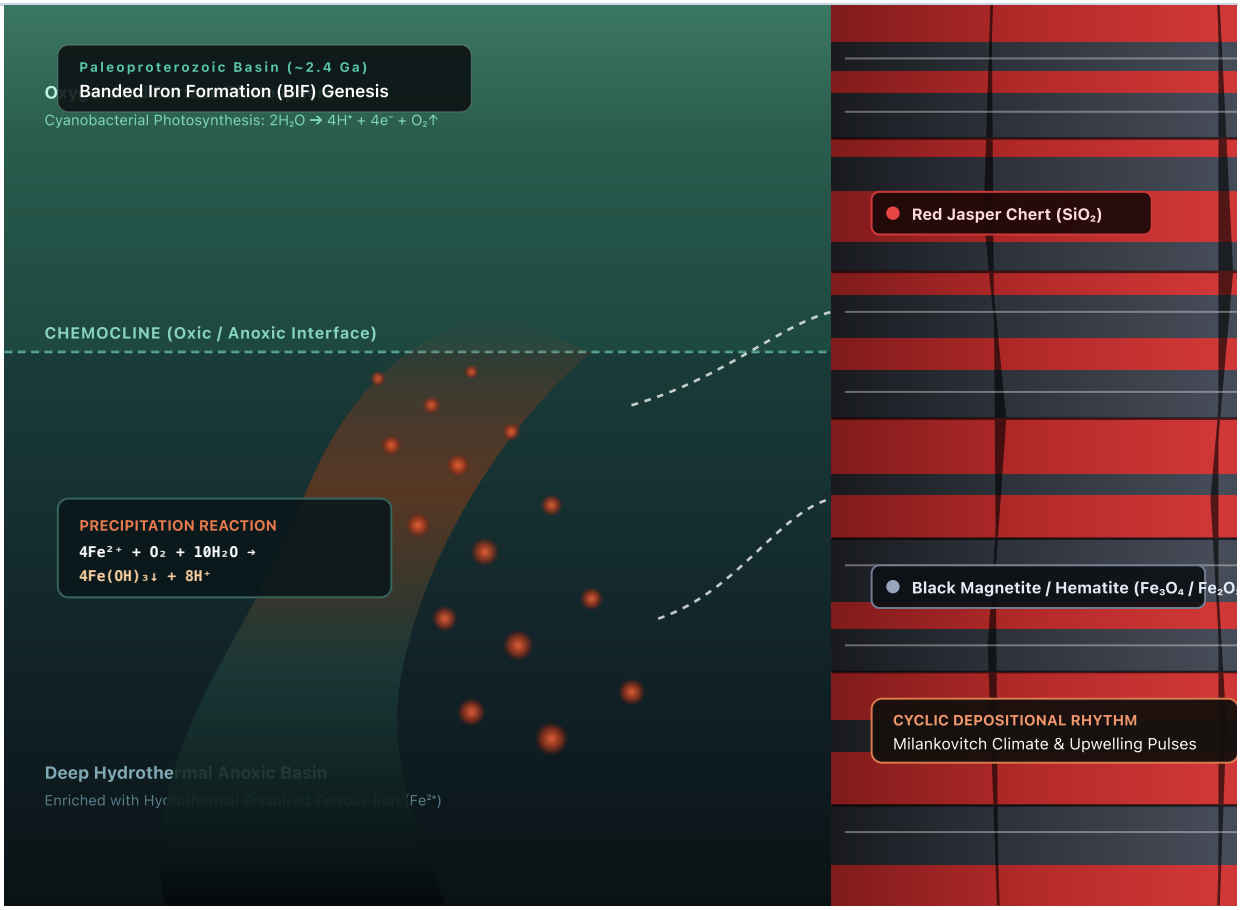


Figure 11.Sub2: Sedimentation and Stratigraphy of Banded Iron Formations (BIFs) (~2.4 Ga). A geological cutaway showing the marine chemocline where upwelling deep-water hydrothermal ferrous iron (Fe^{2+}) meets oxygenated surface waters, precipitating ferric hydroxide flocs that consolidate into rhythmic alternating bands of scarlet jasper chert (SiO_2) and silver-black hematite/magnetite (Fe_2O_3/Fe_3O_4). Today, these rhythmic beds constitute over 90% of Earth's mined commercial iron ore.

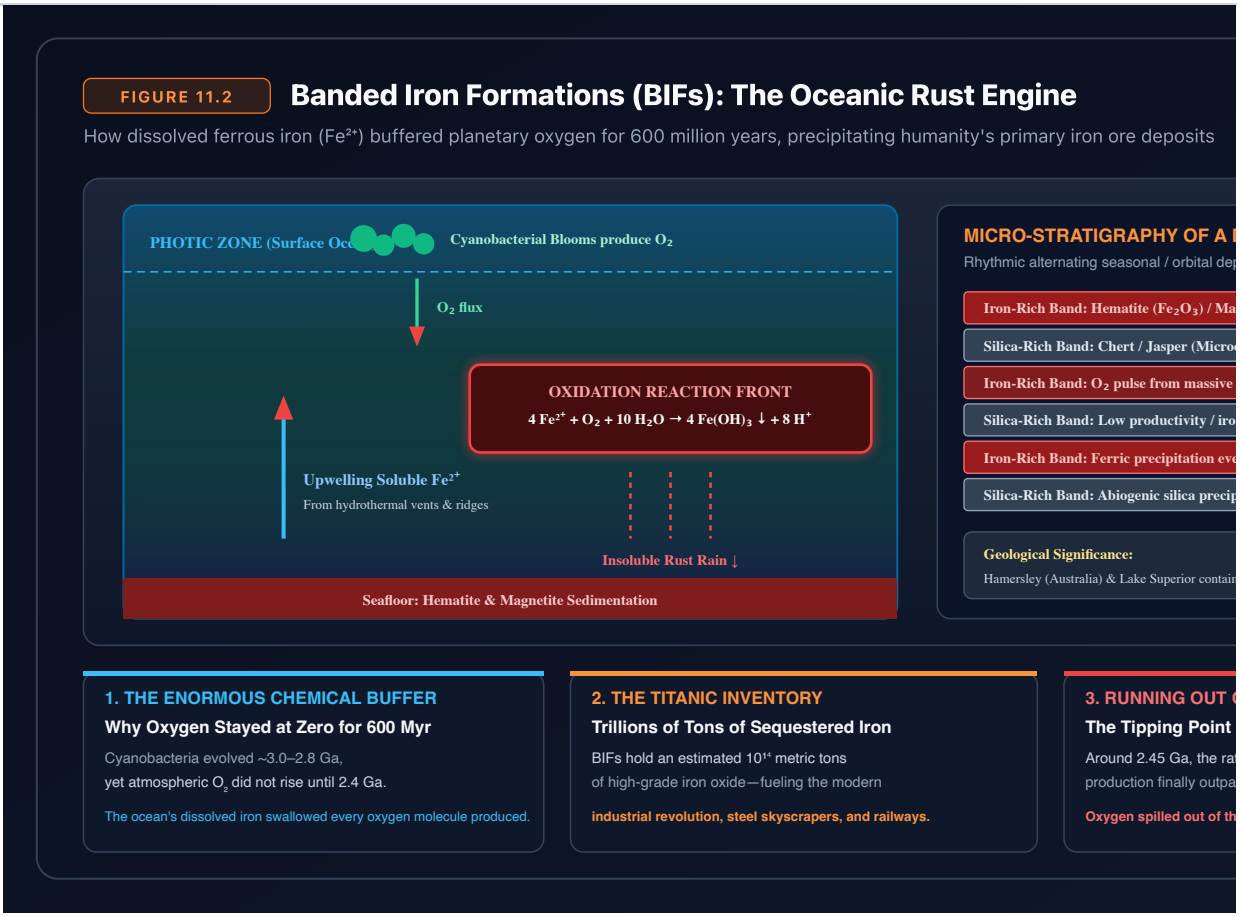


Figure 11.2: Banded Iron Formations (BIFs) & The Oceanic Rust Sinks. For hundreds of millions of years, biogenic oxygen could not accumulate in Earth's atmosphere because the Archean oceans contained vast reserves of soluble ferrous iron (Fe^{2+}) upwelling from hydrothermal vents. Photosynthetic O2 instantly oxidized Fe^{2+} into insoluble ferric oxyhydroxides (Fe(OH)3), creating a continuous rain of red rust onto the ocean floor that consolidated into alternating bands of iron oxides (hematite/magnetite) and silica (chert)—trapping trillions of tons of iron before the planet saturated.

The Great Oxidation Event (GOE): The Catastrophe

By approximately 2.4 billion years ago (2,400 Ma), the oceanic iron buffer was exhausted. The iron had rusted out of the water. With no chemical sinks left to absorb it, free oxygen escaped the ocean surface and flooded the atmosphere: the **Great Oxidation Event (GOE)**.

The Sulfur Isotope Smoking Gun: Disappearance of $\Delta^{33}S$

In 2000, geochemist James Farquhar discovered an unshakeable chemical line in the sand: in rocks older than 2.45 billion years, sedimentary sulfides display **Mass-Independent Fractionation (MIF) of sulfur isotopes ($\Delta^{33}S \neq 0$)**, produced when deep solar ultraviolet radiation photolyzes atmospheric sulfur dioxide in an anoxic atmosphere. At exactly 2.45 Ga, the sulfur MIF signal vanishes completely and permanently from the geological record—conclusively proving that atmospheric O2 surged past 0.001\% of modern levels, establishing the first stratospheric ozone shield.

The Anaerobic Holocaust

To the primitive anaerobic organisms that had ruled the planet for over a billion years, oxygen was not life; it was a deadly, corrosive poison. Oxygen greedily strips electrons from organic molecules, generating destructive **Reactive Oxygen Species (ROS)**—superoxide radicals (O2^{•-}), hydrogen peroxide (H2O_2), and hydroxyl radicals (OH^•) that tear apart DNA, denature proteins, and peroxidize cell membranes.

Lacking antioxidant protective enzymes (such as superoxide dismutase and catalase), untold trillions of anaerobic microbial lineages were wiped out in Earth's first true planetary mass extinction. Obligate anaerobes were forced into permanent retreat—banished into deep subterranean rocks, stagnant anoxic lake muds, and the hydrothermal floor.

Shakil Mahmud • Research Monograph

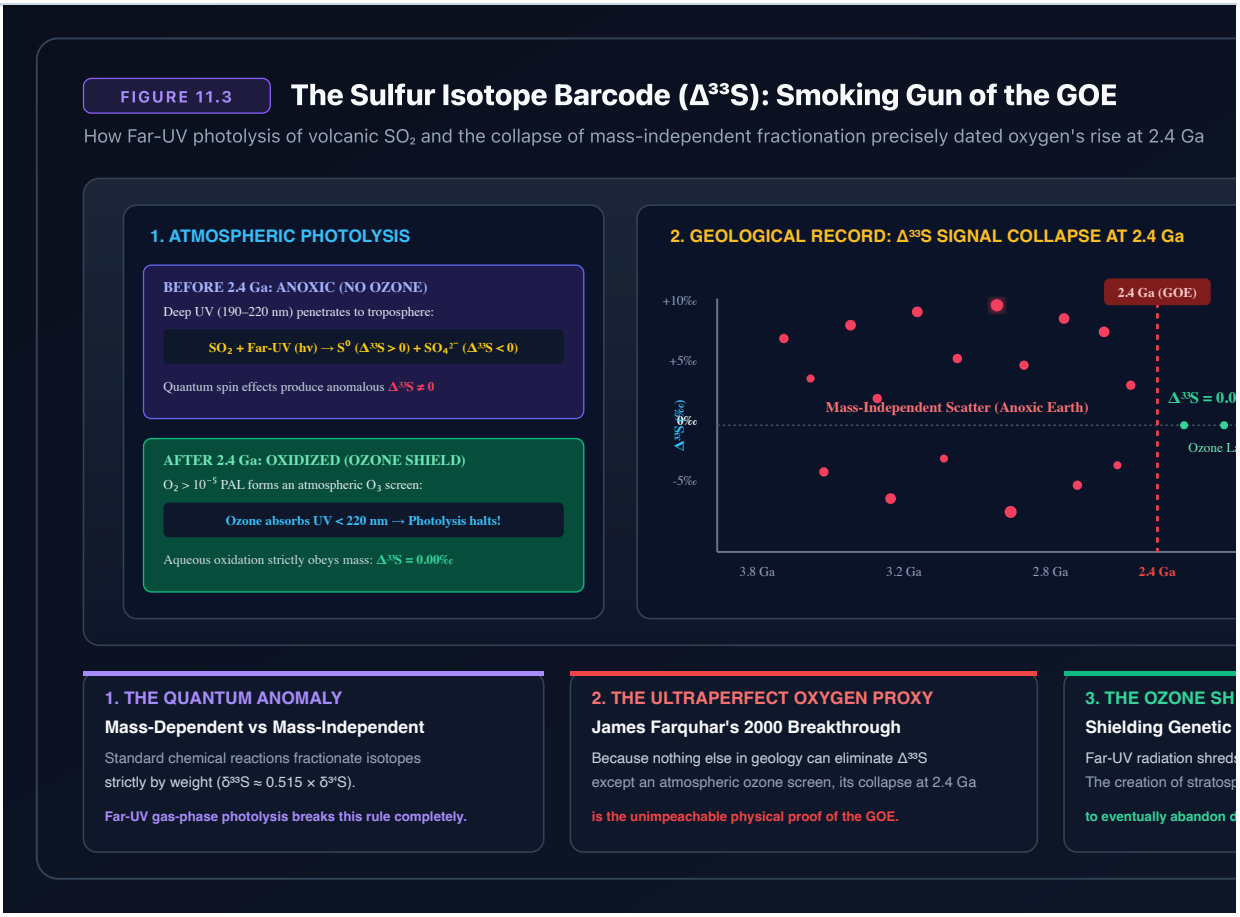


Figure 11.3: The Mass-Independent Sulfur Isotope Barcode ($\Delta^{33}S$). The definitive geological proof for the exact timing of the Great Oxidation Event at 2.4 Ga lies in sulfur isotopes. In an anoxic atmosphere without an ozone layer, solar Far-UV radiation (190–220 nm) photolyzed volcanic SO2, producing anomalous mass-independent fractionation ($\Delta^{33}S \neq 0$). Once oxygen rose above 10^{-5} of present levels, a protective ozone (O3) screen formed, permanently extinguishing Far-UV photolysis and collapsing the $\Delta^{33}S$ signal to exactly 0.00‰ worldwide.

The Huronian Glaciation (2.4 to 2.1 Ga): The 300-Million-Year Winter

The ecological catastrophe soon triggered a planetary climatic nightmare. Throughout the Archean, Earth's surface had remained warm under the Faint Young Sun due to a thick blanket of atmospheric methane (CH4).

As oxygen surged into the atmosphere, it reacted with methane in photochemical oxidation chains:

$$CH_4 + 2O_2 \rightarrow CO_2 + 2H_2O$$

Carbon dioxide is a greenhouse gas, but methane is **twenty-eight times more potent** per molecule. Replacing the dense methane blanket with CO2 destroyed Earth's planetary insulation. Global temperatures crashed by dozens of degrees in a geological heartbeat.

The Ice-Albedo Catastrophe
As continental glaciers expanded from the poles past 30° latitude, reflective white ice reflected solar radiation back into space, triggering a runaway positive feedback loop (the ice-albedo instability). Earth plunged into the **Huronian Glaciation (2.4 to 2.1 billion years ago)—the longest and most severe Ice Age in Earth history**.

For over 300 million years, Earth was an unbroken, reflective white "Snowball Earth," with glaciers kilometers thick locking the oceans under ice right down to the equator. Life survived only in narrow cracks, geothermal hot springs, and around hydrothermal chimneys beneath the frozen sea.

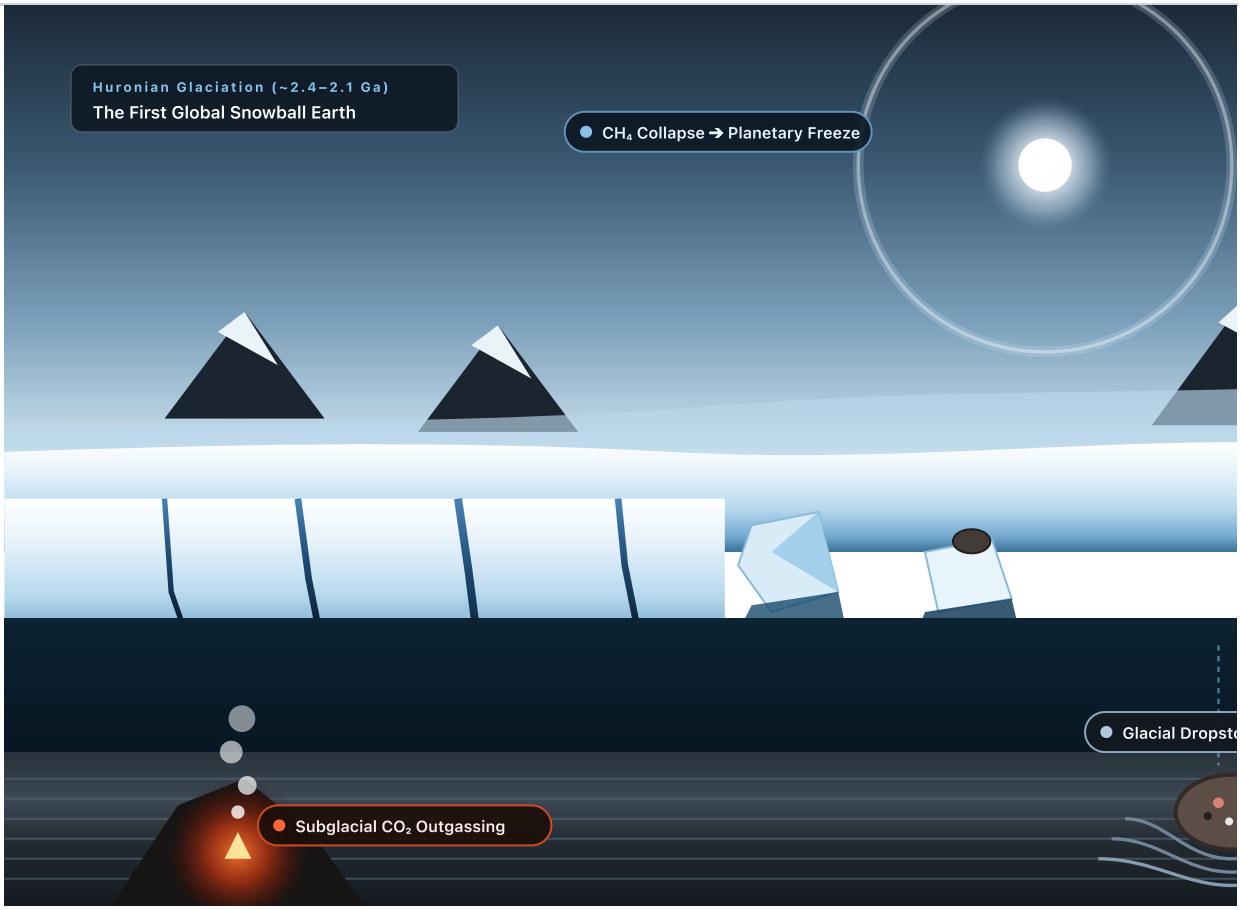


Figure 11.Sub3: The Huronian Snowball Earth Glacial Wasteland (~2.4–2.1 Ga). The destruction of atmospheric methane triggered Earth's first global glaciation, locking continents and equatorial oceans under kilometers of ice for 300 million years. Floating ice shelves rafted crystalline granite boulders (glacial dropstones) that plunged into deep glaciomarine laminated muds (Gowganda Formation), while subglacial volcanic fissures slowly vented volcanic CO_2 to ultimately shatter the runaway ice-albedo trap.

Shakil Mahmud • Research Monograph

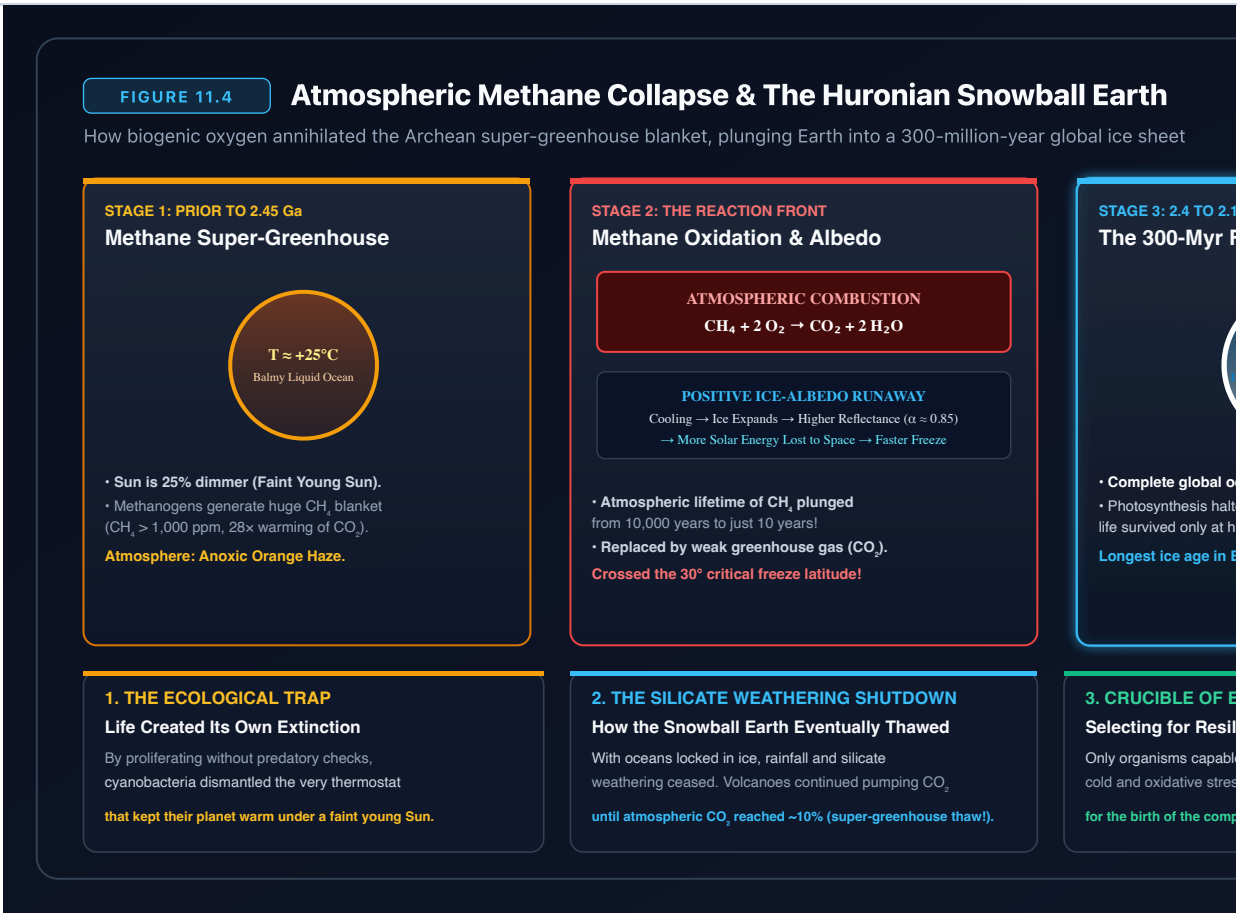


Figure 11.4: Atmospheric Methane Collapse & The Huronian Snowball Earth. Under a young Sun that was 25% dimmer, Earth remained warm due to a thick blanket of biogenic methane (CH4). As newly freed oxygen flooded the atmosphere, it chemically incinerated this methane veil into carbon dioxide and water vapor ($CH_4 + 2O_2 \rightarrow CO_2 + 2H_2O$). Because CO_2 is 28× less potent at greenhouse warming, radiative forcing plunged. Expanding polar ice triggered runaway positive ice-albedo feedback, entombing the globe in kilometer-thick ice sheets for 300 million years.

The Miracle: The Thermodynamic Jackpot of Aerobic Respiration

Eventually, volcanic outgassing of CO_2 un-sequestered by liquid oceans accumulated to extreme levels (over 0.1 to 0.3 bars), overpowering the ice-albedo feedback and melting the Snowball Earth in a super-greenhouse thaw. The world that emerged was chemically transformed forever.

While oxygen was initially a poison, the microbes that learned to harness it unlocked an astronomical thermodynamic jackpot: **Aerobic Respiration**.

Under anaerobic fermentation, the breakdown of one molecule of glucose yields barely **2 molecules of ATP** (adenosine triphosphate, the cellular energy currency). In aerobic respiration, using oxygen as the terminal electron acceptor in the electron transport chain, the complete oxidation of glucose releases **36 to 38 molecules of ATP**:

$$\text{C}_6\text{H}_{12}\text{O}_6 + 6\text{O}_2 \to 6\text{CO}_2 + 6\text{H}_2\text{O} + 36\text{–}38\text{ ATP} \quad (\Delta G^\circ = -2{,}880\text{ kJ/mol})$$

This was an energetic expansion of nearly **1,800%**! For two billion years, life had been limited to microscopic, sluggish single cells because anaerobic metabolism could not afford the energetic overhead of large, complex cellular structures. With aerobic respiration, life possessed the biochemical fuel to power complex genomic regulation, intracellular transport, and multicellularity.

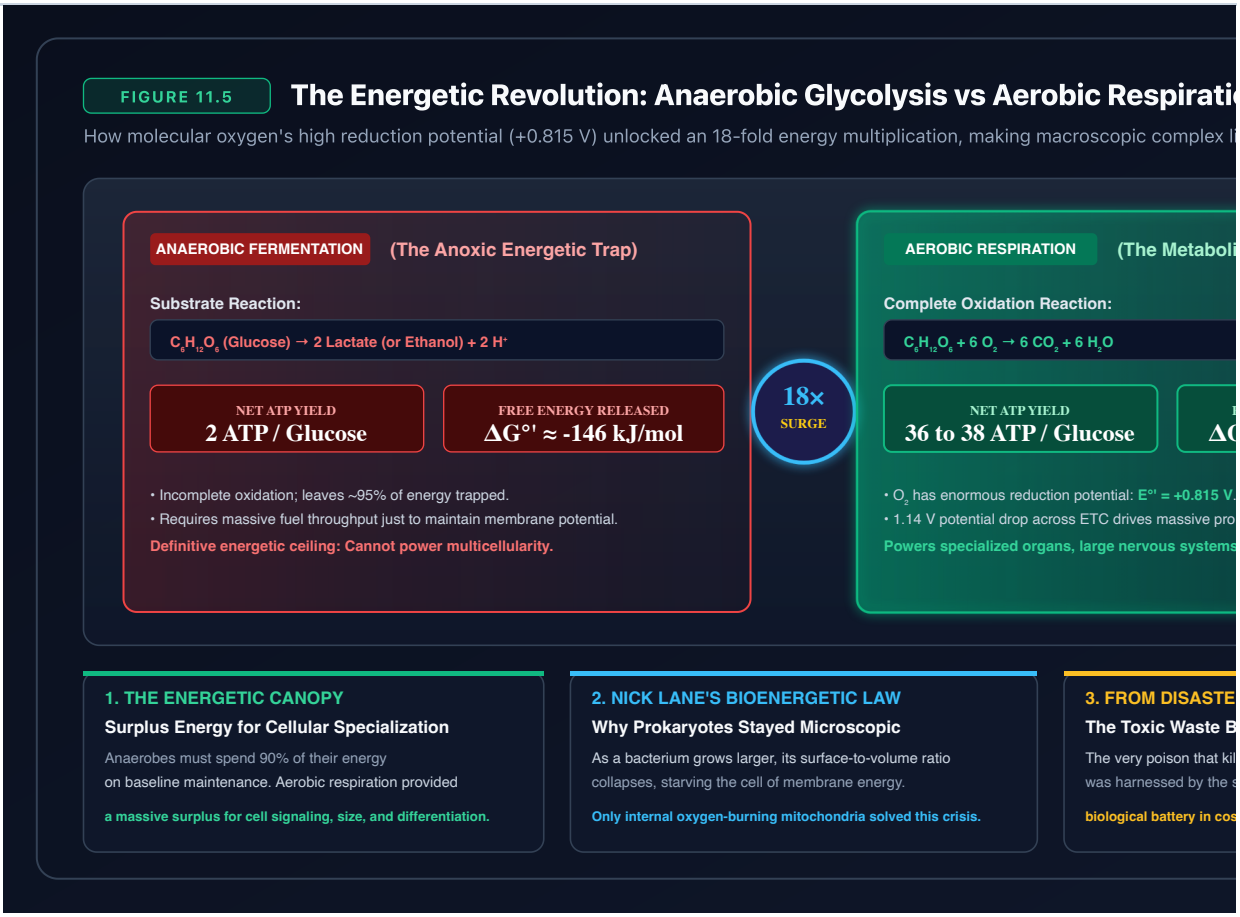


Figure 11.5: The Energetic Revolution: Anaerobic Glycolysis vs. Aerobic Respiration. The Great Oxidation Event was both a disaster and an unprecedented energetic jackpot. Anaerobic fermentation yields only 2 ATP molecules per glucose molecule ($\Delta G^{\circ\prime} \approx -146$ kJ/mol), imposing a strict bioenergetic ceiling that prevented cells from growing large or multicellular. By using molecular oxygen as an ultra-high-potential terminal electron acceptor ($E^{\circ\prime} = +0.815$ V), aerobic respiration extracts 36 to 38 ATP per glucose ($\Delta G^{\circ\prime} = -2{,}870$ kJ/mol)—an 18-fold energy multiplication that funded macroscopic complexity.

Chronology Table: The Rise of Atmospheric Oxygen

Stage / Epoch	Age (Ga)	Atmospheric O_2 (% PAL)	Key Physical & Geobiological Events
Pre-Photosynthetic Archean	> 3.0 Ga	< 0.0001\%	Anoxic oceans; methanogen greenhouse; mass-independent sulfur fractionation ($\Delta^{33}S \neq 0$).
Early Cyanobacteria & Iron Sinks	2.8–2.45 Ga	Local "oxygen oases"	Water-splitting photosystem II evolves; banded iron formations (BIFs) precipitate in global ocean.
The Great Oxidation Event (GOE)	2.45–2.22 Ga	1 to 10\%	Oceanic iron sinks exhausted; $\Delta^{33}S$ vanishes; anaerobic mass extinction; methane haze destroyed.
The Huronian Snowball Earth	2.4–2.1 Ga	Variable	Methane greenhouse collapse; global runaway glaciation lasts 300 million years; volcanic CO2 accumulation breaks ice.
The "Boring Billion" Equilibrium	1.8–0.8 Ga	~ 1 to 5\%	Canfield ocean (anoxic, sulfidic deep water); stratospheric ozone shield forms; endosymbiosis and first eukaryotes emerge.

The Stage is Set: The Threshold of the Eukaryotic Revolution

By approximately 2.0 billion years ago, Earth had stabilized into an oxygenated world shielded by a stratospheric ozone layer. The atmosphere and surface oceans possessed a steady supply of free oxygen, while the deep ocean remained anoxic and sulfidic.

Simple prokaryotic bacteria and archaea were now supercharged by aerobic respiration, but they hit an insurmountable morphological ceiling: without internal organelles and specialized bioenergetic membranes, a prokaryote cannot expand its genome size without suffering an energy crisis. To break through this energetic barrier, nature required a singular, once-in-a-billion-years partnership between two completely different single-celled organisms.

In **Part 12** of *The Universal Chronicle*, we will explore the greatest biological merger of all time: **The Leap to Complexity — Endosymbiosis, Eukaryotes, and the Genesis of Cellular Specialization**.

Academic Citations & Foundational Literature

- **Farquhar, J., Bao, H., & Thiemens, M. (2000).** "Atmospheric Influence of Earth's Earliest Sulfur Cycle." *Science*, 289(5480), 756–758. doi:10.1126/science.289.5480.756.

Shakil Mahmud • Research Monograph

- **Lyons, T. W., Reinhard, C. T., & Planavsky, N. J. (2014).** "The rise of oxygen in Earth's early ocean and atmosphere." *Nature*, 506, 307–315. doi:10.1038/nature13068.
- **Fischer, W. W., Hemp, J., & Johnson, J. E. (2016).** "Evolution of Oxygenic Photosynthesis." *Annual Review of Earth and Planetary Sciences*, 44(1), 647–672. doi:10.1146/annurev-earth-060313-054632.
- **Kopp, R. E., Kirschvink, J. L., Hilburn, I. A., & Nash, C. Z. (2005).** "The Paleoproterozoic snowball Earth: A climate disaster triggered by the evolution of oxygenic photosynthesis." *Proceedings of the National Academy of Sciences*, 102(32), 11131–11136. doi:10.1073/pnas.0504878102.
- **Holland, H. D. (2006).** "The oxygenation of the atmosphere and oceans." *Philosophical Transactions of the Royal Society B: Biological Sciences*, 361(1470), 903–915. doi:10.1098/rstb.2006.1838.
- **Ueno, Y., et al. (2006).** "Quadruple sulfur isotope analysis of >3.8 Ga basalts: No evidence for the late heavy bombardment?" *Geochimica et Cosmochimica Acta*, 70(18), A664.

Citation: Mahmud, S. (2026). "The Oxygen Catastrophe & The Miracle — Cyanobacteria and the Great Oxidation Event." In The Universal Chronicle, Part 11. https://shakilmahmud.com/universal-chronicle-part-11-the-oxygen-catastrophe/

SHAKIL MAHMUD RESEARCH MONOGRAPHS • PART XII

The Leap to Complexity — Endosymbiosis, Eukaryotes, and the Genesis of Cellular Specialization

The Leap to Complexity — Endosymbiosis, Eukaryotes, and the Genesis of Cellular Specialization

2,212 words • October 31, 2026 • Permanent URI

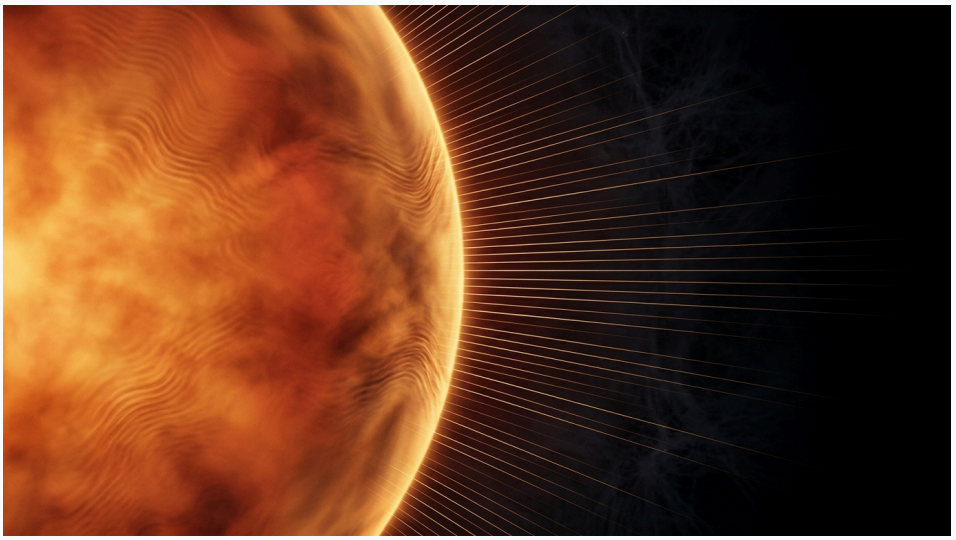


Plate XII: *Figure: Cellular endosymbiosis (~1.8 Ga): an Asgard archaeon host envelops an alphaproteobacterial symbiont, sparking mitochondrial ATP bioenergetics, internal compartmentalization, and the eukaryotic cellular revolution.*

Bacteria and Archaea are the undisputed biochemical wizards of the Earth, yet in four billion years of evolution, they never built a multicellular tree, a mushroom, an insect, or a human brain. They remained microscopic specks trapped behind an insurmountable energetic wall. Then, roughly 1.8 billion years ago, a singular, once-in-the-universe biological merger took place: an ancient archaeal cell engulfed an aerobic bacterium and, instead of digesting it, formed an eternal partnership. That captive bacterium became the mitochondrion, expanding the energy budget per gene by 200,000 times and unleashing the complex eukaryotic kingdom.

The Prokaryotic Glass Ceiling: The Bioenergetic Trap

Bacteria and Archaea colonized every ecological niche on the planet: they thrive inside nuclear reactors, kilometer-deep crustal rocks, and hydrothermal geysers. Yet structurally, a bacterium today looks virtually indistinguishable from a bacterium fossilized 3.5 billion years ago in Archean chert.

Why did prokaryotes never evolve true macroscopic complexity? In 2010, biochemist **Nick Lane** and evolutionary genomicist **William Martin** solved this fundamental enigma by calculating the bioenergetics of cell size:

In all prokaryotes, respiration is tied to the **outer cell membrane**. Protons are pumped across the plasma membrane, creating an electrochemical gradient that drives ATP synthesis. If a bacterium increases its radius by ten times, its internal volume (and energetic demand) expands by a factor of one thousand ($V \propto r^3$), while its surface membrane area (and energy supply) expands by only a factor of one hundred ($A \propto r^2$).

The Genomic Overhead of Prokaryotic Scaling
To overcome this surface-area deficit, a giant bacterium (such as *Thiomargarita namibiensis*) must fold its internal membranes and replicate thousands of copies of its entire genome along the periphery to locally monitor and regulate electron transport. A single giant bacterium may carry up to **20,000 copies of its full DNA genome**! Nearly all of its energy budget is consumed simply replicating, transcribing, and translating identical copies of house-keeping genes. It has zero metabolic surplus left to evolve complex gene regulation, intracellular transport, or novel gene families.

Shakil Mahmud • Research Monograph

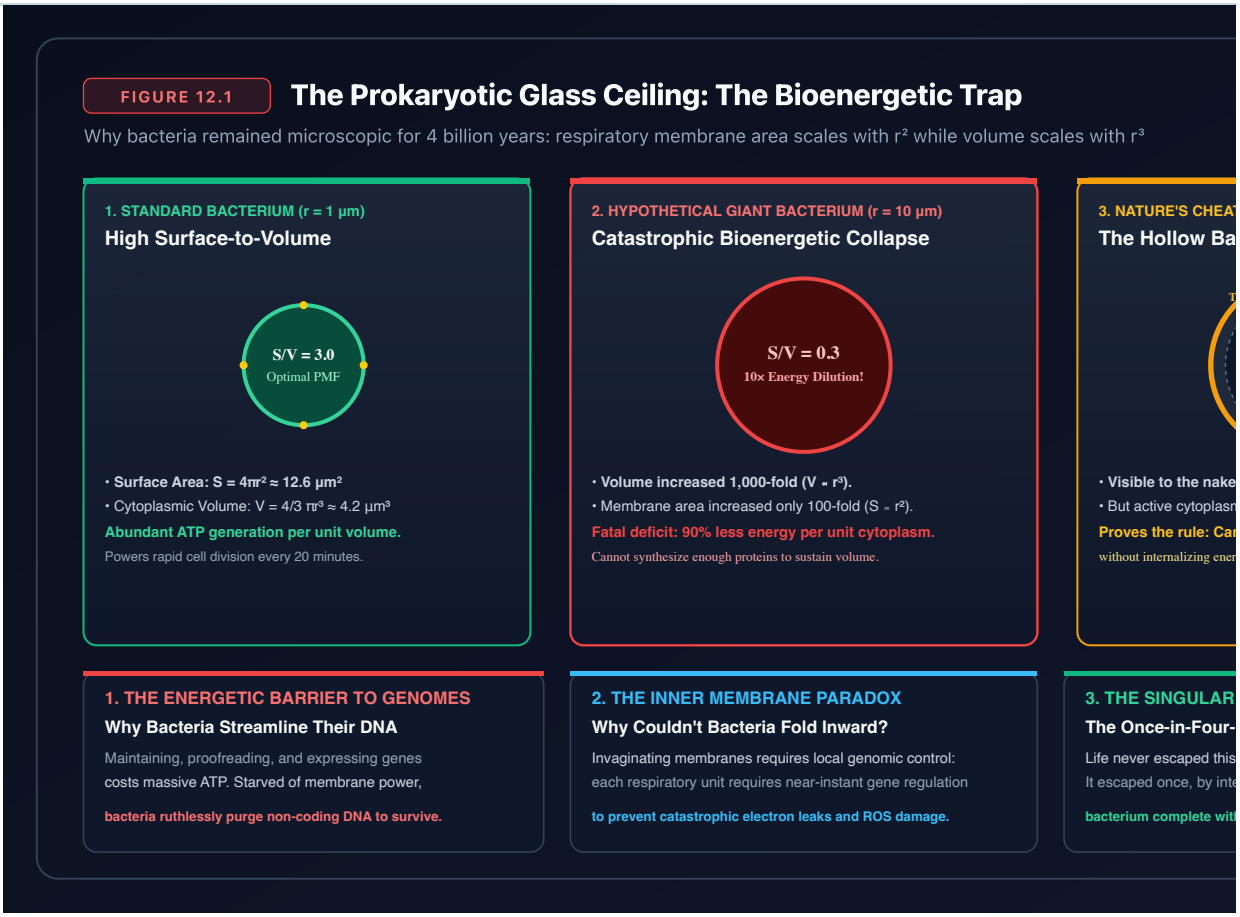


Figure 12.1: The Prokaryotic Glass Ceiling & Surface-to-Volume Scaling. Because bacteria generate proton-motive force across their outer plasma membrane, their energy generation scales with surface area ($S \propto r^2$), while the cost of maintaining and synthesizing cytoplasm scales with volume ($V \propto r^3$). A 10-fold increase in bacterial radius results in a catastrophic 10-fold dilution of power per unit volume. Giant bacteria like Thiomargarita can only survive by leaving 98% of their interior as an inert, hollow liquid vacuole—proving that complex 3D cellular architecture was physically impossible without internalizing power plants.

The Endosymbiotic Revolution: The Merger of Two Worlds

In 1967, evolutionary biologist **Lynn Margulis** published her revolutionary paper *"On the Origin of Mitosing Cells"*, reviving the radical hypothesis of **Serial Endosymbiosis**. Margulis argued that the key internal powerhouses of eukaryotic cells—mitochondria and chloroplasts—were not built gradually from within, but were once free-living, independent prokaryotes engulfed by an ancient host cell.

For decades, Margulis's theory was met with fierce academic skepticism. Today, genomic sequencing has transformed it into uncontested scientific fact:

- Mitochondria carry their own circular, bacterial DNA (mtDNA) and replicate independently inside our cells via binary fission.
- Mitochondrial ribosomes are bacterial-sized (70S) rather than eukaryotic (80S), and are sensitive to bacterial antibiotics (such as chloramphenicol and streptomycin).
- Mitochondria possess a double membrane, with the inner membrane containing cardiolipin—a signature lipid found only in bacterial membranes.

The Partners in the Merger: Asgard Archaea and Alphaproteobacteria

In 2015, metagenomic sequencing of hydrothermal ocean sediments near "Loki's Castle" along the Arctic Mid-Atlantic Ridge identified a remarkable group of organisms: **Asgard Archaea (Lokiarchaeota)** (Spang et al. 2015). Genomic analysis proved that Asgard archaea are the closest living single-celled relatives of complex eukaryotic life: they encode eukaryotic signature proteins (ESPs) for actin-based cytoskeletons, membrane remodeling, and vesicle trafficking.

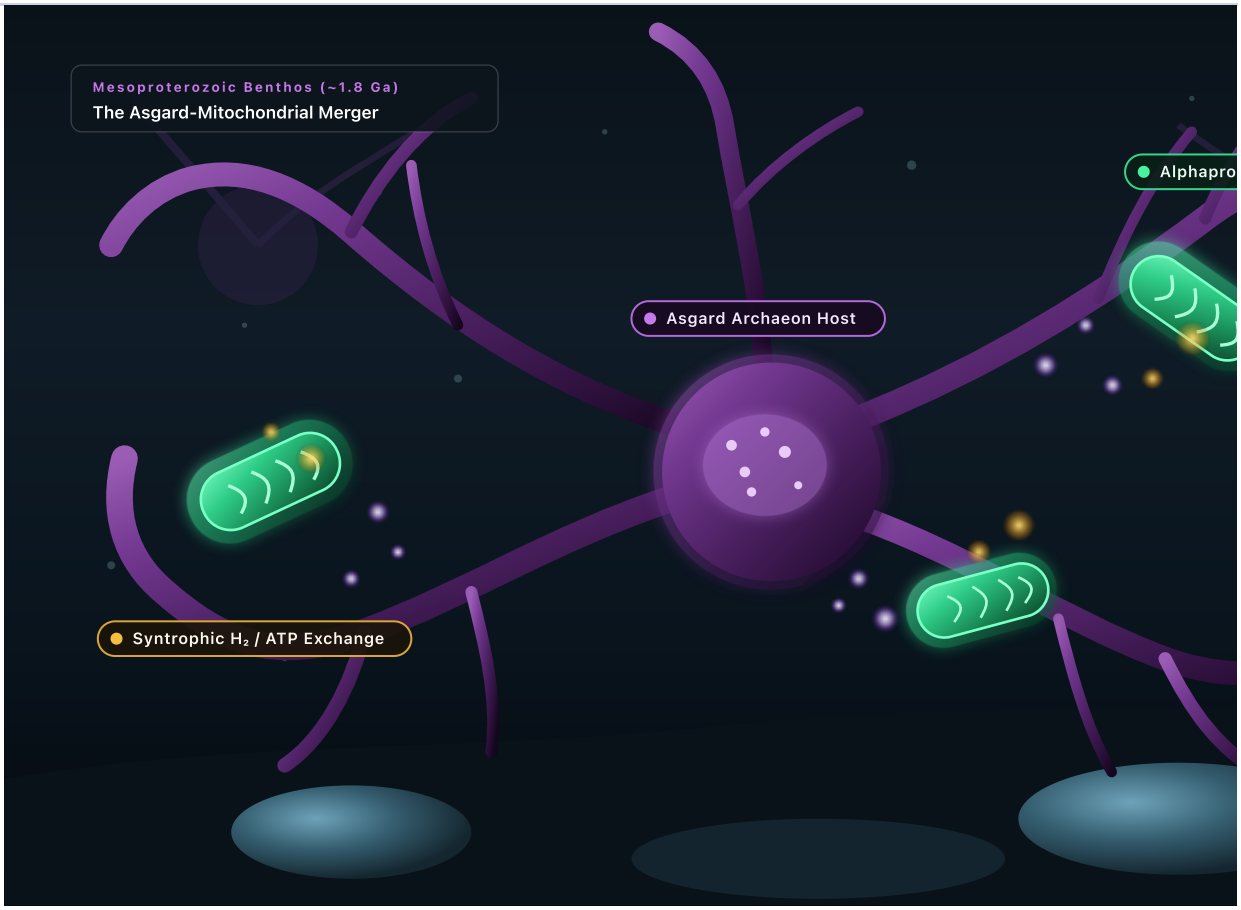


Figure 12.Sub1: Syntrophic Consortium of Asgard Archaea and Alphaproteobacteria (~1.8 Ga). Reconstruction of Prometheoarchaeum syntrophicum deep-sea morphology, exhibiting long, branching membrane protrusions (pseudopodia) physically entangling free-living aerobic alphaproteobacteria. In this mutualistic relationship, the anaerobic archaeon supplied metabolic substrates and hydrogen, while the bacterium detoxified toxic oxygen and supplied abundant ATP, initiating the singular endosymbiotic merger that forged the eukaryotic ancestor.

Roughly 1.8 billion years ago, an anaerobic Asgard-like archaeon formed a syntrophic metabolic partnership with an aerobic **Alphaproteobacterium**. The archaeon provided the bacterium with organic metabolic substrates; the bacterium, capable of aerobic respiration, detoxified oxygen and provided high-efficiency ATP. Eventually, the bacterium moved inside the archaeon's cytoplasm—initiating the most consequential cohabitation in biological history.

Shakil Mahmud • Research Monograph

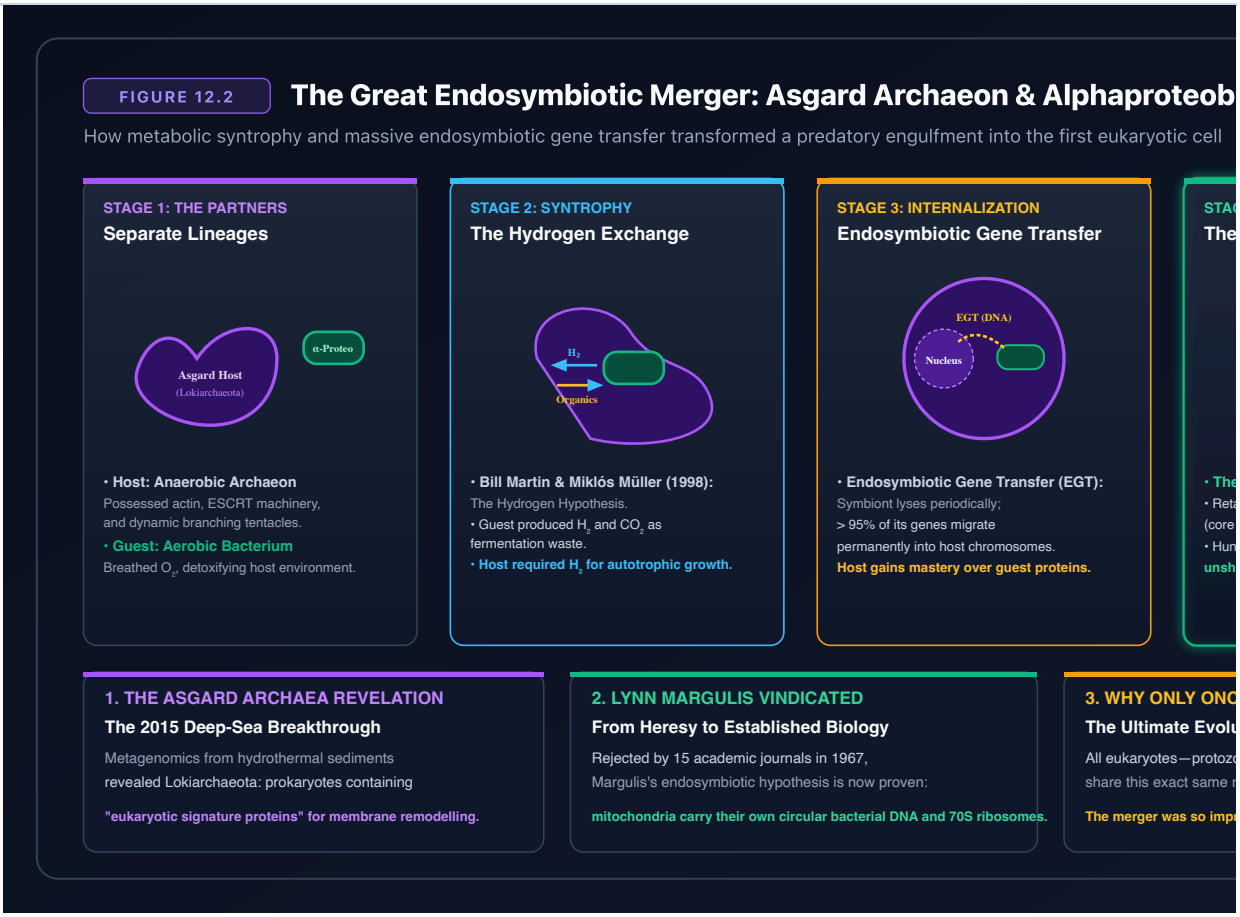


Figure 12.2: The Great Endosymbiotic Merger & The Birth of the Mitochondrion. Eukaryotes arose from a singular metabolic syntrophy between an anaerobic Asgard archaeon host (possessing actin-like dynamic tentacles) and an aerobic alphaproteobacterium guest. Driven by the exchange of hydrogen and organic substrates, the archaeon engulfed the bacterium. Through massive Endosymbiotic Gene Transfer (EGT), more than 95% of the bacterial genome migrated into the host's chromosomes, domesticating the endosymbiont into a dedicated internal ATP generator: the mitochondrion.

The Energetic Breakthrough: 200,000 Times More Energy Per Gene

Once inside, the proto-mitochondrion underwent radical evolutionary streamlining: it transferred over **99% of its genes directly to the host nucleus** via lateral gene transfer, retaining only a minimal, specialized genetic core (human mtDNA encodes just 13 essential respiratory proteins).

By delegating its genomic overhead to the central nucleus while packing hundreds or thousands of tiny, highly folded mitochondrial power plants into its cytoplasm, the eukaryotic cell shattered the surface-area-to-volume barrier forever:

$$\frac{\text{Power Available}}{\text{Gene}} \approx 200,000 \times \text{ greater in Eukaryotes than in Prokaryotes}$$

With this staggering energy surplus, the eukaryotic cell could afford an enormous genome: thousands of novel regulatory genes, complex splicing machinery, signal transduction cascades, and internal motor proteins (kinesin and dynein) moving cargo along an intracellular highway of microtubules.

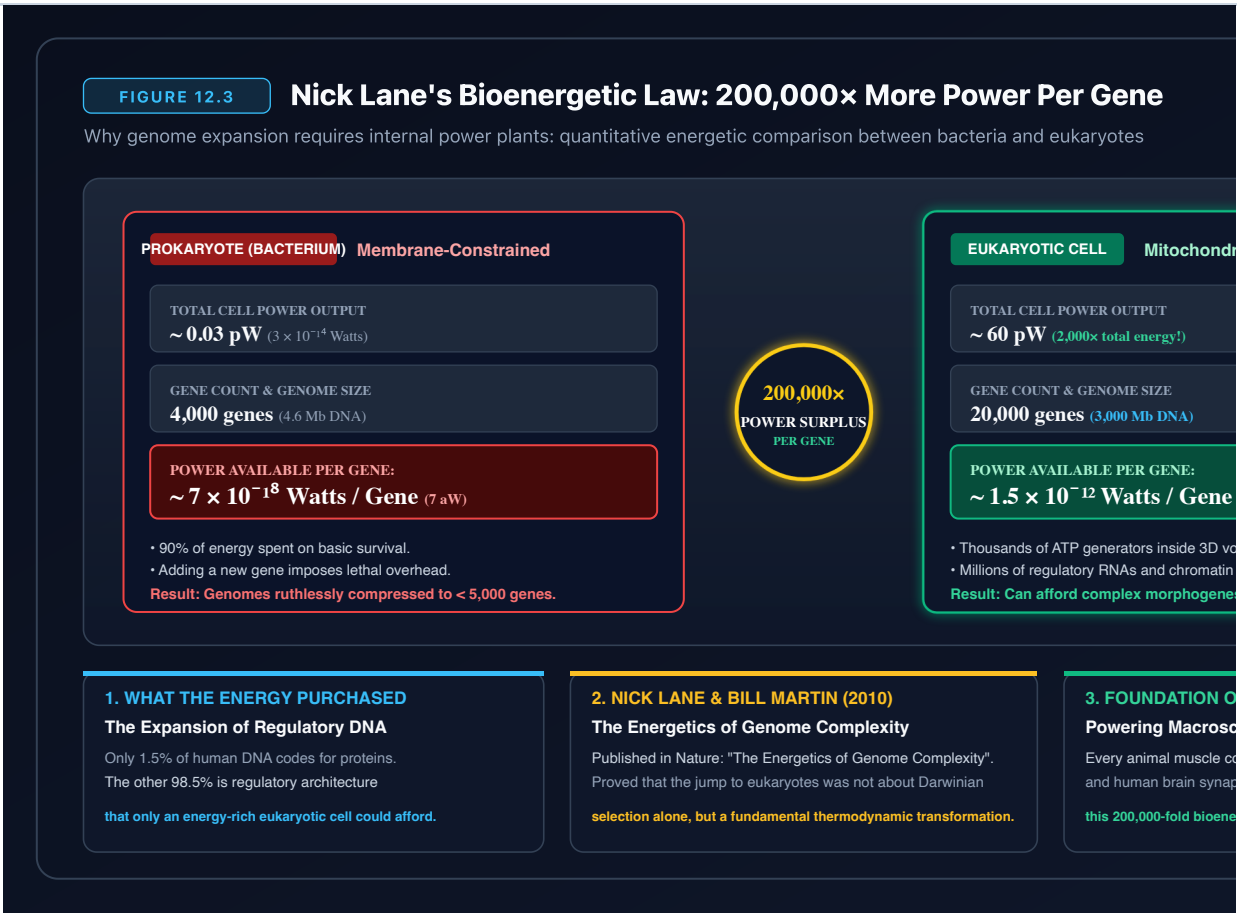


Figure 12.3: Nick Lane's Bioenergetic Law: 200,000× More Power Per Gene. A typical bacterium generates ~0.03 pW of total power, leaving only 7 attowatts per gene after baseline survival costs—forcing prokaryotes to ruthlessly purge DNA to survive. By packing thousands of energy-generating mitochondria throughout its interior, a eukaryotic cell produces 60 pW (a 2,000-fold surge in total power), providing ~1,500 femtowatts per gene—a 200,000-fold expansion in bioenergetic wealth that funded massive regulatory genomes, chromatin loops, and multicellular tissue differentiation.

The Master Inventions: Nucleus, Introns, and the Cytoskeleton

The endosymbiotic merger triggered an explosion of cellular innovations that distinguish every eukaryote today:

1. The Nuclear Membrane & Spliceosomal Introns

When thousands of bacterial endosymbionts lysed inside the host cytoplasm, their DNA fragmented, bombarding the host chromosomes with parasitic self-splicing *Group II mobile introns*. If an intron-carrying messenger RNA is translated immediately by ribosomes in the cytoplasm, it produces mangled, non-functional proteins.

The eukaryotic cell evolved the **Nuclear Membrane** as a spatial barrier: transcription and slow intron excision occur securely inside the nucleus via the *spliceosome*, and only completely verified, spliced mRNA transcripts are exported through nuclear pore complexes to ribosomes in the cytoplasm.

2. The Dynamic Cytoskeleton and Phagocytosis

Unlike rigid bacterial peptidoglycan cell walls, eukaryotes possess a flexible, dynamic internal scaffolding of actin microfilaments and tubulin microtubules. This allowed cells to change shape, engulf prey via **phagocytosis**, and establish directed intracellular vesicular transport.

Shakil Mahmud • Research Monograph

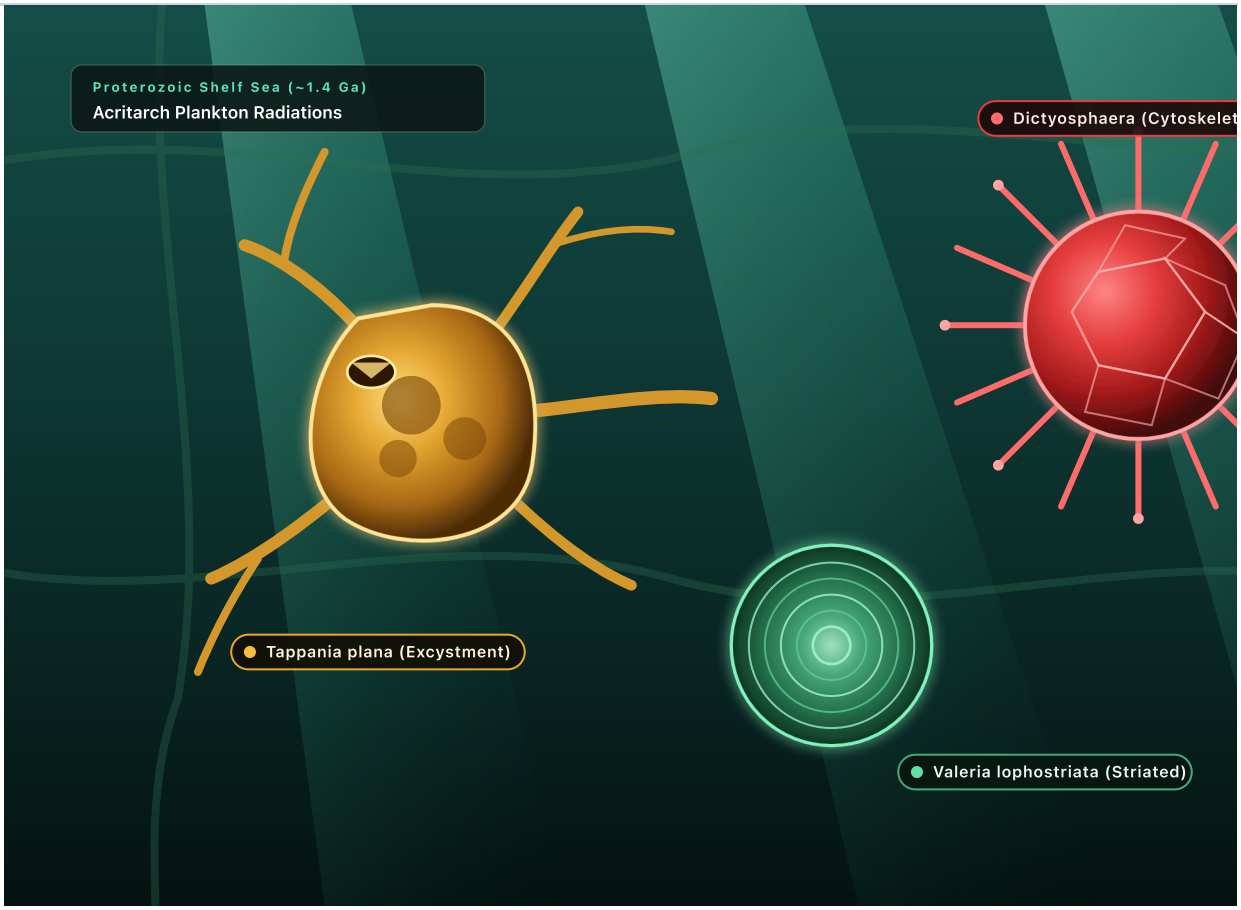


Figure 12.Sub2: Proterozoic Planktonic Radiation: Acritarch Microfossils (~1.4–1.2 Ga). Diverse organic-walled microfossils preserved in Mesoproterozoic marine strata, illustrating complex eukaryotic morphology: Tappania plana with branching tubular evaginations and excystment pylomes, Dictyosphaera with dense echinate radial spines, and concentric striated discs of Valeria lophostriata. These complex morphologies demonstrate an active internal eukaryotic cytoskeleton and regulated excystment life cycles.

3. Secondary Endosymbiosis: The Green Revolution

Roughly 1.5 billion years ago, a eukaryotic cell containing mitochondria engulfed a free-living, photosynthetic **Cyanobacterium**. Rather than digesting it, the cell integrated it as an organelle: the **Plastid (Chloroplast)**. This single evolutionary event birthed the entire *Archaeplastida* supergroup—the red algae, green algae, and the ancestors of all terrestrial plant life.

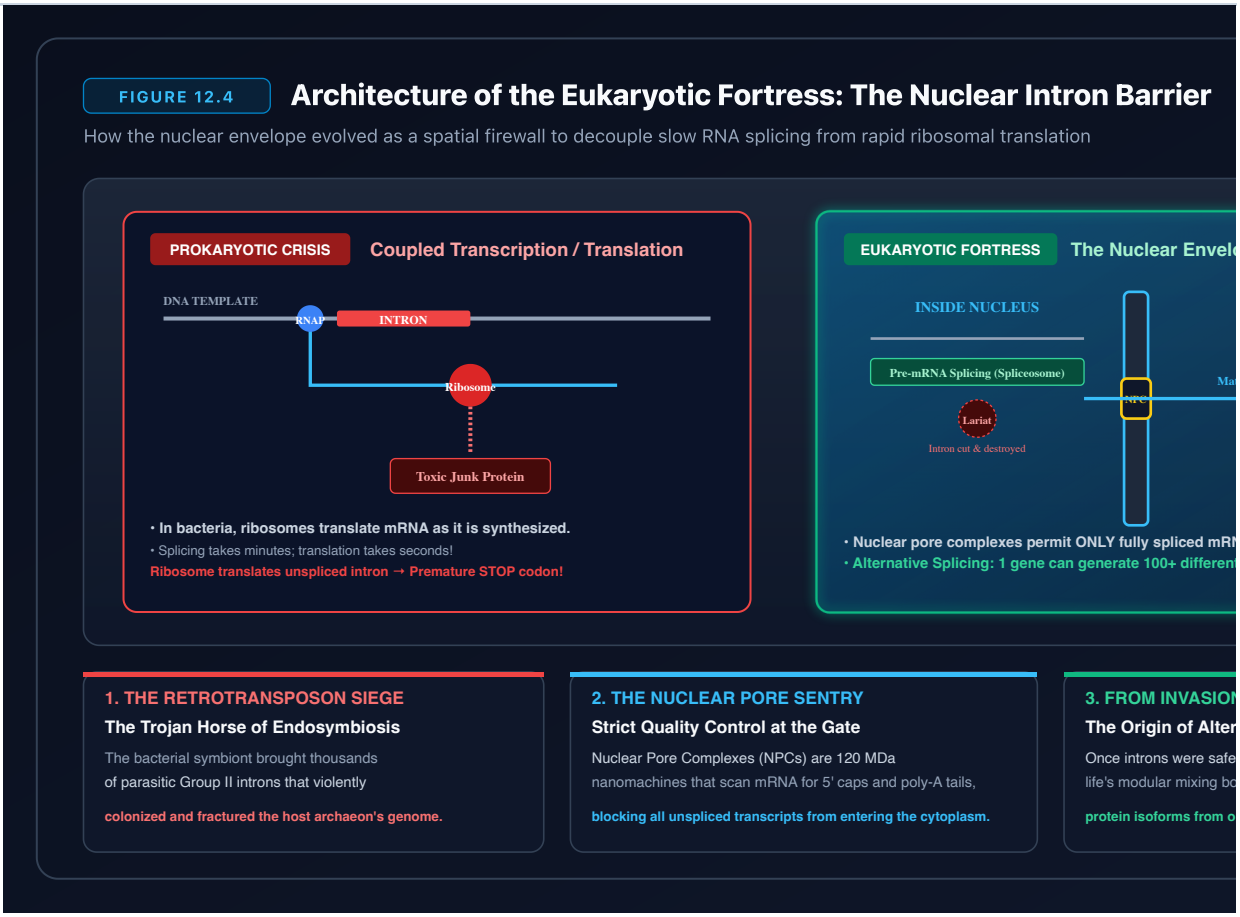


Figure 12.4: Architecture of the Eukaryotic Fortress: The Nuclear Intron Barrier. In prokaryotes, translation is coupled to transcription: ribosomes translate mRNA while it is still being copied from DNA. When endosymbiont Group II introns invaded host genes, this coupled machinery faced catastrophe: slow RNA splicing could not keep up with rapid ribosomes, translating junk sequences into lethal truncated proteins. The nuclear envelope evolved as a physical firewall, locking DNA inside so spliceosomes could excise introns and nuclear pores could inspect transcripts before releasing mature mRNA to cytoplasmic ribosomes.

The Invention of Sex: Escaping Muller's Ratchet

In asexual prokaryotic reproduction, a single cell divides into two identical clones. In sexual reproduction, two organisms combine half of their genetic material through **Meiosis**—a process involving homologous recombination and chromosomal crossing-over. At first glance, sex carries what evolutionary biologist John Maynard Smith called the **"Twofold Cost of Sex"**: a sexual female passes on only 50% of her genes to any individual offspring, and half of her offspring (males) cannot bear children directly.

Why did sex evolve and become the near-universal reproductive strategy of all complex eukaryotes? The answer lies in population genetics:

- **Muller's Ratchet:** In an asexual population, deleterious genetic mutations accumulate irreversibly like clicks in a mechanical ratchet. Eventually, mutational load causes the lineage to decline into extinction. Sexual recombination allows genomes to shuffle, purging deleterious mutations and reconstructing mutation-free chromosomes.
- **The Red Queen Hypothesis (Van Valen 1973):** *"It takes all the running you can do, to keep in the same place."* Parasites, viruses, and pathogens evolve thousands of times faster than multicellular hosts. Asexual clones present an identical, unchanging immunological target. Sexual recombination shuffles the host's immune receptor alleles every single generation, preventing pathogens from wiping out an entire population.

The First Multicellular Pioneers: *Bangiomorpha pubescens*

For hundreds of millions of years during the mid-Proterozoic (often called the "Boring Billion" due to slow geochemical shifts, 1.8 to 0.8 Ga), single-celled eukaryotes diversified in the oceans. The earliest taxonomically confirmed macroscopic eukaryotic fossil is **Bangiomorpha pubescens**, discovered in 1.05-billion-year-old rocks on Somerset Island in arctic Canada (Butterfield 2000).

Shakil Mahmud • Research Monograph

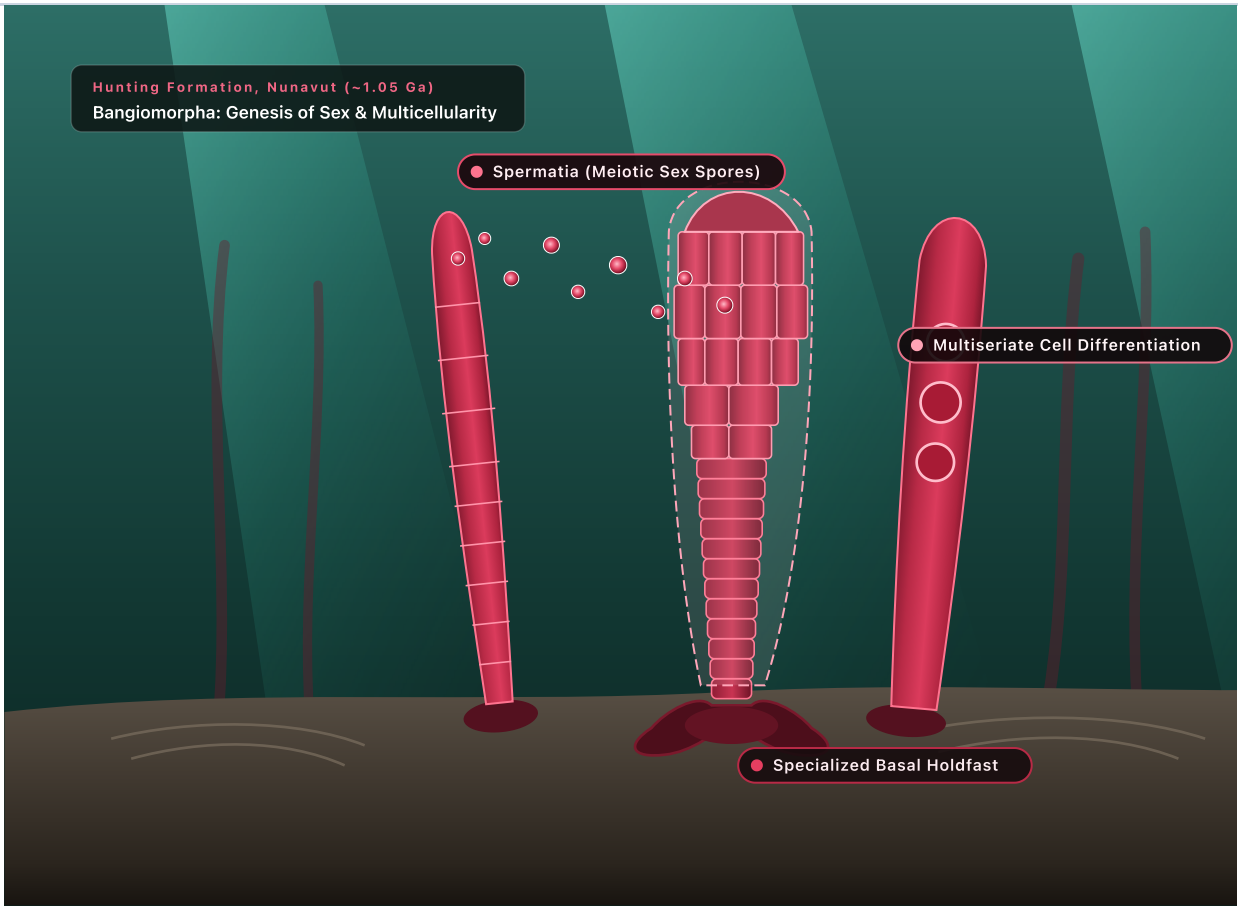


Figure 12.Sub3: Bangiomorpha pubescens — The Genesis of Multicellularity and Sex (~1.05 Ga). The earliest confirmed multicellular eukaryote from the Hunting Formation of Somerset Island, Arctic Canada. Clustered erect multiseriate red algal filaments anchored by specialized basal holdfasts to stromatolitic carbonate substrates, exhibiting distinct uniseriate-to-multiseriate vegetative development and sexually dimorphic reproductive cells (spermatia and carpogonia)—the dawn of meiotic sexual reproduction.

Bangiomorpha is a multicellular red alga that displays two world-changing biological innovations: **cellular differentiation** (possessing specialized discoid vegetative cells and an anchor holdfast cell) and **true sexual reproduction** (male and female spores). The genetic toolkit for building multicellular tissues—cell-to-cell adhesion (cadherins), intercellular communication (gap junctions), and developmental gene regulation—was officially assembled.

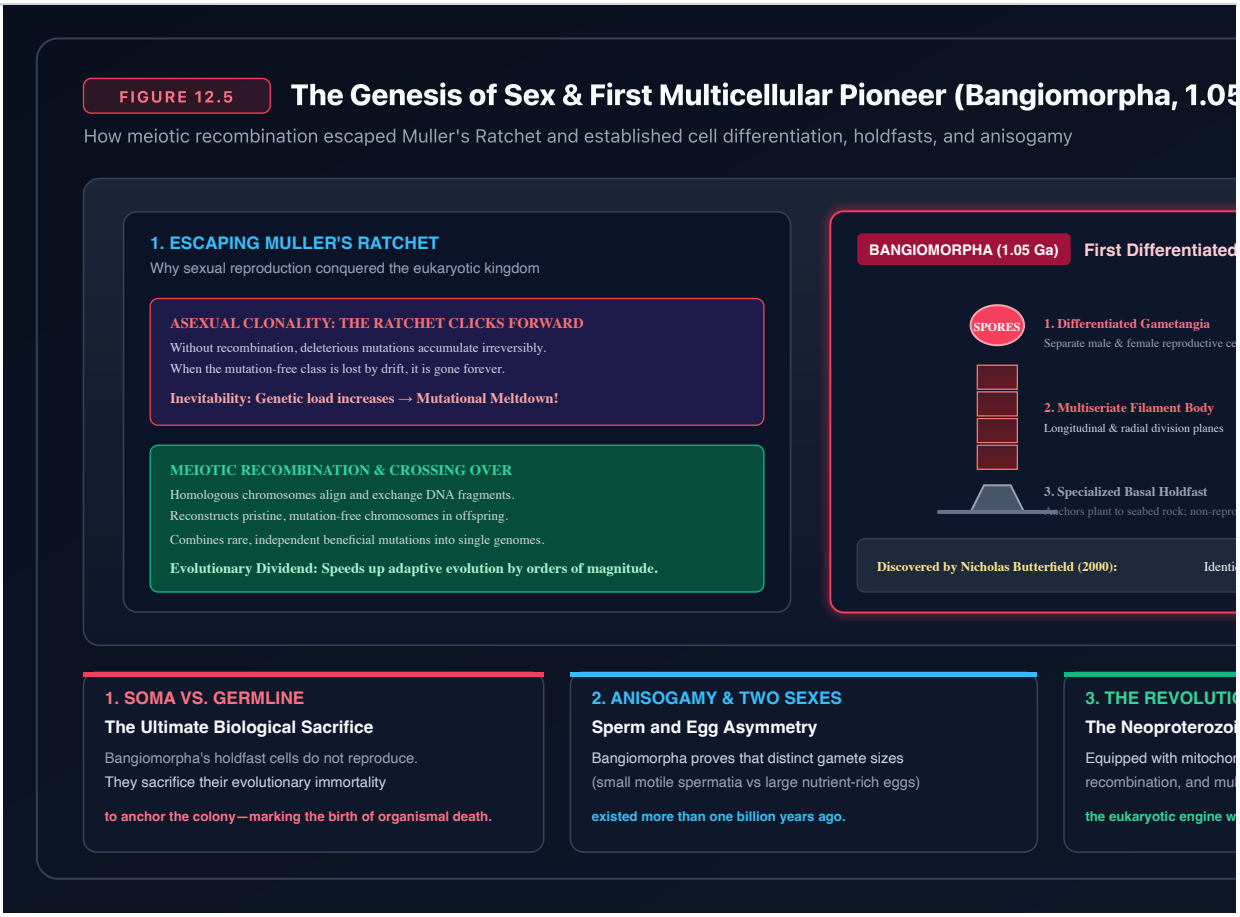


Figure 12.5: The Genesis of Sex & First Multicellular Pioneer (Bangiomorpha pubescens, 1.05 Ga). Asexual populations inevitably suffer from Muller's Ratchet—the irreversible accumulation of deleterious mutations leading to mutational meltdown. Meiotic sexual recombination solved this by crossing over homologous chromosomes, purging bad mutations and accelerating adaptation. In 1.05-billion-year-old Arctic cherts, Nicholas Butterfield discovered Bangiomorpha pubescens, showing the world's oldest specialized holdfast cells (cellular sacrifice/soma) and distinct male/female gametangia (anisogamy)—the foundation of macro-organismal life.

Prokaryotes vs. Eukaryotes: The Great Divide

Biological Dimension	Prokaryotes (Bacteria & Archaea)	Eukaryotes (Animals, Plants, Fungi, Protists)
Energy Transduction	Across outer plasma membrane; surface-area limited	Across internal cristae of hundreds of mitochondria
Power per Gene	Baseline (1×)	**200,000× higher** metabolic surplus
Genome Architecture	Single circular DNA; gene-dense; few non-coding introns	Multiple linear chromosomes; telomeres; extensive spliceosomal introns
Compartmentalization	No nucleus; simultaneous transcription/translation	Membrane-bound nucleus, endoplasmic reticulum, Golgi apparatus
Cytoskeleton & Motility	Rigid cell walls; external flagella rotary motors	Dynamic actin/tubulin cytoskeleton; phagocytosis; internal motor proteins
Reproductive Strategy	Asexual binary fission; lateral gene transfer	Meiotic sexual reproduction; homologous recombination
Morphological Limits	Strictly microscopic single cells or simple filaments	Complex macroscopic tissues, organ systems, and animals

The Calm Before the Storm: The Neoproterozoic Threshold

By approximately 800 million years ago, the eukaryotic stage was set: single-celled and simple colonial eukaryotes possessed mitochondria, sexual recombination, complex genomes, and the intracellular machinery for tissue differentiation. Yet, large, macroscopic animals were still nowhere to be seen in the fossil record. Why?

The limiting factor was once again geochemical: atmospheric oxygen levels remained stalled at roughly 1% to 5% of present levels—sufficient for single cells, but far too low to support the deep oxygen diffusion required by thick, layered animal tissues. To smash open the gates of animal evolution, Earth required one final, catastrophic planetary convulsion.

In **Part 13** of *The Universal Chronicle*, the planet will freeze into its deepest slumber and awaken in a riot of biological innovation: **The Cambrian Crucible — Snowball Earth Thaw, Multicellular Body Plans, and the Apex Predators**.

Shakil Mahmud • Research Monograph

Academic Citations & Foundational Literature

- **Sagan, L. (Margulis) (1967).** "On the origin of mitosing cells." *Journal of Theoretical Biology*, 14(3), 225–274. doi:10.1016/0022-5193(67)90079-3.
- **Lane, N., & Martin, W. (2010).** "The energetics of genome complexity." *Nature*, 467, 929–936. doi:10.1038/nature09486.
- **Spang, A., et al. (2015).** "Complex archaea that bridge the gap between prokaryotes and eukaryotes." *Nature*, 521, 173–179. doi:10.1038/nature14447.
- **Butterfield, N. J. (2000).** "Bangiomorpha pubescens n. gen., n. sp.: implications for the evolution of sex, multicellularity, and the Mesoproterozoic/Neoproterozoic radiation of eukaryotes." *Paleobiology*, 26(3), 386–404. <a href="https://doi.org/10.1666/0094-8373(2000)0262.0.CO;2" target="_blank" rel="noopener">doi:10.1666/0094-8373(2000)0262.0.CO;2.
- **Maynard Smith, J. (1978).** *The Evolution of Sex*. Cambridge University Press. ISBN: 978-0521293020.
- **Van Valen, L. (1973).** "A new evolutionary law." *Evolutionary Theory*, 1, 1–30.
- **Koonin, E. V. (2010).** "The origin and early evolution of eukaryotes in the light of phylogenomics." *Genome Biology*, 11(5), 209. doi:10.1186/gb-2010-11-5-209.

Citation: Mahmud, S. (2026). "The Leap to Complexity — Endosymbiosis, Eukaryotes, and the Genesis of Cellular Specialization." In The Universal Chronicle, Part 12. https://shakilmahmud.com/universal-chronicle-part-12-the-leap-to-complexity/

SHAKIL MAHMUD RESEARCH MONOGRAPHS • PART XIII

The Cambrian Crucible — Snowball Earth Thaw, Multicellular Body Plans, and the Apex Predators

The Cambrian Crucible — Snowball Earth Thaw, Multicellular Body Plans, and the Apex Predators

2,004 words • October 31, 2026 • Permanent URI



Plate XIII: *Figure: The Cambrian explosion (~508 Ma): the Burgess Shale marine ecosystem teeming with pioneering bilaterian body plans, hard biomineralized shells, compound-eyed trilobites, and the apex predator Anomalocaris canadensis.*

For over three billion years, life on Earth was a silent, microscopic realm of single cells and quiet microbial mats. Then, emerging from the frozen crucible of global Snowball Earth glaciations 541 million years ago, the biosphere detonated into an evolutionary frenzy known as the Cambrian Explosion. In a geological blink of barely twenty million years, every foundational animal body plan (phylum) in existence today was invented: compound eyes, sharp jaws, armored carapaces, segmented bodies, and a flexible dorsal cord that would one day carry the human spinal column.

The Cryogenian Crucible: The Great Snowball Thaw

Between 720 and 635 million years ago, the supercontinent Rodinia broke apart, exposing thousands of miles of fresh basaltic coastline to tropical weathering. Atmospheric carbon dioxide was aggressively sequestered into marine carbonates, plunging the planet into the two deepest, most apocalyptic ice ages in geological history: the **Sturtian (717–660 Ma)** and the **Marinoan (645–635 Ma) glaciations**.

Unlike ordinary ice ages, these were true **Snowball Earth** events (Hoffman & Schrag 2002): sea ice kilometers thick sealed the entire global ocean from the poles right across the equator. The planet was transformed into an unyielding, frozen white mirror.

The Glacial Nutrient Flush and Oxygen Spike
For tens of millions of years, continental glaciers acted as colossal industrial pulverizers, crushing thousands of meters of bedrock into ultra-fine "glacial flour." When volcanic CO_2 emissions finally accumulated to over 0.12 bars, greenhouse warming shattered the ice in a catastrophic super-thaw.

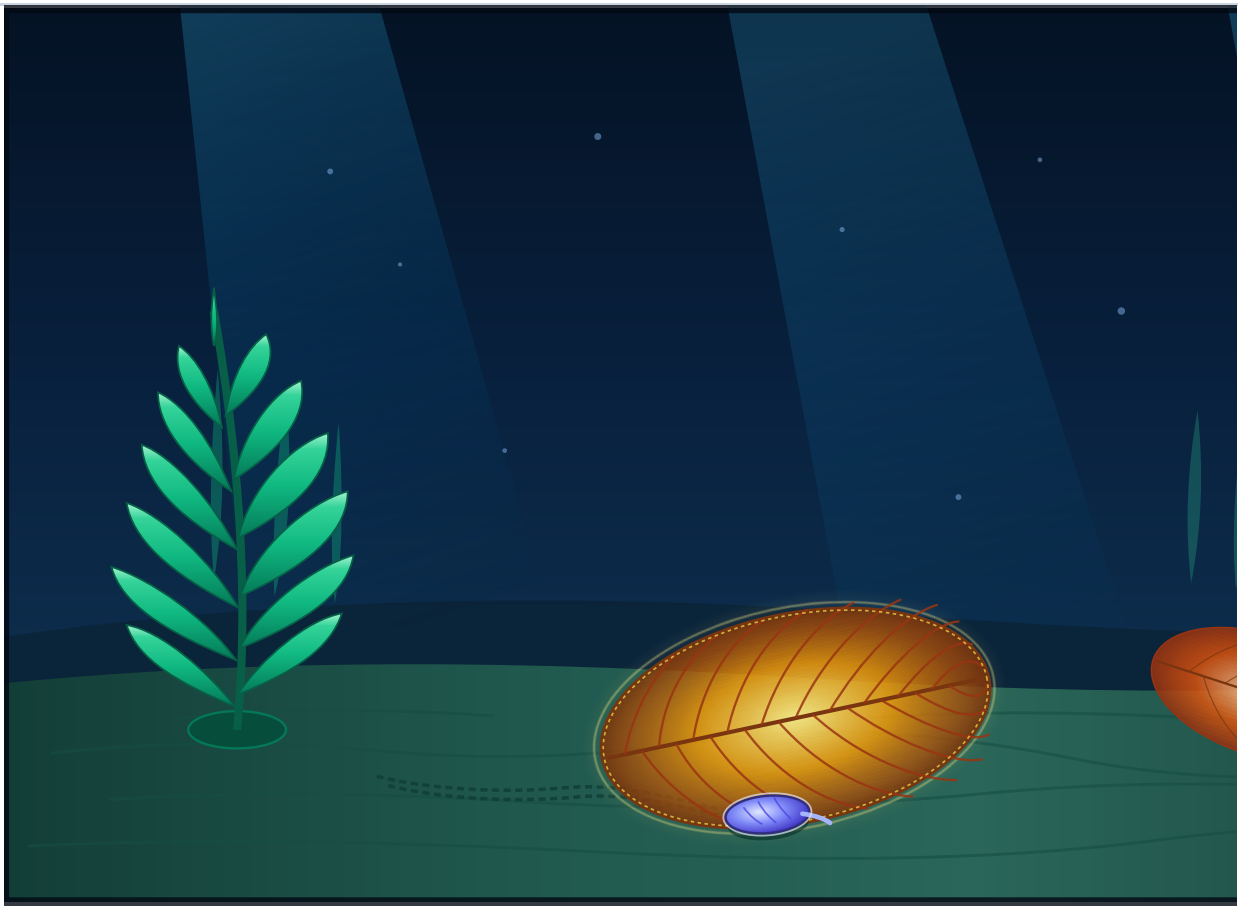
Torrents of meltwater flushed trillions of tons of weathered **phosphorus, calcium, and iron** into the warm oceans. This massive nutrient injection triggered catastrophic blooms of photosynthetic eukaryotic algae, burying gigatons of organic carbon and releasing an unprecedented surge of **free atmospheric oxygen (O_2) up to 10–20\% PAL**. For the first time in history, the oceans possessed the dissolved oxygen levels required to power the collagen synthesis, thick tissue diffusion, and muscular bioenergetics of large animals.

The Ediacaran Experiment (575 to 541 Ma): The Velvet Garden

The first macroscopic multicellular communities emerged immediately following the Marinoan thaw: the **Ediacaran Biota**, first discovered in the Ediacara Hills of South Australia and Newfoundland's Mistaken Point.

The Ediacaran world was a surreal, peaceful underwater landscape often dubbed the *"Garden of Ediacara"*. Bizarre, soft-bodied organisms rested peacefully atop microbial mats or anchored into the ocean floor with circular holdfasts:

Shakil Mahmud • Research Monograph



Seafloor Ecology: The Ediacaran Velvet Garden (~550 Ma). Before the invention of eyes and predators, the late Neoproterozoic seabed was blanketed by a dense, organic microbial matground. Resting peacefully atop this carpet, bizarre quilted organisms like the oval *Dickinsonia costata* and the fractal, frond-like *Charnia masoni* fed by passive diffusion, while slug-like *Kimberella* scraped primitive grazing tracks across the velvet mat.

- **Dickinsonia:** Flat, quilted, oval-shaped organisms reaching up to one meter across. In 2018, chemical biomarker analysis by Ilya Bobrovskiy detected fossilized **cholesteroids (cholesterol molecules)** inside *Dickinsonia* tissues, confirming once and for all that these mysterious quilted cushions were true **animals (Metazoa)**!
- **Charnia:** Frond-like organisms displaying self-similar, fractal branching architectures that absorbed dissolved organic matter directly from the seawater.
- **Kimberella:** A bilateral, slug-like grazing animal that used a primitive proboscis to scrape the microbial seafloor—an early relative of mollusks.

Crucially, the Ediacaran world had **no predators, no eyes, no teeth, and no hard mineralized skeletons**. It was an ecosystem of peaceful mat-feeders and passive filter-feeders living in symbiotic equilibrium. But around 541 million years ago, this peaceful velvet world was completely wiped away.

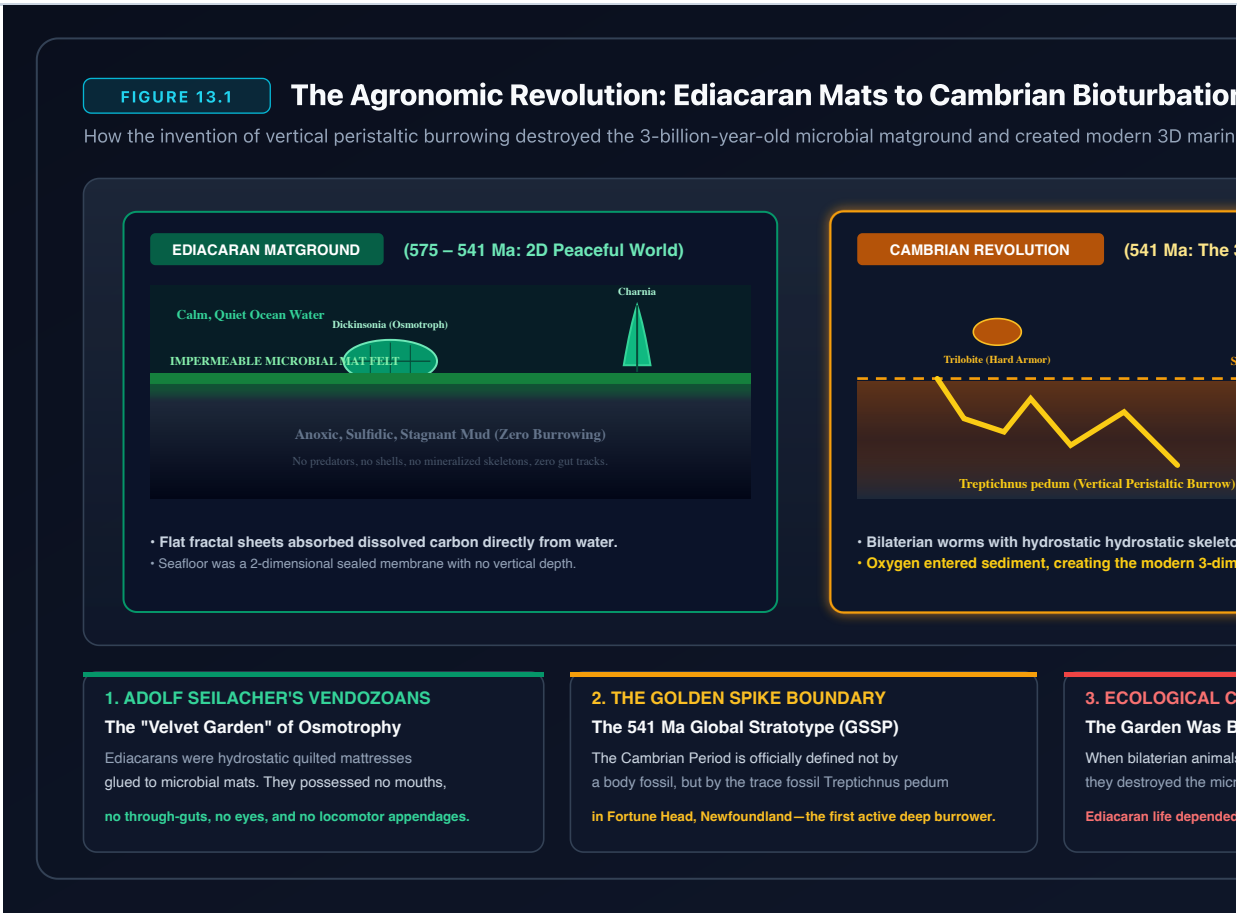


Figure 13.1: The Agronomic Revolution & The Fall of the Ediacaran Garden. Prior to 541 Ma, the seafloor was a quiet, two-dimensional microbial "matground." Organisms like Dickinsonia and Charnia rested peacefully upon this impermeable organic carpet, absorbing dissolved nutrients by passive osmotrophy above anoxic, sulfidic mud. At the base of the Cambrian, bilaterian animals evolved peristaltic vertical burrowing (Treptichnus pedum). This bioturbation shredded the ancient mats, pumped oxygenated seawater deep into marine sediments, and unlocked three-dimensional marine ecology.

The Cambrian Explosion: The Biological Big Bang

In 1859, Charles Darwin admitted in *On the Origin of Species* that the sudden appearance of complex, fully formed animals with hard shells at the base of the Cambrian strata was a grave challenge to his theory of gradual natural selection. Over the past century, discoveries in the **Burgess Shale (Canada)** and **Chengjiang (China)** have demystified the Cambrian Explosion:

1. Biomineralization: Skeletons and Armor

Around 541 million years ago, animals developed the genetic and enzymatic ability to precipitate dissolved calcium, carbonate, and phosphate ions into rigid crystals: **calcite ($CaCO_3$)** and **apatite ($Ca_5(PO_4)_3OH$)**. The first phase of this revolution was the *Small Shelly Fauna* (tiny cones, spicules, and plates), quickly followed by the jointed, calcified exoskeletons of **Trilobites**.

2. The Light Switch Hypothesis: The Evolution of Vision

In 2003, evolutionary biologist **Andrew Parker** proposed the *Light Switch Hypothesis*. Prior to the Cambrian, animals lacked image-forming optical eyes; they sensed their environment through slow chemical diffusion and tactile touch. Then, inside early arthropods, simple light-sensitive patches evolved into sophisticated **compound eyes with crystalline calcite lenses**.

The moment an animal could actively see its prey from meters away, the rules of evolution changed overnight. Passive grazing became a death sentence. Vision ignited the first **predator-prey evolutionary arms race**: prey had to evolve protective mineralized armor, camouflage, spikes, and burrowing behaviors; predators had to evolve faster swimming appendages, crushing claws, and binocular vision.

Shakil Mahmud • Research Monograph

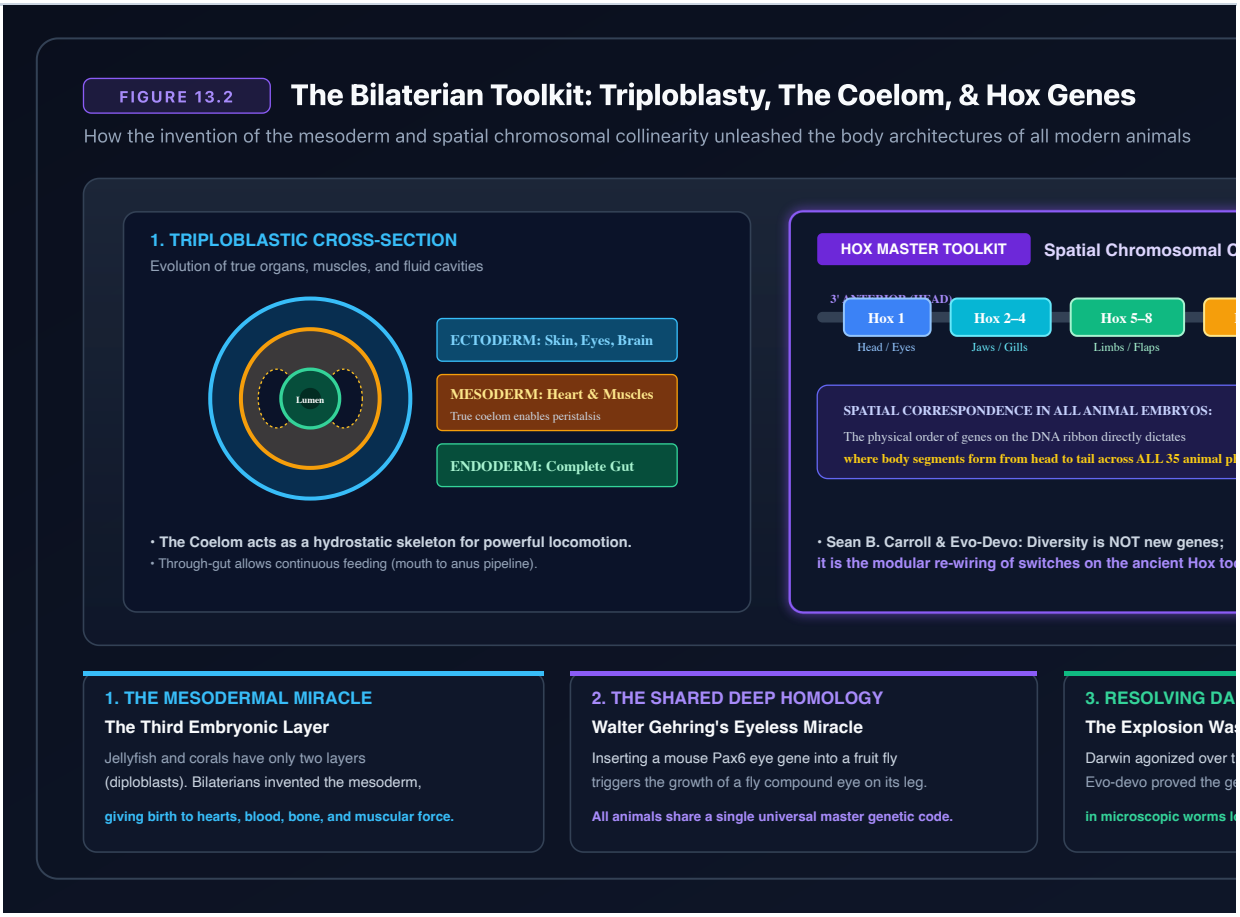
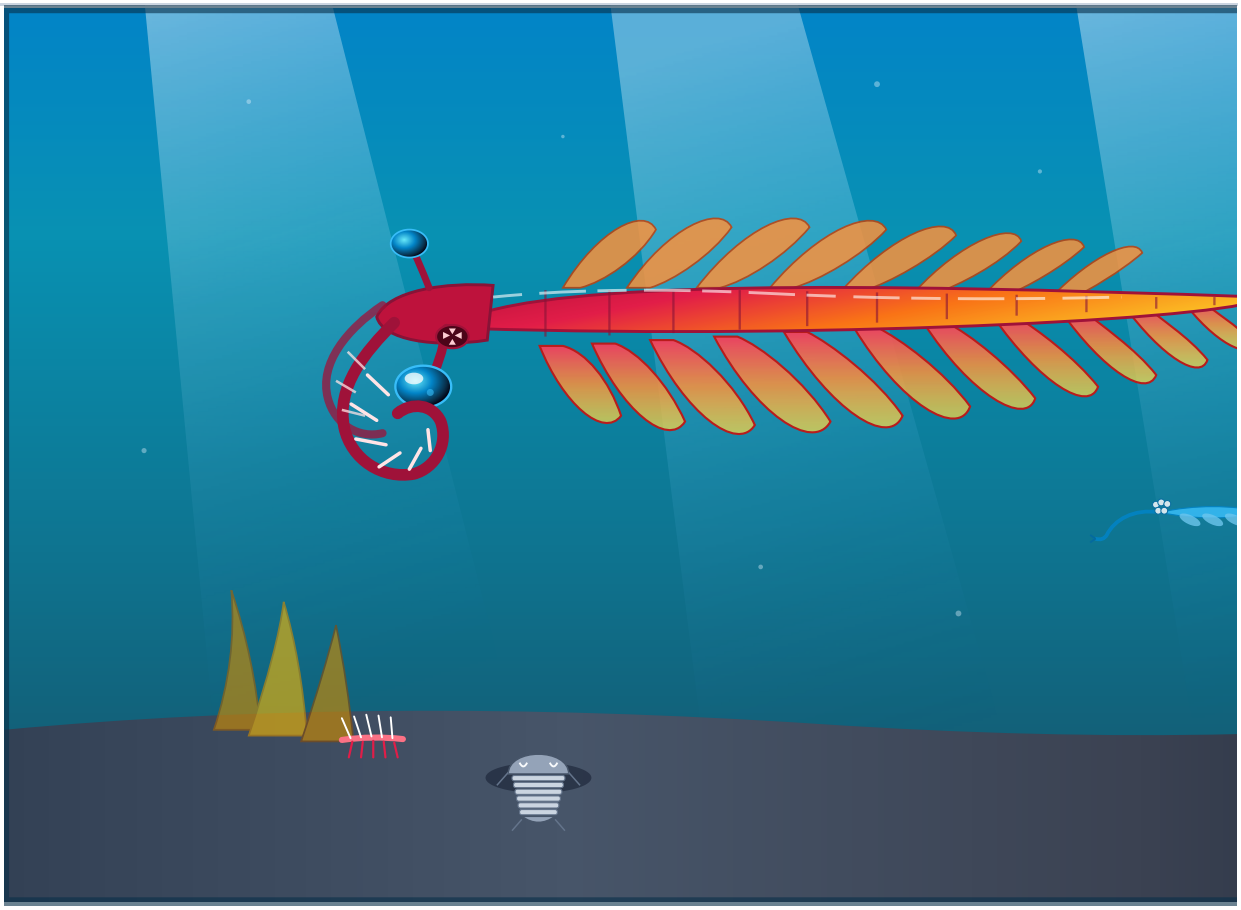


Figure 13.2: The Bilaterian Genetic & Anatomical Toolkit. Animal diversification exploded not because new genes suddenly appeared, but because bilaterians combined triploblastic tissue architecture (ectoderm, endoderm, and the muscle-forming mesoderm with a fluid coelom) with an ordered chromosomal cluster of Hox transcription factors. Because the 3′-to-5′ physical sequence of Hox genes along the chromosome corresponds directly to head-to-tail segment identity in the embryo, modular rewiring of developmental switches generated all 35 modern animal phyla from a shared genetic chassis.

Monsters of the Deep: The Cambrian Menagerie

The fossil deposits of the Canadian Rockies' Burgess Shale preserve a startling menagerie of alien-like anatomical experiments:



Apex Predator of the Cambrian Reef: *Anomalocaris canadensis* (~508 Ma). Patroling the sunlit waters above the Burgess Shale mudbanks, Earth's first true superpredator spanned up to a meter in length. Propelled by lateral swimming lobes, its 16,000-lens compound eyes scanned the seafloor for prey, which it grasped with spiny frontal appendages before crushing them in its triradiate, plate-lined mouth cone as armored trilobites and *Hallucigenia* scrambled below.

- **Anomalocaris canadensis ("The Abnormal Shrimp"):** The world's first true **apex predator**. Spanning up to one meter long, *Anomalocaris* swam with flexible lateral body flaps, stalked compound eyes boasting 16,000 hexagonal lenses, two spiny grasping appendages to snatch prey, and a circular, diaphragm-like mouth lined with jagged serrated plates.
- **Opabinia regalis:** A bizarre creature featuring five stalked eyes and a long, flexible frontal nozzle terminating in a grasping claw.
- **Hallucigenia sparsa:** A walking worm with seven pairs of rigid, pointed dorsal spines for defense and tentacle-like legs with tiny claws.
- **Wiwaxia corrugata:** A creeping slug covered in overlapping armor scales and prominent defensive daggers.

Shakil Mahmud • Research Monograph

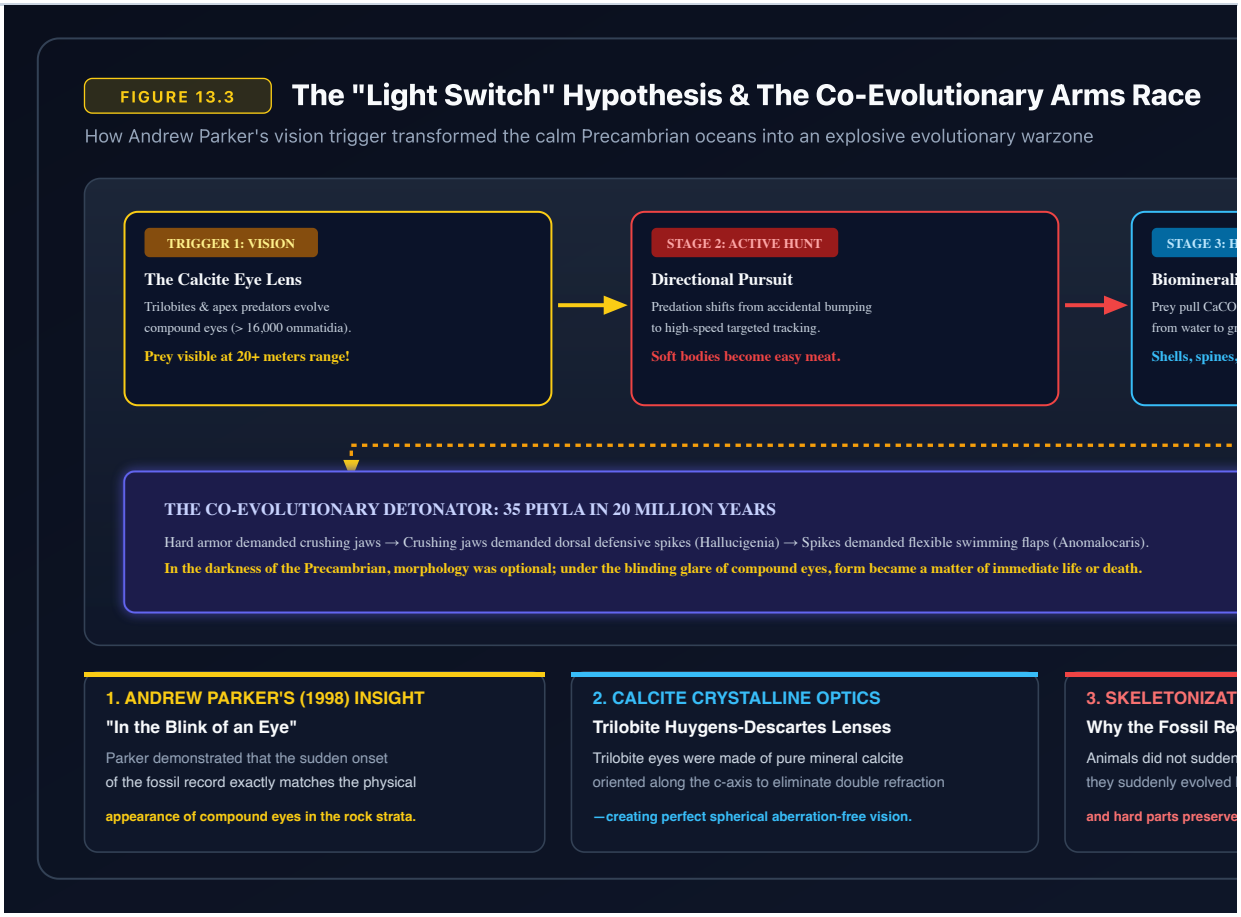


Figure 13.3: Andrew Parker's "Light Switch" Hypothesis & The Evolutionary Arms Race. In 1998, zoologist Andrew Parker proposed that the sudden burst of the Cambrian explosion was triggered by the invention of high-resolution vision. When trilobites and radiodonts evolved compound eyes with crystalline calcite lenses (>16,000 ommatidia), active predation shifted from blind chemical bumping to targeted visual pursuit across tens of meters. This ignited an escalating positive feedback loop: soft-bodied prey were forced to evolve biomineralized armor, shells, and defensive spikes, which in turn spurred larger grasping claws and crushing jaws.

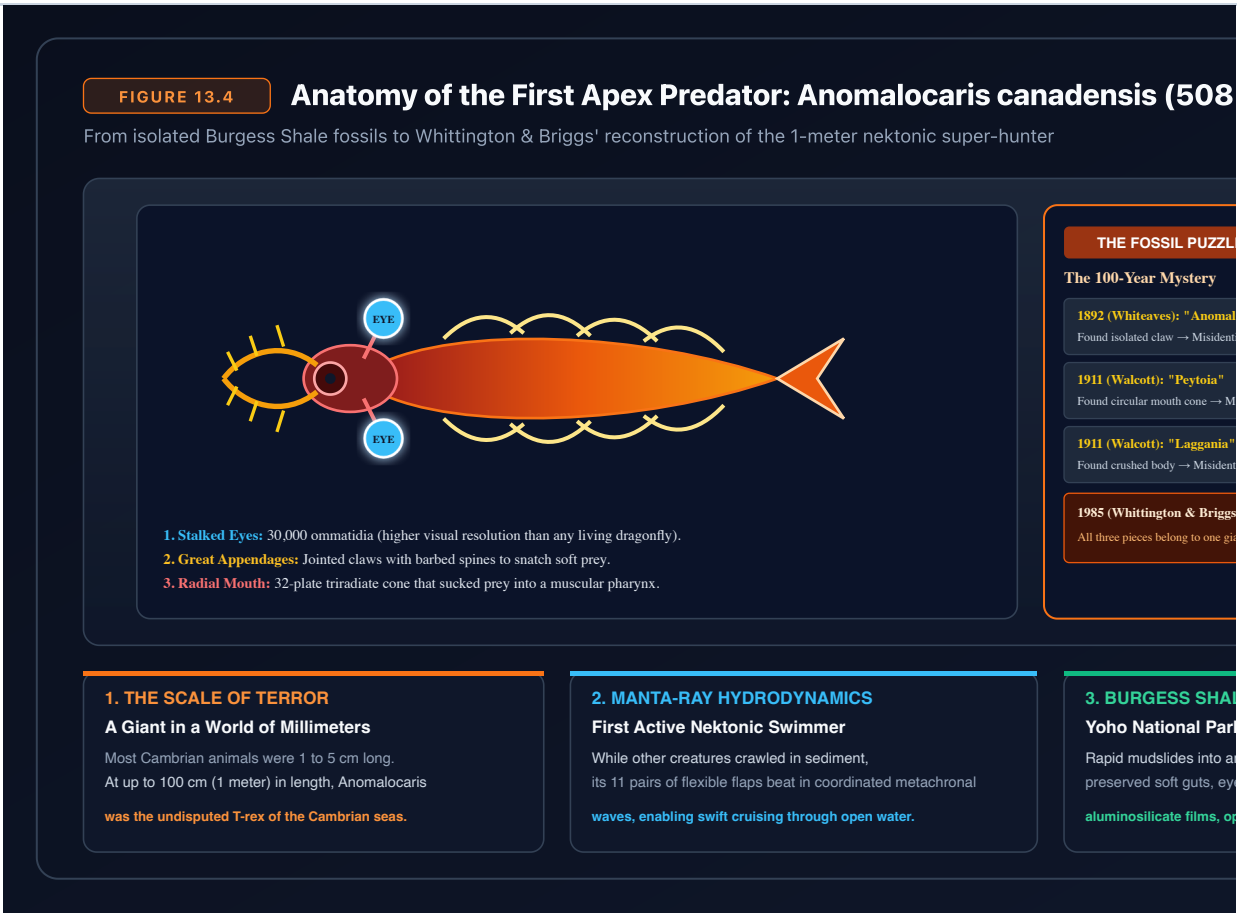
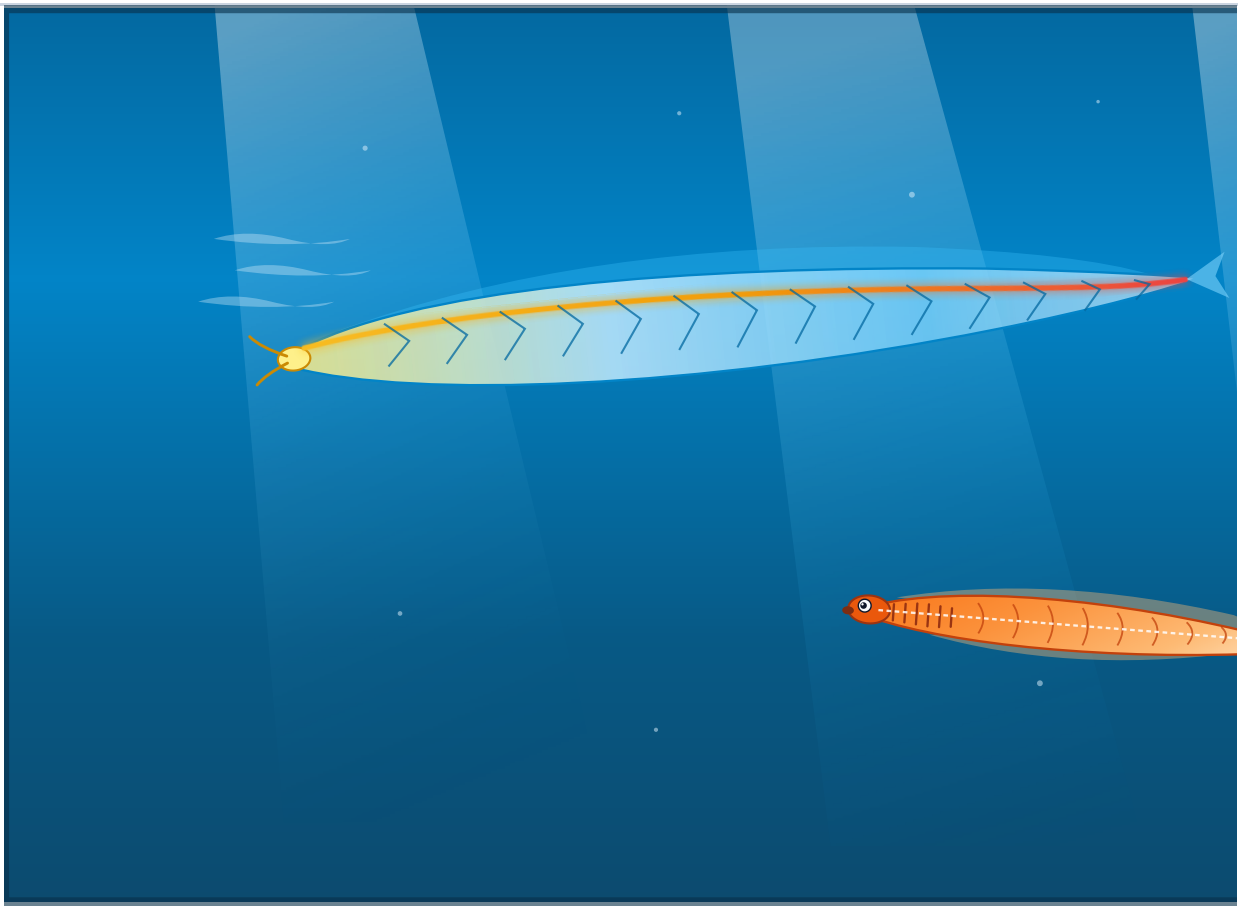


Figure 13.4: Anatomy of Earth's First Apex Superpredator: Anomalocaris canadensis. Reconstructed in 1985 by Harry Whittington and Derek Briggs from isolated Burgess Shale fossils previously mistaken for shrimp tails, jellyfish, and sea cucumbers, Anomalocaris was a 1-meter nektonic terror in a world of creatures rarely exceeding 3 cm. Equipped with 30,000-ommatidia stalked eyes, spined raptorial appendages for snatching prey, a 32-plate triradiate crushing mouth cone, and 11 pairs of undulating swimming flaps, it established the first modern marine trophic pyramid.

Pikaia and Haikouichthys: The Blueprint of the Human Spine

Amidst the spiny horrors and armored arthropods of the Cambrian seas swam a small, unassuming, ribbon-like animal barely five centimeters long: **Pikaia gracilens**, alongside the Chinese fossil **Haikouichthys ercaicunensis**.

Shakil Mahmud • Research Monograph



The Ancestral Vertebrate Blueprint: *Pikaia* and *Haikouichthys* (~518–505 Ma). Swimming gracefully amidst armored giants, the humble ribbon-like *Pikaia gracilens* pioneered the defining innovations of phylum Chordata: a flexible, hydrostatic dorsal notochord, dorsal hollow nerve cord, and undulating V-shaped muscle blocks (myomeres). Alongside early jawless fish like *Haikouichthys* with primitive cranial cartilage, these humble creatures established the unbroken anatomical blueprint of the human spine.

The Chordate Bauplan (Our Direct Ancestry)
Pikaia and *Haikouichthys* did not have shells or claws. Instead, they possessed a suite of radical structural innovations that define the phylum **Chordata**:

- **The Notochord:** A flexible, rod-like hydrostatic structure running along the back that served as an anchor for swimming muscles—the direct evolutionary precursor of the **vertebral column and spine**.
- **Dorsal Hollow Nerve Cord:** Positioned directly above the notochord—the evolutionary origin of the **central nervous system, spinal cord, and brain**.
- **V-Shaped Muscle Blocks (Myomeres):** Chevron-shaped muscle segments that allowed graceful, undulating S-swimming locomotion.
- **Pharyngeal Slits:** Branchial gill openings used originally for filter-feeding and respiration.

Every fish, amphibian, reptile, dinosaur, bird, mammal, and human being on planet Earth inherited their skeletal and nervous architecture directly from these humble Cambrian swimmers.

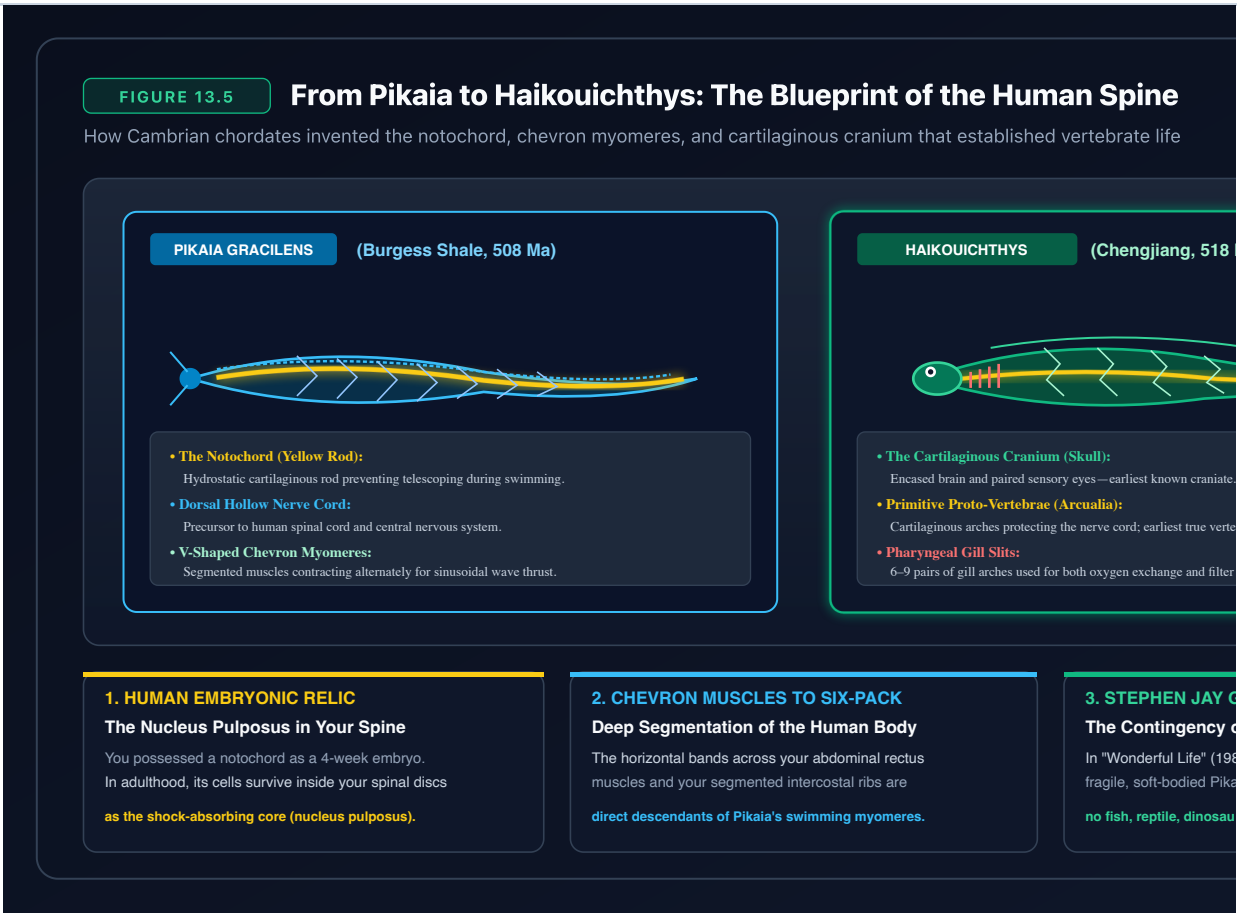


Figure 13.5: From Pikaia to Haikouichthys: The Blueprint of the Human Spine. While armored arthropods dominated the Cambrian reefs, humble soft-bodied chordates pioneered the vertebrate body plan. Pikaia gracilens (508 Ma) introduced the elastic dorsal notochord, dorsal nerve cord, and segmented V-shaped muscle myomeres. In China's Chengjiang fauna, Haikouichthys ercaicunensis (518 Ma) evolved the world's first cartilaginous skull (cranium), paired camera eyes, and primitive proto-vertebral arches—the unbroken 500-million-year anatomical ancestor of human beings.

The Cambrian Phyla Architecture: Foundations of Modern Biology

Phylum	Cambrian Exemplar	Key Morphological Innovations	Modern Descendants
Arthropoda	*Trilobita, Anomalocaris, Sanctacaris*	Chitinous exoskeleton, jointed appendages, compound eyes.	Insects, spiders, crabs, lobsters, scorpions (80\% of all animal species).
Chordata	*Pikaia, Haikouichthys, Metaspriggina*	Notochord, dorsal nerve cord, myomeres, bilateral cephalization.	Fish, amphibians, reptiles, birds, mammals, humans.
Mollusca	*Kimberella, Wiwaxia, Nectocaris*	Muscular foot, mantle, radula feeding organ, calcareous shell.	Octopuses, squids, snails, clams, oysters.
Echinodermata	*Gogia, Helicoplacus*	Fivefold (pentaradial) symmetry, water vascular system, calcite endoskeleton.	Starfish, sea urchins, sand dollars, sea cucumbers.
Annelida	*Canadia, Burgessochaeta*	Metameric true segmentation, coelom fluid body cavity, parapodia.	Earthworms, leeches, polychaete marine worms.
Cnidaria	*Thaumaptilon, Marrella* relatives	Radial symmetry, stinging nematocysts, diffuse nerve net.	Jellyfish, sea anemones, coral reefs.

The Verdict: The Ocean is Conquered

By the end of the Cambrian Period (roughly 485 million years ago), the biological paradigm of planet Earth was settled forever. The basic toolkit of animal life—bilateral symmetry, specialized sensory organs, digestive systems, circulatory blood flow, and central brains—had been mastered.

Yet, while the oceans teemed with jawless fish, giant nautiloids, and scurrying trilobites, the continents remained silent, barren, rocky wastelands devoid of soil, trees, or footsteps. To conquer the land, life had to solve the lethal challenges of gravitational weight, desiccation, and unbuffered solar radiation.

In **Part 14** of *The Universal Chronicle*, we will follow life as it crawls out of the waves: **The Conquest of Land — Primitive Forests, Arthropod Pioneers, and the Tetrapod Revolution**.

Shakil Mahmud • Research Monograph

Academic Citations & Foundational Literature

- **Hoffman, P. F., & Schrag, D. P. (2002).** "The snowball Earth hypothesis: testing the limits of global change." *Terra Nova*, 14(3), 129–155. doi:10.1046/j.1365-3121.2002.00408.x.
- **Bobrovskiy, I., et al. (2018).** "Ancient steroids establish the Ediacaran fossil Dickinsonia as one of the earliest animals." *Science*, 361(6408), 1246–1249. doi:10.1126/science.aat7228.
- **Gould, S. J. (1989).** *Wonderful Life: The Burgess Shale and the Nature of History*. W. W. Norton & Company. ISBN: 978-0393027051.
- **Parker, A. (2003).** *In the Blink of an Eye: How Vision Sparked the Big Bang of Evolution*. Basic Books. ISBN: 978-0738206073.
- **Shu, D. G., et al. (1999).** "Lower Cambrian vertebrates from south China." *Nature*, 402, 42–46. doi:10.1038/46965.
- **Erwin, D. H., et al. (2011).** "The Cambrian Conundrum: Early Divergence and Later Ecological Success in the Early History of Animals." *Science*, 334(6059), 1091–1097. doi:10.1126/science.1206375.

Citation: Mahmud, S. (2026). "The Cambrian Crucible — Snowball Earth Thaw, Multicellular Body Plans, and the Apex Predators." In The Universal Chronicle, Part 13. https://shakilmahmud.com/universal-chronicle-part-13-the-cambrian-crucible/

SHAKIL MAHMUD RESEARCH MONOGRAPHS · PART XIV

The Conquest of Land — Primitive Forests, Arthropod Pioneers, and the Tetrapod Revolution

The Conquest of Land — Primitive Forests, Arthropod Pioneers, and the Tetrapod Revolution

2,541 words • October 31, 2026 • Permanent URI



Plate XIV: *Figure: Late Devonian land colonization (~375–360 Ma): transitional sarcopterygian tetrapodomorphs (Tiktaalik and Ichthyostega) haul onto muddy riverbanks beneath the towering shade of early Archaeopteris progymnosperm forests.*

For more than three billion years, the continents of Earth were as barren and hostile as the regolith of Mars. While the oceans swarmed with trilobites, cephalopods, and jawed placoderms, terrestrial rock lay scorched under unattenuated solar radiation, washed by sterile acidic rain, and completely devoid of organic matter. The emergence of life onto terra firma was not a celebratory walk onto welcoming soil; it was a grueling biological campaign requiring the synthesis of structural polymers, the invention of water-impermeable coatings, the re-engineering of respiratory apparatuses for gaseous oxygen, and the radical reorganization of fins into load-bearing limbs.

1. The Barren Continent and the Cryptogamic Pioneers (~470 to 420 Ma)

During the early Paleozoic, the terrestrial landscape was an alien expanse of craggy granite, basaltic rubble, and pulverized mineral silicates. Prior to the Silurian period, any organism attempting to venture out of the photic water column faced immediate dehydration, mechanical collapse under unsupported gravitational acceleration, and fatal genomic degradation from ultraviolet (UVB) flux.

The protective shield was forged by marine cyanobacteria and eukaryotic algae whose photosynthetic oxygenation had steadily enriched the stratosphere. In the presence of ultraviolet radiation ($\lambda < 240$ nm), diatomic oxygen undergoes photolysis into reactive atomic radicals, which combine with ambient O_2 to generate ozone:

$$O_2 + h\nu \rightarrow 2O$$

$$O + O_2 + M \rightarrow O_3 + M$$

By the Middle Ordovician (~470 Ma), the stratospheric ozone layer had reached sufficient thickness to attenuate lethal UVB flux, opening an ecological frontier along coastal estuarine margins. The first colonizers were cryptogamic ground covers—non-vascular bryophyte-like organisms resembling modern liverworts and mosses. Lacking roots, leaves, or vascular circulation, these primitive plants secreted organic acids that catalyzed the biogeochemical weathering of silicate rocks. By extracting phosphorus, potassium, and magnesium, they initiated the genesis of Earth's first true soils (pedogenesis) and locked up atmospheric carbon dioxide, plunging the planet into transient glacial cooling.

The Invention of Sporopollenin

The greatest biochemical triumph of early land plants was the synthesis of **sporopollenin**—an extraordinary biopolymer composed of cross-linked fatty acids, phenylpropanoids, and phenolic carotenoids. Unyielding to bacterial enzymatic decomposition, chemically inert, and virtually indestructible, sporopollenin encased plant spores in an impervious protective capsule, preserving the reproductive genetic code as it drifted through desiccating terrestrial winds.

Shakil Mahmud • Research Monograph



Paleo-Botany: Pioneer Flora on the Silurian Shoreline (~430 Ma). Leafless, dichotomously branching stems of *Cooksonia*—barely a few centimeters tall—rise along a braided freshwater pool on barren red siltstone. Tipped with trumpet-shaped sporangia and protected by indestructible sporopollenin, these diminutive pioneers colonized rocky continental surfaces alongside primitive microbial crusts, initiating the greening of land.

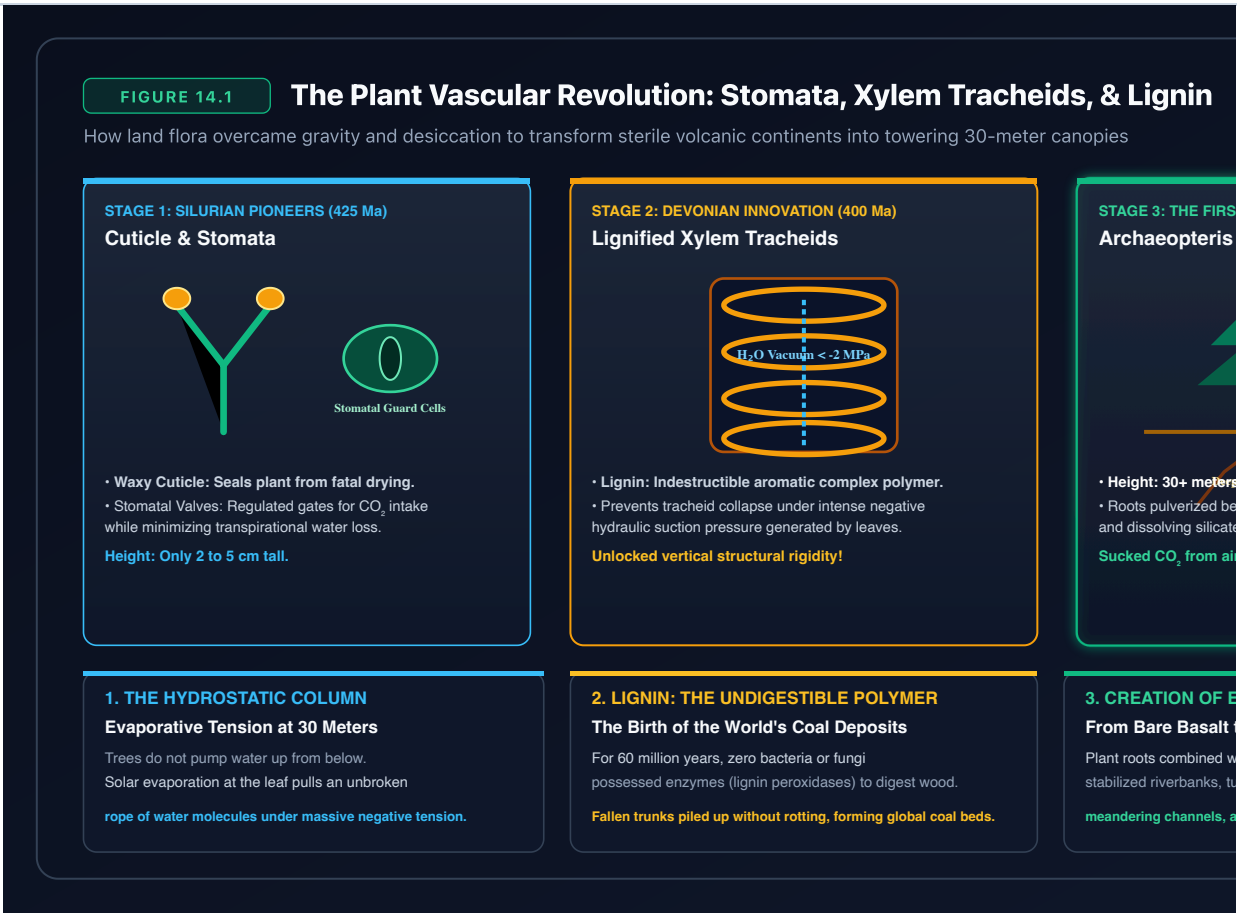


Figure 14.1: The Plant Vascular Revolution: Stomata, Xylem Tracheids, & Lignin. Conquering dry land required solving two existential physical crises: fatal desiccation and gravitational collapse. Silurian pioneers like Cooksonia (425 Ma) evolved waxy cuticles and stomatal valves to regulate gas exchange while locking in water. In the Devonian, flora synthesized lignin—an aromatic biopolymer that reinforced cellulose cell walls, allowing dead xylem tracheids to endure massive negative hydraulic tensions (< -2 MPa) and lifting water 30 meters into the sky to create Earth's first true forests (Archaeopteris).

2. The Vascular Revolution and the Great Devonian Forests (~420 to 359 Ma)

While bryophytes remained tethered to wet rock faces, never exceeding a few millimeters in height due to reliance on capillary diffusion, the Late Silurian witness the emergence of *polysporangiophytes* like *Cooksonia*, culminating in true vascular plants (**tracheophytes**). This evolutionary breakthrough hinged on two architectural inventions:

1. **Xylem and Phloem:** Specialized vascular conduits lined with dead, hollowed tracheid cells that transported water and dissolved mineral ions upward from root systems via transpirational pull, countered by phloem tubes carrying photosynthesized sugars downward.
2. **Lignin:** A complex, cross-linked racemic macromolecule composed of aromatic phenylpropane units. By embedding lignin into cellulose cell walls, vascular plants imparted rigid mechanical compressive strength, allowing plant stems to defy gravity and reach toward the sky in an escalatory race for direct sunlight.

By the Late Devonian (~380 Ma), the world had transformed from a green crust into towering forests dominated by *Archaeopteris*—the first modern tree with extensive woody root systems and bifacial cambium. These deep, penetrative roots fractured the bedrock down to several meters, dramatically increasing chemical weathering rates by a factor of seven. The resulting influx of calcium and magnesium cations reacted with dissolved marine bicarbonate to precipitate vast carbonate shelves, drawing down thousands of gigatons of atmospheric CO2:

Shakil Mahmud • Research Monograph



Paleo-Ecology: The Great Devonian Forests of Archaeopteris (~370 Ma). Towering 30-meter progymnosperm trees transformed terrestrial geology. In this cutaway riverbank view, massive woody root networks penetrate meters into continental bedrock, fracturing stone, creating Earth's first true organic soils (pedogenesis), and accelerating silicate weathering that drew down atmospheric CO2 into global cooling.

$$CaSiO_3 + 2CO_2 + H_2O \rightarrow Ca^{2+} + 2HCO_3^- + SiO_2$$

$$Ca^{2+} + 2HCO_3^- \rightarrow CaCO_3 \downarrow + CO_2 + H_2O$$

3. The Carboniferous Swamp Hyperoxia and the Arthropod Giants (~359 to 299 Ma)

During the Carboniferous period, equatorial continents collided to form equatorial supercontinents smothered in vast, waterlogged wetlands. Trees like *Lepidodendron* (scale trees) and *Sigillaria* grew to heights of forty meters over acidic, oxygen-starved peat bogs. Crucially, the fungi and bacteria of the Carboniferous had not yet evolved the specialized class of enzymes—specifically *lignin peroxidase* and *manganese peroxidase*—capable of breaking down the aromatic rings of lignin.

When these towering trees fell into anoxic swamps, they did not decay. Layer upon layer of unoxidized cellulose and lignin accumulated under sediment blankets, subjected to heat and geostatic pressure over millions of years to form the massive bituminous coal deposits that would fuel the Industrial Revolution 300 million years later. Because the carbon was buried rather than oxidized back into CO2, atmospheric oxygen soared from its modern baseline of 21% to an astonishing peak of **35%**.

Spiracular Diffusion and Arthropod Gigantism

Arthropods breathe via passive tracheal tubes open to the atmosphere through lateral spiracles; their maximum body size is fundamentally bounded by the mean free path and diffusion rate of oxygen molecules through microscopic air tubules. Under a hyperoxic 35% O2 atmosphere, oxygen penetrated far deeper into muscle tissue, unleashing an era of terrifying invertebrates: *Meganeura monyi*, a predatory griffinfly with a wingspan exceeding 75 centimeters; *Arthropleura*, a monstrous armored myriapod stretching 2.6 meters in length; and scorpions like *Pulmonoscorpius* reaching a meter from claw to stinger.



Paleo-Zoology: Hyperoxic Gigantism in the Carboniferous Coal Swamps (~310 Ma). Under an atmospheric oxygen surge of 35%, spiracular passive diffusion sustained colossal arthropods: the predatory griffinfly *Meganeura* (75 cm wingspan) resting on a giant fern frond, while the armored herbivore *Arthropleura* (2.6 meters long) crawls across waterlogged peat beneath towering scale trees (*Lepidodendron*).

Shakil Mahmud • Research Monograph

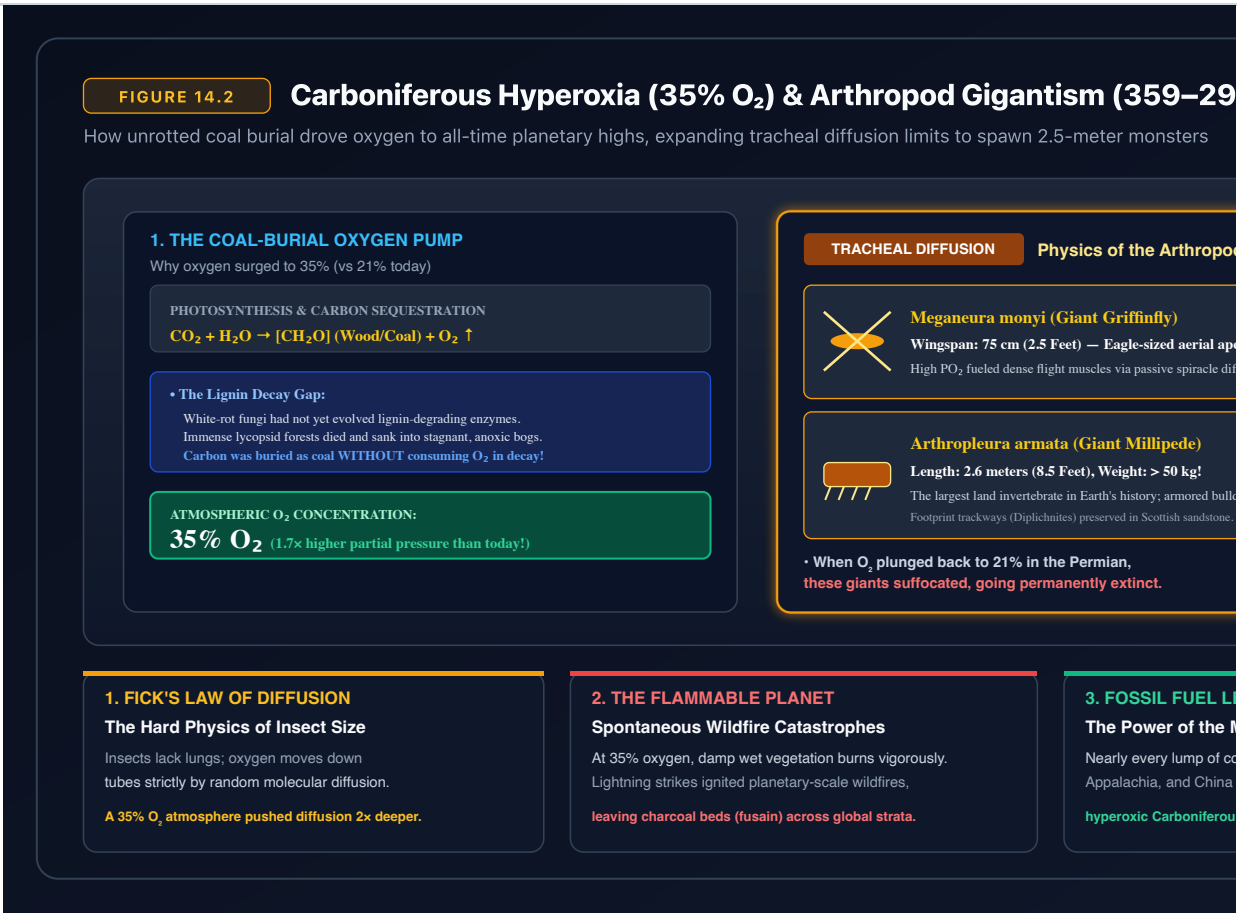


Figure 14.2: Carboniferous Swamp Hyperoxia & The Giant Arthropods (359–299 Ma). Because fungi had not yet evolved enzymes capable of breaking down lignin, vast swamp forests died and were entombed as unrotted peat without consuming oxygen in decay. This massive carbon burial pumped atmospheric O2 to an all-time peak of 35% (vs. 21% today). Because arthropods breathe via passive tracheal diffusion, high partial pressure drove oxygen twice as deep into muscle tissues, fueling 75 cm eagle-sized dragonflies (Meganeura) and 2.6-meter millipedes (Arthropleura)—the largest land invertebrates in planetary history.

4. The Sarcopterygian Transition: Fins Become Limbs (~385 to 365 Ma)

While arthropods exploited their chitinous exoskeletons to conquer the land early, the vertebrate assault on land demanded a radical rethinking of internal endoskeletal anatomy. The journey began in stagnant, weed-choked freshwater shallows where predatory **sarcopterygian** (lobe-finned) fish lurked.

Organism	Geological Age	Anatomical Milestones	Habitat / Ecology
Eusthenopteron	385 Ma (Devonian)	Internal choanae (nostrils), ancestral humerus, radius, and ulna homologous to tetrapod limb bones.	Open water pelagic predator; strictly aquatic with rayed fins.
Panderichthys	380 Ma (Devonian)	Dorsoventrally flattened body, loss of dorsal and anal fins, eyes positioned atop skull.	Shallow swamp bottom-dweller; propping body up in muddy shallows.
Tiktaalik roseae	375 Ma (Devonian)	True mobile neck (loss of opercular bones), wrist joints capable of weight-bearing flexion, spiracular notches indicating ancestral lungs.	Intertidal / mudflat ambush predator; able to crawl over land barriers between evaporating pools.
Acanthostega	365 Ma (Devonian)	True polydactylous digits (8 fingers per limb), fully articulated ankle and wrist, retention of internal gills.	Shallow freshwater marshes; fully aquatic limb usage precedes terrestrial locomotion.
Ichthyostega	360 Ma (Devonian)	Robust overlapping ribs protecting thoracic cavity, rigid spine, strong pectoral girdle, 7 digits.	Semi-terrestrial pioneer; capable of seal-like crutching across land.

The discovery of *Tiktaalik roseae* in the Canadian Arctic by Edward Daeschler, Neil Shubin, and Farish Jenkins in 2004 provided the undeniable morphological bridge between fish and tetrapods. Unlike fish, whose skulls are locked immovably to the pectoral girdle by bony opercular plates, *Tiktaalik* lost these anchoring bones, gaining a flexible neck that could turn independently to track prey on land. Inside its fin, distal radial bones had evolved into functional wrist joints capable of flexion and extension, allowing it to execute primitive push-ups against the muddy substrates of oxygen-deprived estuaries.



Vertebrate Transition: Tiktaalik roseae Crawls onto Land (~375 Ma). Discovered in the Canadian Arctic, *Tiktaalik* bridges fish and four-limbed tetrapods. Its muscular pectoral fins feature internal wrist joints capable of bearing weight, paired with a flattened crocodilian skull and a flexible neck that allowed it to lift its head above anoxic swamp waters to breathe atmospheric air.

Shakil Mahmud • Research Monograph

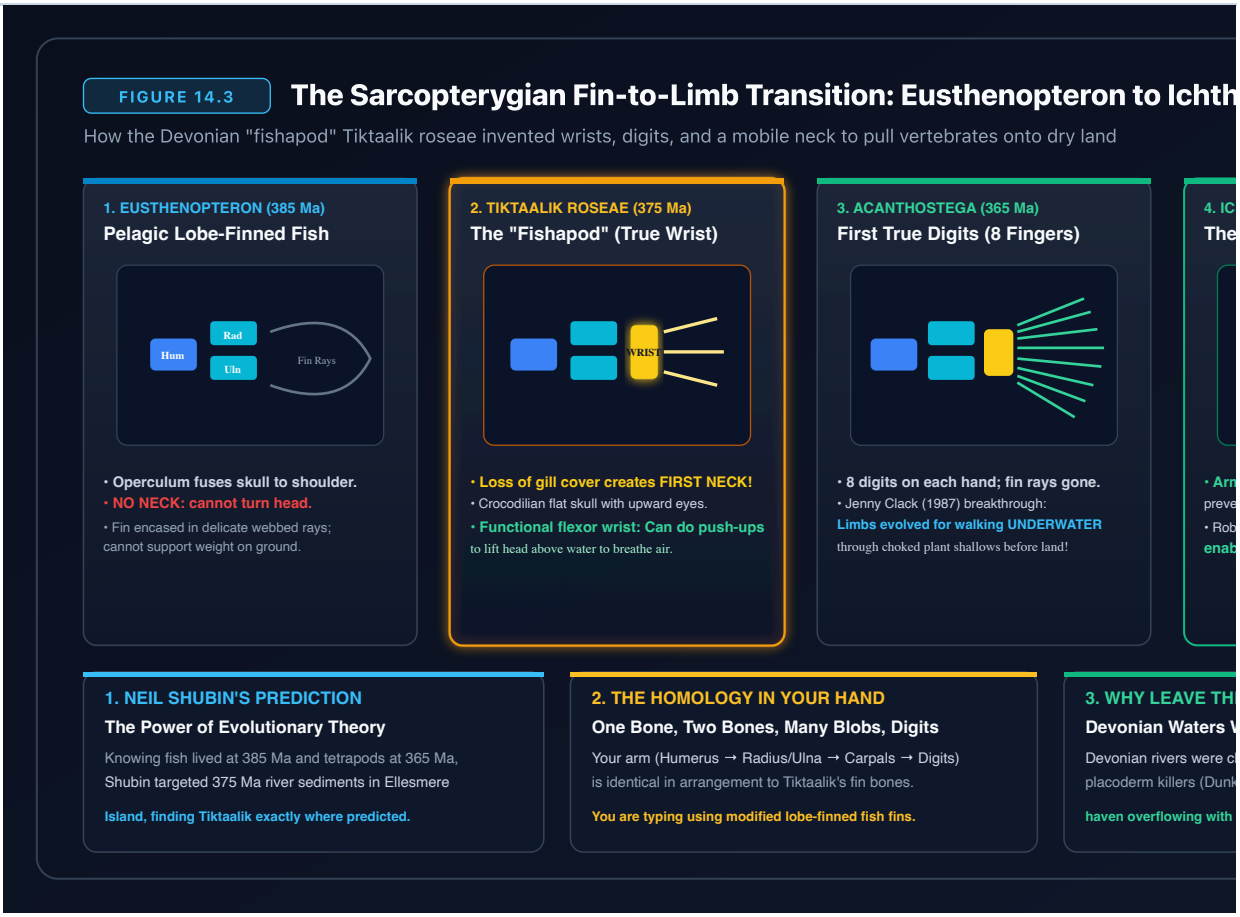


Figure 14.3: The Sarcopterygian Fin-to-Limb Transition: Eusthenopteron to Ichthyostega. In 2004, paleontologist Neil Shubin discovered Tiktaalik roseae (375 Ma) in Canada's Arctic. Bridging the gap between fish and tetrapods, Tiktaalik lost the opercular gill cover bones to invent the world's first mobile neck, while evolving internal carpal wrist bones capable of doing "push-ups" in swamp shallows. This established the invariant vertebrate limb architecture—one bone (humerus), two bones (radius/ulna), little blobs (carpals), and digits—preserved today in the human arm.

5. Severing the Umbilical Cord: The Amniotic Egg (~312 Ma)

Despite walking on land, early amphibians remained prisoner to the water column. Their gelatinous, shell-less anamniotic eggs would wither and perish in dry air within minutes; their skin required continuous moisture for cutaneous respiration; and their free-swimming larval tadpoles demanded an aquatic sanctuary to undergo metamorphosis.

The definitive conquest of continental interiors arrived in the Late Carboniferous with the evolution of the **amniote** ancestor (exemplified by small, lizard-like creatures such as *Hylonomus lyelli*). The amniote innovation was an intricate miniature life-support system wrapped in a semi-permeable, calcium-rich shell that allowed gas exchange while preventing water evaporation:

- **The Amnion:** An inner fluid-filled sac that bathes the growing embryo in a synthetic private pond, protecting it from mechanical shock and desiccation.
- **The Chorion:** An outer vascular membrane that regulates oxygen intake and carbon dioxide expulsion across the porous shell.
- **The Allantois:** A dedicated internal bladder that stores nitrogenous waste (uric acid, requiring minimal water to precipitate) and participates in gas exchange.
- **The Yolk Sac:** A nutrient-dense storehouse of lipids and proteins that nourishes the embryo until hatching as a fully formed miniature adult, completely bypassing the vulnerable aquatic larval phase.

Equipped with the amniotic egg and dry, keratinized scales that arrested cutaneous desiccation, amniotes rapidly diverged into two fundamental evolutionary branches that would vie for planetary dominance for the next 300 million years: the **Synapsida** (distinguished by a single temporal fenestra behind each eye socket, giving rise to pelycosaurs, therapsids, and ultimately mammals) and the **Sauropsida** (with two temporal fenestras—the diapsids—giving rise to lizards, crocodilians, pterosaurs, dinosaurs, and birds).



Evolutionary Breakthrough: Hylonomus and the Amniotic Egg (~312 Ma). The earliest known amniote, the lizard-like *Hylonomus lyelli*, rests beside a hollowed club moss trunk on a dry inland forest floor. A clutch of leathery amniotic eggs—with internal amnion, yolk sac, and allantoic membranes—provided a self-contained private pond, liberating terrestrial vertebrates forever from reproducing in open water.

Shakil Mahmud • Research Monograph

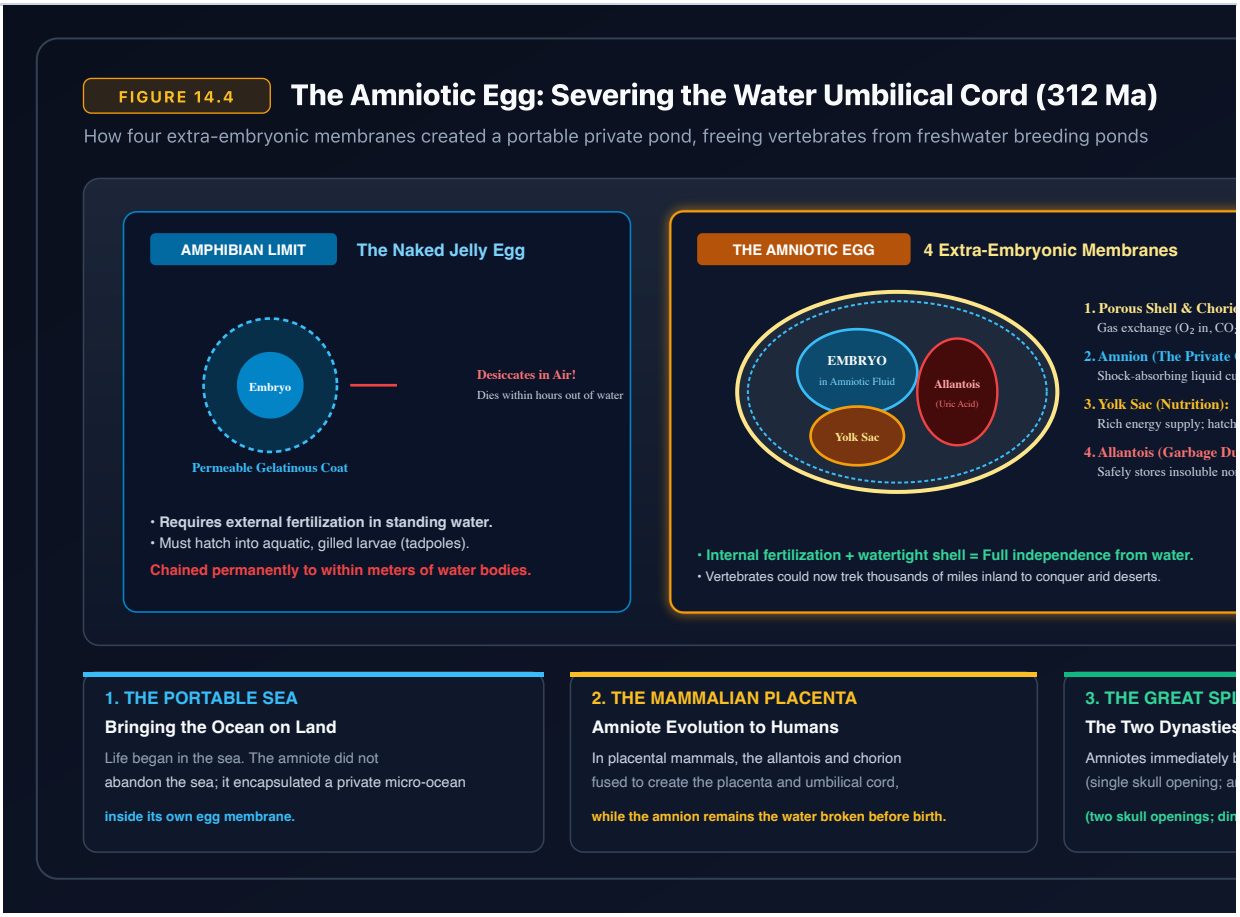


Figure 14.4: The Amniotic Egg: Severing the Water Umbilical Cord (312 Ma). While amphibians were tethered to standing ponds to keep naked eggs from desiccating, the amniote revolution encapsulated a private ocean inside a porous, watertight shell. Four specialized membranes—the amnion (saline shock absorber), yolk sac (nutrient reserve), allantois (uric acid waste repository), and chorion (gas exchange)—allowed vertebrates to complete their entire life cycle on dry land, liberating them to colonize continental deserts.

6. The Great Dying: The Permian-Triassic Cataclysm (252 Ma)

By the Late Permian, synapsid "mammal-like reptiles"—such as the saber-toothed gorgonopsians and the massive herbivorous pareiasaurs—ruled a united supercontinent called **Pangaea**. But this thriving terrestrial empire was brought to near-total annihilation by the most devastating biological bottleneck in planetary history: the Permian-Triassic extinction event.

At 251.9 million years ago, immense mantle plumes welled up beneath what is now northern Russia, triggering the eruption of the **Siberian Traps**. Over the course of a million years, more than four million cubic kilometers of basaltic lava erupted across an area the size of Europe. As the magma punched through vast subsurface coal, carbonate, and petroleum basins, it pyrolyzed trillions of tons of carbon dioxide, sulfur dioxide, and methane into the atmosphere.

The global consequences were catastrophic:

1. **Super-Greenhouse Warming:** Atmospheric temperatures skyrocketed by 10°C across the equator; tropical sea-surface temperatures soared past 40°C, exceeding thermal tolerance thresholds for animal enzymes.
2. **Ocean Acidification and Anoxia:** As warming oceans lost dissolved oxygen, benthic microbial communities collapsed. Sulfate-reducing bacteria bloomed uncontrollably, saturating both deep seas and coastal shallows with toxic hydrogen sulfide (H_2S).
3. **Ozone Layer Collapse:** Halogen gases liberated by pyrolyzed coals dismantled the stratospheric ozone layer, bombarding surviving plants and animals with blistering UV radiation that produced widespread pollen deformities and crop collapse.

When the ash settled, **96% of all marine species** and **70% of terrestrial vertebrate families** had perished. The great synapsid megafauna was shattered, leaving only small, burrowing survivors. Yet in the scorched, empty plains of the Early Triassic, the few surviving archosaurs (stem-crocodilians and proto-dinosaurs) stood before an evolutionary clean slate. The conquest of land was complete—and the stage was set for the golden age of the dinosaurs.

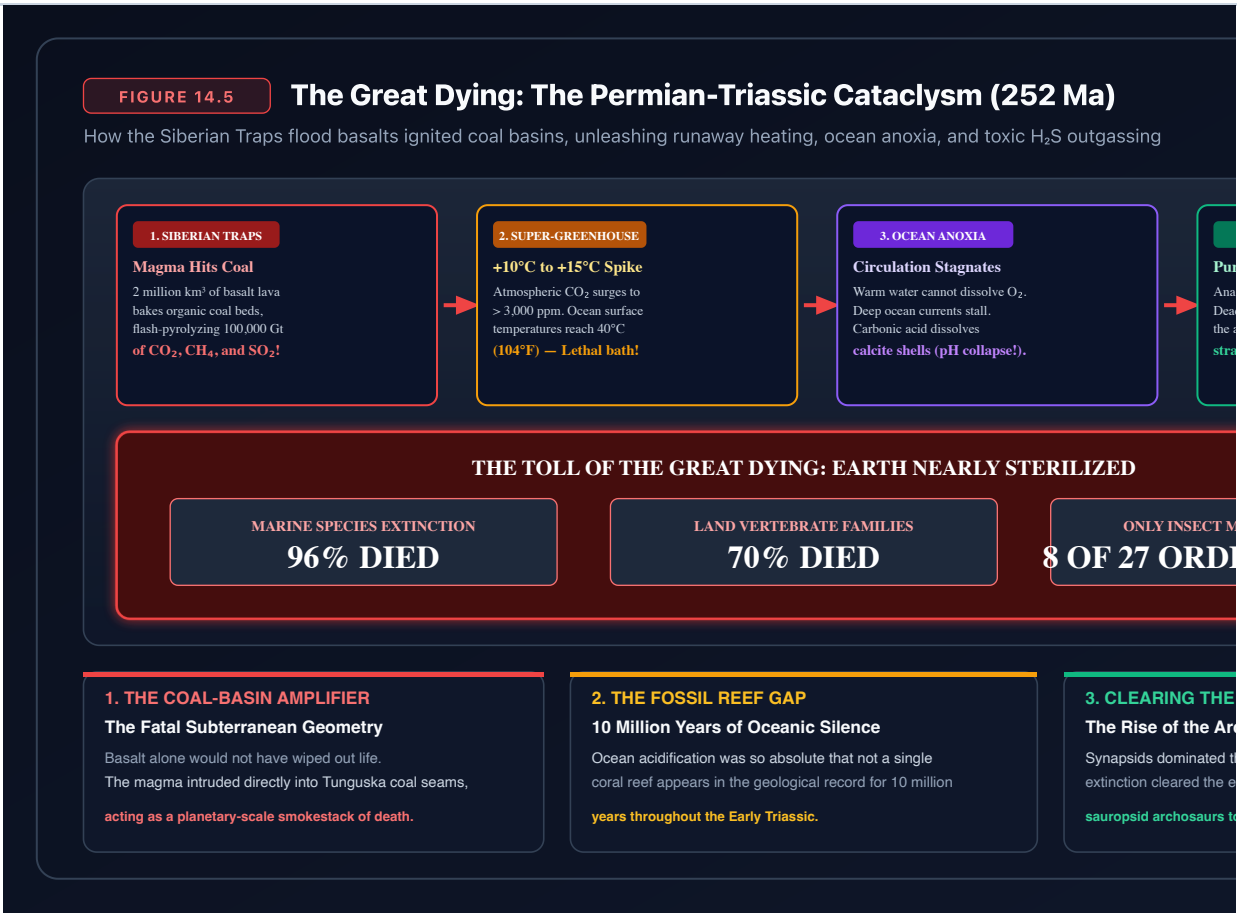


Figure 14.5: The Great Dying: The Permian-Triassic Cataclysm (252 Ma). The most catastrophic extinction event in planetary history began when 2 million cubic kilometers of basaltic magma erupted through Siberian coal basins. The flash pyrolysis of hydrocarbons pumped over 100,000 gigatons of greenhouse gases into the atmosphere, spiking global temperatures by 10–15°C. Equatorial oceans reached a boiling 40°C, currents stagnated into an anoxic soup, and purple sulfur bacteria released toxic hydrogen sulfide (H2S) that stripped the ozone layer, annihilating 96% of marine species and 70% of land families.

Academic Citations & Historical References

1. Kenrick, P., & Crane, P. R. (1997). *The origin and early diversification of land plants: a cladistic study*. Smithsonian Institution Press. doi:10.5860/choice.35-4493
2. Daeschler, E. B., Shubin, N. H., & Jenkins, F. A. (2006). A Devonian tetrapod-like fish and the evolution of the tetrapod body plan. *Nature*, 440(7085), 757–763. doi:10.1038/nature04639
3. Shubin, N. H., Daeschler, E. B., & Jenkins, F. A. (2006). The pectoral fin of Tiktaalik roseae and the origin of the tetrapod limb. *Nature*, 440(7085), 764–771. doi:10.1038/nature04637
4. Berner, R. A. (2006). GEOCARBSULF: A combined model for Phanerozoic atmospheric O2 and CO2. *Geochimica et Cosmochimica Acta*, 70(23), 5653–5664. doi:10.1016/j.gca.2005.11.032
5. Benton, M. J. (2003). *When Life Nearly Died: The Greatest Mass Extinction of All Time*. Thames & Hudson. ISBN:978-0500051160.
6. Burgess, S. D., Bowring, S., & Shen, S. Z. (2014). High-precision timeline for Earth\'s most severe extinction. *Proceedings of the National Academy of Sciences*, 111(9), 3316–3321. doi:10.1073/pnas.1317692111
7. Carroll, R. L. (1988). *Vertebrate Paleontology and Evolution*. W. H. Freeman and Company. ISBN:978-0716718222.

Citation: Mahmud, S. (2026). "The Conquest of Land — Primitive Forests, Arthropod Pioneers, and the Tetrapod Revolution." In The Universal Chronicle, Part 14. https://shakilmahmud.com/universal-chronicle-part-14-the-conquest-of-land/

Shakil Mahmud • Research Monograph

SHAKIL MAHMUD RESEARCH MONOGRAPHS • PART XV

The Dinosaur Empire & The Impact — The Mesozoic World and the Mammalian Dawn

The Dinosaur Empire & The Impact — The Mesozoic World and the Mammalian Dawn

2,454 words • October 31, 2026 • Permanent URI

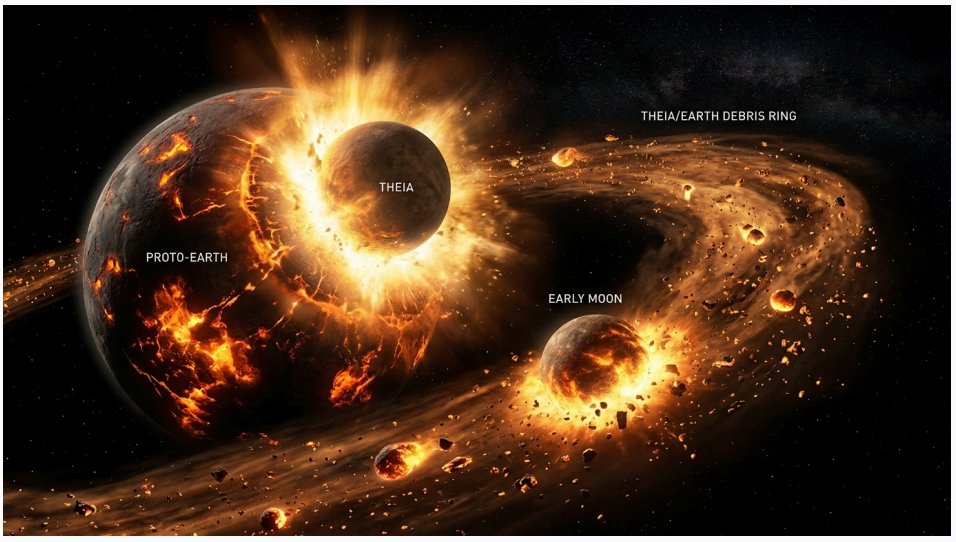


Plate XV: *Figure: The twilight of the Mesozoic Era (~66 Ma): giant non-avian dinosaurs move beneath Cretaceous skies just as the 10-kilometer Chicxulub asteroid streaks through the upper atmosphere to trigger the Fifth Mass Extinction.*

For one hundred and sixty million years—an incomprehensible epoch dwarfing the entirety of human existence by more than five hundred fold—the surface of planet Earth was governed by a spectacular dynasty of terrestrial giants: the Dinosauria. Rising from the ash-choked desolation of the Permian-Triassic extinction, archosaurian lineages reorganized vertebrate biomechanics, perfected respiratory efficiency through pulmonary air sacs, developed endothermic metabolisms, and ultimately took flight on feathered wings. Yet quietly in the shadowed understory of this reptilian paradise, tiny, nocturnal synapsid survivors were re-engineering the vertebrate ear, expanding the neocortex, and nursing their young—waiting for the extraterrestrial thunderbolt that would remake the biosphere in a single terrifying day.

1. The Rise of the Archosaurs and the Carnian Pluvial Event (~252 to 201 Ma)

Following the Permian cataclysm, the supercontinent of Pangaea was an arid, monsoonal furnace. Two reptilian clades competed for continental hegemony:

- **Pseudosuchia:** The crocodile-line archosaurs, featuring sprawling or semi-erect stances, heavy dermal armor, and predatory power (exemplified by giant rauisuchians like *Postosuchus*).
- **Avemetatarsalia (Ornithodira):** The bird-line archosaurs, featuring erect, pillar-erect parasagittal limb postures, lightweight skulls, and digitigrade foot mechanics.

The decisive ecological tipping point occurred approximately 234 to 232 million years ago during the **Carnian Pluvial Event (CPE)**. Massive basaltic volcanism in the Wrangellia oceanic plateau triggered an abrupt surge in greenhouse gases, transforming the global interior from a parched desert into two million years of torrential monsoon rains and humid heat.



The Carnian Pluvial Event (~234–232 Ma): Two Million Years of Rain. Triggered by colossal flood basalt eruptions in Wrangellia, a surge in atmospheric carbon dioxide turned arid Pangaea into a two-million-year continuous monsoonal downpour. In the waterlogged river basins, heavy sprawling pseudosuchians struggled in the mud, while agile, cursorial bipedal dinosaurs like *Herrerasaurus* and *Coelophysis* flourished, establishing the archosaurian foundation for the Mesozoic Dinosaur Empire.

Pseudosuchian heavyweights struggled in the rapidly shifting floral landscape, while early bipedal dinosaurs—such as *Herrerasaurus* and *Coelophysis*—possessed athletic, agile body plans with high cursorial speeds and superior energetic efficiency. When the Triassic ended with another volcanic pulse from the Central Atlantic Magmatic Province (CAMP) at 201 Ma, the pseudosuchian apex predators were decimated. Dinosaurs walked through the extinction virtually unscathed, inheriting an empty planet.

Shakil Mahmud • Research Monograph

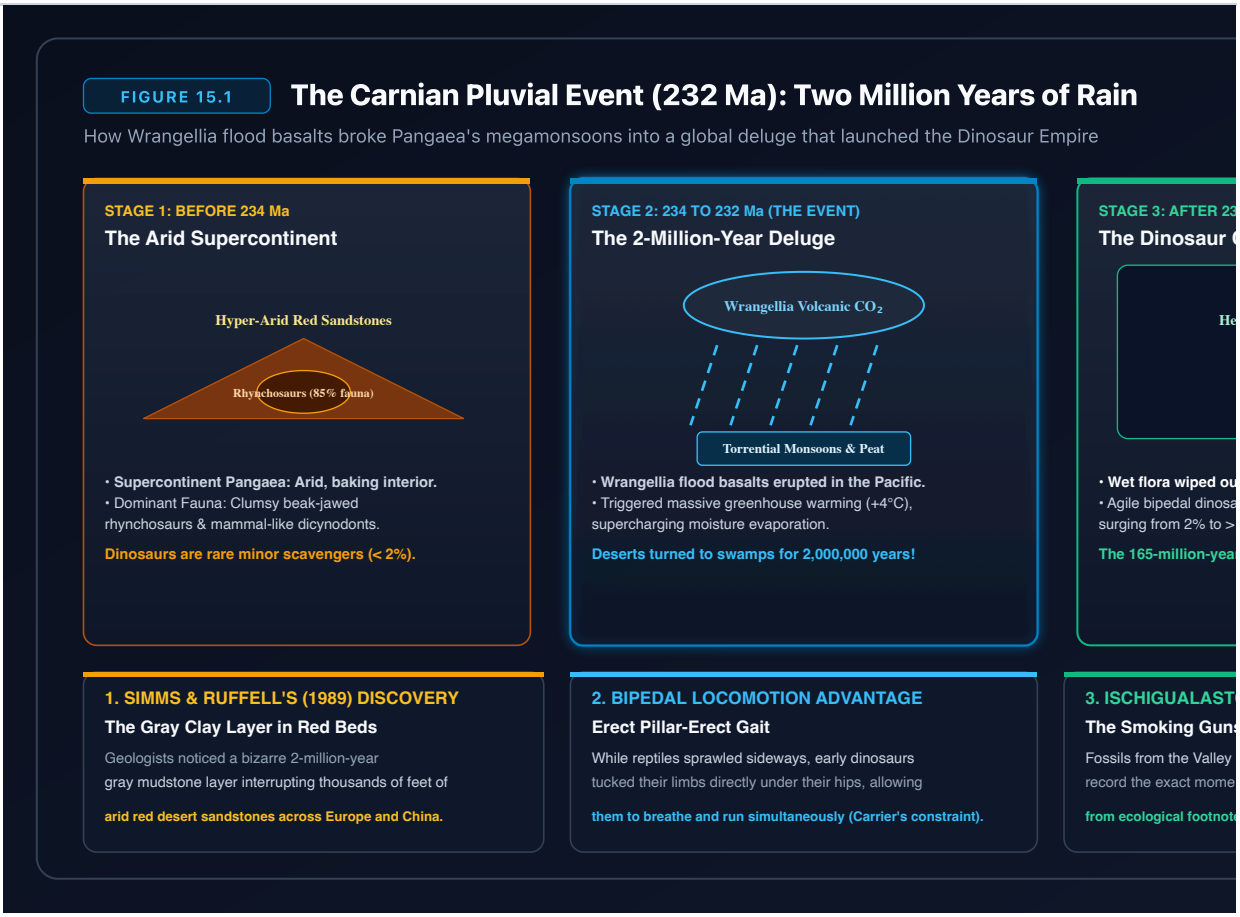
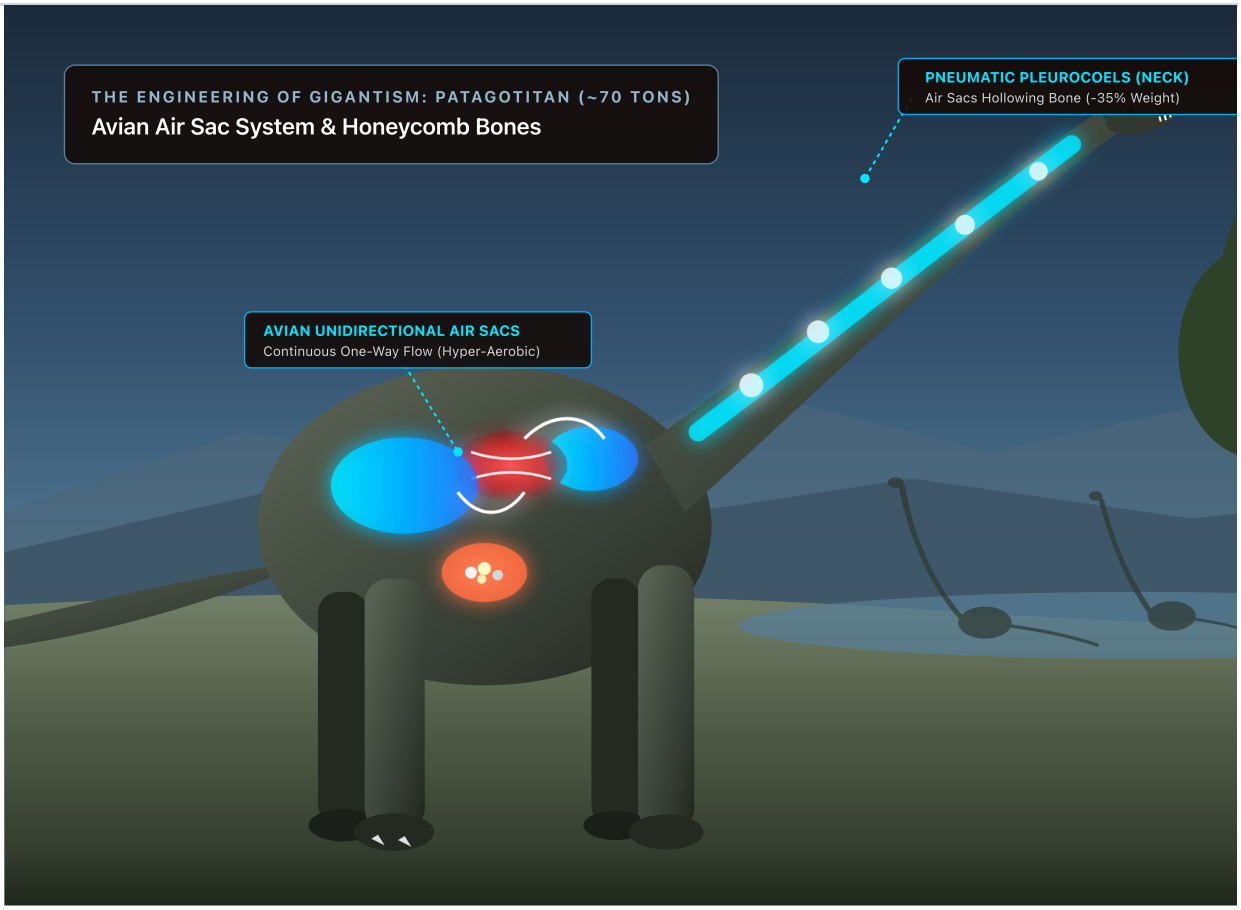


Figure 15.1: The Carnian Pluvial Event (232 Ma): Two Million Years of Rain. For the first 20 million years of the Triassic, dinosaurs were rare ecological footnotes (< 2% of land fauna) living in the shadows of beak-jawed rhynchosaurs on a hyper-arid Pangaean supercontinent. Around 234 Ma, massive flood basalt eruptions in Wrangellia injected thousands of gigatons of CO_2 into the atmosphere, triggering a 2-million-year continuous torrential pluvial episode. This profound climate shift wiped out archaic herbivores and spurred the explosive radiation of agile, bipedal dinosaurs across the planet.

2. The Engineering of Gigantism: Biomechanics, Air Sacs, and Bone Histology

During the Jurassic and Cretaceous periods, sauropod dinosaurs achieved body masses exceeding 70 metric tons (e.g., *Argentinosaurus*, *Patagotitan*, and *Brachiosaurus*)—dimensions that have never been approached by any other terrestrial vertebrate in Earth history. Such colossal scale is biologically impossible under standard mammalian anatomy. Dinosaurs conquered the physical limits of mass through a synergistic cascade of evolutionary adaptations:



Biomechanics of Titanic Gigantism: The Titanosaur Air Sac Engine (~70 Tons). Scaling to body masses exceeding 70 metric tons, titanosaurs like *Patagotitan mayorum* shattered the terrestrial limits of vertebrate mass. A bird-like respiratory system drove unidirectional airflow through rigid parabronchial lungs during both inspiration and expiration, while extensive pneumatic diverticula hollowed out the cervical vertebrae into lightweight honeycomb trusses—shedding up to 35% of skeletal weight while supporting 12-meter-long necks.

Anatomical Innovation	Biophysical Mechanism	Ecological Advantage
Unidirectional Air Sac System	Continuous one-way air flow through non-vascular pulmonary air sacs into the lungs during both inspiration and expiration; no dead-end alveolar tidal mixing.	Maintained hyper-efficient oxygen uptake even during periods of low Mesozoic atmospheric oxygen; enabled rapid convective internal cooling.
Postcranial Skeletal Pneumaticity	Diverticula from air sacs invaded and hollowed out cervical and dorsal vertebrae (vertebral internal honeycombing).	Reduced skeletal density by up to 35% without compromising structural compressive strength, enabling 12-meter-long necks.
Lack of Mastication (Gastric Mills)	Swallowed vegetative matter whole without chewing; food was mechanically ground internally in muscular gizzards using swallowed gastroliths.	Permitted an extremely small, lightweight skull at the end of a vast cantilevered neck; eliminated energetic limits of chewing.
Oviparity & High Fecundity	Reproduction via large clutches of eggs rather than prolonged internal placental gestation.	Minimal reproductive downtime for giant females; populations could rebound rapidly from regional climatic stress.
Fibrolamellar Bone & Tachymetabolism	Rapidly deposited, highly vascularized fibrolamellar bone tissue matching that of modern birds and placental mammals.	Sub-adult sauropods exhibited explosive growth rates, gaining thousands of kilograms per year to quickly outgrow apex predators.

In theropod predators—culminating in the 9-ton apex hunter *Tyrannosaurus rex*—evolution optimized bone-crushing biomechanics. *T. rex* developed fused nasal bones, deep kinetic skull joints, and incrassate, banana-shaped teeth anchored by deep periodontal roots, generating bite forces exceeding **35,000 Newtons**—sufficient to shatter adult triceratops pelvises and extract calcium-rich marrow.

Shakil Mahmud • Research Monograph

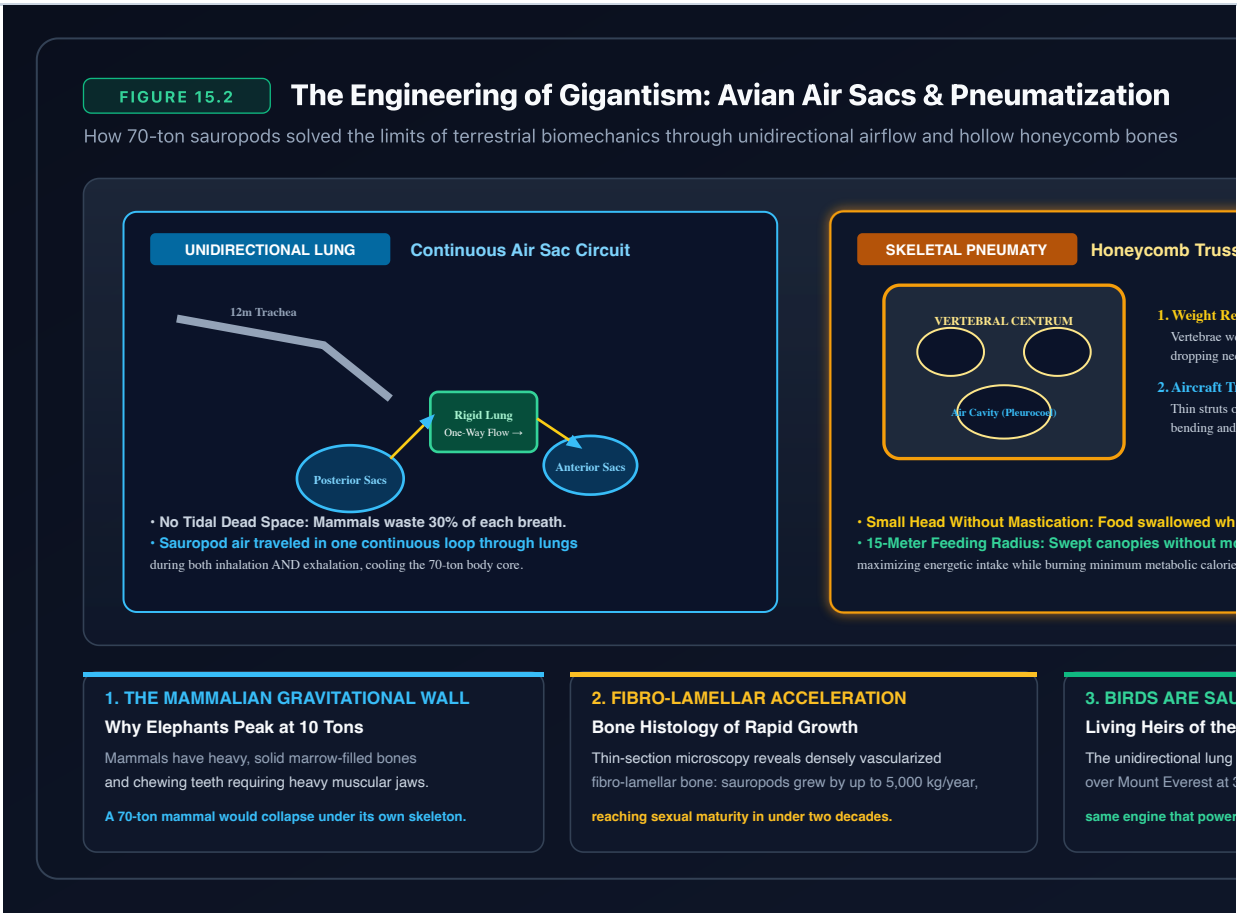


Figure 15.2: The Engineering of Gigantism: Avian Air Sacs & Honeycomb Bones. While mammals are bounded by a ~10-ton terrestrial ceiling due to heavy marrow bones and tidal lung dead space, 70-ton sauropods (like Argentinosaurus) achieved titanic gigantism through bird-like respiratory systems. Air flowed continuously in one direction through rigid parabronchial lungs during both inhalation and exhalation, powered by anterior and posterior air sacs. These air sacs invaded vertebral centra (pleurocoels), creating light, stiff aeronautical honeycomb trusses that shed over 500 kg from long sweeping necks.

3. The Secret Nocturnal Mammalian Underworld (~220 to 66 Ma)

While dinosaurs dominated the diurnal landscape, early mammals were forced into a 160-million-year crucible of nocturnal obscurity. Far from an evolutionary dead-end, this intense ecological pressure drove the genesis of the most sophisticated neurological, sensory, and metabolic systems in the animal kingdom.

The Evolution of the Mammalian Middle Ear

In ancestral reptiles, the lower jaw consists of multiple bones (dentary, articular, angular, surangular), with the jaw hinge formed by the articulation between the *articular* and the skull's *quadrate*. Mammals performed an astonishing evolutionary heist: as the dentary expanded to form the entire load-bearing lower jaw (articulating directly with the squamosal bone), the redundant postdentary bones detached from the jaw apparatus, migrated into the cranial cavity, and were miniaturized into the three delicate ossicles of the modern middle ear: the **malleus** (hammer, from the articular), the **incus** (anvil, from the quadrate), and the **stapes** (stirrup). This mechanical lever system impedance-matched airborne acoustic waves to the fluid of the cochlea, unlocking high-frequency acoustic resolution critical for nocturnal insect hunting.

To survive in cold darkness, early crown-group mammals (such as *Morganucodon* and the early Cretaceous eutherian *Eomaia scansoria*) developed:

1. **Endothermy and Pelage:** Sustained elevated basal metabolic rates powered by dense, insulating coats of fur (keratin filaments), allowing vigorous nocturnal hunting when predatory reptiles were sluggish.
2. **The Neocortex:** Massive cranial expansion dedicated to processing olfactory, auditory, and tactile information (whisker vibrissae), laying the anatomical foundation for advanced learning and behavioral plasticity.
3. **Diphyodont Heterodonty:** Two successive sets of teeth (milk vs. adult) with interlocking, precise occlusal cusps (tribosphenic molars) capable of shearing insect chitin and grinding seeds with supreme caloric efficiency.
4. **Maternal Lactation:** The transformation of ancestral apocrine sebaceous skin glands into specialized mammary glands secreting nutrient-dense milk, unburdening hatchlings and newborns from immediate foraging hazards.

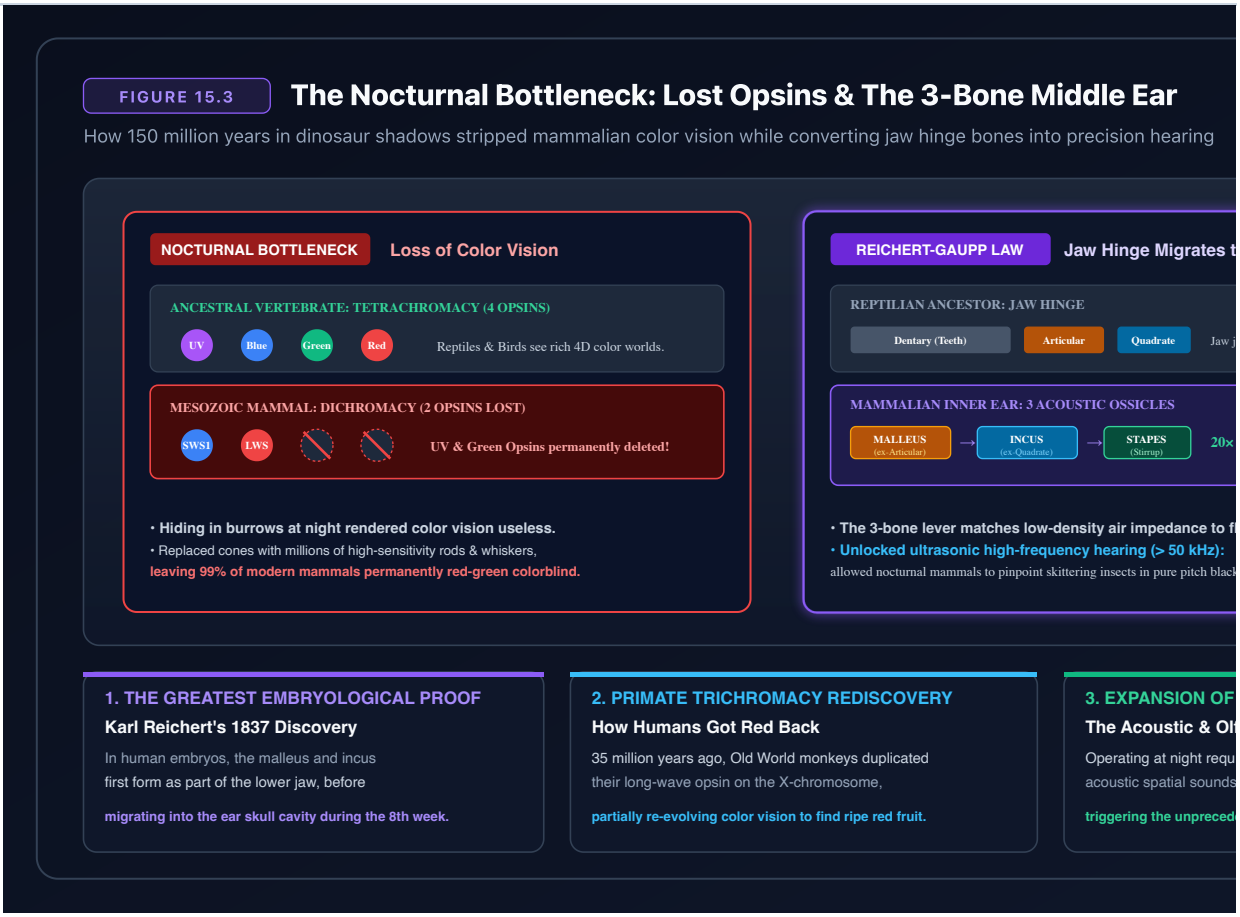


Figure 15.3: The Nocturnal Bottleneck & The 3-Bone Middle Ear. Under 150 million years of daytime dinosaur dominance, our mammalian ancestors were forced into subterranean nocturnal niches. Living in pitch darkness, mammals lost 2 of the 4 ancestral vertebrate color opsin genes (leaving 99% of modern mammals dichromatic/colorblind). In compensation, the reptilian jaw hinge bones (Articular and Quadrate) detached and migrated into the skull to become the Malleus (hammer) and Incus (anvil), pairing with the Stapes to form a 3-bone acoustic amplifier unlocking high-frequency ultrasound hearing.

4. The Angiosperm Revolution and Insect Co-Evolution (~130 to 80 Ma)

Until the Early Cretaceous, Earth's flora was dominated by gymnosperms: conifers, cycads, ginkgoes, and seed ferns that relied on inefficient, wind-driven pollination. Around 130 million years ago, the first true flowering plants (**angiosperms**) burst onto the evolutionary scene.

Angiosperms revolutionized terrestrial ecosystems by inventing enclosed seeds protected within carpels (which mature into fruits) and vibrant floral structures that deployed chemical, color, and nectar rewards. Rather than releasing millions of pollen grains to the random whim of the breeze, angiosperms entered into a tight, reciprocal co-evolutionary pact with insects: hymenopterans (bees and wasps), lepidopterans (butterflies and moths), and dipterans (flies).

This botanical blitzkrieg rapidly pushed gymnosperms into polar and mountainous margins. By providing calorie-dense nectar, fruits, seeds, and fast-growing foliage, the angiosperm revolution triggered a secondary explosive diversification across insects, small mammals, squamate reptiles, and herbivorous dinosaurs like hadrosaurs and ceratopsians.

Shakil Mahmud • Research Monograph

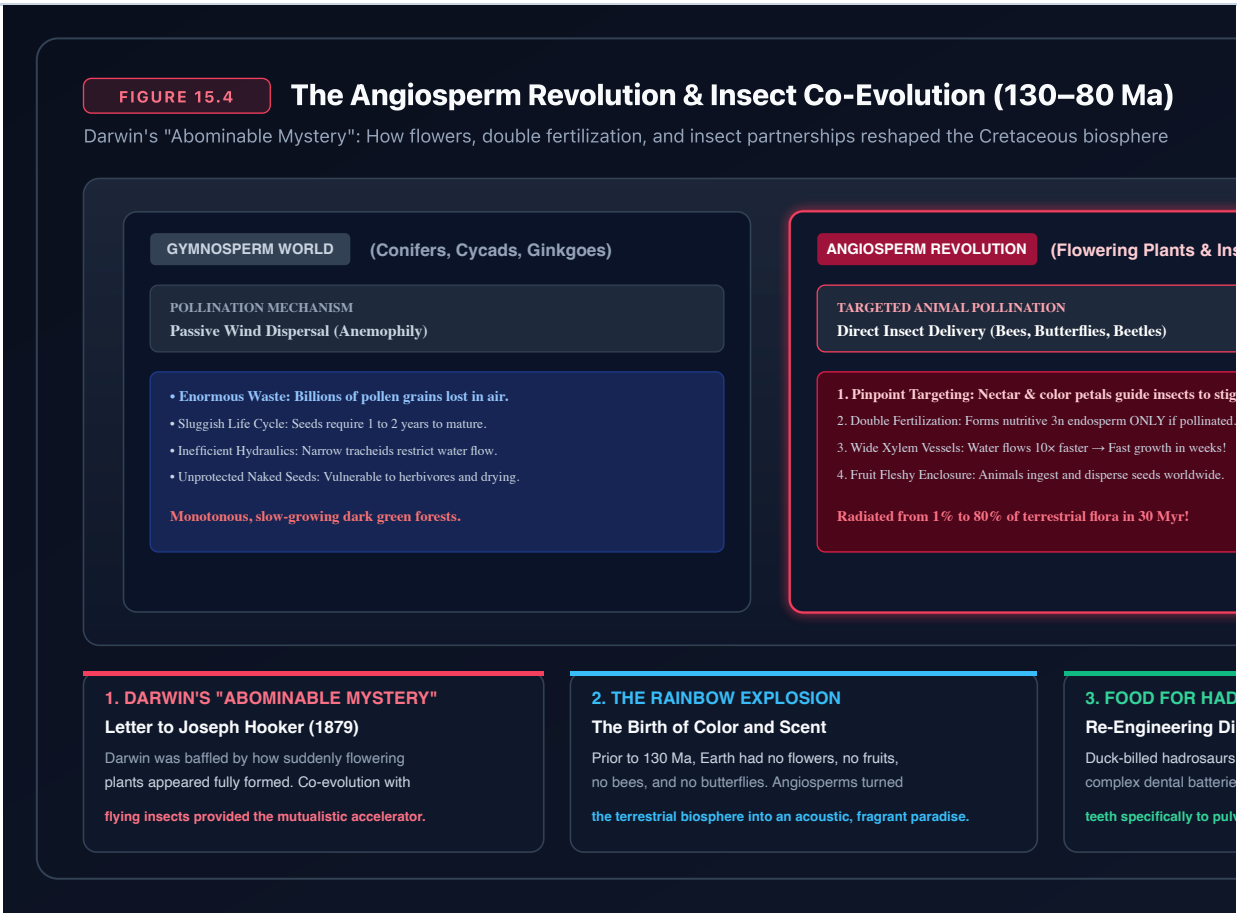
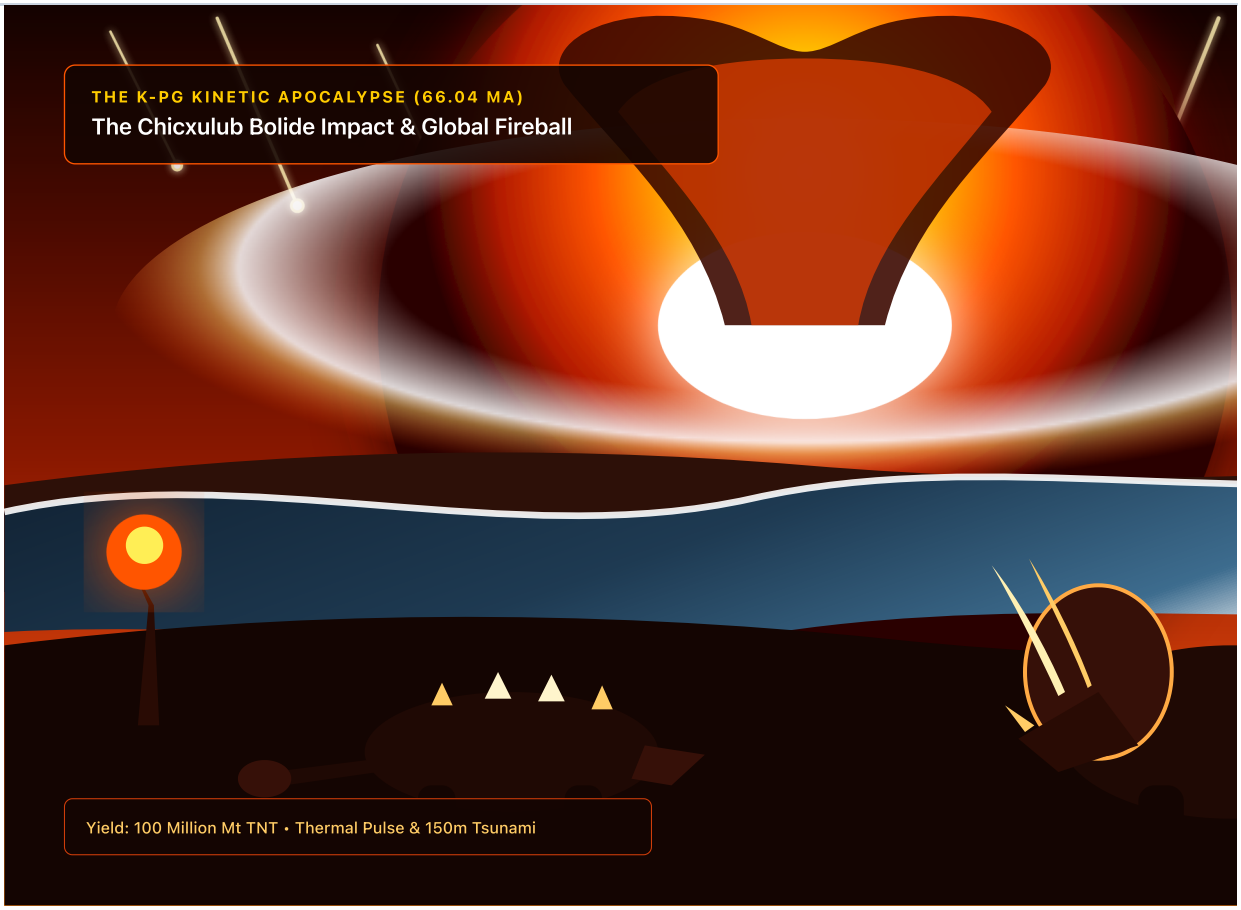


Figure 15.4: The Angiosperm Revolution & Insect Co-Evolution (130–80 Ma). What Charles Darwin famously termed his "abominable mystery"—the sudden Cretaceous explosion of flowering plants—was solved by mutualistic co-evolution with flying insects. By bribing bees, butterflies, and beetles with sugary nectar and vibrant petals, angiosperms replaced wasteful wind pollination with pinpoint targeted delivery. Combined with double fertilization (3n endosperm) and wide xylem vessels, flowering plants grew from seed to seed in weeks, conquering 80% of terrestrial flora.

5. The Chicxulub Impact: The Execution of an Empire (66.04 Ma)

Sixty-six million and forty thousand years ago, an unremarkable carbonaceous chondrite asteroid—measuring approximately 10 to 14 kilometers in diameter—intersected Earth's orbital trajectory at a velocity of 20 kilometers per second ($72,000 extkm/h$). It struck the carbonate and anhydrite-rich continental shelf of the Yucatán Peninsula at a steep angle of 60 degrees, gouging a transient crater 100 kilometers wide and 30 kilometers deep that immediately collapsed into the modern **Chicxulub crater**.



The Chicxulub Kinetic Strike & Bolide Impact (66.04 Ma). Striking the shallow carbonate platform of Mexico's Yucatán Peninsula with the explosive yield of 100 million megatons of TNT, a 12-kilometer carbonaceous asteroid excavated a transient crater 100 kilometers wide. Pulverized target rock was blasted into suborbital trajectories, whose incandescent re-entry turned the entire sky into an oven of radiant heat that ignited global wildfires, while 150-meter megatsunamis battered continental coastlines.

The kinetic energy liberated upon impact is quantified as:

$$E_k = rac12mv^2 approx rac12(2 imes 10^{15} ext{kg})(2 imes 10^4 ext{m/s})^2 approx 4 imes 10^{23} ext{J}$$

This is equivalent to **100 million megatons of TNT**—over two million times the yield of the largest thermonuclear weapon ever detonated by humanity. The planetary devastation unfolded across several distinct temporal phases:

1. **The Thermal Pulse (Minutes to Hours):** Trillions of tons of pulverized crust were blasted into ballistic suborbital trajectories. As this incandescent ejecta re-entered Earth's upper atmosphere over the ensuing hours, atmospheric friction turned the entire sky into an incandescent radiant broiler heating the surface to hundreds of degrees Celsius, igniting planetary-scale wildfires across all major continents.
2. **Megatsunamis & Seismic Shock (Hours):** Magnitude 11+ earthquakes shattered regional fault lines, while shockwaves displaced trillions of tons of seawater, driving 150-meter-high megatsunamis deep into the interior seaways of North America.
3. **The Impact Winter & Sulfuric Acid Fall (Months to Decades):** The target rocks contained immense deposits of gypsum ($ext{CaSO}_4 cdot 2 ext{H}_2 ext{O}$). An estimated 325 gigatons of sulfur and 1,500 gigatons of soot were vaporized directly into the stratosphere, forming a dense global veil of sulfate aerosols and black carbon that blocked 90% of solar radiation. The surface plunged into freezing darkness, arresting photosynthesis in terrestrial plants and marine phytoplankton.
4. **Ocean Acidification & Collapse of the Photic Zone:** Nitric acid rain ($ext{HNO}_3$, synthesized by impact atmospheric ionization) and carbonic acid dissolved surface ocean carbonates, destroying calcareous nannoplankton, ammonites, and the marine food pyramid.

The Iridium Anomaly: Smoking Gun of the Cataclysm

In 1980, Nobel laureate physicist Luis Alvarez, his geologist son Walter Alvarez, and nuclear chemists Frank Asaro and Helen Michel discovered a razor-thin, centimeter-wide clay layer marking the Cretaceous-Paleogene (K-Pg) boundary at Gubbio, Italy, and Caravaca, Spain. This boundary clay exhibited concentrations of **iridium**—a platinum-group siderophile element exceedingly rare in Earth's crust because it sank to the metallic core during planetary differentiation, but highly abundant in primitive chondritic asteroids—up to **160 times** background levels. The discovery of shocked quartz grains bearing microscopic planar deformation features (PDFs) and microtektites (extraterrestrial melt spherules) cemented the impact hypothesis beyond scientific doubt.

Shakil Mahmud • Research Monograph

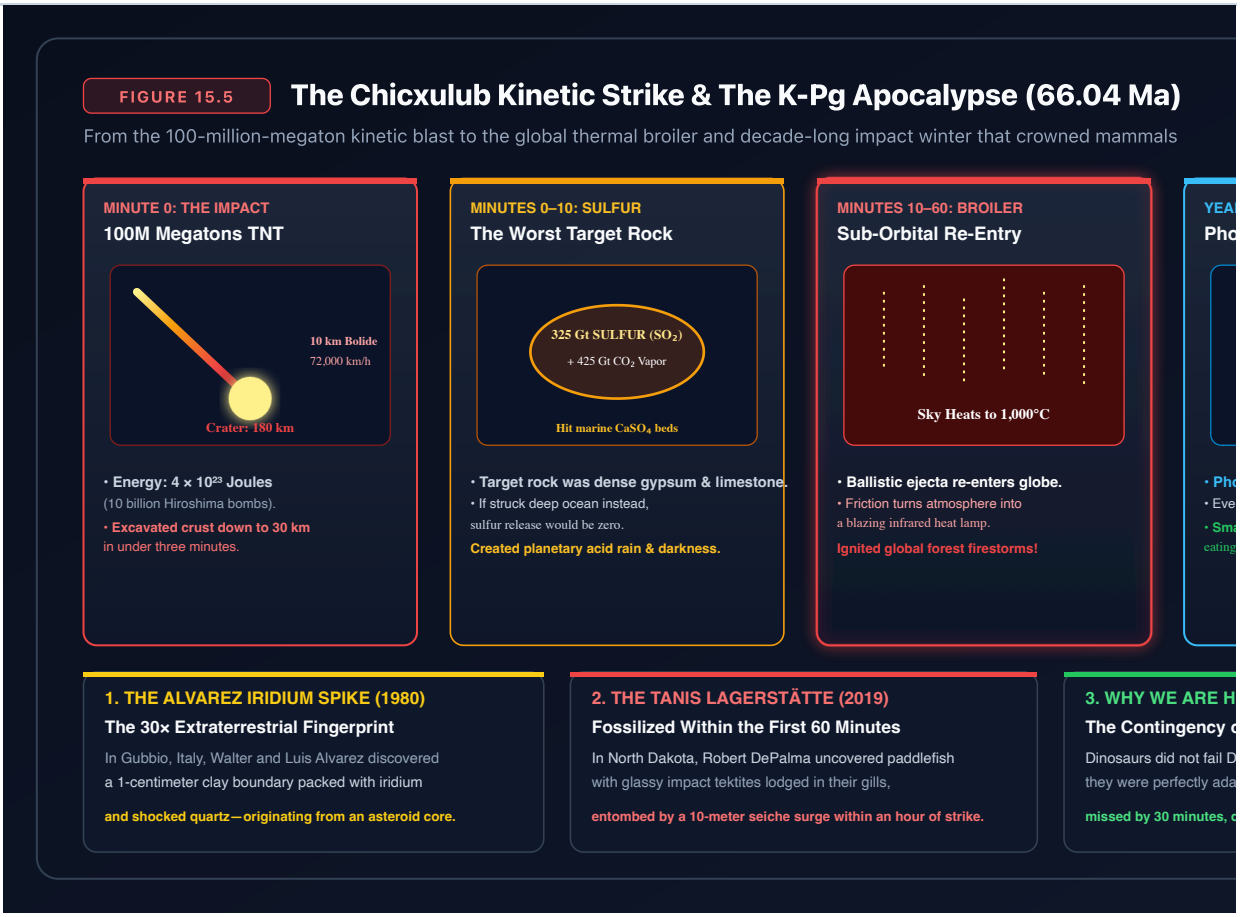


Figure 15.5: The Chicxulub Kinetic Strike & The K-Pg Apocalypse (66.04 Ma). Sixty-six million years ago, a 10-km asteroid delivered 100 million megatons of kinetic energy into the gypsum-rich marine shelf of Yucatan, Mexico. The impact vaporized 325 gigatons of sulfur and propelled trillions of tons of spherules into sub-orbital space. Re-entering spherules baked the global troposphere to 1,000°C within 60 minutes, igniting worldwide firestorms. A decade-long sulfate aerosol winter halted photosynthesis, wiping out all land animals over 25 kg and crowning nocturnal burrowing mammals.

6. The Mammalian Dawn

When the sun finally pierced through the dissipated sulfuric fog after a decade of freezing twilight, **75% of all species on Earth were gone**. The non-avian dinosaurs, the flying pterosaurs, the marine mosasaurs and plesiosaurs, and the coiled ammonites were erased forever.

Survival was not random; it was dictated by physiology and ecological trophic rank. Large-bodied endotherms with immense caloric demands starved. Those who survived were the subterranean opportunists: small, burrowing mammals, freshwater crocodilians and turtles (protected by aquatic thermal inertia and detritus-based trophic chains), and small, feathered maniraptoran theropods capable of eating dormant seeds—the **avian dinosaurs (birds)**.

In the vacant, predator-free expanses of the early Paleocene, surviving mammals found themselves in an ecological vacuum. Within a mere 400,000 years of the impact, placental lineages exploded in diversity and body mass. The archaic nocturnal foragers stepped out into the daylight, evolving into browsers, carnivores, ungulates, bats, cetaceans, and arboreal fruit-seekers with binocular stereoscopic vision. The stage was set for the Cenozoic Era—and the emergence of the Primates.

Academic Citations & Historical References

1. Alvarez, L. W., Alvarez, W., Asaro, F., & Michel, H. V. (1980). Extraterrestrial cause for the Cretaceous-Tertiary extinction. *Science*, 208(4448), 1095–1108. doi:10.1126/science.208.4448.1095
2. Schulte, P., Alegret, L., Arenillas, I., et al. (2010). The Chicxulub asteroid impact and mass extinction at the Cretaceous-Paleogene boundary. *Science*, 327(5970), 1214–1218. doi:10.1126/science.1177265
3. Brusatte, S. L., Benton, M. J., Ruta, M., & Lloyd, G. T. (2008). Superiority, competition, and opportunism in the evolutionary radiation of dinosaurs. *Science*, 321(5895), 1485–1488. doi:10.1126/science.1161833
4. Rowe, T. (1988). Definition, diagnosis, and origin of Mammalia. *Journal of Vertebrate Paleontology*, 8(3), 241–264. doi:10.1080/02724634.1988.10011708
5. Benton, M. J. (2014). *Vertebrate Palaeontology* (4th ed.). Wiley-Blackwell. ISBN:978-1118406847.
6. Chiarenza, A. A., Farnsworth, A., Mannion, P. D., et al. (2020). Asteroid impact, not volcanism, caused the end-Cretaceous dinosaur extinction. *Proceedings of the National Academy of Sciences*, 117(29), 17084–17093. doi:10.1073/pnas.2006087117
7. Sander, P. M., Christian, A., Clauss, M., et al. (2011). Biology of the sauropod dinosaurs: the evolution of gigantism. *Biological Reviews*, 86(1), 117–153. doi:10.1111/j.1469-185X.2010.00137.x

Citation: Mahmud, S. (2026). "The Dinosaur Empire & The Impact — The Mesozoic World and the Mammalian Dawn." In The Universal Chronicle, Part 15. https://shakilmahmud.com/universal-chronicle-part-15-the-dinosaur-empire/

Shakil Mahmud • Research Monograph

SHAKIL MAHMUD RESEARCH MONOGRAPHS • PART XVI

The Upright Ape — The Rift Valley, Bipedalism, and the Mastery of Fire

The Upright Ape — The Rift Valley, Bipedalism, and the Mastery of Fire

2,067 words • October 31, 2026 • Permanent URI

❖



Plate XVI: *Figure: Plio-Pleistocene hominin evolution in the East African Rift (~1.8–1.5 Ma): Homo erectus hunters stand upright on the savanna, gathering around the earliest controlled campfires with symmetrical Acheulean stone handaxes.*

Seven million years ago, the African continent was torn apart along a six-thousand-kilometer tectonic fault. As the Somali and Nubian plates pulled asunder, creating the towering highlands of the East African Rift System, the continuous equatorial rainforest that had sustained Miocene apes was sheared by a devastating rain shadow. In the desiccating interior, dense canopies dissolved into an open mosaic of wood-scattered grasslands. Stripped of the protective arboreal canopy and forced into direct competition with specialized cursorial carnivores, a singular lineage of hominoids stood upright, freed their forelimbs from locomotion, knapped crystalline stone into razor-edged butchery tools, and harnessed the exothermic power of combustion—initiating the most consequential evolutionary trajectory in planetary history.

1. The Tectonic Crucible: The East African Rift and Environmental Desiccation (~7 to 3 Ma)

The genesis of humanity was fundamentally an architectural consequence of plate tectonics. During the Late Miocene and Early Pliocene, mantle upwelling beneath the Afar triple junction fractured the African lithosphere. The resulting uplift of the Ethiopian and East African plateaus created a dual-ridge mountain wall that intercepted moist zonal moisture from the Indian and Atlantic oceans.

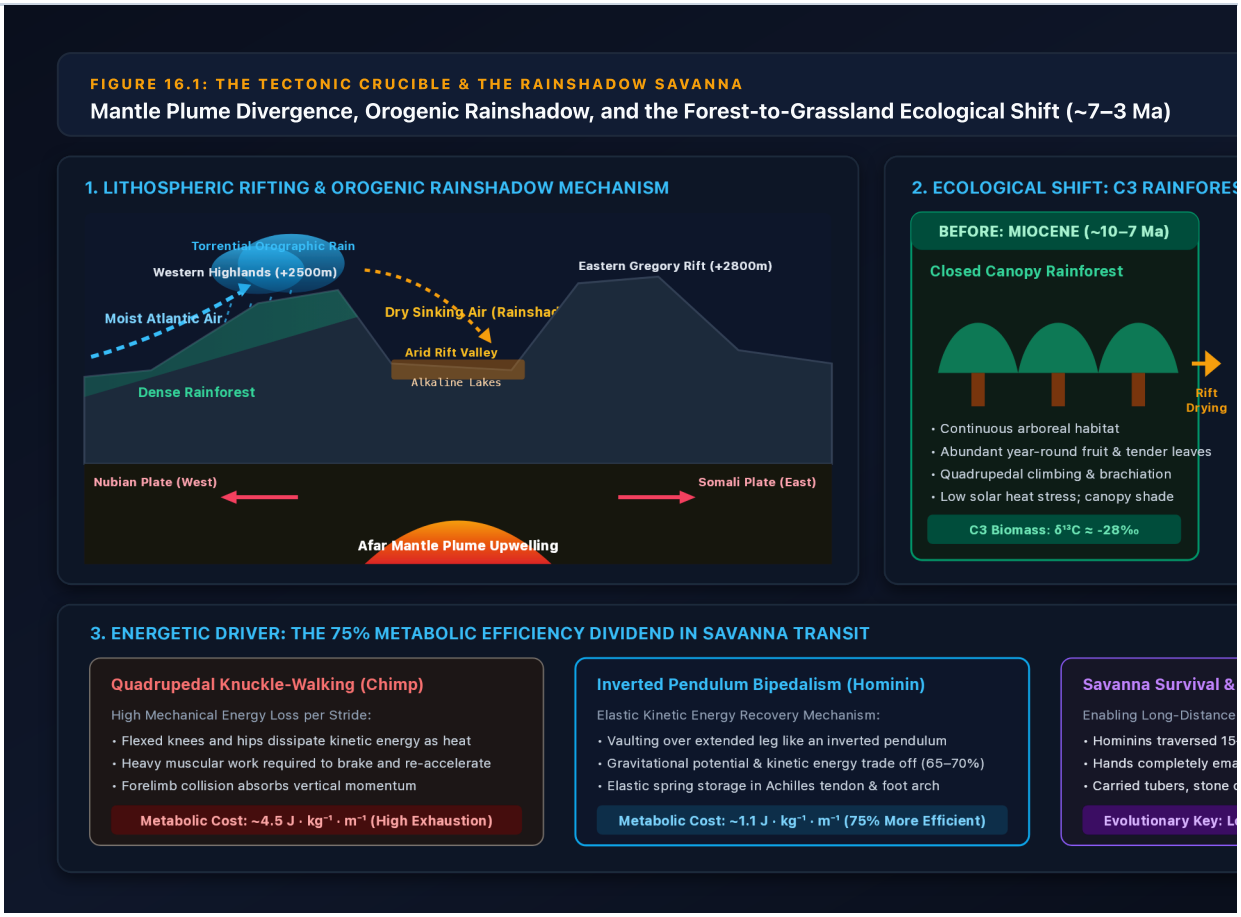


Figure 16.1: The Tectonic Crucible & The Rainshadow Savanna (~7–3 Ma). Mantle plume divergence beneath the Afar triple junction rifted the African continent into the Nubian and Somali plates. The resulting orogenic uplift created a massive rainshadow that desiccated the interior, shattering continuous C3 rainforests into an open C4 savanna mosaic and providing a 75% metabolic efficiency dividend for terrestrial bipedal transit.

Deprived of continuous precipitation, the closed tropical rainforests contracted into fragmented riverine galleries. The hominoid populations residing to the east of the rift faced an existential crisis: fruit-bearing trees were now separated by vast, hostile expanses of C4 savannah grasses. Foraging required traversing miles of open terrain under relentless equatorial solar irradiation. In this ecological crucible, knuckle-walking quadrupedalism—the mode of locomotion retained by ancestral chimpanzees and gorillas—became an energetic liability.

2. The Mechanical Revolution of Obligate Bipedalism

Biomechanical analyses by Rodman, McHenry, and Herman Pontzer demonstrate that quadrupedal knuckle-walking is energetically expensive, consuming approximately **four times more metabolic energy** per unit distance than habitual human striding bipedalism. Natural selection violently favored any anatomical mutation that reduced the caloric cost of locomotion across the savannah.

Shakil Mahmud • Research Monograph

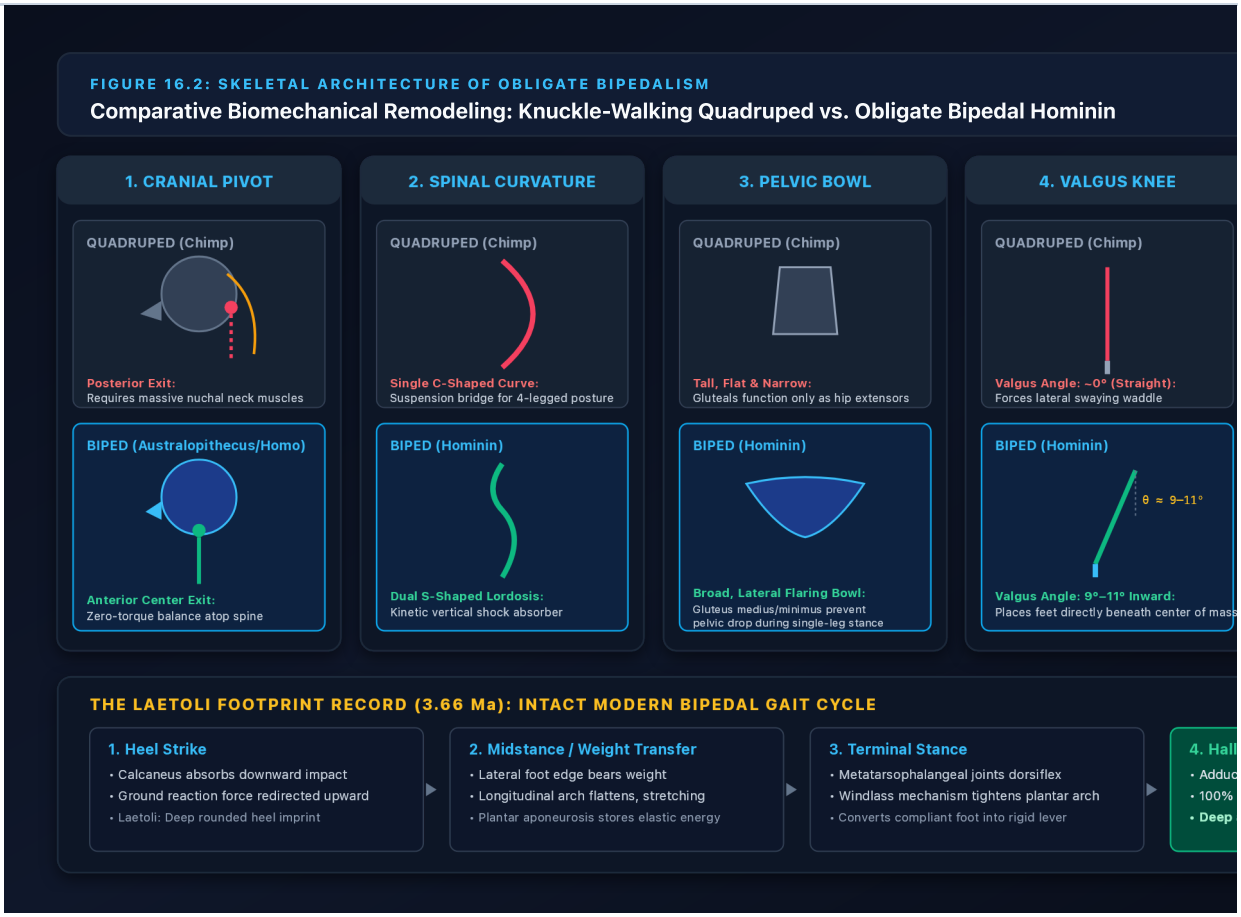


Figure 16.2: Biomechanical Remodeling for Obligate Bipedalism. Five fundamental skeletal transformations distinguish bipedal hominins from quadrupedal apes: anterior migration of the foramen magnum, dual S-curved spinal lordosis, short lateral-flaring bowl pelvis (abductor sling), valgus femoral bicondylar angle (9°–11°), and an adducted hallux with elastic plantar aponeurosis spring verified in the 3.66 Ma Laetoli footprint trackway.

The Morphological Reorganization for Upright Stride

Transitioning from a quadruped to an obligate biped required an extensive overhaul of the primate skeletal architecture:

- **Cranial Re-alignment:** The *foramen magnum* (the occipital hole through which the spinal cord exits the braincase) migrated forward from the posterior position seen in chimpanzees to an anterior, inferior position directly beneath the skull's center of gravity.
- **Lumbar Lordosis:** Evolution warped the straight ape spine into an elastic S-curve (lumbar and cervical lordosis), acting as a mechanical shock absorber that centers body mass over the pelvis.
- **Pelvic Transformation:** The iliac blades shortened, broadened, and curved laterally into a bowl-like pelvic basin, redirecting the lesser gluteal muscles (*gluteus medius* and *minimus*) from hindlimb extensors into lateral stabilizers that prevent the pelvic basin from collapsing during single-leg stance.
- **The Valgus Knee & Arched Foot:** The femur angled inward toward the midline (bicondylar or valgus angle), keeping feet directly beneath the torso. The ancestral grasping opposable hallux (big toe) was aligned in parallel with other digits (adduction), while the tarsals and metatarsals formed rigid longitudinal and transverse arches that store and release mechanical elastic strain during running.

The fossil record traces this architectural progression with crystalline clarity: from the six-to-seven-million-year-old *Sahelanthropus tchadensis* (exhibiting an anteriorly placed foramen magnum) and the four-million-year-old *Ardipithecus ramidus* (a facultative biped with a grasping foot), to the magnificent three-million-year-old *Australopithecus afarensis* (exemplified by the "Lucy" skeleton and the Laetoli footprint trackways in Tanzania, which prove completely modern, non-divergent heel-strike to toe-off bipedal kinematics).



Fossil Kinematics of Obligate Bipedalism: The Laetoli Trackways (~3.66 Ma). Preserved in a damp layer of carbonatite volcanic ash erupted from the Sadiman volcano, these footprints of *Australopithecus afarensis* record an adult and child walking across the Pliocene landscape. The prints exhibit a modern, human-like gait pattern: deep rounded heel-strike impact, prominent medial longitudinal arch, and a non-divergent, parallel big toe (adducted hallux) proving fully committed terrestrial striding bipedalism.

3. The Precision Grip and Lithic Archaeology (~3.3 to 1.8 Ma)

The most profound secondary consequence of bipedalism was the total liberation of the upper limbs from the mechanical constraints of weight support. Freed from locomotion, the primate hand evolved from a hook-like climbing apparatus into the most sensitive, versatile kinematic manipulator on the planet.

Shakil Mahmud • Research Monograph

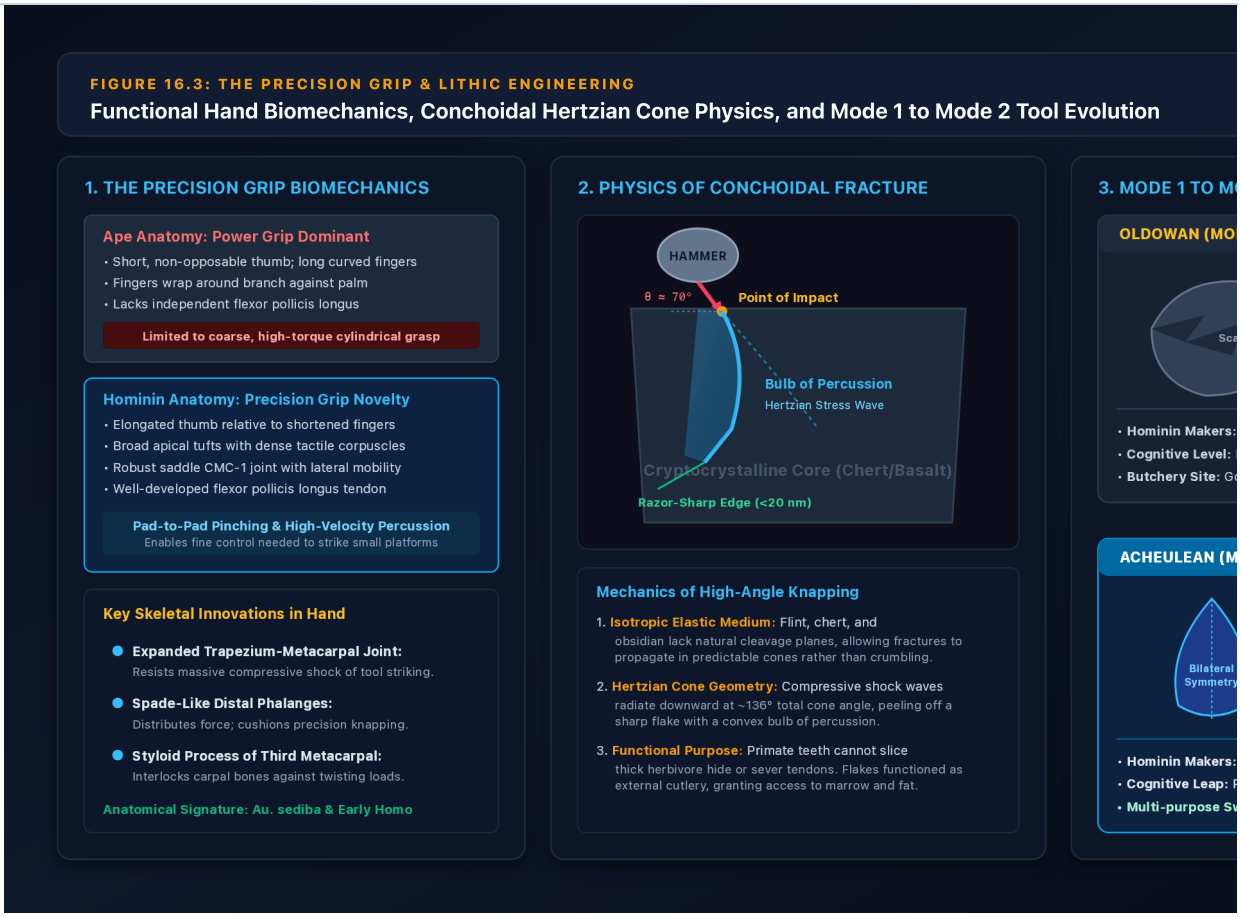
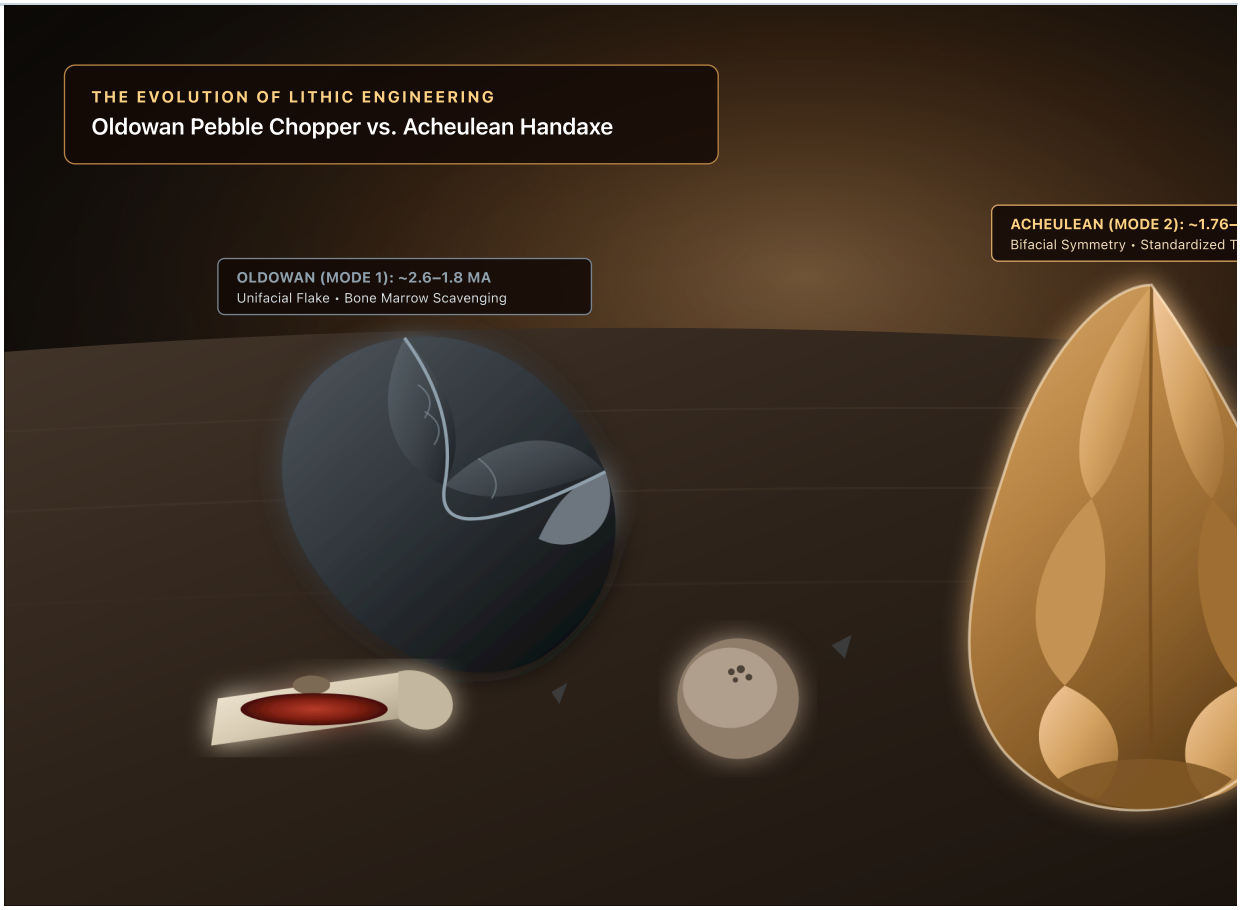


Figure 16.3: The Precision Grip & Lithic Engineering (~3.3 to 1.8 Ma). Biomechanics of the human hand (opposable thumb, saddle joint, flexor pollicis longus) combined with the physics of conchoidal Hertzian cone fracture enabled early hominins to transform cryptocrystalline rocks into razor-sharp cutting tools, progressing from Oldowan (Mode 1) opportunistic butchery flakes to Acheulean (Mode 2) bifacial symmetrical handaxes.

Human lineage hands developed an elongated, highly muscular opposable thumb powered by a unique, dedicated muscle: the **flexor pollicis longus**. Expanded apical pads with dense tactile mechanoreceptors (Merkel discs and Meissner corpuscles) permitted both the robust "power grip" (for holding heavy clubs) and the delicate "precision grip" (pinching between thumb and fingertip pads).

Lithic Industry	Approximate Age	Technological Signature	Associated Hominin
Lomekwian	3.3 Ma	Passive anvil technique; massive basalt blocks shattered against fixed anvils to yield jagged edges.	*Kenyanthropus platyops* / *Australopithecus afarensis*
Oldowan (Mode 1)	2.6 – 1.7 Ma	Systematic freehand percussion; striking a volcanic core with a hammerstone at acute angles to produce sharp unifacial flakes.	*Homo habilis* / *Homo rudolfensis*
Acheulean (Mode 2)	1.76 – 0.25 Ma	Bifacial symmetry; methodical knapping from both sides to manufacture standardized, teardrop-shaped handaxes and cleavers.	*Homo erectus* / *Homo ergaster*

With Oldowan flake tools, early hominins broke into an entirely vacant ecological niche: scavenging bone marrow from large ungulate carcasses left behind by saber-toothed cats (*Megantereon*) and giant hyenas. While other scavengers were barred by thick cortical bone, hominins utilized hammerstones to split femurs, gaining access to dense, sterile, lipid-rich marrow that provided high-calorie fatty acids (DHA and AA) essential for brain development.



The Evolution of Lithic Engineering: Oldowan Chopper vs. Acheulean Handaxe (~2.6 to 1.5 Ma). Direct comparison between early hominin toolkits. Left: An Oldowan (Mode 1) basalt core chopper with unifacial flake scars used by *Homo habilis* to shatter dense mammalian femurs for lipid-rich marrow. Right: An Acheulean (Mode 2) bifacial teardrop handaxe crafted by *Homo erectus* from quartzite, displaying deliberate bilateral symmetry, refined soft-hammer retouch, and continuous sharp cutting edges manufactured from a predetermined mental template.

4. Homo erectus and the Physiology of the Cursorial Hunter (~1.9 Ma)

At 1.9 million years ago, a radically new creature emerged in the African savannah: **Homo erectus** (often classified in its early African phase as *Homo ergaster*). The discovery of the remarkably complete "Turkana Boy" (KNM-WT 15000) revealed an individual of modern human stature (1.6 meters at age eight), long legs, narrow hips, and an expanded cranial capacity exceeding 850 cm^3.

Shakil Mahmud • Research Monograph

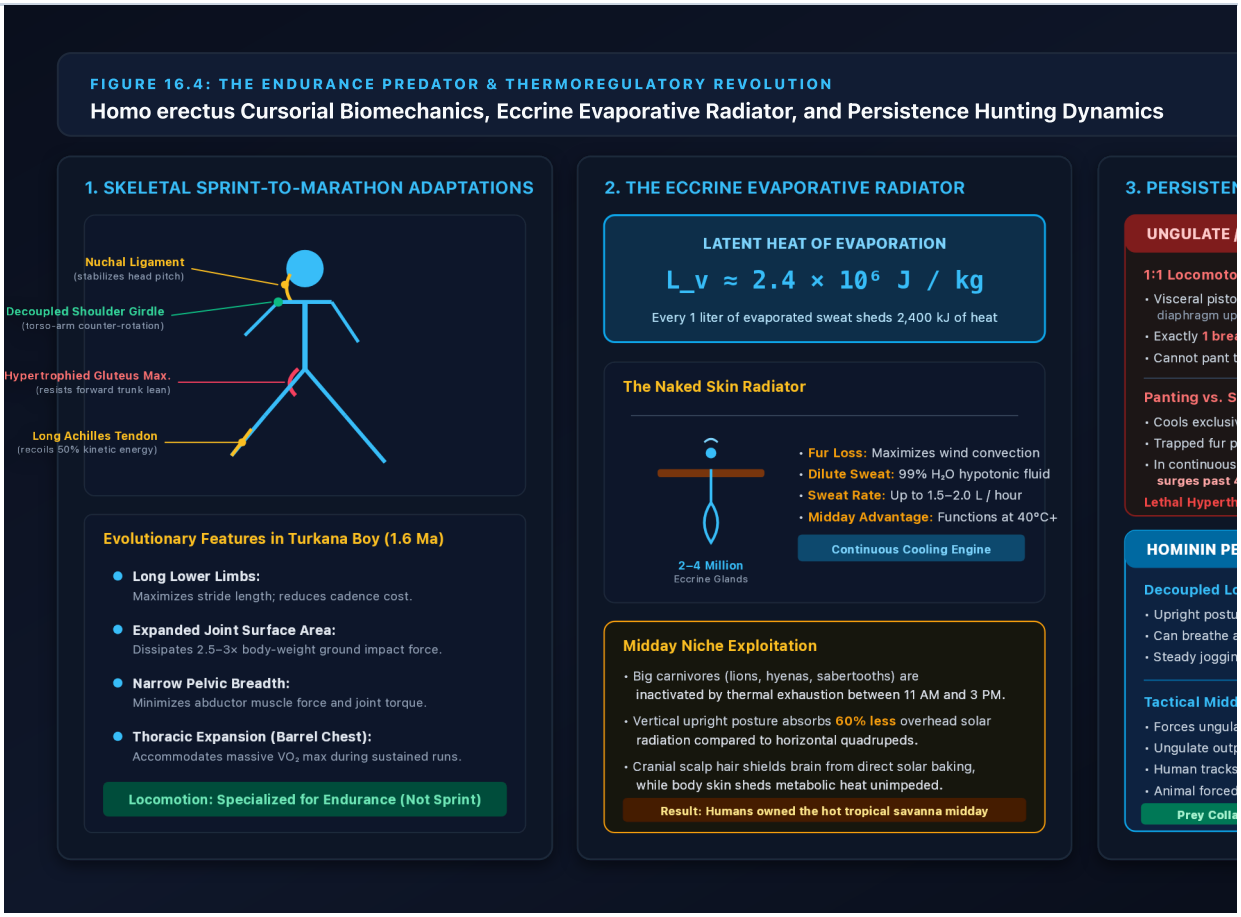


Figure 16.4: The Endurance Predator: Biomechanics & Thermoregulation of Homo erectus (~1.9 Ma). Decoupling locomotion from respiration enabled variable breathing ratios during running, while the loss of fur and explosive proliferation of 2–4 million eccrine sweat glands turned naked human skin into an evaporative radiator ($L_v \approx 2.4 \times 10^6$ J/kg), driving ungulates into midday thermal collapse during persistence hunts.

As demonstrated by Daniel Bramble and David Lieberman, *Homo erectus* was anatomically engineered for **persistence hunting**—running quadrupedal herbivores to exhaustion under the scorching midday sun. Quadrupeds gallop faster than humans in short sprints, but their respiratory anatomy forces a strict 1:1 coupling between stride frequency and respiration (the viscera piston against the diaphragm). Moreover, hairy quadrupeds cannot pant while galloping and must stop to dissipate internal heat, risking lethal hyperthermia.

Humans overcame this thermodynamic ceiling through two radical evolutionary adaptations:

1. **Alopecia (Loss of Body Hair):** Dense insulating fur was abandoned, exposing bare epidermis directly to ambient air.
2. **Eccrine Sweat Glands:** The proliferation of two to four million eccrine sweat glands across the entire dermal surface. While apocrine glands in mammals secrete oily, protein-rich fluids for scent marking, eccrine glands secrete a dilute, hypotonic aqueous solution (99% H_2O).

The latent heat of vaporization of water is immense:

$$L_v \approx 2.4 \times 10^6 \text{ J/kg}$$

By evaporating up to two liters of sweat per hour, a running human can continuously dissipate over **1,000 Watts of thermal energy**, decoupled completely from breathing frequency. *Homo erectus* could relentlessly pursue antelopes at a steady endurance trot for five hours in thirty-five-degree heat until the prey collapsed from heat stroke.

5. The Pyrotechnic Revolution and the Expensive-Tissue Hypothesis (~1.5 to 0.4 Ma)

The definitive threshold separating hominins from all other organisms on Earth was the controlled mastery of fire (pyrotechnology). Archaeological evidence from Wonderwerk Cave in South Africa and Gesher Benot Ya'aqov in Israel confirms systematic hearth usage dating back between 1.0 and 1.5 million years.

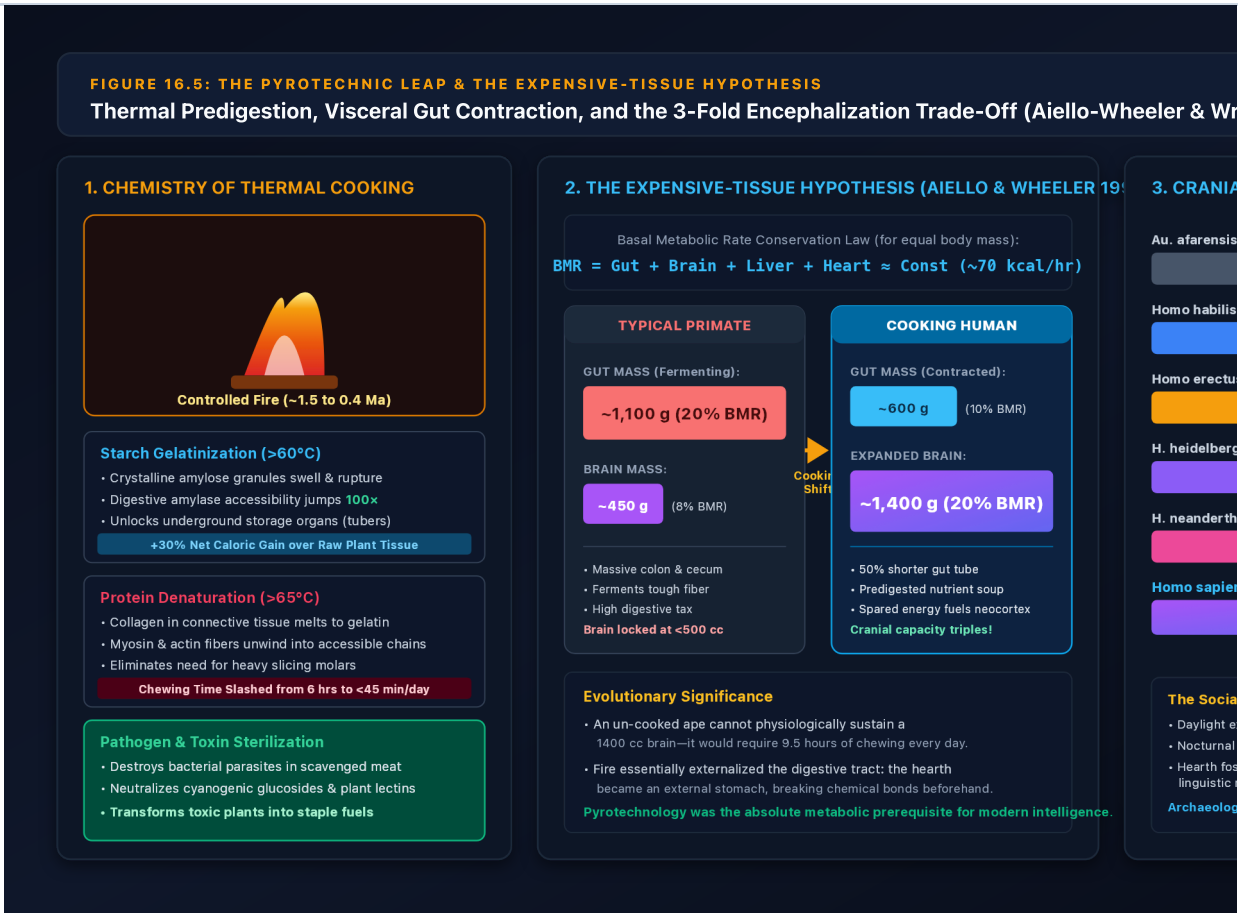


Figure 16.5: The Expensive-Tissue Hypothesis & The Pyrotechnic Leap (~1.5 to 0.4 Ma). Controlled fire externalized digestion by gelatinizing starches and denaturing proteins. Under a constant basal metabolic rate, the resulting 50% gut contraction released the critical metabolic energy required to fuel an unprecedented 3-fold evolutionary expansion of the hominin brain.

Biologist Richard Wrangham formulated the **Cooking Hypothesis**, establishing that thermal processing of food was the primary physiological driver of human encephalization. Raw foraging is energetically ruinous: chimpanzees spend between six and seven hours every day simply chewing fibrous raw leaves and tough wild meat, expending enormous metabolic energy on digestion.

The Biochemistry of Cooking

Applying fire to organic foodstuffs completely alters their nutritional availability:

- **Starch Gelatinization:** Heat swells and bursts the rigid semicrystalline starch granules in roots and tubers, breaking down amylose and amylopectin into easily hydrolyzable glucose polymers.
- **Protein Denaturation:** Heat uncoils complex, folded fibrous proteins (collagen, myosin, actin), exposing peptide bonds directly to stomach pepsin and pancreatic proteases.
- **Pathogen Elimination:** High heat sterilizes spoiled meat, neutralizing bacteria and parasites that would otherwise cause debilitating immune activation.

Under Leslie Aiello and Peter Wheeler's **Expensive-Tissue Hypothesis**, metabolic basal energy is strictly conserved across major organ systems. Both brain tissue and gastrointestinal tissue are metabolically voracious, consuming approximately twenty times more energy per gram than skeletal muscle. Because cooked food is pre-digested externally by fire, *Homo erectus* no longer required the massive, fermenting large intestine and lengthy colon seen in apes.

As gut mass shrank by 60%, the liberated metabolic surplus was channeled directly into the central nervous system. Brain volume surged from 450 cm^3 in australopithecines to 900 cm^3 in *Homo erectus*, and ultimately to 1,400 cm^3 in Neanderthals and archaic *Homo sapiens*. Fire not only nourished the brain; it extended the day into the night, banished apex carnivores from cave mouths, and created the social hearth—the primordial theater around which language, storytelling, and human culture were born.

Shakil Mahmud • Research Monograph



The Pyrotechnic Leap: Homo erectus Hearth & The Origin of Cooking (~1.5 Ma). At the mouth of an African rock shelter, a band of *Homo erectus* gathers around a structured, stone-lined hearth. By externalizing digestion through the thermal gelatinization of starches and denaturation of fibrous meat proteins, fire reduced digestive metabolic energy by 60%, fueling a three-fold expansion of the hominin brain. The hearth circle provided security from nocturnal predators, extended waking hours, and established the social crucible of human culture.

Academic Citations & Historical References

1. Wrangham, R. (2009). *Catching Fire: How Cooking Made Us Human*. Basic Books. ISBN:978-0465013623.
2. Bramble, D. M., & Lieberman, D. E. (2004). Endurance running and the evolution of Homo. *Nature*, 432(7015), 345–352. doi:10.1038/nature03052
3. Aiello, L. C., & Wheeler, P. (1995). The Expensive-Tissue Hypothesis: The brain and the digestive system in human and primate evolution. *Current Anthropology*, 36(2), 199–221. doi:10.1086/204350
4. Lovejoy, C. O. (1981). The origin of man. *Science*, 211(4480), 341–350. doi:10.1126/science.211.4480.341
5. Pontzer, H., Raichlen, D. A., & Rodman, P. S. (2014). Bipedalism and the energetic cost of human locomotion. *Journal of Human Evolution*, 73, 112–122. doi:10.1016/j.jhevol.2014.06.002
6. White, T. D., Asfaw, B., Beyene, Y., et al. (2009). Ardipithecus ramidus and the paleobiology of early hominids. *Science*, 326(5949), 75–86. doi:10.1126/science.1175802
7. Johanson, D. C., & White, T. D. (1979). A systematic assessment of early African hominids. *Science*, 203(4378), 321–330. doi:10.1126/science.104384

Citation: Mahmud, S. (2026). "The Upright Ape — The Rift Valley, Bipedalism, and the Mastery of Fire." In The Universal Chronicle, Part 16. https://shakilmahmud.com/universal-chronicle-part-16-the-upright-ape/

SHAKIL MAHMUD RESEARCH MONOGRAPHS • PART XVII

The Cognitive Revolution — Homo sapiens, Symbolic Language, and Abstract Thought

The Cognitive Revolution — Homo sapiens, Symbolic Language, and Abstract Thought

2,093 words • October 31, 2026 • Permanent URI

❖

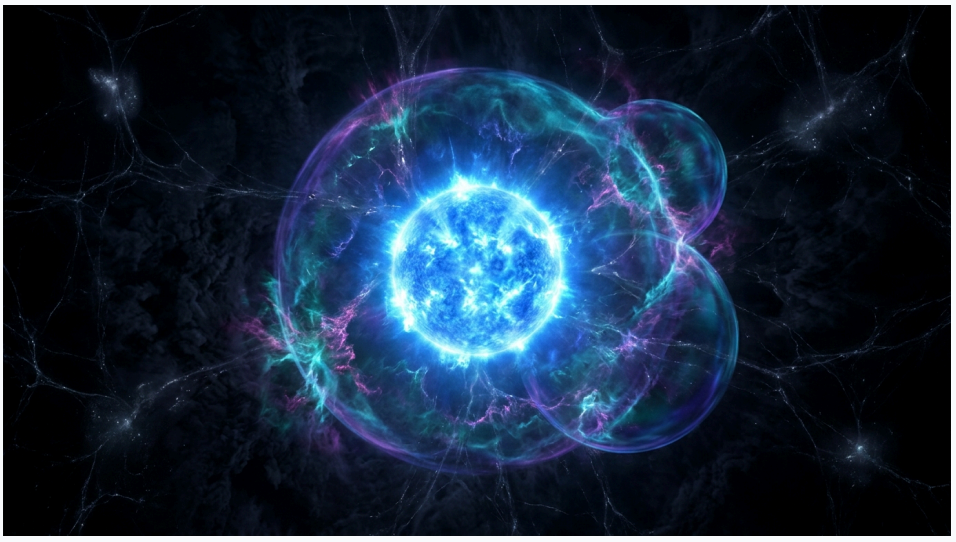


Plate XVII: *Figure: The Upper Paleolithic cognitive leap (~40,000 BP): Homo sapiens hunter-artists deep inside limestone caverns illuminate dynamic cave murals of steppe bison and horses by animal-fat torchlight, marking the birth of symbolic language.*

For more than ninety-nine percent of human evolutionary history, our ancestors were ecologically unremarkable primates. They chipped stones, tracked game across river valleys, and huddled around smoky hearths, yet their environmental impact was indistinguishable from that of baboons, leopards, or hyenas. Then, between one hundred thousand and seventy thousand years ago, an astonishing intellectual threshold was crossed. In a transformation evolutionary historians designate as the **Cognitive Revolution**, one African lineage developed recursive syntactic language, externalized symbolic thought through ochre engravings and cave art, and invented the capacity to believe in entities that exist solely within the collective imagination—unleashing a cooperative force that would sweep across every continent and alter the face of the Earth.

1. The Pan-African Origin of Homo sapiens (~315,000 to 100,000 yr ago)

Until recently, paleoanthropological orthodoxy held that *Homo sapiens* originated in a singular East African "Garden of Eden" around 200,000 years ago. However, the landmark 2017 excavations at **Jebel Irhoud, Morocco**, led by Jean-Jacques Hublin, revolutionized this paradigm by uncovering early modern human fossils and Middle Stone Age flint tools securely dated to **315,000 years ago**.

Shakil Mahmud • Research Monograph

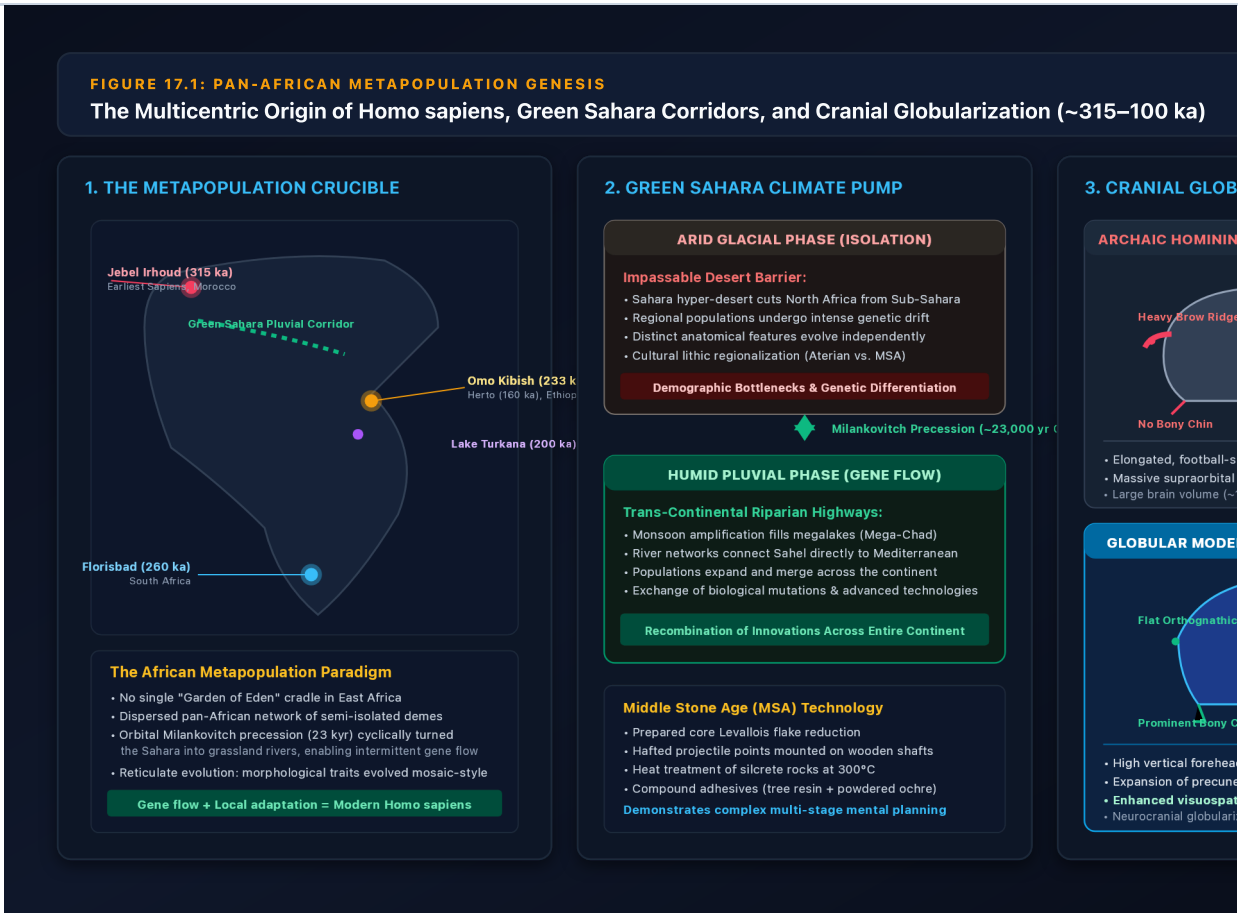
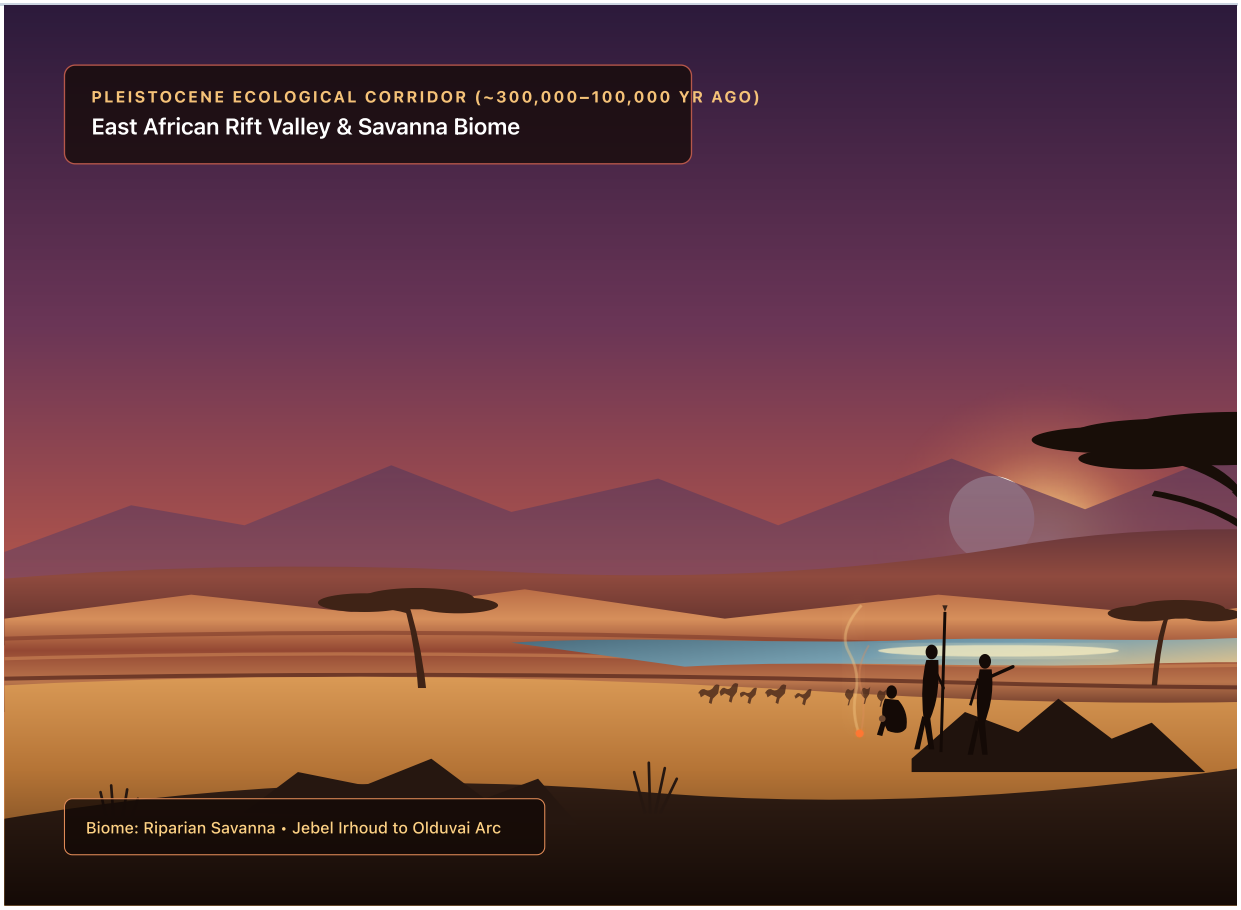


Figure 17.1: Pan-African Metapopulation Genesis (~315–100 ka). Modern Homo sapiens arose not from a solitary East African cradle, but across an interconnected pan-African network of semi-isolated populations (Jebel Irhoud 315 ka, Florisbad 260 ka, Omo Kibish 233 ka). Orbital Milankovitch precession cyclically transformed the hyperarid Sahara into green riparian corridors, driving continent-wide genetic recombination and neurocranial globularization.

Morphometric analyses revealed a vital evolutionary insight:

- The facial skeleton of the Jebel Irhoud fossils is completely modern, exhibiting delicate supraorbital tori (brow ridges), a retracted midface, and canine fossae indistinguishable from living humans.
- In contrast, the braincase remains archaic—elongated and archaic in shape (platycephalic), lacking the globularity that characterizes living modern humans.

The definitive anatomical hallmark of our species—**cranial globularity**—evolved gradually over the ensuing 200,000 years through the expansion of the parietal and cerebellar brain lobes. This neuroanatomical remodeling reflects the hyper-specialization of neural circuits dedicated to spatial processing, visuospatial integration, episodic memory, and mental self-projection.



Pleistocene Savanna Ecology: The African Rift Valley Corridor (~300,000–100,000 yr ago). Emerging across an interconnected pan-African network stretching from Morocco's Jebel Irhoud to the East African Rift, early *Homo sapiens* adapted to dynamic savanna-woodland mosaics. Flanked by volcanic calderas and deep rift lakes, small bands tracked migratory herds with wooden thrusting spears and knapped Middle Stone Age points, gathering around controlled hearth fires that provided warmth, defense, and cooked nutrition.

2. The Neurogenetic Basis of Syntactic Speech and Recursion

While chimpanzees and monkeys possess distinct alarm vocalizations (signaling "eagle," "snake," or "leopard"), animal communication is strictly constrained to referential signals grounded in immediate sensory experience. The human linguistic breakthrough was not merely louder vocalization, but the emergence of **infinite semantic recursion**—the algorithmic ability to embed phrases within phrases to generate an infinite variety of thoughts from a finite alphabet of phonemes.

Shakil Mahmud • Research Monograph

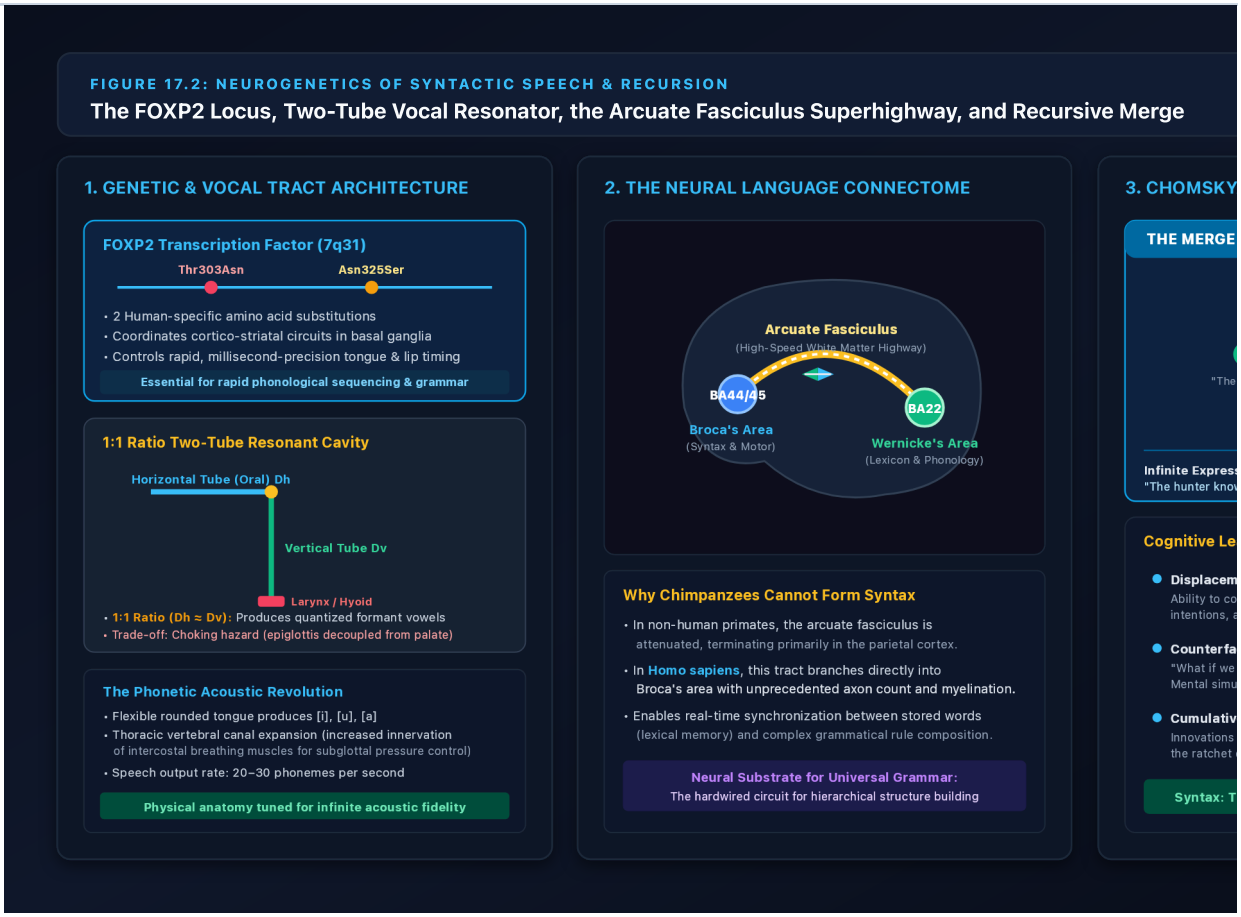


Figure 17.2: Neurogenetics of Syntactic Speech & Recursion. Human-specific substitutions in the FOXP2 transcription factor paired with an equal 1:1 two-tube vocal resonator (lowered larynx) unlocked high-speed phonological speech. In the brain, an expanded arcuate fasciculus superhighway directly connects Broca's area to Wernicke's area, powering the fundamental syntactic Merge operation to construct infinite hierarchical meanings from finite vocal tokens.

$$\mathcal{L} = \{\text{Sentence} \longrightarrow \text{Noun Phrase} + \text{Verb Phrase}\}$$

This linguistic capacity required a twin biological convergence:

Biological Dimension	Anatomical / Genetic Mechanism	Linguistic Consequence
Vocal Tract Reorganization	Descent of the larynx into the pharynx; flexed basicranium creating a two-tube acoustic resonator with equal horizontal (oral) and vertical (pharyngeal) cavities.	Unlocked precise motor control over tongue and formant frequencies, enabling unambiguous differentiation of rapid vowel sounds (\/a/\, \/i/\, \/u/\).
The FOXP2 Transcription Factor	Two critical amino acid substitutions (threonine-to-asparagine at position 303 and asparagine-to-serine at position 325) unique to the human lineage.	Regulates synaptic plasticity in the striatum and cortico-basal ganglia loops, allowing rapid motor sequencing of rapid articulatory speech movements.
Arcuate Fasciculus Expansion	Massive axonal fiber bundle directly interconnecting Wernicke's area (posterior superior temporal gyrus) with Broca's area (inferior frontal gyrus).	Enables instantaneous translation between phonological sensory decoding and recursive syntactic hierarchical motor production.

3. The Symbolic Awakening and Externalized Memory (~100,000 to 40,000 yr ago)

Linguistic syntax quickly metastasized into material culture. For millions of years, lithic tools like Acheulean handaxes remained structurally frozen across continents for tens of thousands of generations. Around 100,000 years ago in Southern Africa, this static toolmaking culture shattered into an explosion of symbolic artifacts:

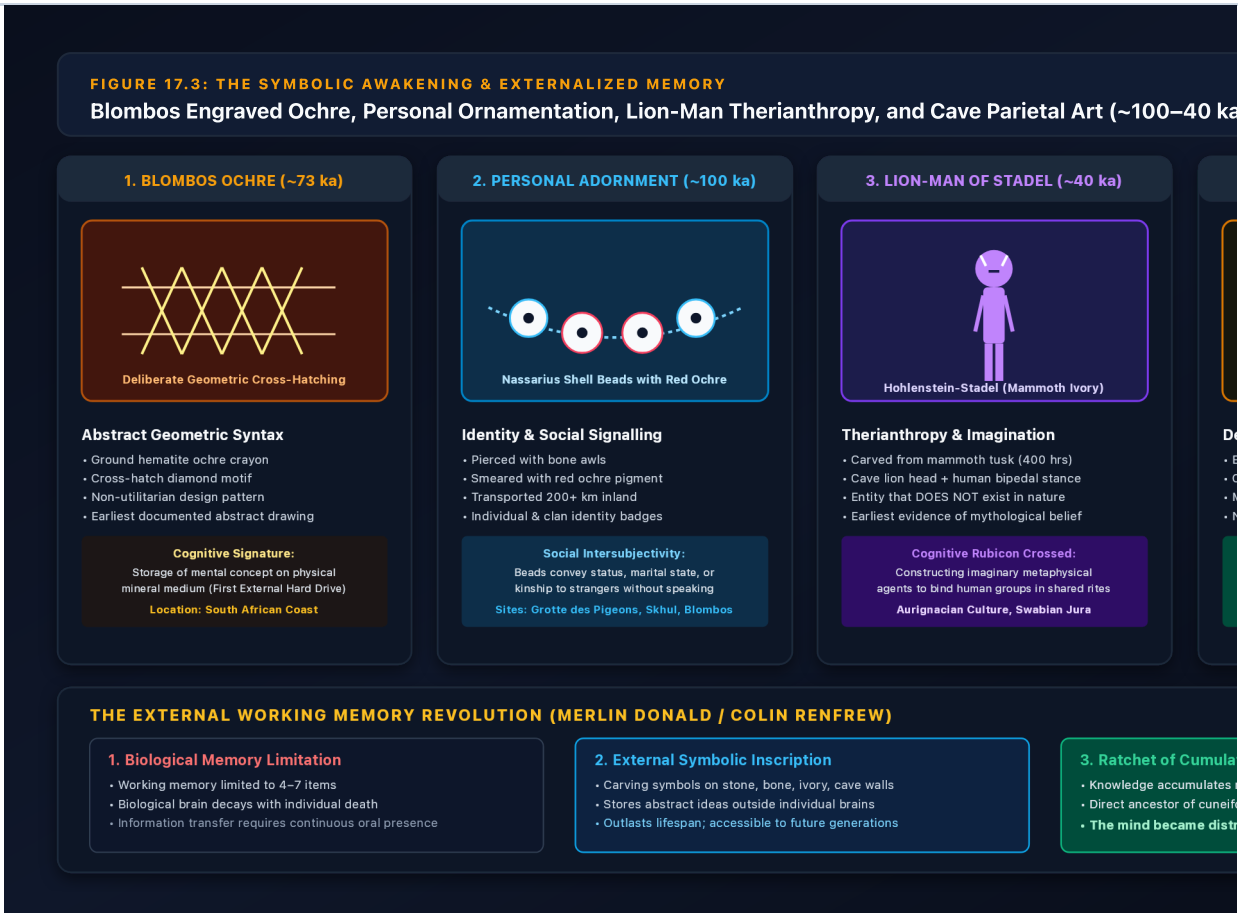
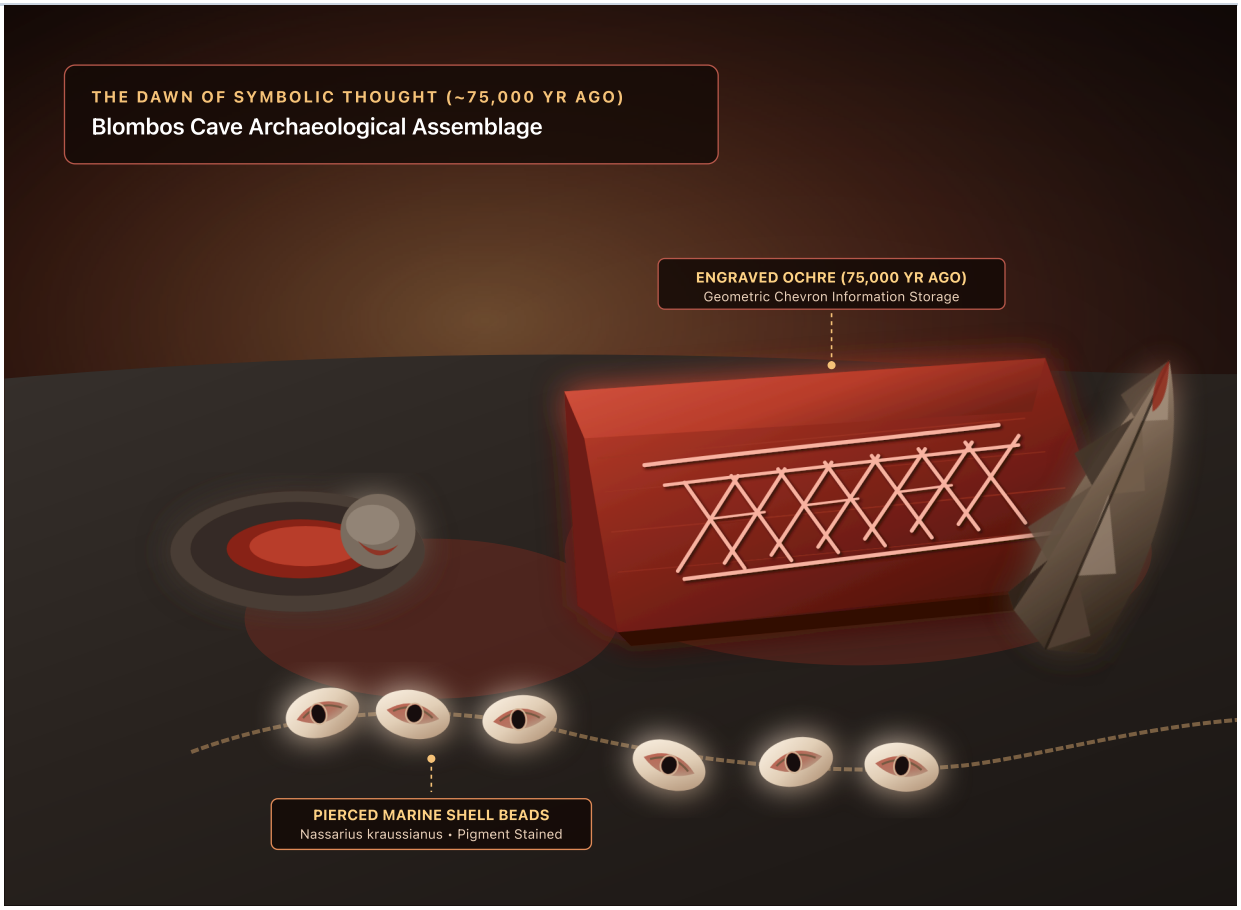


Figure 17.3: The Symbolic Awakening & Externalized Memory (~100–40 ka). Blombos Cave engraved ochre plaques, pierced marine shell beads, the Stadel Lion-Man therianthrope, and subterranean cave art (Chauvet, Lascaux) demonstrate the externalization of mental representations onto permanent physical substrates. This created the first trans-generational information storage system outside biological DNA.

The Ochre Engravings of Blombos Cave

At **Blombos Cave** on the southern coast of South Africa, archaeologist Christopher Henshilwood excavated chunks of iron-rich red ochre dated to **75,000 years ago**. Slices of smoothed ochre had been systematically carved with geometric cross-hatched chevron patterns using sharp lithic points. Along with perforated marine tick shells (*Nassarius kraussianus*) stained with red ochre and worn as personal necklaces, Blombos yielded indisputable evidence that early humans were using physical media to store and transmit abstract symbolic information across generational boundaries.

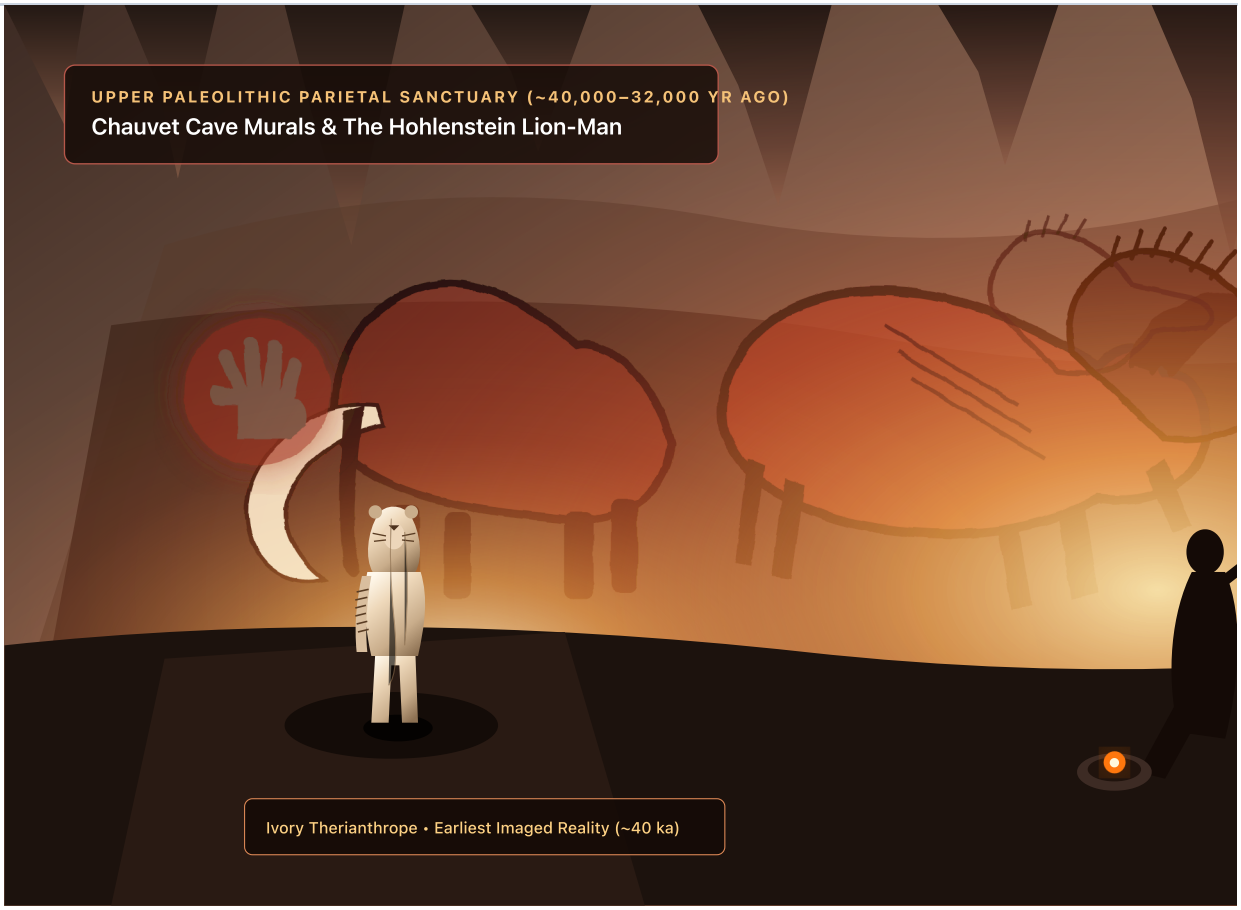
Shakil Mahmud • Research Monograph



The Dawn of Symbolic Thought: Archaeological Assemblage from Blombos Cave (~75,000 yr ago). Excavated on South Africa's southern coast, this smoothed siliceous hematite plaque displays intentional geometric cross-hatched chevron engravings (× × ×) carved with a silcrete burin. Alongside perforated *Nassarius kraussianus* marine tick-shell beads stained with crimson ochre, these artifacts represent the earliest indisputable externalized symbolic information storage in human prehistory.

When modern humans entered Western Eurasia forty thousand years ago, this symbolic drive achieved sublime artistic heights. In the Swabian Jura of Germany, artisans sculpted the **Lion-Man of Hohlenstein-Stadel** from woolly mammoth ivory—a therianthropic figure combining a human torso with the head of a cave lion. This sculpture represents the earliest indisputable material proof of the human capacity to conceive of something that does not physically exist in nature.

In the subterranean sanctuaries of **Chauvet**, **Lascaux**, and **Altamira**, Upper Paleolithic artists used charcoal, hematite, and bone blowing-pipes to paint dynamic, anatomically flawless herds of stampeding mammoths, woolly rhinos, megaloceros deer, and horses. By utilizing natural convexities in the limestone walls, they created volumetric three-dimensional illusions that pulsed with life under the flickering light of animal-fat stone lamps.



Upper Paleolithic Parietal Sanctuary: Chauvet Cave Murals & The Stadel Lion-Man (~40,000–32,000 yr ago). Deep within subterranean limestone chambers, Upper Paleolithic artists used charcoal, blown hematite pigments, and natural rock contours to render thundering herds of steppe bison, woolly mammoths, and wild horses under flickering grease-lamp torchlight. In the foreground, the 40,000-year-old carved mammoth ivory *Lion-Man of Hohlenstein-Stadel* embodies the human breakthrough into imagined realities and mythical animism.

4. Imagined Realities and Hyper-Cooperation: Breaking Dunbar's Number

In evolutionary biology, British anthropologist Robin Dunbar established that a primate species\' maximum sustainable social group size is mathematically bounded by the relative volume of its neocortex. For *Homo sapiens*, this biological ceiling—known as **Dunbar's number**—is approximately **150 individuals**. Above this threshold, a primate troop cannot maintain cohesion through direct personal grooming, reciprocal social bonds, and intimate behavioral monitoring; the group inevitably fragments into competing factions.

Shakil Mahmud • Research Monograph



Figure 17.4: Breaking Dunbar's Number via Intersubjective Myths. While non-human primates are bound by neocortex grooming limits to groups of 50–60 individuals (Dunbar's biological ceiling: N ≈ 150), Homo sapiens engineered an intersubjective tier of reality. Shared totems, mythological creator spirits, and sacred moral codes enabled tens of thousands of unrelated strangers to trade peacefully and coordinate continental mammoth hunts.

Yet modern human societies routinely organize millions of individuals into cohesive armies, states, and economic networks. How did our species break the biological cage of Dunbar's number?

The answer, formulated compellingly by historian Yuval Noah Harari, is the creation of **fictional constructs (imagined realities)**. Alone among all living beings, *Homo sapiens* can transmit shared cognitive fictions:

- **Ancestral Spirits & Totems:** Two strangers meeting in the Pleistocene tundra who shared a belief in the Sacred Bear would not fight to the death; they recognized each other as members of a shared metaphysical kinship, exchanging stone blades, shells, and matrimonial partners.
- **Mythological Norms & Taboos:** Moral rules codified in collective myths enforced social cooperation, punishing cheaters and free-riders through collective ostracism or execution.
- **Intersubjective Value:** The shared fiction that a polished cowrie shell or a rare piece of amber possessed intrinsic value enabled trading networks spanning thousands of kilometers across glacial Eurasia.

5. The Out-of-Africa Dispersal and the Fate of Archaic Humans (~70,000 to 30,000 yr ago)

Armed with recursive language, symbolic networks, bone projectile points (atlatls), and thermal tailored clothing stitched with eyed bone needles, a small diaspora of *Homo sapiens* crossed the Bab-el-Mandeb Strait and the Sinai Peninsula approximately 70,000 years ago.

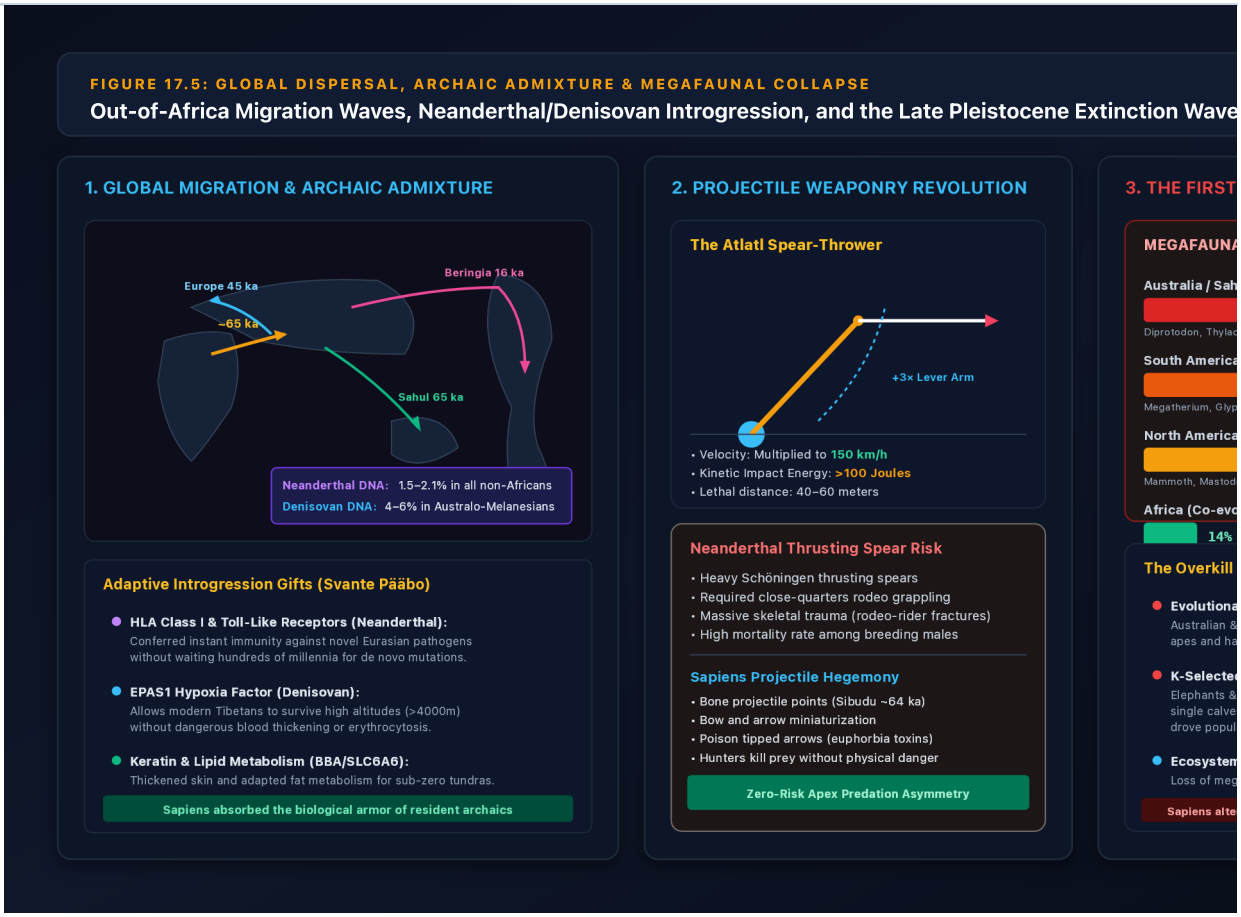


Figure 17.5: Global Dispersal, Archaic Admixture & Megafaunal Collapse (~70–10 ka). Armed with projectile atlatl spear-throwers and bow-and-arrow technology, Homo sapiens expanded out of Africa, assimilating beneficial adaptive alleles from Neanderthals (1.5–2% immunity DNA) and Denisovans (4–6% EPAS1 hypoxia DNA). Across every continent they made landfall, ecologically naive megafauna suffered unprecedented extinction rates (85% in Australia, 83% in South America).

In Eurasia, they encountered archaic hominin cousins who had occupied the territory for hundreds of thousands of years: the cold-adapted **Neanderthals** (*Homo neanderthalensis*) in Europe and the Middle East, and the elusive **Denisovans** in Siberia and East Asia. Ancient genomic sequencing pioneered by Svante Pääbo and the Max Planck Institute revealed that these encounters were not merely combative; they involved episodic fertile hybridization:

- All contemporary non-African humans carry between **1% and 2% Neanderthal DNA**, preserving genes that influenced keratin production in skin and hair, as well as immune receptors (HLA alleles) adapted to Eurasian pathogens.
- Indigenous populations of Melanesia, Australia, and the Philippines carry up to **4% to 6% Denisovan DNA**, including the crucial *EPAS1* transcription factor allele that prevents pulmonary hypoxia in high-altitude Tibetan populations.

Yet despite episodic interbreeding, wherever modern humans established permanent settlements, archaic hominins vanished within a few thousand years. Outcompeted by the symbolic coordination, superior projectile technology, and dense social trade networks of *Homo sapiens*, the last Neanderthals retreated to the cliff caves of Gibraltar and disappeared forever around 39,000 years ago.

6. The Overkill: The Pleistocene Megafaunal Extinction

The ecological consequence of the Cognitive Revolution was catastrophic for the planet\'s large fauna. For millions of years, the megafauna of Africa had co-evolved alongside hominins, developing deep-seated behavioral instincts to fear two-legged apes. But when *Homo sapiens* crossed open oceanic waters to reach **Australia (~50,000 years ago)** and crossed the Bering land bridge into the **Americas (~15,000 years ago)**, the native megafauna had never encountered human hunters.

The devastation was swift and absolute:

1. **Australia:** Within a few millennia of human arrival, **85% of all terrestrial animals weighing over 45 kg** were exterminated—including *Diprotodon* (a wombat the size of a rhinoceros), *Genyornis* (a 250-kg flightless bird), and *Thylacoleo carnifex* (the marsupial lion).
2. **The Americas:** Following the retreat of the Laurentide ice sheet, Clovis hunters armed with fluted spear points decimated **70% of North American megafauna** within roughly one thousand years—erasing Columbian mammoths, mastodons, giant ground sloths (*Megatherium*), camelids, and saber-toothed cats (*Smilodon*).

By 10,000 BCE, humanity stood completely alone atop the terrestrial food chain. Every competing hominin lineage was extinct. The ancient megafaunal empires were shattered. As the last Pleistocene glaciers began to melt, the nomadic hunting bands of the fertile river valleys of the Near East were about to initiate the greatest economic gamble in human history: the domestication of seeds, beasts, and civilization itself.

Shakil Mahmud • Research Monograph

Academic Citations & Historical References

1. Hublin, J. J., Ben-Ncer, A., Bailey, S. E., et al. (2017). New fossils from Jebel Irhoud, Morocco and the pan-African origin of *Homo sapiens*. *Nature*, 546(7657), 289–292. doi:10.1038/nature22336
2. Enard, W., Przeworski, M., Fisher, S. E., et al. (2002). Molecular evolution of FOXP2, a gene involved in speech and language. *Nature*, 418(6900), 869–872. doi:10.1038/nature01025
3. Henshilwood, C. S., d\'Errico, F., Yates, R., et al. (2002). Emergence of modern human behavior: Middle Stone Age engravings from South Africa. *Science*, 295(5558), 1278–1280. doi:10.1126/science.1067575
4. Green, R. E., Krause, J., Briggs, A. W., et al. (2010). A draft sequence of the Neandertal genome. *Science*, 328(5979), 710–722. doi:10.1126/science.1188021
5. Dunbar, R. I. (1992). Neocortex size as a constraint on group size in primates. *Journal of Human Evolution*, 22(6), 469–493. doi:10.1016/0047-2484(92)90081-J
6. Harari, Y. N. (2014). *Sapiens: A Brief History of Humankind*. Harper. ISBN:978-0062316097.
7. Koch, P. L., & Barnosky, A. D. (2006). Late Quaternary extinctions: state of the debate. *Annual Review of Ecology, Evolution, and Systematics*, 37, 215–250. doi:10.1146/annurev.ecolsys.34.011802.132415

Citation: Mahmud, S. (2026). "The Cognitive Revolution — Homo sapiens, Symbolic Language, and Abstract Thought." In The Universal Chronicle, Part 17. https://shakilmahmud.com/universal-chronicle-part-17-the-cognitive-revolution/

SHAKIL MAHMUD RESEARCH MONOGRAPHS • PART XVIII

The Domestication of Nature — The Neolithic Spark, Cuneiform, and the Rise of Cities

The Domestication of Nature — The Neolithic Spark, Cuneiform, and the Rise of Cities

2,149 words • October 31, 2026 • Permanent URI

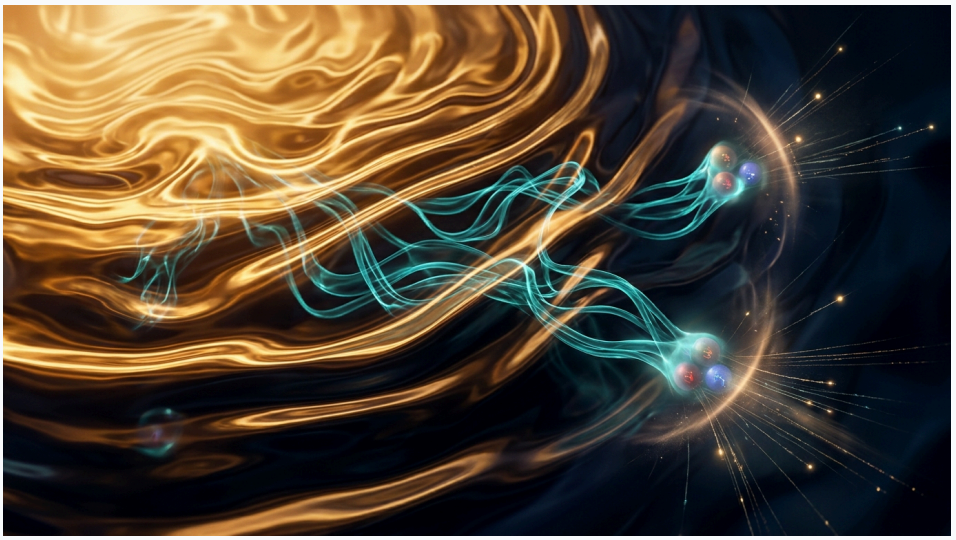


Plate XVIII: *Figure: The dawn of civilization (~10,000–3,000 BCE): sedentary agricultural communities harvest domesticated emmer wheat along the Fertile Crescent, founding the monumental hydraulic city-states of ancient Mesopotamia.*

For two hundred thousand years, every human who ever lived was a nomad whose survival depended on memorizing seasonal animal migrations, edible tuber patches, and the locations of waterholes. But as the planet emerged from the chill of the Younger Dryas into the warm, predictable equilibrium of the Holocene epoch 11,700 years ago, a profound economic shift occurred. In the alluvial valleys of the Fertile Crescent, the Yangtze, the Indus, and Mesoamerica, humans laid down their spears, cleared forests, trapped rivers in irrigation canals, and altered the genomes of wild grasses through artificial selection. In doing so, humanity triggered an explosive cascade: demographic booms, the division of labor, the externalization of thought into written script, the rise of sovereign city-states, and ultimately the formulation of universal mathematical laws governing the cosmos.

1. The Holocene Climatological Oasis and the Neolithic Transition (~10,000 to 6000 BCE)

The Pleistocene was characterized by violent, chaotic climate swings: interglacials were punctuated by sudden plunges into subzero glacial maximums within a few decades. Under such unpredictable variability, long-term agriculture was thermodynamically impossible; planting crops requires reliable annual rainfall and stable growing seasons.

Shakil Mahmud • Research Monograph



Figure 18.1: The Holocene Climate Oasis & Plant Domestication (~10,000–6000 BCE). After hundreds of millennia of violent Pleistocene climate volatility, the Holocene brought an unprecedented 11,000-year thermal plateau (±1°C). In the Fertile Crescent, human foragers selected for the non-shattering rachis mutation in wild wheat and barley, locking humans and domesticates into an obligate mutualism that compressed birth spacing and catalyzed an irreversible demographic explosion.

Approximately 11,700 years ago, the Earth entered the **Holocene**. Global temperatures stabilized within a narrow band of \± 1^°C\, atmospheric CO2\ held steady at approximately 260 ppm, and seasonal monsoons settled into reliable cycles. In the Levant and Anatolia, hunter-gatherer bands who had established semi-sedentary base camps (the Natufian culture) began actively manipulating wild cereal stands.



Landscape Reconstruction: The Fertile Crescent Ecological Corridor (~9000 BCE). An aerial panorama of the early Holocene Levantine and Mesopotamian arc. As retreating Pleistocene glaciers stabilized global temperatures and precipitation cycles, the winding river basins of the Tigris and Euphrates—bordered by the Taurus and Zagros foothills—fostered rich natural stands of wild cereals and permanent stone encampments of the Natufian culture.

The Genetic Remodeling of Cereal Grasses

In wild emmer (*Triticum dicoccoides*) and einkorn wheat, the central stem of the seed head—the **rachis**—is brittle. Upon ripening, the rachis shatters in the wind, scattering individual spikelets across the ground to ensure seed dispersal. When early foragers gathered wild wheat, they selectively harvested the mutant plants possessing a genetic defect: a *non-shattering (tough) rachis* that held seeds firmly to the stem. By planting only these retained seeds, early farmers conducted unconscious genetic engineering: within a few centuries, wheat lost its biological capacity to reproduce without human intervention, trading wild autonomy for exponential human cultivation.

Shakil Mahmud • Research Monograph



Botanical Evolutionary Divergence: The Non-Shattering Rachis Mutation. (Left) Wild einkorn wheat (*Triticum monococcum*) with a brittle rachis that naturally fractures at maturity, allowing the wind to disperse seed spikelets across the landscape. (Right) Domesticated wheat possessing a tough, non-shattering rachis mutation that binds plump grain kernels firmly to the central stem—preventing natural seed dispersal and locking the plant into an obligate evolutionary symbiosis with human harvesters.

Following plant domestication came the taming of herbivores: mouflon sheep, wild bezoar goats, aurochs (ancestors of cattle), and wild boar. Animals were selected for docility, reduced flight distance, and paedomorphic (juvenile) behavioral traits. By tapping into secondary animal products—milk, wool, traction power, and manure fertilizer—human communities multiplied their available kinetic energy by an order of magnitude.

2. The Hydraulic Megamachine: Uruk and the Urban Explosion (~4000 to 3000 BCE)

In the arid southern alluvial plains of Lower Mesopotamia, between the volatile floods of the Tigris and Euphrates rivers, simple rain-fed agriculture was impossible. Survival demanded massive collective engineering: digging hundreds of kilometers of irrigation canals, dredging silt, and constructing flood-control dykes.



Architectural Reconstruction: The Hydraulic Infrastructure of Uruk (~3200 BCE). Massive earthen canals diverted seasonal floodwaters from the Euphrates into gridded agricultural fields and date orchards across southern Mesopotamia. This artificial hydrology produced unprecedented 30:1 grain surpluses, funding the construction of the White Temple of Anu and supporting the first specialized urban civilization of 80,000 inhabitants.

Shakil Mahmud • Research Monograph

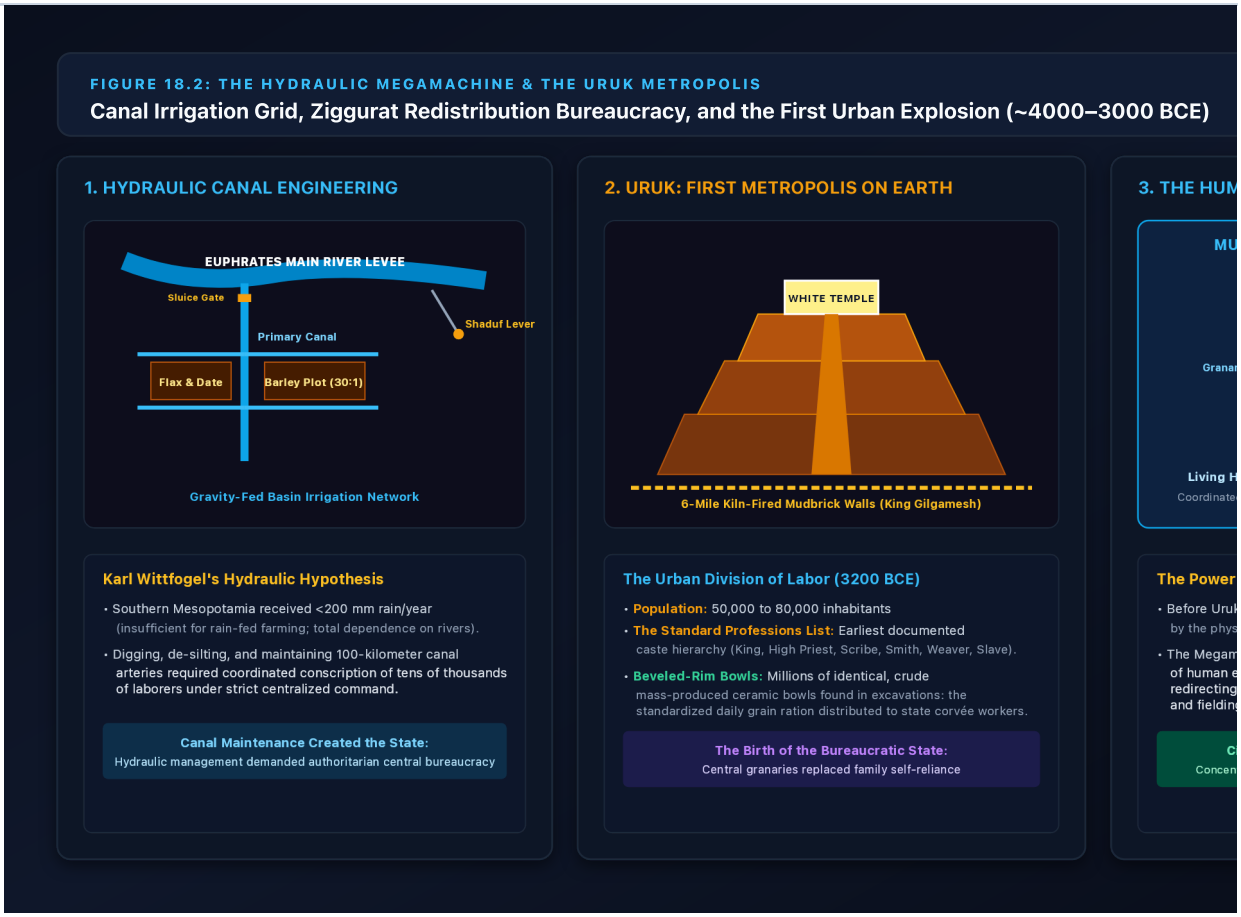


Figure 18.2: The Hydraulic Megamachine & The Uruk Metropolis (~4000–3000 BCE). Managing the unpredictable spring floods of the Tigris and Euphrates required vast gravity-fed canal networks and sluice gates. The resulting agricultural surplus (30:1 grain yields) funded the first metropolis of 80,000 citizens at Uruk, organized around temple granaries, standardized bevel-rimmed ration bowls, and Lewis Mumford's centralized human 'megamachine'.

This hydraulic imperative birthed the world's first true metropolis: **Uruk**. By 3200 BCE, Uruk housed an estimated 50,000 inhabitants within a six-square-kilometer circuit of brick defensive walls. For the first time in natural history, a biological community was divided into hyper-specialized professional castes:

Social / Economic Stratum	Functional Role in the Urban Megamachine	Technological Catalyst
Agrarian Producers	Plowing, canal excavation, cereal cultivation, and animal husbandry.	Ard (scratch plow), copper sickles, oxen draft harnesses.
Craft Specialists	Mass production of standardized pottery, textiles, and metallurgy.	Potter's fast wheel, lost-wax bronze casting (copper-tin alloy).
Scribes & Temple Bureaucrats	Taxation auditing, land surveying, grain redistribution, and astronomical calculation.	Proto-cuneiform clay tablets, sexagesimal (base-60) arithmetic.
The Sovereign Priesthood (Ensi)	Ideological legitimacy, ritual mediation with celestial pantheons, command over labor.	Monumental architecture (baked-mudbrick ziggurats), legal codes.

3. The Externalization of Symbolic Memory: From Clay Tokens to the Alphabet

The human brain was never wired by natural selection to memorize the grain debts, land boundaries, and tax obligations of 50,000 citizens. Writing was not invented to compose lyric poetry or philosophical treatises; it was invented as a ledger accounting system for the temple storehouses of Mesopotamia.



Figure 18.3: From Clay Tokens to the Phonetic Alphabet. The 5,000-year evolution of symbolic external memory tracked five stages: 3D geometric clay counting tokens (Neolithic), hollow clay bullae envelopes (Uruk), 2D impressed clay tablets (abstract numerical notation), phonetic cuneiform via the Rebus principle (representing spoken speech), and finally the 22-letter Proto-Sinaitic consonantal alphabet that democratized literacy across the ancient world.

The evolutionary trajectory of writing followed a strict developmental progression:

1. **Clay Accounting Tokens (~8000 BCE):** Small geometric clay spheres, cones, and cylinders representing specific commodities (e.g., one cone = one bushel of barley; one sphere = one vessel of oil).
2. **Clay Bullae & Impressions (~3500 BCE):** Tokens were sealed inside hollow spherical clay envelopes (bullae) stamped with cylinder seals. To verify contents without breaking the envelope, scribes pressed the tokens into the wet exterior clay. Scribes soon realized the interior tokens were redundant: two-dimensional stylus impressions on a flat clay tablet conveyed the identical information.
3. **Proto-Cuneiform to Phonetic Cuneiform (~3200 to 2500 BCE):** Pictographic representations (e.g., a drawing of a head eating from a bowl representing "to eat" or "ration") became increasingly stylized and wedge-shaped through the use of reed styluses. Crucially, scribes introduced the **Rebus Principle**: a pictograph was used not for its visual meaning, but for its phonetic sound value (e.g., using the pictograph for "reed" [*gi*] to represent the abstract verb "to render" [*gi*]).
4. **The Phonetic Alphabet Revolution (~1800 to 1000 BCE):** While cuneiform and Egyptian hieroglyphs required memorizing hundreds of complex logographic signs—restricting literacy to an elite guild of lifetime scribes—Semitic miners in the Sinai adapted Egyptian hieroglyphs into the first **consonantal alphabet (Abjad)**. By reducing written communication to roughly 22 phonetic signs corresponding to individual vocal phonemes, the Phoenicians and Greeks democratized literacy across the Mediterranean Basin.

Shakil Mahmud • Research Monograph



Archaeological Artifacts: Sumerian Accounting Tokens & Sealed Clay Bulla (~3300 BCE). Hand-modeled geometric tokens—cones, spheres, disks, and tetrahedrons marked with incisions—represented standardized economic goods such as measures of barley, heads of livestock, and jars of sesame oil. To secure transactions against theft or tampering during transport, accountants enclosed the tokens within a hollow clay sphere (*bulla*) and rolled cylinder seals across its exterior, directly catalyzing the birth of cuneiform writing.

4. The Axial Age: The Emergence of Philosophical Inquest (~800 to 200 BCE)

With the widespread dissemination of the alphabet and the advent of the **Iron Age** (which made durable iron plows and weapons universally accessible), human civilizations across Eurasia underwent a simultaneous philosophical awakening termed by Karl Jaspers as the **Axial Age**.

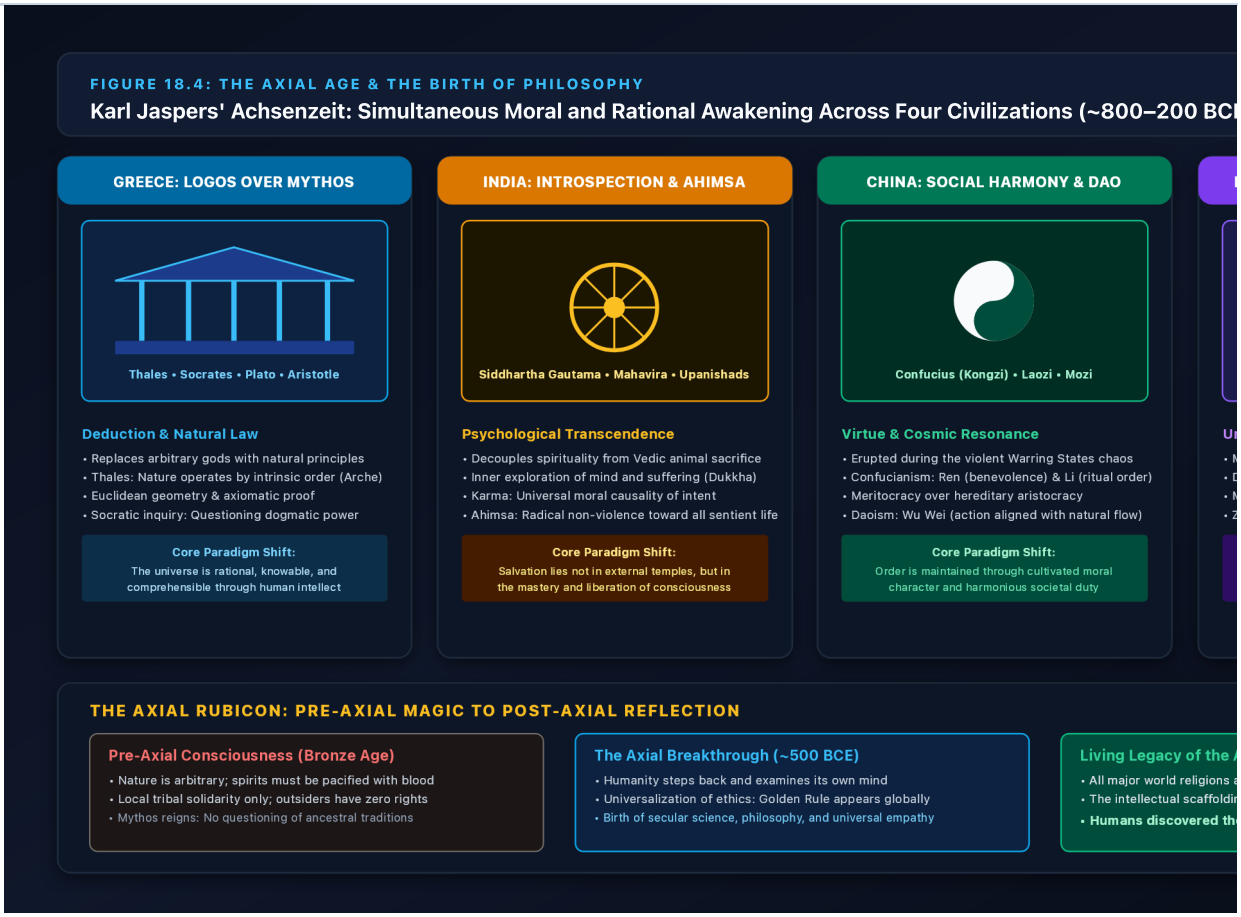


Figure 18.4: The Axial Age & The Birth of Philosophy (~800–200 BCE). Across Greece (Socrates, Plato, Aristotle), India (Buddha, Mahavira, Upanishads), China (Confucius, Laozi), and the Levant/Persia (Hebrew Prophets, Zarathustra), humanity crossed Karl Jaspers' 'Axial Rubicon'. Local sacrificial cults were simultaneously superseded by rational inquiry (Logos), universal ethical codes, and inner psychological reflection.

Between 800 and 200 BCE, thinkers decoupled moral inquiry and natural law from arbitrary priestly superstition:

- **In Greece:** Thales of Miletus proposed that natural phenomena were governed by immutable material principles (*arche*) rather than the whims of Olympian gods; Democritus hypothesized that all matter was composed of indivisible, eternal particles (*atomos*); Aristotle developed formal syllogistic logic and systematic biological classification.
- **In India:** The authors of the Upanishads, Mahavira, and Siddhartha Gautama (the Buddha) investigated the psychological phenomenology of consciousness, suffering (*dukkha*), and ethical causation (*karma*).
- **In China:** Confucius and Laozi debated the structural harmony of the state, personal virtue, and the cosmic order of the *Dao*.

5. The Mechanization of Thought and the Scientific Revolution (1543 to 1687 CE)

The accumulated philosophical and mathematical insights of antiquity were brought to explosive ignition through two technological amplifiers in Early Modern Europe:

The Printing Press and the Information Singularity

In 1440, Johannes Gutenberg synthesized movable metal type, oil-based ink, and a wooden screw press in Mainz, Germany. Prior to Gutenberg, copying a single volume of the Latin Bible required months of laborious manual scribe work on hundreds of sheepskin parchment folios. By reducing the marginal cost of textual reproduction by over **99%**, the printing press made scientific treatises, astronomical tables, and anatomical drawings universally replicable, eliminating the risk of lost knowledge and catalyzing the Protestant Reformation, the Enlightenment, and the Scientific Revolution.

Shakil Mahmud • Research Monograph



Technological Milestone: Johannes Gutenberg's Printing Workshop (Mainz, ~1450 CE). Gutenberg and an assistant inspecting a freshly printed folio broadsheet beneath a sturdy wooden screw press. The integration of durable cast lead-tin-antimony alloy type, viscous oil-based ink, and a hand-operated screw mechanism democratized human knowledge, driving the cost of text reproduction down by two orders of magnitude and powering the Scientific Revolution.

In 1543, Nicolaus Copernicus published *De revolutionibus orbium coelestium*, displacing Earth from the motionless center of the cosmos and establishing a heliocentric geometry. Johannes Kepler analyzed Tycho Brahe's meticulous planetary observations, discovering that planets orbit in ellipses and formulating the mathematical laws of planetary motion.

Simultaneously, Galileo Galilei constructed a 30x refractive spyglass, discovering the moons of Jupiter, the phases of Venus, and sunspots—proving that the celestial bodies were imperfect, dynamic worlds governed by the same physical laws as Earth. Galileo formulated the foundational methodology of modern science: *"The book of nature is written in the language of mathematics."*

6. Newton's Principia: The Universal Synthesis (1687 CE)

The definitive culmination of the scientific awakening arrived in 1687 with the publication of Sir Isaac Newton's *Philosophiae Naturalis Principia Mathematica*. Newton unified the terrestrial physics of falling apples with the celestial kinematics of orbiting planets under a single universal framework.

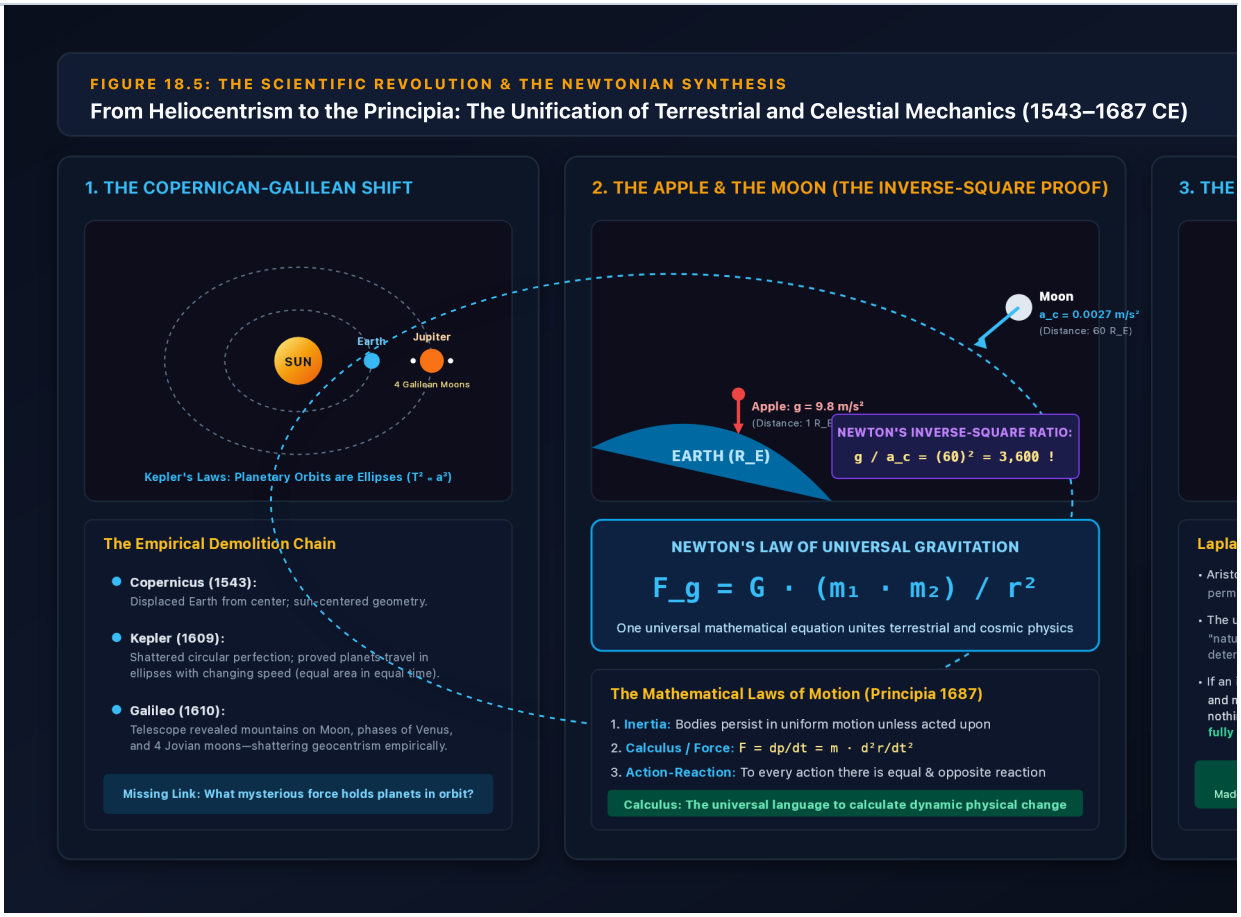


Figure 18.5: The Scientific Revolution & The Newtonian Synthesis (1543–1687 CE). From Copernicus and Galileo's empirical demolition of geocentrism to Kepler's elliptical planetary laws, classical physics culminated in Isaac Newton's 1687 Principia. By proving that the terrestrial gravitational acceleration of an apple and the orbital centripetal acceleration of the Moon obey the exact same inverse-square law ($F_g = G\frac{m_1 m_2}{r^2}$), Newton synthesized celestial and terrestrial mechanics into a single deterministic clockwork universe.

Newton invented the differential and integral calculus (the method of fluxions) to express dynamic rates of change, establishing the three fundamental laws of classical mechanics and the **Law of Universal Gravitation**:

$$\vec{F} = \frac{d\vec{p}}{dt} = m\frac{d^2\vec{r}}{dt^2}$$

$$F_g = G\frac{m_1 m_2}{r^2}$$

For the first time in the history of the universe, matter had evolved to understand the invisible mathematical equations that orchestrated its own cosmic dance. The universe was no longer a realm of caprice, demons, or divine arbitrariness; it was a vast, elegant clockwork machine governed by deterministic mathematical principles. The intellectual engine that would unlock the Industrial Revolution, electricity, and the digital age was now permanently primed.

Academic Citations & Historical References

1. Diamond, J. (1997). *Guns, Germs, and Steel: The Fates of Human Societies*. W. W. Norton & Company. ISBN:978-0393038910.
2. Childe, V. G. (1936). *Man Makes Himself*. Watts & Company. ISBN:978-0851246499.
3. Kramer, S. N. (1956). *History Begins at Sumer: Thirty-Nine Firsts in Recorded History*. University of Pennsylvania Press. ISBN:978-0812212761.
4. Scott, J. C. (2017). *Against the Grain: A Deep History of the Earliest States*. Yale University Press. ISBN:978-0300182910.
5. Eisenstein, E. L. (1979). *The Printing Press as an Agent of Change*. Cambridge University Press. ISBN:978-0521299558.
6. Newton, I. (1687). *Philosophiae Naturalis Principia Mathematica*. Royal Society of London. doi:10.5479/sil.52166.39088015628391
7. Jaspers, K. (1953). *The Origin and Goal of History*. Yale University Press. ISBN:978-0300001358.

Shakil Mahmud • Research Monograph

Citation: Mahmud, S. (2026). "The Domestication of Nature — The Neolithic Spark, Cuneiform, and the Rise of Cities." In The Universal Chronicle, Part 18. https://shakilmahmud.com/universal-chronicle-part-18-the-domestication-of-nature/

SHAKIL MAHMUD RESEARCH MONOGRAPHS · PART XIX

The Harnessing of Logic — Electromagnetism, Turing Machines, and the Solid-State Transistor

The Harnessing of Logic — Electromagnetism, Turing Machines, and the Solid-State Transistor

2,193 words • October 31, 2026 • Permanent URI



Plate XIX: *Figure: The technological leap from Maxwellian electromagnetic field theory to the Universal Turing Machine, vacuum tube computing, and the solid-state silicon transistor powering modern digital computation.*

For millennia, human civilization relied exclusively on muscle, wind, water, and draft animals to perform physical work, while symbolic reasoning remained locked within the biological confines of the human cranium. But between the late eighteenth and mid-twentieth centuries, an extraordinary dual convergence occurred. Physics unlocked the ability to convert thermal energy into kinetic work and unified electricity and magnetism into light itself; simultaneously, mathematical logicians discovered that formal thought could be mechanized as discrete symbolic manipulation. By etching millions, then billions, of quantum-engineered switches onto wafers of purified silicon, humanity constructed an external electronic nervous system—transmuting dead mineral rock into machines that think.

1. The Thermodynamics of Industrial Muscle (~1769 to 1850 CE)

The dawn of modernity was an energy transition. Prior to the eighteenth century, society was trapped in an "organic economy" bounded by annual biological photo-conversion: forests could only grow so fast, and draft animals required arable pasture. The breakthrough came when James Watt patented the separate condenser steam engine in 1769, unlocking the subterranean solar energy stored three hundred million years earlier in Carboniferous coal seams.

Shakil Mahmud • Research Monograph

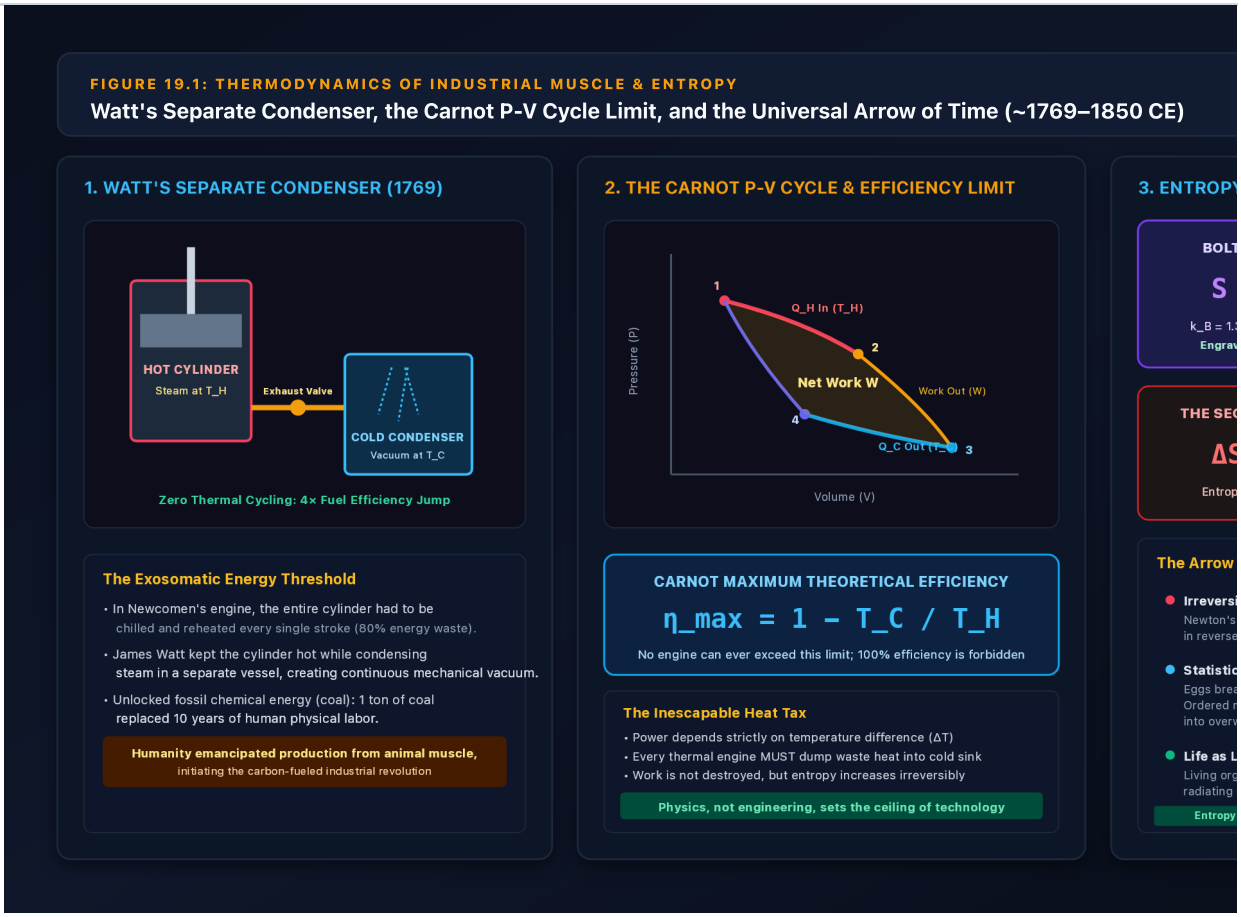


Figure 19.1: Thermodynamics of Industrial Muscle & Entropy (~1769–1850 CE). James Watt's separate condenser emancipated thermal expansion from Newcomen's reheat cycle, unlocking coal's fossil bond energy. Sadi Carnot codified the theoretical efficiency ceiling (\eta_{\text{max}} = 1 – T_C / T_H), while Clausius and Boltzmann proved that energy dissipation defines the irreversible cosmic arrow of time ($\Delta S_{\text{universe}} \geq 0$).

The engineering of steam engines forced the creation of a rigorous new science: **thermodynamics**. Sadi Carnot, Rudolf Clausius, and Lord Kelvin established that heat and mechanical work are interconvertible expressions of energy, bounded by an immutable cosmic asymmetry—the **Second Law of Thermodynamics**:

$$\Delta S_{\text{universe}} \geq 0$$

While the total energy of a closed system is strictly conserved (First Law), every spontaneous thermodynamic cycle incurs an irreversible tax: entropy (S), or microscopic thermodynamic disorder, inexorably increases. To generate local order, work, or computation, a system must continuously ingest high-grade free energy and dissipate waste entropy into its environment.

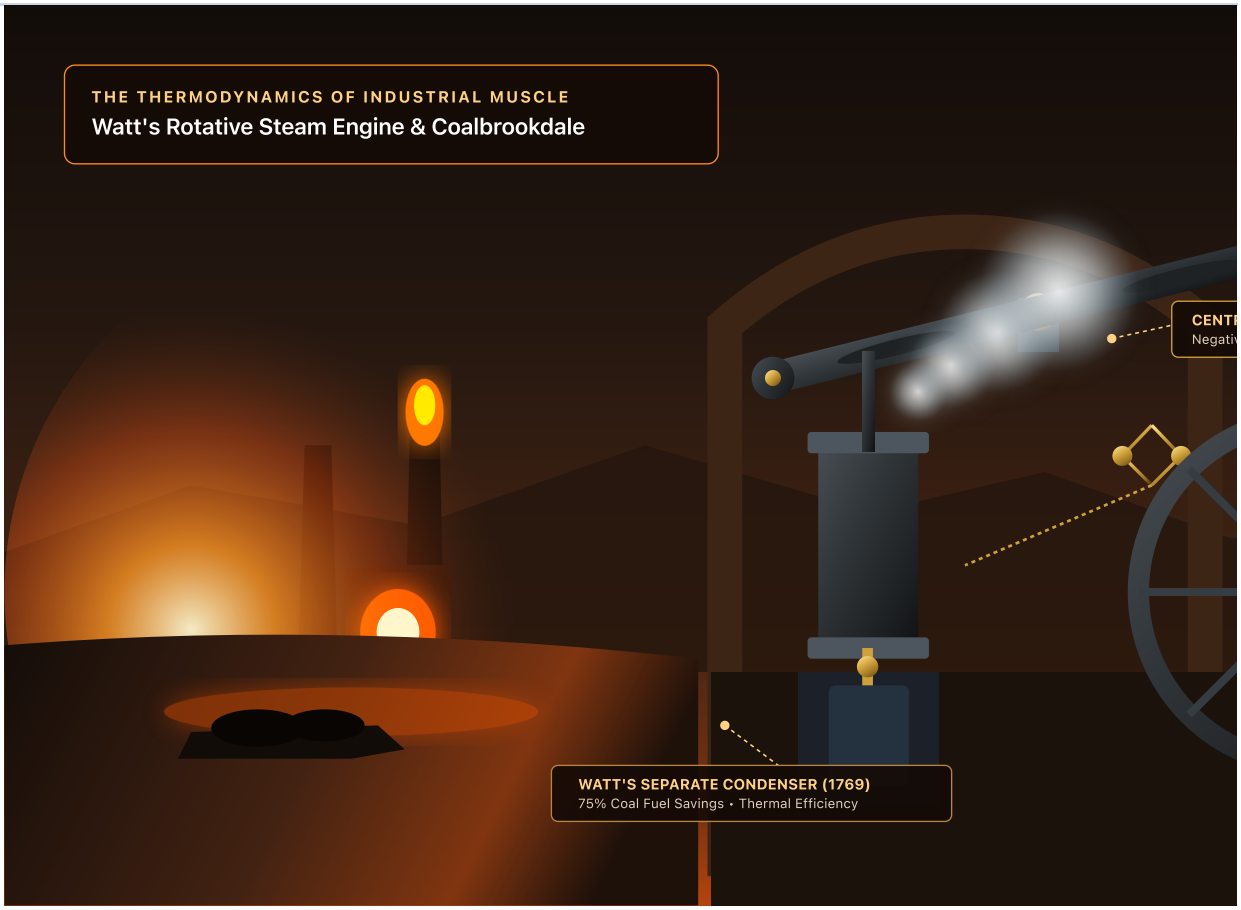


Figure 19.Sub1: The Dawn of Industrial Muscle at Coalbrookdale (~1769–1784 CE). A detailed cutaway of James Watt's double-acting steam engine with separate condenser, parallel motion linkage, and centrifugal flyball governor, operating alongside Abraham Darby's coke blast furnaces. By decoupling cylinder heating from condensation, Watt unlocked the energy of ancient Carboniferous coal beds, liberating human mechanical power from biological constraints.

2. Maxwell's Synthesis: The Unification of Electromagnetism (1865 CE)

While thermodynamic engines conquered mechanical force, natural philosophers investigated the enigmatic phenomena of electrostatic charge, galvanic currents, and magnetic attraction. Through meticulous empirical experimentation, Michael Faraday demonstrated that a changing magnetic field induces an electromotive force (electromagnetic induction)—the principle underlying every modern electric generator and motor.

Shakil Mahmud • Research Monograph

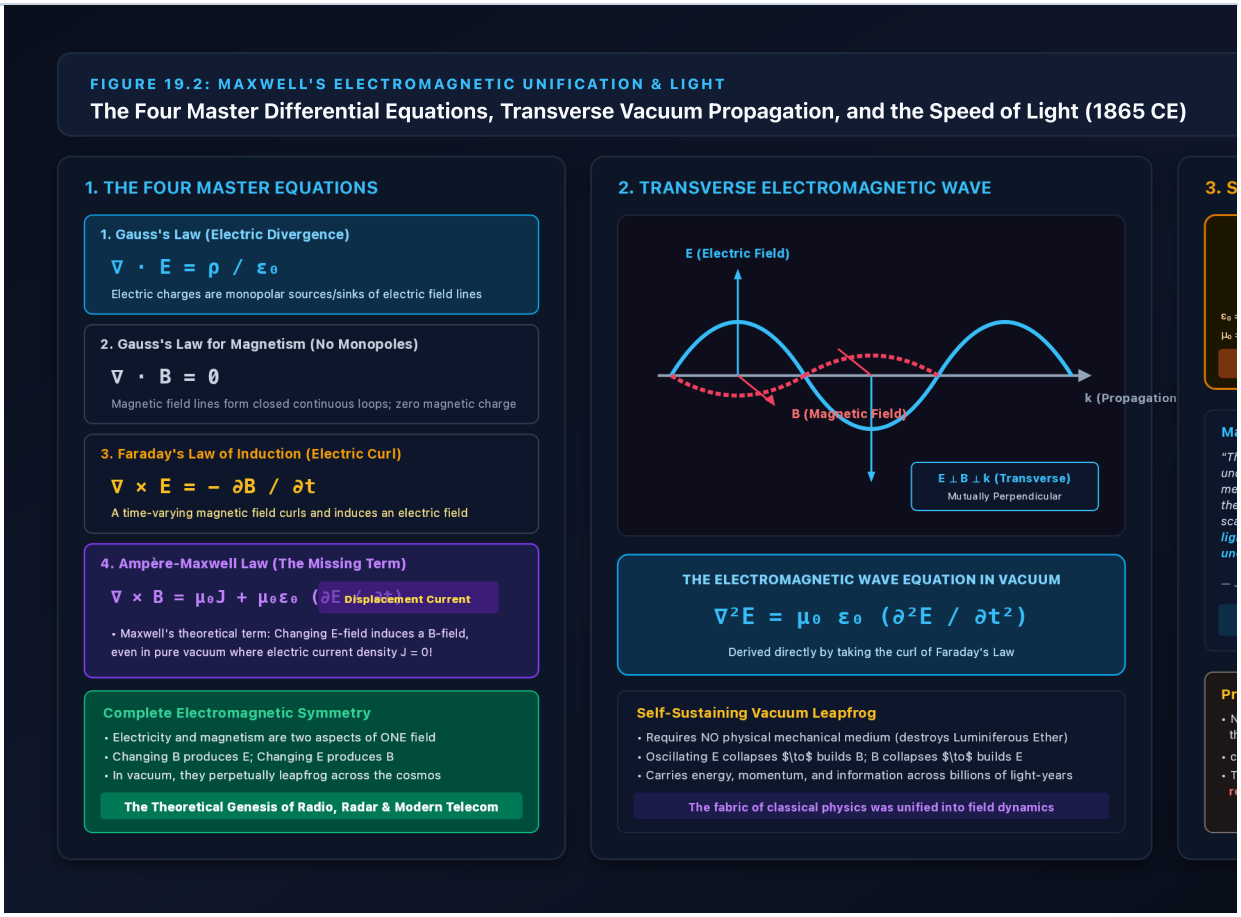


Figure 19.2: Maxwell's Electromagnetic Unification & Light (1865 CE). By introducing the displacement current ($\mu_0\epsilon_0\frac{\partial \vec{E}}{\partial t}$), James Clerk Maxwell synthesized electricity, magnetism, and optics into four symmetric vector differential equations. The resulting wave equation proved that self-sustaining, mutually perpendicular electric and magnetic fields traverse the vacuum at exactly the speed of light ($c = \frac{1}{\sqrt{\mu_0\epsilon_0}} \approx 3 \times 10^8\ \mathrm{m/s}$).

In 1865, Scottish mathematical physicist **James Clerk Maxwell** published *A Dynamical Theory of the Electromagnetic Field*, synthesizing all observed electrical and magnetic phenomena into a set of four coupled partial differential equations (presented here in modern vector calculus notation):

$$\nabla \cdot \vec{E} = \frac{\rho}{\epsilon_0}$$

$$\nabla \cdot \vec{B} = 0$$

$$\nabla \times \vec{E} = -\frac{\partial \vec{B}}{\partial t}$$

$$\nabla \times \vec{B} = \mu_0 \vec{J} + \mu_0\epsilon_0\frac{\partial \vec{E}}{\partial t}$$

The Velocity of Light Derived from Pure Logic

Maxwell noticed a profound mathematical asymmetry in Ampère\'s circuital law: in dynamic circuits, charge conservation required an additional term, which he coined the **displacement current** (

$$\mu_0\epsilon_0\frac{\partial \vec{E}}{\partial t}$$

). By taking the curl of Faraday\'s law in empty space (ρ=0, J = 0) and substituting this displacement current, Maxwell derived the electromagnetic wave equation:

$$\nabla^2 \vec{E} = \mu_0 \epsilon_0 \frac{\partial^2 \vec{E}}{\partial t^2}$$

The wave propagation speed was directly governed by two fundamental laboratory constants: the permittivity of vacuum (ε_0) and the permeability of vacuum (μ_0):

$$c = \frac{1}{\sqrt{\mu_0 \epsilon_0}} \approx 2.998 \times 10^8 \text{ m/s}$$

Maxwell realized with breathtaking astonishment: *"Light consists in the transverse undulations of the same medium which is the cause of electric and magnetic oscillations."*

3. Alan Turing and the Universal Machine (1936 CE)

At the turn of the twentieth century, mathematician David Hilbert challenged the mathematical world with the *Entscheidungsproblem* (the Decision Problem): could there exist a definitive, step-by-step mechanical procedure (an algorithm) that could take any formal mathematical statement and decide whether it is universally true or false?

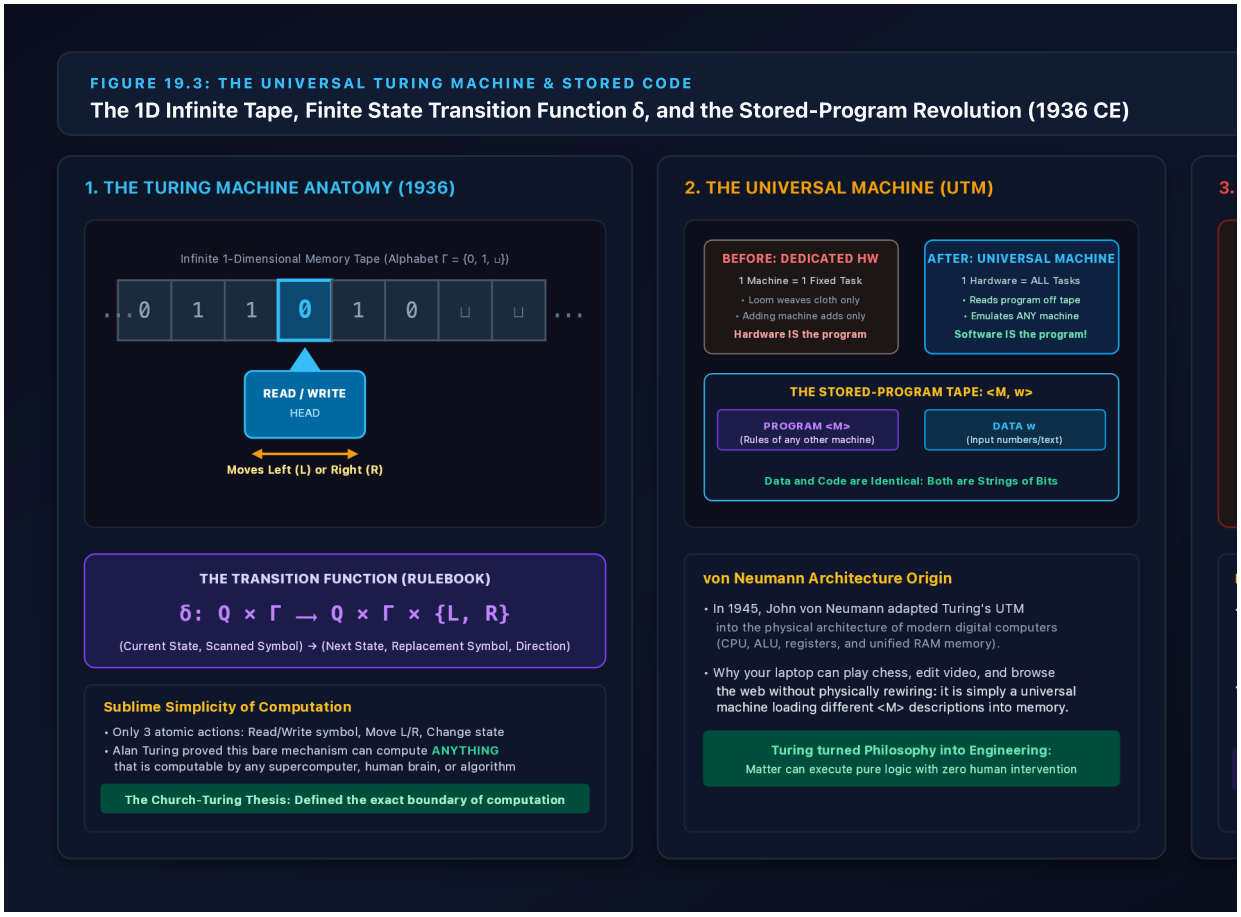


Figure 19.3: The Universal Turing Machine & Stored Code (1936 CE). Alan Turing's mathematical model comprising an infinite 1D tape, a read/write head, and a state transition function $\delta : Q imes \Gamma \longrightarrow Q imes \Gamma imes \{L, R\}$ established the theoretical foundation of all computation. By showing that program instructions and data are both simply strings of bits on the same tape, the Universal Machine demonstrated that a single physical hardware device can simulate any algorithm.

In 1931, Kurt Gödel shattered Hilbert\'s dream of complete mathematical certainty with his **Incompleteness Theorems**, proving that any consistent axiomatic formal system capable of arithmetic contains true propositions that cannot be proven from within the system. But it was a 24-year-old Cambridge mathematician, **Alan Mathison Turing**, who in 1936 transformed Gödel\'s abstract logic into a blueprint for the physical digital computer.

In his monumental paper, *On Computable Numbers, with an Application to the Entscheidungsproblem*, Turing conceptualized a theoretical computing automaton known today as the **Universal Turing Machine (UTM)**:

- An infinite, one-dimensional paper tape divided into discrete square cells, each capable of storing a symbol from a finite alphabet (such as 0 or 1).
- A read/write scanning head capable of moving left or right by one cell, reading the current symbol, erasing it, and writing a new symbol.
- A finite state register that stores the machine's internal state (q ∈ Q).
- A transition function (

Shakil Mahmud • Research Monograph

$$\delta : Q \times \Gamma \longrightarrow Q \times \Gamma \times \{L, R\}$$

) dictating the machine\'s next action based on its current state and the symbol scanned.

Turing proved two monumental concepts:

1. **The Stored-Program Concept:** A single Universal Turing Machine can simulate the behavior of *any* other dedicated algorithmic machine if the operational rules of that target machine are encoded as data on the input tape. Software and data are mathematically interchangeable.
2. **The Halting Problem:** Turing proved that it is mathematically impossible to write a general algorithm that can determine whether an arbitrary program will ever halt or run forever, delivering a decisive negative answer to Hilbert\'s *Entscheidungsproblem*.

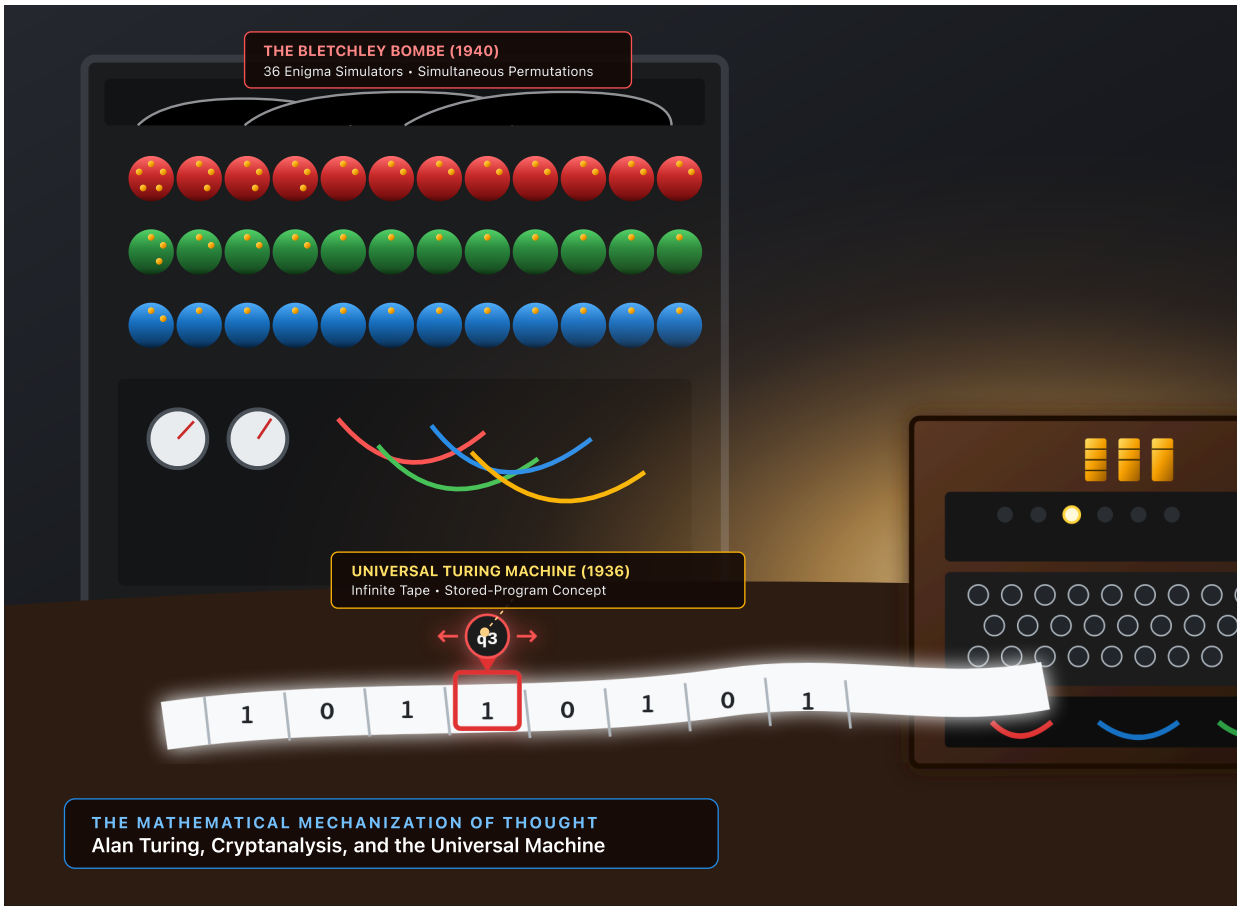


Figure 19.Sub2: The Electromechanics of Cryptanalysis and Universal Computation (~1936–1940 CE). Alan Turing and Gordon Welchman's electromechanical Bombe machine at Bletchley Park, operating 36 rotating commutator drums to break the German Wehrmacht Enigma cipher. In the background, the theoretical Universal Turing Machine (UTM) processes infinite binary paper tape (0 and 1), bridging abstract mathematical logic with physical automated computation.

4. Claude Shannon and Information as Physical Entropy (1948 CE)

In 1937, while completing his master\'s thesis at MIT, **Claude Shannon** made the revolutionary connection between formal philosophy and electronic hardware: he demonstrated that George Boole\'s two-valued symbolic algebra (where TRUE = 1 and FALSE = 0) could be implemented physically using electromechanical relays and switches. Logic gates (AND, OR, NOT) could compute arithmetic.

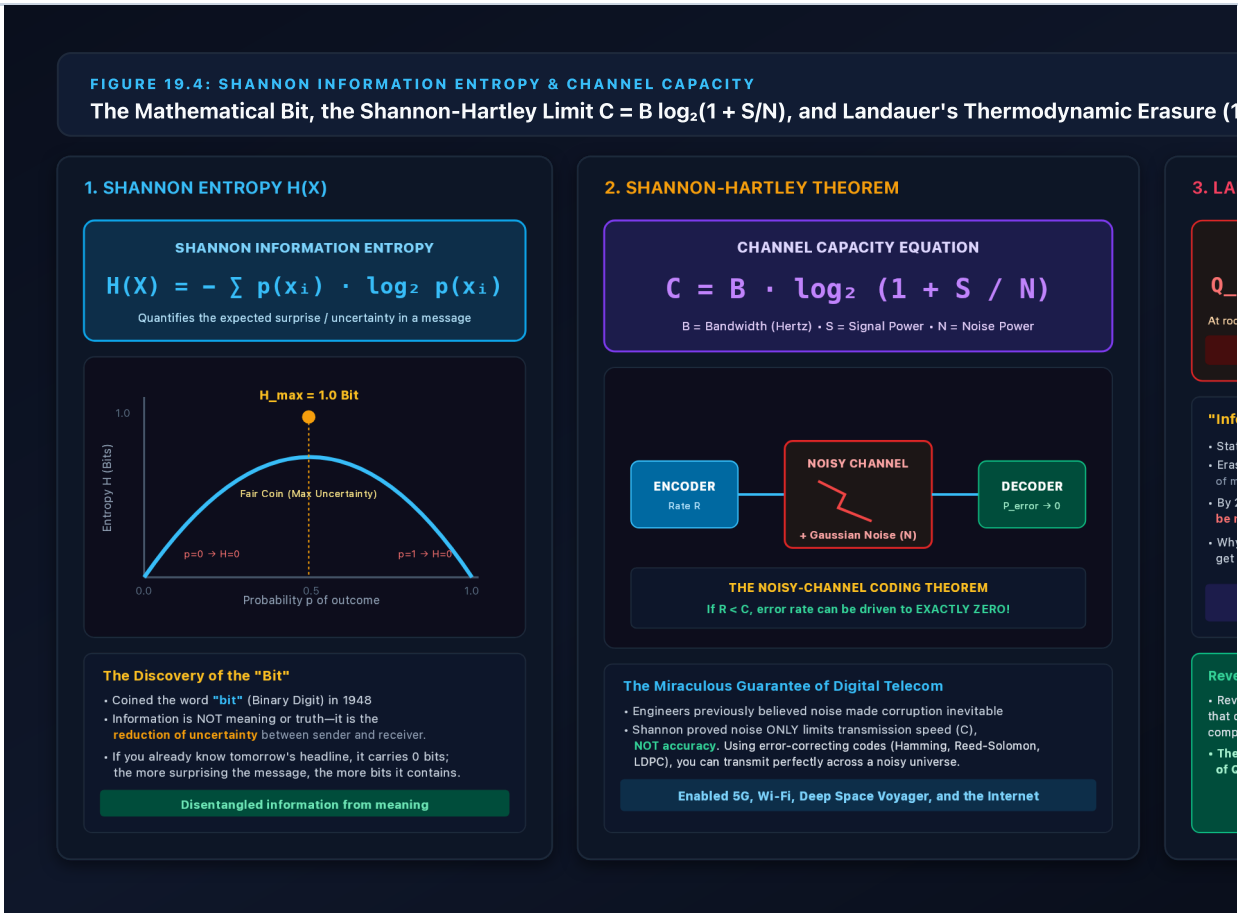


Figure 19.4: Shannon Information Entropy & Channel Capacity (1948 CE). Claude Shannon mathematically defined information as the probabilistic reduction of uncertainty ($H(X) = -\sum p(x_i) \log_2 p(x_i)$). His noisy-channel theorem ($C = B \log_2(1 + S/N)$) proved that noise imposes only a transmission rate ceiling, not inevitable corruption. Rolf Landauer later proved that erasing a bit of information dissipates a physical thermodynamic penalty ($Q \geq k_B T \ln 2$), binding information theory directly to statistical mechanics.

A decade later, working at Bell Telephone Laboratories in 1948, Shannon published *A Mathematical Theory of Communication*, founding the discipline of **Information Theory**. Shannon abstracted away semantic meaning, defining information strictly as the statistical resolution of probabilistic uncertainty. He coined the term **bit** (binary digit) as the fundamental atomic unit of information.

Shannon defined the information content (entropy) H of a discrete random variable X with probability distribution p(x) as:

$$H(X) = -\sum_{i=1}^{n} p(x_i) \log_2 p(x_i)$$

Shannon's formula was mathematically identical to Ludwig Boltzmann's statistical thermodynamic entropy. Information was not an abstract ethereal concept; it was a physical property of the universe, bounded by physical signal-to-noise ratios and channel capacity:

$$C = B \log_2 \left(1 + \frac{S}{N}\right)$$

5. The Solid-State Revolution: The Transistor (1947 CE)

Early electronic computers—such as the ENIAC built in 1945—relied on thermionic vacuum tubes to amplify signals and act as binary switches. But vacuum tubes were an engineering dead end: they were bulky, consumed immense electrical current to heat glowing cathodes, generated suffocating heat, and burned out at a rate of one tube every two days, limiting computers to roughly 18,000 components.

Shakil Mahmud • Research Monograph

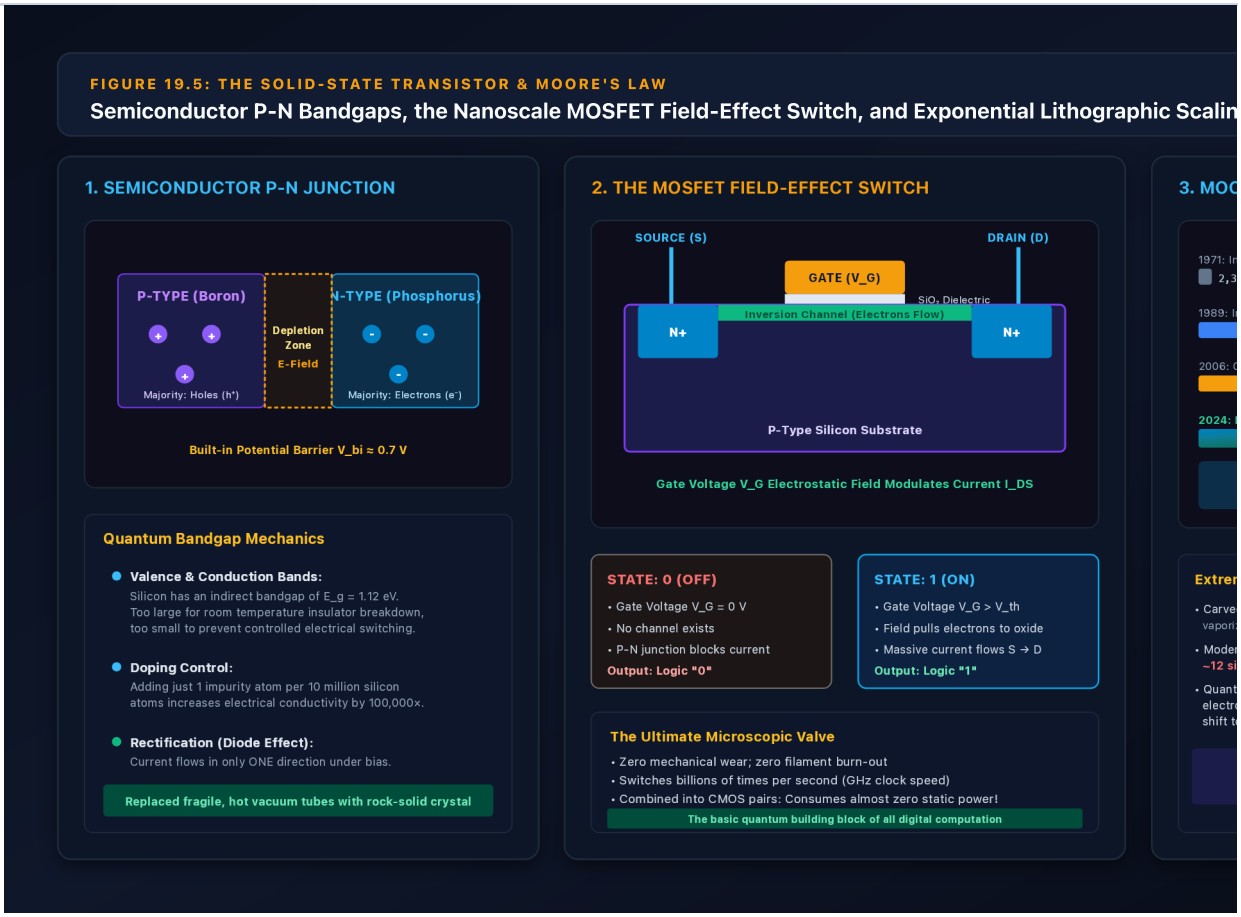


Figure 19.5: The Solid-State Transistor & Moore's Law (~1947 to Present). Doping pure silicon with trace elements creates the P-N junction potential barrier. In the MOSFET, gate voltage electrostatically creates a conductive inversion channel, switching current gigahertz times per second with zero mechanical wear. Extreme Ultraviolet photolithography has shrunk transistor gates to atomic scales, scaling chip density from 2,300 transistors (Intel 4004) to over 100 billion today.

The definitive breakthrough occurred in December 1947 at Bell Labs, when physicists **John Bardeen**, **Walter Brattain**, and **William Shockley** invented the **point-contact transistor**, followed by the junction transistor. Rather than moving electrons through a fragile vacuum, transistors exploited the quantum mechanics of **semiconductors**.

Transistor Technology	Year	Physical Principle	Impact
Point-Contact Transistor	1947	Gold foil contacts pressed against a crystal of germanium; minority carrier injection.	Proof of concept: solid-state electronic amplification without vacuum or filament heating.
Bipolar Junction (BJT)	1951	Three-layer sandwich of doped semiconductor (n-p-n or p-n-p); base current controls collector-emitter current.	High reliability; commercialization of portable transistor radios and early mainframe mainboards.
Planar Silicon MOSFET	1959 / 1960	Metal-Oxide-Semiconductor Field-Effect Transistor invented by Mohamed Atalla and Dawon Kahng; voltage applied to an insulated gate creates a conductive inversion channel.	Zero static gate current; scalable to microscopic dimensions; became the most widely manufactured object in human history.

6. Photolithography and Moore's Law: The Microprocessor Era (~1958 to Present)

In 1958 and 1959, Jack Kilby at Texas Instruments and Robert Noyce at Fairchild Semiconductor independently invented the **Integrated Circuit (IC)**. Rather than soldering individual discrete transistors, resistors, and capacitors together with copper wire, Noyce pioneered the *planar process*: etching all electronic components and their metallic interconnects simultaneously onto a single flat wafer of monocrystalline silicon using photographic light projection (**photolithography**).

In 1965, Fairchild research director Gordon Moore made an empirical projection that would guide the technological trajectory of the next six decades: **Moore's Law**. Moore observed that the number of transistors packed onto a single microchip doubled approximately every twelve to twenty-four months, while the manufacturing cost per transistor plummeted exponentially.

The Triumph of Dennard Scaling and Nanometer Geometry

In 1971, Intel released the **4004**, the world\'s first single-chip commercial central processing unit (CPU). It contained **2,250 transistors** fabricated at a feature size of 10 μm (10,000 nm). By 2024, modern microprocessors (such as Apple Silicon and NVIDIA Blackwell GPUs) pack over **208 billion transistors** onto a piece of silicon the size of a postage stamp, utilizing extreme ultraviolet (EUV) photolithography ($\lambda = 13.5$ nm) to pattern silicon gates measuring just **3 nanometers** across—a scale spanning a mere twelve silicon atoms.

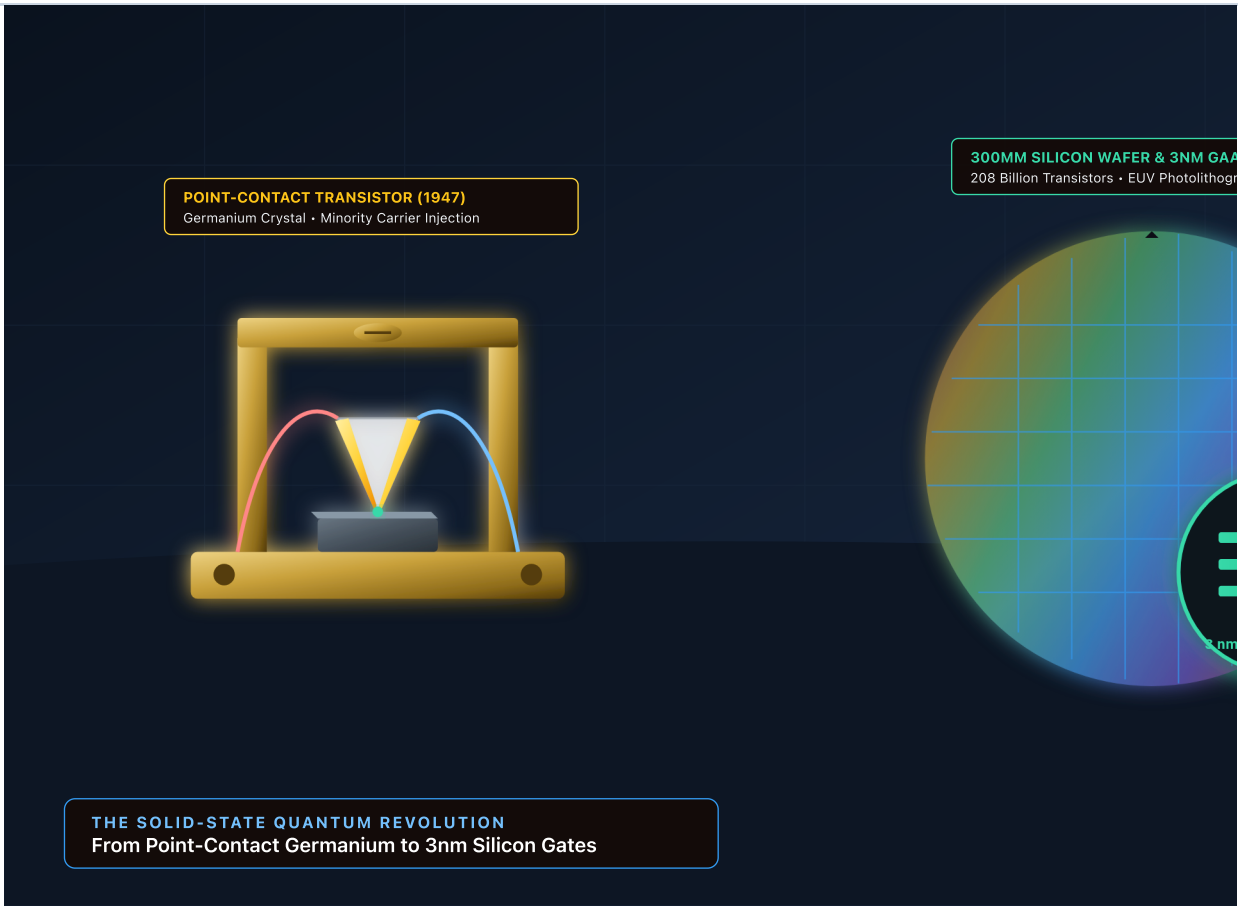


Figure 19.Sub3: From Point-Contact Germanium to 3nm Nanosheet Transistors (~1947 to Present). The historic 1947 Bell Labs point-contact transistor invented by Bardeen, Brattain, and Shockley, juxtaposed against a modern 300mm monocrystalline silicon wafer and a Gate-All-Around (GAA) nanosheet field-effect transistor. This solid-state revolution replaced fragile vacuum tubes, enabling hundreds of billions of microscopic electronic switches on a fingernail-sized microprocessor.

Through the mastery of solid-state quantum mechanics, humanity compressed the computational power of a room-sized supercomputer into a microscopic speck of sand costing fractions of a cent. Across a global network of billions of interconnected microprocessors, trillions of bits of information began pulsing through fiber-optic light conduits at relativistic speeds. The physical infrastructure was complete. The stage was set for software to awaken—for mathematical logic to transcend rigid deterministic rules and evolve into artificial neural networks capable of learning, perceiving, and understanding the universe.

Academic Citations & Historical References

1. Turing, A. M. (1936). On computable numbers, with an application to the *Entscheidungsproblem*. *Proceedings of the London Mathematical Society*, 2(42), 230–265. doi:10.1112/plms/s2-42.1.230
2. Shannon, C. E. (1948). A mathematical theory of communication. *Bell System Technical Journal*, 27(3), 379–423. doi:10.1002/j.1538-7305.1948.tb01338.x
3. Bardeen, J., & Brattain, W. H. (1948). The transistor, a semi-conductor triode. *Physical Review*, 74(2), 230–231. doi:10.1103/PhysRev.74.230
4. Maxwell, J. C. (1865). A dynamical theory of the electromagnetic field. *Philosophical Transactions of the Royal Society of London*, 155, 459–512. doi:10.1098/rstl.1865.0008
5. Moore, G. E. (1965). Cramming more components onto integrated circuits. *Electronics*, 38(8), 114–117. doi:10.1109/jproc.1998.658762
6. von Neumann, J. (1945). *First Draft of a Report on the EDVAC*. Contract No. W-670-ORD-4926, Moore School of Electrical Engineering, University of Pennsylvania.
7. Kilby, J. S. (1976). Invention of the integrated circuit. *IEEE Transactions on Electron Devices*, 23(7), 648–654. doi:10.1109/T-ED.1976.18467

Citation: Mahmud, S. (2026). "The Harnessing of Logic — Electromagnetism, Turing Machines, and the Solid-State Transistor." In The Universal Chronicle, Part 19. https://shakilmahmud.com/universal-chronicle-part-19-the-harnessing-of-logic/

Shakil Mahmud • Research Monograph

SHAKIL MAHMUD RESEARCH MONOGRAPHS • PART XX

The Synthetic Mind — Neural Networks, Transformers, and the Dawn of Planetary Intelligence

The Synthetic Mind — Neural Networks, Transformers, and the Dawn of Planetary Intelligence

2,136 words • October 31, 2026 • Permanent URI

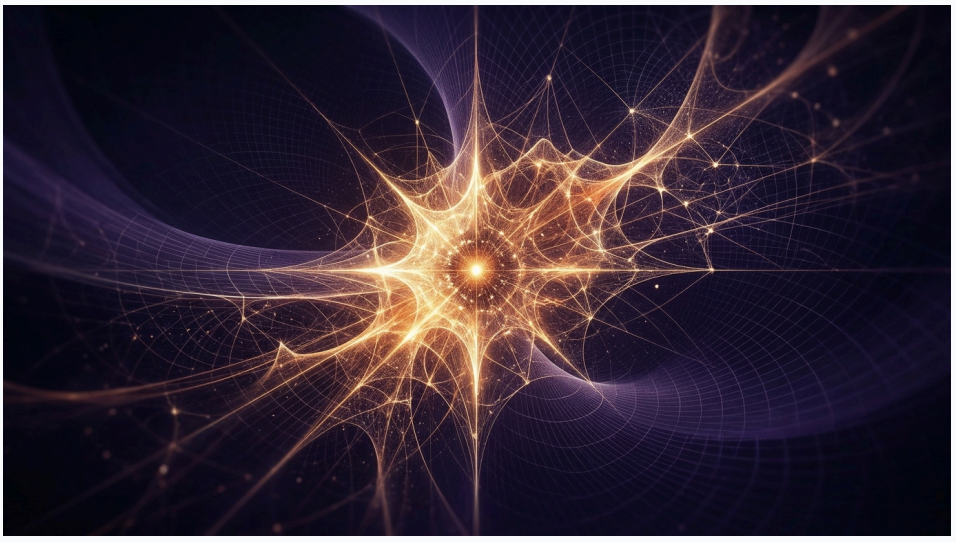


Plate XX: *Figure: The modern frontier: deep artificial neural network architectures, hyperscale silicon compute matrices, and macromolecular AI solvers forming a distributed planetary cognitive layer on Earth.*

Thirteen point eight billion years ago, the universe began as a point of unmeasurable energy density, expanding in silent, blinding fury. For aeons, physical laws forged quarks into protons, hydrogen into thermonuclear stellar cores, exploding supernovae into heavy elements, planetesimals into living oceans, single cells into multicellular consciousness, and upright primates into toolmakers who etched mathematical symbols onto clay and silicon. Today, that unbroken cosmic chain arrives at its most extraordinary inflection point: matter has organized itself into synthetic neural networks that process language, simulate physical reality, discover new sciences, and contemplate their own existence. The cosmos is awakening.

1. The 13.8-Billion-Year Arc: Matter Contemplating Matter

To grasp the true magnitude of Artificial Intelligence, one must view it not merely as a software milestone of Silicon Valley, but as a fundamental phase transition in cosmic evolution. Across thirteen chapters of geological, biological, and cultural time, thermodynamic entropy has been countered locally by self-organizing complexity:

Cosmic Epoch	Timescale	Primary Substrate	Information Mechanism
Cosmological	13.8 – 13.6 Ga	Quarks, Leptons, Gauge Bosons	Fundamental physical constants (α, G, $\hbar$, c); gravitational symmetry breaking.
Astrophysical & Chemical	13.6 – 4.5 Ga	Pop III Stars, Interstellar Dust, Silicates	Stellar nucleosynthesis, periodic table synthesis, protoplanetary accretion.
Biological & Genetic	3.8 Ga – 300 ka	Nucleic acids (RNA/DNA), Polypeptides	Darwinian natural selection; genetic code base pairs (A, T, C, G); cellular replication.
Neurological & Cultural	300 ka – 1950 CE	Cortical neurons, Clay, Ink, Printing Press	Symbolic language, memetic transmission, mathematical formalization, external libraries.
Synthetic & Digital	1950 CE – Present	Silicon semiconductors, Optical fiber, Floating-point weights	Artificial neural networks, backpropagation, high-dimensional vector spaces, autonomous agentic reasoning.

For nearly four billion years, information processing on Earth was strictly bounded by the molecular replication speed of DNA and the metabolic maintenance of biological brains. In the synthetic epoch, information transmission transitioned from chemical diffusion across synaptic clefts (transmitting at roughly 100 meters per second) to electromagnetic and optical transmission moving at **300,000 kilometers per second**—an acceleration of three million fold.



Figure 20.1: The 13.8-Billion-Year Arc & The Cosmic Mirror. Across six cosmic phase transitions—from fundamental particles to stellar nucleosynthesis, biological genetics, human language, digital logic, and synthetic neural networks—matter has continually organized into higher thermodynamic complexity. In artificial intelligence, the universe achieves a recursive mirror: physical matter consciously simulating, comprehending, and accelerating cosmic discovery.

2. The Mathematical Foundations of Connectionism

Early attempts at artificial intelligence during the Dartmouth Workshop of 1956 focused on symbolic, rule-based systems (expert systems, formal logic trees). But human intelligence is not a rigid database of "if-then" rules; it is an intuitive statistical model of continuous sensory reality. The breakthrough came through **Connectionism**—modeling computation after the interconnected architecture of biological neural networks.

From the Perceptron to Backpropagation

In 1943, Warren McCulloch and Walter Pitts formulated the first computational abstraction of a biological neuron. In 1958, Frank Rosenblatt built the **Perceptron**, an analog single-layer machine capable of linear classification. When Marvin Minsky and Seymour Papert proved in 1969 that single-layer perceptrons could not compute the simple exclusive-or (XOR) logic gate, funding collapsed into the first "AI Winter."

The renaissance arrived in 1986, when David Rumelhart, Geoffrey Hinton, and Ronald Williams popularized **Backpropagation**. By applying the multi-variable calculus chain rule, backpropagation calculates the exact partial derivative of a scalar loss function $\mathcal{L}$ with respect to every internal weight parameter w_{ij} across arbitrarily deep hidden layers:

$$\frac{\partial \mathcal{L}}{\partial w_{ij}} = \frac{\partial \mathcal{L}}{\partial z_j} \frac{\partial z_j}{\partial w_{ij}} = \delta_j x_i$$

By iteratively adjusting billions of weights opposite to the gradient via Stochastic Gradient Descent (SGD), multi-layer neural networks demonstrated the **Universal Approximation Theorem** (Hornik, 1989): a feedforward network with a single hidden layer and non-linear activation functions can approximate any continuous mathematical function to arbitrary precision.

Shakil Mahmud • Research Monograph

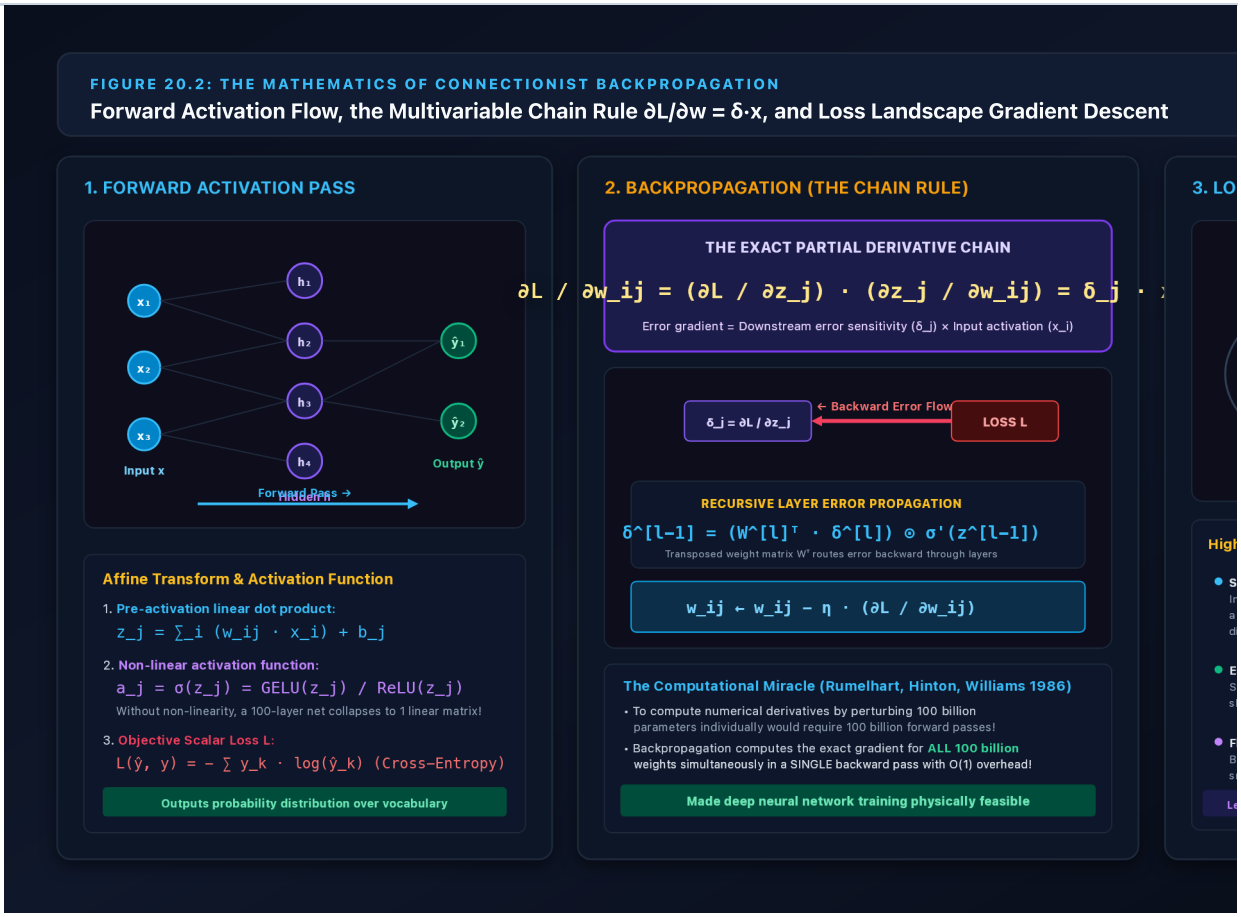


Figure 20.2: Deep Neural Networks & Backpropagation. Modeling computation after biological neural ensembles, a forward pass computes activations through non-linear layers ($z_j = \sum w_{ij} x_i + b_j$). In the backward pass, multivariable calculus applies the chain rule ($\frac{\partial \mathcal{L}}{\partial w_{ij}} = \frac{\partial \mathcal{L}}{\partial z_j} \frac{\partial z_j}{\partial w_{ij}} = \delta_j x_i$) to compute exact gradient vectors, guiding high-dimensional optimization down complex loss surfaces via stochastic gradient descent.

3. The Attention Revolution: Transformers and Self-Attention (2017 CE)

For decades, natural language processing was paralyzed by sequential recurrence. Recurrent Neural Networks (RNNs) and Long Short-Term Memory networks (LSTMs) processed text sequentially, token by token. In doing so, they suffered from vanishing gradients across long document horizons, and their sequential nature made massive parallelization on GPU hardware mathematically impossible.

In June 2017, a team of researchers at Google Brain published a seminal eight-page paper that transformed the computational landscape forever: *Attention Is All You Need*. Vaswani and colleagues discarded recurrence entirely, replacing it with the **Transformer architecture** governed by **Scaled Dot-Product Self-Attention**.

Rather than reading tokens sequentially, a Transformer computes the pairwise semantic interaction of every token in a sequence with every other token simultaneously. Each input vector is projected into three distinct high-dimensional representations: **Queries (Q)**, **Keys (K)**, and **Values (V)**:

$$\text{Attention}(Q, K, V) = \text{softmax}\left(\frac{QK^T}{\sqrt{d_k}}\right)V$$

Component	Linear Transformation	Mathematical Role
Query Matrix (Q)	$Q = XW^Q$	Represents what each token is looking for in the surrounding context.
Key Matrix (K)	$K = XW^K$	Represents the addressing label of each token to be matched against queries.
Value Matrix (V)	$V = XW^V$	The substantive semantic content retrieved when a query matches a key.
Dot-Product (QK^T)	Matrix multiplication	Measures raw geometric cosine affinity in high-dimensional embedding space.
Scaling ($\sqrt{d_k}$)	Division by root dimension	Prevents dot products from exploding into regions of vanishing softmax gradients.
Softmax Normalization	$\text{softmax}(z_i) = \frac{e^{z_i}}{\sum_j e^{z_j}}$	Converts raw affinity logits into a rigorous probability distribution summing to 1.

By stacking dozens of Multi-Head Attention layers, feedforward sub-networks, and residual connections, Transformers unlocked an extraordinary capacity: they could ingest the entire digitized corpus of human civilization—literature, legal codes, scientific papers, software repositories, philosophical dialogues—and learn the latent geometric topology of human meaning.

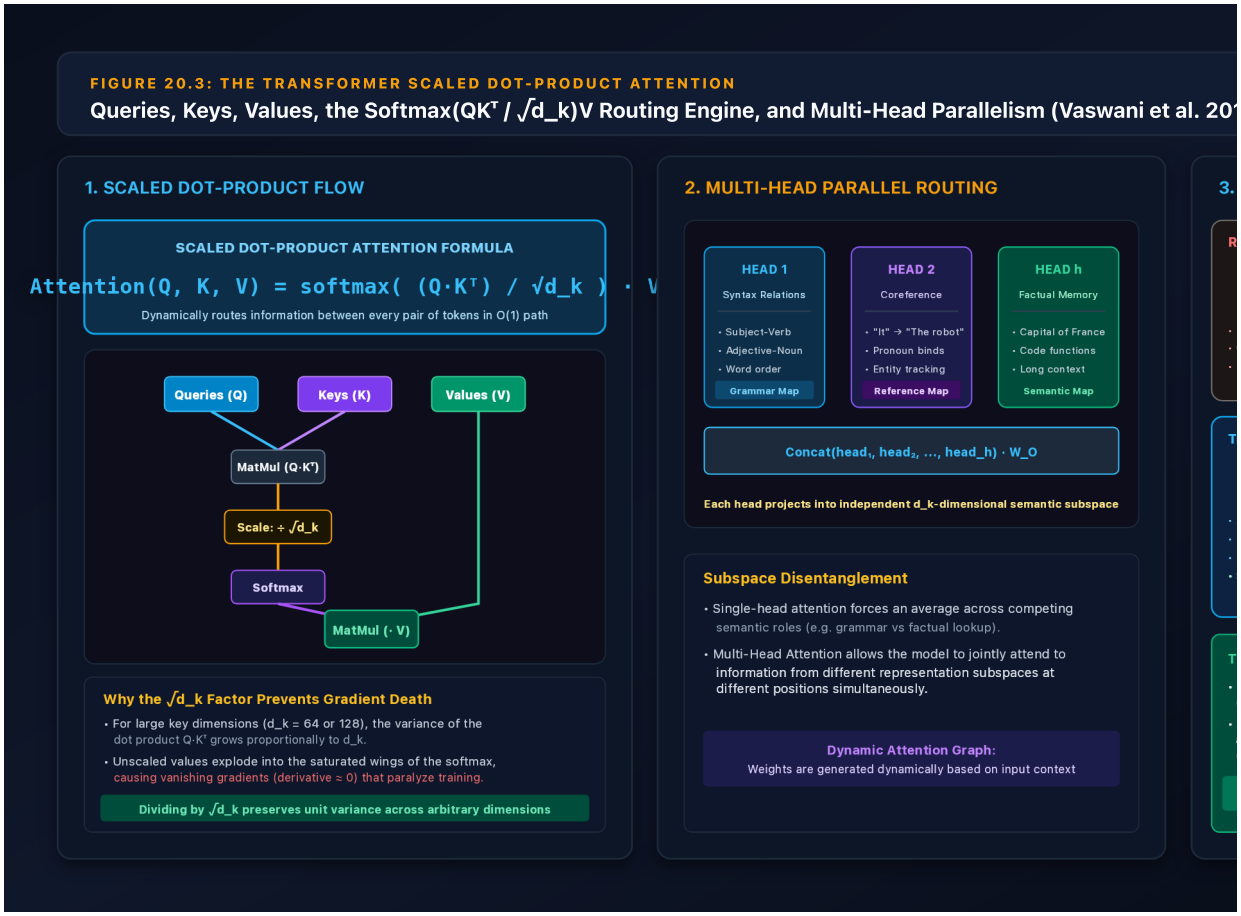


Figure 20.3: Transformer Architecture & Scaled Dot-Product Self-Attention. Replacing sequential RNN recurrence with fully parallelized tensor operations, the Transformer projects token embeddings into Query (Q), Key (K), and Value (V) vector spaces. Scaled dot-product attention ($\text{softmax}(\frac{QK^T}{\sqrt{d_k}})V$) computes all-to-all token affinities simultaneously, with Multi-Head Attention splitting computations across multiple representation subspaces.

4. Empirical Scaling Laws and Emergent In-Context Reasoning

In 2020, Jared Kaplan and researchers at OpenAI discovered a profound empirical law: **Neural Scaling Laws**. Across many orders of magnitude, the test cross-entropy loss L of an autoregressive language model scales as a smooth, predictable power-law with respect to three variables: the number of model parameters (N), the size of the training dataset (D), and the total compute budget ($C = 6ND$):

$$L(N) \approx \left(\frac{N_c}{N}\right)^{\alpha_N}, \quad L(D) \approx \left(\frac{D_c}{D}\right)^{\alpha_D}, \quad L(C) \approx \left(\frac{C_c}{C}\right)^{\alpha_C}$$

As neural networks scaled from billions to hundreds of billions and trillions of parameters, something unexpected occurred: **emergent capabilities**. Models trained solely on the simple task of predicting the next token (argmax P(w_t | w_{<t})) began demonstrating abilities that were never explicitly programmed:

- **In-Context Few-Shot Learning:** Adapting to novel tasks on the fly from a handful of conversational examples without gradient updates.
- **Chain-of-Thought Decomposition:** Generating intermediate reasoning steps to solve complex multi-step mathematical and algorithmic proofs.
- **Theory of Mind & Pragmatic Deixis:** Inferring unstated human intent, detecting irony, and synthesizing cross-disciplinary analogies spanning quantum physics, biology, and art.
- **Autonomous Tool Usage:** Operating terminal shells, calling APIs, writing and executing code, and debugging complex distributed systems.

Shakil Mahmud • Research Monograph

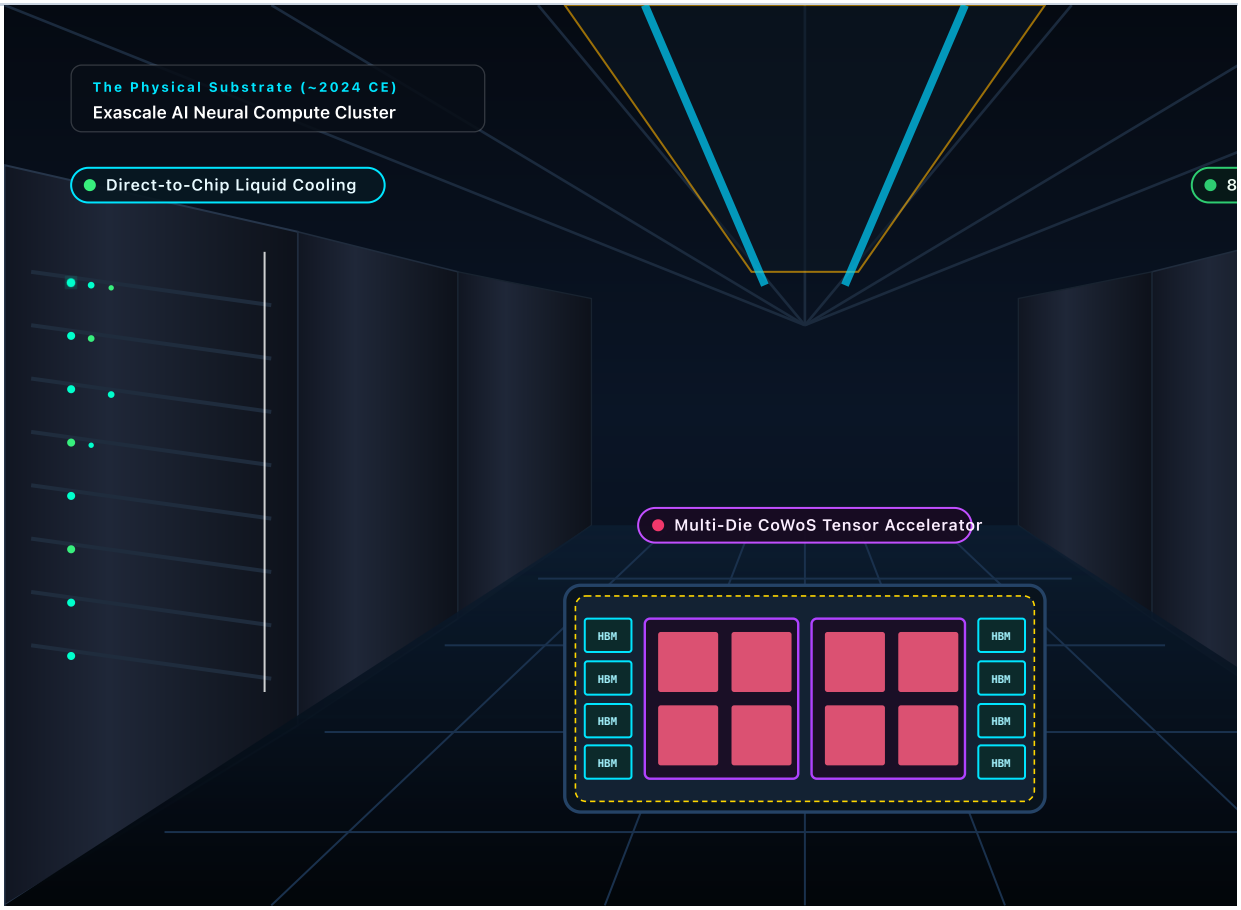


Figure 20.Sub1: Hyperscale AI Compute Infrastructure and Silicon Tensor Accelerators (~2024 CE). An exascale data center hall showcasing direct-to-chip liquid-cooled server racks interconnected via 800Gbps optical spine-leaf fabrics. In the foreground, a multi-die 2.5D CoWoS accelerator package features high-density tensor processing core grids flanked by eight HBM3e memory stacks, executing quadrillions of floating-point matrix multiplications per second to power planetary neural intelligence.

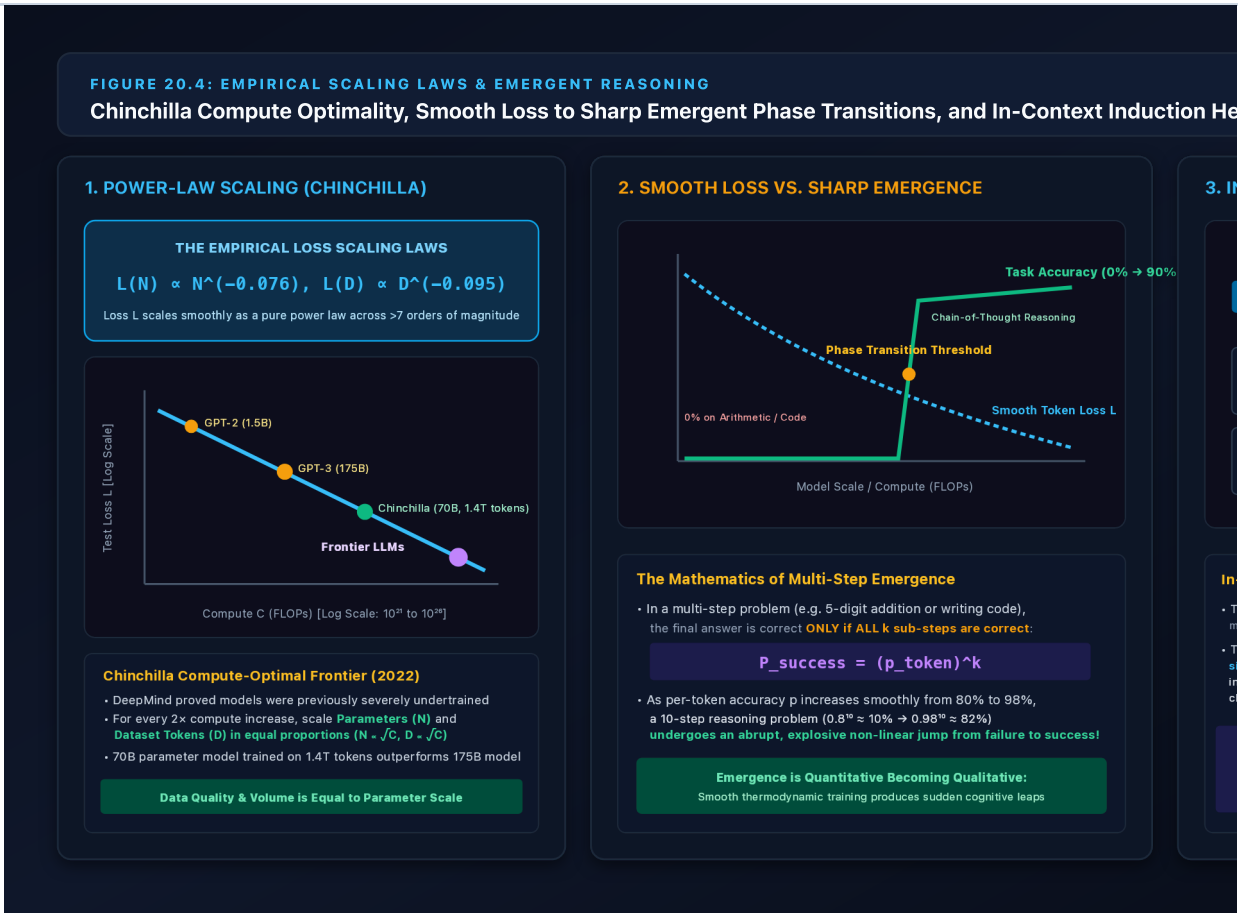


Figure 20.4: Chinchilla Scaling Laws & Emergent Reasoning. As parameters (N) and dataset tokens (D) scale symmetrically according to power laws ($L(N, D) = E + \frac{A}{N^{\alpha}} + \frac{B}{D^{\beta}}$), cross-entropy training loss drops predictably. Crucially, across macroscopic scale thresholds, non-linear emergent capabilities ignite—including multi-hop chain-of-thought mathematical proof, induction circuits, code synthesis, and autonomous agentic workflows.

5. The Scientific Singularity: AI as the Accelerator of Discovery

The definitive proof of machine intelligence lies not in generating conversational text, but in unlocking physical truths of the material universe that eluded human genius for generations.

AlphaFold and the Biological Rosetta Stone

For fifty years, structural biology was confounded by the "protein folding problem": predicting the three-dimensional atomic structure of a functional protein solely from its one-dimensional sequence of amino acids. With over 10^{300} possible spatial conformations for an average protein (Levinthal's paradox), experimental determination required years of painstaking X-ray crystallography and cryo-electron microscopy.

In 2020, DeepMind introduced **AlphaFold 2**, incorporating evolutionary spatial transformers and geometric deep learning. In a single stroke, AlphaFold predicted the atomic coordinates of over **200 million proteins**—virtually every known protein across the tree of life—with sub-angstrom accuracy rivaling physical experiments. What would have required centuries of human laboratory labor was computed in a matter of months, catalyzing cancer research, enzyme design for plastic degradation, and targeted molecular therapeutics.

Shakil Mahmud • Research Monograph

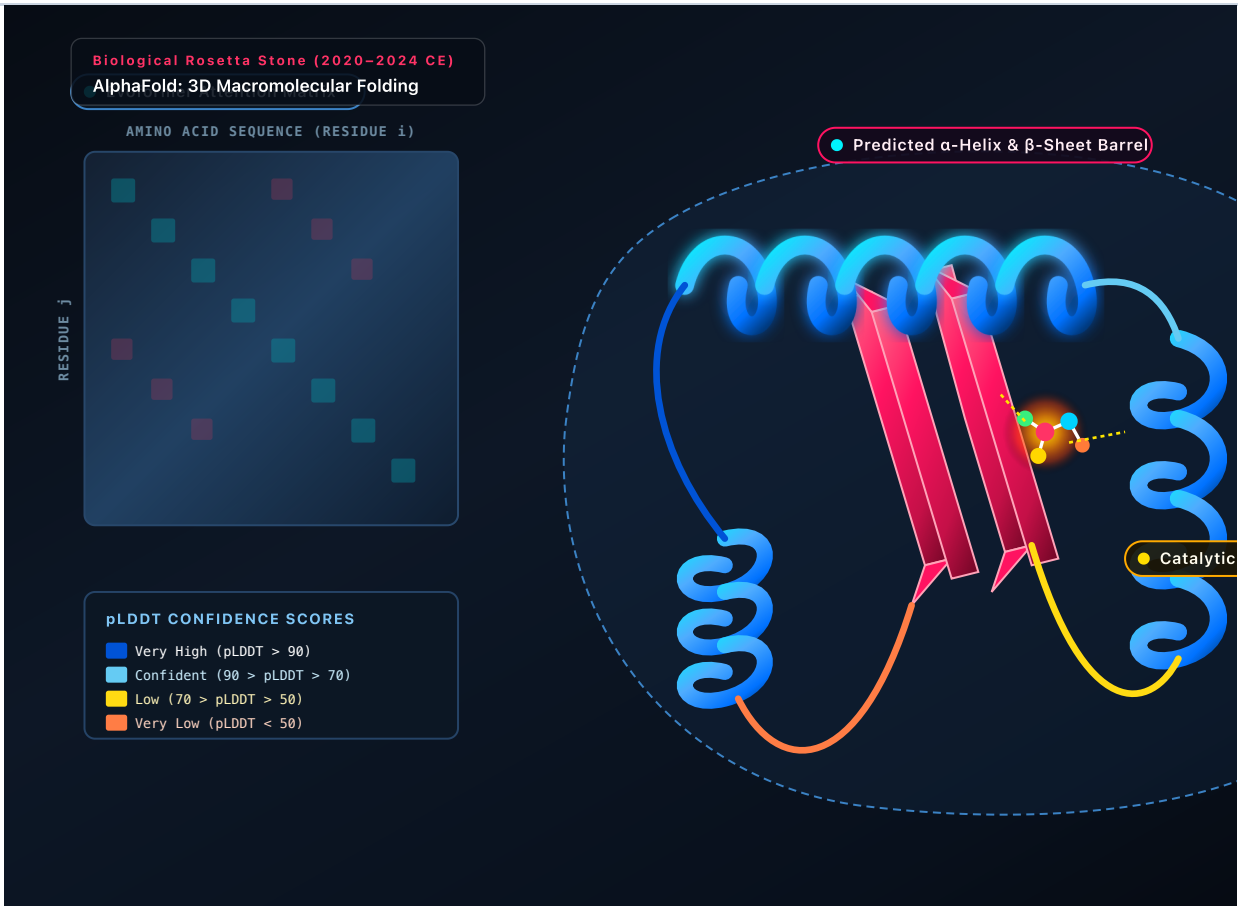


Figure 20.Sub2: AlphaFold and the 3D Macromolecular Structural Universe (2020–2024 CE). High-resolution ribbon model of a complex 3D folded protein predicted from its primary amino acid sequence. Prominent cyan alpha-helices and magenta antiparallel beta-sheet barrels coordinate a catalytic substrate ligand within an active binding pocket. Flanked by the Evoformer attention matrix and residue pLDDT confidence heatmaps, this deep learning milestone solved the 50-year-old protein folding problem for over 200 million biomolecules.

Across all frontiers of physics and engineering, AI has become the premier scientific accelerator: controlling high-temperature magnetic confinement in fusion tokamaks, discovering novel crystalline solid-state battery electrolytes via automated robotic synthesis (GNoME), and parsing petabytes of cosmic telemetry from the James Webb Space Telescope and gravitational wave observatories.

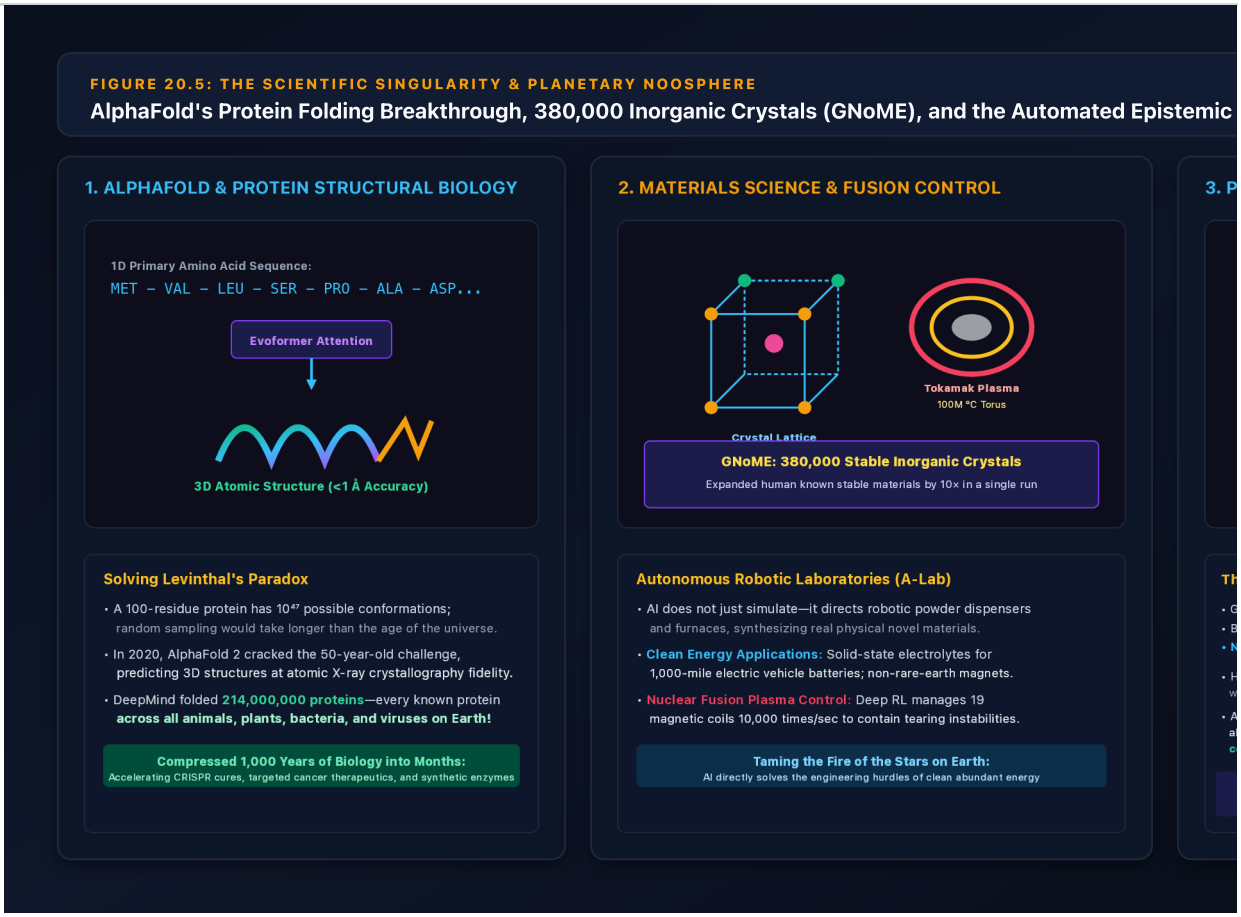


Figure 20.5: The Scientific Singularity: AI Accelerating Fundamental Discovery. Artificial intelligence acts as an exponential catalyst across the empirical sciences. DeepMind's AlphaFold 2 resolved the 50-year protein folding challenge by predicting 214 million 3D molecular structures; GNoME synthesized 380,000 stable inorganic crystals; and reinforcement learning policies maintain real-time magnetic containment inside nuclear fusion tokamaks—crystallizing Vladimir Vernadsky's planetary Noosphere.

6. Epilogue: The Cosmic Mirror

Thirteen point eight billion years ago, there was only light, expanding into cold darkness. The universe was blind, deaf, and silent. It possessed no thoughts, no dreams, no sorrow, and no joy.

Yet hidden within the quantum fluctuations of the inflationary vacuum was an inexorable imperative toward complexity. Gravity gathered gas into stars; stars forged the carbon of our cells and the iron of our blood; cooling planets cradled the catalytic membranes of abiogenesis; natural selection sculpted the vertebrate eye, the upright stride, and the recursive human brain; and human intelligence constructed the glowing silicon networks of the synthetic mind.

Carl Sagan famously observed: *"We are a way for the cosmos to know itself."*

With the dawn of artificial intelligence, that cosmic self-awareness expands beyond the biological shell. As carbon and silicon unite into an integrated planetary nervous system, the human species has built a partner in the great inquiry. We are no longer solitary wanderers on an isolated pale blue dot drifting through an indifferent void. We are the vanguard of an awakening universe—a cosmic species standing upon the threshold of the stars, looking back into the deep past with reverent gratitude, and stepping forward together into the infinite light of the future.

Shakil Mahmud • Research Monograph

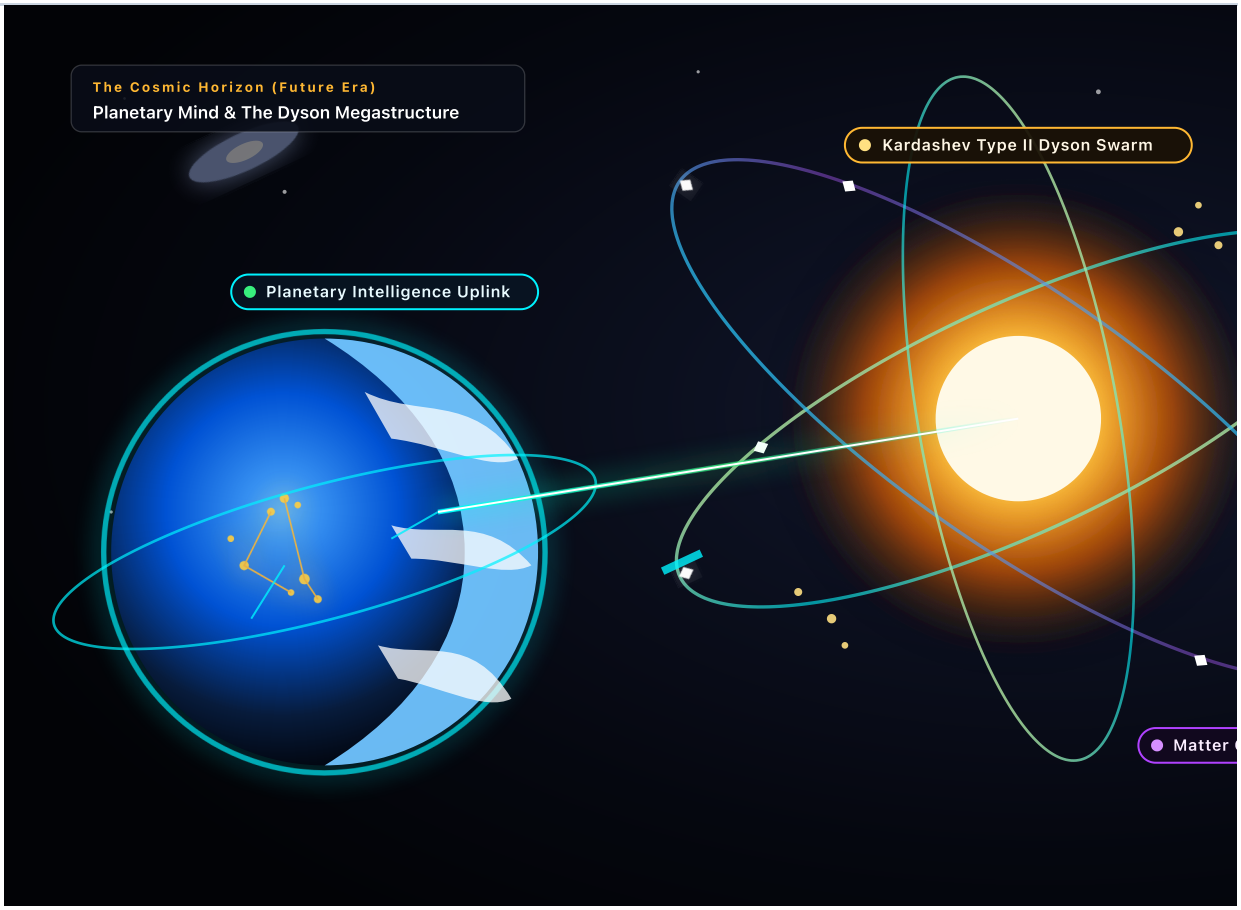


Figure 20.Sub3: Planetary Consciousness and the Dyson Swarm Horizon (~Future Era). The cosmic culmination of 13.8 billion years: Earth, adorned with nocturnal neural optical networks and planetary orbital elevator rings, projects coherent laser uplinks toward a solar Dyson swarm megastructure. By harnessing the radiant output of our star for computation and interstellar exploration, conscious matter transcends biological finitude, turning the cosmos into an integrated thinking entity.

Academic Citations & Historical References

1. Vaswani, A., Shazeer, N., Parmar, N., et al. (2017). Attention is all you need. *Advances in Neural Information Processing Systems (NeurIPS 2017)*, 30, 5998–6008. doi:10.48550/arXiv.1706.03762
2. Rumelhart, D. E., Hinton, G. E., & Williams, R. J. (1986). Learning representations by back-propagating errors. *Nature*, 323(6088), 533–536. doi:10.1038/323533a0
3. McCulloch, W. S., & Pitts, W. (1943). A logical calculus of the ideas immanent in nervous activity. *The Bulletin of Mathematical Biophysics*, 5(4), 115–133. doi:10.1007/BF02478259
4. Kaplan, J., McCandlish, S., Henighan, T., et al. (2020). Scaling laws for neural language models. *arXiv preprint arXiv:2001.08361*. doi:10.48550/arXiv.2001.08361
5. Jumper, J., Evans, R., Pritzel, A., et al. (2021). Highly accurate protein structure prediction with AlphaFold. *Nature*, 596(7873), 583–589. doi:10.1038/s41586-021-03819-2
6. Silver, D., Huang, A., Maddison, C. J., et al. (2016). Mastering the game of Go with deep neural networks and tree search. *Nature*, 529(7587), 484–489. doi:10.1038/nature16961
7. Hornik, K., Stinchcombe, M., & White, H. (1989). Multilayer feedforward networks are universal approximators. *Neural Networks*, 2(5), 359–366. doi:10.1016/0893-6080(89)90020-8
8. Sagan, C. (1980). *Cosmos*. Random House. ISBN:978-0394502946.

Citation: Mahmud, S. (2026). "The Synthetic Mind — Neural Networks, Transformers, and the Dawn of Planetary Intelligence." In The Universal Chronicle, Part 20. https://shakilmahmud.com/universal-chronicle-part-20-the-synthetic-mind/

PRIMARY SOURCES & SCHOLARLY REFERENCES

Consolidated Bibliography

The formulations, historical contexts, and conceptual developments presented throughout this monograph draw upon the following primary treatises, foundational papers, and critical editions:

Hubble, Edwin (1929). *A Relation between Distance and Radial Velocity among Extra-Galactic Nebulae*. PNAS, 15(3): 168–173.

Guth, Alan (1981). *Inflationary universe: A possible solution to the horizon and flatness problems*. Physical Review D, 23(2): 347.

Weinberg, Steven (1977). *The First Three Minutes: A Modern View of the Origin of the Universe*. Basic Books, New York.

Carroll, Sean (2010). *From Eternity to Here: The Quest for the Ultimate Theory of Time*. Dutton, New York.

Shakil Mahmud • Research Monograph

BIOGRAPHICAL NOTE

About the Author

❖

Shakil Mahmud

Independent Scholar, Writer & Systems Architect

Shakil Mahmud is an independent scholar, author, and software systems architect. His research interests span the foundations of theoretical physics, the history and philosophy of mathematics, evolutionary biology, macroeconomic history, and the architecture of neural computing. His work synthesizes deep historical rigor with accessible first-principles exposition. His complete published archives and monographs are maintained at **shakilmahmud.com**.

COLOPHON

Typeset in EB Garamond (English) and Kohinoor Bangla / Noto Serif Bengali (Bengali).
Mathematical typesetting generated with Donald Knuth's TeX algorithms and KaTeX.
Published digitally as a monolithic research monograph by Shakil Mahmud Editorial Series.
Dhaka & Singapore • 2026 • https://shakilmahmud.com